MA 982

NAS 1.55 : 2221

NASA Conference Publication 2221

16th Aerospace Mechanisms Symposium

COMPLETED

ORIGINAL

Proceedings of a symposium held at
John F. Kennedy Space Center
Kennedy Space Center, Florida
May 13-14, 1982

NASA

NASA Conference Publication 2221

16th Aerospace Mechanisms Symposium

Proceedings of a symposium co-sponsored by
National Aeronautics and Space Administration,
California Institute of Technology, and
Lockheed Missiles and Space Company, Inc., and
held at John F. Kennedy Space Center
Kennedy Space Center, Florida
May 13-14, 1982

NASA
National Aeronautics
and Space Administration

**Scientific and Technical
Information Branch**

1982

Blank Page

PREFACE

The proceedings of the 16th Aerospace Mechanisms Symposium held at the John F. Kennedy Space Center on May 13-14, 1982, are in this NASA Conference Publication. The symposium was sponsored by the National Aeronautics and Space Administration, the California Institute of Technology, and Lockheed Missiles and Space Company, Inc.

The purpose of the symposium was to provide a forum for the interchange of information among those active in the field of mechanisms technology. To that end, 24 papers were presented on aeronautics and space flight, with special emphasis on actuators and aerospace applications for ground support equipment, latches, connectors, and other mechanisms for large space structures. The papers were prepared by engineers from a broad aerospace background including the U.S. aerospace industry, NASA, and European participants.

At this turning point in the American space-flight program, we are entering the operational era, and there must be an improvement in productivity and a reduction in the costs of operation. These symposia, with the active interchange of experience, assist in a growth of better design and operational performance.

The efforts of the review committee, session chairmen, and speakers contributing to the technical excellence and professional character of the conference are especially appreciated.

The use of trade names or names of manufacturers in this publication does not constitute an official endorsement of such products or manufacturers, either expressed or implied, by the National Aeronautics and Space Administration.

Peter A. Minderman
Host Chairman

Blank Page

ORGANIZING AND REVIEWING COMMITTEE

The papers presented at the symposium were selected and reviewed by the Organizing Committee. Responsibility for content and technical accuracy lies with each respective author. The committee included the following members:

General Chairman:	Charles W. Coale, Lockheed Missiles and Space Company, Inc.
Operations/Executive Chairman:	Alfred L. Rinaldo, Lockheed Missiles and Space Company, Inc.
Administrative/Executive Chairman:	David F. Welch, California Institute of Technology
Host Chairman:	Peter A. Minderman, NASA-Kennedy Space Center
Committee Members:	Paul W. Bomke, Jet Propulsion Laboratory
	Aleck C. Bond, NASA-Johnson Space Center
	Tom F. Bonner, Jr., NASA-Langley Research Center
	H. Mervyn Briscoe, European Space Technology Center
	Kenneth C. Curry, Jet Propulsion Laboratory
	Charles R. Darwin, NASA-Marshall Space Flight Center
	David F. Englebert, NASA-Ames Research Center
	Otto H. Fedor, NASA-Kennedy Space Center
	Angelo Giovannetti, NASA-Ames Research Center
	Harvey H. Horiuchi, Jet Propulsion Laboratory
	Allen J. Louviere, NASA-Johnson Space Center
	Frank T. Martin, NASA-Goddard Space Flight Center
	James B. Sterett, Jr., NASA-Marshall Space Flight Center
	Bowden W. Ward, NASA-Goddard Space Flight Center
	Nathan D. Watson, NASA-Langley Research Center

Blank Page

TABLE OF CONTENTS

Preface iii

Organizing and Reviewing Committee v

1. Baggie: A Unique Solution to an Orbiting Icing Problem 1
   L. J. Walkover

2. Flight Support System Mechanisms 23
   William A. Leavy

3. The Design and Development of an End Effector for the Shuttle Remote Manipulator System 45
   Robert G. Daniell and Savi S. Sachdev

4. Centerline Latch Tool for Contingency Orbiter Door Closure 63
   Robert C. Trevino

5. Spacecraft Launch Vehicle Event Sequencing System 73
   Vincent R. Noel

6. Development of an Ultra-Low-Shock Separation Nut 87
   William Woebkenberg, Donald N. Matteo, and Vaughn D. Williams

7. A Ball Trunnion Capture Latch 99
   David V. Adams and Brendan Alchorn

8 A Movable Stop Mechanism for the SIRE Telescope 109
   R. E. Tweedt and R. N. Poulsen

9. Dual Drive Actuators 123
   Douglas T. Packard

10. Design Aspects of a Solar Array Drive for SPOT, With a High Platform Stability Objective 143
    J. Cabillic, J. P. Fournier, P. Anstett, M. Souliac, and G. Thomin

11. Development of a High Stability Pointing Mechanism for Wide Application 159
    A. J. D. Brunnen and R. H. Bentall

12. Computer-Aided Design and Analysis of Mechanisms 175
    Frank L. Knight

13. Estimation of Bearing Contact Angle In-Situ by X-Ray Kinematography 189
Peter H. Fowler and Frank Manders

14. National Geotechnical Centrifuge 201
James A. Hallam, Nans Kunz, and Wilbur C. Vallotton

15. Design and Analysis Considerations for Deployment Mechanisms in a Space Environment 211
P. L. Vorlicek, J. V. Gore, and C. T. Plescia

16. A Deployment Mechanism for the Double Roll-Out Flexible Solar Array on the Space Telescope 223
T. R. Cawsey

17. Solar Drum Positioner Mechanisms 235
L. W. Briggs

18. Deployment/Retraction Ground Testing of a Large Flexible Solar Array 249
Darius T. Chung

19. The Development of a Universal Diagnostic Probe System for Tokamak Fusion Test Reactor 265
Richard Mastronardi, Richard Cabral, and Dennis Manos

20. Elastic Suspension of a Wind Tunnel Test Section 277
Russell Hacker, Stephen Rock, and Daniel B. DeBra

21. Space Shuttle External Tank Gaseous Oxygen Vent System 299
William G. Franklin

22. Design, Development and Mechanization of a Precision Deployable Truss With Optimized Structural Efficiency for Spaceborne Applications 315
N. D. Craighead, T. D. Hult, and R. J. Preliasco

23. The Mechanical Design of a Vapor Compressor for a Heat Pump To Be Used in Space 329
F. Berner, H. Oesch, K. Goetz, and C. J. Savage

24. Design of a 7kW Power Transfer Solar Array Drive Mechanism 341
J. S. Sheppard

BAGGIE: A UNIQUE SOLUTION TO AN ORBITER ICING PROBLEM

L. J. Walkover*

ABSTRACT

Solving the orbiter icing problem that is located in two lower surface mold line cavities presented a challenging assignment on the Space Shuttle program. These two cavities are open during Shuttle ground operations and ascent, and are then closed after orbit insertion. If not protected, these cavities may be coated with ice, which may be detrimental to the adjacent thermal protection system (TPS) tiles if the ice breaks up during ascent, and may hinder the closing of the cavity doors if the ice does not break up. The problem of ice in these cavities was solved by the use of a passive mechanism called baggie, which is a purge curtain used to enclose the cavity and is used in conjunction with gaseous nitrogen as the local purge gas. The baggie, the final solution, is unique in its simplicity, but its design and development were not. This paper discusses the final baggie design and emphasizes its development testing. Also discussed are the baggie concepts and other solutions not used. This work was done under contract to NASA's Johnson Space Center (JSC) in Houston, Texas.

INTRODUCTION

The Space Shuttle consists of the reusable orbiter, expendable external tank (ET), and the reusable solid rocket boosters (SRB), which are protected from the various environments during ground operations, launch, orbit, and reentry (Figure 1). The environmental protection systems for the Shuttle elements vary, depending on the requirement, e.g., the TPS on the external surface of the orbiter, and the external spray-on foam insulation on the ET. On the orbiter, there are two local areas that are protected against the ground environments by the subject of this paper.

The mated Shuttle has two 17-inch diameter propellant feedlines that transfer liquid hydrogen (LH_2) on the left-hand side, and liquid oxygen (LO_2) on the right-hand side from the ET to the orbiter. The feedlines are connected and separated at the two interfaces between the two vehicles via each of the ET-to-orbiter umbilical separation disconnects. Each of these installations in the orbiter results in a local large-size mold line umbilical cavity that is open during ground operations and ascent, and is then closed by the respective left-hand and right-hand umbilical cavity doors after orbit insertion. Each cavity is approximately 50 inches by 50 inches wide by 6 inches deep. Figure 2 shows the location of the left-hand and right-hand cavities on the underside of the orbiter toward the rear of the vehicle.

---

*L. J. Walkover is manager of Structure Design for the Space Shuttle Progrem at the Rockwell International Space Transportation and Systems Group in Downey, California.

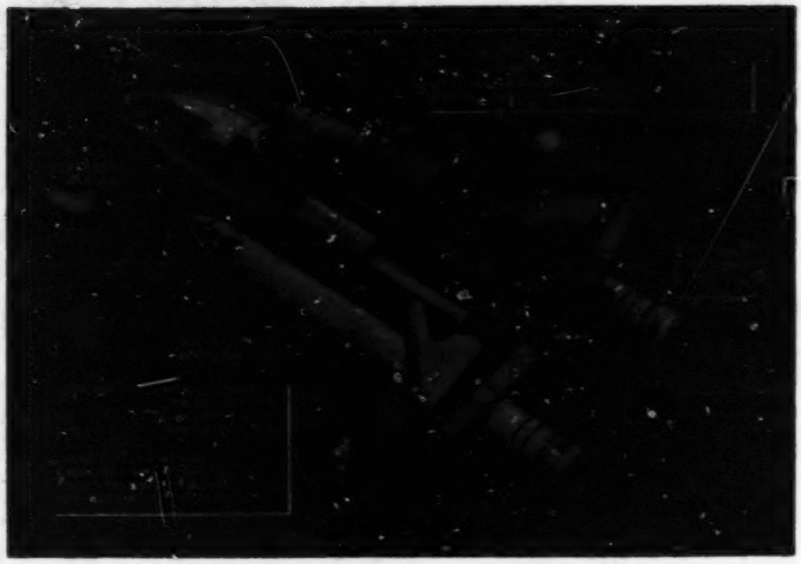

Figure 1 – Space Shuttle Vehicle

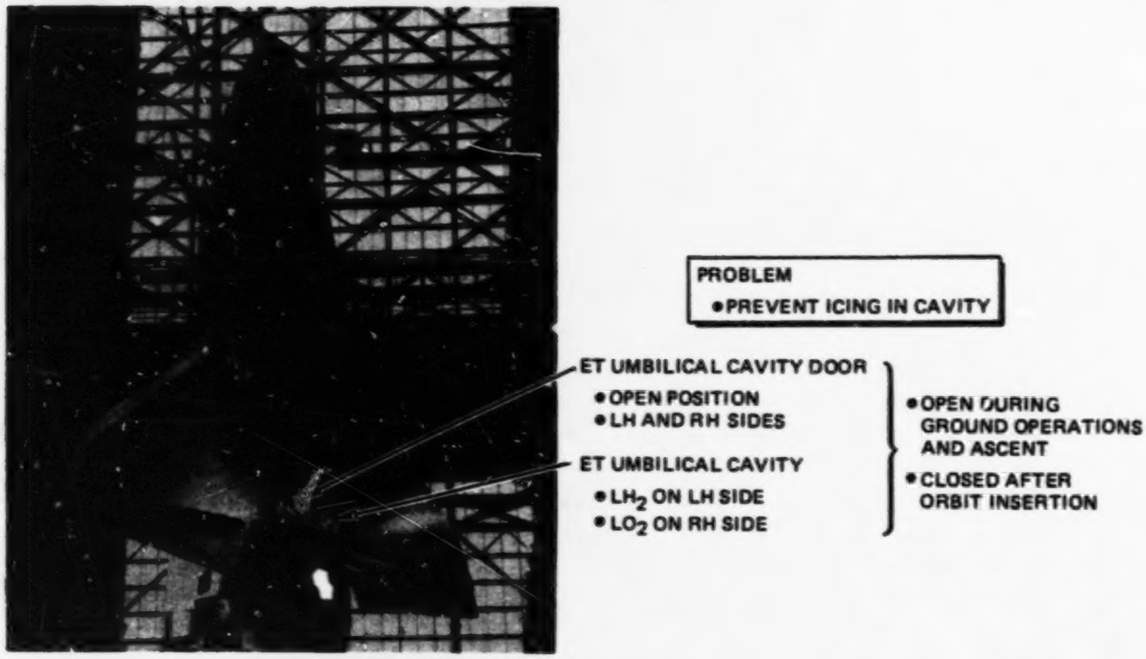
PROBLEM
• PREVENT ICING IN CAVITY
ET UMBILICAL CAVITY DOOR
• OPEN POSITION
• LH AND RH SIDES
ET UMBILICAL CAVITY
• LH_2 ON LH SIDE
• LO_2 ON RH SIDE
• OPEN DURING GROUND OPERATIONS AND ASCENT
• CLOSED AFTER ORBIT INSERTION

Figure 2 – Space Shuttle Orbiter

The local temperatures on the structure and the umbilicals in the cavity areas are influenced by the cryogenic temperatures of the local propellant feedlines and the payload when the payload contains cryogenic stages. The feedlines and payload cryogenic temperatures result in local, below-freezing temperatures that may cause icing because of condensation or rain on the structure at the cavity surface areas. The icing may be thick and dense enough to prevent the doors from closing by either jamming the door closure/locking mechanism or blocking the door/cavity interfaces. In addition, ice breakup during Shuttle ascent may damage the TPS tiles that cover most of the orbiter's exterior surface. It must be emphasized that the doors must be closed or a successful reentry will not be accomplished.

Many studies were made to solve the icing problem. The solutions had to be compatible with the orbiter's cost, schedule, manufacturing, weight, and installation. One of the main obstacles in finding a solution was that there was not much space available. This severely limited the design concepts and the details of any solution. In addition, the baggie design, as it matured during design, development, fabrication, and installation, required a step-by-step approach that was planned and executed in real time instead of being planned before the time of execution.

Because of its simplicity, the baggie design is a unique solution to a perplexing problem. It was developed from design efforts, expedient ground testing, and sophisticated transonic wind tunnel testing that yielded negative results until the final solution was determined.

REQUIREMENTS

The cavity icing solution was designed to satisfy, to various degrees, the listed requirements.

1. Prevent ice formation that could inhibit or harm ET umbilical separation, ET umbilical cavity door closure, or TPS tiles
2. No dedicated purge system: GN_2 vented from aft fuselage
3. Pad wind environment: 100 mph locally at ET umbilical cavity
4. Does not have to survive launch firing
5. Does not have to be reusable
6. Provide vision for cameras located in cavity, which are used on development test flights only, to record ET separation from the orbiter
7. No delta separation force requirement by orbiter or ET
8. Least impact on adjacent orbiter, ET, and launch facility structures and systems
9. Installation capability at Kennedy Space Center (KSC) both prior and subsequent to mating
10. Minimum weight and cost

DESIGN CONCEPTS

The icing problem in the cavities was determined late in the orbiter development program. At the time it was identified, the structure in and about the cavity had been designed, the door and its operating (closure and locking) mechanism were relatively complete, most of the local systems including the ET umbilical separation disconnect and its supporting closeout curtain were in their final stages, local TPS tile and TPS seals were far along in their design stages, and, most important of all, the size of the cavity and door was fixed. The late start, combined with the requirement that any icing problem solution have minimum impact on released or built orbiter structure and systems, and if possible, no impact on the ET or launch facilities, severely limited the scope and feasibility of any design solution.

Design concepts for the icing solution are listed in Table 1.

As shown in Table 1, the initial approach for the icing solution was to limit or raise the local temperatures to above the freezing temperature to simply prevent any ice formation. Two basic concepts used this method. One was to utilize insulation by coating local areas or, if required, the entire cavity. It was quickly determined that insulation by itself was not adequate. The next

TABLE 1 – DESIGN CONCEPTS

Method	Objective
1. Insulation and/or electrical heaters a. Complex b. Active system c. Heavy 2. Hot gas blower a. Ground-supplied equipment (GSE) b. Removed before launch c. High pad reach (36 feet) d. Additional GSE disconnects	• Increase local temperature above freezing
3. Hard enclosure a. ET supported b. Δ ET/orbiter interfaces c. Δ separation forces d. Heavy 4. Purge barrier a. GSE b. Removed before launch (lanyard) c. High pad reach (36 feet) d. Additional GSE pad disconnects → 5. Purge curtain a. Thin film/frangible b. Nonreusable c. Very lightweight d. Development requirements	• Provide purge chamber • Keep moisture and rain out

attempt was to utilize electrical heaters, but the power requirements became excessive. Insulation was then combined with the use of local electrical heaters. This option was eliminated because of the complexity involved (insulation, heaters, and exposed mechanisms), the use of an active system (heaters), the lack of clearance room, the power requirements (approximately 622 watts), and the weight (approximately 110 pounds).

The second concept was to utilize a hot gas blower system supplied by GSE. This system used a blower feeding hot gas into two main ducts that reached approximately 36 feet up from the pad to each cavity. The ends of the blowers were fitted with either fixed or oscillating nozzles to direct the hot air to the required locations. This concept was quickly eliminated because the two main ducts had to be removed just prior to launch so as not to impede the vehicle launch. (KSC would not tolerate another ground separation system.) In addition, the excessive reach required and the limited clearance between the orbiter and the ET made this concept impractical.

The second approach to the icing problem (Table 1) was to provide a purge chamber that could be filled with a purge gas, and, at the same time, keep any rain or moisture out. One concept was to utilize a hard enclosure that would be mounted on the ET and enclose the cavity. This would be a typical structural approach utilizing a structural assembly. This design was eliminated because it required additional interfaces with and changes to the ET, required a change in the orbiter/ET separation force, and was relatively heavy. The next concept was to utilize a purge barrier that would essentially be a flexible external enclosure to the cavity (Figure 3). Covering the outer surface of the cavity essentially isolated all structures, systems, and mechanisms from the local

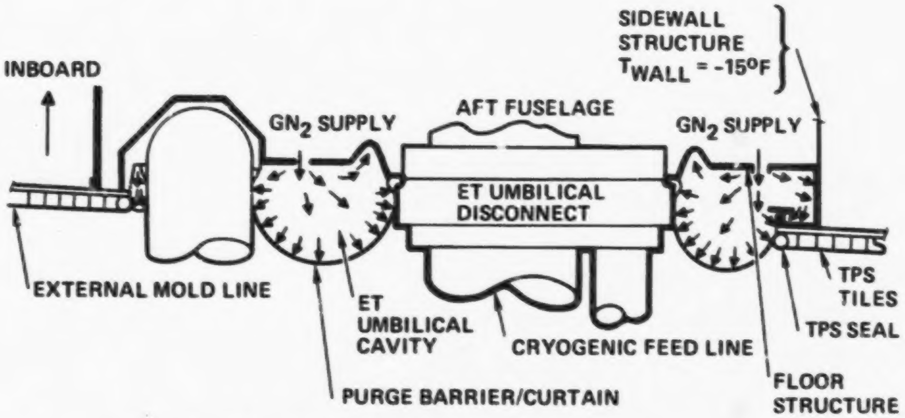

- PURGE CHAMBER ISOLATES COLD SOAKED STRUCTURE, SYSTEMS AND MECHANISM FROM PAD HUMID/RAIN ENVIRONMENTS
- GN_2 PURGE PREVENTS ICE FORMATION (BLOCKS AMBIENT AIR INTRUSIONS)

Figure 3 – Purge Chamber Concept

humid and rain environment. The enclosure was then filled with GN_2 purge gas, which prevents ice formation by blocking ambient air intrusion. The purge barrier was to be installed on the orbiter, and was to be removed immediately before or at launch by a GSE pad lanyard. This concept was dropped because of the required lanyard reach, approximately 36 feet. The limited clearance between the orbiter and the ET made it questionable as to whether the lanyard and purge barrier could be pulled free without damaging the Shuttle. And again, KSC was not in favor of another ground separation system.

The final concept was the frangible purge curtain, now called the baggie. (The basic concept is shown on Figure 3.) The concept was appealing because it was simple, lightweight, could be designed with the least impact on the adjacent structure and systems, and required no changes to the ET structure or separation force. The concept used a curtain made of a thin, frangible film material that did not have to survive the launch environment. It was accepted that new baggies would be installed for flight readiness firing and for each launch. It was also accepted that the material would be selected as the design progressed and that some development would be required, but how much development would be required to select and fabricate the material, the curtain shape, and the curtain attachments was not known. In addition, a major limitation was the cavity size, and the fixed door/cavity clearance, thus severely limiting the space for curtain attachments.

BAGGIE EVOLUTION

The evolution of the baggie is shown in Table 2, which lists the basic features that were changed during the design, development, and testing phases.

TABLE 2 – BAGGIE EVOLUTION

Item	Hemispherical Baggie ⟶	Flat Baggie
Shape	Hemispherical	Flat
Material	2 mil Kel F 800	2 mil Kapton
Fabrication	Spray-on mold	Cut from sheet stock
Attachment	• Tape to tiles, structure, umbilical • Zip lock • Zip lock + clips	• Zip lock + clips • Plate attached by screws (outer) • Drawstring (inner)) • Plate attached by screws (outer/inner)
Development	• Mold for shape • Material fabrication • Separation agent • Material reinforcement • Installation technique	• Assembly tool • Material assembly
Testing	• Door closure • AEDC transonic wind tunnel • Wind machine	• Wind machine • Door closure • AEDC transonic wind tunnel • Baggie/retainer integrity deviation test

Hemispherical Baggie

The original baggie (Figure 4) utilized a radial cross-section, which is the natural form to react to internal pressure, especially with a material with weak structural properties. The radius at various locations about the baggie periphery varied, depending on the distance between the umbilical and the cavity opening as defined by the cavity sill. The radial cross-section was tangent at the TPS thermal barrier (outer periphery) and to the umbilical (inner periphery). The baggie tangencies are to keep moisture and rain out of the cavity and away from the cavity edges (Figure 5). The actual shape of the LO_2 baggie is shown by Figure 6, which is the tool used for the baggie assembly. The material was 2 mil Kel F 800, which has a low tensile strength (1,500 psi), a low service temperature (+250°F), and was self-extinguishing; all characteristics picked to allow separation during boost. The baggie material is clear, which allows cameras to take separation pictures through the material.

Figure 7 indicates a possible baggie installation–if it survives the launch. There is no installation problem if the baggie is totally enclosed within the door. This was demonstrated by door closure tests, which proved the door mechanisms will penetrate through the baggie material, and by additional door closure tests in which the bunched baggie material was stuffed in and about the individual mechanisms without affecting door mechanism or closure. Thermal data indicated that there would be no problem if the baggie locally protrudes external to the door: the door closure will not jam, the baggie will not burn past the thermal barrier, and it will not trip the boundary layer. Figure 8 is an example of the problem of designing the baggie to fit about the door hinge mechanism when the door is open, but still not prevent proper hinge movement to allow the door to close.

The original thoughts on attaching the baggie to the structure and umbilical were to simply use tape of a suitable nature (Kapton tape). The tape attachment would be either external at the outer surface of the tiles or internal at the structure. These concepts were eliminated because no relatively smooth and uninterrupted surfaces (tiles or structures) were available for attachment, and, possibly more important, the pull action of the baggie tended to peel the tape off the surface it was attached to. The requirement for no delta separation forces meant that the baggie must be attached to the orbiter side of the umbilical disconnect.

The selected design used for baggie attachment to both the cavity structure (outer periphery) and the umbilical (inner periphery) is shown in Figure 9. It is similar to the zip-lock closure of commercial plastic bags by the same name. The outer periphery locking retainer (aluminum extrusion) is attached by No. 4-40 screws tapped into the adjacent structural aluminum skin. The inner periphery locking retainer uses No. 4-40 screws and nuts. The outer and inner periphery of the baggie were wrapped around a silicone rubber locking cord and reinforced with Kapton tape. The baggie cord assembly was hand forced into the preinstalled locking retainer. An interference fit at the retainer opening assured a positive retention force. The radial shape of the baggie resulted in a shear retention reaction rather than a direct tension pullout. The baggie was designed to tear and separate at the edge of the Kapton reinforcing tape. The zip-lock installation was also judged to be

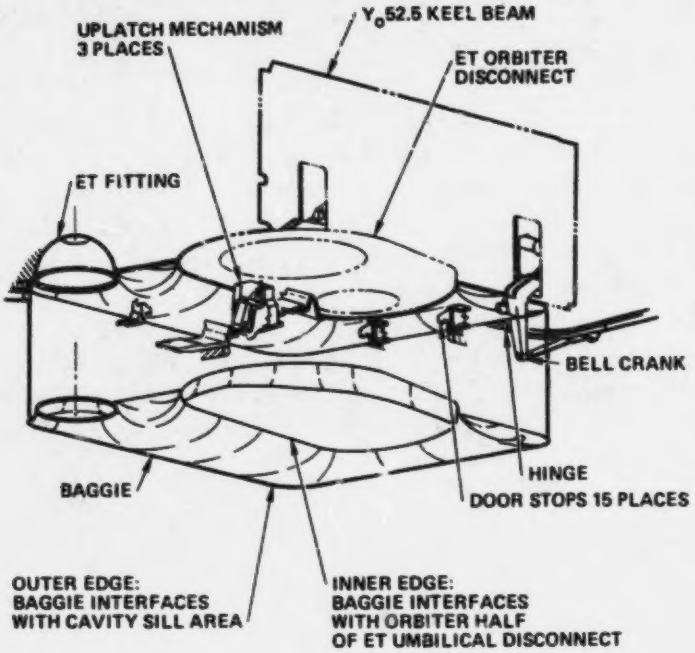
UPLATCH MECHANISM
3 PLACES
$Y_0$52.5 KEEL BEAM
ET ORBITER
DISCONNECT
ET FITTING
BELL CRANK
BAGGIE
HINGE
DOOR STOPS 15 PLACES
OUTER EDGE:
BAGGIE INTERFACES
WITH CAVITY SILL AREA
INNER EDGE:
BAGGIE INTERFACES
WITH ORBITER HALF
OF ET UMBILICAL DISCONNECT

BAGGIE MATERIAL
- 2 MIL KEL F 800

FABRICATION
- SPRAY ON MOLD

ATTACHMENT
- ZIP LOCK + CLIPS

FIRST INSTALLATION
- BAGGIE FIT AND PRESSURE CHECKED AT PALMDALE VIA AFT FUSELAGE PURGE PRESSURE TEST
- BAGGIE REMOVED FOR FERRY AND KITTED
- BAGGIE REINSTALLED AT KSC AND VERIFIED VIA AFT FUSELAGE PURGE PRESSURE TEST

FIRST INSTALLATION
- POST-MATING AT KSC

Figure 4 – Baggie Design; Hemispherical

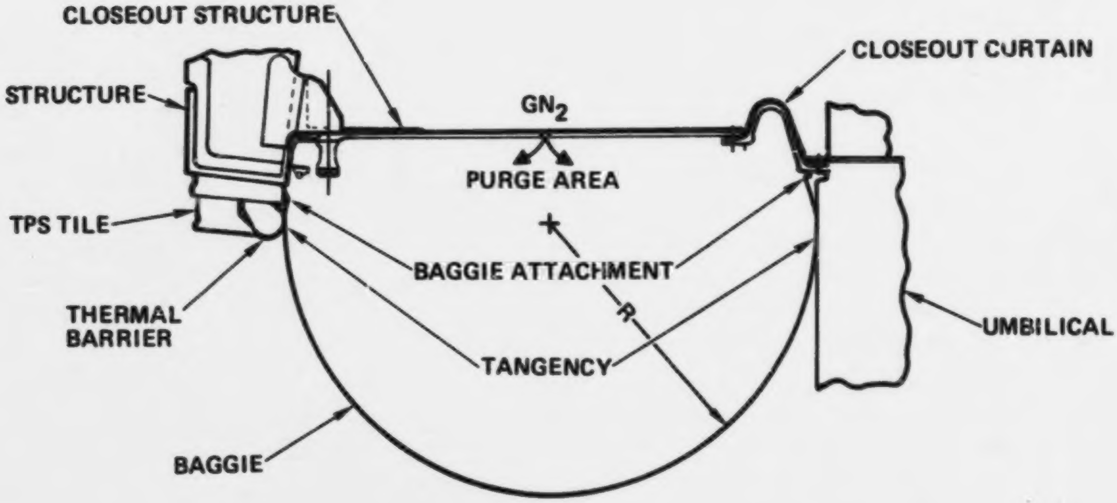
CLOSEOUT STRUCTURE
CLOSEOUT CURTAIN
STRUCTURE
GN_2
PURGE AREA
TPS TILE
BAGGIE ATTACHMENT
R
THERMAL
BARRIER
UMBILICAL
TANGENCY
BAGGIE

✓ **IDEAL BAGGIE INSTALLATION**

PROVIDE PURGE CHAMBER AND KEEP MOISTURE AND RAIN OUT

Figure 5 – Typical Baggie Cross-Section; Hemispherical

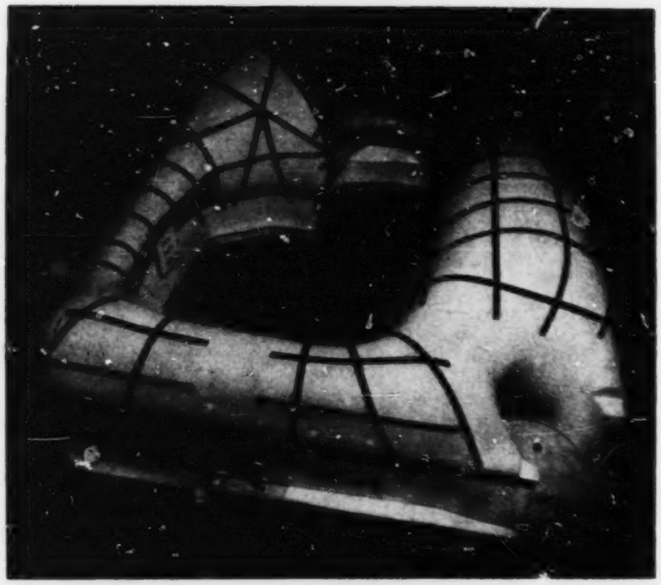

- BAGGIE SHAPE SHOWN BY TOOL CONTOURS
- STRIPS INDICATE CRISSCROSS KAPTON TAPE REINFORCEMENT
- TOOL USED TO ASSEMBLE BAGGIE TO INNER AND OUTER PERIPHERY ZIP LOCK LOCKING CORD

Figure 6 – Hemispherical Baggie (LO_2) Assembly Tool

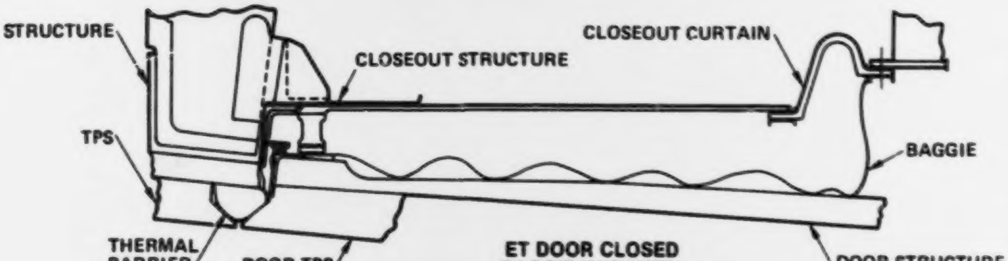
STRUCTURE
CLOSEOUT CURTAIN
CLOSEOUT STRUCTURE
TPS
BAGGIE
THERMAL BARRIER
DOOR TPS
DOOR STRUCTURE

ET DOOR CLOSED
BAGGIE IN CAVITY

ET DOOR CLOSED; BAGGIE PROTRUDING PAST DOOR

✓ BAGGIE WILL NOT
  - PREVENT DOOR CLOSURE
  - BURN PAST THERMAL BARRIER
  - TRIP BOUNDARY LAYER

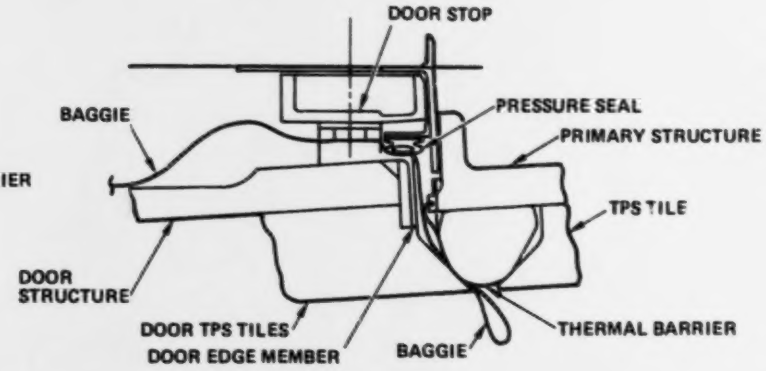
DOOR STOP
BAGGIE
PRESSURE SEAL
PRIMARY STRUCTURE
TPS TILE
DOOR STRUCTURE
DOOR TPS TILES
DOOR EDGE MEMBER
BAGGIE
THERMAL BARRIER

Figure 7 – If Baggie Survives Launch

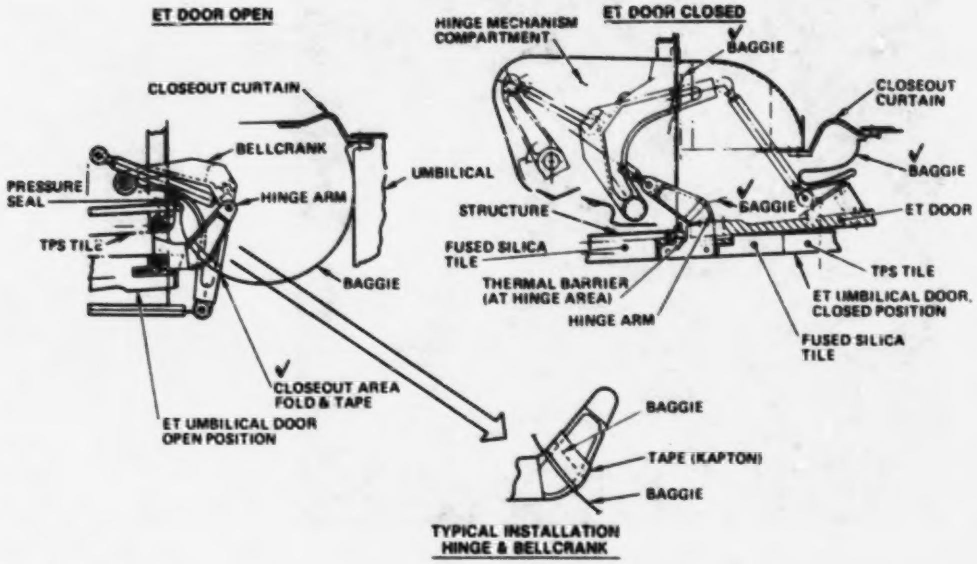
ET DOOR OPEN
CLOSEOUT CURTAIN
BELLCRANK
PRESSURE SEAL
HINGE ARM
UMBILICAL
TPS TILE
BAGGIE
✓ CLOSEOUT AREA FOLD & TAPE
ET UMBILICAL DOOR OPEN POSITION
HINGE MECHANISM COMPARTMENT
ET DOOR CLOSED
✓ BAGGIE
CLOSEOUT CURTAIN
✓ BAGGIE
STRUCTURE
✓ BAGGIE
ET DOOR
FUSED SILICA TILE
THERMAL BARRIER (AT HINGE AREA)
HINGE ARM
TPS TILE
ET UMBILICAL DOOR, CLOSED POSITION
FUSED SILICA TILE
BAGGIE
TAPE (KAPTON)
BAGGIE
TYPICAL INSTALLATION HINGE & BELLCRANK

Figure 8 – Hemispherical Baggie Installation; Hinge Area

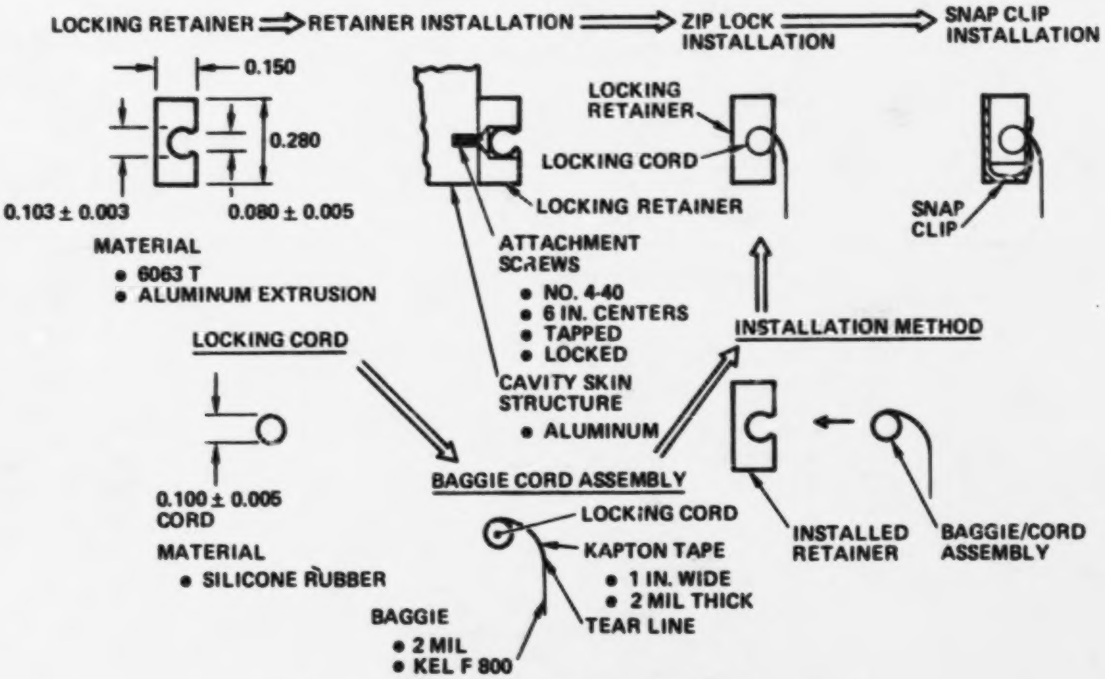
LOCKING RETAINER
RETAINER INSTALLATION
ZIP LOCK INSTALLATION
SNAP CLIP INSTALLATION
0.150
0.280
0.103 ± 0.003
0.080 ± 0.005
MATERIAL
• 6063 T
• ALUMINUM EXTRUSION
LOCKING RETAINER
LOCKING CORD
LOCKING RETAINER
SNAP CLIP
ATTACHMENT SCREWS
• NO. 4-40
• 6 IN. CENTERS
• TAPPED
• LOCKED
CAVITY SKIN STRUCTURE
• ALUMINUM
INSTALLATION METHOD
LOCKING CORD
0.100 ± 0.005 CORD
MATERIAL
• SILICONE RUBBER
BAGGIE CORD ASSEMBLY
LOCKING CORD
KAPTON TAPE
• 1 IN. WIDE
• 2 MIL THICK
TEAR LINE
BAGGIE
• 2 MIL
• KEL F 800
INSTALLED RETAINER
BAGGIE/CORD ASSEMBLY

Figure 9 – Hemispherical Baggie Attachment

reasonably easy to do. A special hand tool was developed to help install the baggie and cord into the retainer.

Because of the unusual shape of the baggie (Figure 6), Kel F 800 sheet stock could not be used because there was not a way to transform the flat sheet stock to fit the complicated shape of the baggie. Instead, a spray-on mold technique was selected. Kel F 800 is adaptable to spraying, which is one of the reasons it was chosen. The procedure for spray-on mold is to spray 0.5 mil on the mold, and cure at 425°F. This is repeated four times. The result is a 2 mil Kel F 800 baggie of the correct shape, which is then peeled off the mold and assembled on an assembly tool (Figure 6) with the locking cord at both the inner and outer peripheries.

Fabrication development was required for the actual spraying, the mold materials, and the parting agent. The spraying techniques had to be developed to control the actual thickness of each spray and the total final thicknesses. (Technicians were trained as to this technique.) The original mold was made of glass epoxy from a plaster master. The glass epoxy molds would not take the repeated high temperature required during each spray curing cycle--they deteriorate. The glass epoxy molds were replaced by electro-formed nickel molds, which were also made from the plaster masters. These latter molds were successful in that they stood up to repeated temperature usage. Various parting agents (to allow the baggie to be peeled off the mold without tearing) were utilized and did not work satisfactorily. It was found that a Teflon coating sprayed on the electro-formed nickel molds allowed the baggies to be successfully peeled off the molds.

The baggies were tested for proper separation from the orbiter. The testing was done at the transonic wind tunnel at the Arnold Engineering Development Center (AEDC) in Tullahome, Tennessee. The baggie testing was piggy-backed to the planned aerodynamic flow tests used in the development testing of the TPS tiles. Figure 10 shows the baggie test bed for the LO_2 right-hand side, which included the cavity structure, the adjacent TPS tiles, the ET structural crossbeam, the umbilical, and the installed baggie. The baggie shown is not the hemispherical baggie, but the flat baggie to be discussed later. Five runs were made: one with strips of Kel F 800 and four runs with the installed baggie. Problems were encountered when a long section of the locking cord separated from the locking retainer, slapped, and damaged some downstream TPS tiles before total baggie separation occurred. Snap clips (Figure 9) were designed to slip about the locking retainer and the locking cord. These were installed approximately six inches on center and the locking cords, after installation, were slit at each snap ring to limit the length of cord that could separate from the retainer (if it were to come out) and possibly damage the adjacent tiles. The last runs were successful in that the baggie separated properly (at approximately 0.25 Mach) and the locking cord did not come out of the locking retainer.

The original plan was to install the baggies on Orbiter 102 during manufacturing operations at Palmdale. This would verify the installation (fit and pressure check), provide training for manufacturing personnel, and turn up any required changes or installation difficulties. It was not done because certified baggies were not available, i.e., the baggie was not designed, developed, and tested in time; therefore, two complete sets of baggies (one set plus one spare set) were sent to KSC to be installed on the mated Shuttle. The two field splices (per cavity) were in a difficult location to reach. They were relocated by cut and fit with baggie material segments and Kapton tape. Numerous tears occurred in the baggies during handling and installation, which were spliced by Kapton tape. There were problems in closing out and taping the baggie in the hinge areas, and the baggies did not fit properly (tangency) about the inner and outer periphery. The baggies were finally installed and the installation accepted for the first flight of Orbiter 102—space transportation system flight 1 (STS-1).

The following day, the local winds at KSC increased in velocity. This resulted in one of the baggies being torn away. It was estimated that the ground winds were at 50 mph, but the local cross wind in the vicinity of the cavities was as high as 80 mph. Higher cross wind velocities (relative to the vertically oriented Shuttle) are expected in the cavity area because of the maze of structures surrounding the cavity and the reduced area between the orbiter and the ET as the winds pass crosswise between the two vehicles. Immediately, the spare set of baggies was installed, but a few days later they also failed in a moderate wind.

An immediate program was set up for ground testing of the hemispherical baggies. A limited number of spare LO_2 baggies were available for the tests. As time (the launch schedule) was a major factor, ground testing had to be as expeditious as possible. The thought was to mount the baggie test bed (Figure 10) on a flat bed truck with a long ground run to attain the required velocity. The test runs were to be done on either the long runways or the flat test salt bed available at Palmdale and Edwards Air Force Base. This was reluctantly discarded as being too unreliable, and probably too dangerous.

Ground testing was done at the Downey plant facilities utilizing a wind machine owned by Controlled Airstreams, Inc. (See Figure 11.) The machine was immediately available, and would provide controlled air flow over the baggie test bed (Figure 10). The wind machine utilized a Continental gasoline engine mounted behind a flow screen; the combination adjustable for flow orientation and installed on a trailer for mobility. The machine normally is used by various fire services for agricultural spraying and for creating special effects for television and the movies.

During the first run, the baggie failed at approximately 50 mph. Another baggie was immediately reinforced by crisscross strips of Kapton tape spaced four to six inches apart (Figure 6). This baggie assembly also failed. It was planned to then increase the thickness to provide more material strength, but this was nullified because it would take approximately three weeks to fabricate the baggie, and, more important, it was realized that the basic material, shape, and retention had to be changed. The final plan for GSE ground protection of the baggie from the winds was not considered because 36 feet of access stands and GSE protection would have to be removed before launch. Figure 12 is a summary of the problems with the hemispherical baggie and the reasons for stopping work on this design.

The first flight of the Shuttle did not contain baggies because baggies of proper design and certification were not available in time for the launch. Additional thermal analysis also indicated that there would be no ice in the ET umbilical cavity at launch unless it rained after the propellant tanks had been filled. During previous tanking tests and launch tanking, there had been no rain and

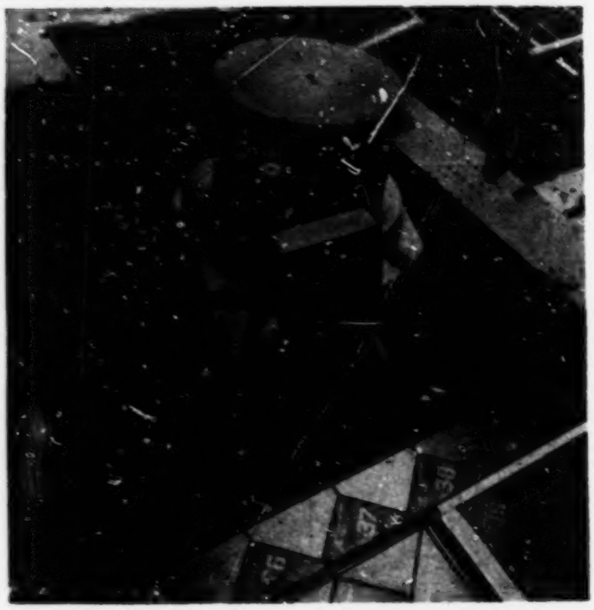

- USED FOR
  - GROUND TESTING WITH WIND MACHINE AT DOWNEY, CA.
  - WIND TUNNEL TESTING AT AEDC SUPERSONIC TUNNEL
- ASSEMBLY OF
  - CAVITY STRUCTURE
  - UMBILICAL
  - ET CROSS BEAM
  - ADJACENT TPS TILES
  - BAGGIE

- LO_2 UMBILICAL
- RH SIDE

- ORIGINALLY USED FOR
  - AERODYNAMIC FLOW TESTS FOR TPS TILES

Figure 10 – Baggie Test Bed

- WIND MACHINE, WHICH IS OWNED BY CONTROLLED AIRSTREAM INC., IS USED FOR
  - FIRE SERVICE
  - AGRICULTURAL SPRAYING
  - SPECIAL EFFECTS FOR TV AND MOVIES

- CONTINENTAL GASOLINE ENGINE
- FLOW SCREEN
- ADJUSTABLE FLOW DIRECTION
- ON TRAILER FOR MOBILITY

- BAGGIE TESTING
  - CROSS WIND FLOW
  - MAXIMUM VELOCITY AT BAGGIE = 100 MPH
  - AT DOWNEY CA.

Figure 11 – Ground Testing

only frost was indicated in the ET umbilical cavities. By itself, humidity is not an icing problem; therefore, management decided to launch STS-1 without baffies. Figure 13 is a summary of the basic development sequence for the hemispherical baggie.

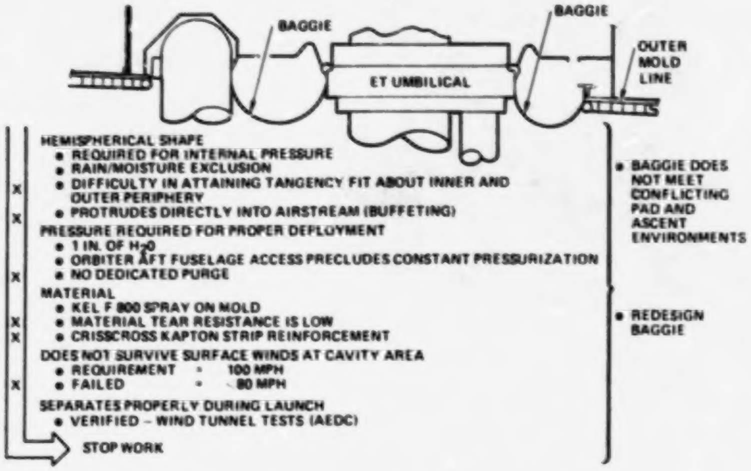
BAGGIE
BAGGIE
ET UMBILICAL
OUTER MOLD LINE
HEMISPHERICAL SHAPE
• REQUIRED FOR INTERNAL PRESSURE
• RAIN/MOISTURE EXCLUSION
X • DIFFICULTY IN ATTAINING TANGENCY FIT ABOUT INNER AND OUTER PERIPHERY
X • PROTRUDES DIRECTLY INTO AIRSTREAM (BUFFETING)
PRESSURE REQUIRED FOR PROPER DEPLOYMENT
• 1 IN. OF H2O
• ORBITER AFT FUSELAGE ACCESS PRECLUDES CONSTANT PRESSURIZATION
X • NO DEDICATED PURGE
MATERIAL
• KEL F 800 SPRAY ON MOLD
X • MATERIAL TEAR RESISTANCE IS LOW
X • CRISSCROSS KAPTON STRIP REINFORCEMENT
DOES NOT SURVIVE SURFACE WINDS AT CAVITY AREA
• REQUIREMENT = 100 MPH
X • FAILED = 80 MPH
SEPARATES PROPERLY DURING LAUNCH
• VERIFIED – WIND TUNNEL TESTS (AEDC)
STOP WORK
• BAGGIE DOES NOT MEET CONFLICTING PAD AND ASCENT ENVIRONMENTS
• REDESIGN BAGGIE

Figure 12 – Hemispherical Baggie; Problem Summary

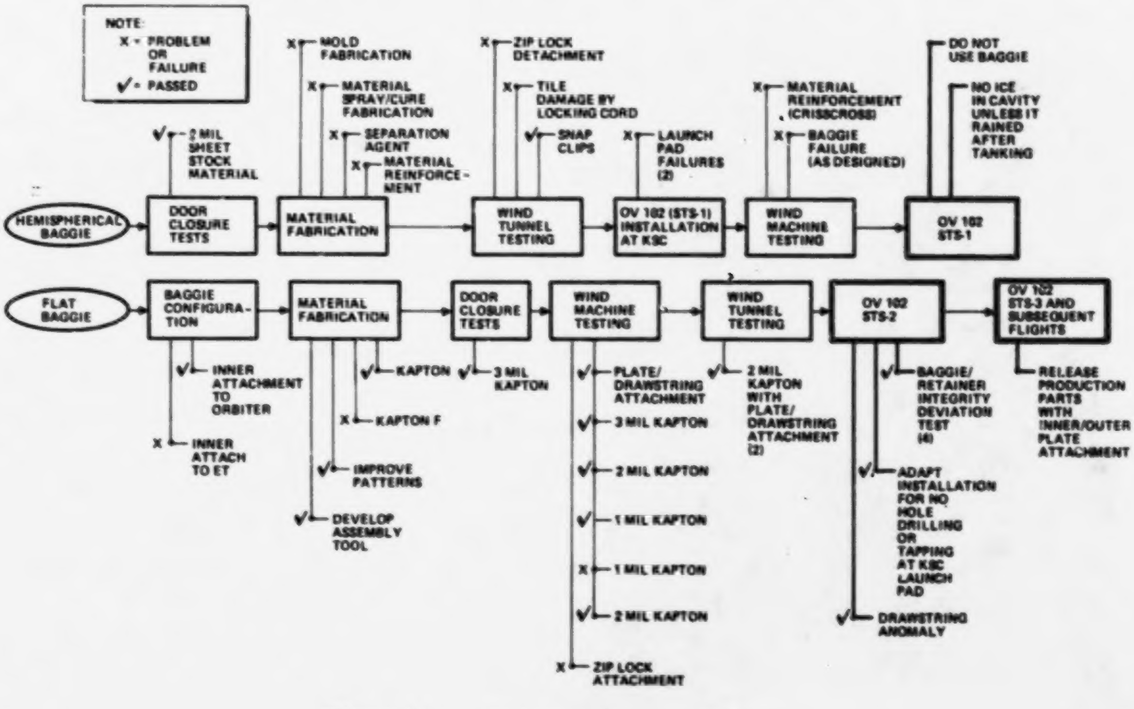
NOTE:
X = PROBLEM OR FAILURE
✓ = PASSED
HEMISPHERICAL BAGGIE
DOOR CLOSURE TESTS
✓ 2 MIL SHEET STOCK MATERIAL
MATERIAL FABRICATION
X MOLD FABRICATION
X MATERIAL SPRAY/CURE FABRICATION
X SEPARATION AGENT
X MATERIAL REINFORCEMENT
WIND TUNNEL TESTING
X ZIP LOCK DETACHMENT
X TILE DAMAGE BY LOCKING CORD
✓ SNAP CLIPS
OV 102 (STS-1) INSTALLATION AT KSC
X LAUNCH PAD FAILURES (2)
WIND MACHINE TESTING
X MATERIAL REINFORCEMENT (CRISSCROSS)
X BAGGIE FAILURE (AS DESIGNED)
OV 102 STS-1
DO NOT USE BAGGIE
NO ICE IN CAVITY UNLESS IT RAINED AFTER TANKING
FLAT BAGGIE
BAGGIE CONFIGURATION
✓ INNER ATTACHMENT TO ORBITER
X INNER ATTACH TO ET
MATERIAL FABRICATION
✓ KAPTON
X KAPTON F
✓ IMPROVE PATTERNS
✓ DEVELOP ASSEMBLY TOOL
DOOR CLOSURE TESTS
✓ 3 MIL KAPTON
WIND MACHINE TESTING
✓ PLATE/DRAWSTRING ATTACHMENT
✓ 3 MIL KAPTON
✓ 2 MIL KAPTON
✓ 1 MIL KAPTON
X 1 MIL KAPTON
✓ 2 MIL KAPTON
X ZIP LOCK ATTACHMENT
WIND TUNNEL TESTING
✓ 2 MIL KAPTON WITH PLATE/DRAWSTRING ATTACHMENT (2)
OV 102 STS-2
✓ BAGGIE/RETAINER INTEGRITY DEVIATION TEST (4)
✓ ADAPT INSTALLATION FOR NO HOLE DRILLING OR TAPPING AT KSC LAUNCH PAD
✓ DRAWSTRING ANOMALY
OV 102 STS-3 AND SUBSEQUENT FLIGHTS
RELEASE PRODUCTION PARTS WITH INNER/OUTER PLATE ATTACHMENT

Figure 13 – Basic Development Sequence

Flat Baggie

The failure evaluations of the hemispherical baggies indicated the configuration should be changed from hemispherical to flat to remove the baggie from the direct effects of the wind velocity coming across the cavity. The hemispherical baggie extends beyond the mold line and was being buffeted by the wind; a flat baggie would be within the mold line and be semiprotected within the cavity. The hemispherical baggie required constant internal pressure (1 inch of H_2O) to sustain its shape and minimize buffeting in the wind. The internal pressure was not always available, especially when the aft fuselage access doors were open. The flat baggie did not require internal pressure, but it did require a controlled minimum inner pressure in the cavity to absolutely reduce the tension pull loads on the locking retainer; therefore, the baggie leak rate was increased. This was done by not closing out the hinge area, which both simplified the installation at the hinge and reduced the retainer load. In addition, a flat baggie could be made from flat sheet stock, and cut and fit to form the total assembly, which was an improvement over the spray-on mold technique.

The flat baggie configuration (Figure 14) was a flat sheet of material retained at the outer periphery of the cavity by a newly designed retainer system (plate attached by screws) and at the inner periphery about the orbiter side of the umbilical by a drawstring contained in a channel. A skirt was added to limit rain on the exposed umbilical separation attachment structure. This

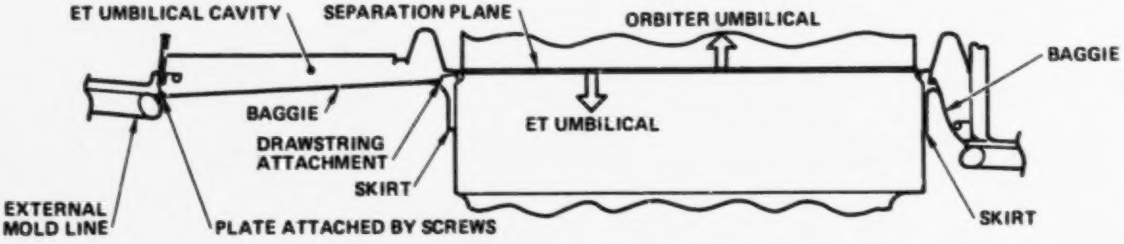

✓ CONFIGURATION
- SEMI-PROTECTED WITHIN CAVITY

✓ FABRICATION
- MADE FROM FLAT STOCK
- SIMPLER ASSEMBLY
- SKIRT REQUIRED AT UMBILICAL

✓ CONTROLLED INNER PRESSURE REQUIRED
- VENT AT INNER AREA
- SIMPLER INTERFACE AT HINGE AREA

INSTALLATION LESS DIFFICULT
- ✓ PLATE ATTACHED BY SCREWS (OUTER)
- ✓ DRAWSTRING IN CHANNEL (INNER)

✓ IF BAGGIE SURVIVES LAUNCH
- NO IMPACT TO ET SEPARATION
- DOOR MUST CLOSE THROUGH BAGGIE

TESTING REQUIRED
- DOOR CLOSURE
- WIND TUNNEL
- WIND MACHINE

SELECTION FACTORS

Figure 14 – Selected Flat Baggie Design

design completely enclosed all the critical icing areas. The cavity outer edge was now not as critical for moisture or rain freezing, and the flat baggie protection was considered adequate. Complete testing was required for this design.

A series of new designs was investigated for retaining both the outer and inner baggie attachments. The zip-lock and snap clip attachment used for the hemispherical baggie (Figure 9) were not adequate for the flat baggie, which would apply loads to the retention device in a tension direction. This was demonstrated during wind machine ground testing of a 1 mil flat baggie with zip-lock outer and inner attachment. During testing, some of the locking cord came out of the locking retainer, and part of the locking retainer moved away from the attachment structure.

As noted before, a major limitation for the design of the retention device was the fact that the cavity size and door/cavity clearances were fixed. The volume available for the retention devices was limited, and attachments to the adjacent primary structure (primarily the structural skin) were also limited. To complicate matters further, on Orbiter 102 the TPS thermal barrier about the outer periphery of the ET umbilical cavity was not exactly as per the released drawing, but it was still acceptable, and no changes to the actual location of the thermal barrier would be tolerated. Figure 15 indicates some of the designs that were not used, primarily because of impractical installations.

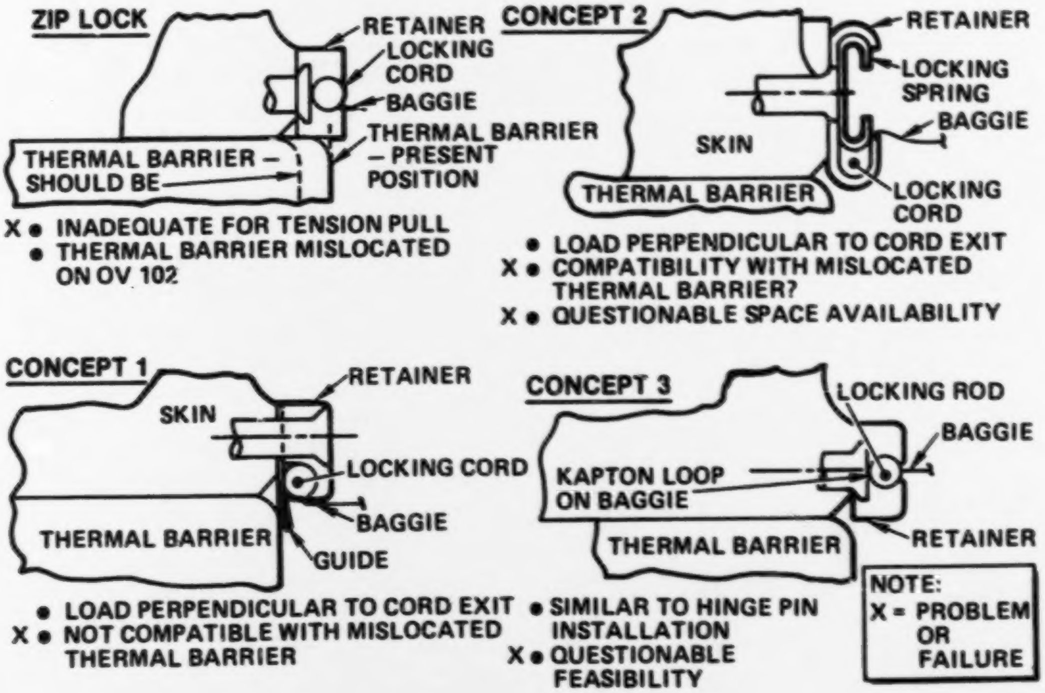
ZIP LOCK
RETAINER
LOCKING CORD
BAGGIE
THERMAL BARRIER – PRESENT POSITION
THERMAL BARRIER – SHOULD BE
X • INADEQUATE FOR TENSION PULL
• THERMAL BARRIER MISLOCATED ON OV 102
CONCEPT 2
RETAINER
LOCKING SPRING
BAGGIE
SKIN
THERMAL BARRIER
LOCKING CORD
• LOAD PERPENDICULAR TO CORD EXIT
X • COMPATIBILITY WITH MISLOCATED THERMAL BARRIER?
X • QUESTIONABLE SPACE AVAILABILITY
CONCEPT 1
RETAINER
SKIN
LOCKING CORD
BAGGIE
THERMAL BARRIER
GUIDE
• LOAD PERPENDICULAR TO CORD EXIT
X • NOT COMPATIBLE WITH MISLOCATED THERMAL BARRIER
CONCEPT 3
LOCKING ROD
BAGGIE
KAPTON LOOP ON BAGGIE
THERMAL BARRIER
RETAINER
• SIMILAR TO HINGE PIN INSTALLATION
X • QUESTIONABLE FEASIBILITY
NOTE: X = PROBLEM OR FAILURE

Figure 15 – Not Utilized Flat Baggie Attachment

The selected design for the flat baggie retainer is shown in Figure 16. For the outer periphery, the selected retainer system utilizes a plate attached by screws, and for the inner periphery, a drawstring enclosed in a retainer channel. The drawstring provided a very simplified final attachment method, which was well received by KSC. To provide reusability for the outer periphery retainer, a fixed ring is attached by tapped No. 4-40 screws (3-inch spacing) into the adjacent aluminum skin. The baggie is held by the removable ring that, in turn, is attached to the fixed ring by tapped No. 4-40 screws at 3-inch spacing. The fixed ring becomes the steel tapping ring that provides the reusability. Tapped screws into aluminum are not recommended for reusability. Both rings are 718 Inconel. The use of Inconel rings and more screws increased the strength of the retention design. The retainer channel supporting the drawstring is attached by No. 4-40 screws and nuts (6-inch spacing) to the orbiter side of the separation plate structure. The drawstring was made of lacing tape.

The materials considered for the flat baggie are listed in Table 3. Kel F 800 was immediately eliminated as being too weak. Kapton F was seriously considered until it was realized that the material has a memory, e.g., a piece cut from rolled stock would roll up again, making it hard to work with this material. Reinforced Kapton with its extremely high tear strength (internal mesh cord) would only be considered as a last resort. Kapton was selected as the material, but the thickness would be determined from the test results. The testing philosophy was to start with the

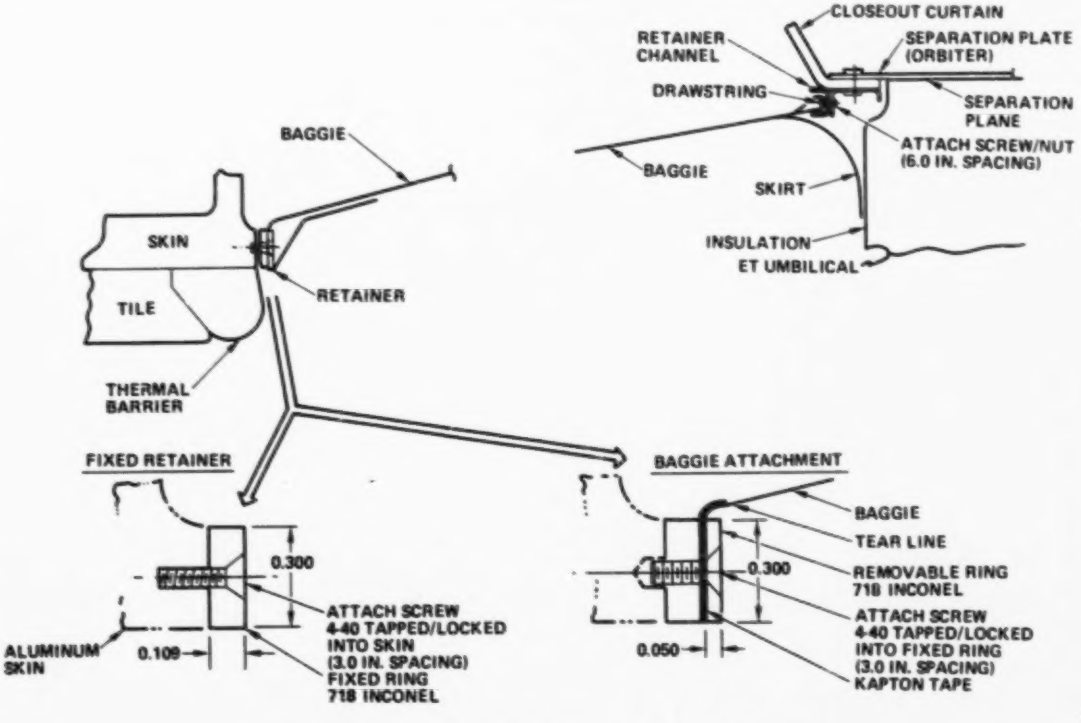
CLOSEOUT CURTAIN
RETAINER CHANNEL
SEPARATION PLATE (ORBITER)
DRAWSTRING
SEPARATION PLANE
ATTACH SCREW/NUT (6.0 IN. SPACING)
BAGGIE
SKIRT
INSULATION
ET UMBILICAL
BAGGIE
SKIN
TILE
RETAINER
THERMAL BARRIER
FIXED RETAINER
0.300
ATTACH SCREW 4-40 TAPPED/LOCKED INTO SKIN (3.0 IN. SPACING) FIXED RING 718 INCONEL
ALUMINUM SKIN
0.109
BAGGIE ATTACHMENT
BAGGIE
TEAR LINE
0.300
REMOVABLE RING 718 INCONEL
ATTACH SCREW 4-40 TAPPED/LOCKED INTO FIXED RING (3.0 IN. SPACING)
KAPTON TAPE
0.050

Figure 16 – Selected Flat Baggie Attachment

TABLE 3 – FILM MATERIAL OPTIONS FOR FLAT BAGGIE

Property	Film Materials						
	Kel F 800	Kapton	Kapton F	Tedlar	Aclar	Fep	Reinforced Kapton
Tensile (psi)	1,500	25,000	25,000	7,000	7,000	2,500	25,000
Elongation (%)	350	70	105	150	15	300	5-9
Tear gm/mil							
Initiation	–	510	500	620	450	270	1,800
Propagation	–	8	38	40		125	
Service Temperature							
Maximum	250	750	450	225	350	450	250
Minimum	-200	-400	-400	-100	-320	-400	-320
Flammability		SE	SE	SE		SE	
Color	Clear	Clear Amber	Clear Amber	Clear	Clear	Clear	Amber Opaque

Kel F 800 used for hemispherical baggie • Low tensile • Low tear resistance	• Do not use for flat baggie
Kapton F • High tear resistance • Rolled material has memory	• Not usable for flat baggie
Reinforced Kapton • Integral mesh cord • Too high tear strength	• Not usable for flat baggie
→ Kapton	• Selected for flat baggie

estimated thickest material and work toward the thinner materials until one of the materials failed. The preceding thicker material test would then be repeated.

Individual LO_2 baggies were made of various thicknesses of Kapton 1 mil through 3 mil. The baggies were cut from sheet stock to a pattern that was developed during the assembly operations. The assembly tool was a simple, flat tool fabricated in the model shop mostly of wood and some metal. The flat baggie assembly was much easier than the previous hemispherical baggies.

Door closure tests were repeated using 3 mil Kapton, which were successful. The ground wind tests (baggie test bed shown in Figure 10, and the wind machine in Figure 11) using the wind machine were again activated with the following results: 3 mil Kapton passed, 2 mil Kapton passed, 1 mil Kapton passed, 1 mil Kapton failed, 2 mil Kapton passed, and 2 mil Kapton was selected to be tested at the AEDC wind tunnel with the baggie test bed shown in Figure 10. Two tests passed. No further work was done with any of the thicker Kapton materials or with reinforced Kapton.

The flat baggie was released for installation on STS-3. Meanwhile, a compromise retention installation was designed and released for STS-2, as noted in Table 4 and in Figure 17.

TABLE 4 – BAGGIE INSTALLATION FOR ORBITER 102 (STS-2)

Item	Deviation
1. Requirements a. No additional drilling or tapping on the vehicle b. Utilize existing attachment holes c. Minimize possibility of vehicle damage d. Installation post-mating • Reduced access to cavity • Tight schedule to launch	
2. Baggie retention modifications a. LH umbilical cavity (LH_2 umbilical); outer periphery • Fixed retainer only • Traps baggie • Attachment screws 6.0 inch spacing	Certified by baggie retainer integrity test
b. LH umbilical cavity (LH_2 umbilical); inner periphery • Drawstring attachment in retainer channel	
c. RH umbilical cavity (LO_2 umbilical); outer periphery • Fixed retainer only • Traps baggie • Attachment screws 6.0 inch spacing	Certified by baggie retainer integrity test
d. RH umbilical cavity (LO_2 umbilical); inner periphery • Fixed retainer only • Traps baggie	Certified by baggie retainer integrity test

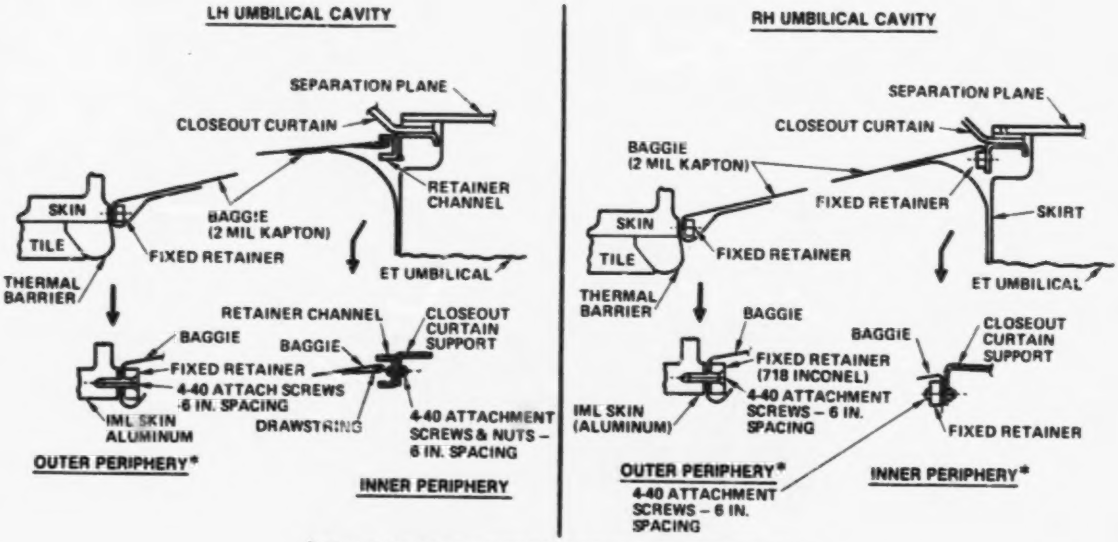
LH UMBILICAL CAVITY
SEPARATION PLANE
CLOSEOUT CURTAIN
RETAINER CHANNEL
SKIN
TILE
BAGGIE (2 MIL KAPTON)
FIXED RETAINER
THERMAL BARRIER
ET UMBILICAL
RETAINER CHANNEL
CLOSEOUT CURTAIN SUPPORT
BAGGIE
BAGGIE
FIXED RETAINER
4-40 ATTACH SCREWS 6 IN. SPACING
IML SKIN ALUMINUM
DRAWSTRING
4-40 ATTACHMENT SCREWS & NUTS – 6 IN. SPACING
OUTER PERIPHERY*
INNER PERIPHERY
RH UMBILICAL CAVITY
SEPARATION PLANE
CLOSEOUT CURTAIN
BAGGIE (2 MIL KAPTON)
FIXED RETAINER
SKIRT
SKIN
TILE
FIXED RETAINER
THERMAL BARRIER
ET UMBILICAL
BAGGIE
BAGGIE
CLOSEOUT CURTAIN SUPPORT
FIXED RETAINER (718 INCONEL)
4-40 ATTACHMENT SCREWS – 6 IN. SPACING
IML SKIN (ALUMINUM)
FIXED RETAINER
OUTER PERIPHERY*
INNER PERIPHERY*
4-40 ATTACHMENT SCREWS – 6 IN. SPACING

* DEVIATION CERTIFIED BY BAGGIE/RETAINER INTEGRITY TEST

Figure 17 – Baggie Installation; OV-102 (STS-2) Only

The baggie installation in STS-2 would be done after the mating. Access to the ET umbilical cavity combined with installation just prior to launch did not involve any additional hole drilling or tapping operations on the vehicle to install the baggie. The compromise did not violate the baggie design, testing, or certification. A final baggie and retainer integrity test, which was repeated four times, certified the STS-2 installation deviations. Figure 13 summarizes the basic development sequence for the flat baggie.

SUMMARY

In summary, the late start of the design, the space limitations, the real time testing (using sophisticated and expedient facilities), and the use of materials for purposes never utilized before created a challenging assignment that led to a unique solution to an orbiter icing problem, which was successfully used on STS-2.

The baggie performed successfully on this mission (including the prolonged ground stay capability because of the launch delay), except for one flight anomaly: the left-hand baggie drawstring broke, hung up, and slightly damaged some adjacent tiles.

A design review of the anomaly determined that the drawstring about the umbilical (inner periphery) be replaced by a positive mechanical retention similar to the retainer design used at the outer periphery (plate attached by screws). Figure 18 shows the final attachment design as released for Orbiter 102 (STS-3) and subsequent Shuttle flights.

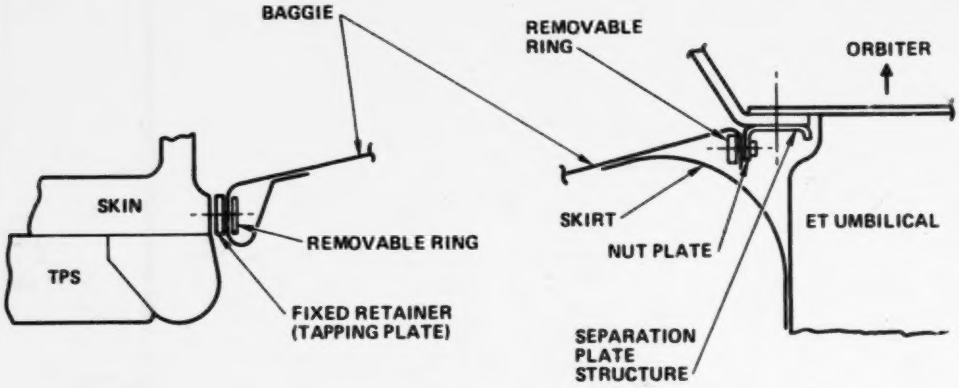

POSITIVE BAGGIE RETENTION

- MECHANICAL ATTACHMENT
- INNER/OUTER PERIPHERY

Figure 18 – Flat Baggie Attachment–Final Selection; OV-102 (STS-3) and Subsequent Vehicles

Louis J. Walkover
Rockwell Space Transportation and Systems Group
12214 Lakewood Boulevard
Downey, California 90241

Mr. Walkover is currently Structure Design Manager at Rockwell Space Transportation and Systems Group. During his 32 years at Rockwell, he has been involved in the design phase of several different programs, ranging from the Navaho and Hound Dog through the Apollo and onto the Shuttle. Mr. Walkover graduated from New York University in 1940 with a B.S. degree in Aeronautical Engineering.

Blank Page

FLIGHT SUPPORT SYSTEM MECHANISMS

William A. Leavy
Goddard Space Flight Center

SUMMARY

The Flight Support System (FSS) contains twelve mechanisms (six different types) which are used for retention and positioning of a Multimission Modular Spacecraft (MMS) within the Space Shuttle's cargo bay during launch, retrieval, and servicing missions. Retention latches were designed to provide the capability for structural support of the MMS during launch and retrieval, and during servicing operations the mechanisms on the Positioning Platform provide the capability for positioning the MMS in virtually any orientation necessary for the work to be performed. In addition, there are mechanisms for mating and demating umbilical connectors and a mechanism for locking the Positioning Platform during maneuvers. Each mechanism is driven by a Common Drive Unit. Manual overrides have been provided for those mechanisms that would present a safety hazard for the crew, if they should fail.

INTRODUCTION

The Flight Support System (FSS) is a reuseable piece of equipment which provides the mechanical, thermal, and electrical interfaces between the Multimission Modular Spacecraft (MMS) and the Space Shuttle for launch, retrieval, and on-orbit servicing missions.

The MMS is a reuseable platform which provides a user with systems for attitude control, power, commands and data handling. It was designed to be compatible with both the Delta launch vehicle and the Space Shuttle. The interface with the Space Shuttle is through the FSS.

The first user of the MMS was the Solar Maximum Mission (SMM), which was launched into earth orbit by a Delta 3910 in the first quarter of 1980. The SMM was originally scheduled for retrieval in 1985, but malfunctions which developed in the Attitude Control Subsystem caused it to become a candidate for a servicing mission now planned in 1983.

Figure 1 shows the SMM spacecraft affixed to the baseline FSS in a typical position within the Shuttle cargo bay. The FSS baseline configuration (see Figure 2) consists of three structural cradles, avionics, and twelve mechanisms for spacecraft retention and positioning. The twelve mechanisms are shown in Figure 3, and include three retention latches for supporting the spacecraft during launch or landing, three berthing latches which hold the spacecraft to the Positioning Platform during orbital operations, one mechanism each for pivoting, rotating, and translating the Positioning Platform, two mechanisms for mating and demating the spacecraft umbilical connectors, and a mechanism (identical to the retention latches) which locks the Positioning Platform to the cradles during launch or landing.

COMMON DRIVE UNIT

Each of the twelve FSS mechanisms is driven by a Common Drive Unit (CDU), of which there are two types: high speed and low speed. Both have the same mounting and output shaft interfaces and both provide the same amount of stall torque, 31 Nm (275 in. lb.).

Each CDU (see Figure 4) consists of two (three-phase, 115-V, 400-Hz) motors, gearing, an automatic electromagnetic brake and an automatic overload switch. Full redundancy is provided up to the output shaft. The high-speed unit uses the larger motor to provide a no-load output speed of 90 rpm. The low-speed unit has an additional gear reduction and gives a no-load output speed of 9 rpm. If both motors of a CDU are powered simultaneously, the speed would be twice these values, and the stall torque would be the same.

The electromagnetic brake locks the motor shaft when power is removed, and thereby prevents the motor from being backdriven in either direction. The overload switch prevents damage to the motor during stall conditions.

SWITCHES

End-of-travel limit switches have been included in the design of each mechanism. These switches are used for automatic cutoff of the CDU's and provide status data to the crew. In the event of failure of a switch, the mechanism is driven to a hard stop. All mechanisms were designed to withstand this condition.

RETENTION LATCHES

Three retention latches are attached to Cradle A. They are used to support the MMS during Shuttle launch and return. Each mechanism was designed to a limit load of 127,000 Newtons (28,500 lb.), using a factor of safety of 2 based on yield. (Design yield load 254,000 N.)

As shown in Figures 5 and 6, the latch operates as follows: a high-speed CDU drives an Acme screw which causes a linear motion of the barrel. A segmented collet closes around the MMS trunnion pin as the barrel moves forward. At the end of travel, the collet very nearly fills the volume between the barrel and the pin. A gap of about 0.025 mm (0.001 in.) is left. This gap enables the latch to restrain the pin radially while allowing it to move freely in the axial direction. By using three latches on Cradle A (as shown in Figure 3), an MMS is self-aligned during Shuttle maneuvers.

In order to meet the requirement that the latch be capable of withstanding being driven against a hard stop, a torque-limiting clutch had to be incorporated between the CDU and the gears (to protect the gears). The torque limiter operates at about 1600 Nm (180 in. lb.).

Design of the retention latch includes a means for an astronaut to manually drive it in the event of a failure in the CDU or in the driver electronics. As shown in Figure 7, the astronaut inserts a standard-size socket tool into a fitting on the side of the cradle. He engages a clutch by depressing the shaft until it locks (by means of the ball detents). The output of the clutch drives the Acme screw of the latch through a gear box at the rear of the mechanism.

PLATFORM LOCK

The mechanism which is used to lock the Positioning Platform to the cradles during launch or landing is identical to the three retention latches just described. Its location is shown in Figure 3.

BERTHING LATCH

Three berthing latches are used to hold the MMS to the Positioning Platform. Each latch consists of a pair of jaws which close around a berthing pin attached to the lower MMS structure. The jaws were designed to capture a pin if it is within ±5 cm (2 in.) of the desired final position. They were designed for an impact load of 6,450 N (1,450 lb.) when open, and for a limit load of 40,000 N (9,000 lb.) when closed. Both design loads assume a factor of safety of 2 based on yield.

As shown in Figure 8, the berthing latch operates by means of an Acme screw which actuates a linkage for each jaw. The screw is driven by a high-speed CDU through a gear train. As with the retention latches, a small gap exists between the fully closed jaws and the berthing pin so that only radial loads are reacted. By using three latches, as on the FSS, the MMS is automatically aligned.

The design includes means whereby an astronaut can manually open the jaws in the event a failure occurs while an MMS is secured. As shown in Figure 9, an astronaut can use a standard-sized tool to unscrew the jaw pivot pins. Note that this method only allows for release of a spacecraft. No means is provided for berthing one under failure conditions, because this situation does not present a safety hazard for the crew or the orbiter.

UMBILICAL CONNECTOR ACTUATOR

Two umbilical connector actuators are mounted to the Positioning Platform as shown in Figure 3. Each one provides a remotely controlled means for mating and demating a spacecraft umbilical connector. Each has a stroke of 10 cm (4 in.) and can press the connectors together or pull them apart with a force of 1,800 N (400 lb.).

The mechanism, shown in Figure 10, consists of a connector holder which rides on two parallel rails driven by a low-speed CDU through a bellcrank. The connector is mounted to the holder on a spring-loaded frame, which takes up misalignment up to 0.3 cm (1/8 in.).

In the event of a failure while the connectors are mated, an astronaut can demate them manually as shown in Figure 11. The entire mechanism is mounted to a moveable frame. Using a standard-size tool, an astronaut turns the override screw and the mechanism is pulled away from the spacecraft, demating the connectors. This override is a one-way device in that it can only be used for demating. Failure to mate is not considered a safety hazard.

ROTATOR

The rotator is a mechanism which is used to rotate the Positioning Platform ring about its centerline through ±175 degrees. It can be operated for any pivot position, thus providing considerable flexibility for servicing operations.

As shown in Figure 12, it drives a large ring gear mounted to the moveable platform. It simply consists of a low-speed CDU and a gear box and can supply a torque of 210 Nm (24,000 in. lb.). If a failure occurs, it can be overriden manually by an astronaut using a standard-size tool. He must loosen two drive unit bolts, slide a spacer under one of them and retighten the bolts. This frees the ring gear from the CDU and permits it to be driven manually through an idler. It can be driven in either direction.

PIVOTER

The pivoter is a mechanism which moves the Positioning Platform from the horizontal position to the vertical position, or to any desired position in between. The horizontal position is used for launch, landing and orbital maneuvers, the vertical position is used for deploy-retrieve requirements, and other positions are used during servicing operations.

The pivoter is shown in Figure 13. It consists of a compound planetary gear assembly driven by a low-speed CDU. It drives the Positioning Platform through a splined output shaft, and is capable of supplying an output torque of 800,000 Nm (90,000 in. lb.).

If a failure occurs which prevents pivoter operation, it can be driven manually (see Figure 14). With a standard-size tool an astronaut can remove the bolts which fasten the two turnbuckles on the pivoter housing to the stationary part of the Positioning Platform. Using the same tool, he can then turn the idler which operates the pivoter. The pivoter can be moved manually in either direction.

TRANSLATOR

The translator is a device designed to prevent impact between a stowed MMS and the Positioning Platform during dynamic loading conditions. It is capable of moving the platform to a position 9 cm (3.5 in.) away from a stowed MMS.

Figure 14 shows the overall configuration of the translator. A low-speed CDU located at the top center of the ring drives two shafts extending on either side. As shown in Figure 15, each shaft drives a large Acme screw through a set of helical gears. Since translator failure is not considered a safety hazard, no means for manual operation was provided.

CONCLUSION

A summary of data for all twelve mechanisms is listed in Table 1. Operating times shown are for single motor operation. For dual motor operation, times are one-half of those given. Structurally, the design of each mechanism incorporates a limit-to-yield safety factor of 2.0.

All mechanisms have been fabricated and assembled, and are presently undergoing testing.

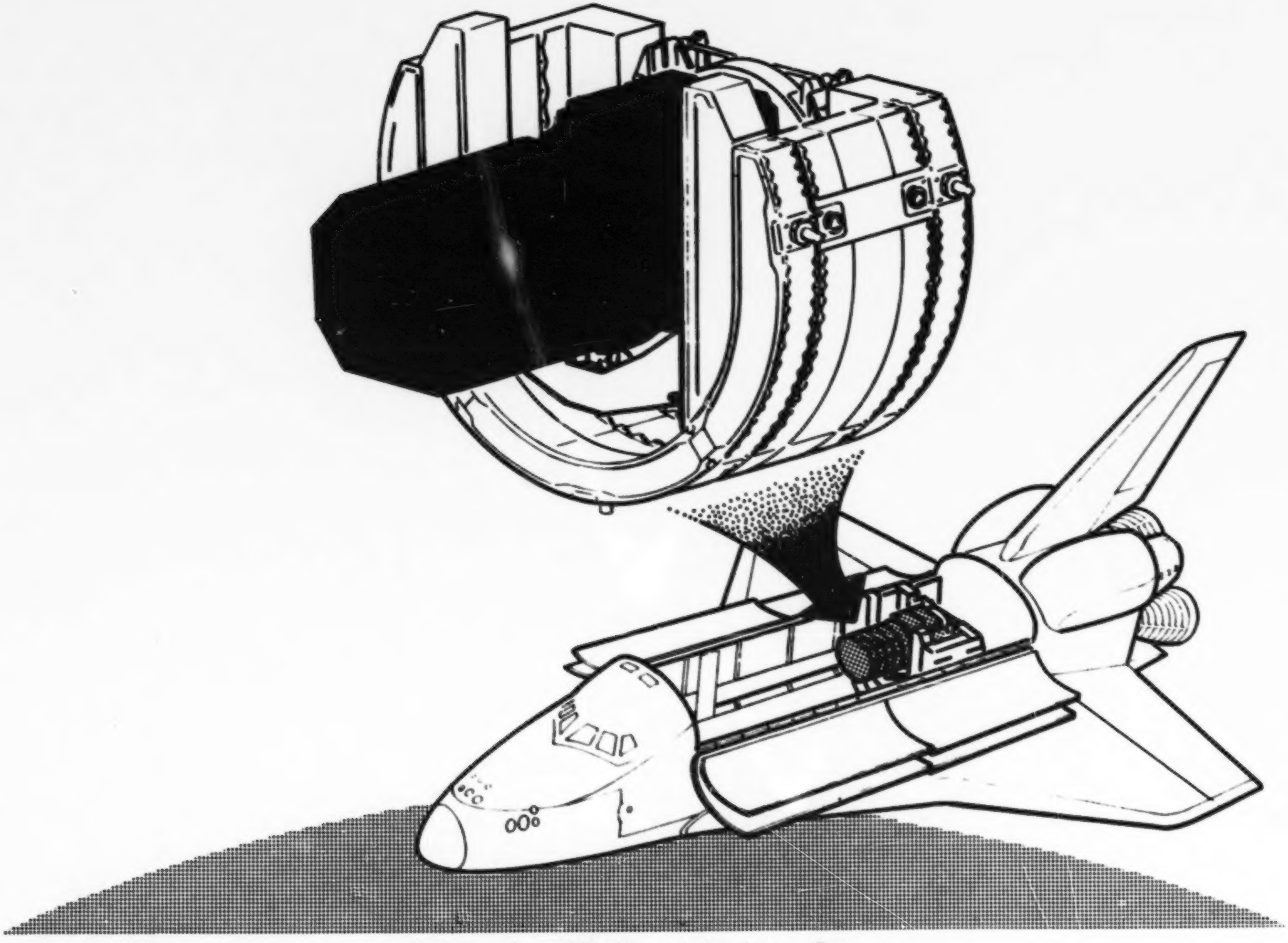

Figure 1. SMM Stowed in Cargo Bay

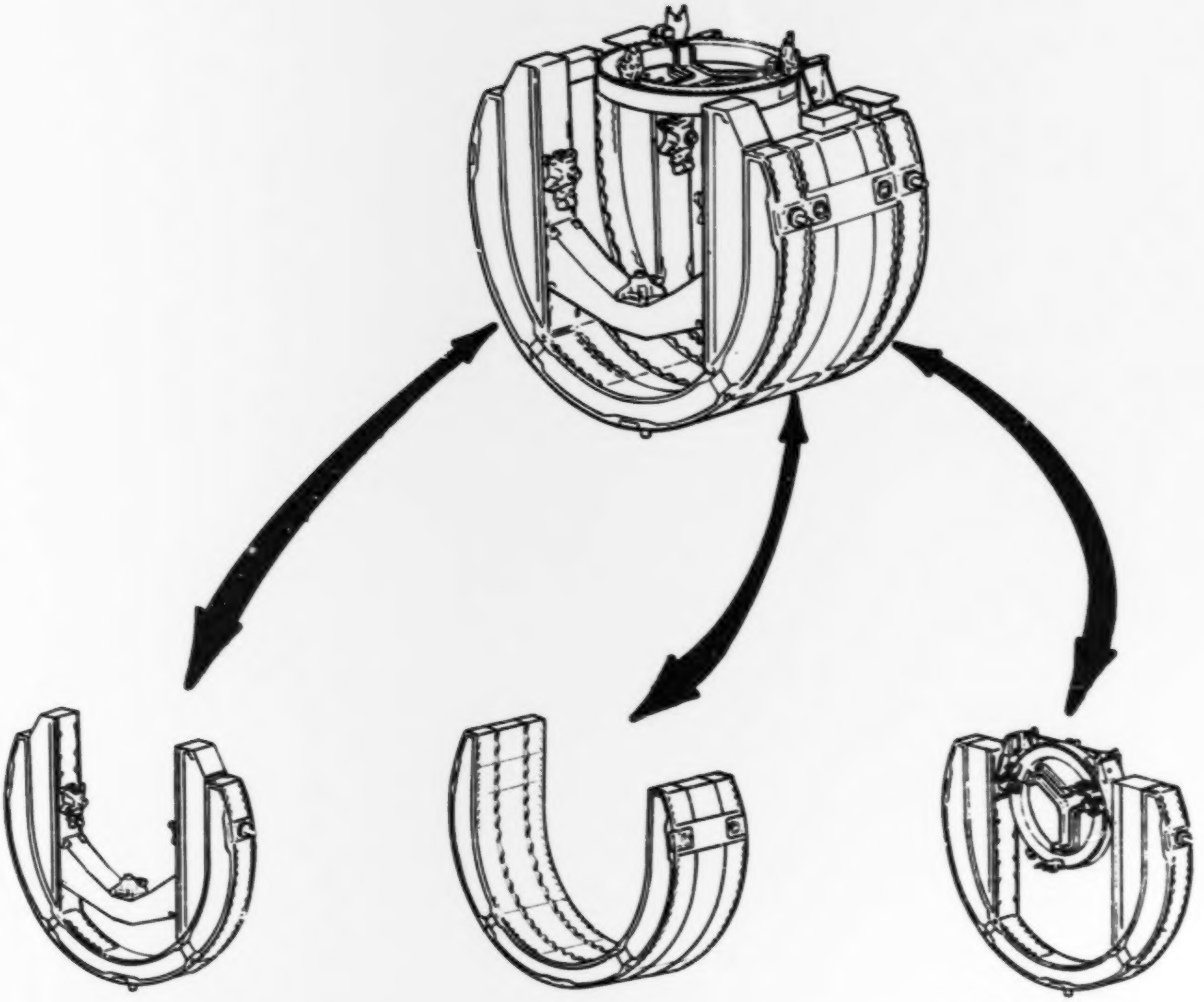

CRADLE A WITH LATCH BEAM

CRADLE B

CRADLE A' WITH POSITIONING SYSTEM

Figure 2. Flight Support System

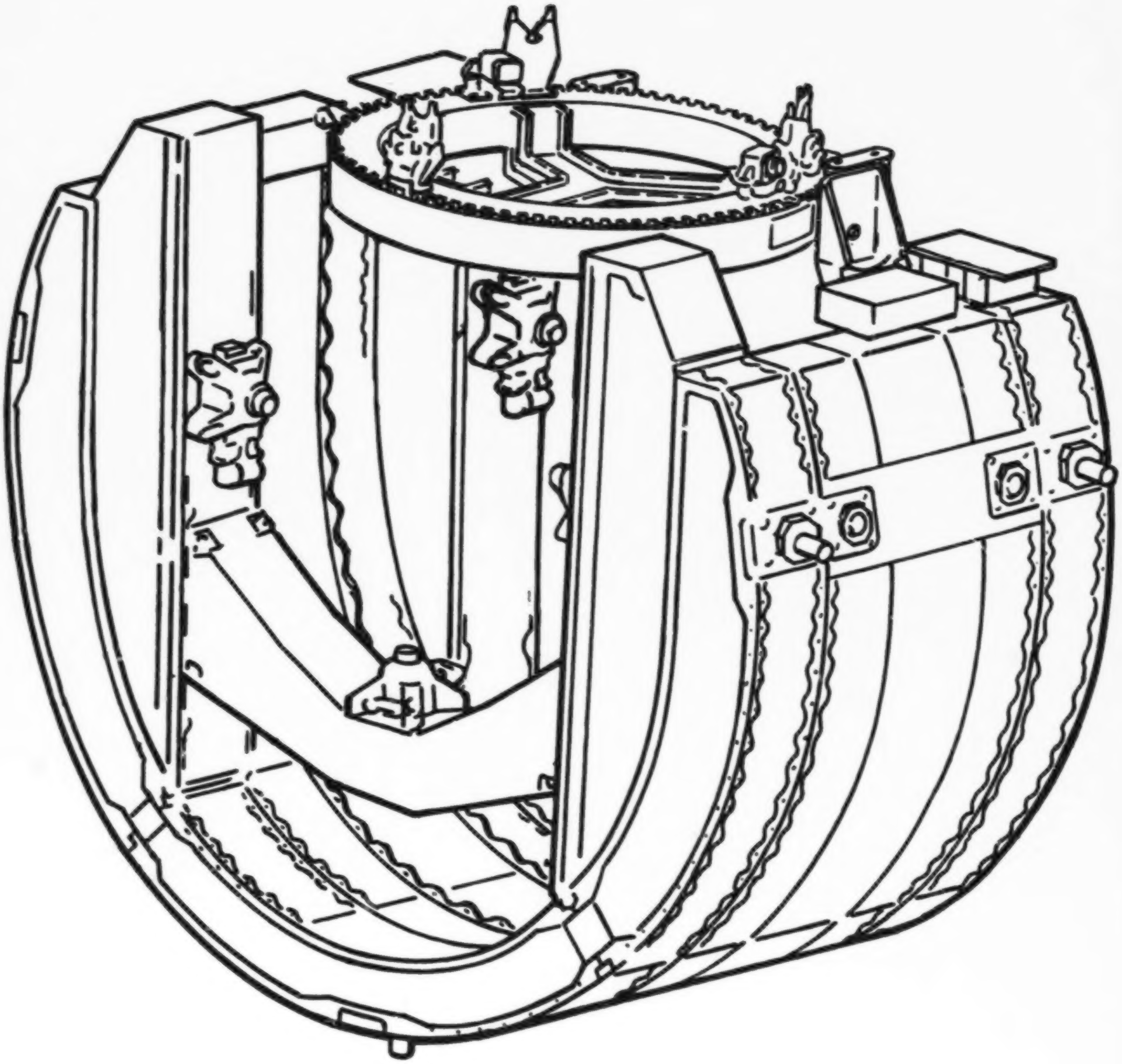

Figure 3. Flight Support System

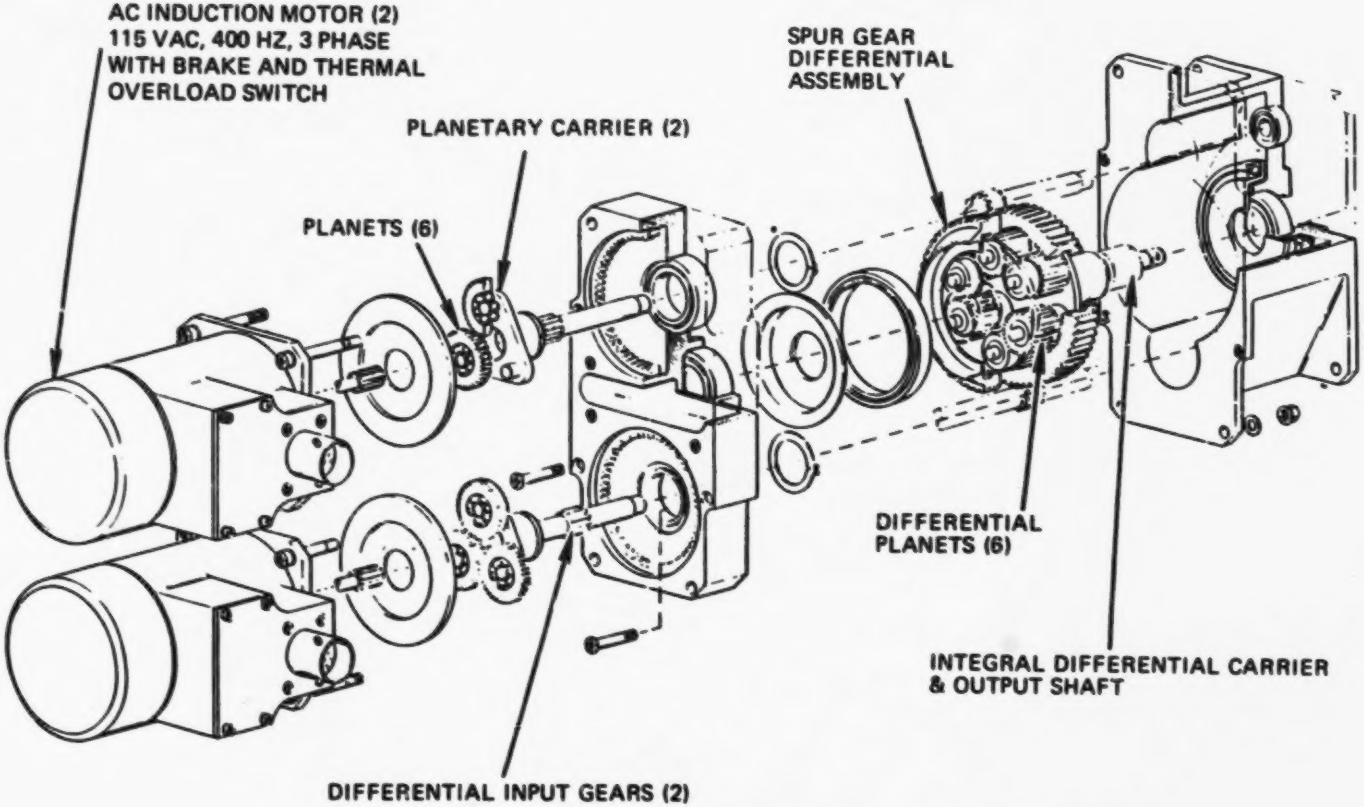
AC INDUCTION MOTOR (2)
115 VAC, 400 HZ, 3 PHASE
WITH BRAKE AND THERMAL
OVERLOAD SWITCH
SPUR GEAR
DIFFERENTIAL
ASSEMBLY
PLANETARY CARRIER (2)
PLANETS (6)
DIFFERENTIAL
PLANETS (6)
INTEGRAL DIFFERENTIAL CARRIER
& OUTPUT SHAFT
DIFFERENTIAL INPUT GEARS (2)

Figure 4. Common Drive Unit (Large Motor Size)

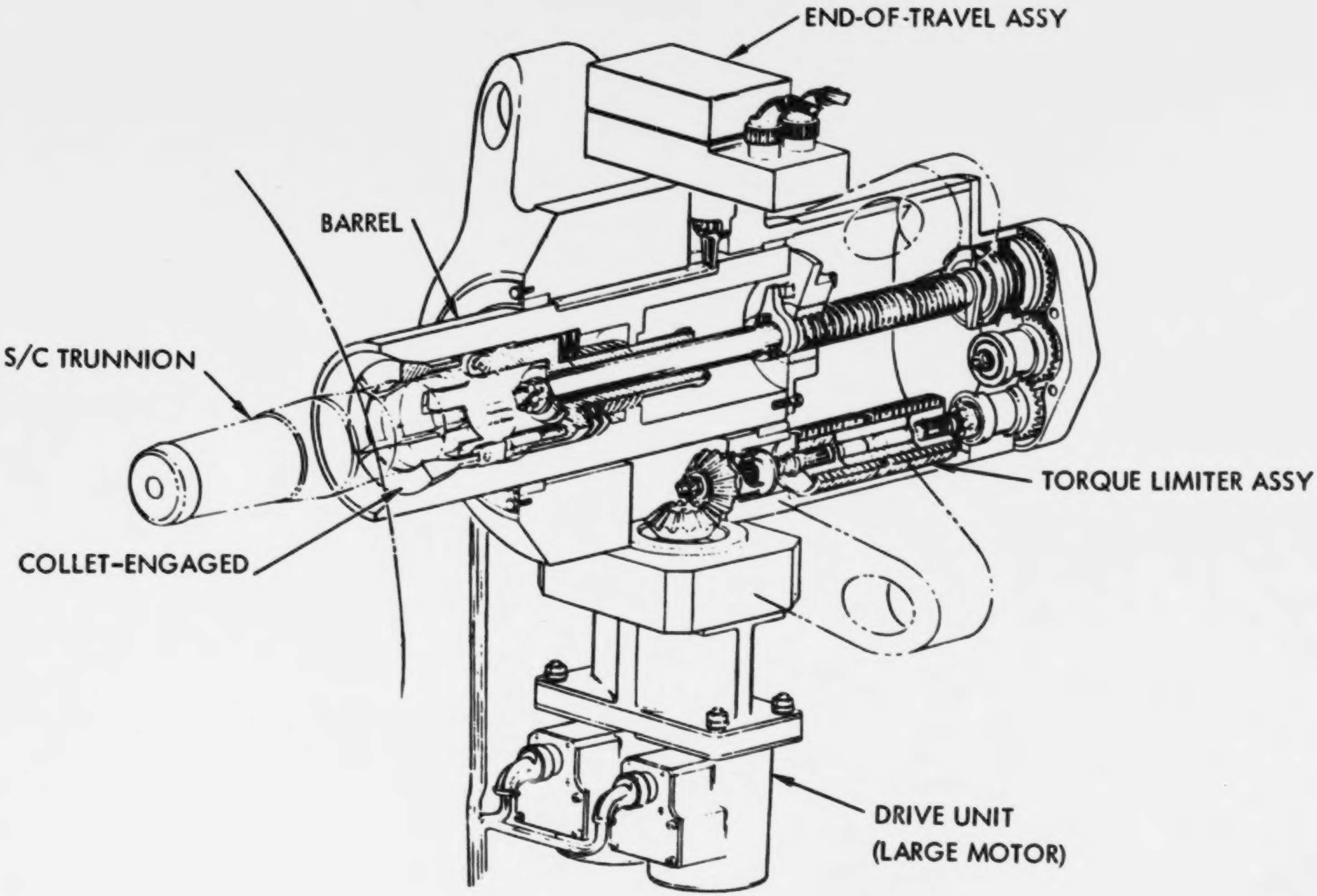
END-OF-TRAVEL ASSY
BARREL
S/C TRUNNION
TORQUE LIMITER ASSY
COLLET-ENGAGED
DRIVE UNIT
(LARGE MOTOR)

Figure 5. Spacecraft Retention Latch-Engaged

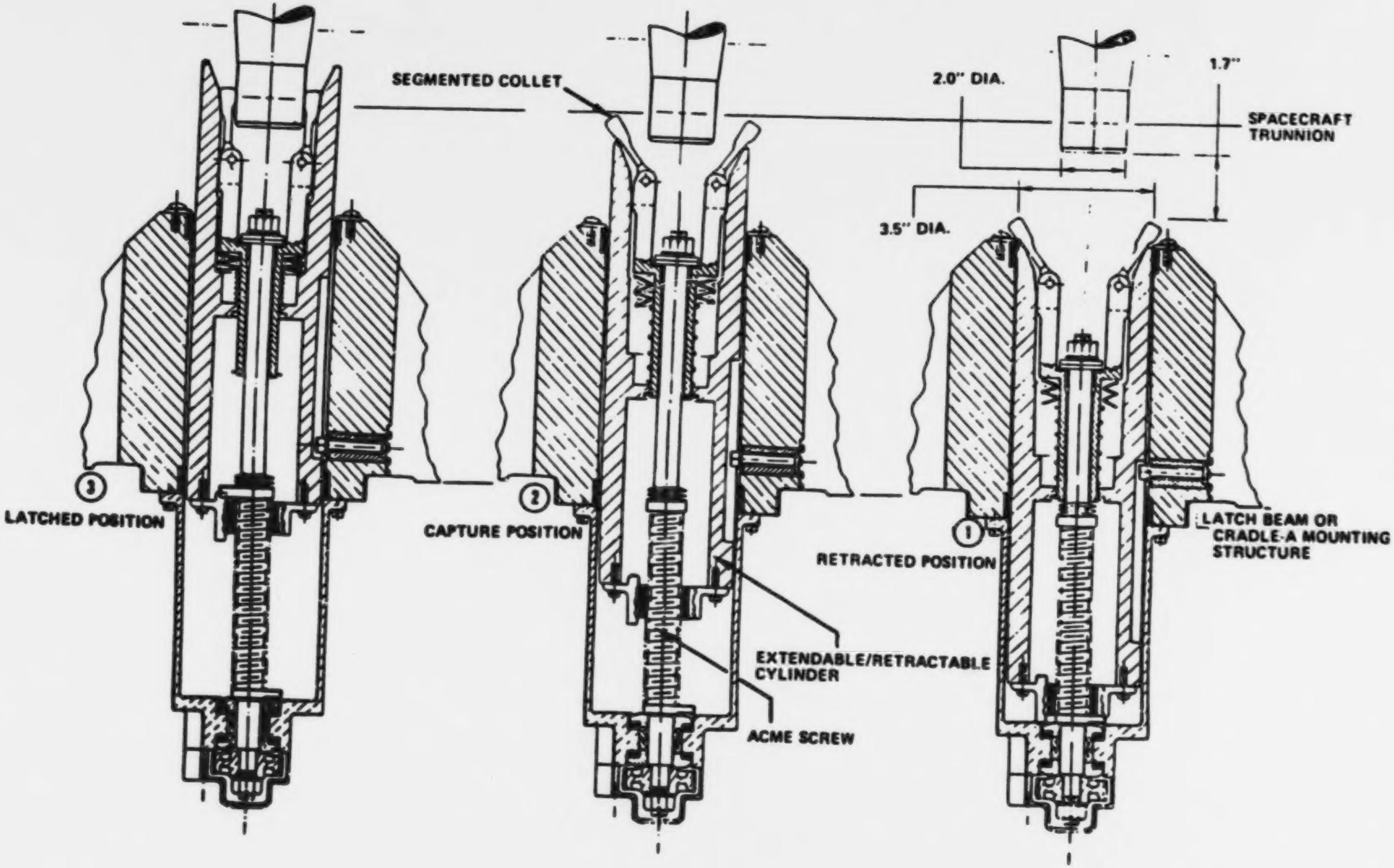
SEGMENTED COLLET
2.0" DIA.
1.7"
SPACECRAFT TRUNNION
3.5" DIA.
③
LATCHED POSITION
②
CAPTURE POSITION
①
RETRACTED POSITION
LATCH BEAM OR CRADLE-A MOUNTING STRUCTURE
EXTENDABLE/RETRACTABLE CYLINDER
ACME SCREW

Figure 6. Retention Latch Operational Sequence

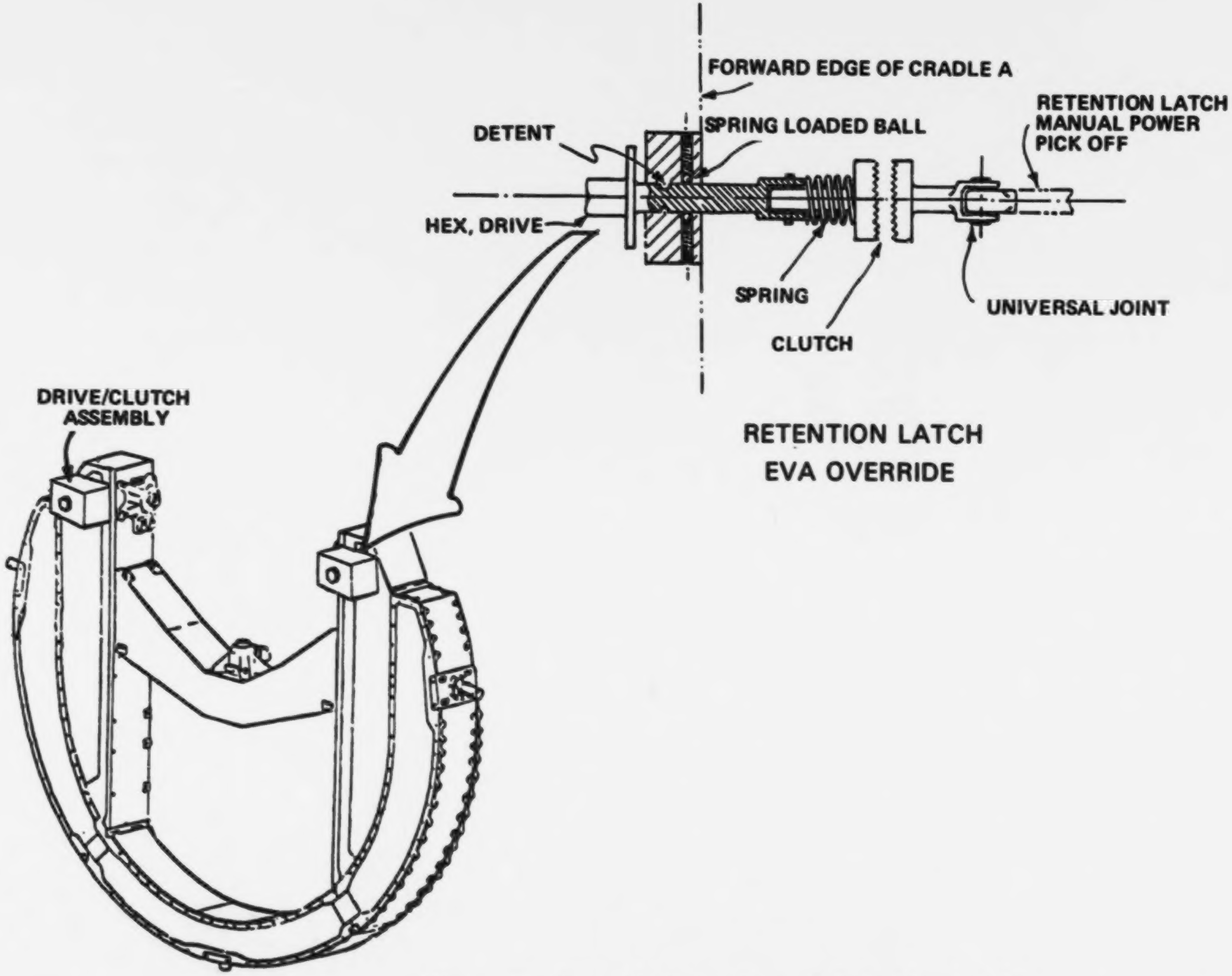
FORWARD EDGE OF CRADLE A
RETENTION LATCH MANUAL POWER PICK OFF
DETENT
SPRING LOADED BALL
HEX, DRIVE
SPRING
UNIVERSAL JOINT
CLUTCH
DRIVE/CLUTCH ASSEMBLY
RETENTION LATCH EVA OVERRIDE

Figure 7. Override Drive Concept Retention Latches

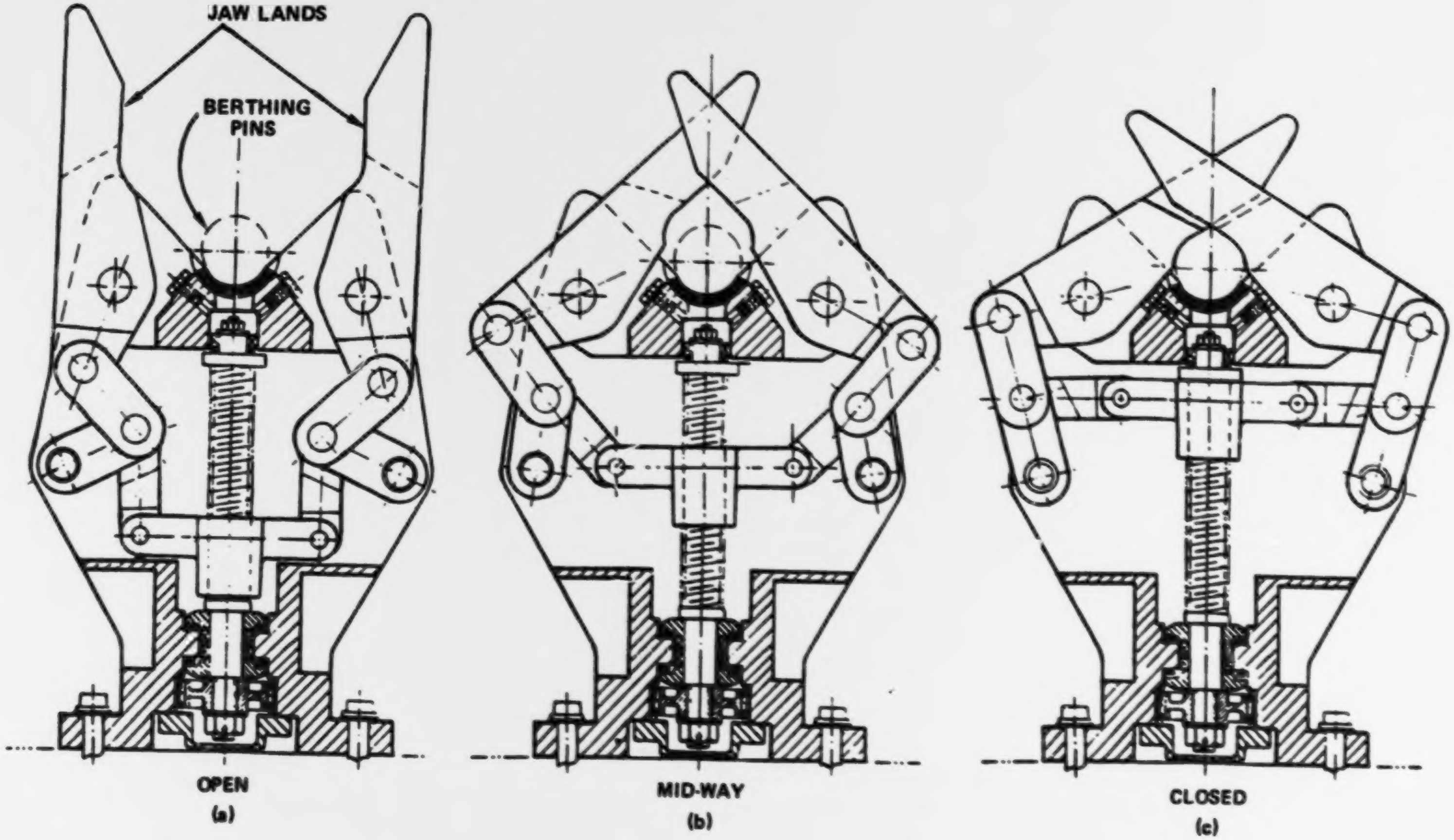
JAW LANDS
BERTHING PINS
OPEN
(a)
MID-WAY
(b)
CLOSED
(c)

Figure 8. Berthing Latch Mechanism Operating Sequence

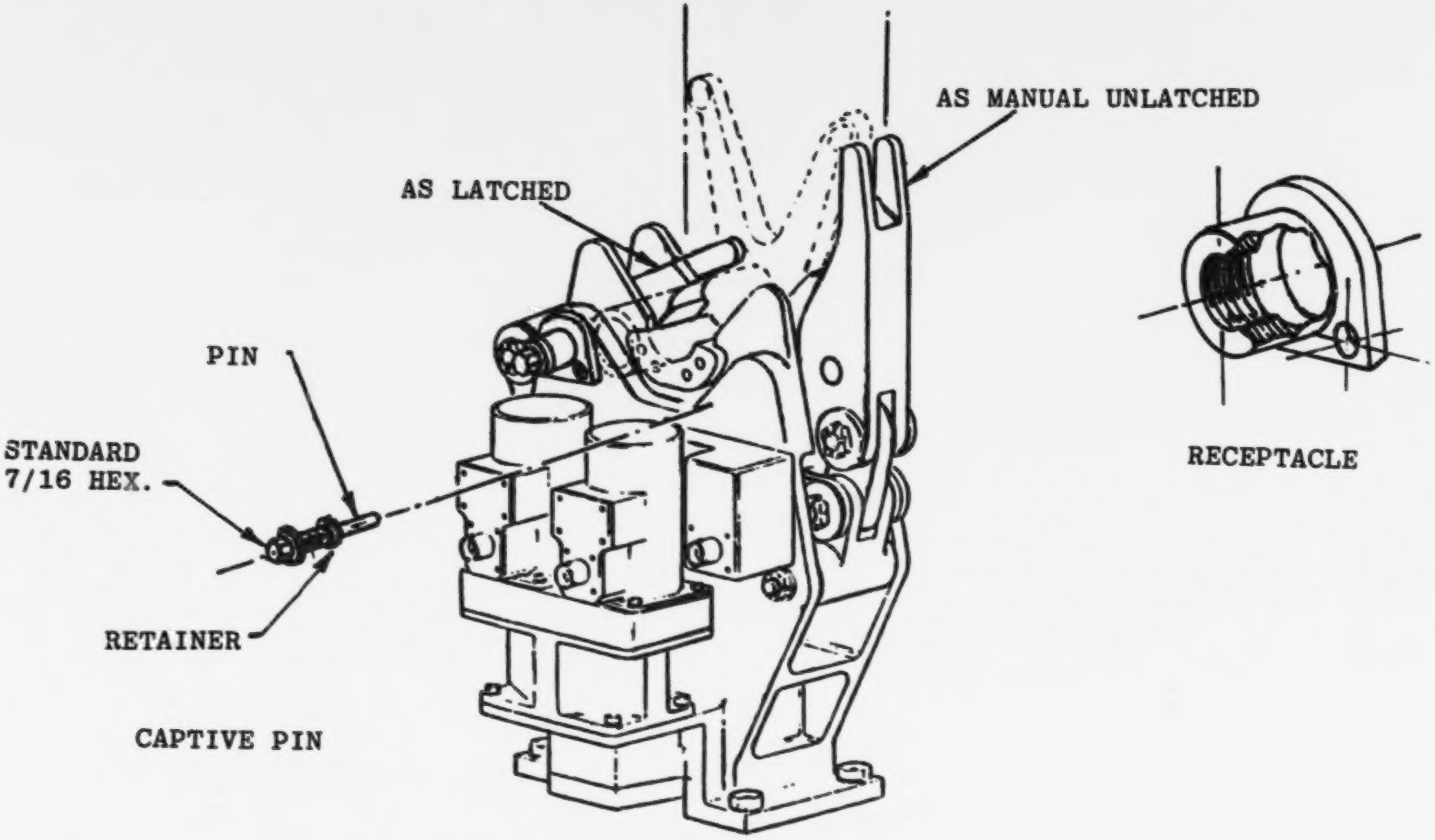
AS MANUAL UNLATCHED
AS LATCHED
PIN
STANDARD
7/16 HEX.
RETAINER
CAPTIVE PIN
RECEPTACLE

Figure 9. Berthing Latch Manual Unlatch

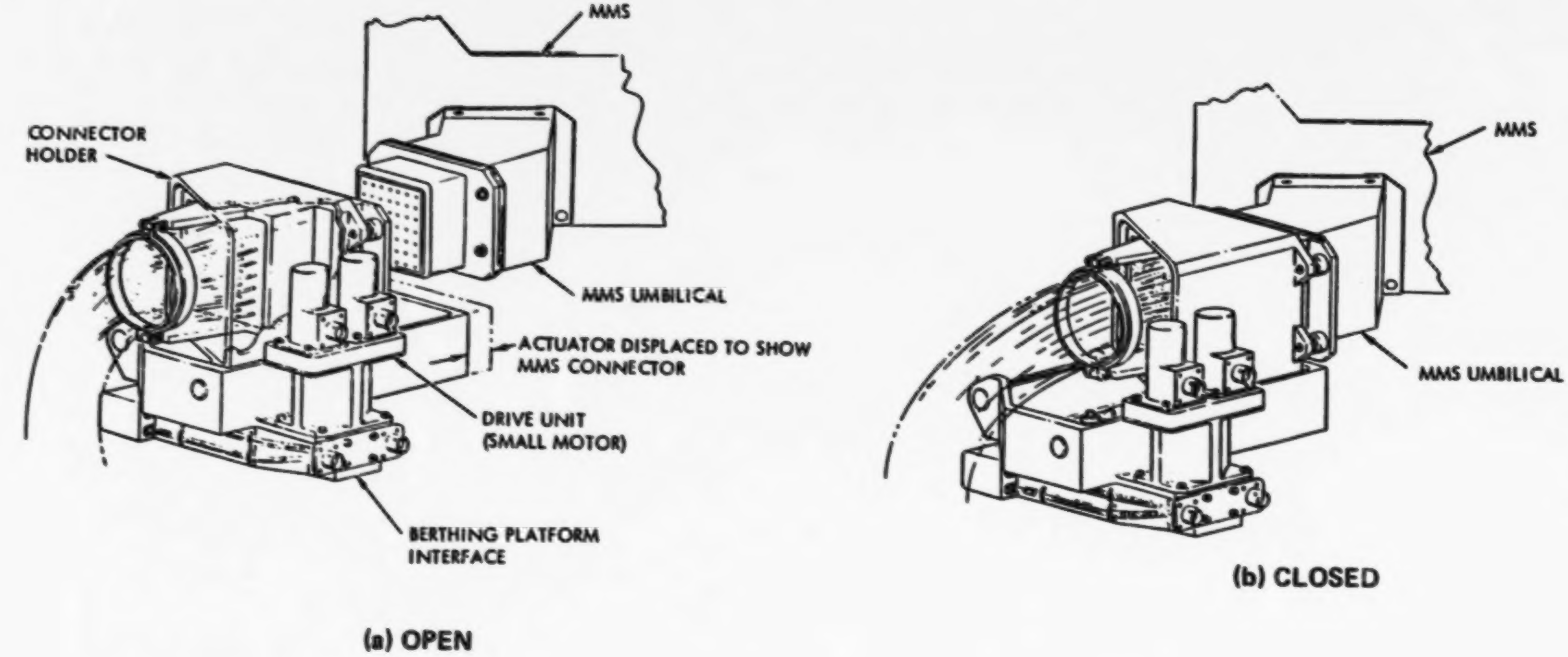
MMS
CONNECTOR HOLDER
MMS UMBILICAL
ACTUATOR DISPLACED TO SHOW MMS CONNECTOR
DRIVE UNIT (SMALL MOTOR)
BERTHING PLATFORM INTERFACE
MMS
MMS UMBILICAL

(a) OPEN

(b) CLOSED

Figure 10. Umbilical Actuator Positions

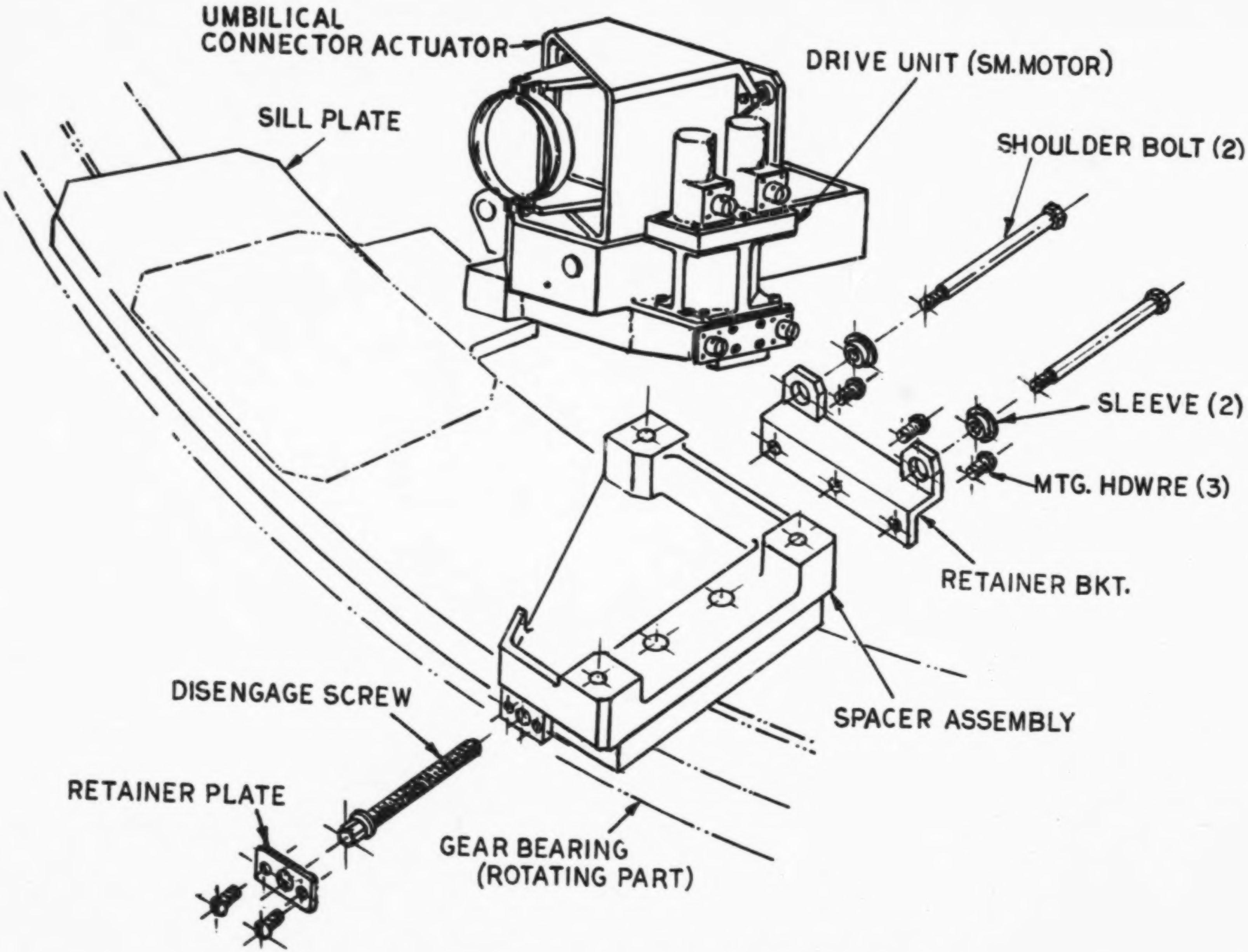
UMBILICAL CONNECTOR ACTUATOR
DRIVE UNIT (SM.MOTOR)
SILL PLATE
SHOULDER BOLT (2)
SLEEVE (2)
MTG. HDWRE (3)
RETAINER BKT.
SPACER ASSEMBLY
DISENGAGE SCREW
RETAINER PLATE
GEAR BEARING (ROTATING PART)

Figure 11. Umbilical Actuator-Manual Disengage

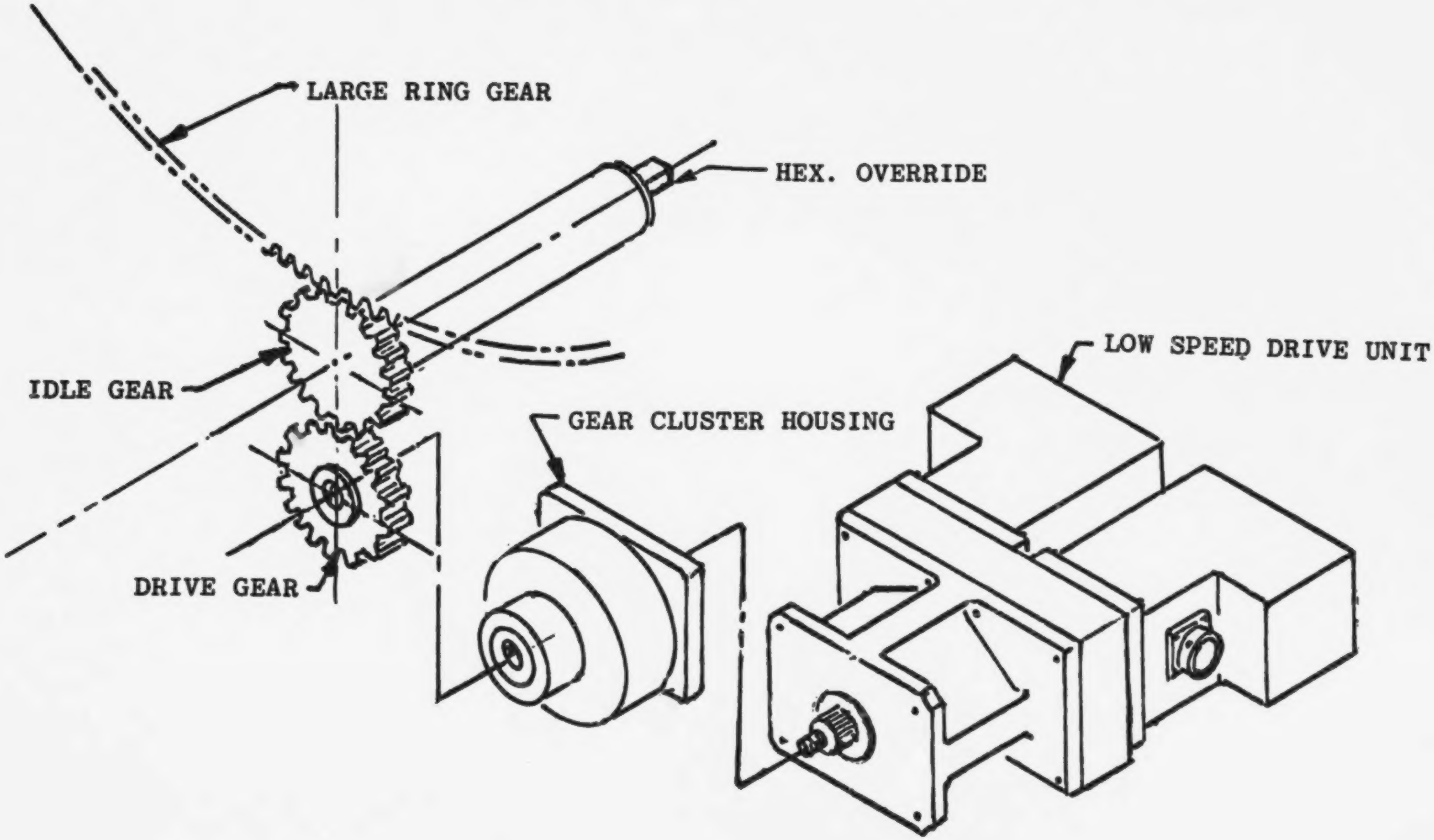
LARGE RING GEAR
HEX. OVERRIDE
LOW SPEED DRIVE UNIT
IDLE GEAR
GEAR CLUSTER HOUSING
DRIVE GEAR

Figure 12. Rotator

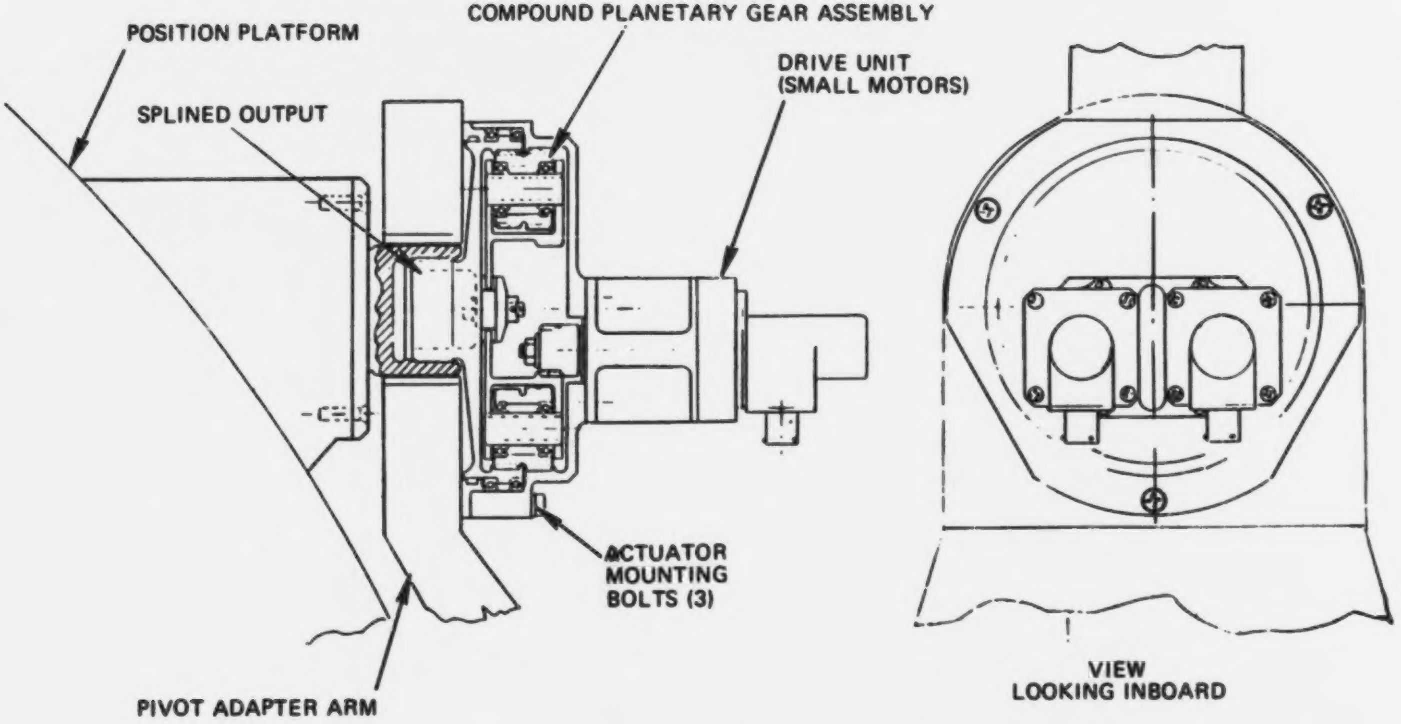
POSITION PLATFORM
COMPOUND PLANETARY GEAR ASSEMBLY
DRIVE UNIT (SMALL MOTORS)
SPLINED OUTPUT
ACTUATOR MOUNTING BOLTS (3)
PIVOT ADAPTER ARM
VIEW LOOKING INBOARD

Figure 13. Platform Pivot Actuator Detail

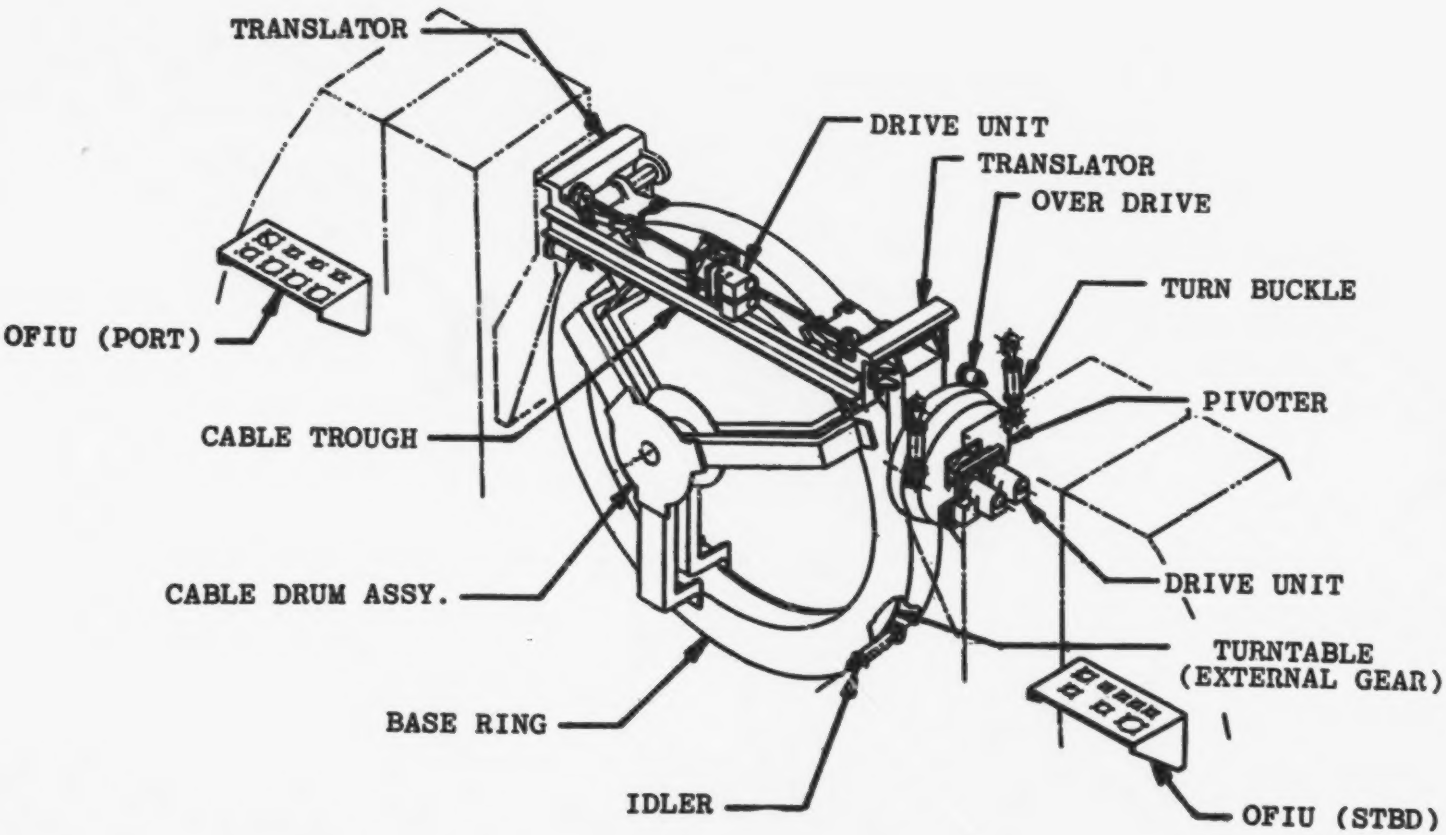
TRANSLATOR
DRIVE UNIT
TRANSLATOR
OVER DRIVE
TURN BUCKLE
OFIU (PORT)
PIVOTER
CABLE TROUGH
CABLE DRUM ASSY.
DRIVE UNIT
TURNTABLE (EXTERNAL GEAR)
BASE RING
IDLER
OFIU (STBD)

Figure 14. Manual Pivoter Operation

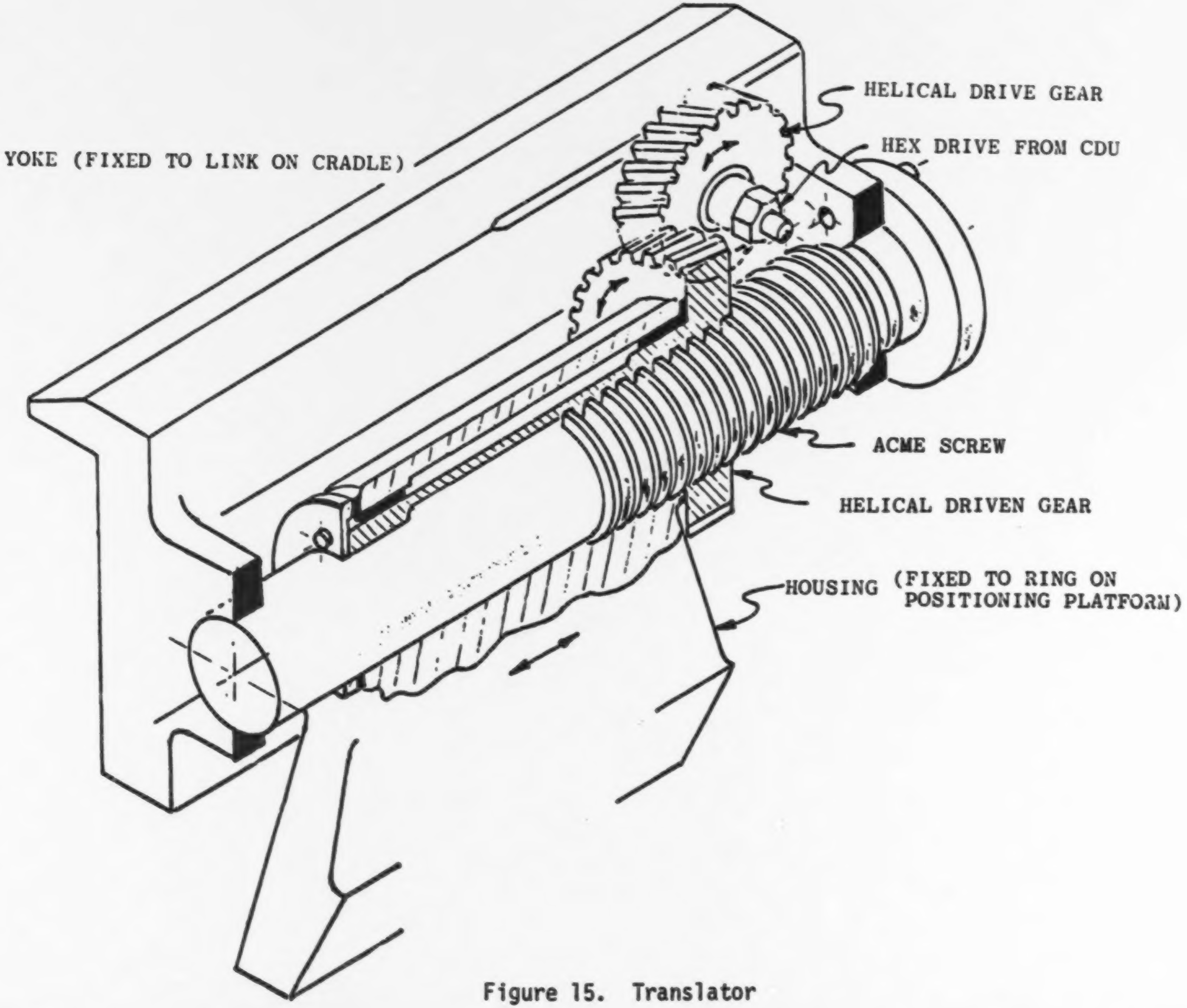
HELICAL DRIVE GEAR
YOKE (FIXED TO LINK ON CRADLE)
HEX DRIVE FROM CDU
ACME SCREW
HELICAL DRIVEN GEAR
HOUSING (FIXED TO RING ON POSITIONING PLATFORM)

Figure 15. Translator

Table 1. FSS Mechanisms

Mechanism	Number	Operating Time, Sec	Drive Unit		Weight Newtons (lbs.)
			High Speed	Low Speed	
Positioning System					
o Pivot	(1)	600 (90°)		X	406 (91.2)
o Rotator	(1)	100 (180°)		X	130 (30)
o Translator	(1)	320		X	210 (47.2)
o Lock	(1)	24	X		486 (109.2)
Berthing Platform					
o Berthing Latches	(3)	18	X		268 (60.2)
o Umbilical Drive	(2)	10		X	102 (22.9)
Retention System					
o Spacecraft Retention Latch	(3)	24	X		486 (109.2)

William A. Leavy
National Aeronautics and Space Administration
Goddard Space Flight Center
Mail Code 408
Greenbelt, Maryland 20771

Mr. Leavy has been employed as an aerospace engineer for NASA-Goddard Space Flight Center since 1959. He holds two patents for mechanisms used on spacecraft. Mr Leavy received his B.S. degree in Aeronautical Engineering from Polytechnic Institute of Brooklyn in 1958 and an M.S. degree in Aerospace Engineering from Catholic University in 1965.

THE DESIGN AND DEVELOPMENT OF AN END EFFECTOR FOR THE SHUTTLE REMOTE MANIPULATOR SYSTEM

Robert G. Daniell and Savi S. Sachdev*

ABSTRACT

This paper describes the design requirements, the design, and qualification and development test problems encountered on the Remote Manipulator End Effector. The constraints and interfaces with the arm, the Orbiter, and the payload are identified. The design solution to meet the requirements is a unique device that provides a soft-docking feature termed capture and a hard-docking feature termed rigidization.

INTRODUCTION

The Shuttle Remote Manipulator System (SRMS) is required to deploy payloads to and from the payload bay of the Orbiter. The SRMS consists of a 6-degree-of-freedom, 15.24-m (50-ft) long manipulator arm mounted on a longeron of the Orbiter. The arm, which comprises a shoulder, elbow, and wrist joint, is operated from the crew compartment. At the free end of the arm is located an end effector that interfaces with and captures a grapple fixture on the payload. The capture mechanism is a three-cable system that closes around the grapple fixture. Once capture is completed, rigidization consists of pulling the payload toward the end effector and achieving a rigid interface. The mechanism is fail-safe in that a single failure will not lead to crew hazard. A backup release system is incorporated into the design that will permit release of the payload in the event of a prime channel failure.

The end effector has been designed to perform the above functions within severe constraints:

- o Size:
  - Diameter: 0.34 m (13.5 in)
  - Length: 0.46 m (18 in)
- o Weight: 29.5 kg (65 lb)
- o Misalignment (end effector to payload):
  - Lateral: ±0.1 m (4 in)
  - Axial: 0.1 m (4 in)

---

*Spar Aerospace Limited, Toronto, Canada

- Vibration: launch environment
- Thermal: orbital environment

Several problems were encountered during the development and qualification program. These are described in this paper, as well as design changes implemented to overcome the problems and produce a qualified unit for future Space Transportation System flights.

SPECIFICATION REQUIREMENTS

The following are basic requirements defined by the user, NASA-Johnson Space Center, and those derived by Spar Aerospace Limited as a result of overall SRMS and subsystem concept and design evolution:

- The standard end effector will be attached to the wrist of the manipulator arm and used primarily for grappling or releasing payloads and applying loads and/or motions to the payload.
- Capability for ground change-out of end effectors is to be provided, as well as the ability for the standard end effector to interface on orbit with a special-purpose end effector. (Actuation of the electrical interface will be provided by the special-purpose end effector.)
- The system will be fail-safe, with a single operational channel for payload grappling and release. The backup channel will provide payload release capability only.
- When operated in conjunction with the SRMS manipulator arm, by the SRMS operator, the end effector will grapple a payload grapple fixture with both linear and angular misalignments (delineated later in this paper).
- Should the end effector fail to acquire the grapple fixture for any reason, no alternate mating or hangup will result.
- Release impulse to be imparted to the payload is limited to $9.5\text{X}10^{-6}$ N-m ($7\text{X}10^{-6}$ ft-lb) in the prime mode and 0.068 N-m (0.05 ft-lb) in the backup mode. No force is to be imparted to the grapple fixture during end effector withdrawal, after release.
- A single, detachable EVA handhold is required on the outside of the end effector.

- Grappling of a payload is to be carried out using a soft-docking feature to initially center out radial misalignment. This is to be followed with removal of axial misalignment. Angular payload-to-end-effector misalignment will be carried out against a limped arm; i.e., an arm that has low backdrive resistance in each joint, except wrist roll, which is active.

- Load transfer capability between end effector and payload is to be as follows (assuming a rigid grapple fixture/payload):

  - No interface separation up to 474.5 N-m (350 ft-lb) cross-axis (pitch/yaw) bending moment

  - Interface angular separation up to 3° permitted with a cross-axis bending moment as large as 1,627 N-m (1,200 ft-lb)

  - Full torsional (roll) load transfer capability required (even with 3° separation) for roll moments as large as 949 N-m (700 ft-lb)

- Postrigidization roll accuracy of ±0.4° and pitch/yaw accuracy of ±0.15° are to be assured between end effector axes and grapple fixture axes. Axes are to be positioned within ±0.0025 m (0.1 in) in X, Y, and Z.

- Bending and torsional stiffness will be greater than 7,864 N-m/° (5,800 ft-lb/°) and 3389.5 N-m (2,500 ft-lb/°), respectively, for maximum applied moments of 474.5 N-m (350 ft-lb).

- Capture and rigidization times are to be less than 3 s and 20 s, respectively. Payload-to-Orbiter relative velocity at moment of capture may be as high as 0.031 m/s (0.1 ft/s) maximum.

- Impact loads are defined by maximum relative velocity (payload to end effector) of 0.122 m/s (0.4 ft/s).

- Sighting aids are required on the payload side of the interface. Also, special markings are required on the end effector surface.

- Operating life will be 100 mission cycles (5 operations per mission cycle) with a useful life of 10 years. Mean time between failures must be 8,333 h.

- Operational, acceptance, qualification, and survival temperatures to be tolerated are as defined in Table 1. Also defined are payload (grapple fixture) temperature extremes.

- Maximum allowable electrical power is 125 W for operation and 88 W for heaters.

- Key vibration and load environments are shown in Table 2.
- Maximum mass of the end effector will be 29.5 kg (65 lb).
- Two modes of operation are required:
  - Manual - operator-commanded capture, rigidization, derigidization, and release
  - Automatic - operator-commanded capture; automated rigidization
- Status switch signals as defined in Table 3 are to be provided to the operator.

OVERALL DESIGN SUMMARY

The end effector, which was designed and developed to meet the specifications that have been outlined, is shown in Figure 1. The details of this mechanism will be described in the following sections. Figure 2 displays a schematic functional diagram of the end effector system. The end effector is designed to mate with a grapple fixture of the type shown in Figure 3, which also shows the target used to visually assist in the grappling operation. Figure 4 illustrates the capture envelope within the end effector. This figure also outlines the details of the allowable linear and angular misalignments as given by the specifications.

The capture and rigidization mechanisms within the end effector are actuated by a single dc-brushless-motor drive as shown in Figure 1. Clutches are used to separate the mechanisms, and brakes prevent unwanted rotation. In the event of a failure within the prime channel, the backup release motor (spring drive) is automatically actuated upon release of the backup clutch. Spur gearing is used to provide the required output torques, and both wet (Bray grease 3L-38RP) and dry (Lubeco 905) lubricants are used within the assembly. In general, wet lubricant is used in the small bearings and dry lubricant in other bearings, gears, ball screws, and ball spline.

CAPTURE MECHANISM

Prior to attempting a capture, the snare carriage is fully forward and the snare wires are stored within grooves in the fixed and rotating rings (Figure 5, views 1 and 2). The operator maneuvers the manipulator arm such that the payload grapple shaft (Figure 3) is within the capture envelope. The capture-clutch-and-rigidize brake is closed; the rigidize-clutch-and capture brake is open.

To capture a payload, the inner rotating ring is driven through an 80° angle (Figure 5, views 3 and 4) to close the snare wires over the grapple shaft. Snare-closed and payload-present switches give flat indications of a successful capture and, in an automatic sequence, would automatically initiate rigidization. The snare-closed switch is contacted at the end of snare travel, and the payload-present switch is actuated by the increased cable tension that occurs when the cable passes over a grapple shaft. In this case, movement of a spring in the cable end actuates the switch.

Torque is transmitted to the end effector rotating ring from the backplate, where the motor module is located, via a ball spline assembly. During the rigidization sequence, when the carriage is pulled toward the backplate, torque is maintained on the snare system as the ball spline shaft travels through the backplate into a protective cover provided in the wrist roll joint.

RIGIDIZATION MECHANISM

Following a successful capture, the capture-clutch-and-rigidize brake is opened, and the rigidize-clutch-and-capture brake is closed. Motor torque acts through a spur gear train to three ball screws, the ball nuts of which are attached to the carriage. The ball nuts travel axially toward the backplate, along the ball screws, to effect the rigidization sequence. At the commencement of carriage travel, a flag on the D&C panel shows that carriage movement has started. The carriage travel continues until all misalignments have been pulled out and the grapple fixture baseplate is flush against the end effector end ring. At this point, a zero-tension flag is actuated on the D&C panel. (To release a payload, the snare wires are opened at this carriage position.) Continued carriage travel [approximately 0.025 m (1 in)] is required to fully rigidize the payload. A rigidize flag is activated at approximately 3,560 N (800 lb) of load in the grapple fixture probe. Since the rigidize flag (carriage position actuated) is adjusted to be actuated at a specific grapple fixture pull load, its sensitivity to changes in position as a result of temperature fluctuations required compensation. To this end, a Belleville spring system, preloaded 2,670 N (600 lb) to 3,114 N (700 lb), was installed (Figure 1) in the carriage between the ball screw nuts and the snare ring assembly, and the rigidize switch is adjusted to actuate within the Belleville system's range of travel. Thermal vacuum testing has confirmed that between high- and low-temperature limits, the rigidize switch is contacted within the grapple pin load range of 3,290 N (740 lb) to 3,650 N (820 lb).

BACKUP RELEASE MECHANISM

A spring motor is located on the backplate, near the motor module, to provide backup release capability. Testing has confirmed that this system will open the snare wires at any carriage position from fully rigidized to fully forward. A schematic of the end effector drive mechanisms including backup release is shown in Figure 6.

The spring motor is connected to the motor drive via spur gearing and a backup dog-tooth-type clutch. During normal operation, the negator spring is continuously wound and unwound between its two spools (Figure 1) as the snare system is opened and closed. In the snare-closed position, the spring (which is backwound on the drive spool) provides a constant torque of approximately 70.6 mN-m (10 oz-in) to open the snare system, when the backup clutch is opened.

DEVELOPMENT PROBLEMS AND SOLUTIONS

Capture Mechanism - Main Bearing Thermal Compensation

The large 0.3-m (12-in) diameter ball bearing that supports the rotating ring is mounted into an aluminum structure. At cold temperature, the increase in bearing preload raised friction torques beyond the capability of the backup release mechanism to open the snare system. This was corrected by the provision of a looser bearing fit in the structure, but at the expense of slightly increased virbration wear at the snare drive output gearing because of the increased radial play. The provision of additional carriage or bearing support in the launch configuration is currently being reviewed.

Rigidization Mechanism - Alignment

Development testing demonstrated the need, in this design, for precise relative alignment of the three ball screws, the ball spline, the rigidization spring assemblies, and the carriage guide rollers. Close tolerance fixtures (Figure 7) were developed to meet this need.

Lubrication

The end effector was originally lubricated with Lubeco 905 dry lubricant throughout. However, certain bearings, which were required to accelerate very rapidly to high speed (e.g., approximately 7,000 r/min in 1 s), failed due to clogging with dry-lubricant debris. A design change to wet lubricant (Braycote 3L-38RP) in these bearings has resulted in no further problems to date.

Backup Release Spring Motor

Under certain rapid stop-start conditions, the spring would unwind from the drive spool faster than it could play onto the takeup spool. This resulted in failure of the system. Backwind roller restraints were added around the periphery of each spool to act as low-friction devices to contain the spring within each spool. Satisfactory performance of the spring motor resulted from this modification.

Motor Modules - Brakes and Clutches

During certain portions of the capture-and-rigidize cycle, the brakes and clutches are required to slip at their preset slip-torque values. Although these devices successfully completed a representative-life test program, friction pad wearout, with a resultant drop in slip torque below specified minimums, has been experienced after prolonged use. No design changes were incorporated to correct this problem, but the devices have been declared as life-limited items (50 missions).

CONCLUSIONS

An innovative design for the capturing and docking of payloads has been produced that meets very severe envelope, loading, and environmental requirements. Problems that have occurred during the performance of development- and qualification-level environmental testing have been corrected, and the test program to formally qualify the design for the Orbiter mission is currently underway.

Several other areas of potential product improvement have been identified and are being evaluated for possible incorporation in follow-on production units. These items are:

- Reduced vibration wear and damage to the rigidize-carriage guide tracks and snare-drive output gearing may be accomplished through improved support to these assemblies in the launch configuration (carriage fully forward). Design methods under consideration are:
    - Taper-fit support to the carriage and rotating ring at the carriage-to-housing interface
    - Carriage track bearings that are preloaded against the guide tracks to eliminate free play
    - Steel inserts in the aluminum guide tracks to provide increased tolerance to severe vibration loads

  - O-ring-type support to the large 12-in carriage bearing at the housing and shaft interface; again, to eliminate free play

- Increased use of wet lubrication may eliminate any risks related to bearing or mechanism clogging from debris generation. Research and development in this area is, in some instances, confirming the increased reliability of this approach.

- Further, some specification changes related to force-moment and proximity sensing are under consideration and these, if approved, will undoubtedly result in mechanical design impact.

ACKNOWLEDGMENT

The authors wish to thank the National Research Council of Canada and Spar Aerospace Limited for their permission to publish this paper and would like to acknowledge the contributions of the many engineers and technicians at Spar who contributed to this project.

Table 1. End Effector Temperature Limits (°C)

	OPERATIONAL		ACCEPTANCE		QUALIFICATION		SURVIVAL	
	MAX.	MIN.	MAX.	MIN.	MAX.	MIN.	MAX.	MIN.
ELECTRONICS UNIT	65	-20	70	-25	81	-36	81	-50
MOTOR MODULE COMPONENTS	80	-5	85	-10	96	-36	101	-36
EVA HANDHOLD	69	-94	76	-99	N/A	N/A	N/A	N/A
PAYLOAD (GRAPPLE FIXTURE)	121	-156						

Table 2. Key Loads and Environments

MAXIMUM ACCELERATION (CRASH CASE)	9 g
SHOCK	20 g 11 ms
RANDOM VIBRATION (HARD MOUNTED)	0.8 g^2/Hz, 80 to 100 Hz
ARM OPERATION (INCLUDING RCS FIRING)	1085 Nm (800 FT LB) BENDING, 515 Nm (380 FT LB) ROLL
ARM BRAKING	976 Nm (720 FT LB) BENDING, 651 Nm (480 FT LB) ROLL
ARM JOINT LOCKED MOTOR	1627 Nm (1200 FT LB) BENDING, 949 Nm (700 FT LB) ROLL

Table 3. Status Switch Signals

1. SNARES OPEN
2. SNARES CLOSED
3. RIGIDIZATION COMPLETE
4. END EFFECTOR DE-RIGIDIZED (ZERO TENSION)
5. END EFFECTOR EXTEND
6. PAYLOAD PRESENT

54

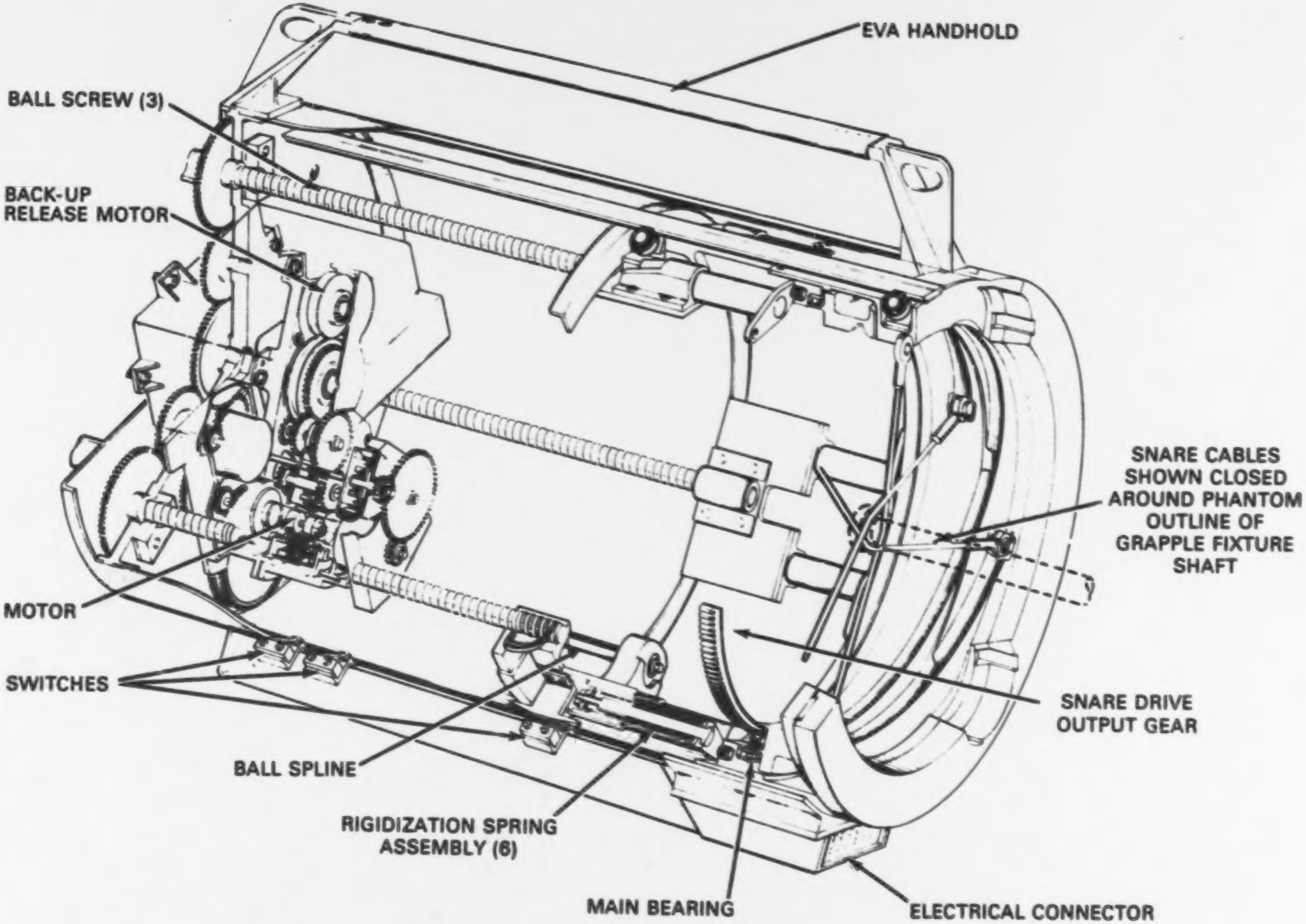
EVA HANDHOLD
BALL SCREW (3)
BACK-UP RELEASE MOTOR
SNARE CABLES SHOWN CLOSED AROUND PHANTOM OUTLINE OF GRAPPLE FIXTURE SHAFT
MOTOR
SWITCHES
SNARE DRIVE OUTPUT GEAR
BALL SPLINE
RIGIDIZATION SPRING ASSEMBLY (6)
MAIN BEARING
ELECTRICAL CONNECTOR

Figure 1. Standard Snare-Type End Effector

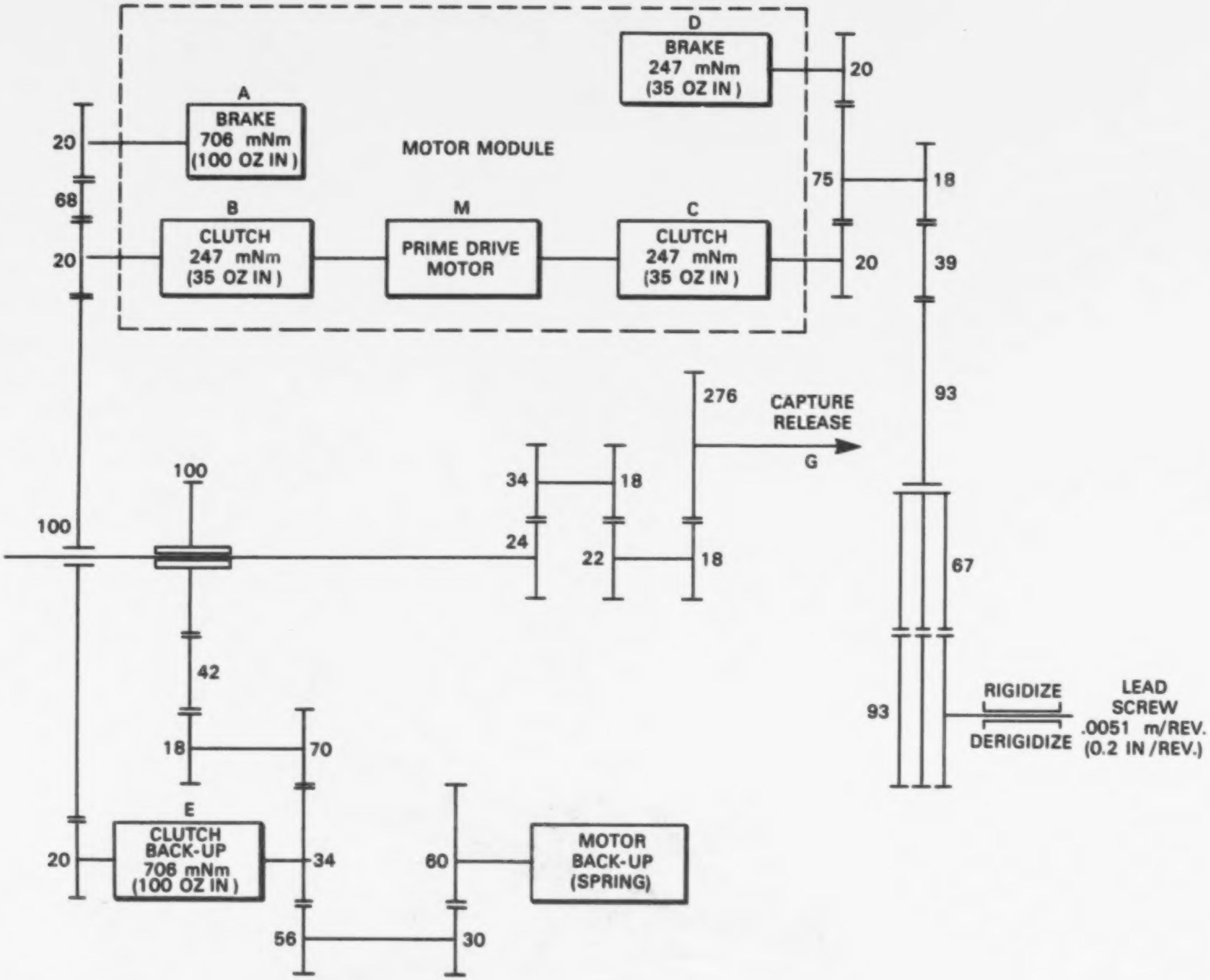
MOTOR MODULE
A
BRAKE
706 mNm
(100 OZ IN)
B
CLUTCH
247 mNm
(35 OZ IN)
M
PRIME DRIVE
MOTOR
C
CLUTCH
247 mNm
(35 OZ IN)
D
BRAKE
247 mNm
(35 OZ IN)
20
68
20
20
75
20
18
39
93
276
CAPTURE
RELEASE
G
100
100
34
18
24
22
18
67
93
42
18
70
RIGIDIZE
DERIGIDIZE
LEAD
SCREW
.0051 m/REV.
(0.2 IN/REV.)
E
CLUTCH
BACK-UP
706 mNm
(100 OZ IN)
20
34
60
MOTOR
BACK-UP
(SPRING)
56
30

Figure 2. End Effector Schematic Functional System

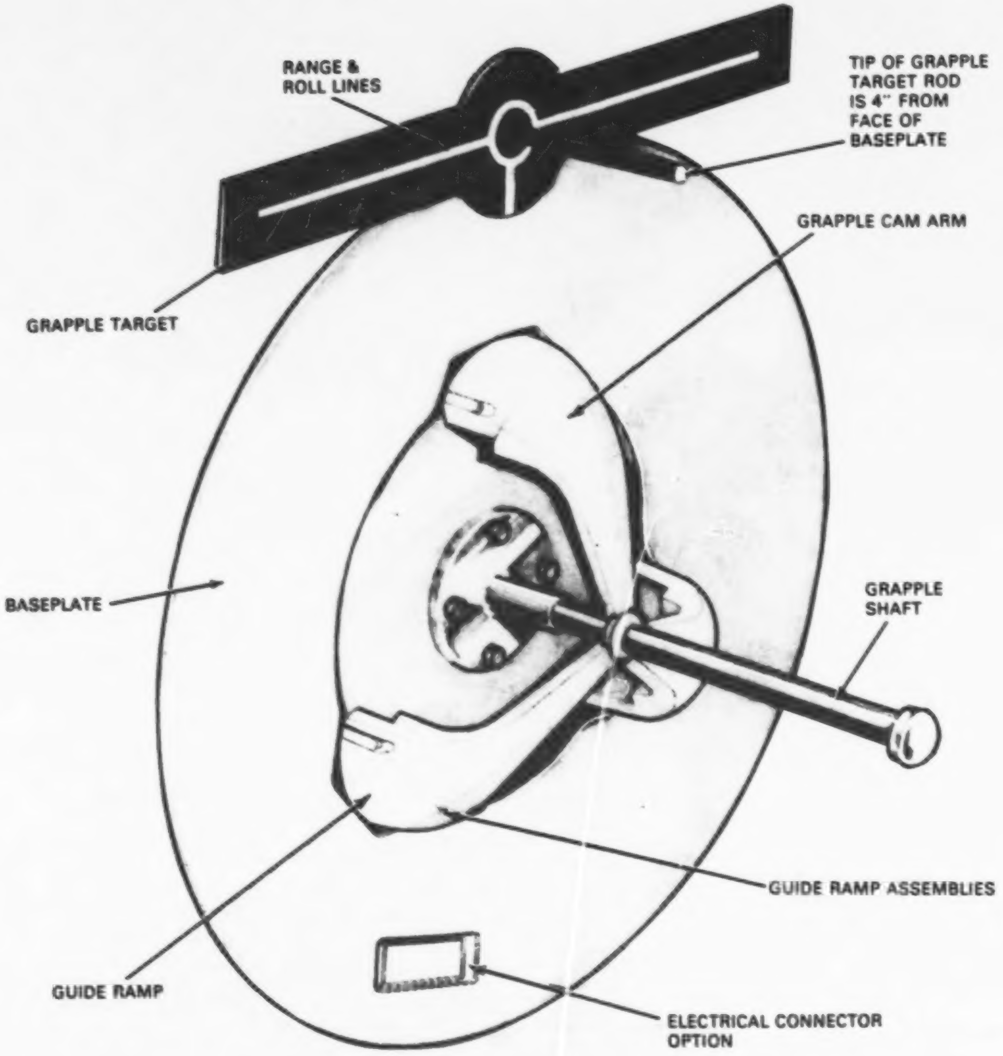
RANGE & ROLL LINES
TIP OF GRAPPLE TARGET ROD IS 4" FROM FACE OF BASEPLATE
GRAPPLE CAM ARM
GRAPPLE TARGET
BASEPLATE
GRAPPLE SHAFT
GUIDE RAMP ASSEMBLIES
GUIDE RAMP
ELECTRICAL CONNECTOR OPTION

Figure 3. Grapple Fixture and Target Assembly

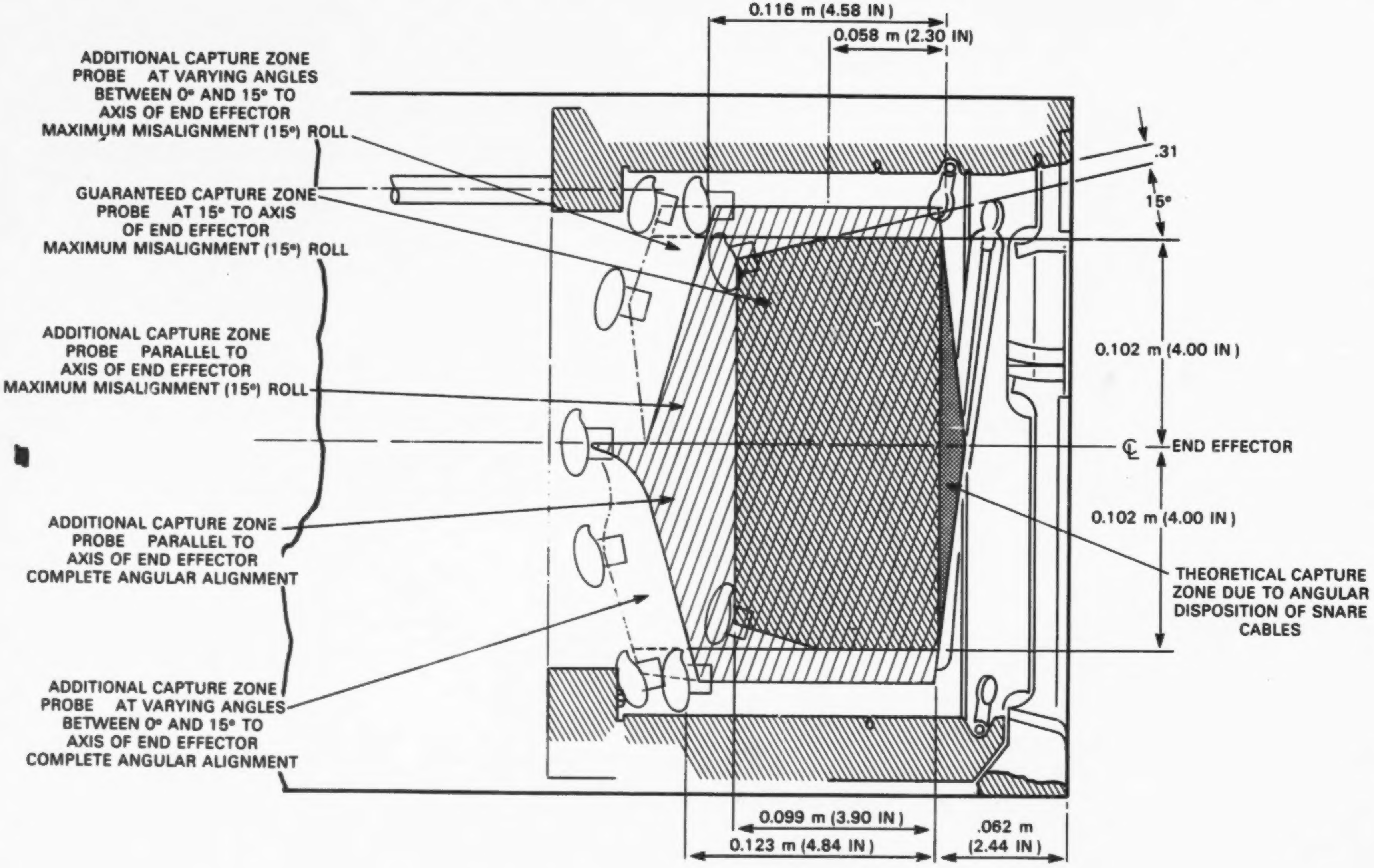
0.116 m (4.58 IN)
0.058 m (2.30 IN)
ADDITIONAL CAPTURE ZONE PROBE AT VARYING ANGLES BETWEEN 0° AND 15° TO AXIS OF END EFFECTOR MAXIMUM MISALIGNMENT (15°) ROLL
GUARANTEED CAPTURE ZONE PROBE AT 15° TO AXIS OF END EFFECTOR MAXIMUM MISALIGNMENT (15°) ROLL
ADDITIONAL CAPTURE ZONE PROBE PARALLEL TO AXIS OF END EFFECTOR MAXIMUM MISALIGNMENT (15°) ROLL
ADDITIONAL CAPTURE ZONE PROBE PARALLEL TO AXIS OF END EFFECTOR COMPLETE ANGULAR ALIGNMENT
ADDITIONAL CAPTURE ZONE PROBE AT VARYING ANGLES BETWEEN 0° AND 15° TO AXIS OF END EFFECTOR COMPLETE ANGULAR ALIGNMENT
.31
15°
0.102 m (4.00 IN)
℄ END EFFECTOR
0.102 m (4.00 IN)
THEORETICAL CAPTURE ZONE DUE TO ANGULAR DISPOSITION OF SNARE CABLES
0.099 m (3.90 IN)
0.123 m (4.84 IN)
.062 m (2.44 IN)

Figure 4. Capture Envelope - End Effector

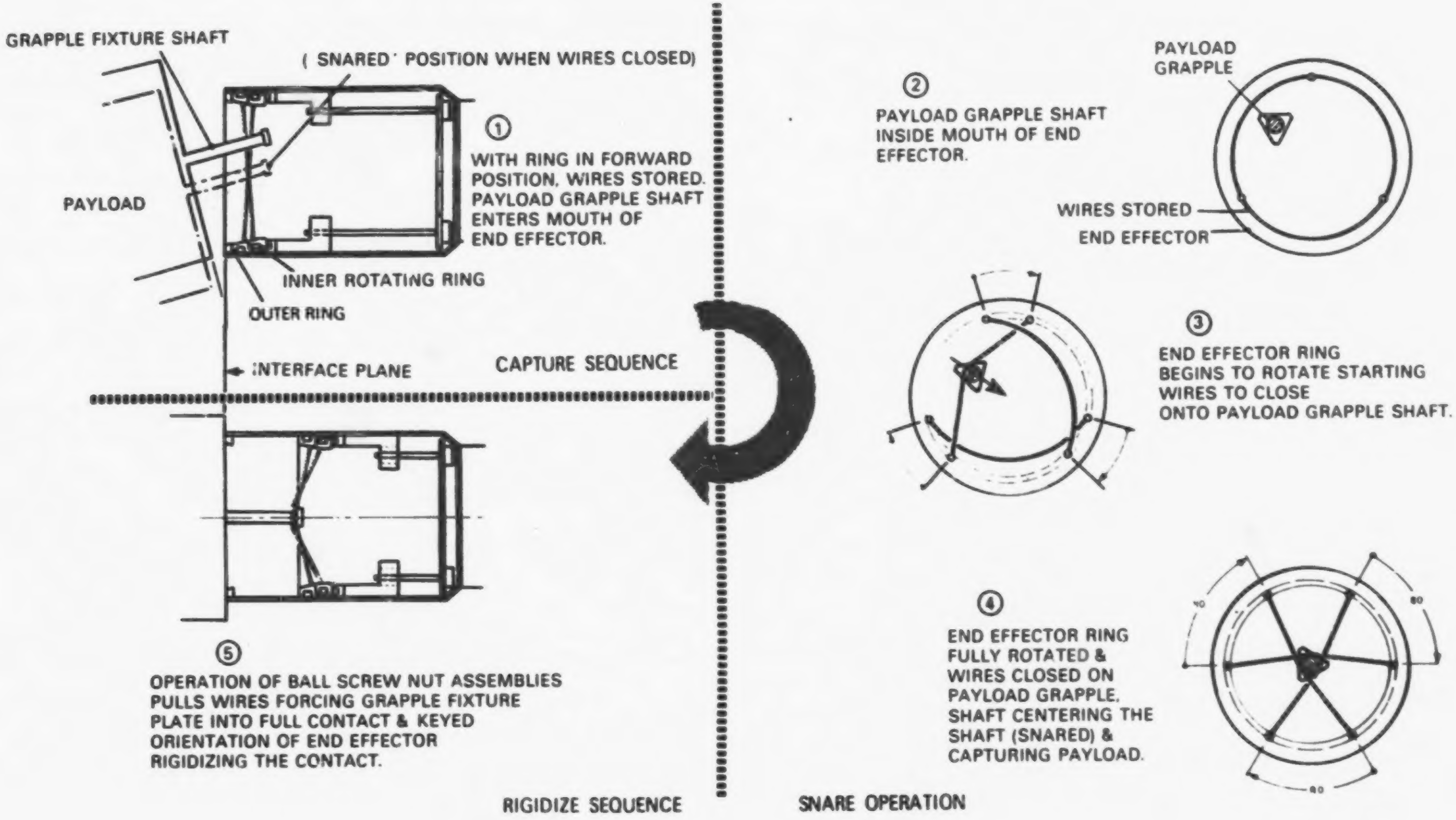
GRAPPLE FIXTURE SHAFT
(SNARED' POSITION WHEN WIRES CLOSED)
①
WITH RING IN FORWARD POSITION, WIRES STORED. PAYLOAD GRAPPLE SHAFT ENTERS MOUTH OF END EFFECTOR.
PAYLOAD
INNER ROTATING RING
OUTER RING
INTERFACE PLANE
CAPTURE SEQUENCE
②
PAYLOAD GRAPPLE SHAFT INSIDE MOUTH OF END EFFECTOR.
PAYLOAD GRAPPLE
WIRES STORED
END EFFECTOR
③
END EFFECTOR RING BEGINS TO ROTATE STARTING WIRES TO CLOSE ONTO PAYLOAD GRAPPLE SHAFT.
④
END EFFECTOR RING FULLY ROTATED & WIRES CLOSED ON PAYLOAD GRAPPLE, SHAFT CENTERING THE SHAFT (SNARED) & CAPTURING PAYLOAD.
⑤
OPERATION OF BALL SCREW NUT ASSEMBLIES PULLS WIRES FORCING GRAPPLE FIXTURE PLATE INTO FULL CONTACT & KEYED ORIENTATION OF END EFFECTOR RIGIDIZING THE CONTACT.
RIGIDIZE SEQUENCE
SNARE OPERATION

Figure 5. End Effector Operation

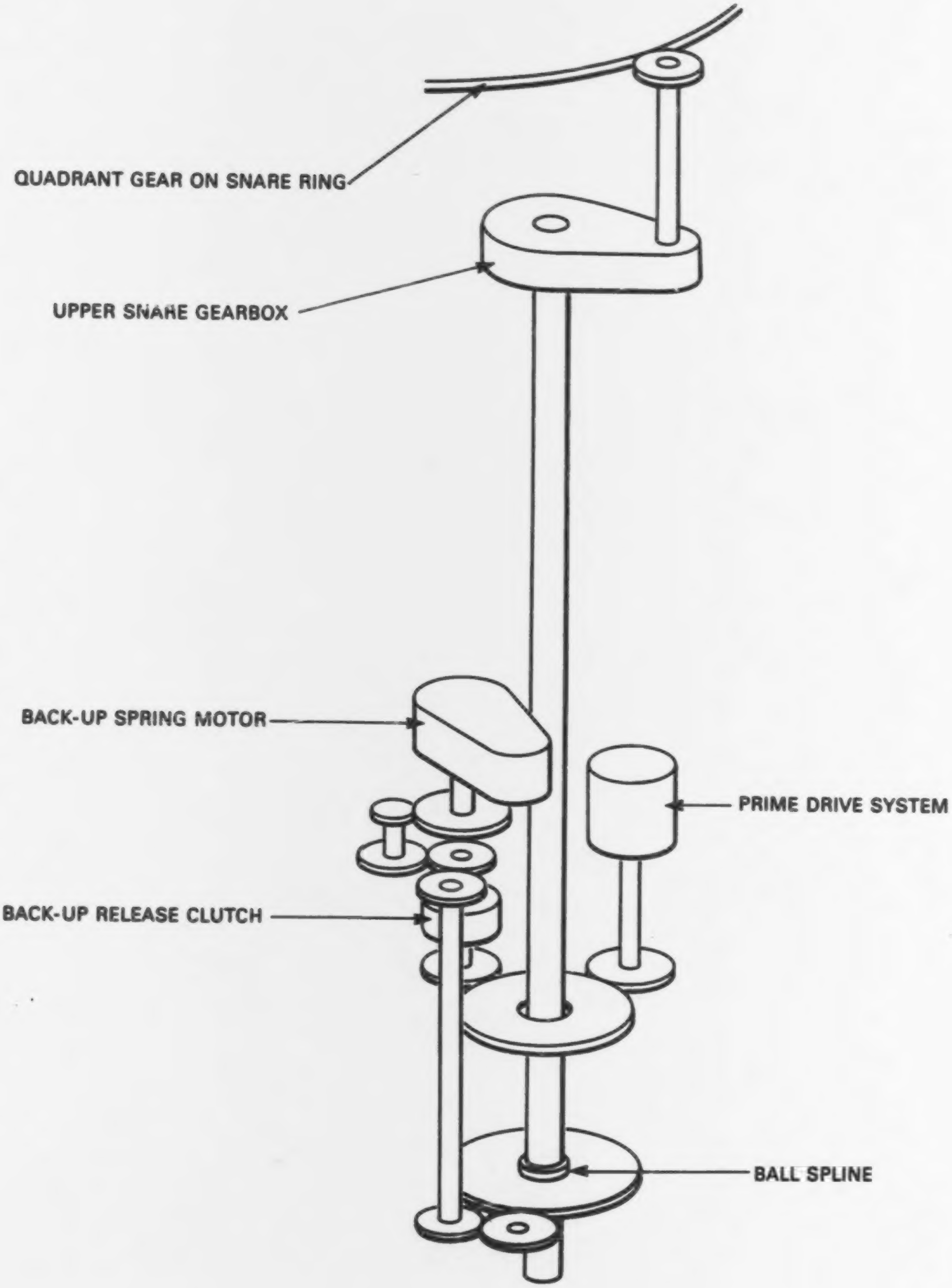
QUADRANT GEAR ON SNARE RING
UPPER SNARE GEARBOX
BACK-UP SPRING MOTOR
PRIME DRIVE SYSTEM
BACK-UP RELEASE CLUTCH
BALL SPLINE

Figure 6. Schematic End Effector Backup Release System

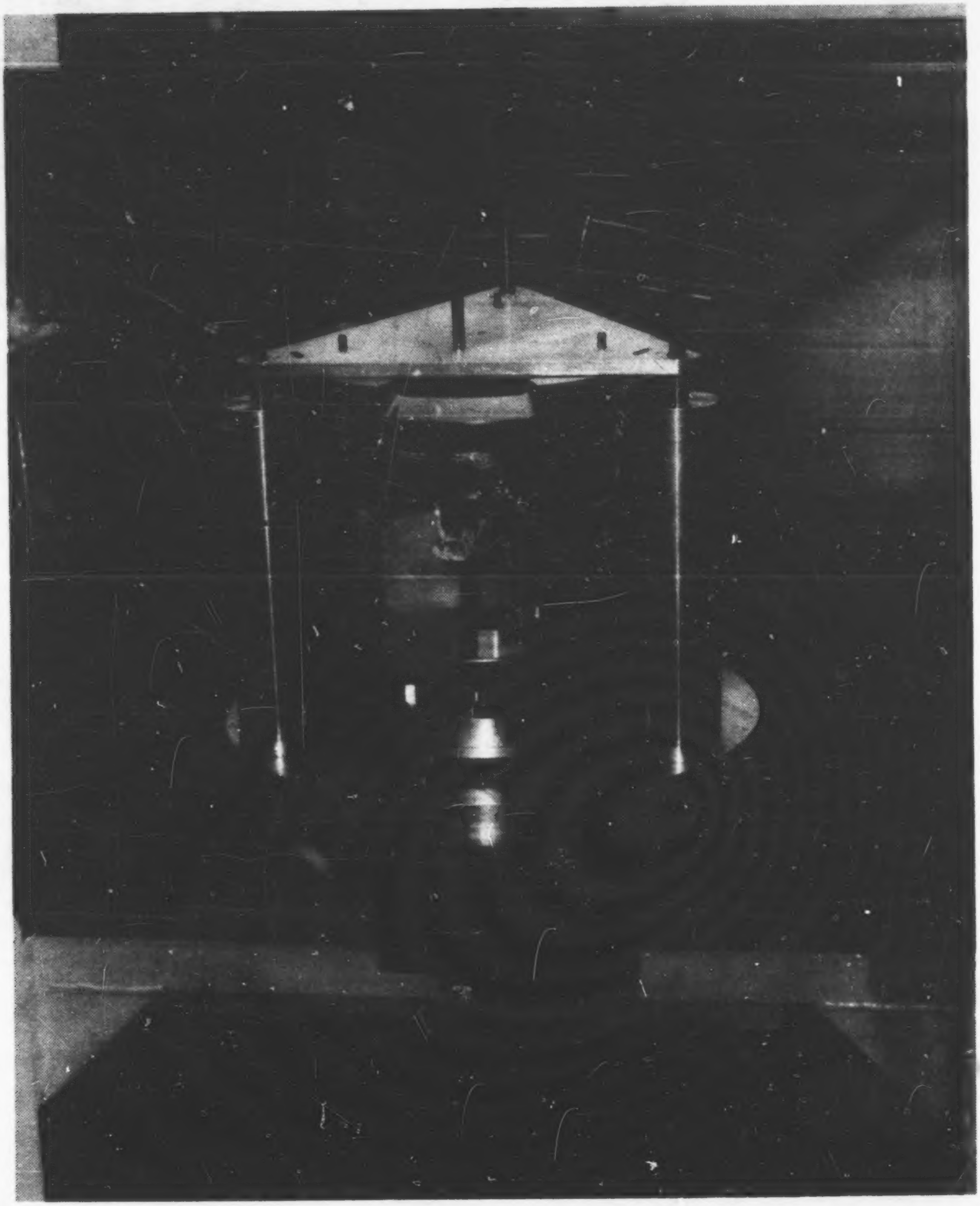

Figure 7. End Effector Alignment Fixture

Robert G. Daniell
Spar Aerospace Ltd.
1700 Ormont Drive
Weston, Ontario, Canada M9L 2W7

Mr. Daniell joined Spar Aerospace in 1962 and has since held mechanical engineering responsibilities for a variety of space and terrestrial projects. In 1972, he joined the Communications Technology Satellite (CTS) program team. In November 1973, he was appointed CTS Structure Subsystem Manager and later became Assistant Solar Array Subsystem Supervisor. In 1975, he joined the SRMS team as Section Chief, Mechanical Arm Subsystem. Currently, Mr. Daniell is the Manager, Mechanical Engineering, responsible for all mechanical design activity within Spar's Remote Manipulator Systems Division.

Co-author of this paper is Mr. Savi S. Sachdev who is also affiliated with Spar Aerospace in Ontario.

Blank Page

CENTERLINE LATCH TOOL FOR
CONTINGENCY ORBITER DOOR CLOSURE

Robert C. Trevino
Lyndon B. Johnson Space Center

ABSTRACT

The centerline latch tool was designed and developed as an EVA manual backup device for latching the Space Shuttle Orbiter's payload bay doors for reentry in case of a failure of the existing centerline latches to operate properly. The tool was designed to satisfy a wide variety of structural, mechanical, and EVA requirements. It provides a load path for forces on the payload bay doors during reentry. Since the tool would be used by an EVA crewmember, control, handgrips, operating forces, and procedures must be within the capabilities of a partially restrained, suited crewmember in a zero-gravity environment. The centerline latch tool was designed, developed, and tested at the Johnson Space Center to meet these requirements.

INTRODUCTION

The Space Shuttle Orbiter's payload bay doors are opened soon after entering orbit and remain open until just before reentry. The doors are opened/closed and latched sequentially, either manually from the on-board control panel or automatically from the on-board computer, by electromechanical actuators. A detailed description of the complex payload bay door system is discussed in a paper entitled "Space Shuttle Orbiter Payload Bay Door Mechanisms" (Ref. 1) given during the 13th Aerospace Mechanisms Symposium at Johnson Space Center, Houston, Texas.

The door mechanisms consist of four basic subelements: door drive actuation, forward bulkhead latches, aft bulkhead latches, and centerline latches (Fig. 1). The door drive system moves the doors to a designated position by two actuator systems, one on either side of the payload bay. Each system drives one 18.3-meter (60-foot) door and consists of an electromechanical actuator that drives six gear boxes interconnected by torque tubes. Each gear box then rotates the drive linkage to the door. The forward bulkhead latches connect the doors to the forward structural bulkhead. These latches consist of a right-hand gang of four latches and a left-hand gang of four latches that operate sequentially. The active latch mechanism is mounted on the door, and the mating passive hook rollers are mounted on the bulkhead. Each gang of latches is driven by a single electromechanical rotary actuator with two motors. In the same manner, the aft bulkhead latches operate and connect the doors to the aft structural bulkhead. Finally, the centerline latches connect the right-hand and left-hand doors along the centerline. There are four gangs of latches (four latches per gang). The active latch mechanisms are on the right-hand door and the passive mating rollers are on the left-hand door. The four latches within each gang are connected by torque tubes to each other and to a single electromechanical rotary actuator. The centerline latch system is shown on Fig. 2 and 3.

A failure in any of the four basic door mechanisms could require a manual EVA operation using one or more specially designed Orbiter door closure tools. These tools would disconnect a disabled door or latch system and close and secure the doors if the normal system failed. The set of EVA Orbiter door closure tools consists of a tubing cutter, a winch, a 3-point latch tool, and a centerline latch tool. The tubing cutter, the winch, and the 3-point latch tool have been previously discussed in detail in a paper entitled "Orbiter Door Closure Tools" (Ref. 2) given during the 14th Aerospace Mechanisms Symposium at NASA Langley Research Center, Hampton, Virginia.

The basic types of potential failures, their causes, and the required EVA actions are described in Table 1. For a door drive system failure such that the door can neither be opened or closed, the EVA crewmember uses the tubing cutter to cut the upper or lower drive tubes. Once the door drive tubes have been cut, the EVA winch rope hook is routed over the number 4 bulkhead hook roller and attached to the number 4 latch bellcrank at the tip of the door. The rope is then reeled back in by the winch until the door has been fully closed. If a gang of bulkhead latches on either end of one or both doors fails to operate properly, the EVA crewmember uses the 3-point latch tool to fully close and secure the door.

CENTERLINE LATCH TOOL

If a gang of centerline latches on the right-hand payload bay door fails to operate properly, the doors must be safely secured by some other means. The centerline latch tool is an EVA manual backup device for latching the Orbiter's payload bay doors for reentry. Four of these tools (enough to bypass one gang of latches) are carried onboard the Orbiter.

Design criteria required that the tool fit all 16 centerline latches. It had to be able to interface with the existing centerline latch mechanisms and payload bay doors. The problem of misalignment due to thermal distortion was also considered. The tool had to close the doors having 5.05 cm (1.99 inches) misalignment in the y-axis and 10.97 cm (4.32 inches) misalignment in the z-axis. Misalignment in the x-axis was considered negligible because the four passive shear fittings align the doors in the x-direction. The tool provides a load path for y and z forces on the payload bay doors to maintain the Orbiter's structural integrity during reentry.

The centerline latch tool's controls, handgrips, operating forces, and procedures had to be within the capabilities of a partially restrained, EVA crewmember in a zero-gravity environment. These design requirements are set by the Shuttle EVA Description and Design Criteria Document (JSC-10615). Another requirement is that the tool be provided a safety tether attach point since it will be transported or handled during EVA. The tool also had to retain itself in position while being used by the crewmember.

The centerline latch tool (Fig. 4) consists of a frame, a screw/nut drive assembly turned by a ratchet that pivots in the frame, and the latch. The ratchet handle folds down into a stowed position to conserve space. The release button, which is used to deploy the tool latch, can be depressed from either side of the tool frame. It has a safety catch, also on both sides, such that it cannot be inadvertently depressed. The installation sequence is shown on Fig. 5.

INSTALLATION

The tool is installed by first inserting it on the failed centerline hook latch. Then the tool is rotated to brace it in place (Fig. 6). The safety catch is removed on the release button to be depressed. When the release button is depressed, the tool latch is deployed. The tool latch bypasses the existing hook latch regardless of the position of the centerline hook latch. The ratchet-handle is now unfolded. In this configuration, the crewmember holds the tool and extends the screw by ratcheting until a force is applied on the centerline latch passive roller, closing and securing the door. The sleeve on the ratchet handle is raised and the handle folded to the stowed position.

One tool is installed on each centerline latch in the disabled gang in the same sequence as normal door closure. After installing the last tool, the crewmember is ready to reenter to the crew module.

TESTING

The centerline latch tool has undergone development and evaluation by crewmembers and NASA personnel. Extensive testing and training have also been done using the full-scale mockup of the Orbiter in the Weightless Environment Training Facility (WETF) at the Johnson Space Center. This testing determined that the centerline latch tool was within extravehicular capabilities and workload limits.

A qualification test fixture was also built to simulate the loading on the latches. The centerline latch tool was installed on the test fixture latches. Then, using a hydraulic cylinder, the tool reacted the loads that it would see during reentry.

CONCLUDING REMARKS

The flight tools are stored onboard the Cargo Bay Stowage Assembly, a stowage container located in the payload bay, during the Shuttle flights. The centerline latch system is a reliable mechanical system; however, like any mechanical system, it is possible that a malfunction could occur that could cause an unsafe reentry of the Orbiter. This backup tool will be available as a safety device for the Orbiter.

REFERENCES

1. McAnally, Bill M.: Space Shuttle Orbiter Payload Bay Door Mechanisms. Paper presented at the 13th Aerospace Mechanisms Symposium (Johnson Space Center, Texas), April 26-27, 1979.

2. Acres, William R.: Orbiter Door Closure Tools. Paper presented at the 14th Aerospace Mechanisms Symposium (NASA Langley Research Center, Hampton, Virginia), May 1-2, 1980.

TABLE 1.- DOOR CLOSURE FAILURES

TYPE OF FAILURE	CAUSE	ACTION
One or both doors will not close	Door drive system failure	Attach the winch hook to the affected door and manually close the door. Actuate the bulkhead latch system.
	Door drive system failure and jam	Cut the six drive tubes on the affected door with the tubing cutter and manually close the door using the winch. Actuate the bulkhead latch system.
Bulkhead latch system fails with the latch hook greater than 37° from the closed position	Latch actuator fails or jams	Install the three-point latch tool on the end of the affected door starting with the number 1 latch. Proceed in order to the number 4 latch, closing the door at each position before proceeding to the next latch.
Bulkhead latch system fails with the latch hook less than 37° from the closed position	Latch actuator fails or jams	Remove the connector bolt from the actuator linkage with the bolt extractor. Manually backdrive the latch hooks until the three-point latch tool can be installed on the number 1 latch; proceed in order to the number 4 latch, closing the door at each position before proceeding to the next latch.
Centerline latch system fails with the hook latch in any position	Latch actuator fails or jams	Install the centerline latch tool on the affected centerline latch. Proceed in order to the next centerline latch.

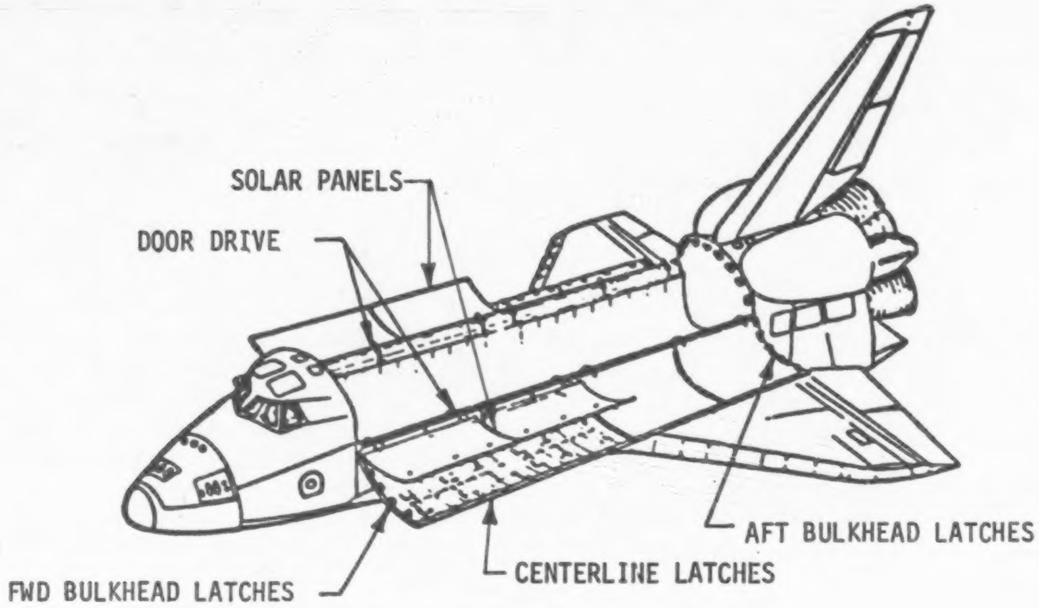
SOLAR PANELS
DOOR DRIVE
AFT BULKHEAD LATCHES
CENTERLINE LATCHES
FWD BULKHEAD LATCHES

FIGURE 1. - PAYLOAD BAY DOOR SYSTEM

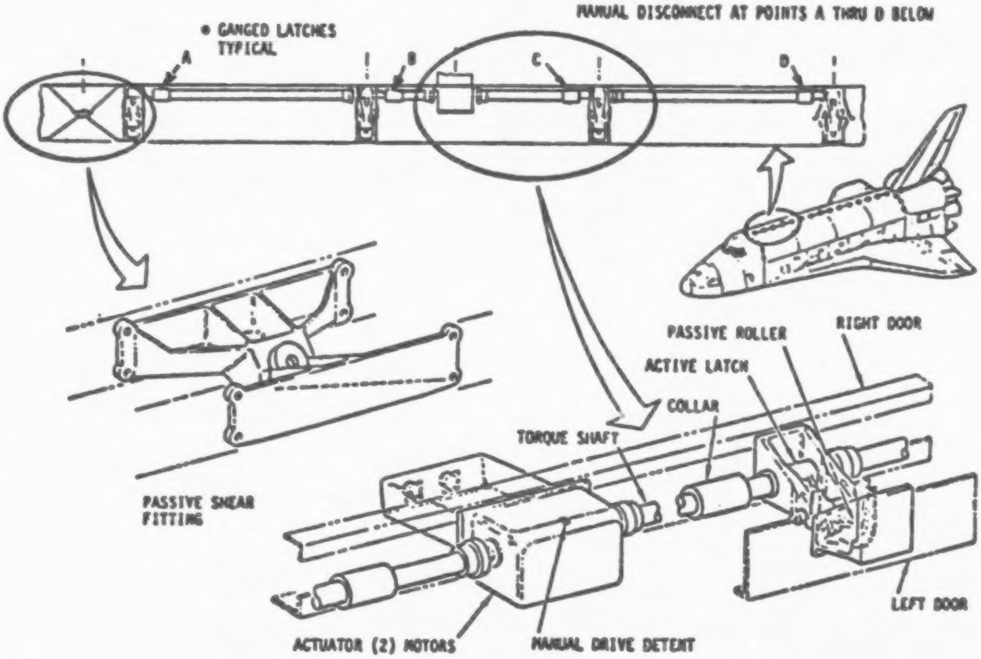
MANUAL DISCONNECT AT POINTS A THRU D BELOW
• GANGED LATCHES TYPICAL
A
B
C
D
PASSIVE ROLLER
RIGHT DOOR
ACTIVE LATCH
COLLAR
TORQUE SHAFT
PASSIVE SHEAR FITTING
LEFT DOOR
ACTUATOR (2) MOTORS
MANUAL DRIVE DETENT

FIGURE 2. - PAYLOAD BAY DOOR CENTERLINE
LATCH SYSTEM

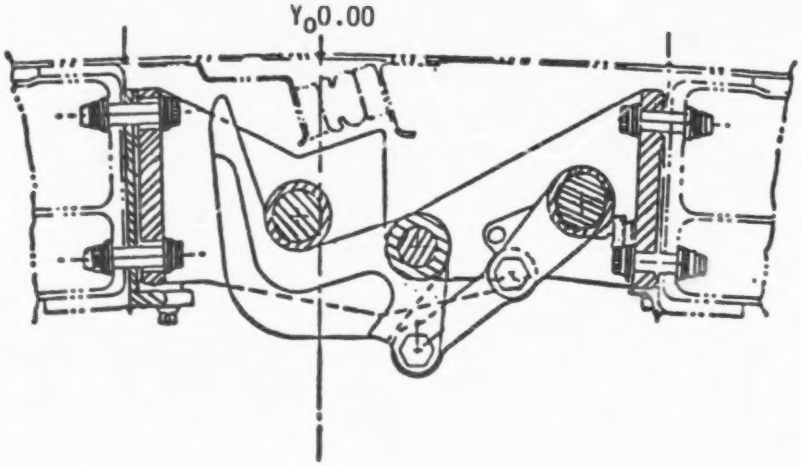

FIGURE 3. - CENTERLINE LATCH ASSEMBLY, TYPICAL (16 LOCATIONS), VIEW LOOKING FWD

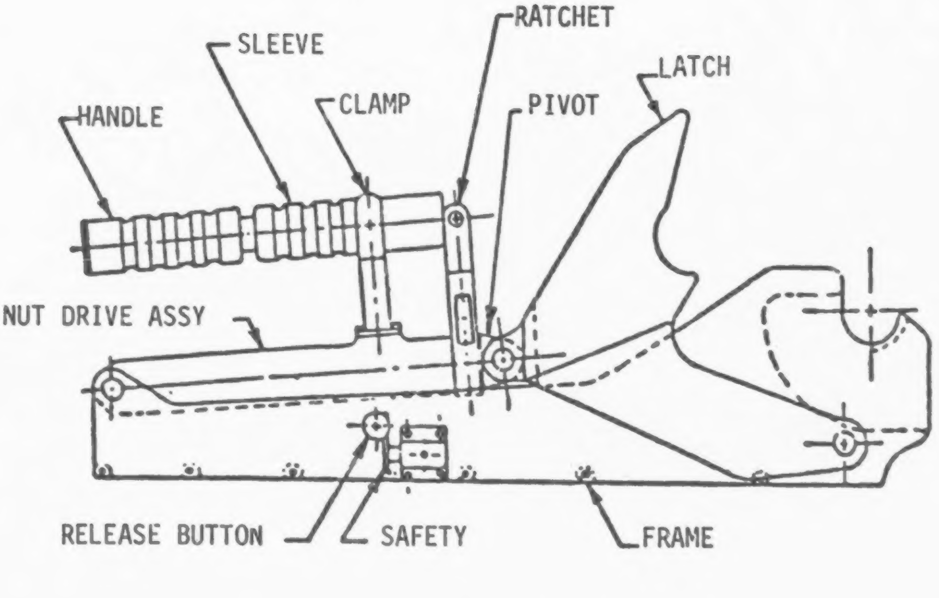
RATCHET
SLEEVE
LATCH
HANDLE
CLAMP
PIVOT
NUT DRIVE ASSY
RELEASE BUTTON
SAFETY
FRAME

FIGURE 4. - CENTERLINE LATCH TOOL

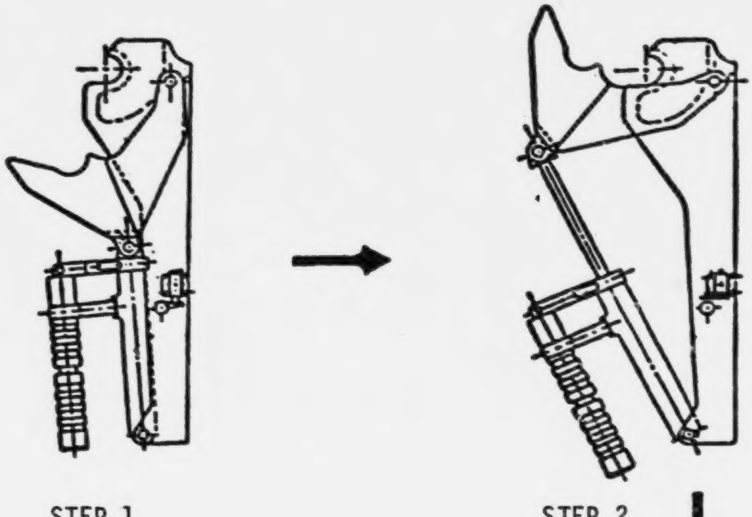

STEP 1
INSTALL ON DISABLED LATCH

STEP 2
RELEASE HOOK

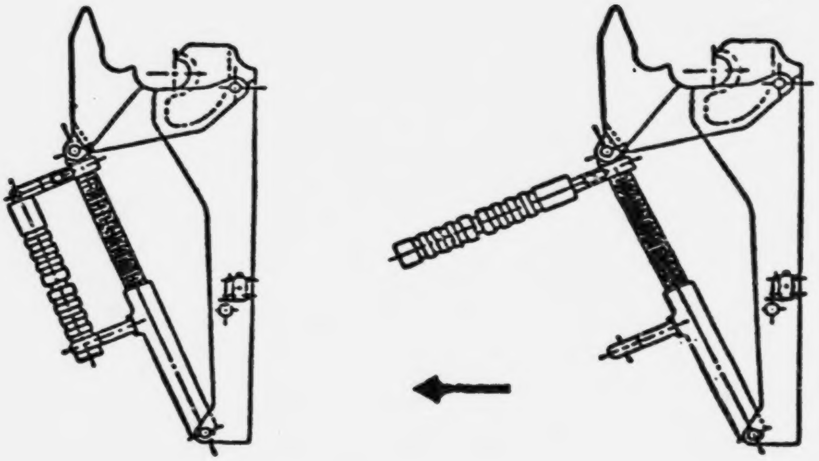

STEP 4
STOW HANDLE

STEP 3
EXTEND DRIVE SCREW

FIGURE 5. - CENTERLINE LATCH TOOL
INSTALLATION SEQUENCE

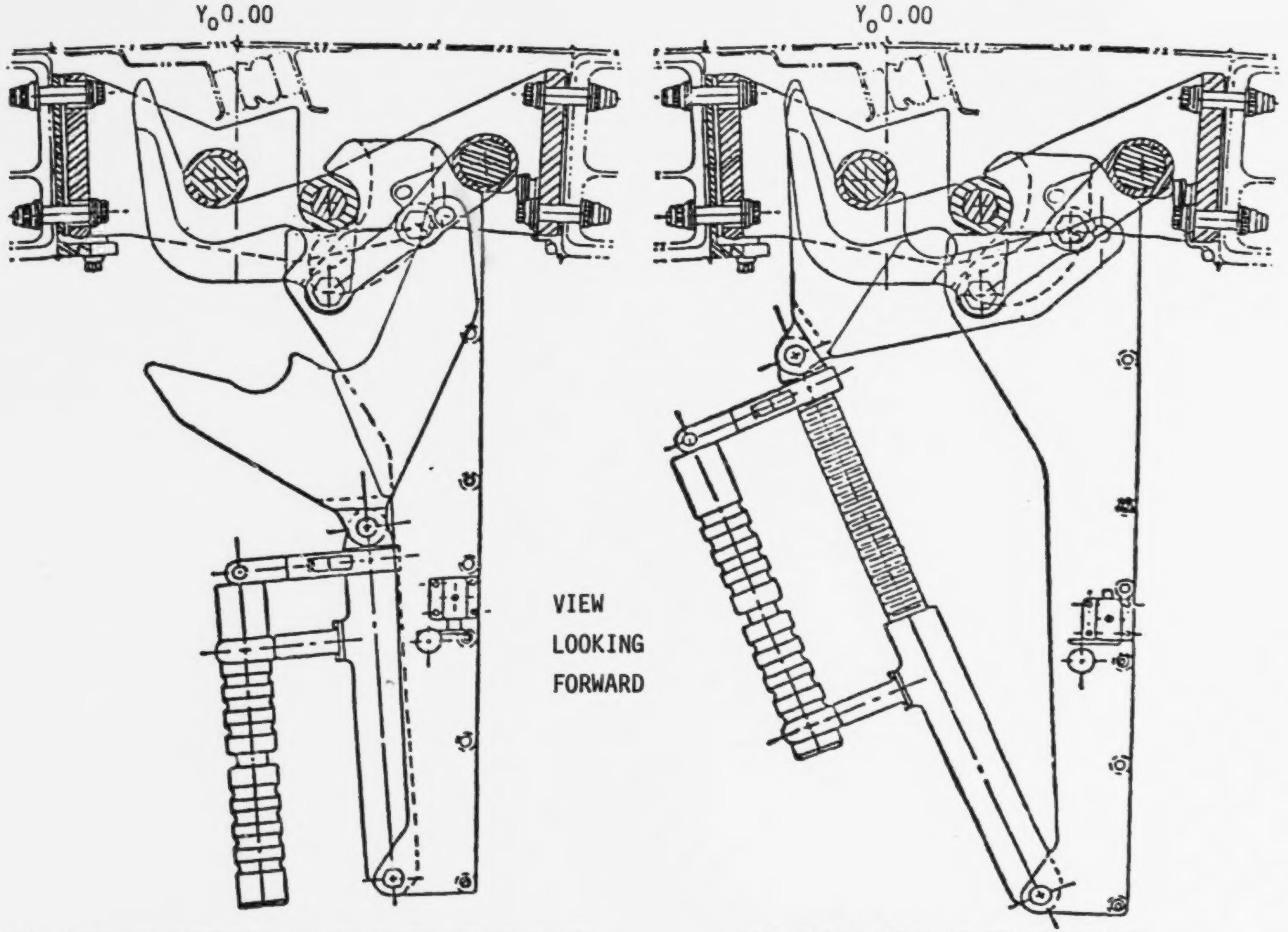
$Y_0$0.00
$Y_0$0.00
VIEW
LOOKING
FORWARD

(1) TOOL IS INSERTED ON THE HOOK PIVOT SHAFT AND BRACED AGAINST THE BELLCRANK.

(2) TOOL LATCH IS RELEASED AND LOCKED IN PLACE.

FIGURE 6. - CENTERLINE LATCH TOOL INSTALLATION

Robert C. Trevino
National Aeronautics and Space Administration
Johnson Space Center
Mail Code EW34
Houston, Texas 77058

Mr. Trevino is assigned to the Mechanisms Design Section, Spacecraft Design Division, of the Engineering and Development Directorate, NASA-Johnson Space Center. Before joining NASA, he was a naval flight officer in the United States Navy and is presently a Lieutenant Commander in the Naval Reserve attached to an Office of Naval Research/Naval Research Laboratory reserve unit. Mr. Trevino received his B.S. degree in Aerospace Engineering from the University of Texas in 1972.

SPACECRAFT LAUNCH VEHICLE

EVENT SEQUENCING SYSTEM

By

Vincent R. Noel*

ABSTRACT

This paper describes the design and operation of a combination of explosive devices and mechanisms that are used to provide sequencing signals and events for the upper stages of a multistage launch vehicle. The launch vehicle is a three-stage vehicle with the Atlas booster as the first stage and Thiokol Star 48 solid motors providing propulsion for the 2nd and 3rd stages. The 1st/2nd stage separation is initiated by redundant discrete electrical signals that originate in the Atlas booster. All subsequent events are controlled by explosive/mechanical components assembled and installed in a subsystem called the Event Sequencing System. No electrical power or signal is required for subsequent events.

The upper stages are designated the SGS-II Stage Vehicle System.

INTRODUCTION

The Event Sequencing System evolved from a requirement commencing with separation from an Atlas E/F booster to perform all functions necessary to place a NAVSTAR Global Positioning satellite into a transfer orbit. Two tandem Star 48 solid-propellant motors provided sufficient total impulse to achieve the necessary apogee velocity. A method of providing the following functions in a sequential manner was required:

1. 1st/2nd Stage Separation
2. Simultaneous Ignition of 8 Spin Gas Generators
3. 2nd Stage Solid Motor Ignition
4. 2nd/3rd Stage Separation
5. 3rd Stage Solid Motor Ignition
6. 3rd Stage/Spacecraft Stage Separation
7. Release of Tumble Weights

The Event Sequencing System is an integrated system which performs items 2 through 7.

---

*McDonnell Douglas Astronautics Company, Huntington Beach, California

TRADE STUDIES AND RISK ASSESSMENT

Three major types of systems were studied for Event Sequencing: Electromechanical, Electronic and Explosive. Safety, reliability, simplicity of design (including telemetry interfaces), cost, weight, flight environment, implementation schedule, field station operations and procedures, amount of ground support equipment required, and extent of company experience with each system were considered. Cost and schedule were of paramount importance. The system had to be designed, developed and qualified for flight within one year.

The major alternative to the explosive/mechanism system was the use of electromechanical timers. The complexity of electrical system design and checkout, the historical problems associated with electromechanical timers, the additional amount of telemetry required, and the severe schedule problems involved with electromechanical timers led to selection of the explosive/mechanism system.

The explosive/mechanism system was selected because it was safe, simple, highly reliable, weighed less than competing systems, and could be designed, developed and tested within the allotted schedule. The selected system used less electrical power, required no telemetry, and eliminated the need for field checkout and ground support equipment.

SYSTEM DESCRIPTION

The system consists of components listed below, together with Explosive Transfer Assemblies (ETA), and inert parts necessary to connect the components together.

QUANTITY	NOMENCLATURE
2	1-second delay
2	2.1-second delay
2	10.2-second delay
2	128.4-second delay
2	141.7-second delay
2	203.6-second delay
20	Through-Bulkhead-Initiator (TBI)
4	TBI Operated Bolt Cutters
2	TBI Operated Cable Cutters
4	Separation Plane Initiators (SPI)

A functional schematic showing the organization of the components into the system is shown in Figure 1 and 1A. An exploded view of the SGS-II Stage Vehicle System is shown in Figure 2. Figure 3 is a photograph of the SGS-II taken during development testing.

SYSTEM OPERATION

The system sequencing is initiated by the separation of the 1st/2nd stages which pulls an activating rod from each of two Separation Plane Initiator Mechanisms (SPIM). The SPIM output initiates the following sequence of events:

Sequence 1

Initiates redundant one-second pyrotechnic time delays whose output is used to:

A. Ignite 8 gas generators that are used to spin the 2nd and 3rd stages and the spacecraft to 75 RPM.

B. Initiate redundant 141.7-second pyrotechnic delays.

Sequence 2

Output from the 141.7-second delays initiate:

A. The second stage Star 48 motor.

B. Redundant 128.4-second time delays.

Sequence 3

Output from the 128.4-second delays initiates redundant bolt cutter mechanisms which sever the bolts on a V-band clamp assembly, thus releasing the structural attachment between the 2nd/3rd stages. Coiled helical compression spring actuators provide the separation force.

Sequence 4

The third stage segment of the system is initiated by the separation motion which activates two SPIM.

Sequence 5

Output of the two SPIM initiate redundant 10.2-second pyrotechnic time delays. Output of each time delay is manifolded to accomplish the following:

A. Initiate the 3rd stage Star 48 motor.

B. Initiate redundant 203.6-second time delays.

Sequence 6

Output from each 203.6-second delay initiates:

A. Redundant bolt cutter mechanisms which sever the bolts on a V-band clamp assembly, thus releasing the structural attachment between the 3rd stage and spacecraft. Coiled helical compression springs provide the separating force.

B. Redundant 2.1-second time delays.

Sequence 7

Output from each 2.1-second delay initiates redundant cable cutters which release a tumble weight that prevents the expended third stage from recontacting the spacecraft.

COMPONENT DESCRIPTION

Explosive Transfer Assemblies (ETA)

The ETA consists of a metal-clad explosive core (mild detonating cord) assembled into a stainless steel tube which contains all the products of detonation. This material is fabricated into ETA lines of the required length by adding identical end tips and the appropriate size threaded fitting at each end (Figure 4). All explosive material is hexanitrostilbene, especially developed for high-temperature applications. The ETA transfers the sequencing signal from component to component with a detonation velocity of approximately 6000 meters/sec (20,000 ft/sec). The ETA can be formed into any shape in which a similar piece of stainless steel tubing could be formed using a one inch minimum bend radius. Approximately three-quarter million ETA lines have been manufactured to date.

Through-Bulkhead-Initiator (TBI)

A TBI is a bar of steel with non-connecting holes bored on its centerline from each end. Figure 5 shows a cross-sectional view of a TBI configured for an ETA tip input. A high-explosive donor charge is press loaded into the cavity against the bulkhead on the input side, and a receptor charge is loaded against the bulkhead on the output side. The donor charge is initiated by the ETA tip, and resulting shockwaves are transmitted through the bulkhead to initiate the receptor charge, which then ignites the TBI output charge. The output charge is tailored and sized to a specific objective. The bulkhead remains intact and is designed to retain a pressure of 5516 $\frac{N}{CM^2}$ (8000 PSI) at a temperature of 149°C (300°F).

Bolt and Cable Cutters

The bolt cutter (Figure 5) is a self-contained device consisting of an explosive cartridge (TBI), a bolt cutter body, a guillotine piston/knife blade held and positioned in the body by a shear pin, and an anvil. In operation, the pressure resulting from the output of the explosive charge builds up behind the piston/knife blade, causing it to shear the shear pin and impact against the anvil. The bolt cutter is used to cut a 0.792 CM (.312 IN) diameter A-286 stainless steel stud heat treated to 117 K $\frac{N}{CM^2}$ - 138K $\frac{N}{CM^2}$ (170-200 KSI). The cable cutter is similar in operation to the bolt cutter except that it has a removeable anvil, which allows the cutter to be installed on a cable with fixed ends.

Pyrotechnic Time Delays

Figure 6 shows the incorporation of Small Column Insulated Delay (SCID) fuse into a delay module designed for ETA end-tip initiation. Shock/pressure from an ETA end tip drives a firing pin into a percussion primer, and hot gases from the primer ignite a pickup charge on the end of the SCID. Burning rate and length of SCID control the length of time delay. The other end of the SCID is fitted with a booster charge that produces a high-order detonation output to initiate the interconnecting ETA lines and the other time delay in the module. SCID fuse is a deflagrating pyrotechnic (32.8 grains/meter [10 grains/ft]) encased in a continuous lead sheath. It is similar in appearance to lead solder. Burning rates of SCID in this application vary from .20 $\frac{SEC}{CM}$ (.5 $\frac{SEC}{IN}$) to 1.38 $\frac{SEC}{CM}$ (3.5 SEC/IN).

TIME DELAY REQUIREMENTS/RESULTS

The delay limits imposed were a 3 sigma value of ± 10% from the nominal over a temperature range of 10°C to 26.7°C (50°F to 80°F).

Representative actual time delay periods from production delays are shown in Table 1. Pyrotechnic delays are temperature sensitive and tend to time out faster at high temperature and slower at low temperatures. Nominal times also tend to increase at the rate of 1% to 2% a year as a result of aging.

TABLE 1. TIME DELAY TEST RESULTS

TEMP	DELAY TIME (SEC)					
	1.0	141.7	128.4	10.2	203.6	2.1
10°C(50°F)	1.01	146.90	127.15	10.95	209.10	2.05
18.3°C(65°F)	1.00	135.60	125.68	10.98	209.45	2.09
	1.00	136.75	123.73	10.69	202.55	2.12
	1.01	139.15	124.35	10.65	199.50	2.11
	1.00	138.76	122.53	10.84	193.05	2.06
	.99	132.56	129.35	10.61	209.65	2.10
	.99	138.64	129.40	10.68	203.45	2.13
26.7°C(80°F)	1.05	134.45	125.45	10.21	196.50	2.03

SEPARATION PLANE INITIATOR MECHANISM (SPIM)

The SPIM is a simple mechanism which performs a very important function. The explosive components installed on the second and third stages are initiated by redundant SPIM mounted at the separation planes. The SPIM is fired by a standard firing pin and percussion primer arrrangement. The separation motion between stages cocks the spring-driven firing pin and in the same movement releases the sear and allows the pin to drive into the percussion primer (Figure 7). The percussion primer initiates a pickup charge which initiates a standard ETA end tip.

A similar design is commonly used on military aircraft escape systems for initiation of the escape system and for parachute reefing line cutters. The Apollo space vehicle used such devices in its parachute recovery system.

SAFETY ASPECTS

The system met all the range safety requirements of SAMTEC 127-1, CHANGE 3, with the exception of Para. 3.4.6.4, Volume I, which required the use of a remotely controlled safe and arm (S&A) device in the solid motor ignition system. The need for an S&A device was obviated by the use of the non-electric SPIM which initiates the motor-ignition explosive trains only upon stage separation.

Inadvertent motor ignition is prevented by the following: installation of the output ETA line to the SPIM late in the launch preparation cycle; use of a flagged removeable safety pin and safety plug for the output port; placement of a shoulder on the firing pin to prevent the pin from being pushed in; and installation of integral mounting bracketry on the aft stage to prevent the pin from being pulled out except by stage separation. The weight of one motor and the space vehicle is greater than the force the separation springs provide; therefore, no separation would occur at either first/second or second/third separation planes if a clamp band assembly inadvertently separated while on the launch pad.

The use of the SPIM concept was approved by Range Safety and the upper stages designated the SGS-II Stage Vehicle System are scheduled to be launched from Vandenberg Air Force Base in 1982.

CONCLUSION

The Event Sequencing System represents a unique application of explosives and mechanisms to accomplish operations formerly performed by electromechanical and electronic systems. Application of such a system is recommended for sequencing events where the timing variations inherent in the system are acceptable; and high reliability, safety, relatively low cost and weight, and absence of field station checkout and equipment are desired.

ACKNOWLEDGMENTS

The system was designed for the Space Division of the Air Force Systems Command. All component parts were designed and built by Teledyne McCormick Selph, Hollister, California, to a system specification provided by McDonnell Douglas Astronautics Company, Huntington Beach, California.

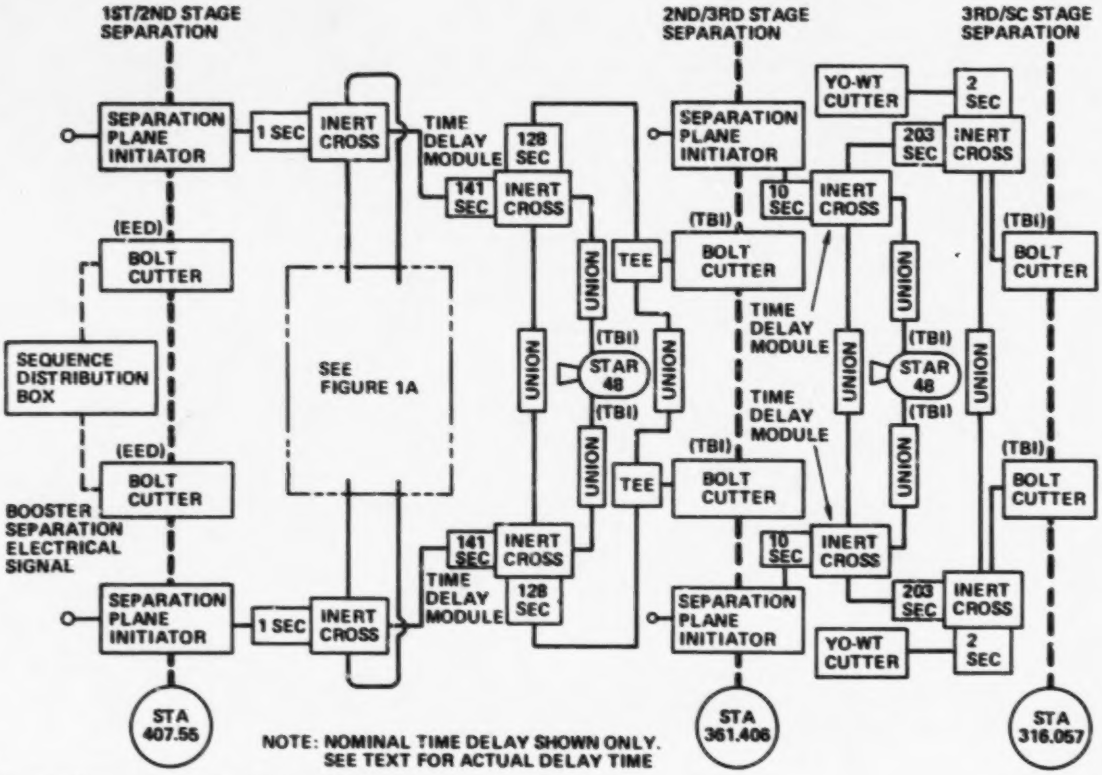
1ST/2ND STAGE SEPARATION
2ND/3RD STAGE SEPARATION
3RD/SC STAGE SEPARATION
SEPARATION PLANE INITIATOR
1 SEC
INERT CROSS
TIME DELAY MODULE
128 SEC
141 SEC
(EED)
BOLT CUTTER
SEQUENCE DISTRIBUTION BOX
SEE FIGURE 1A
BOOSTER SEPARATION ELECTRICAL SIGNAL
UNION
TEE
(TBI)
STAR 48
YO-WT CUTTER
2 SEC
203 SEC
10 SEC
STA 407.55
STA 361.406
STA 316.057

NOTE: NOMINAL TIME DELAY SHOWN ONLY.
SEE TEXT FOR ACTUAL DELAY TIME

Figure 1. Event Sequencing System Schematic

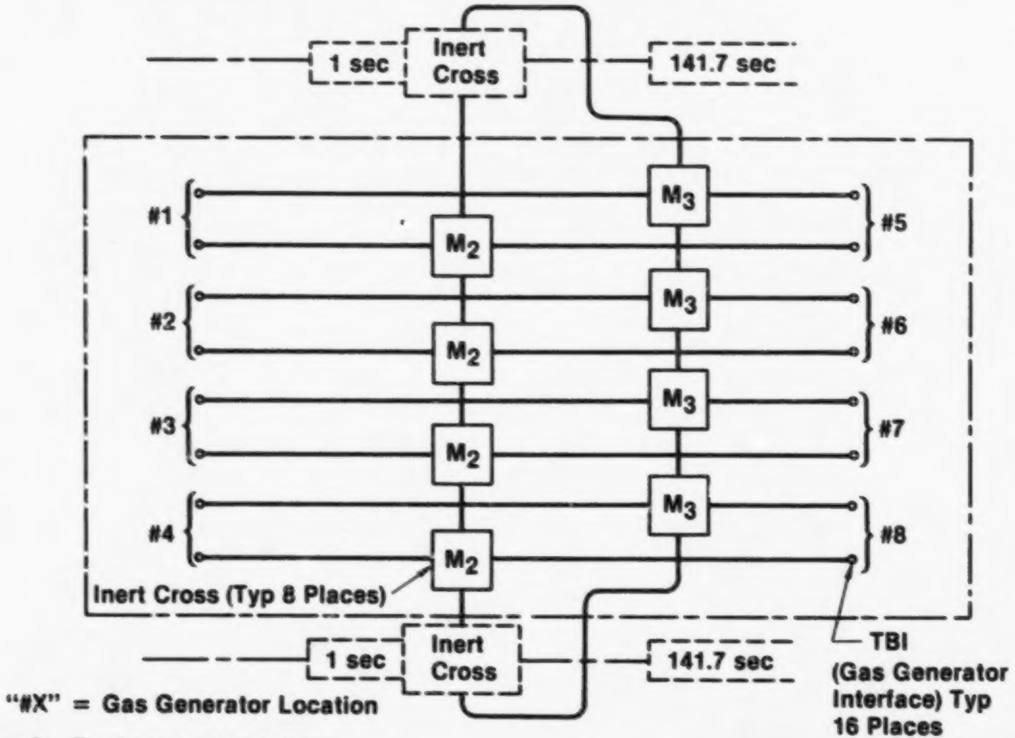
1 sec
Inert Cross
141.7 sec
#1
#2
#3
#4
#5
#6
#7
#8
M3
M2
Inert Cross (Typ 8 Places)
TBI (Gas Generator Interface) Typ 16 Places

"#X" = Gas Generator Location

Figure 1a. Gas Generator Manifolding

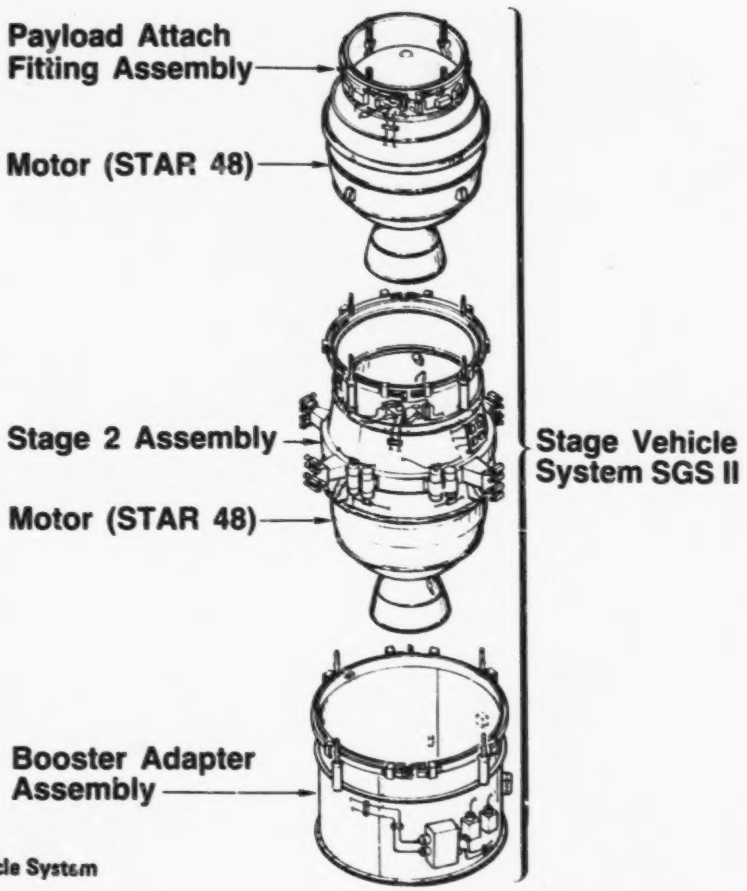
Payload Attach Fitting Assembly
Motor (STAR 48)
Stage 2 Assembly
Motor (STAR 48)
Booster Adapter Assembly
Stage Vehicle System SGS II

Figure 2. Stage Vehicle System

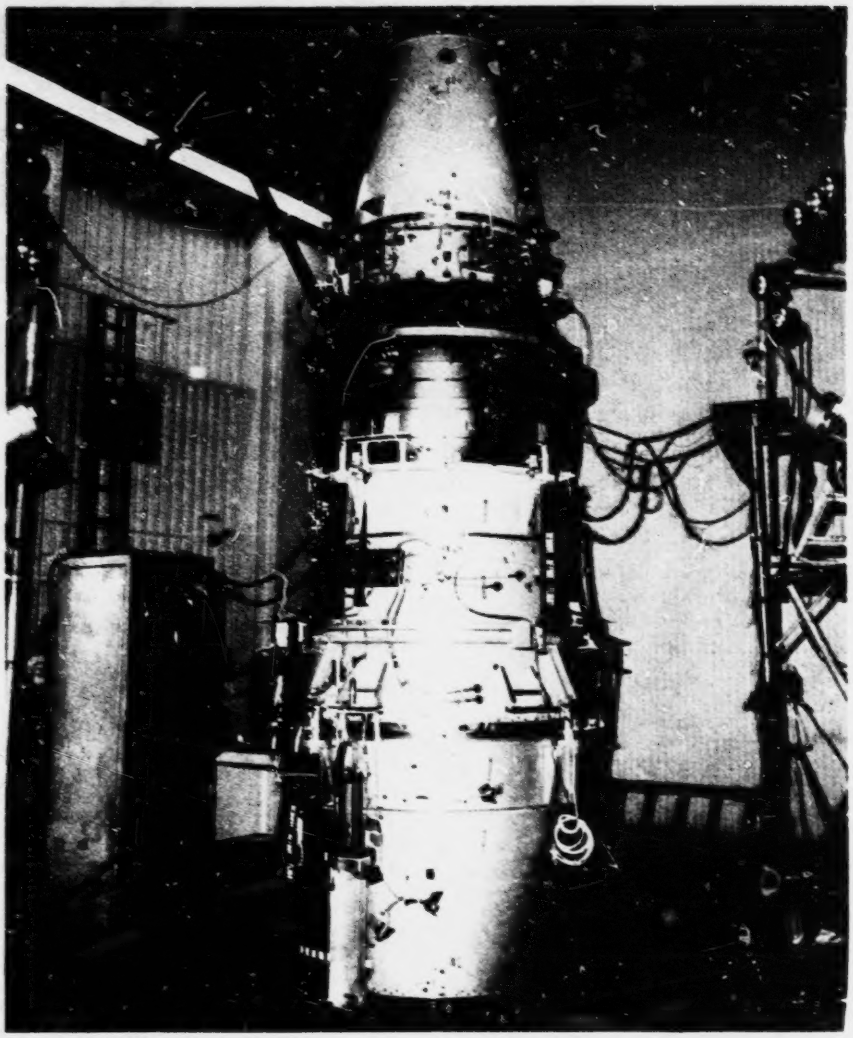

Figure 3. Stage Vehicle Systen

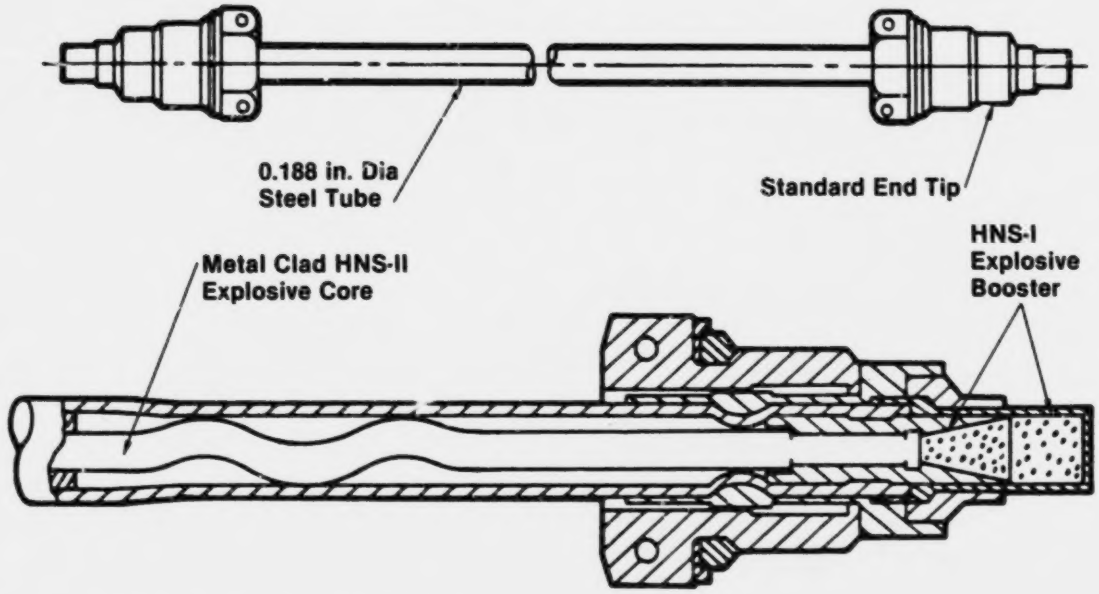
0.188 in. Dia
Steel Tube
Standard End Tip
Metal Clad HNS-II
Explosive Core
HNS-I
Explosive
Booster

Figure 4. Explosive Transfer Assembly (ETA) Line

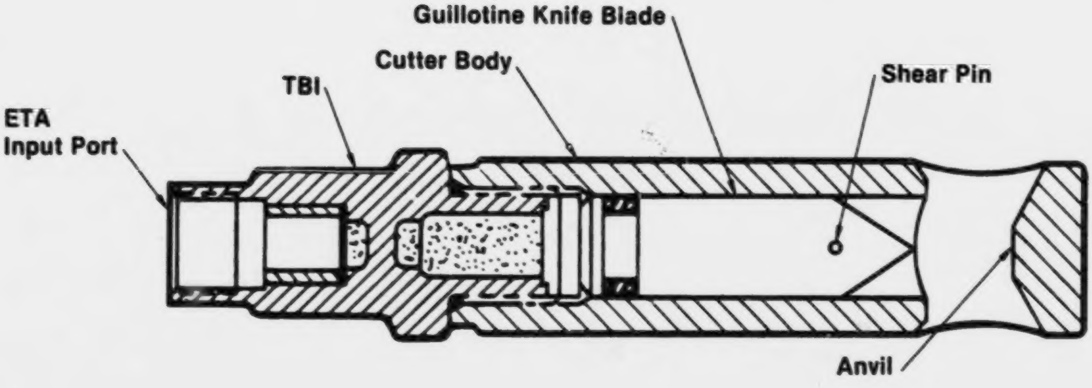
Guillotine Knife Blade
Cutter Body
TBI
Shear Pin
ETA
Input Port
Anvil

Figure 5. Through Bulkhead Initiator (TBI)/Bolt Cutter Cross Section

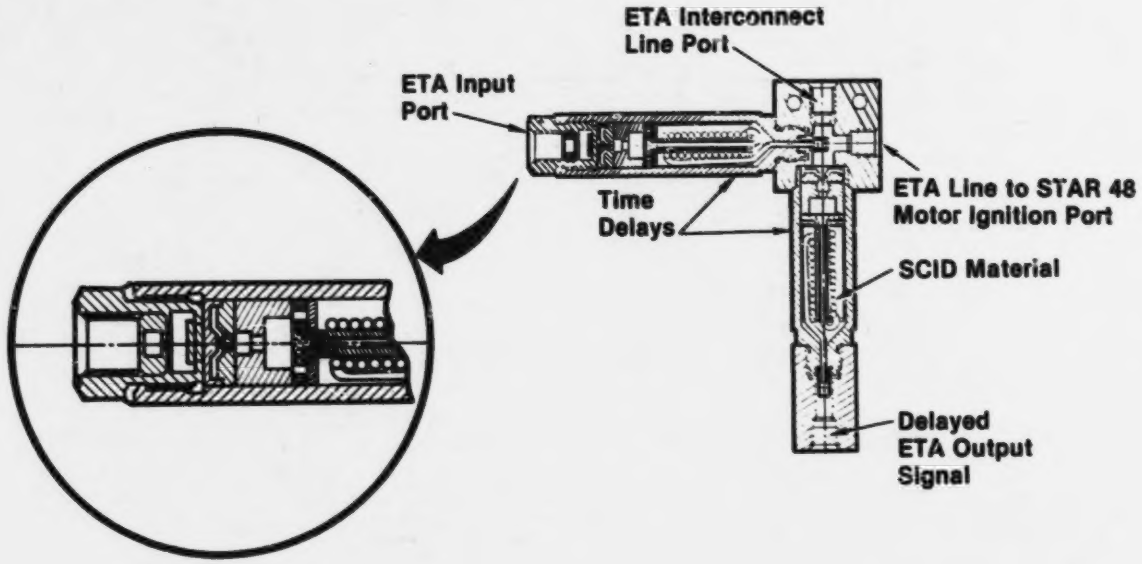
ETA Interconnect Line Port
ETA Input Port
ETA Line to STAR 48 Motor Ignition Port
Time Delays
SCID Material
Delayed ETA Output Signal

Figure 6. Pyrotechnic Time Delay Modules

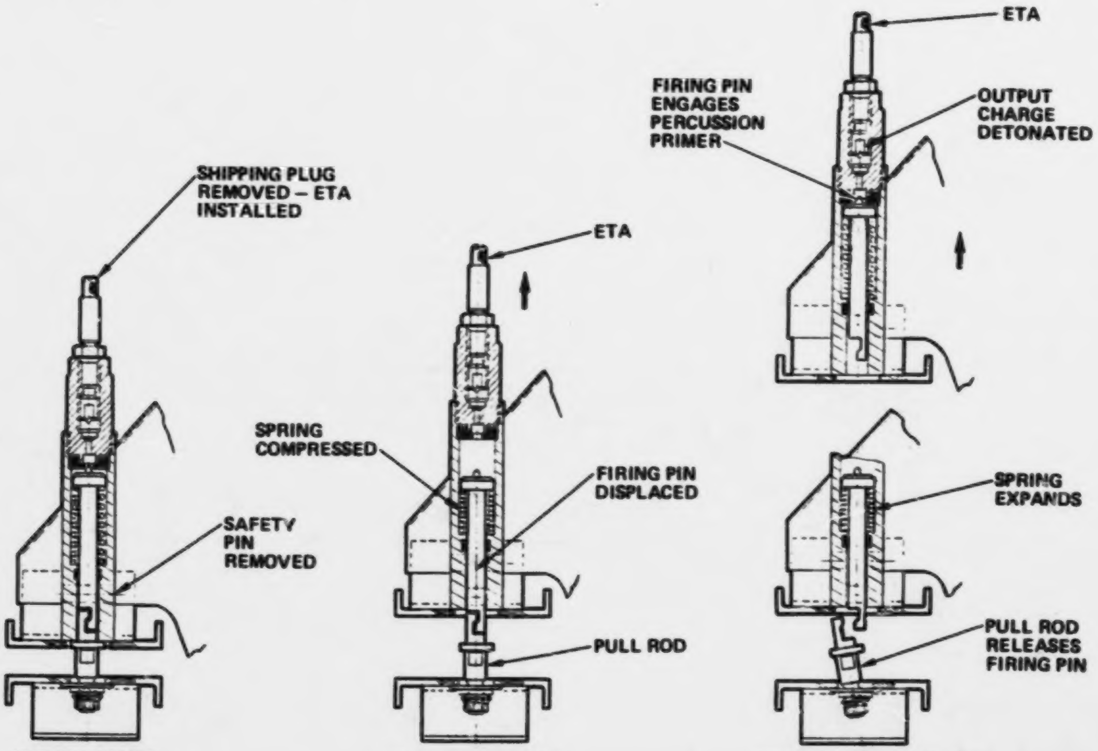
ETA
FIRING PIN ENGAGES PERCUSSION PRIMER
OUTPUT CHARGE DETONATED
SHIPPING PLUG REMOVED – ETA INSTALLED
ETA
SPRING COMPRESSED
FIRING PIN DISPLACED
SAFETY PIN REMOVED
SPRING EXPANDS
PULL ROD
PULL ROD RELEASES FIRING PIN

SYSTEM ARMED

STAGE SEPARATION

INITIATOR FUNCTIONS

Figure 7. SPIM Separation Sequence

Vincent R. Noel
McDonnell Douglas Astronautics Company
5301 Bolsa Avenue
Huntington Beach, California 92647

Mr. Noel is currently a senior engineer/scientist with McDonnell Douglas Astronautics Company. His experience includes that of being mechanical group engineer on the SGS-II program and principal designer of the event sequencing system. He has previously been the principal designer for the Delta launch vehicle 8-foot fairing separation system and the explosive system used to ignite and separate the Delta solid boosters. He participated in the design and testing of explosively actuated mechanisms and systems on several programs including the Gemini, Manned Orbiting Laboratory, and Spartan missile. Mr. Noel received his B.S. degree in Aeronautical Engineering from Northrup Institute of Technology in 1960 and has pursued additional studies at the University of California-Los Angeles.

Blank Page

DEVELOPMENT OF AN ULTRA-LOW-SHOCK SEPARATION NUT

William Woebkenberg*, Donald N. Matteo*, and Vaughn D. Williams**

ABSTRACT

This paper describes the technical problems encountered in the development of an advanced separation nut design which is capable of sustaining large preload and releasing that load with low level of induced pyrotechnic shock, while demonstrating a tolerance for extremely high shock imposed by other pyrotechnic devices.

INTRODUCTION

Separation nuts have been used by the aerospace community for over twenty (20) years to achieve remote, rapid and/or simultaneous disassembly of spacecraft and missile components. Separation nuts differ from so-called "frangible" nuts in that the latter depend on a detonation to structurally fail the nut and allow the stud to be released, while in separation nuts, no structural failure is required.

The typical separation nut utilizes a set of threaded collets to engage the threads of the attachment bolt. Those collets are held in position by the relative position of the internal parts of the nut. When separation is desired, the pyrotechnic charge is ignited and the gas thus generated is released into the working volume of the nut and acts upon piston surfaces to cause motion of the internal parts of the nut. This action releases the retaining feature of the collets and allows the separation bolt to be released. Figure 1 shows a standard separation nut before and after actuation.

Increasing sophistication of typical modern spacecraft has brought about the utilization of payloads/instruments which are increasingly sensitive to dynamic environments such as the shock induced by pyrotechnically actuated devices. Standard shock isolation techniques are, in many cases, not feasible due to functional constraints such as the required strength and stiffness of the load path from the separation nut mounting surface to the vehicle structure and precise alignment requirements between the sensitive instruments and vehicle structure. Accordingly, virtually the entire burden of limiting the shock level input to sensitive instruments has been placed on the source of shock, the separation nut.

---

*Space Systems Operations, General Electric Company
**Ad-Tech Division (Ordnance), Hi-Shear Corporation

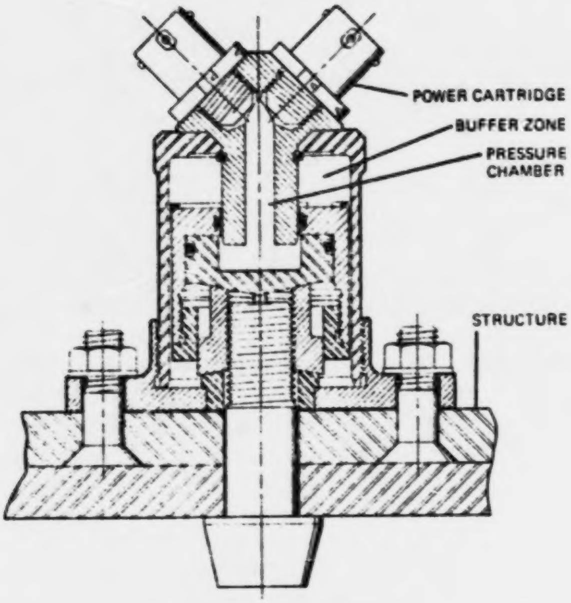
POWER CARTRIDGE
BUFFER ZONE
PRESSURE CHAMBER
STRUCTURE

BEFORE ACTUATION

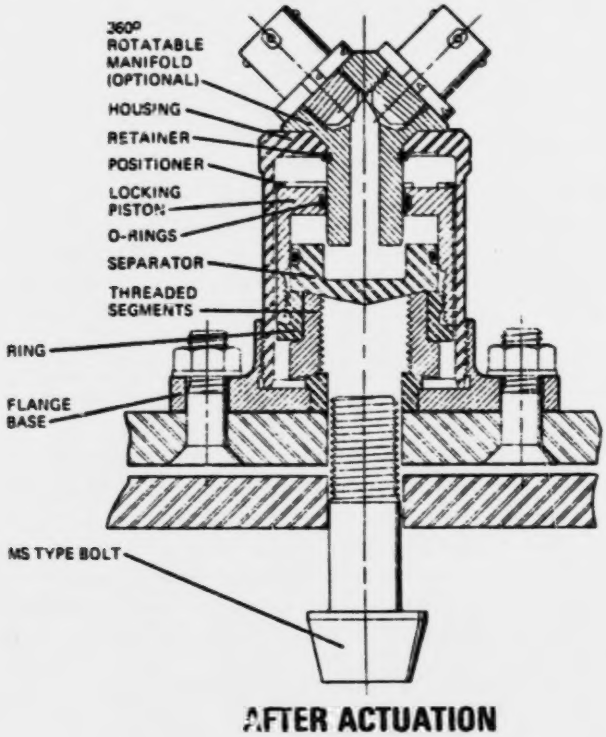
360° ROTATABLE MANIFOLD (OPTIONAL)
HOUSING
RETAINER
POSITIONER
LOCKING PISTON
O-RINGS
SEPARATOR
THREADED SEGMENTS
RING
FLANGE BASE
MS TYPE BOLT

AFTER ACTUATION

Figure 1. Standard Separation Nut

CONSTRAINTS

A combination of three (3) mutually conflicting requirements has placed the designer of pyro-actuated separation nuts in a rather tightly bounded situation. His design must perform satisfactorily within a requirements "triangle": bounded on one side by the requirement to reliably actuate under the worst combination of loads and environments (including the requirement to demonstrate margin by functioning with underloaded cartridges); bounded on the second side by the requirement to severely limit the pyro shock pulse induced by the device to levels more than an order of magnitude lower than those generated by previously produced devices (such as the separation nut of Figure 1); and bounded on the third side by the requirement that the device must not prematurely actuate at shock levels similar to those which it itself produces upon actuation.

DESIGN

One such device, designed to the mutually conflicting requirements of the above-mentioned triangle, is the separation nut developed by Hi-Shear Corporation for General Electric for use in satellite-to-satellite separation and in boost-vehicle separation on the Air Force's DSCS-III Communications Satellite.

Early in the development program, the Hi-Shear 9400 Series Standard low-shock separation nut was selected for DSCS-III Spacecraft separation function to retain and release a 1/2-inch bolt. The cartridge charge was sized such that the minimum output charge which would reliably actuate the nut (under worst-case temperature and preload conditions) was defined as the 80% output charge, and 100% charge was determined accordingly. This is due to the requirement that, during qualification, the nut must demonstrate release at maximum preload and worst-case temperature utilizing a single cartridge loaded to only 80% of nominal output charge.

As a schedule expedient, induced pyro shock testing was performed on a vehicle simulator using engineering separation nuts and cartridges to determine response at critical component locations. These test data defined the shock qualification requirements for critical components.

Subsequently, separation nuts and cartridges were fabricated and subjected to component qualification testing. A failure to release with single 80% output charge cartridge was incurred. Two approaches were available to cause release at specified conditions:

- Increase output charge of cartridge
- Cause separation nut to release at lower applied pressure

Because the component qualification shock environment for panel-mounted components had been established at the low energy level, additional output charge could not be added without providing for energy absorption in the separation nut itself. Therefore, effort was directed towards reducing required actuation pressure in the separation nut.

Actuation pressure was approximately 34.47 megapascals (5000 psi) in the as-produced separation nut. Some reduction in actuation pressure was realized by burnishing the dry film lubricant which is applied to segments, key seat and retainer ring. Burnishing was accomplished by cold gas release of the nut while at maximum preload. The retaining ring was undercut slightly to provide easier release.

An energy-absorbing honeycomb cushion was added to the base to reduce shock induced by impact of piston on the housing.

The segments were "slotted" at the retaining ring interface area to reduce area of contact and permit better compliance at that interface.

Figure 2 shows the separation nut configuration with changes incorporated.

The combination of changes reduced actuation pressure to approximately 3.45 - 4.83 megapascals (500-700 psi), and reduced the shock-generating capability of the nut.

Separation nuts were built to the modified configuration for component qualification testing. Again the separation nut failed. Mode of failure was inadvertent release in pyro shock environment, the second leg of the requirements triangle. Qualification test shock requirement was 2300 g at 1300 Hz.

All effort was now concentrated on construction of a dynamic model of the separation nut.

DESIGN ANALYSIS

An analysis of the separation nut was performed to acquire additional understanding of the phenomena affecting operation of the nut and to provide quantitative evaluation of design modification.

Physical evidence indicated that rotation of segments under preload may provide a component of the preload acting in a direction to "push" the retaining ring off the segments. Therefore, the separation nut was modelled to investigate segment rotation. Additionally, a theory that deflection of housing under shock load may permit contact between the housing and piston, causing the piston retaining ring to "walk" off the segment, was considered in the analysis.

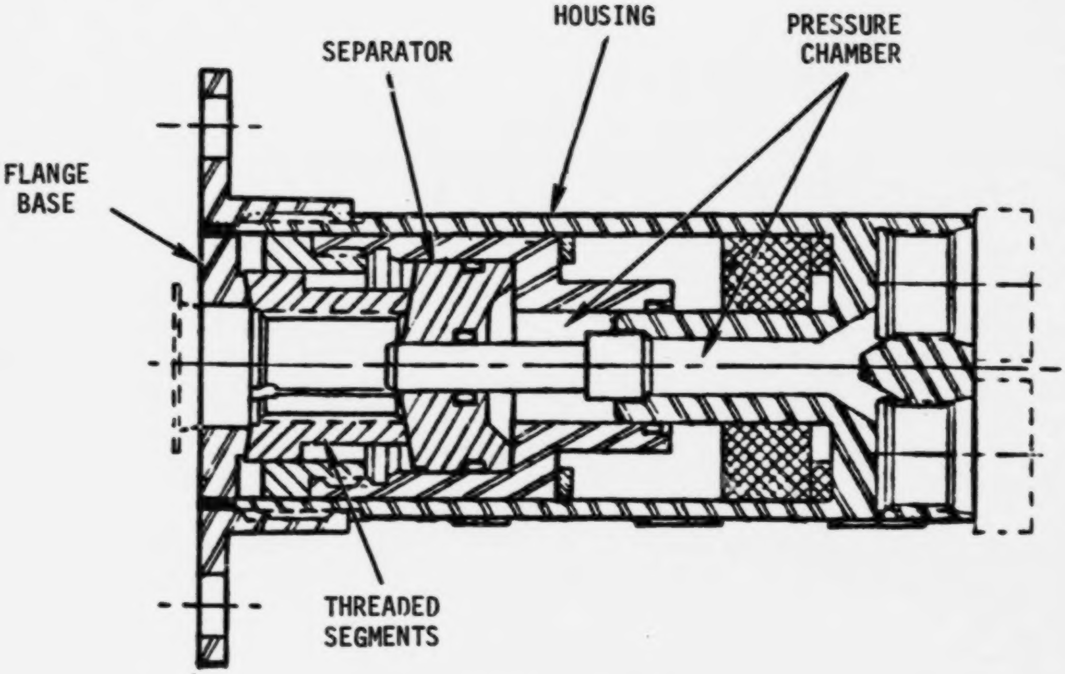
HOUSING
SEPARATOR
PRESSURE CHAMBER
FLANGE BASE
THREADED SEGMENTS

BEFORE ACTUATION

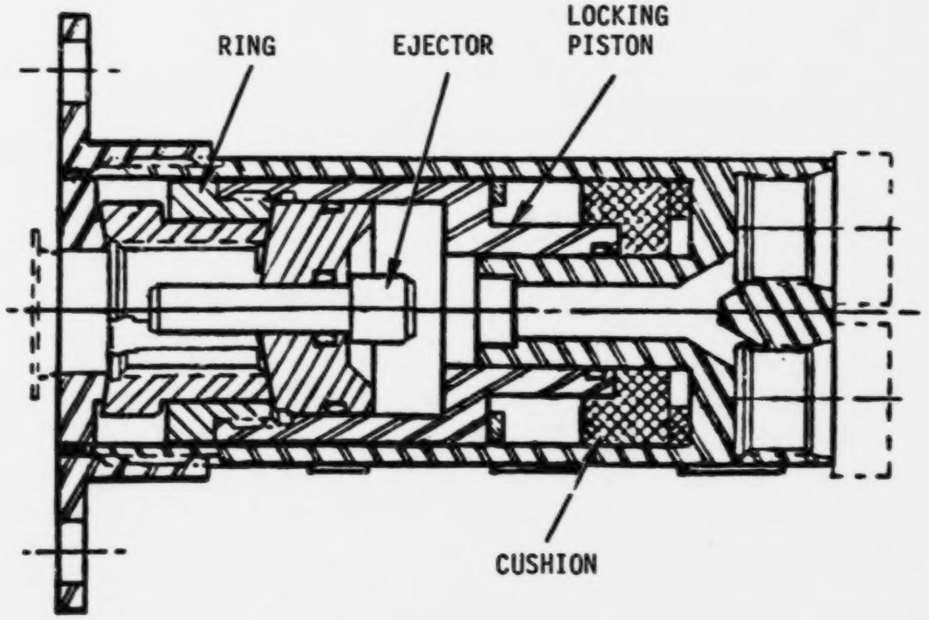
LOCKING PISTON
RING
EJECTOR
CUSHION

AFTER ACTUATION

Figure 2. Initial Separation Nut Design

The analysis used the NASTRAN finite element method. A 3-D model of the separation nut was required to account for the fact that the nut is segmented. Symmetry permitted modelling of only half of the nut. Careful selection of boundary conditions for the many elements of the nut was required since in normal functioning, parts slip with respect to one another.

Results of the analysis showed that the segments did indeed rotate under preload and predispose the nut to premature release. The analysis also confirmed that the retaining ring slips 0.025mm (.001 inches) when the top of the case moves laterally 0.229mm (.009 inches) as was measured in shock testing of the original design. A design fix, increasing the length of engagement between segments and retaining ring, was prepared. This was done by increasing the length of ring. The increased interface length stabilized the segments and inhibited rotation under load. Indeed measurements taken later in the program showed segment cocking of 0.19 degrees average compared to a predicted value of 0.18 degrees.

FINAL DESIGN

Increasing the length of interface between segments and ring increased pressure required to actuate the separation. Consequently, more output charge was required for reliable function. It was therefore necessary to absorb more energy within the separation nut to avoid increasing the baseline vehicle pyro shock environment which had been established early in the program.

The aluminum honeycomb energy absorber was redesigned for the nut case to perform two functions. The primary function was to limit shock induced by actuation of the nut. The second function was to bear against the piston in the assembled state to provide added insurance that the piston would not move during preloading and environmental exposure. Figure 3 shows the final configuration with extended honeycomb.

Engineering tests of this configuration in dynamic environments were successful. Engineering tests were also performed to verify that shock induced into the spacecraft by this design was within the program baseline. Again, the tests showed the design was good.

Figures 4 and 5 show comparative induced shock data at 2 vehicle locations for the standard low-shock separation nut and the ultra-low-shock separation nut. A new lot of hardware was procured and 27 separation nuts were subjected to qualification test environments including a shock test of 2300 g at 1300 Hz. Each unit was X-rayed after each dynamic environment.

There was no relative motion between segments and ring in any of the test units. All units survived environmental exposure and functioned normally.

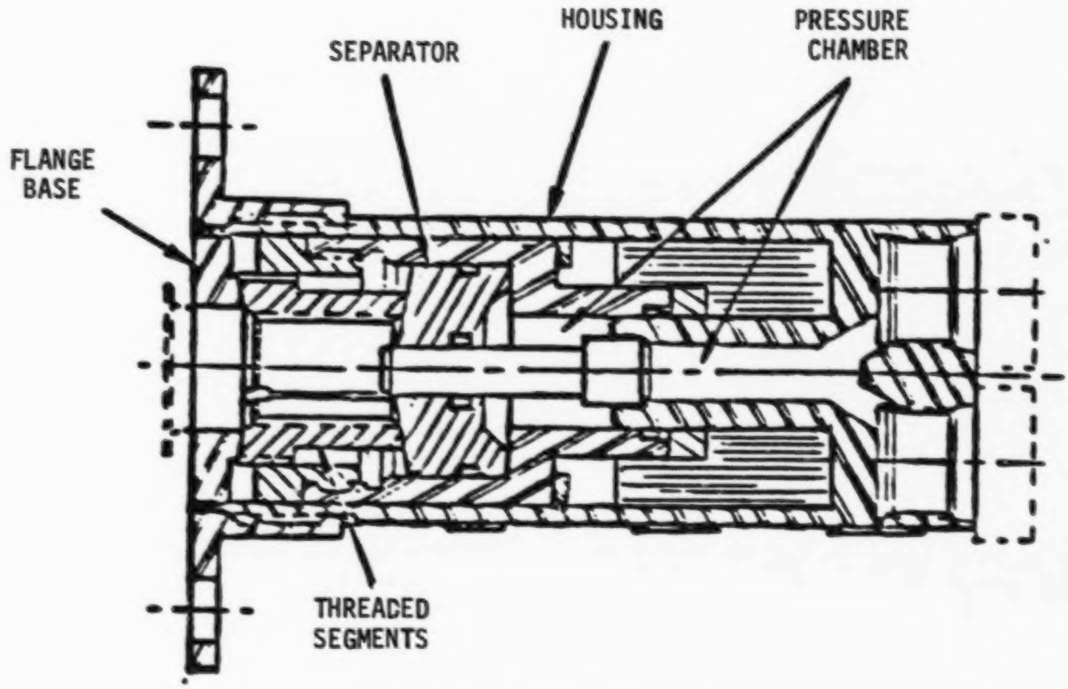
HOUSING
PRESSURE
CHAMBER
SEPARATOR
FLANGE
BASE
THREADED
SEGMENTS

BEFORE ACTUATION

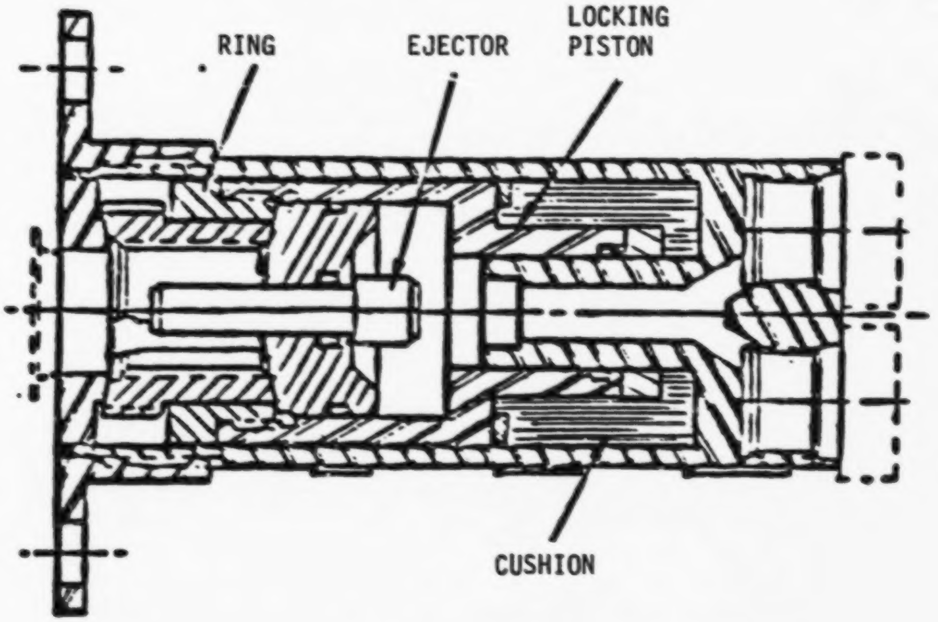
LOCKING
PISTON
RING
EJECTOR
CUSHION

AFTER ACTUATION

Figure 3. Final Separation Nut Design

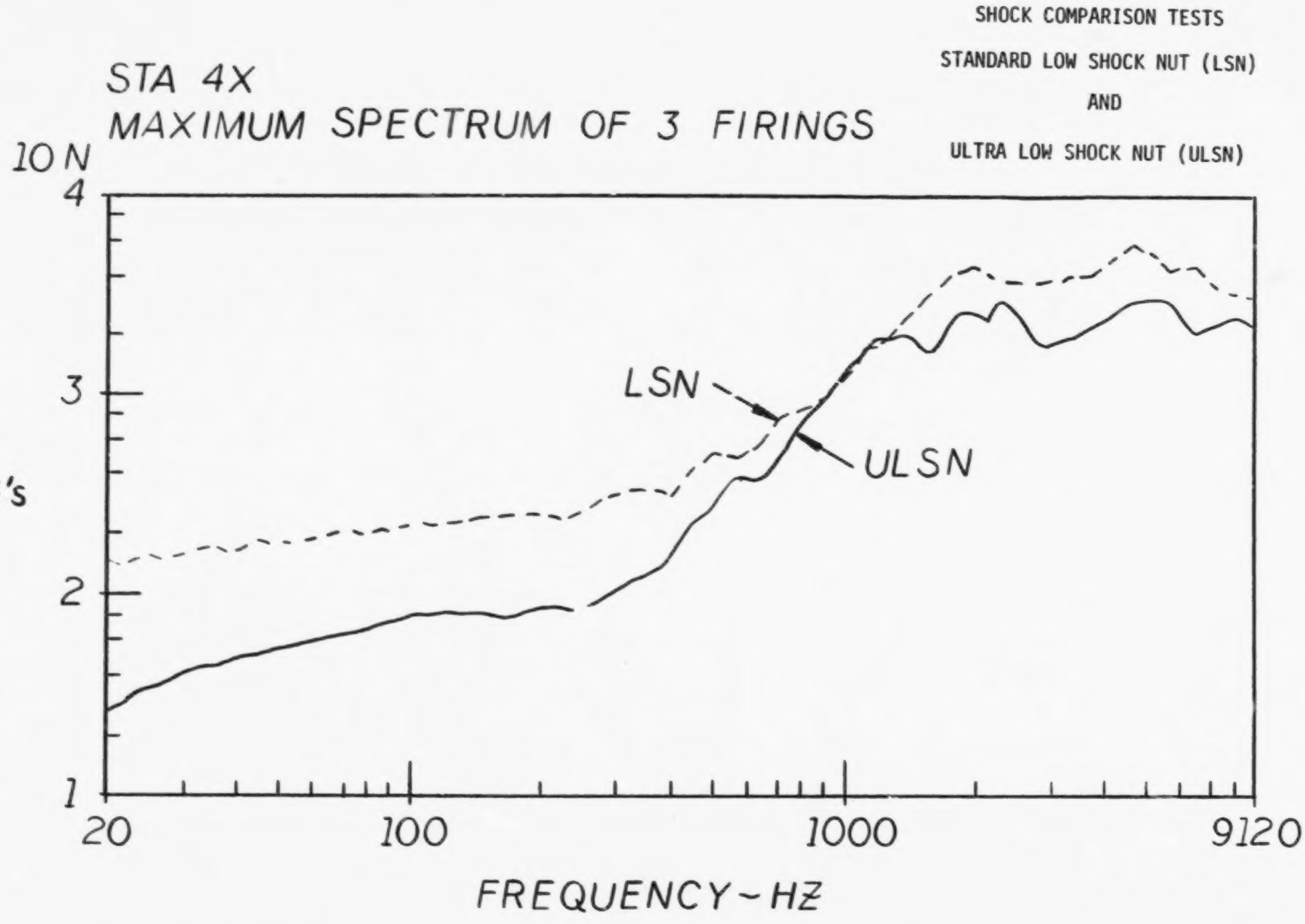

Figure 4. Station 4X Shock Comparison Tests

SHOCK COMPARISON TESTS

STANDARD LOW SHOCK NUT (LSN)

AND

ULTRA LOW SHOCK NUT (ULSN)

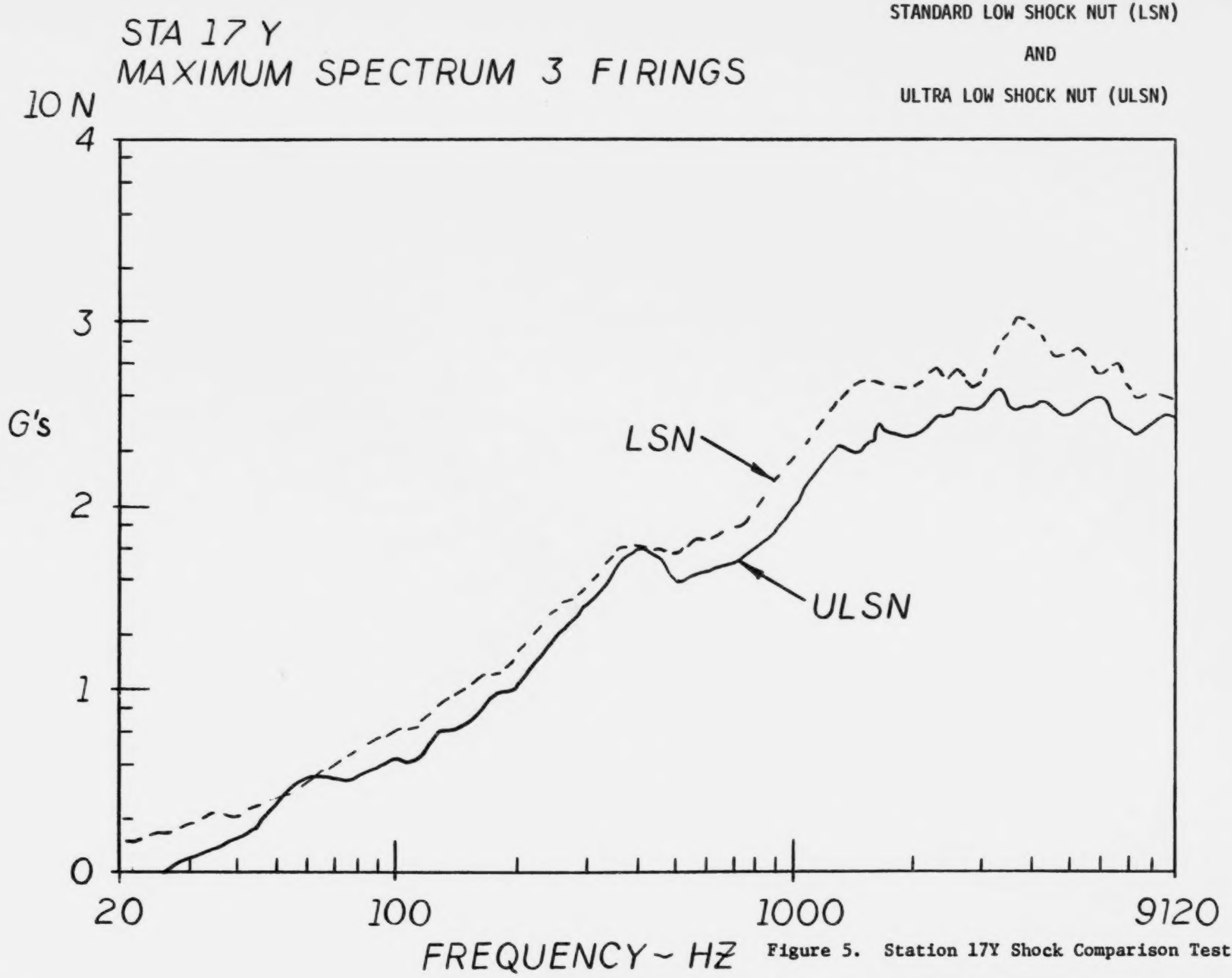

Figure 5. Station 17Y Shock Comparison Tests

VALIDATION OF DESIGN AT HIGHER SHOCK LEVEL

Subsequent to the qualification of the separation nut to the 2300-g environment, a new and much more severe shock environment of 4500 g peak, as defined in Figure 6, was identified for a second candidate booster combination. A new lot of hardware was prepared and tested to the increased environmental level. Qualification testing was completed successfully without problems.

ACKNOWLEDGEMENT

The authors thank Dr. E. R. Jones and Mr. R. D. Page of General Electric Company, Space Systems Division, for their support in creating the analytical model which pointed the way to resolution of the inadvertent release problem.

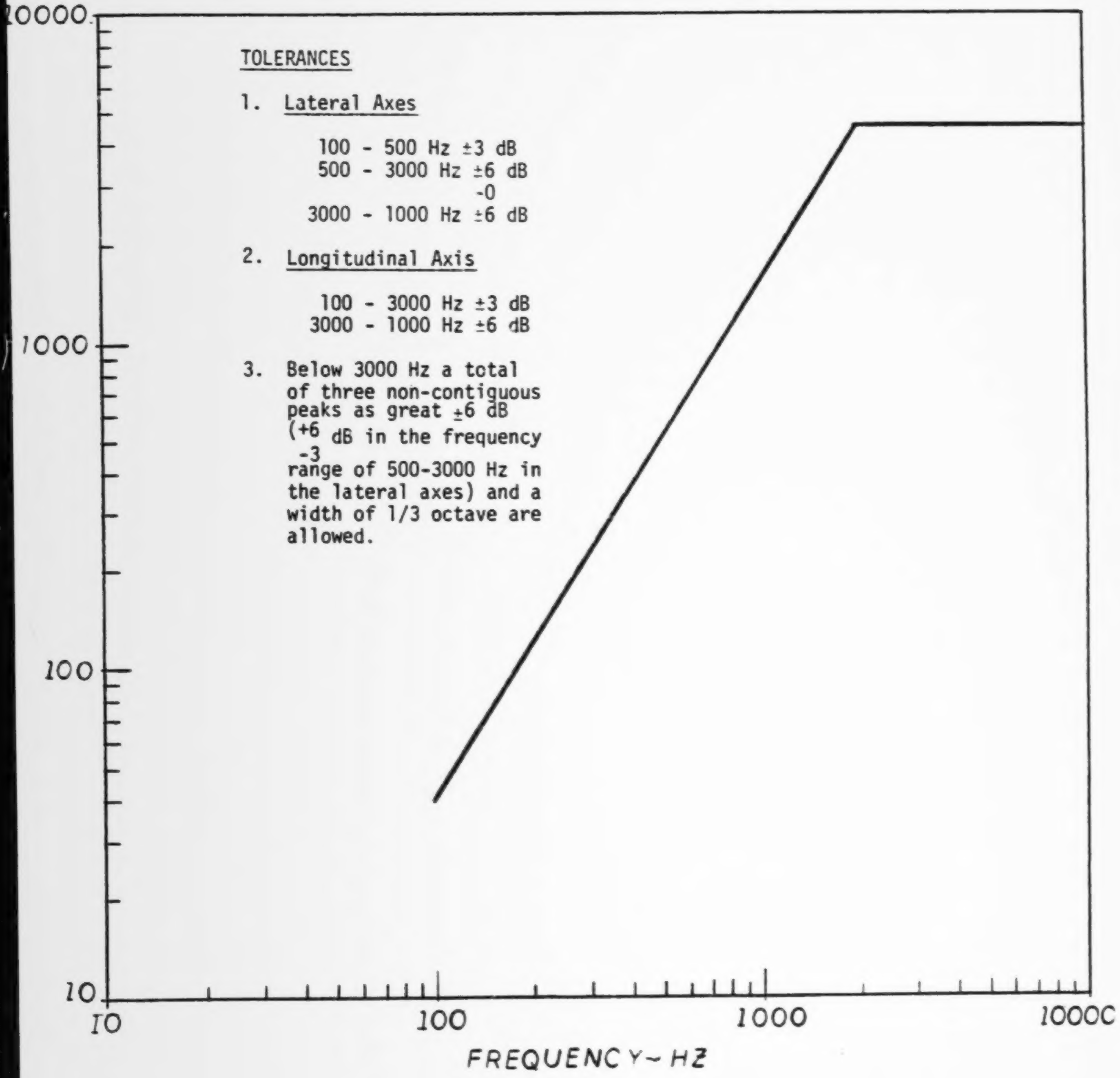

TOLERANCES

1. Lateral Axes

100 - 500 Hz ±3 dB
500 - 3000 Hz ±6 dB
-0
3000 - 1000 Hz ±6 dB

2. Longitudinal Axis

100 - 3000 Hz ±3 dB
3000 - 1000 Hz ±6 dB

3. Below 3000 Hz a total of three non-contiguous peaks as great ±6 dB (+6 dB in the frequency
-3
range of 500-3000 Hz in the lateral axes) and a width of 1/3 octave are allowed.

Figure 6. DSCS-III 1/2-in Separation Nut Shock Response Spectrum (Q = 10)

William Woebkenberg
General Electric Company
Space Systems Operation
P.O. Box 8555
Philadelphia, Pennsylvania 19101

Mr. Woebkenberg has 22 years' experience in the design, development, and test of aerospace components and subsystems, including satellite recovery systems, spacecraft separation subsystems, solar array drive mechanisms, and ordnance-actuated devices. He received his B.S. degree in Aeronautical Engineering from Purdue University in 1959.

Co-authors of this paper are Mr. Donald N. Matteo who is also with General Electric's Space Systems Operation in Philadelphia and Mr. Vaughn D. Williams who is with the Hi-Shear Corporation in Torrance, California.

A BALL TRUNNION CAPTURE LATCH

David V. Adams and Brendan Alchorn*

ABSTRACT

The Ball Trunnion Capture Latch, developed under a research and development program conducted by Lockheed Missiles and Space Company, was designed to restrain a spacecraft deployable appendage in three translational directions. The latch is capable of supporting an appendage during STS ascent and landing events and is capable of releasing and restowing an appendage distorted in three translational directions by thermal growth. This paper discusses requirements, design, analyses, and tests conducted on a development unit of the latch.

INTRODUCTION

The function of the Ball Trunnion Capture Latch is to restrain a spacecraft deployable appendage through ascent and landing conditions. The latch must also recapture and preload the appendage during on-orbit conditions, when relative thermal growth may occur between the deployable appendage and the spacecraft supporting structure. Since the latch is to be of general utility, it must be insensitive to thermal growth in three orthogonal translational directions. The latch must be tolerant of the spatial distortion of such an appendage, and it must overcome any loads associated with pulling a distorted appendage back into place. The latch consists of dual four-bar linkages which are actuated by a motor-driven ball screw. In the over-center position, one link, called the latch jaw, closes down on a ball (spherical) trunnion, locking it between two conical cups. The ball trunnion provides the interface between the latch and the deployable appendage.

REQUIREMENTS

The latch must be capable of withstanding a limit opening load of 44,500 N (10,000 lb) against the jaw when the latch is closed. This load includes any opening loads induced by side loads reacting against the conic slopes of the two capture cups. Additionally, the latch must supply a ball trunnion preload of 4,450 N (1,000 lb) to prevent rattle during typical acoustic conditions seen at launch.

---

*Lockheed Missiles and Space Company, Sunnyvale, California

The latch must also be capable of pulling a trunnion displaced 0.762 cm (0.3 in) in the direction of actuation against a load varying from 0 to 4,450 N (1,000 lb). This must be accomplished while the trunnion is also offset 0.254 cm (0.1 in) in both directions [0.359 cm (0.141 in) total] orthogonal to the direction of jaw travel, overcoming an orthogonal load varying from 0 to 9,900 N (2,000 lb, vector sum). The latch must be capable of a minimum on-orbit life of 3 years, and single-point failures (excluding structure) must be minimized. The latch must operate between temperature extremes of -34°C (-30°F) and +88°C (+190°F) under conditions ranging from 0- to 100-percent humidity. The envelope of the latch measures 45.7 cm by 22.9 cm by 11.4 cm (18 in by 9 in by 4.5 in). An acoustic vibration criterion of 16.7 GRMS was selected based on typical responses measured on components of this type during launch of Lockheed-built spacecraft.

DESIGN DESCRIPTION

A ball-end trunnion caught between two conical cups was chosen as the design solution. This design configuration permits capture and restraint of the trunnion in three translational directions, while it allows some relief from rotational loads (depending on friction). Figure 1 shows the latch in the over-center position. The latch jaw is shown closed down on the ball trunnion, locking it between the two conical cups. One conical cup is located on the latch jaw while the other cup is fixed rigidly to the latch structure. A half-cone angle of 45° was selected for both cups, based on a trade-off between lock-down capability and capture capability. A narrower cone would have reduced the vertical reaction on the jaw but would have increased the distance required for jaw travel. The peak load on the ball screw actuator would have increased because loading would have begun when the mechanical advantage was lower. A shallow half-cone angle would have required higher jaw vertical loads to pull the trunnion into place.

Preload is achieved by placing a shim under the fixed cup. Motive power is supplied to the ball screw through a 1:2 speed-increasing gear train from redundant motors driving through a planetary differential into a common output shaft.

The link pivots and the ball screw supports are redundant. Each joint consists of a pin surrounded by a bushing which is free to rotate on either its inner or outer surface. The latch is shown in the fully open position in Figure 2.

ANALYSIS OF LATCH

Analysis of the latch was conducted in two phases: analysis of ascent loads sustained when the latch is closed and analysis of loads occurring during latch closure.

Ascent loads were treated as a static loading case, since the latch is closed over the ball trunnion and its internal dynamic reactions are insignificant. An analytical model of the capture cups predicts that the latch jaw takes loads only in the direction of its travel (+Y direction at closure). This is due to the fact that the jaw stiffness in the plane orthogonal to the direction of jaw travel (the X-Z plane) is low compared to that of the fixed capture cup. Further analysis shows that this assumption is conservative, since it results in calculating higher jaw vertical loads. The results of these analyses forced a change in the design of the latch. It was determined that pin diameters at each of the joints would have to be increased to accommodate the 44,500-N (10,000-lb) opening load.

An analytical model simulating operational performance of the latch was developed to verify latch closure in the presence of deployable appendage thermal growth. The model simulates latch kinematics, stiffness of the linkages and support structure, bearing friction, and ball trunnion/latch jaw pull-in forces. Dynamic forces were neglected, since actuation speed is low.

The kinematic relationship of the latch linkages is shown in Figure 3. A motor-driven ball screw, represented as link DE, actuates the four-bar linkage consisting of ground link AB, jaw BC, compression link CD, and tension link AD. At the full extension of DE, the jaw angle A6 is 0° and links AD and CD align with the Y (vertical) axis. This is the over-center, or closed, position of the latch.

Figure 4 shows how the stiffnesses of the various linkages, including the support structure, are modeled. Links AD, CD, and DE are considered simple extensional springs. Structural stiffnesses at joints A and B are considered decoupled for simplicity. Joint E, which is the ball screw support, is treated as an eccentrically loaded cantilever beam. Flexibility at E is represented by the two-dimensional flexibility matrix $[f_E]$. Latch jaw stiffness is computed by assuming it to be a simply supported beam with an overhanging load. For each spring shown in Figure 4, an effective stiffness is computed at the jaw based on the kinematic relationship between a unit spring displacement and the corresponding jaw displacement. By the principle of conservation of energy, unit strain energy in each link is equated to unit strain energy of an effective spring located at the jaw. An incremental change in length is computed for each spring due to the unit strain energy. This change in length causes a corresponding change in the position of the jaw. The jaw displacement is considered to be the displacement of an effective spring located at the jaw. Knowing strain energy and effective jaw spring displacement allows the calculation of an effective stiffness (transferred to the jaw) for each element. The effective stiffnesses of all the elements are then added in series to determine the total effective jaw stiffness. The total effective jaw stiffness changes with the geometry of the mechanism. Figure 5 shows the plot of jaw stiffness vs. jaw open angle (0° is the closed position).

If the effective stiffness of the jaw is known, then the position of the ball trunnion during pull-in can be calculated, based on the equations of static equilibrium. The simulation of ball trunnion/latch jaw pull-in forces assumes a rigidly fixed capture cup, a jaw with a finite stiffness in the horizontal (X-Z) plane, and a contact angle (based on the slopes of the capture cups) of 45°. For simplicity, we also assume that the trajectory of the ball trunnion projected onto the horizontal (X-Z) plane would consist of straight lines.

Forces and reactions in the latch linkages are then calculated based on the latch jaw load. Torque losses are computed for each joint due to an incremental change in position. The torque losses are considered work done by the ball screw during an incremental change in length. Since work done by the ball screw is equal to force time displacement, and the displacement and the work done are known, then an added force on the ball screw due to friction is computed for each joint. The various friction losses are then summed to obtain a total force on the ball screw force due only to friction. Frictional forces are then added to the ball screw for screw force assuming no joint friction to obtain the total ball screw force. Total ball screw force is shown vs. ball screw extension for a 13,350-N (3,000-lb) preload case in Figure 6, along with test data collected for this case.

It was thought desirable to check the results of the analytical model internally. To do this, an algorithm was added which compares the work done by the ball screw to work done on the latch in the form of friction, strain energy stored in the compliance of the latch, and work done to pull the trunnion into place. This algorithm helped to point out errors in both the coding and the synthesis of the model. Calculations of work done by the ball screw vs. work done on the latch typically differ by less than 1 percent.

DEVELOPMENT TESTS

A development unit of the latch was subjected to tests in order to verify capture, preload, and release capabilities of the latch and to validate the latch analytical model. A total of 10 tests were conducted on the development unit. The tests conducted fall into three general categories: compliance tests, tests of latch operational performance, and vibration sensitivity tests.

Compliance tests were performed in order to calibrate the jaw vertical load, measure the effective jaw stiffness, and determine the flexibility of the ball screw support structure. Calibration was accomplished by placing strain gages on either side of the tension and compression links and then pulling up with a known force on a ball fixture locked in the latch. Link bending due to friction torque required that the strain gages be wired in a moment-compensating circuit. This was an early indication of the significance of joint friction. This test allowed the determination of vertical jaw load in subsequent tests. Effective stiffness at the jaw was measured by inserting shims of various thicknesses under the fixed cup and recording variations in jaw vertical load. The results showed an effective stiffness of 8,400 N/cm (48,000 lb/in), which contrasts with an expected value of about 350,000 N/cm (200,000 lb/in). The difference between the two values can be attributed to bending and shearing of the linkage pins, phenomena which were not considered in the initial analysis. Later versions of the latch will feature larger diameter pins to accommodate ascent conditions and therefore should have higher effective stiffnesses. Pin stiffnesses were incorporated into the analytical model by merely adding them in series to the stiffness of the existing spring elements in the input of the model.

Two preload tests were conducted by closing the latch over a loose ball fixture resting in the fixed capture cup. The preload tests were conducted to determine the effect of joint friction without cup friction. Cup friction was eliminated, since the ball fixture did not move. Shims were placed under the fixed cup to obtain preloads of 6,230 N and 13,350 N (1,400 lb and 3,000 lb) and the latch was then closed and opened while recordings were taken of ball screw extension and required input torque. These tests indicated that joint friction approximately doubled the peak required drive-unit torque. The tests also verified the simulation of joint friction torque in the analytical model.

The Z direction pull-in test was conducted in order to determine the ability of the latch to capture, pull in, and release a ball fixture offset to the side of the latch. In this test, a ball fixture was attached to the end of a long threaded rod with a known axial stiffness (Figure 7). The threads on the rod allowed for position adjustment of the ball. The surfaces of the capture cups and the ball fixture were coated with solid-film lubrication prior to the test. The ball was positioned to rest on the near side of the fixed cup if not loaded. The latch was then closed, pulling the ball down into the cup. Tensile force developed in the rod was indicated by a load cell. Deflections of the ball, the jaw, and the fixed cup were recorded along with ball screw input torque, ball fixture axial force, and jaw vertical load for various ball screw extensions. Latch capabilities of capture, closure, and release were demonstrated. This test yielded information that verified the simulation of cup friction and side-direction stiffness of the jaw. The test also indicated that side forces on the jaw cause rubbing to occur at the side of the jaw, thus reducing the efficiency of the mechanism. This problem can be alleviated by treating the rubbing surfaces with solid-film lubrication.

The X and Y direction pull-in test was performed in order to determine the capability of the latch to capture, pull in, and release a ball fixture which was offset above (vertically) and forward (horizontally) of the fixed capture cup. The setup was similar to that used in the Z pull-in test, except that the ball fixture was not attached directly to either threaded rod. Instead, the ball was centered on a short rod which was supported at both ends by two U-shaped brackets (Figure 8). The brackets were attached to the threaded rods. As the latch was closed, the ball was pulled in simultaneously in both the X and Y directions. Again, latch capabilities for capturing, pulling in, and releasing a ball trunnion were verified. Data gathered in previous tests allowed the analytical model to simulate this test with fair accuracy.

The final test was a measurement of latch sensitivity to vibration. A free-floating trunnion ball was clamped into the latch so that a preload of 4,450 N (1,000 lb) was developed. The latch was then vibrated along three translational axes to determine the capability of the latch to remain closed and maintain its preload in the presence of vibration. The latch was subjected to sine sweep and random vibration levels of 16.7 GRMS, thus simulating conditions that might be seen during a typical launch. The latch remained closed. Typical landing conditions (with thermally induced loads orthogonal to the direction of jaw actuation) were not simulated, due to the complexity of the required test setup. Response of the latch was termed low (Reference 1). Preload capability was verified by subsequently releasing the ball fixture and then reclosing the latch while taking strain gage measurements.

CONCLUSIONS

A capture latch capable of restraining, releasing, and recapturing a spacecraft deployable appendage in three translational directions was developed by Lockheed Space Systems Division. Performance of the latch and a computer simulation of latch operation were verified by tests conducted on a development unit. Bending stiffness of the joint-connecting pins was found to have significant effect on overall latch stiffness; however, larger pins necessitated by the static opening load of 44,500 N (10,000 lb) will alleviate this condition. The latch is currently under consideration for use on several LMSC payloads.

ACKNOWLEDGMENTS

We wish to acknowledge the efforts of Jim Larson for his work on the initial design of the latch, Joe Wilson for his contribution to the stiffness portion of the analytical model, and Ken Buckley for his supervision in the development of the latch design.

REFERENCES

1. LMSC Test Report No. TA B152, "Test Report for the Capture Latch Development Test," September 16, 1981.

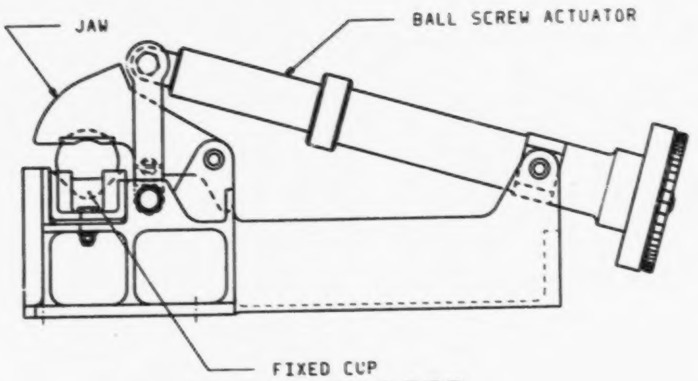
JAW
BALL SCREW ACTUATOR
FIXED CUP

CLAMP CLOSED

FIGURE 1

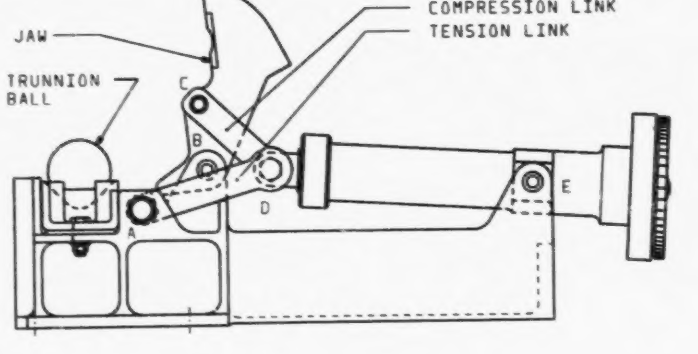
COMPRESSION LINK
TENSION LINK
JAW
TRUNNION BALL
C
B
A
D
E

CLAMP OPEN

FIGURE 2

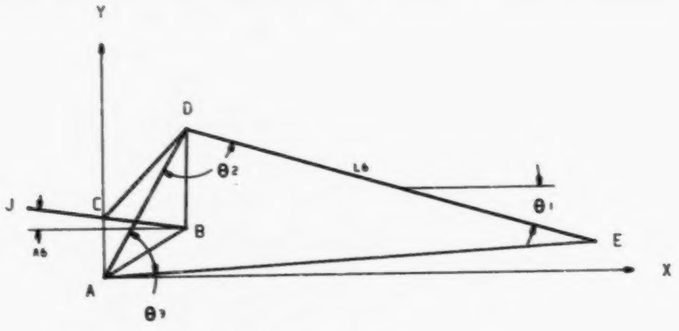
Y
D
θ2
L6
θ1
J
C
B
E
A6
A
X
θ3

LATCH KINEMATICS

FIGURE 3

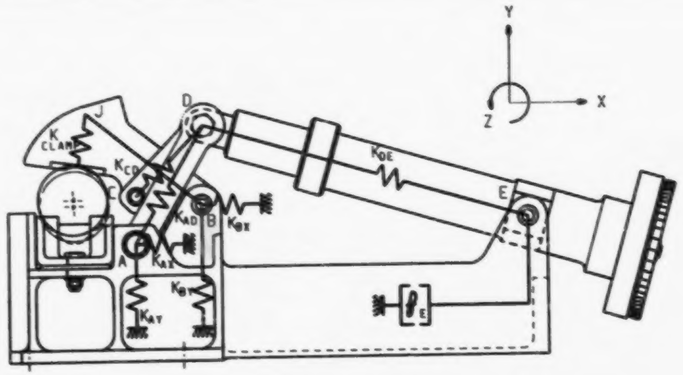
Y
X
Z
D
J
K CLAMP
K_CD
C
K_AD
B
K_BX
K_DE
E
A
K_AX
K_AY
K_BY
θ_E

LATCH STIFFNESS MODEL

FIGURE 4

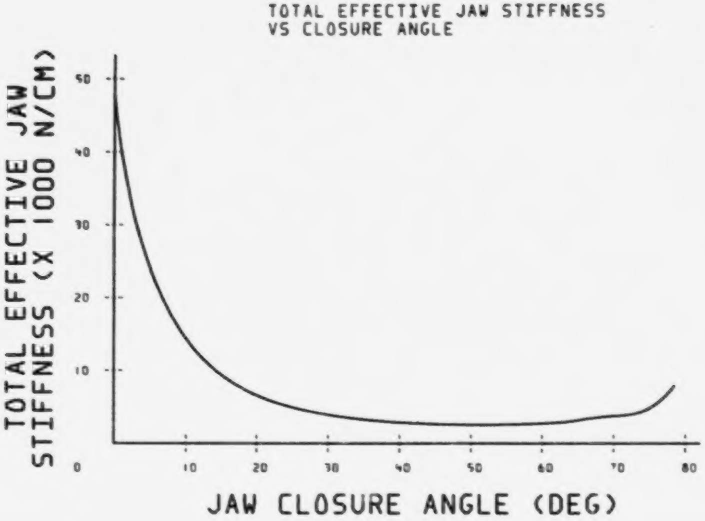
TOTAL EFFECTIVE JAW STIFFNESS
VS CLOSURE ANGLE

FIGURE 5

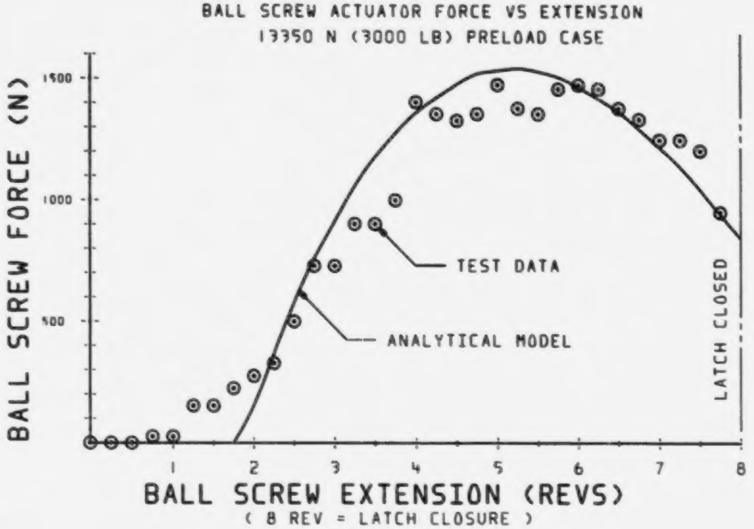
BALL SCREW ACTUATOR FORCE VS EXTENSION
13350 N (3000 LB) PRELOAD CASE

FIGURE 6

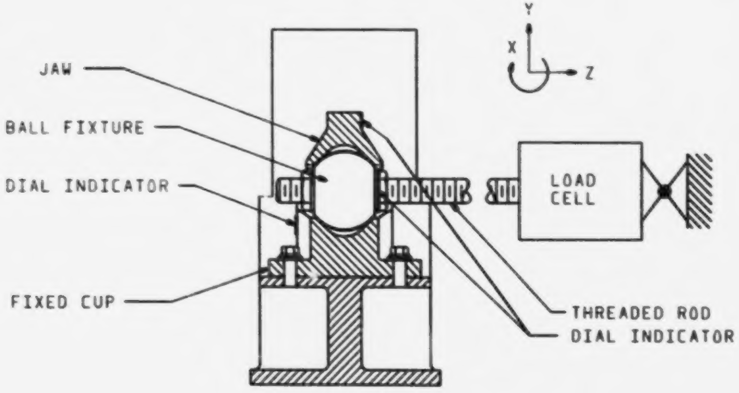
Y
X
Z
JAW
BALL FIXTURE
DIAL INDICATOR
FIXED CUP
LOAD CELL
THREADED ROD
DIAL INDICATOR

Z PULL-IN TEST SET-UP

FIGURE 7

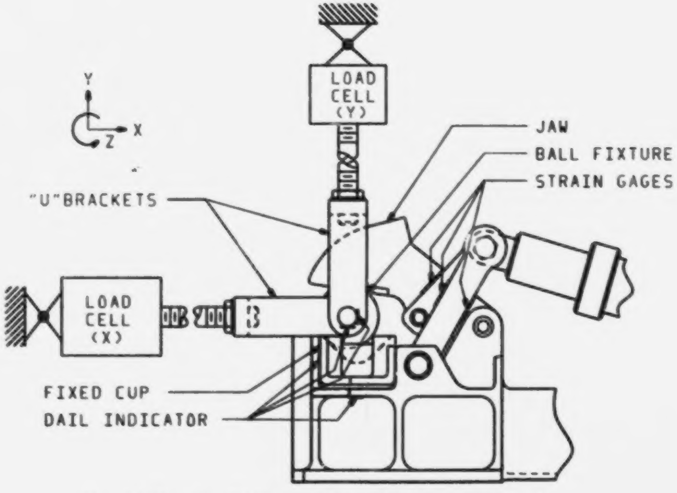
Y
Z
X
LOAD CELL (Y)
JAW
BALL FIXTURE
STRAIN GAGES
"U"BRACKETS
LOAD CELL (X)
FIXED CUP
DAIL INDICATOR

X AND Y PULL-IN TEST SET-UP

FIGURE 8

David V. Adams
Lockheed Missiles and Space Company
P.O. Box 504
Sunnyvale, California 94086

Mr. Adams is an engineering analyst for the Mechanisms and Separation Analysis Group at Lockheed. He received his B.S. degree in General Engineering from the University of Illinois in 1980.

Co-author of this paper is Mr. Brendan Alchorn who is also with Lockheed Missiles and Space Company at Sunnyvale.

Blank Page

A MOVABLE STOP MECHANISM
FOR THE
SIRE TELESCOPE

R. E. Tweedt and R. N. Poulsen
Hughes Aircraft Company

ABSTRACT

The purpose of the movable stop mechanism (MSM) is to activate flaps that change the size and shape of the telescope aperture stop on command. Operating at the cryogenic temperatures of the optical system, it consists primarily of a rotary solenoid that drives (activates) dual four-bar linkages in synchronism that in turn rotate the butterfly flaps into position. This paper discusses the design, performance characteristics, and test of this mechanism. Specific problems that occurred during test and the solutions that were adopted are also described.

INTRODUCTION

The primary objective of the Space Infrared Experiment (SIRE) Program is to develop an infrared sensor system that can make a variety of star and space target measurements from space in several different spectral wavelength regions. During the course of this program, a requirement was added for a dual aperture stop configuration.

Figure 1a indicates the shape and size of the aperture stop during normal operation. The required alternate aperture stop configuration is shown in Figure 1b.

Hence the ability to change the stop from one configuration to the other is the general requirement for this mechanism. The movable stop mechanism (MSM) is pictured in its test fixture in Figures 2 and 3. Figure 2 shows the aperture stop with the flaps closed, and Figure 3 shows the drive solenoid that activates the flaps.

DESIGN REQUIREMENTS

The principal design requirements for the MSM are listed in Table 1. The unique configuration restrictions and cryogenic optics application are the factors that govern these requirements.

TABLE 1 - DESIGN REQUIREMENTS

- Operating temperature: 15° to 25°K
- Power dissipation: ≤200 mW to close aperture stop and to keep it closed
- Power dissipation in open position: ≤10 mW
- Hold in closed position for at least five minutes
- Fail-safe in open position
- Life: 5000 cycles minimum
- Switches to indicate end-point positions
- Time to actuate: ≤1 second
- Noncontamination of cryogenic optics in vacuum
- Compatible with present telescope hardware

DESCRIPTION OF MECHANISM

In the final design of the MSM, shown in Figure 4, the aperture stop and its actuating arm support bracket are made of beryllium. The arm, connecting links, link pins, and flap shafts are made of A-286 steel. The stop flaps are made of 6061 aluminum. The diameters of the journal-type bearing areas of the flap shafts and of the actuating arm shafts are sized to provide 0.015/0.025 mm (0.0006/0.0010 inch) of clearance in the respective mating pivot holes. The link pins are sized to provide 0.010/0.020 mm (0.0004/0.0008 inch) of diametral clearance in the respective mating pivot holes.

It was necessary to make several different-length configurations of the actuating arm and the No. 2 connecting link in length increments of 0.025 mm (0.001 inch) in order to be able to select parts at assembly to ensure symmetrical flap clearances in both the open and the closed positions. Adjustable stop screws are used to set the open and closed positions of the flaps.

The drive shaft connecting the solenoid output shaft to the actuating arm is made of A-286 steel and is designed to float axially in order to accommodate differential thermal expansion. The drive shaft also accommodates slight positional mislocations between the solenoid and the actuating arm.

Although the MSM is to operate in a zero-gravity environment, 1-g loading of contacting link and actuating arm surfaces can occur during ground tests because of the vertical orientation of the unit. To prevent the creation of excessive friction loads during test and during ground operation, Teflon washers are installed as shown in Figure 5.

The solenoid ball bearings and all shafts, link pins, stop flap shims, and pivot holes are coated with 99-percent-pure commercial lead lubricant, ion plated to a thickness of 2000/3000 Å. This lubricant was chosen because of its ability to meet the requirements imposed by operation in space at cryogenic temperature, low friction, and minimum contaminant generation.

The rotary solenoid is shown in Figure 6. The solenoid rotor is mounted on ball bearings in a titanium housing. The radial air gap between the rotor and pole pieces is 0.23/0.30 mm (0.009/0.012 inch). Each of the two pole pieces is wound with 1800 turns of 40-gauge magnet wire. Magnetic detent stops on the pole pieces reduce the air gap to zero at the closed position and thereby allow a reduction in the holding current needed. Redundant torsional springs made of beryllium-copper alloy are installed with an adjustable anchor post at the fixed end to permit the spring output torque to be accurately set. Reed switches indicate position, and in the closed position, the switch causes the actuating current (0.170 ampere) to be reduced to a holding current of 0.050/0.060 ampere. Reed switches housed in glass-filled polycarbonate resin were designed and built for this cryogenic application. A samarium-cobalt magnet attached to the rotor actuates these switches.

PERFORMANCE CHARACTERISTICS

The measured performance characteristics of the MSM are shown in Figures 7 and 8.

Figure 7 is a plot of the measured activating torque delivered by the rotary solenoid versus angle as a function of the current in the solenoid coils. The solenoid is driven by a constant-current power supply that delivers a minimum current of 170 mA. The solenoid pole piece with a zero magnetic air gap in the actuated (closed) position allows a 66-percent reduction in the current needed to maintain closure. The closed position reed switch triggers this reduction in current.

Figure 8 is a plot of the measured torque needed to activate the MSM as a function of angle. The torque needed to overcome friction is approximately constant (15 gram-cm). Redundant return springs have been incorporated to ensure reliability. The spring design criteria were that the rotary solenoid should have a torque margin of 1.0 in order to close the stop when both springs were active; a margin of 1.0 to open the stop when one spring is inactive (broken) was also required. These requirements entailed a delicate balance that required spring adjustments during assembly and test.

TESTING

The test plan originally adopted for the MSM provided for a 5000-cycle life test of an engineering model in a test dewar at a pressure of less than 10^{-4} Torr and at a temperature of less than 25°K. The test equipment provided for automatic cycling to close the movable stop, to maintain this position for 3 seconds, and to then release the stop to the open position for 1.5 seconds. The use of a manual override made it possible to keep the stop in the closed position for extended periods. At regular intervals during the test, the minimum actuating and minimum holding currents as well as the closing and opening times were measured in order to monitor changes in the performance characteristics of the MSM.

During the initial 5000-cycle test of the engineering model, unexplained stoppages occurred; although two subsequent 6000-cycle tests of this model were successfully completed, it was decided that a 20,000-cycle life test of both the engineering model and the flight unit should be conducted in order to establish confidence that this unit would be able to meet its 5000-cycle life requirement.

The refurbishment of the engineering model before this extended life test was begun consisted of relubricating all parts of the linkage with ion-plated lead. The 20,000-cycle life test of the engineering model was completed without failure. However, after the MSM had been brought up to room temperature at the conclusion of the test, the MSM was jammed in the open position, and the solenoid torque was insufficient to operate the linkage. During inspection, a slight pressure applied to one of the flaps released the stoppage, and the unit operated normally at room temperature thereafter. The engineering model was then subjected to an additional 6000-cycle test without failure; again, upon being brought to room temperature, it was jammed in the open position. Inspection established that except for the actuating arm, all parts of the MSM (i.e., solenoid, linkage, and flap shafts) were free to move. Further inspection disclosed that the area of contact between the actuating arm and the stop screws was galled or scuffed and that the line of action between this roughened contact and the pivot axis of the actuating arm could result in a locking force when differential thermal expansion between the steel actuating arm and the stop screws and the beryllium support bracket occurred during warmup. This situation is illustrated in Figure 9a. This stoppage was eliminated by modifying the angle of contact between the stop screw and the actuating arm stop contact surface and by applying a 0.050/0.076-mm (0.002/0.003-inch) coat of plasma-sprayed tungsten carbide to the stop contact surfaces of the actuating arm as shown in Figure 9b.

During the initial tests of the flight version of the MSM, stoppage occurred in the closed position after less than 500 cycles at operating temperature and pressure; however, at room temperature, it operated properly. Inspection of the solenoid revealed evidence of galling and of cold welding of the rotor to the magnetic detent stop of one of the pole pieces; see Figure 10. In a subsequent test of the engineering model, this same type of stoppage occurred after approximately 47,000 cycles. This marked discrepancy in the test results for the engineering model and those for the flight model was the result of differences in the electrical discharge machine tooling and in the different manufacturing setups used in fabricating these two models. As a result of these differences in manufacturing, the solenoid rotor for the flight unit struck a sharp corner of the pole piece magnetic detent stop and made contact with only one magnetic detent stop while the solenoid rotor for the engineering model made simultaneous flat contact with both pole piece magnetic stops (the Winchester Rifle 1-in-10,000 phenomenon). This stoppage was corrected by reworking the pole piece magnetic detent stops to eliminate the possibility of sharp corner contact and to bring the rotor into simultaneous contact with both pole piece magnetic detent stops. In addition to this rework, the solenoid rotor contact area was coated with a 0.050/0.076-mm (0.002/0.003-inch) layer of plasma-sprayed tungsten carbide. This coating increased the minimum holding current from 0.013 to 0.027 ampere.

During continued testing of the MSM flight unit, stoppages occurred in the open and in the partially open positions at operating temperature and pressure; however, at room temperature, the unit operated normally. Careful comparison of the engineering model with the flight unit revealed a slight difference in the diametral clearances between the shafts and the holes. Because of rework on the engineering model, these clearances were 0.0025/0.005 mm (0.0001/0.0002 inch) greater than the drawing tolerance that the flight unit met. The drawings were changed, and the flight unit shaft diameters were reworked to provide the 0.015/0.025-mm (0.0006/0.0010-inch) clearances that characterized the engineering model.

A problem related to the maintenance of end play on the flap shafts was also encountered; see Figure 11. In the engineering model, the flap was keyed to the flap shaft by means of a coiled spring pin. Apparently, the friction between the pin and the flap slot maintained the axial position of the flap on its shaft and thereby ensured that the amount of end play set during assembly was maintained. During the design review, the use of the coiled spring pin was criticized; the attachment of the flap shaft was therefore redesigned. A flattened shaft, a flat-sided hole, and a retaining ring were substituted. The flap can now shift on the shaft in a way that tends to eliminate the shaft end play established at assembly. The attachment of the flight unit flap shaft to the flap was redesigned to incorporate an additional retaining ring and thereby ensure the maintenance of the proper shaft end play.

With these changes in the shaft-to-hole diametral clearances and in the flap-to-flap shaft attachment, the MSM flight unit successfully completed the 20,000-cycle life test.

CONCLUSIONS

Testing an engineering model is useful in debugging the initial design and test procedures for any mechanism that must meet stringent requirements for low friction, close tolerances, and precise balancing of the spring output torque against solenoid output torque. However, each subsequent mechanism assembly must be subjected to a level of testing that will demonstrate that assembly parameters relating to friction, tolerances, and spring/solenoid output torque balance have been satisfied.

The activating current needed to close the MSM exceeds the power dissipation design requirement (465 versus 200 mW), but the current is used for less than 0.1 second and is then reduced to a holding current which dissipates only 40 mW during the rest of the operating cycle, which may last for 5 minutes or more. It is therefore believed that the 200-mW maximum power dissipation requirement has been met. Estimates of reliability based on the life-cycle tests predict that the MSM and the solenoid will meet the 5000-cycle life requirement. All other design requirements were demonstrably met.

The ion-plated lead lubrication has proved to be satisfactory for a lightly loaded journal bearing type of application at cryogenic temperature and in a vacuum.

The tungsten carbide coating was effective in preventing galling and cold welding of the contacting surfaces in the presence of significant impact forces.

The importance of exactly replicating the fits, geometry, and assembly parameters of the engineering models in the subsequent production of flight units has once again been very positively demonstrated.

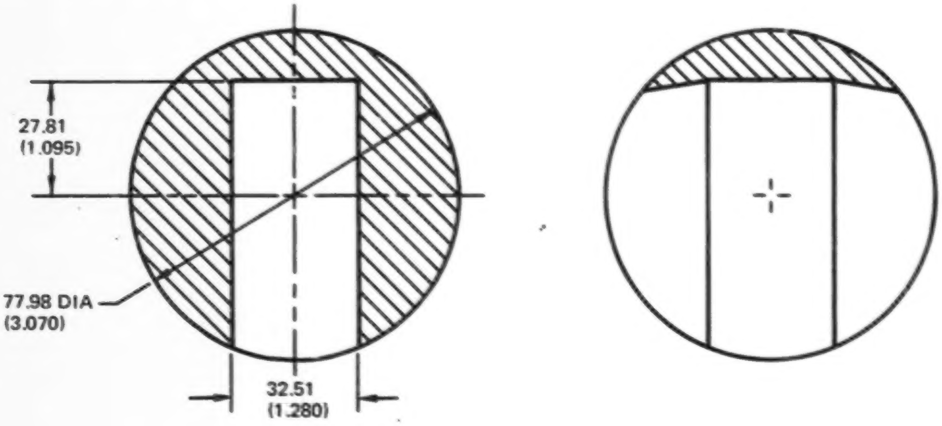

(a) NORMAL CONFIGURATION

DIMENSIONS – MM (INCHES)

(b) ALTERNATE CONFIGURATION

CLEAR APERTURE – ▨

Figure 1. Aperture stop configurations.

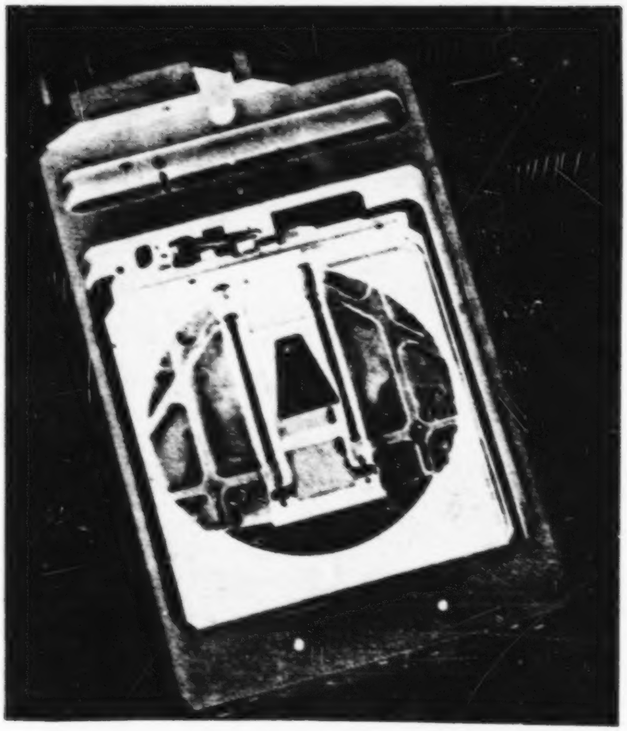

Figure 2. MSM with flaps closed.

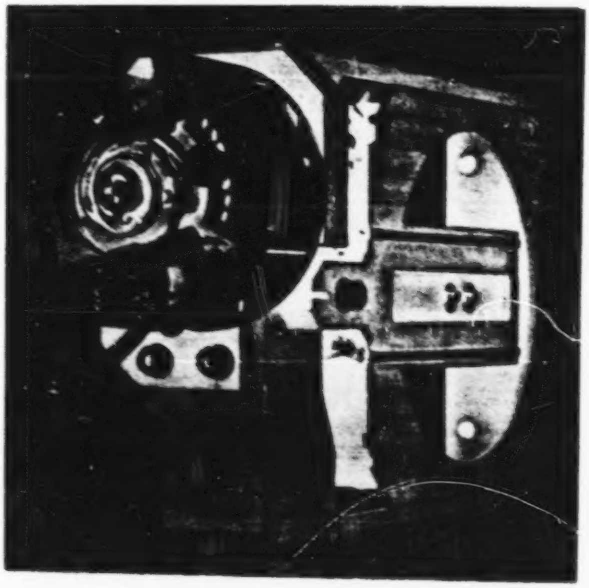

Figure 3. MSM drive solenoid.

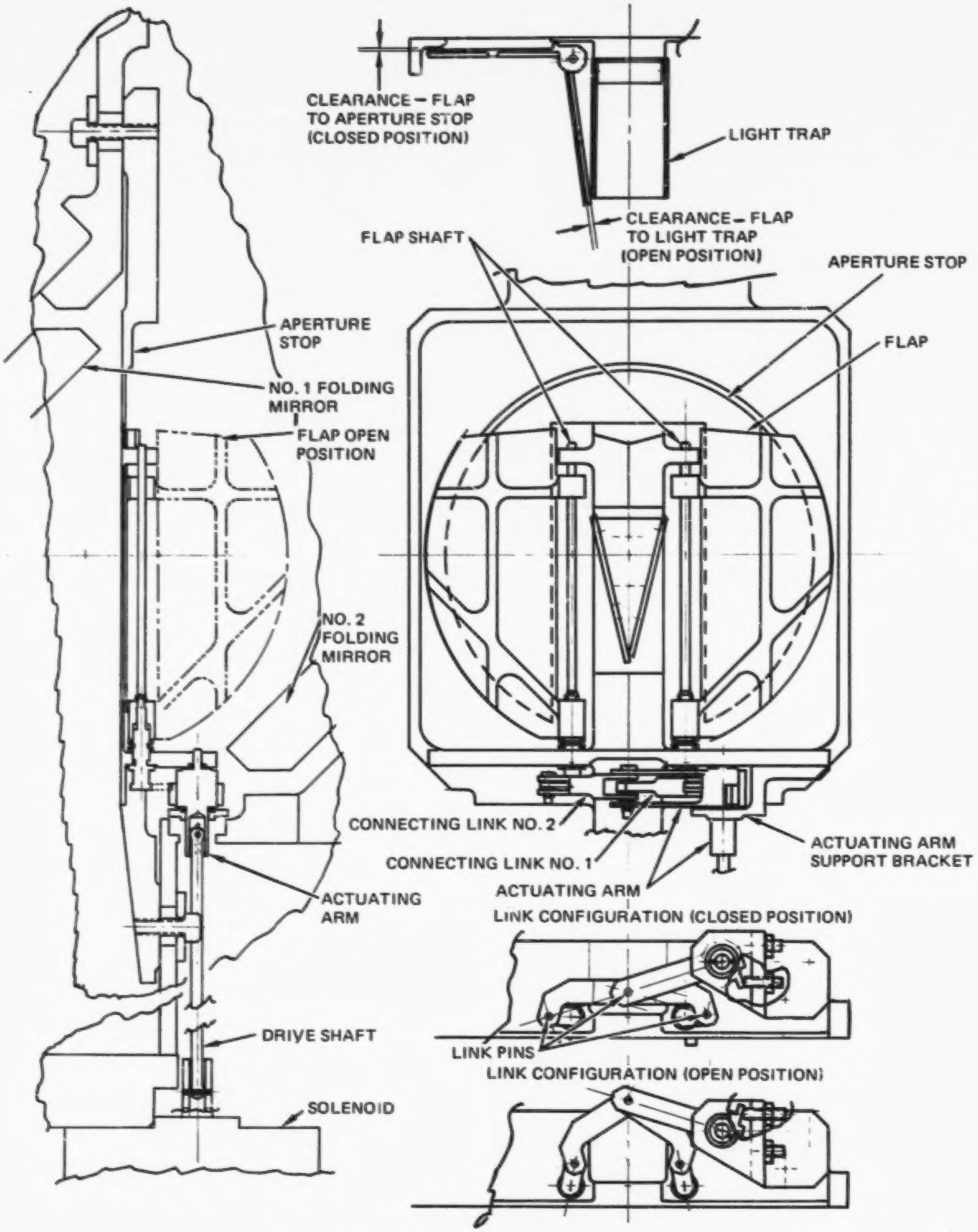
CLEARANCE – FLAP TO APERTURE STOP (CLOSED POSITION)
LIGHT TRAP
CLEARANCE – FLAP TO LIGHT TRAP (OPEN POSITION)
FLAP SHAFT
APERTURE STOP
APERTURE STOP
FLAP
NO. 1 FOLDING MIRROR
FLAP OPEN POSITION
NO. 2 FOLDING MIRROR
CONNECTING LINK NO. 2
CONNECTING LINK NO. 1
ACTUATING ARM SUPPORT BRACKET
ACTUATING ARM
ACTUATING ARM
LINK CONFIGURATION (CLOSED POSITION)
LINK PINS
LINK CONFIGURATION (OPEN POSITION)
DRIVE SHAFT
SOLENOID

Figure 4. Movable stop mechanism.

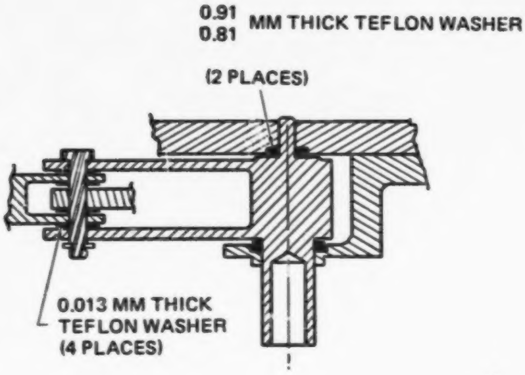
0.91
0.81 MM THICK TEFLON WASHER
(2 PLACES)
0.013 MM THICK
TEFLON WASHER
(4 PLACES)

Figure 5. Teflon washer installation.

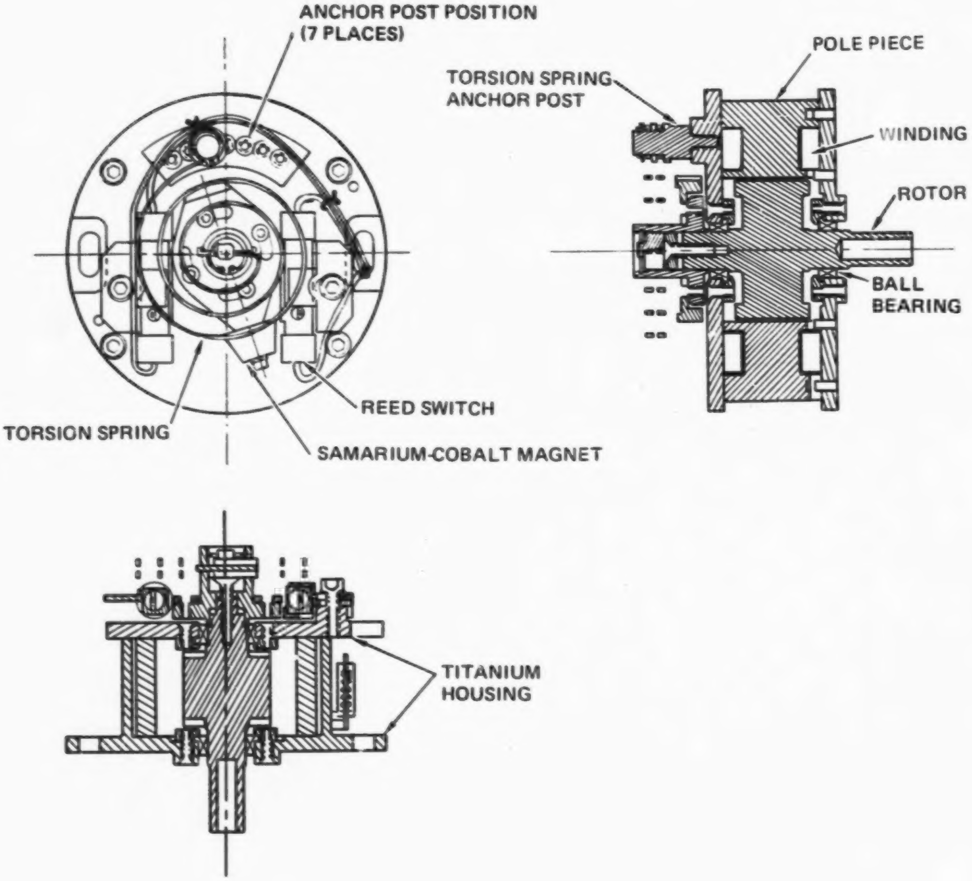
ANCHOR POST POSITION
(7 PLACES)
TORSION SPRING
REED SWITCH
SAMARIUM-COBALT MAGNET
POLE PIECE
TORSION SPRING
ANCHOR POST
WINDING
ROTOR
BALL
BEARING
TITANIUM
HOUSING

Figure 6. Rotary solenoid.

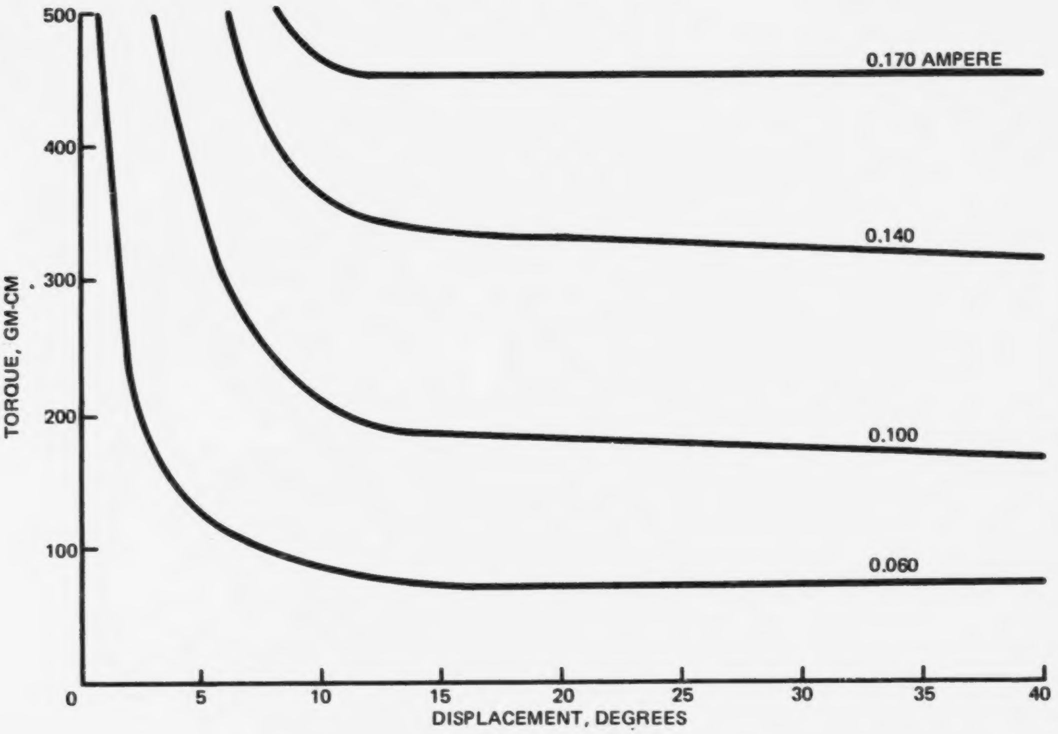

Figure 7. Measured solenoid output torque.

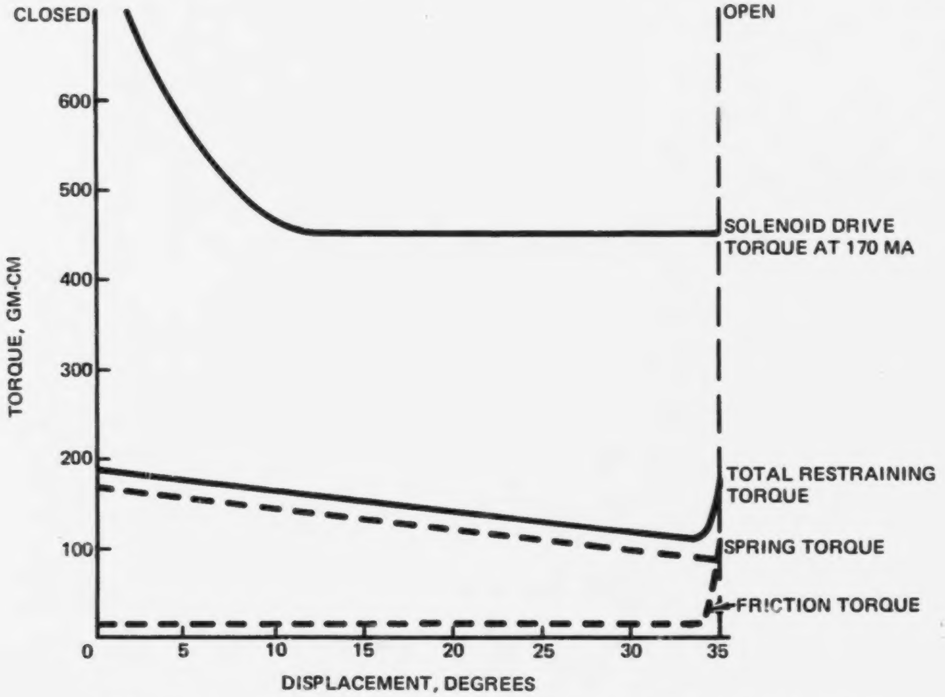

Figure 8. Measured performance at room temperature.

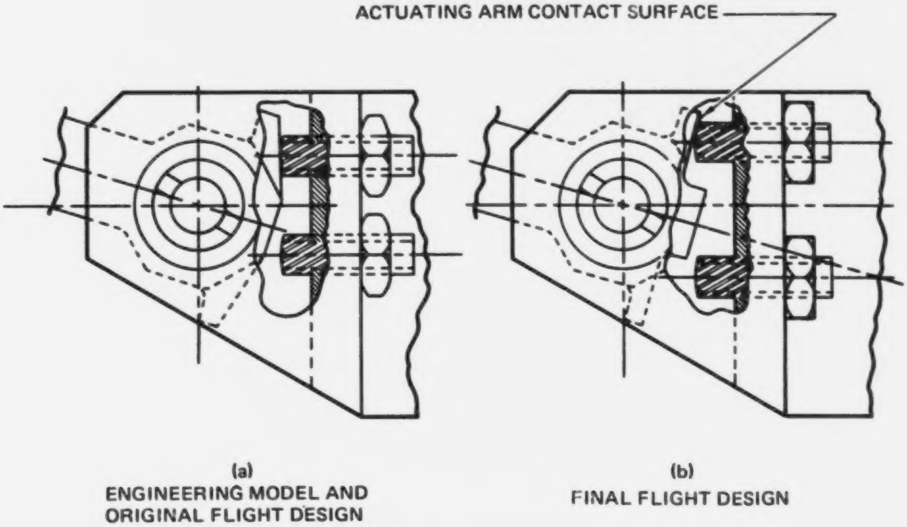
TUNGSTEN CARBIDE COATING
ACTUATING ARM CONTACT SURFACE
(a)
ENGINEERING MODEL AND
ORIGINAL FLIGHT DESIGN
(b)
FINAL FLIGHT DESIGN

Figure 9. Actuating arm stop contact surfaces.

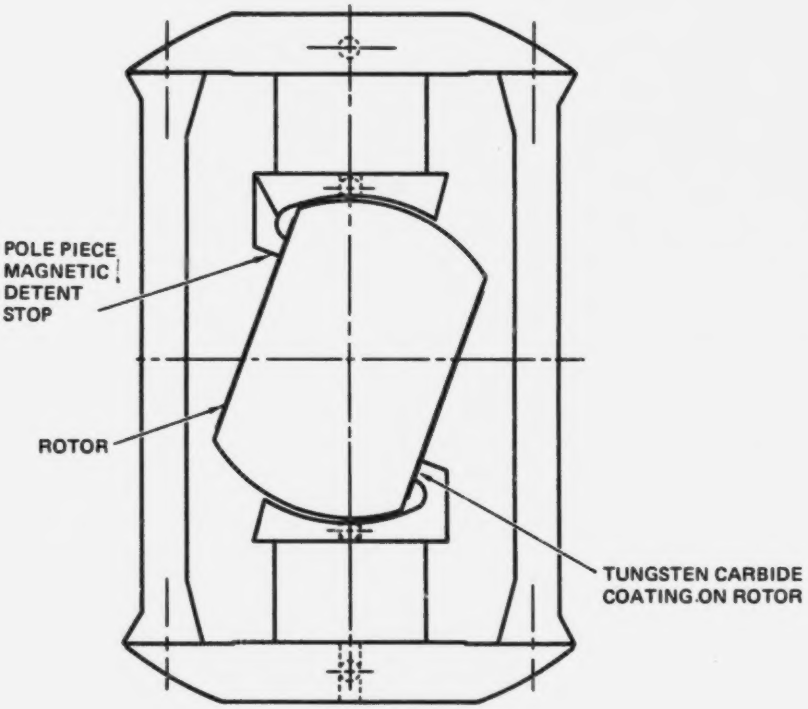
POLE PIECE
MAGNETIC
DETENT
STOP
ROTOR
TUNGSTEN CARBIDE
COATING ON ROTOR

Figure 10. Solenoid rotor/pole piece contact.

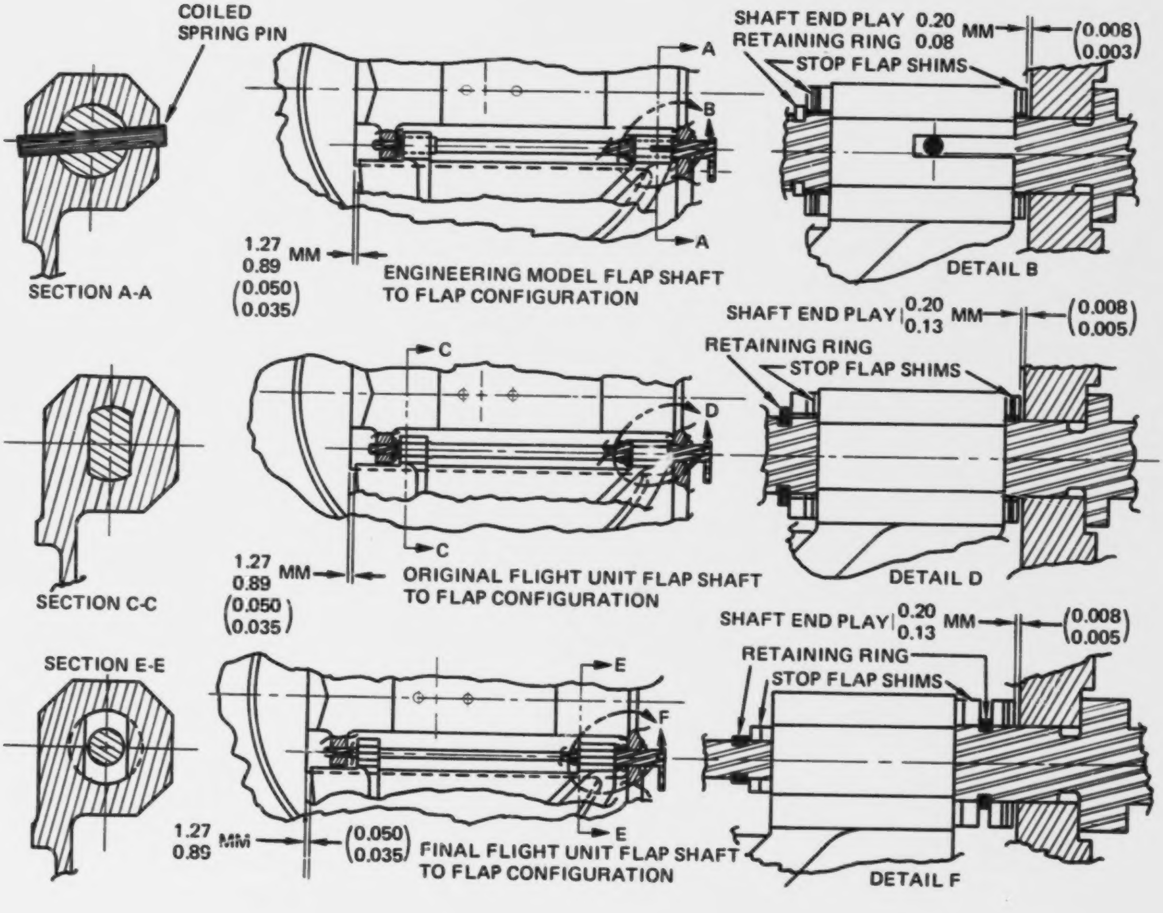
COILED SPRING PIN
SECTION A-A
A
B
A
1.27 0.89 MM (0.050 0.035)
ENGINEERING MODEL FLAP SHAFT TO FLAP CONFIGURATION
SHAFT END PLAY 0.20 MM (0.008)
RETAINING RING 0.08 (0.003)
STOP FLAP SHIMS
DETAIL B
SECTION C-C
C
D
C
1.27 0.89 MM (0.050 0.035)
ORIGINAL FLIGHT UNIT FLAP SHAFT TO FLAP CONFIGURATION
SHAFT END PLAY 0.20 0.13 MM (0.008 0.005)
RETAINING RING
STOP FLAP SHIMS
DETAIL D
SECTION E-E
E
F
E
1.27 0.89 MM (0.050 0.035)
FINAL FLIGHT UNIT FLAP SHAFT TO FLAP CONFIGURATION
SHAFT END PLAY 0.20 0.13 MM (0.008 0.005)
RETAINING RING
STOP FLAP SHIMS
DETAIL F

Figure 11. Flap shaft to flap configurations.

Robert N. Poulsen
Hughes Aircraft Company
2000 El Segundo Boulevard
El Segundo, California 90245

Mr. Poulsen is presently a senior staff engineer with the Space Sensors Division of Hughes Aircraft Company. He was first employed at Hughes as a draftsman in 1949. Work assignments since then have included detail design of helicopter structure and castings; aircraft machine gun and ammunition link design and testing; and mechanical layout design and assembly of infrared seeker heads and space sensor telescopes. Mr. Poulsen graduated from the U.S. Naval Academy in 1945.

Co-author of this paper is Mr. R. E. Tweedt who is also affiliated with Hughes Aircraft.

Blank Page

DUAL DRIVE ACTUATORS

Douglas T. Packard*
Jet Propulsion Laboratory
Pasadena, CA.

ABSTRACT

A new class of electromechanical actuators is described. These dual drive actuators were developed for the NASA-JPL Galileo Spacecraft. The dual drive actuators are fully redundant and therefore have high inherent reliability. They can be used for a variety of tasks, and they can be fabricated quickly and economically.

INTRODUCTION

A new class of electromechanical actuators has been developed for the NASA-JPL Galileo Spacecraft. These actuators perform such diverse functions as deployment of the 4.8-meter-high gain antenna, deployment and pointing control for the 1.0-meter probe relay antenna, and activation of a variable spring rate device in the spacecraft nutation damping system.

The actuators are called dual drives (Figures 1 and 2). They provide two independent electromechanical drive trains that combine at a common output shaft. Both trains are continuously engaged and independently operable without common failure modes.

The dual drive motor is a brushless configuration, containing internal electronics that perform all commutation functions, thereby providing a "two-wire" electrical interface and a motor package having speed/torque/current/weight characteristics equivalent to a standard size 11, permanent magnet brush motor. The dual drive configuration can also be adapted to use typical aerospace motor types, such as brush motors and stepper motors.

These are all desirable features. But, of equal importance, the dual drive can be produced quickly and economically due to its modular construction, manufacturing simplicity, and usage of commercial parts.

---

*The research described in this paper was performed by the Jet Propulsion Laboratory, California Institute of Technology, under contract with the National Aeronautics and Space Administration.

OPERATING SEQUENCE

Figure 3(a) shows a mechanical schematic of the dual drive. The actual operating sequence is as follows:

System 1

Motor 1 drives spur gear 1 which rotates the input shaft of harmonic drive 1. The harmonic drive is a simple compact gear system for achieving large speed reductions and large output torques. The "pancake" harmonic drive, used here, includes four main elements as shown in Figure 3(b). The wave generator is the input member, and either circular spline can serve as the output member. Speed reduction is achieved by engagement of a differential number of teeth on the flex spline and stationary circular spline.

The input shaft to harmonic drive 1 passes through the center of a hollow outer shaft and continues through harmonic drive 2 without physical contact. The inner shaft is connected to the input of harmonic drive 1 through a cone clutch. The clutch is non-functional during normal operation, and its specific purpose will be discussed in a subsequent paragraph.

System 2

Motor 2 drives spur gear 2 which rotates the input shaft to harmonic drive 2. That input shaft is located concentrically around the system 1 drive shaft. The input drive elements of system 1 and system 2 are totally separate and non-contacting. However, operation of system 2 causes the entire system 1 harmonic drive to rotate as a single mass. The torque produced by system 2 is transmitted across harmonic drive 1 by the tooth mesh of flexspline 1.

SLIP CLUTCH FUNCTION

The system 1 harmonic drive is linked mechanically to ground through its wave generator, input gearing, and motor; therefore, relative motion must occur at one or more of these system 1 elements when system 2 is operated (system 2 must be able to rotate the entire system 1 harmonic drive as a single mass).

The required relative motion can occur by rotation of the system 1 wave generator bearing or by backdriving of the system 1 motor; however, when system 1 is not backdrivable, the only remaining point of relative motion will be the system 1 wave generator bearing. Therefore, failure of that bearing represents a potential functional single-point failure because both system 1 and system 2 would become non-operable.

A slip clutch, located within the system 1 input shaft, provides a redundant point of relative motion in the system 1 drive train. The clutch guarantees that regardless of input gear configuration, no functional single-point failures exist in the dual drive. (Functional single-point failures are discussed in additional detail in the paragraph dealing with dual drive reliability.)

SLIP CLUTCH TORQUE MARGIN

The slip clutch must be truly non-functional during normal operation in order to assure that it does not, by itself, become a single-point failure. This is accomplished by providing a very large torque margin between actual operating torques and the threshold torque for clutch slippage.

This arrangement guarantees that the clutch will be non-functional during system 1 operation and also guarantees that relative motion, during system 2 operation, will occur first at the system 1 wave generator bearing and/or motor. The magnitude of the slip clutch torque margin guarantees that the clutch will only operate if all other potential operating modes have failed.

Figure 4 shows the range of input shaft torques for the drive shown in Figure 1. The torque required to slip the clutch is supplied from system 2 output torque, but the clutch must only transmit input torque without slippage.

The ratio of input torque to output torque is, in fact, the harmonic drive numerical gear ratio times an efficiency factor. Thus, the torque required to slip the clutch only slightly reduces available output torque from system 2 while still assuring a significant input torque margin for system 1 operation.

BACKDRIVING

The term "backdriving" refers to the condition in which a torque, applied at the output shaft of a non-operating electromechanical drive, will cause rotation of the unit's input shaft and motor.

The dual drive model, shown in Figures 1 and 5, is a highly efficient low ratio configuration which can be backdriven. Each motor in the drive contains a specified magnetic detent (holding) torque. These detent torques, reflected through each gear system, provide a repeatable and predictable backdrive threshold of approximately 30 inch-pounds.

The operation of either dual drive system produces torque at the unit's output shaft. Also, torques may exist at the output shaft due to externally generated loads. The existance of output torque, regardless of the source, will produce a simultaneous torque reaction across both harmonic drives from the output shaft back to the stationary structure.

This output torque reaction is the source of backdriving torque. For the dual drive configuration under discussion, the torque reaction will cause a non-operating system to begin backdriving at an output torque level of approximately 30 inch-pounds. However, each active drive system, in this dual drive configuration, is capable of producing approximately 50 inch-pounds of output torque, and operation of either drive system while the companion system is non-operating will result in backdriving of that non-operating system.

When backdriving begins, the output speed of the dual drive will decrease to zero as motion is lost into the non-energized system, and the driving system will become torque limited at the backdriving threshold torque level. When both drive systems are operated simultaneously, backdriving cannot occur and the full output torque capability can be produced.

The backdriving action does not damage either system and, in applications where torque limiting or manual over-ride are required, a backdrivable dual drive configuration can satisfy those requirements.

If backdriving must not occur for specific applications, worm input gears should be selected.

DIFFERENTIAL OUTPUT SPEED

Combined operation of both dual drive systems may increase output torque by preventing backdriving, but the output torques of each dual drive system are not additive at the common output shaft. Dual drive configurations containing non-backdrivable systems will produce **similar** output torque levels for single or dual system operations; however, the output speeds of each dual drive system are additive at the common output shaft.

A slight speed differential will exist between system 1 and system 2 because both harmonic drive inputs rotate at the same speed (assuming identical motor speeds) while the body of harmonic drive 1 rotates at the output speed of harmonic drive 2. This speed differential amounts to: $N/N\pm1$, where (N) equals the harmonic drive gear ratio. Thus, the speed difference amounts to 1% or less and can be ignored for most applications.

DUAL DRIVE RELIABILITY

Each dual drive system (drive train) contains a minimum number of functional elements (elements involving relative motion). This alone results in high inherent reliability for each drive train. But, when these truly parallel paths are combined into a single operating system containing no common failure points, the resulting reliability is unmatched by more conventional, partially redundant drives which have at least a few common functional elements.

Conventional reliability analysis of a system containing series elements will show that the overall reliability of that system will always be less than the reliability of the least reliable, series element in the system.

The same analysis will also show that the reliability of a system containing truly parallel elements will be orders of magnitude greater than the reliability of the least reliable element in that system.

The following equations relate load, life, and reliability for ball bearings which are the usual common elements in partially redundant systems.

Life/reliability is shown by

$$\frac{L}{L_o} = \left[\frac{\ln 1/R}{\ln 1/R_o}\right]^{1/1.125} \qquad (1)$$

Reliability (R)	Available Life (L) Revolutions
0.9	1,000,000
0.99	124,000
0.999	16,000
0.9999	2,000
0.99999	265

Life/load is shown by

$$L = L_{10} \left(\frac{C}{P}\right)^3 \tag{2}$$

C = basic (B-10) load ratings
P = actual operating load
L = allowable life for 0.90 reliability
L_{10} = (1) million revolutions.

These equations indicate that a factor of eight decrease in required operating life or a factor of two decrease of operating loads will increase reliability by one additional "9." This means that the very great reliability inherent in the dual drive concept can be traded off against longer operating life and/or higher operating loads with a final calculated reliability equal to or better than the reliability of more common differential drive concepts.

DESIGN DETAILS

Figure 5 shows a cross-sectional view of one dual drive configuration. The input bearings (① and ②) are "DF" mounted in order to simplify alignments. The input gears ③ and ④ are placed near the optimum locations to minimize input shaft/wave generator run-out effects on tooth mesh. These features eliminate the need for special "oldham" type couplings between the input gears and harmonic drives.

All ball bearing housings are fabricated from titanium alloy to allow wide temperature range operations. The output bearings (⑤ and ⑥) are "x-type" four-point contact ball bearings which can transmit axial, radial, and moment loads without the need for bearing pairs.

The motor register diameter ⑦ is slightly eccentric to the motor output shaft ⑧ . This allows adjustment of the "motor pinion-to-input gear" running clearance and also allows input gear ratio changes without the need for gear case modifications. (The ratio changes are accomplished by varying the diameters of driving and driven gears while maintaining an approximately constant gear center distance.)

The dual drive is lubricated with two types of grease. The alloy steel components of the gear systems are grease plated with Bray Oil Company Braycote 3L-38RP which provides lubrication and inhibits corrosion. The smaller corrosion-resistant input ball bearings and gears are lubricated with Braycote 3L-38-1 which is chemically identical to the "RP" material except it contains no rust inhibitor. These materials provide excellent wide temperature range performance and very low vacuum outgassing, such that ambient pressure operations and vacuum operations provide indistinguishable results with regard to post-test lubricant condition.

The dual drive motor is shown in Figure 6. The motor has been specifically developed for spacecraft applications and has the following significant design features:

(1)	Wound Stator	Provides optimum heat transfer
(2)	Separate Magnetic Detent Assembly	Allows independent control of detent torque magnitude and number of detent poles.
(3)	Rare Earth Magnets	Minimize performance changes due to transient voltages, voltage reversals, or overspeeds due to external torques.
(4)	Steel Housing	Provides very low residual magnetic fields and wide temperature operating range.
(5)	Non-Contacting Rotor Position Sensor and Internal Drive Electronics	Provide brushless performance with simple "two-wire" electrical interface

DUAL DRIVE PERFORMANCE

Several dual drive configurations have been tested extensively to identify operating characteristics. The various test configurations are identified as follows:

(Model Number)	Motor Size		Input Gear Ratio & Type		Output Gear Type		Output Gear Ratio
	XX	-	XXX	-	XXX	/	XX
Example:							
	11	-	10S	-	14 F	/	88
	Size 11 Motor		10 to 1 Spur Input Gears		Size 14 HDUF Harmonic Drive		88 TO 1 Harmonic Drive Ratio
			(Overall Ratio = 10 x 88 = 880:1)				
	11	-	30W	-	14 D	/	10,200
	Size 11 Motor		30 to Worm Input Gears		Size 14 HDD Harmonic Drive		10,200 to 1 Harmonic Drive Ratio
			(Overall Ratio = 30 x 10,200 = 306,000:1)				

Figure 7 shows general performance characteristics of three tested configurations. Figure 8 shows the speed/torque/current characteristics of these same configurations. Figure 9 shows the effects of temperature on speed and torque.

ALTERNATIVE DESIGN CONFIGURATIONS

The dual drive design provides for a modular construction in order to facilitate alternative design configurations. This concept is shown in Figure 10 along with estimated weights for several alternate design sizes. Figure 10 shows that approximately 40% of the component parts in the JPL dual drives are interchangeable between configurations.

Interchangeable spur gears or worm gears may be used at the input gear stages. These gears may then be coupled into any one of several available pancake harmonic drive configurations.

The standard pancake harmonic drives are produced in two configurations, "HDUF" (standard duty) and "HDD" (heavy duty). Approximately 127 different sizes and ratios are immediately available or can be readily produced.

As shown in Figure 11, these gearing combinations make it possible to achieve overall gear ratios as low as 432:1 or as high as 612,000:1 within the same basic envelope. This allows great freedom in the selection of operating characteristics for specific user requirements, and significant component interchangeability is also maintained.

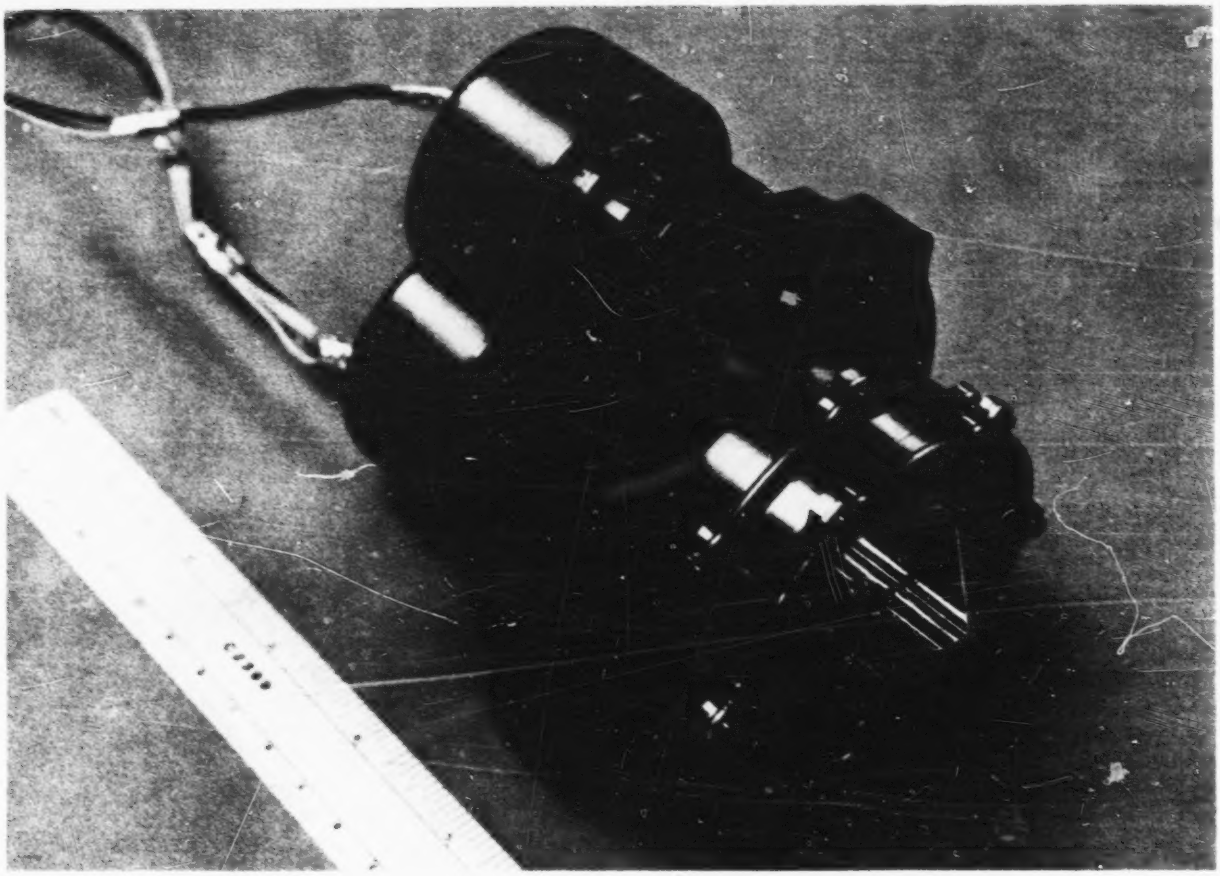

PERFORMANCE SPECIFICATION:

OUTPUT SPEED	0 - 13.4 RPM
OUTPUT TORQUE	0 - 50 in-lb
OVERALL GEAR RATIO	880:1
NORMAL OPERATING VOLTAGE	24 - 30 VDC
ALLOWABLE VOLTAGE	0 - 36 VDC
POWER (PER MOTOR) AT 30 VDC	3 - 11 W
MASS	2.00 lb

Figure 1. Dual Drive Assembly (JPL P/N 10095000)

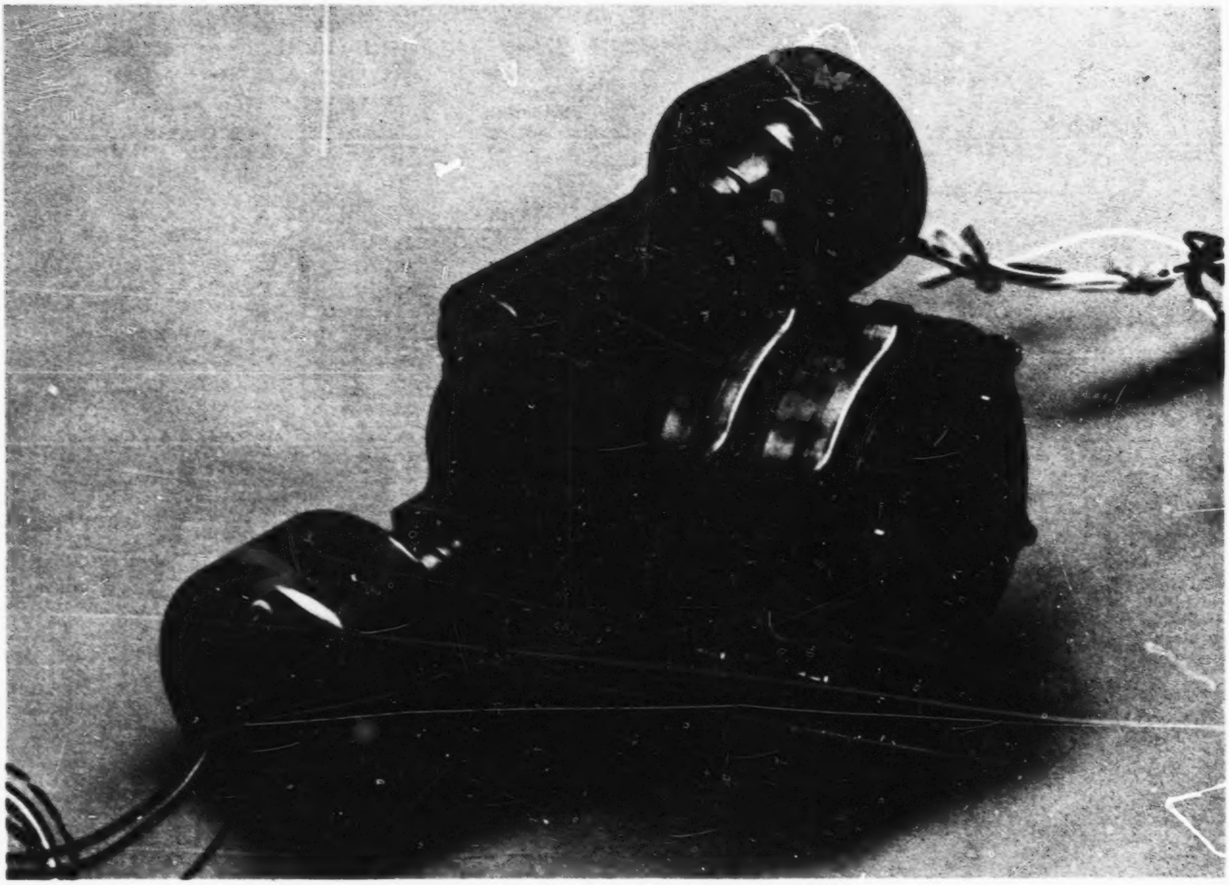

PERFORMANCE SPECIFICATION:

OUTPUT SPEED	0 – 0.018 RPM
OUTPUT TORQUE	0 – 180 in-lb
OVERALL GEAR RATIO	306,000:1
NORMAL OPERATING VOLTAGE	24 - 30 VDC
ALLOWABLE VOLTAGE	0 - 36 VDC
POWER (PER MOTOR) AT 30 VDC	4 – 11 W
MASS	2.50 lb

Figure 2. Dual Drive Assembly (JPL P/N 10100100)

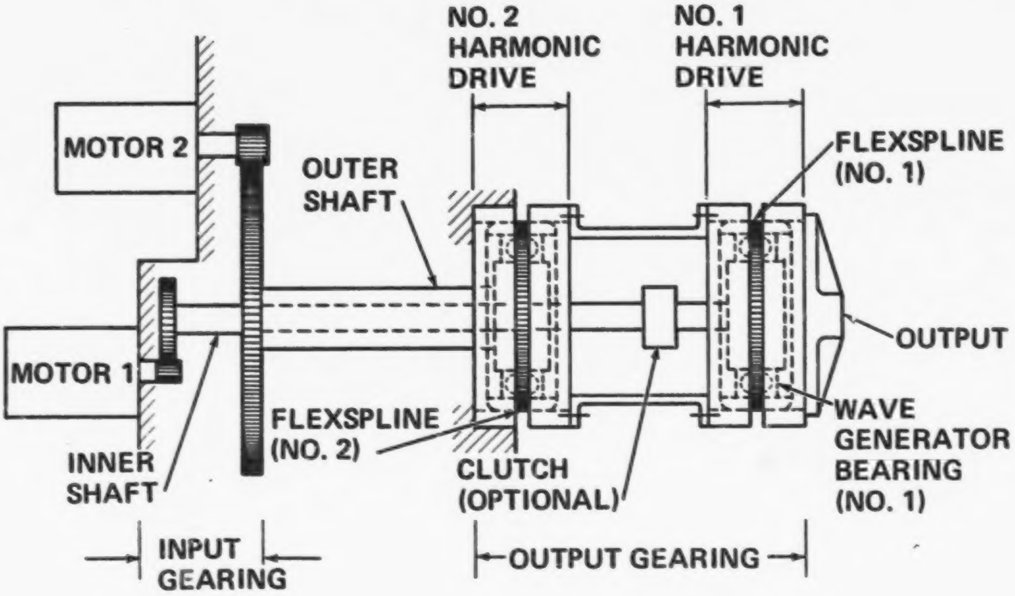
NO. 2
HARMONIC
DRIVE
NO. 1
HARMONIC
DRIVE
MOTOR 2
OUTER
SHAFT
FLEXSPLINE
(NO. 1)
OUTPUT
MOTOR 1
FLEXSPLINE
(NO. 2)
WAVE
GENERATOR
BEARING
(NO. 1)
INNER
SHAFT
CLUTCH
(OPTIONAL)
INPUT
GEARING
OUTPUT GEARING

(a) Overall

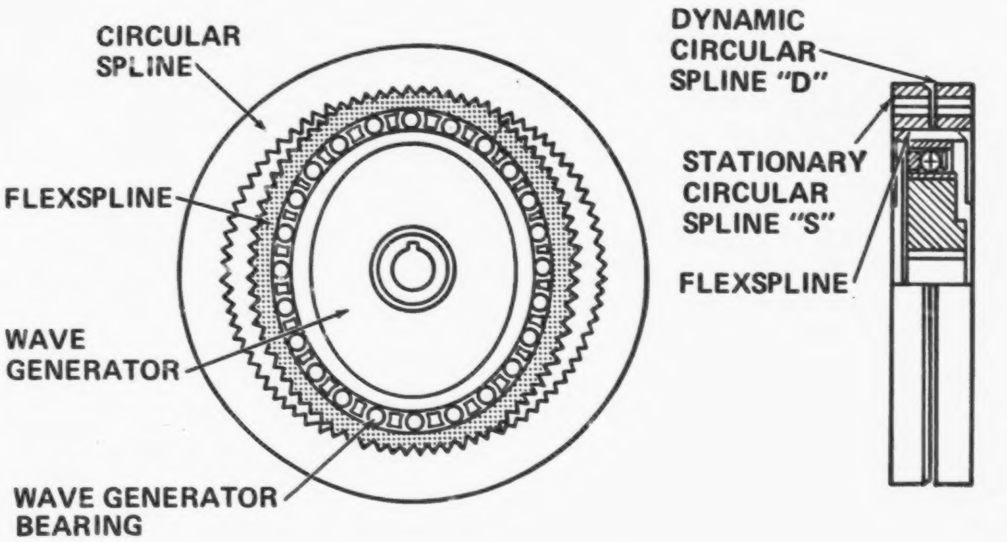
CIRCULAR
SPLINE
DYNAMIC
CIRCULAR
SPLINE "D"
STATIONARY
CIRCULAR
SPLINE "S"
FLEXSPLINE
FLEXSPLINE
WAVE
GENERATOR
WAVE GENERATOR
BEARING

(b) Pancake Harmonic Drive
(Proprietary Product of the Harmonic Drive Div.,
USM Corp., Wakefield, MA)

Figure 3. Dual Drive Mechanical Schematic

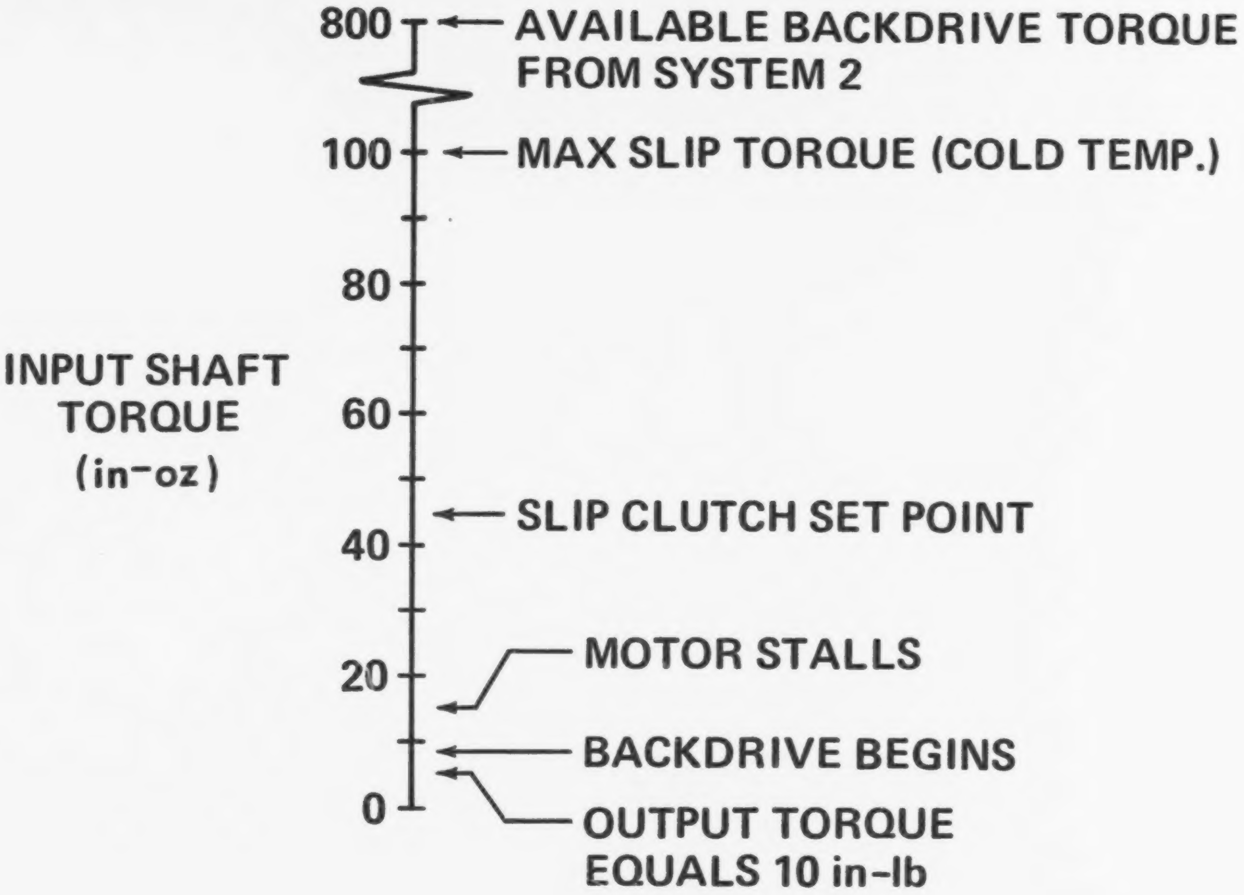
800
AVAILABLE BACKDRIVE TORQUE FROM SYSTEM 2
100
MAX SLIP TORQUE (COLD TEMP.)
80
INPUT SHAFT TORQUE (in-oz)
60
SLIP CLUTCH SET POINT
40
MOTOR STALLS
20
BACKDRIVE BEGINS
0
OUTPUT TORQUE EQUALS 10 in-lb

Figure 4. Input Shaft Torques (System 1)

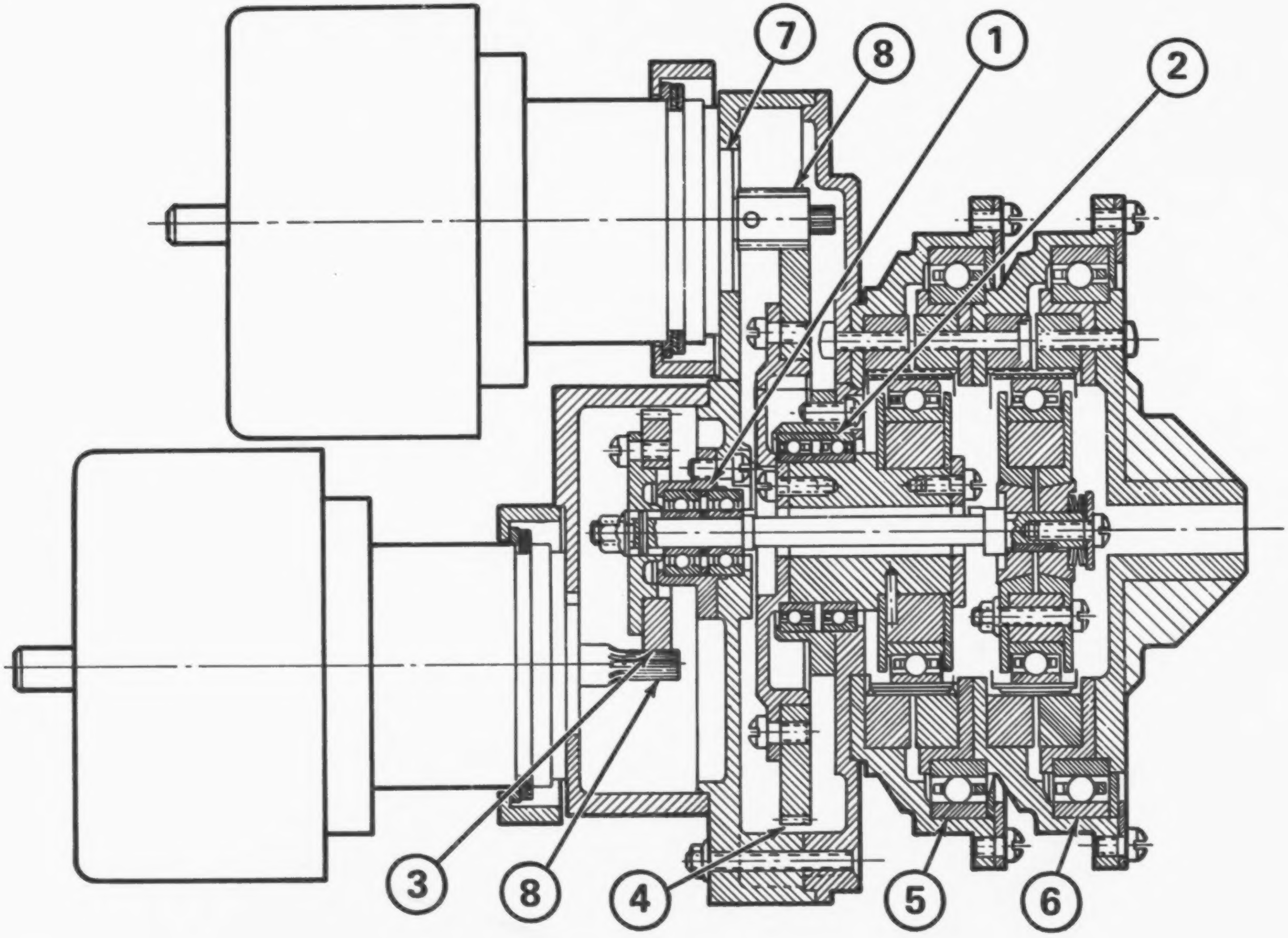

Figure 5. Dual Drive Assembly (Model 11-10S-14F/88)

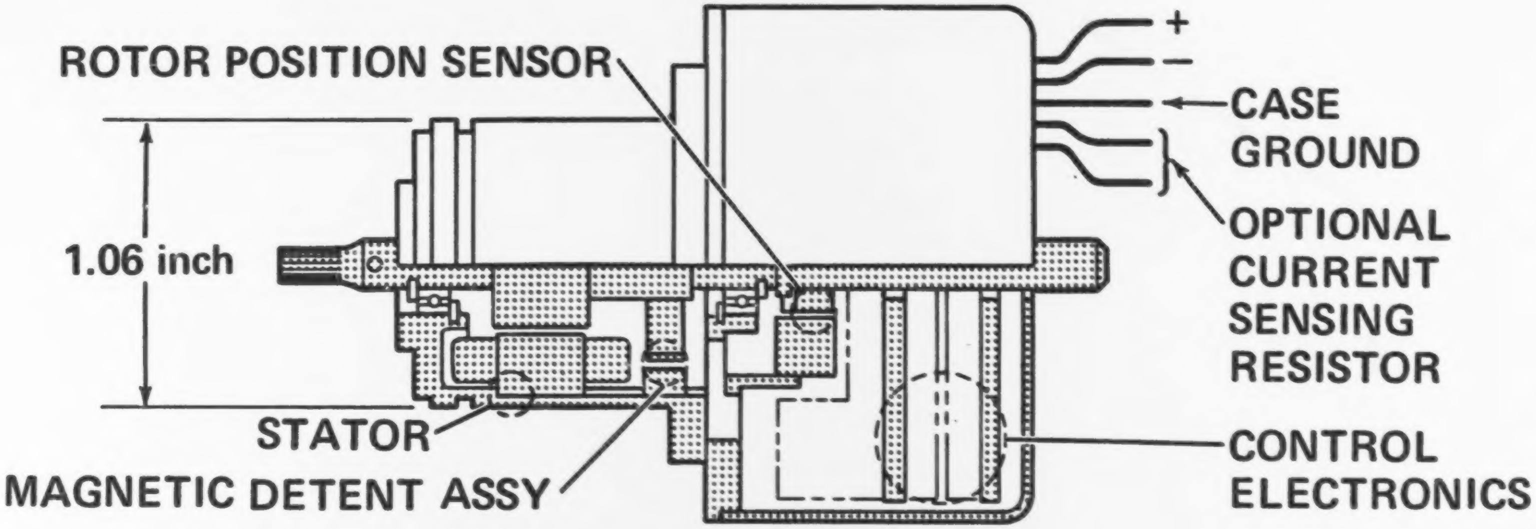
ROTOR POSITION SENSOR
1.06 inch
STATOR
MAGNETIC DETENT ASSY
+
–
CASE GROUND
OPTIONAL CURRENT SENSING RESISTOR
CONTROL ELECTRONICS

MOTOR CHARACTERISTICS

NO LOAD SPEED	6800 RPM AT 30 V
STALL TORQUE	2.5 in-oz AT 30 V
NO LOAD CURRENT	0.05 A
DETENT TORQUE	0.5 in-oz
MASS	6.5 oz
RESIDUAL MAGNETIC FIELD	2 nanotesla AT 1.0 m
HOUSING	416 STAINLESS
MOTOR CONFIG	PM ROTOR/WOUND STATOR 3 ϕ, 4 POLE

Figure 6. Dual Drive Brushless D.C. Motor

PERFORMANCE CHARACTERISTIC		DUAL DRIVE MODEL NO.		
		11-10S-14F/88	11-30W-14F/88	11-30W-14D/10200
BACK LASH		2° OR LESS (STANDARD), 1° OR LESS (SPECIAL)		
OUTPUT SHAFT TORSIONAL WIND-UP		APPROXIMATELY 2000 in-lb/RADIAN		
OUTPUT MOTION LINEARITY		± 2 $\widehat{\text{MIN}}$ (ONE SYSTEM OPERATING) ± 4 $\widehat{\text{MIN}}$ (TWO SYSTEMS OPERATING)		
OPERATING TEMPERATURE		QUALIFIED FOR -60°F TO +160°F		
NON-OPERATING TEMPERATURE		QUALIFIED FOR -100°F TO +160°F		
DEMONSTRATED LIFE		70,000 OUTPUT REVS (NO FAILURES)	IN TEST	IN TEST
OUTPUT BEARING ALLOWABLE LOADING	OPERATING	149 lb (RADIAL) 375 lb (THRUST) 168 in-lb (BENDING)	SAME	SAME
	NON-OPERATING	763 lb (RADIAL) 763 lb (THRUST) 231 in-lb (BENDING)	SAME	SAME
STATIC HOLDING TORQUE		30 in-lb (HOLDING)	GREATER THAN 50 in-lb	NON-BACKDRIVABLE
		20 in-lb (STOP AND HOLD)		
STALL IN A VACUUM		REQUIRED: 2 MINUTES AT 30 VDC AND AMB TEMP ENV DEMONSTRATED: 11 MINUTES AT 30 VDC AND AMB TEMP ENV		

Figure 7. Dual Drive General Performance Characteristics

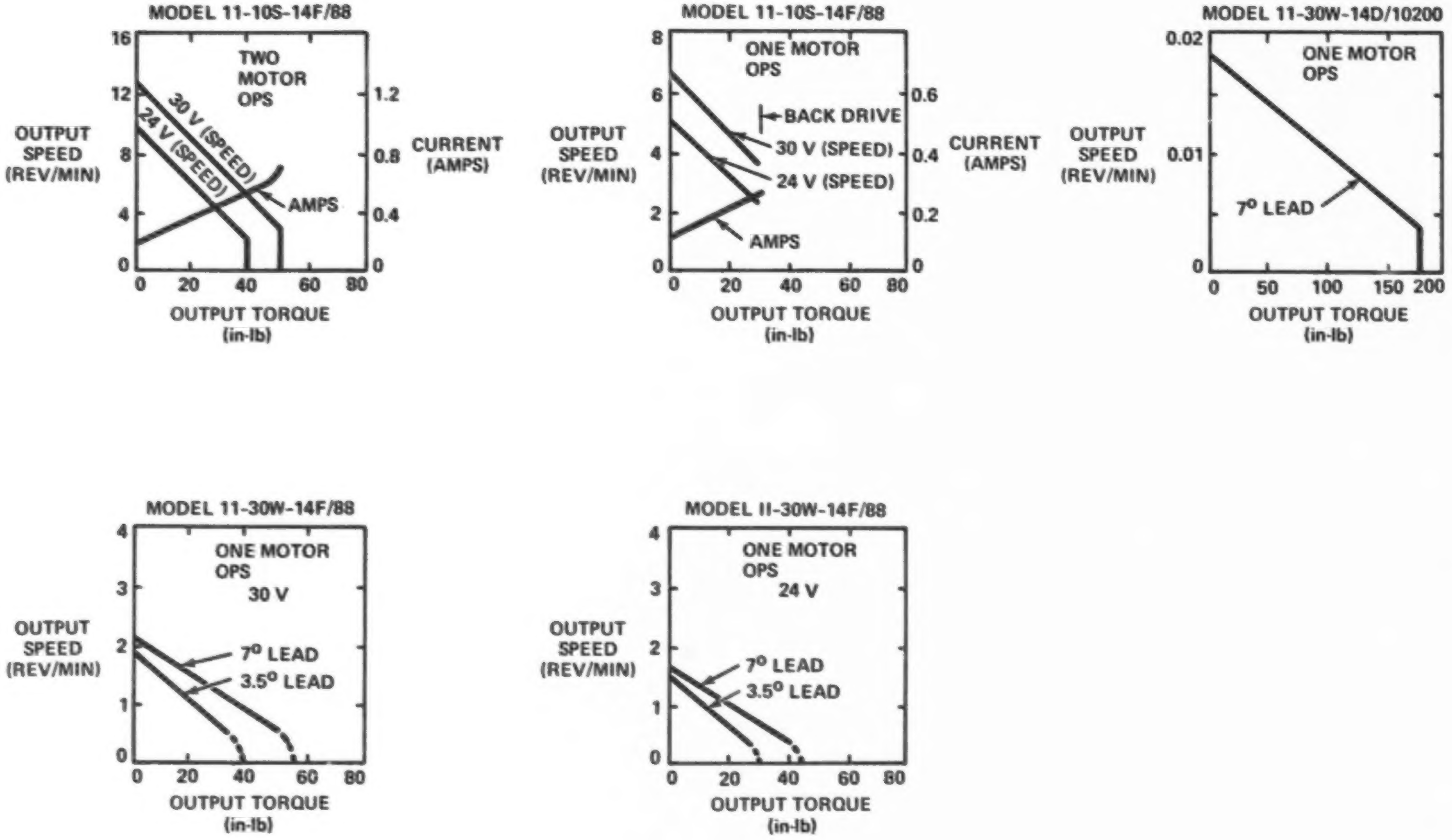

Figure 8. Speed/Torque/Current for Various Dual Drives

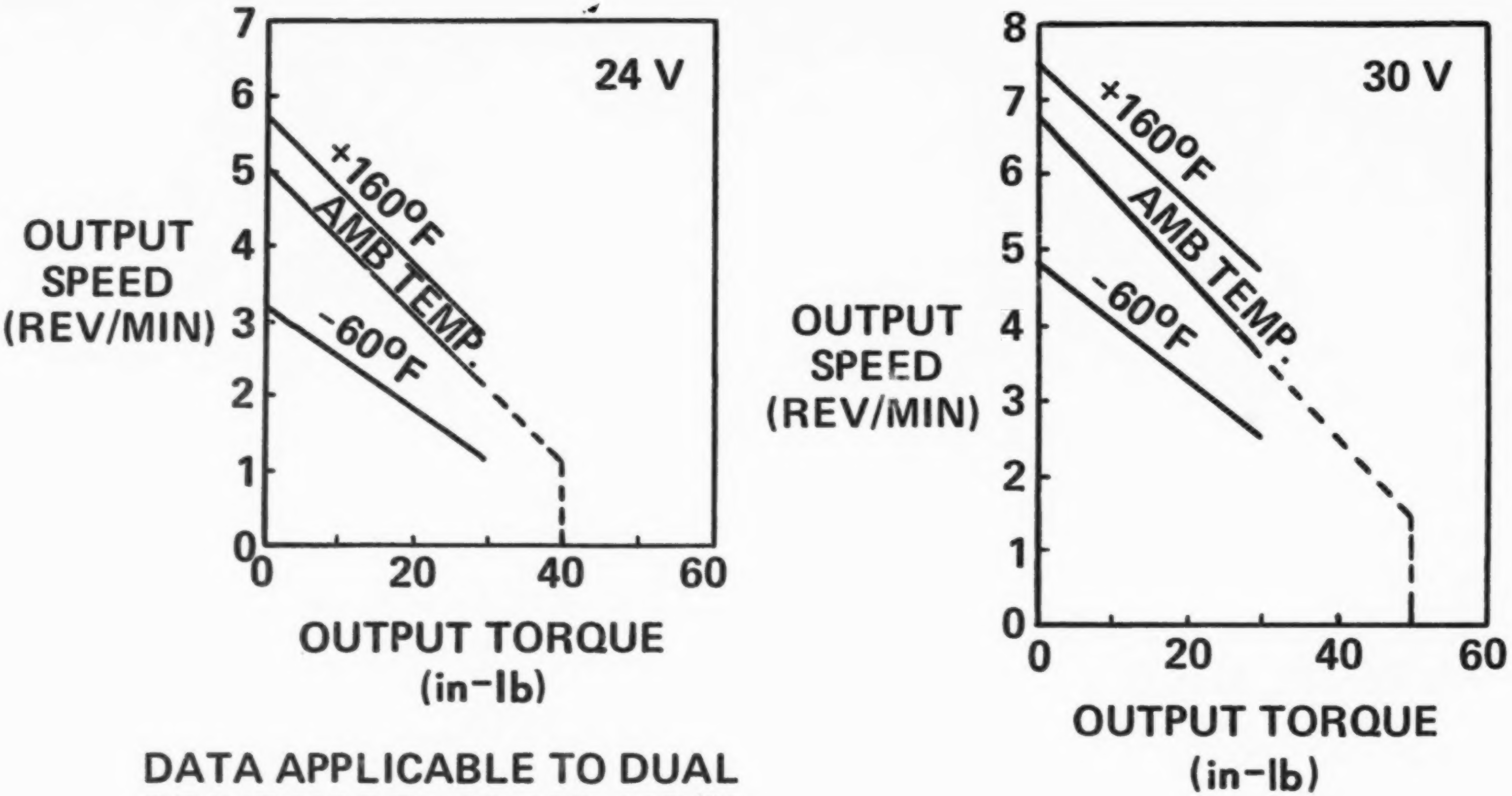

DATA APPLICABLE TO DUAL
DRIVE MODEL 11-10S-14F/88
(ONE DRIVE SYSTEM OPERATING)

Figure 9. Temperature Effects on Dual Drive Performance

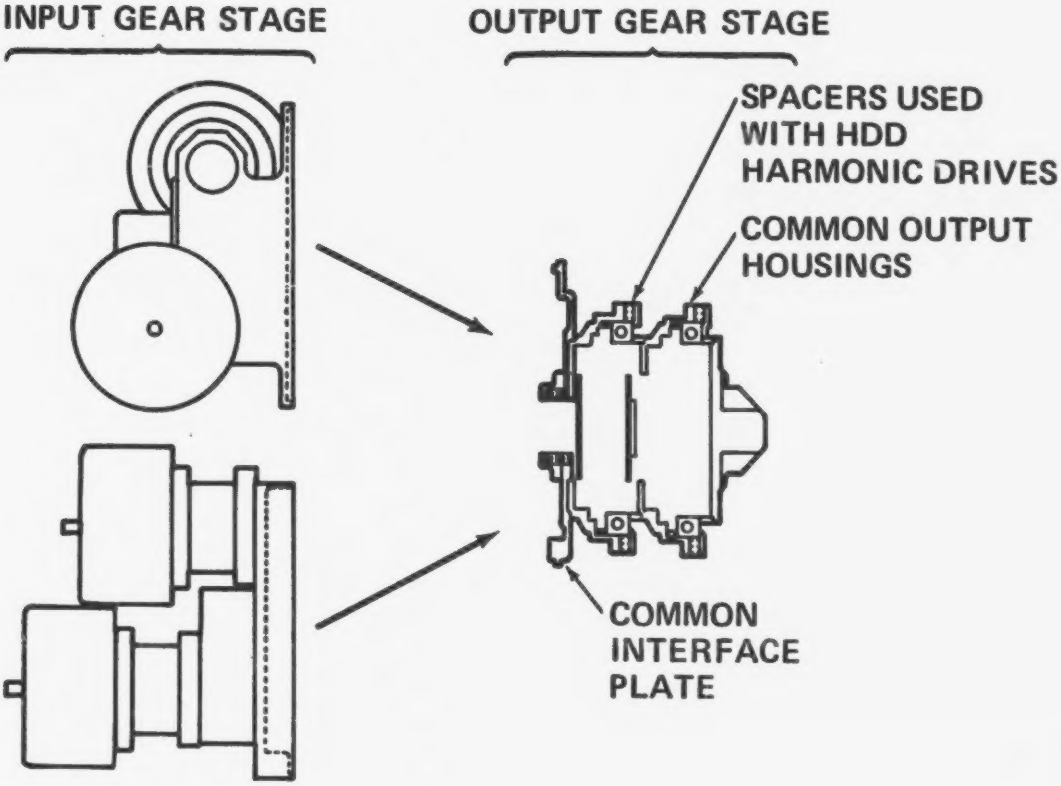
INPUT GEAR STAGE
OUTPUT GEAR STAGE
SPACERS USED WITH HDD HARMONIC DRIVES
COMMON OUTPUT HOUSINGS
COMMON INTERFACE PLATE

APPROXIMATE WEIGHT, lb

	OUTPUT GEARING						
INPUT CONFIG	14F	14D	20F	20D	25F	25D	32D
11-30 11-60	2.15	2.65	3.6	4.5	4.95	6.6	9.3
11-10	2.0	2.5	3.4	4.3	4.8	6.4	9.1
15-30 15-60		3.3	4.2	5.1	5.6	7.2	9.9
15-10		3.1	4.0	5.0	5.4	7.0	9.7

Figure 10. Dual Drive Modular Construction and Weight Estimate for Alternative Configurations

ALTERNATIVE DUAL DRIVE GEAR RATIOS (SIZE 14)*

INPUT GEAR RATIOS	OUTPUT GEAR RATIO										
	SIZE 14F		SIZE 14D								
	88	110	72	80	100	110	296	489	1110	2331	10,200
6:1 SPUR	528	660	432	480	600	660	1776	2994	6660	13,986	61,200
10:1 SPUR	880	1100	720	800	1000	1100	2960	4990	11,100	23,310	102,000
30:1 SPUR	2640	3300	2160	2400	3000	3300	8800	14,970	33,300	69,930	306,000
30:1 WORM	2640	3300	2160	2400	3000	3300	8880	14,970	33,300	69,930	306,000
60:1 WORM	5280	6600	4320	4800	6000	6600	17,760	29,940	66,000	139,860	612,000

*SIMILAR RATIO COMBINATIONS APPLY TO OTHER HARMONIC DRIVE SIZES (20, 25, 32, 40, 50, 65, 80, 100)

Figure 11. Alternative Dual Drives

Douglas T. Packard
Jet Propulsion Laboratory
4800 Oak Grove Drive
Pasadena, California 91109

Mr. Packard has been a member of the Technical Staff at Jet Propulsion Laboratory since 1978. Prior to that time, he was with Lockheed Missiles and Space Company in Sunnyvale. His experience has encompassed design and development involving over 300 spacecraft. Particular areas of knowledge include: deployable structures, pointing control systems, deployment devices, general-purpose space actuators, and pyrotechnic separation systems. Mr. Packard received his B.S. degree in Aeronautical Engineering from California State Polytechnic College in 1960.

Blank Page

DESIGN ASPECTS OF A SOLAR ARRAY DRIVE FOR SPOT, WITH A HIGH PLATFORM STABILITY OBJECTIVE

J. Cabillic and J. P. Fournier*,
P. Anstett and M. Souliac**, and G. Thomin***

ABSTRACT

SEP is developing a solar array drive mechanism (MEGS: mécanisme entraînement générateur solaire) for the SPOT platform, which is a prototype of the multimission platform developed by MATRA under CNES contract.

High-resolution cameras and other optical instruments are carried by the platform, requiring excellent platform stability in order to obtain high-quality pictures.

Therefore, a severe requirement for the MEGS is the low level of disturbing torques it may generate considering the $0.6\text{X}10^{-3}$ deg/sec stability required.

To reduce the mean friction torque and its fluctuations, use has been made of:

- Two angular contact, lead lubricated ball bearings having a very moderate elastic preload on orbit and completely protected against static loads and vibrations during the launch and deployment phases.
- A modular multidisc slip ring assembly of small diameter and a subsystem of electric contacts used only for pyrotechnic orders to the panels.

To reduce the torque fluctuations of the electric motor, a compensation of some defects is achieved.

Finally, the MEGS is used as a secondary actuator for damping of the solar array flexible modes.

INTRODUCTION

Multimission Platform for Earth Observation

SEP is developing a solar array drive mechanism named MEGS (mécanisme entraînement générateur solaire) for the SPOT platform. This platform is the

---

*SEP, Vernon, France
**MATRA EPT, France
***CNES, France

prototype of the so-called multimission platform currently being developed by MATRA under CNES contract.

The platform is, in fact, the service module, to be reused as is (or with minor modifications) on various earth observation satellites having different missions.

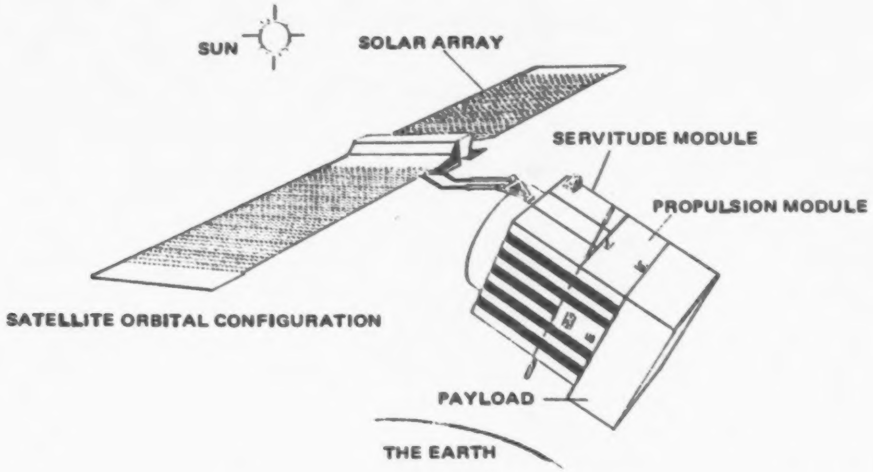

Picture Taking

Pictures can be taken with infrared spaceborne cameras, visible light cameras, side aperture radars, and other devices. One common need for all these instruments is a 0.15-deg/3-sigma pointing accuracy.

However, this pointing specification is not the major one to ensure good image quality; the stability of the platform and instrument is the mandatory condition to obtain high-resolution pictures.

The movement of the camera must be as small as possible during the exposure time, which is in the order of 10 sec for a full-size SPOT camera picture, thus leading to the severe rate stability specification: 0.2 to 0.6×10^{-3} deg/sec.

MEGS Design Aspects to Reach the Stability Required

The angular fluctuations of the platform are produced by disturbing torques resulting from the friction torque fluctuations of the ball bearings and the slip ring assembly and also from some imperfections of the electric motor.

The mechanical design aspects aiming at reducing the mean friction torque, and therefore its fluctuations, are described hereafter, as well as the method of compensation of the motor imperfections. However, this is not sufficient to reach the stability requirement.

A complementary actuation of the MEGS is used also to damp the flexible modes of the solar array.

VARIOUS OPERATION MODES OF THE MEGS

The MEGS cannot be presented as an isolated mechanism. It is, indeed, intimately connected with platform stability: on one hand it is a disturbance generator, and on the other hand it is used as a secondary actuator to provide damping. It is therefore necessary to first examine how it is used.

The multimission platform AOCS (Attitude and Orbit Control System) is detailed on the block diagram below in which the various units involved in the solar array drive function are particularly shown.

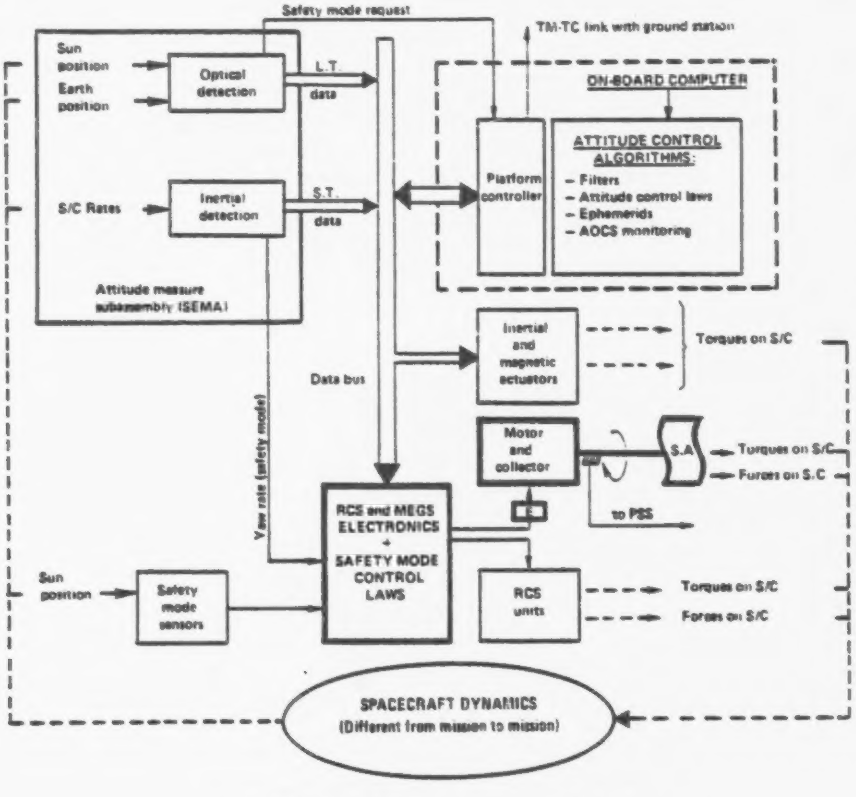

Safety mode request
TM-TC link with ground station
Sun position
Earth position
Optical detection
L.T. data
S/C Rates
Inertial detection
S.T. data
Attitude measure subassembly (SEMA)
ON-BOARD COMPUTER
Platform controller
ATTITUDE CONTROL ALGORITHMS:
– Filters
– Attitude control laws
– Ephemerids
– AOCS monitoring
Inertial and magnetic actuators
Torques on S/C
Data bus
Yaw rate (safety mode)
Motor and collector
S.A
Torques on S/C
Forces on S.C
to PSS
RCS and MEGS ELECTRONICS + SAFETY MODE CONTROL LAWS
Sun position
Safety mode sensors
RCS units
Torques on S/C
Forces on S/C
SPACECRAFT DYNAMICS (Different from mission to mission)

MULTIMISSION AOCS: FUNCTIONAL DIAGRAM

In the various modes of operation of the AOCS, MEGS has the following functions:

- o Pointing of the solar array towards the sun in the normal mode of operation with an accuracy of ±3 deg anywhere within 360 deg.
- o Same function, in the safety mode of operation, with an accuracy of ±3 deg about a fixed position called the canonical position.
- o Complementary actuation, in the normal mode of operation, for damping the solar array flexible modes.

In the subsystem architecture, rotation rate orders which are given to MEGS electronics either come from the AOCS onboard computer through EPRS (an AOCS electronics dedicated to actuator drive) or directly from this equipment in case of safety mode.

Typical Operation in Various Modes

Acquisition Sequence

First, the solar array is deployed; pyro orders transmit through the MEGS. Deployment status is confirmed to the onboard computer, also through the MEGS, which then authorizes the unlocking of the MEGS mechanism.

The solar array, at this time, is in the canonical position; the friction torque of the slip ring assembly and the motor holding torque maintain the arm in that position. When the satellite comes, in its orbit, to a point such that the sun direction enters the yaw-pitch plane, MEGS is automatically started by an AOCS algorithm which sends the proper PROM reading to obtain an angular rate nearly the same as the orbital rate.

Normal Mode

Long-Term Operation. Once per orbit the angular rate of MEGS will be adjusted by a special algorithm which, starting from the digital sun sensor data, compares the theoretical time to be in the canonical position with the actual one. The algorithm then deduces a new mean rate of rotation to be applied for the next orbit. The angular speed of the MEGS in real time is equal to the mean rate, plus small variations imposed by the need to control flexible modes of arm and array, as detailed hereafter.

Short-Term Operation. To achieve the very good stability required, a noiseless and wide-bandwidth AOCS of about 1 Hz will be necessary to react quickly enough to tape recorder starts and to solar array drive perturbations and to keep a safe stability margin relative to solar array flexible modes:

- o The MEGS generates disturbing torques at 0.1, 0.15, 0.2, and 0.4 Hz, which are harmonics 2, 3, 4, and 8, respectively, of the fundamental frequency of the stepper motor drive signals (sine and cosine) at 0.05 Hz.

- The first solar array modal frequencies are 0.11, 0.16, and 0.2 Hz. This shows a potential difficulty if the attitude control does not have sufficient phase margin at these frequencies to damp the oscillations which the drive motor will initiate in the array.
- In addition, the solar array and the electromechanical stiffness of the stepper motor will also form an oscillating system of nearly zero damping. The frequency of this last oscillator is also in the range of 0.1 to 0.2 Hz. To solve this problem, the MEGS has two possible motor stiffnesses (900 and 450 Nm/rad) which will allow selection, once in orbit, of the most favorable one with respect to the real characteristics of the array.

AOCS Control Laws for the Normal Mode of Operation. AOCS makes use of three orthogonal reaction wheels. Gains and filters are put on rate and angle outputs of the attitude detection system to refine torque commands for the wheels. This is actually sufficient to stabilize the platform down to the very low rates aimed at but does not provide damping of solar array oscillations themselves. Indeed, the MEGS excitations, at the same frequency as array modes, can lead to a situation where high wheel torques perpetually counteract high array oscillations. To cure this effect, an additional control law acts on the MEGS itself to provide damping of array oscillations. This control law, based on an in-flight identification of wheel torque oscillation frequency and phase, delivers to the MEGS delta rate commands to generate the damping torques.

The block diagram below summarizes the operation of AOCS and MEGS in the normal mode of operation.

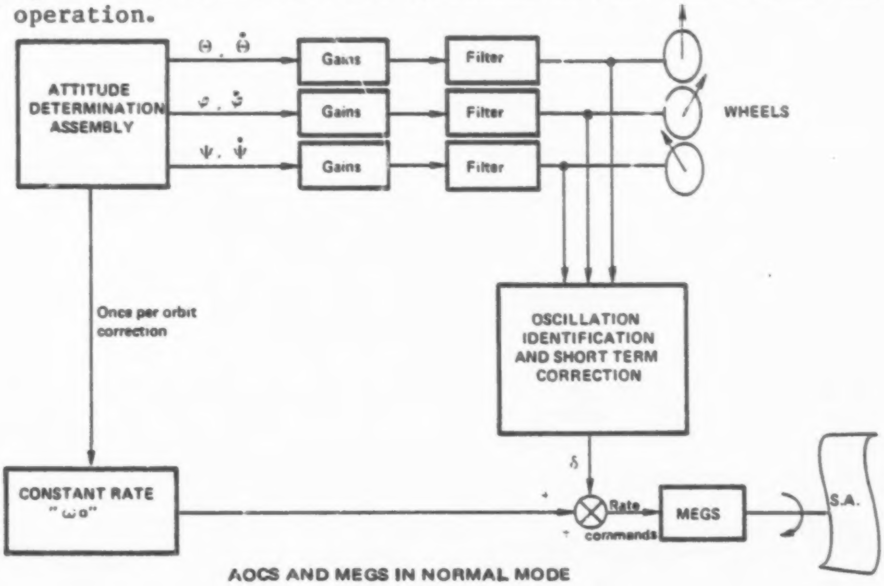
ATTITUDE DETERMINATION ASSEMBLY
$\Theta, \dot{\Theta}$
$\varphi, \dot{\varphi}$
$\Psi, \dot{\Psi}$
Gains
Gains
Gains
Filter
Filter
Filter
WHEELS
Once per orbit correction
OSCILLATION IDENTIFICATION AND SHORT TERM CORRECTION
δ
CONSTANT RATE "ωo"
+
+
Rate commands
MEGS
S.A.

AOCS AND MEGS IN NORMAL MODE

MEGS REQUIREMENTS

Due to its critical role in the stability of the platform, the MEGS is subject to the following requirements:

Nominal speed: 0.055 to 0.063 deg/sec

Speed stability requirement: for $0.05 \text{ Hz} \leq f \leq 0.8 \text{ Hz}$, the speed stability of the MEGS rotor, without additional inertia and in open loop, must be better than 6×10^{-3} deg/sec with the maximum values as follows:

- Harmonic 1 (0.05 Hz) < 2%
- Harmonic 2 (0.1 Hz) < 6%
- Harmonic 3 (0.15 Hz) < 1%
- Harmonic 4 (0.2 Hz) < 1%

Friction requirement: for $0.8 \text{ Hz} \leq f \leq 20 \text{ Hz}$, the torque fluctuations of bearings and slip rings must be < 0.05 Nm and mean friction torque < 0.05 Nm.

Other Constraints

The other constraints put on MEGS by AOCS are:

- Rate range: ±0.48 deg/sec
- Torque capability: ±3 Nm high level
  ±1.5 Nm low level
- Motor stiffness: 900 Nm/rad high-level torque
  450 Nm/rad low-level torque
- Angular position reading over ±180 deg:
  Accuracy between ±0.5 deg at null
  ±4 deg at 180 deg
- Reliability for a 2-year mission: 0.99 (approximately 10,000 revolutions)

Additionally, the loads on the MEGS rotor flange, during the launch and deployment sequence, are relatively high:

- Launching: 1,000 N in any direction
  100 Nm around any axis perpendicular to rotor axis
- Deployment sequence: 100 N in any direction
  ±310 Nm around the deployment axis

MECHANICAL DESIGN

Ball Bearings

We have opted for a classical configuration: two angular contact ball bearings moderately preloaded by a diaphragm.

Lubrication

Our choice for lubrication is a submicron film of lead deposited on the races by an ion plating process, following the ESTL (European Space Tribology Laboratory) procedure, plus the use of a lead bronze cage. This choice was made for the following reasons:

- It is a type of lubrication which suits the very low speeds.
- The level of friction is low and independent of temperature.
- The risk of optical surface pollution is avoided.
- The endurance tests made at ESTL have shown that lead lubricated ball bearings could be operated successfully up to 10^8 revolutions. This is to be compared to the 10,000 revolutions we need!
- The behavior in air is satisfactory.
- The ESTL procedure is well defined and the experience in the field extensive.

Friction

To meet the stiffness requirements and to reduce the mean friction torque and, in a like manner, the noise and peak torques, we have adopted a moderate preload of 100 N and a relatively large angle of contact of 25 deg.

The friction torque measurements on 12 pairs of ball bearings give the following results after vacuum run-in:

Mean torque: between 1.6 and 5.9×10^{-3} Nm

Peak to peak: between 3.8 and 8.2×10^{-3} Nm

The diameter of ball bearings has been chosen as small as possible. The limit was imposed by the desirability of removing the slip ring assembly by passing the three electric connectors through a central tube of the driving mechanism, without having to remove them from the cables.

Unloading the Ball Bearings System

Several considerations led to a decision to unload completely the two angular contact ball bearings and to lock the rotor during the launch and deployment sequence: (1) the high level of forces exerted on the MEGS rotor flange, (2) lack of knowledge of the effect of vibrations on a lead film, and (3) a tight schedule without time for redesign. The solution chosen is a little more complicated than the classical one in which the front ball bearing, alone, is fully unloaded.

Figure 1 presents the two solutions. In the MEGS system, the force to unload the ball bearings is applied to the external ring of ball bearing set no 2. When this force goes beyond the preload value produced by the diaphragm, the deformation increases, causing contact between the first pair of rotor-stator tapers and resulting in dismounting of ball bearing set no. 2. Then as the force is further increased, the rotor goes forward further, causing contact between the second pair of rotor-stator tapers and producing the dismounting of ball bearing set no. 1.

Thus, the rotor is entirely sustained and locked by the tapers, and the ball bearings do not experience any static load or vibrations.

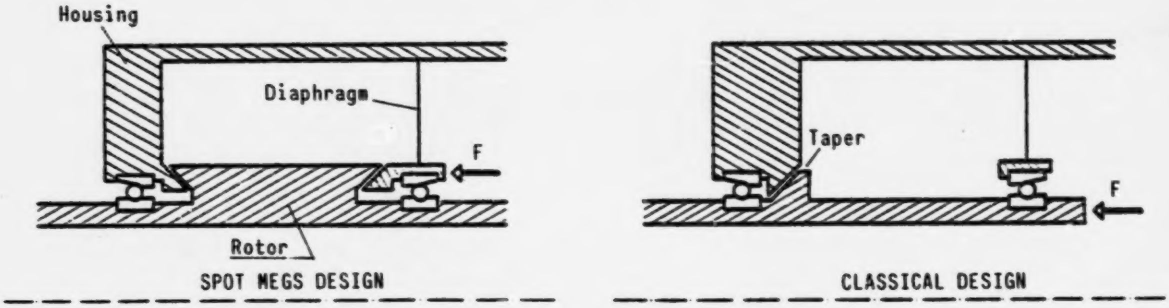

SPOT MEGS DESIGN

CLASSICAL DESIGN

Figure 1. Schemes of Unloading Ball Bearings System

Figure 2 presents the system in the two states: during launch and in orbit.

A redundant pyrotechnic wire cutter is used to release the system.

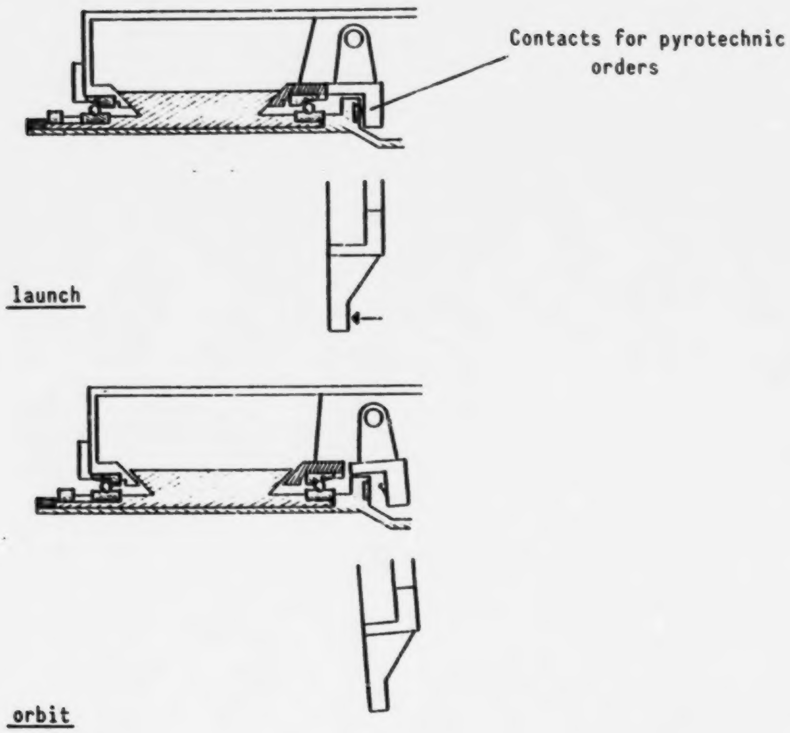
Contacts for pyrotechnic orders
launch
orbit

Figure 2. Scheme of the Unload System in the Two States

Slip Ring Assembly

The slip ring assembly is developed by MECANEX in Geneva, under SEP supervision.

Materials

The choice of materials is classical:

- Rings in coin silver
- Brushes in sintered composite of 82.5% silver, 15% molybdenum disulphide, and 2.5% copper

Design

To minimize the friction torque, we used small-diameter slip ring discs. The disc allows certain positioning defects of brushes which are not tolerated with cylindrical rings (see Figure 3).

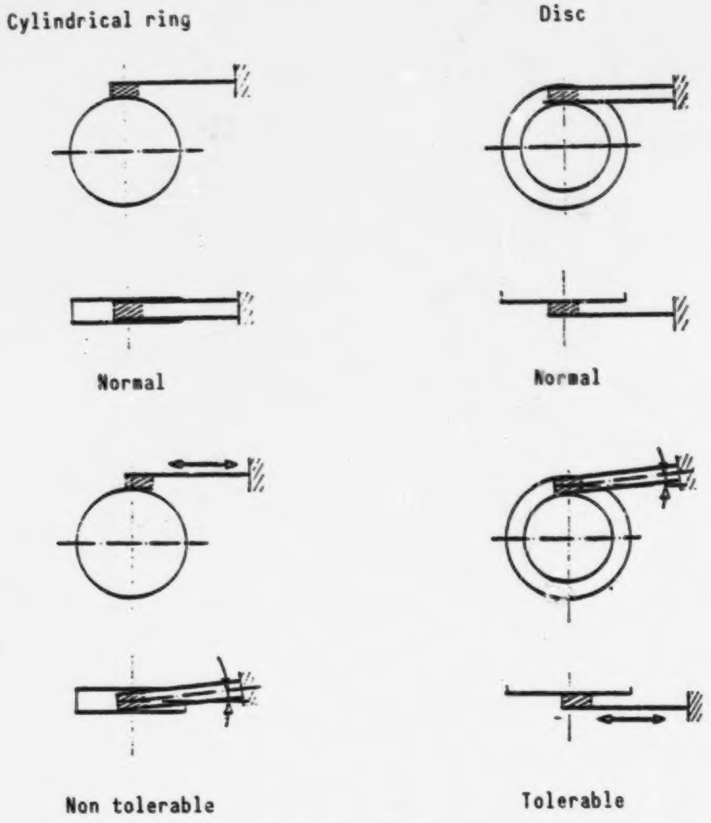
Cylindrical ring
Disc
Normal
Normal
Non tolerable
Tolerable

Figure 3. Advantages of Disc Over Cylindrical Ring

The MEGS slip ring assembly is modular. This presents numerous advantages:

- Lower risks of manufacturing
- Lower costs because of the facility of molding the simplified modular elements
- Possibility of adaptation to different missions

In addition, the design allows for easily separating the slip ring assembly from the driving mechanism. A central tube, which is a part of the slip ring assembly and through which passes the electric cable, goes through the driving unit. It is possible to separate the two subassemblies without disassembling the electrical connectors.

The slip ring disc assembly of MECANEX consists of 11 discs having a power and a signal slip ring on each side. The mean diameter of the power slip rings is 31 mm, and the mean diameter of the signal slip rings is 41 mm.

A subassembly of 10 electrical contacts allows the transmission of the pyrotechnic orders to the solar array. These contacts are broken by the motion of the release lever after array deployment. Thus, a saving of 10 slip rings and their friction has been achieved.

Friction

The mean friction torque measured in the air is 0.25 Nm. The tests in vacuum have not yet been conducted.

COMPENSATION OF THE SAGEM ELECTRIC MOTOR

The SAGEM electric motor is a 1,200-step-per-revolution stepper motor operated in synchronous mode. Although its manufacturing is very carefully done, it presents some defects, the compensation of which is hearafter presented.

First, when the motor, without any load, is energized by two sine and cosine voltages, its angular speed fluctuates around the average speed proportional to the voltage frequency (0.05 Hz). The speed fluctuation of the rotor corresponds to that of the magnetic field, since the load torque is very small (friction torque of ball bearings only).

Second, the motor stiffness is not constant over a voltage period. This appears, for a constant torque load, as a variable lag angle of the rotor referred to the magnetic field during one period and, consequently, a speed fluctuation during the same time.

The aim of the compensation is to reduce to a minimum these fluctuations in order to reduce the disturbances on the platform.

First Method

In this method, the compensation is obtained in two stages: compensation at no load and compensation at fixed load torque.

Compensation at No Load

This consists of energizing the motor by two shaped voltages from the sine and cosine basic voltages so that the amplitude of the magnetic field is constant but its angular speed is opposed to the observed defects.

Experience shows that the distortion observed on one period (which corresponds to four steps) and in which the fourth harmonic is preponderant is approximately the same whatever the period.

The corrections achieved on one period are registered on floppy disc before being PROM programmed. Figure 4 shows the method.

If the motor was perfect, the rotation angle θ versus time would be a straight line Δ. But an actual curve $\theta = f(t)$ is plotted. It can be seen, for instance, that at t_1, the actual position θ_R is smaller than the theoretical position θ_T. To obtain an actual position θ_T at t_1, the two voltage levels applied at this moment must differ from A_1 and A_2 and must be equal to B_1 and B_2, which correspond to θ_T on the actual curve $\theta = f(t)$. The corrections are achieved at 64 points of the period. The results are shown on Figure 5.

Compensation at Fixed Load Torque

The first compensation having been achieved, a load torque approximately equal to the mean friction torque is applied to the rotor.

The second compensation consists of modifying the magnetic field intensity, without changing its direction, in order to modify the stiffness.

Figure 6 shows the method. At t_1, the theoretical angle of lag $\theta'_T - \theta_T$ of the rotor with regard to the position θ_T at no load is not achieved. Actually, it is $\theta_R - \theta_T$.

The compensation consists of modifying both voltages at t_1, in the same ratio

$$\frac{\theta_R - \theta_T}{\theta'_T - \theta_T}$$

This does not modify the direction of the magnetic field but, in the case shown, increases its intensity and therefore the motor stiffness, resulting in an actual position θ_T.

Only the first stage of this mode of compensation has been achieved with success. The second stage will be achieved in January 1982.

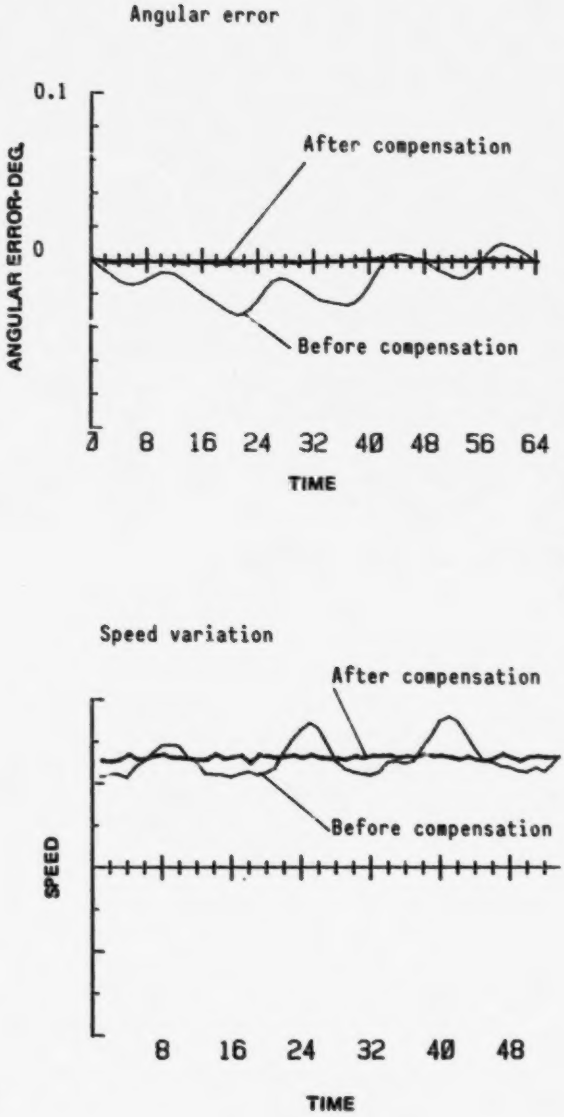

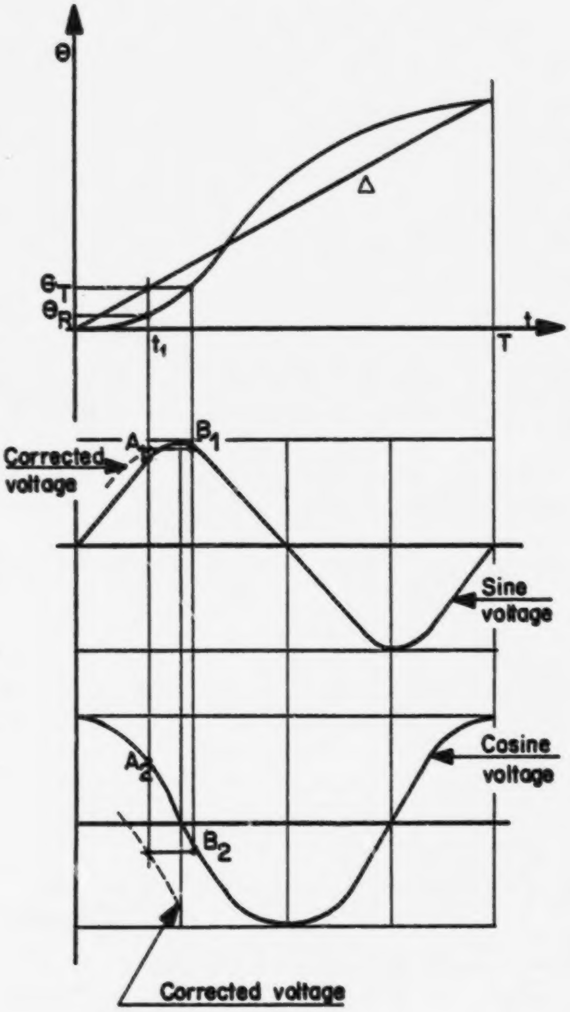
Θ
Δ
Θ_T
Θ_R
t
t₁
T
A₁
B₁
Corrected voltage
Sine voltage
Cosine voltage
A₂
B₂
Corrected voltage

Figure 4. Compensation of the Motor at No Load

Figure 5. Compensated Motor at No Load

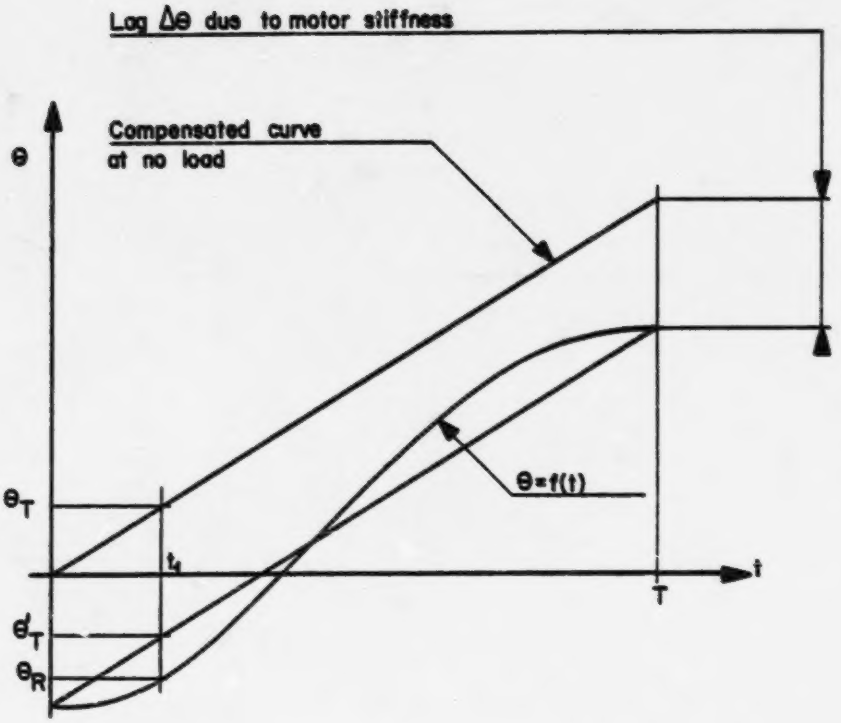
Lag Δθ due to motor stiffness
θ
Compensated curve at no load
θ=f(t)
θ_T
t_1
t
T
θ'_T
θ_R

Figure 6. Compensation of the Motor for a Constant Load

Second Method

This method is accomplished in the same manner as that of the first stage of the first method, but with a load torque of 0.25 Nm.

Experience has shown that the fourth harmonic level, which was about 15%, was reduced to:

1.09% at no load

1.13% for a 0.5-Nm load torque

The choice between the two methods will be decided after testing is completed.

Jacques Cabillic
SEP
Vernon, France

When Mr. Cabillic first joined SEP in 1971, he was responsible for the servo-actuators as well as other equipment on the Ariane. Since 1979, he has been responsible for the electromechanisms in the Space Division. Prior to his joining SEP, he was with the Laboratoire de Recherche Balistique et Aérodynamique as head of the department concerned with servomechanisms, servo-actuators, equipment for launchers, inertial equipment, and testing facilities. Mr. Cabillic graduated from Ecole Nationale Supérieure de Mécanique de Precision.

Co-authors of this paper are Mr. J. P. Fournier who is also with SEP in Vernon, France; Mr. P. Anstett and Mr. M. Souliac who are both with MATRA EPT in France; and Mr. G. Thomin who is affiliated with CNES in France.

Blank Page

DEVELOPMENT OF A HIGH STABILITY POINTING MECHANISM FOR WIDE APPLICATION

A.J.D. Brunnen *

R.H. Bentall **

ABSTRACT

A recurrent requirement of spaceborne instruments and communications equipment is that of accurate pointing. This need is recognisable in such diverse applications as Star Sensor trimming, Momentum Wheel gimballing, in-orbit adjustment or alignment of equipment, inter-satellite communication and Antenna Pointing.

As part of the ESA Advanced Supporting Technology Programme, British Aerospace is developing a pointing mechanism of novel design having several advantages over the more conventional gimbal, centre-pivoted or cross axis pointing concepts currently state-of-the-art.

INTRODUCTION

The 1977 World Administrative Radio Conference (WARC) stipulated that accuracies better that ±0.1° should be achieved on communications beamwidths of typically 1° to 2°, and as a consequence gave rise to an operational requirement for Antenna Pointing Mechanisms (APMs) capable of around ±0.01° pointing accuracy, thus relieving the satellite AOCS from the difficult, if not impossible, task of achieving this accuracy for multi-antenna systems.

Experience with thermal vacuum testing has shown that these high accuracy requirements are very difficult to achieve, particularly when the APM is operating in 'Open Loop' mode (see Ref. 1). Nonlinearities, build errors, non-orthogonality effects and, particularly, thermal expansion effects combine to reduce the accuracy until, typically, an accuracy of around ±0.025° limits the performance of conventional gimbal systems.

* British Aerospace Dynamics Group, Space and Communications Division, Stevenage, England.

** European Space Agency, ESTEC, Noordwijk, Netherlands.

Better 'Closed Loop' performance (i.e. when the APM is responding to an external error signal such as that derived from an RF sensor) can normally be obtained providing that the movement resolution of the actuators is high enough and that mechanism backlash and control response are adequate. (Ref. 2, 3).

The objective of the APM development programme was therefore to achieve an APM design which offered, in addition to other attributes, an improved stability of pointing. Following trade-offs covering the range of existing pointing mechanism concepts, a radically new concept was chosen based on an idea developed at ESTEC. This concept, and its derivatives, is the subject of an ESA patent application.

THE SWASH-PLATE PRINCIPLE

The new mechanism utilises the swash-plate or rotating wedge principle in order to achieve and maintain the pointing vector. Figure 1 shows the operating principle. The device contains 4 main structural elements, A,B,C and D. B and C are wedge-shaped and enabled to rotate about the z-axis by means of bearing systems located at 1, 2 and 3. If mutual z-axis rotation between A and D is prevented by, for example, a bellows E, and the bearings at 1 and 2 are driven, then the device becomes a polar coordinate pointing mechanism.

When B and C are rotated by equal amounts, one clockwise the other anti-clockwise, there results a tilting of the pointing vector away from the z-axis (nodding). If B and C are now rotated together, the vector sweeps around the z-axis at the angle previously achieved. Figure 2 illustrates this by showing the circular paths traced by the pointing vector on a target, due to the rotation of B and C and the combination B + C.

It can readily be seen that if either of the two swash-plates is prevented from rotating, then the pointing vector can be re-aligned with the z-axis by the rotation of the other swash-plate alone. In principle any two of the three bearings may be driven, but it is advantageous to drive bearings 1 and 3 since the actuators may then be mounted on the base and top plates. If the actuators prevent back-driving of the two sections by virtue of their detent positions, then the pointing vector is maintained without the application of power.

MECHANISM DESCRIPTIONS

A cross-sectional view of the BAe High Stability APM is shown in Figure 3. The two swash plates, having a swash angle of 2.15 degrees, can be seen supported by single bearings and the two motors supported off the top (payload) interface and the bottom (satellite) interface, respectively. Figure 4 shows additional views with the installation of the positional encoders.

Main Bearings

The three main bearings are Kaydon four-point contact (Gothic Arch) bearings of 7 inches diameter having a minimal preload within the bearings. This preload, and the thermal design of the mechanism, necessitated careful analysis in order to avoid on the one hand, bearing clearance which would, in principle, result in degraded pointing accuracy, and on the other hand excessive preload and consequent increased torque.

The four-point contact bearings are well suited to the concept allowing a compact design whilst at the same time having a high load-carrying capacity (13,600N radial, 34,000N axial, quoted manufacturer's value for static loading). Substantial mass and dimensional savings are achieved over the use of duplexed pairs of angular contact bearings.

The bearings are lubricated with a low-vapour-pressure oil. The use of a liquid lubricant increases the thermal conductivity of the bearing, reducing the thermal gradients which would otherwise contribute to preload changes. The bellows allow the possibility of hermetic sealing, if required by the application.

Structure

The material selected for the four main structural components of the mechanism is Beryllium. The advantages offered by this material are:

- Extremely low mass
- Thermal expansion close to that of the bearing steel
- Good thermal conductivity
- High specific heat.

The three latter features, combined with the cylindrical nature of the structure and the externally mounted bellows, provide a protected environment within the mechanism, leading to an exceptionally high thermal stability.

The four main structural sections, with the interconnecting bearings, constitute the load path through the mechanism. The large diameter of 180mm is significant in that high strength and stiffness can be obtained for very low mass. The mechanism can typically support unaided a mass of up to 10kg through an Ariane launch, the strength limitations being those of the main bearings having a load capacity as given above. In Figure 4 it can be seen that the central part of the mechanism is free from obstruction. Thus, when desired, an aperture of up to 40mm dia. can be provided through the mechanism for the passage of cables, flexible waveguides, or payload hold-down mechanisms.

Actuators

The actuators, shown mounted off each of the two end sections, are comprised of 15° permanent magnet stepper motors driving through a spur gear train onto ring gears mounted on each of the swash-plates. The motors have an in-line double stacked arrangement such that each motor has a double length rotor and a full set of redundant windings.

The gear ratio is 701:1 from motor shaft to ring gear which, in conjunction with the swash-plate geometry, gives a typical output step size of 0.0008° for each motor step. This high gear ratio also provides a high output torque (>350Nm), permitting a slew rate of 0.24°/sec to be applied to a load of 50kg m^2. The fact that the mechanism is stiff as well makes it suitable for the pointing of complete antennas incorporating relatively stiff 'flexible waveguides'.

Since the actuators prevent back-driving even during launch conditions, no launch lock is needed. As a consequence no pyrotechnics are needed.

Position Sensors

Two-pin contact encoders mounted off the end-plates allow the position of the swash-plates to be determined. The encoders mesh with the ring gears on the swash-plates via a two-pass gear and have a resolution equivalent to 2 motor steps. In addition to the contact encoders, two pairs of redundant optical pick-offs identify the '(0.0)' reference position (where the pointing vector is aligned with the z-axis). These sensors have an accuracy equivalent to ±3 motor steps and provide back-up information in the event of encoder failure or an alternative means of datum identification for applications where encoder information is not required.

THERMAL DESIGN

Pointing mechanisms are normally mounted in exposed conditions, and while the base of an APM may benefit from the relatively controlled temperature of the satellite body, the payload or antenna interface was taken as -170°C to + 120°C and that of the satellite top floor as -20°C to -50°C.

For a satellite-mounted application, the thermal control is completely passive. Thermal insulation is placed between the mechanism and the payload and the mechanism is surrounded by multi-layer insulation. Thermal straps assist the dissipation of heat from the motor so that in the extreme case gradients are limited to:

- 6°C through the main bearings
- 10°C between adjacent swash-plates or end-plates
- 2°C radially across the APM.

For a boom-mounted application, without power supplied to the motors the mechanism can reach very low temperatures. In that case it is necessary to employ heaters either to retain acceptable 'start up' temperatures, or to provide a warm-up capability prior to a re-pointing activity. The motors may act as heaters. In operation the variation in temperatures is expected to have very little impact on the mechanism performance.

OPERATIONAL CHARACTERISTICS

As already described, the High Stability Pointing Mechanism operates in an essentially polar-coordinate fashion such that where the rotation of the two swash-plates is defined by the angles θ_1 and θ_2 the pointing angle of the mechanism in cartesian coordinates is defined by:

$$x = \alpha(\sin \theta_1 - \sin \theta_2)$$

$$y = \alpha(\cos \theta_1 - \cos \theta_2)$$

where α is the swash angle on each of the rotating sections.

For simple open loop repointing it is quite straightforward to calculate the values of θ_1 and θ_2 required and drive the swash-plates to the desired positions on command from the ground. However, in closed loop operation where an RF sensor is employed, it is necessary to respond automatically to the error signals generated in the cartesian axes of the sensor. In this case a number of command strategies are possible.

In a generalised case, where an APM is required to trim about a number of alternative RF beacons, use is made of the quasi-orthogonal nature of the nod and sweep motions. These motions are inclined to the RF sensor axes and an on-board microprocessor is employed in the control electronics to perform the necessary conversion. This is greatly simplified by the use of the algorithm:

$$\Delta\theta_1 = Ae_x + Be_y$$

$$\Delta\theta_2 = Ce_x + De_y$$

where e_x and e_y represent the errors in x and y directions and A, B, C and D are four constants inputted to the electronics by telemetry. These depend on the location of the trimming position within the pointing range and can either be obtained from the encoders or estimated independently. The encoders are not necessary for trimming operations.

This technique allows trimming at any point within the pointing range other than at the centre or at the edge. These 'no-go' areas exist because of reduced slew rates at these positions due to the harmonic character of the pointing vector movement. For a mechanism with a pointing range of 4.3° radius and slew rate requirements of 0.1°/sec. of the boresight the operating range is within an annulus of between 0.7° radius and 4.2° radius.

In a more realistic situation, the trimming position required is fixed and known in advance. Referring to Figure 2, the intersection of the B locus and the C locus at point P represents a point where the two motors, acting independently, comprise their own quasi-cartesian coordinate system. These axes may be chosen to be coincident with the RF axes and thus a simple control system can be achieved. This control philosophy is currently proposed for the European Communication Satellite L-SAT.

While, for trimming operation, the nominal pointing direction is obliged to be off-set from the centre of the range, for re-pointing duty it is advantageous to make the nominal pointing direction coincident with the z-axis or zero reference position. This permits the added feature of a controlled 'return to zero' capability with a single actuator. Since with power off the mechanism will remain fixed, all pointing mechanisms on a spacecraft can be controlled by one electronics unit which multiplexes between them.

TEST RESULTS

A prototype model of the High Stability Pointing Mechanism has been constructed and tested by British Aerospace. It was constructed using commercial standard, off-the-shelf, components for the main bearings and motors. The structural elements were made from aluminium.

Typical results of the test are given in Table 1. Given that the clearance present in the commercial standard bearings employed is theoretically capable of contributing an error of up to ±0.028° without taking into account other error sources such as bearing and housing runout, the results show that the design is inherently highly accurate. In these tests the preload exerted by the bellows tends to compensate for the effects of bearing clearance. Based on these results and supporting analyses, the expected accuracies are given in Table 2. The prototype HSAPM is shown in Figure 5.

PERFORMANCE

Table 3 summarises the main features of the High Stability Pointing Mechanism and its performance. The present design utilises a 2.15° swash angle and 7 inch diameter bearings. However both of these parameters may very easily be changed, thus allowing the pointing range to be greatly extended and the strength and stiffness of the mechanism to be increased dramatically.

The ability to provide a central aperture is a significant advantage for some payloads and, in the case of a steerable antenna dish, is ideally suited to the use of a cassegrain-type feed where defocussing due to re-pointing is avoided.

The incorporation of the pin contact encoder is optional. This is primarily an instrumentational feature since it is not essential for either the trimming or re-pointing duty. A significant reduction in both mass and complexity of the mechanism, compared with other concepts, has been gained by obviating the need for a launch-lock device and a separate fail-safe, return-to-zero facility.

CONCLUSIONS

The High Stability Pointing Mechanism is a new conceptual design which provides a simple and rugged mechanical interface between two structures (see Figure 6) and which is capable of orientating those structures relative to one another on demand. With its high strength, high-stiffness torque output and accuracy the mechanism has been designed to suit a wide variety of applications including antenna pointing for which the mechanism is to be employed on L-SAT (see Figure 7). The pointing range will be increased to 8.6° radius for the L-SAT application.

REFERENCES

1. Thermal Vacuum Tests on the Engineering Model MSDS APM by J.C. Anderson, ESRO(ESTL)15.

2. Systeme d'Orientation Fine D'Antenne by B. Hubert and P. Brunet, Proc. 15th Aerospace Mechanisms Symposium, May 1981.

3. An Antenna Pointing Mechanism for Large Reflector Antennas by H. Heimerdinger, Proc. 15th Aerospace Mechanisms Symposium, May 1981.

TABLE 1 - EXPERIMENTAL POINTING ERRORS

$E\theta_x$	$E\theta_y$
0.002	0.007
0.016	0.001
0.016	0.023
0.010	0.041
0.007	0.017
0.012	0.000
0.005	0.007
0.008	0.004
0.002	0.005
0.008	0.012
0.017	0.000
0.001	0.015
0.002	0.005
0.000	0.000
0.003	0.001
0.018	0.022
0.010	0.020
0.033	0.029
0.015	0.005
0.007	0.013
0.003	0.015
0.006	0.008
0.005	0.009
0.002	0.010

TABLE 2 - HSAPM POINTING ACCURACIES

MODE	ACCURACY
Trimming mode with RF sensor	± 0.006°
Repointing using encoder	± 0.0080°
Repointing (open loop) with encoder set datum	± 0.0085°
Repointing using pipper	± 0.01°
Steady state pointing	± 0.0080°
Launch configuration (relative to interface)	± 0.0080°
Failsafe mode using encoder	± 0.0080°
Failsafe mode using pipper (This assumes use of the encoder on the failed section).	± 0.0094°

For all modes other than the trimming mode the pointing accuracy will be governed by structural component accuracy, bearing run-out, thermal distortion, system backlash and motor step size. The accuracy for these modes is, therefore, dependent on whether it is the encoder or pipper that is used.

TABLE 3 - HSAPM PERFORMANCE CHARACTERISTICS

Mass	:	< 4.2kg , depending on configuration
Dimensions	:	100mm height 235mm diameter
Interface fixation	:	6, M5 bolts on 190mm PCD (antenna) 6, M5 bolts on 215mm PCD (Spacecraft)
Design life	:	10 years continuous trimming duty
Position sensors	:	Pin contact encoder (non-redundant) ± 0.008° Optical datum (redundant) ± 0.01°
Pyrotechnics	:	None
Control aperture	:	Up to 40mm
Load capability (individually applied)	: :	20,000 N axial 8,000 N radial 450 Nm cross axis moment
Ground running capability (individually applied)	: :	4,000 N axial 1,800 N radial 60 Nm cross axis moment
Payload inertia	:	Up to 50kgm^2
Stiffness	:	140×10^6 N/m longitudinal 120×10^6 N/m lateral 450×10^3 Nm/rad cross axis rotation 730×10^3 Nm/rad torsional
Output torque	:	>350 Nm
Swash angle	:	2.15 deg. (4.3 deg for L-SAT)
Pointing range	:	Radius of 4.3° (8.6 deg for L-SAT)
Step size	:	0.0008° from each swash-plate
Slew rate	:	Up to 0.24°/sec.
Accuracy	:	See Table 1
Power consumption	:	Trimming 4W/motor Repointing 4W/motor Steady state pointing 0W/motor
Failsafe return to zero	:	Available for repointing applications

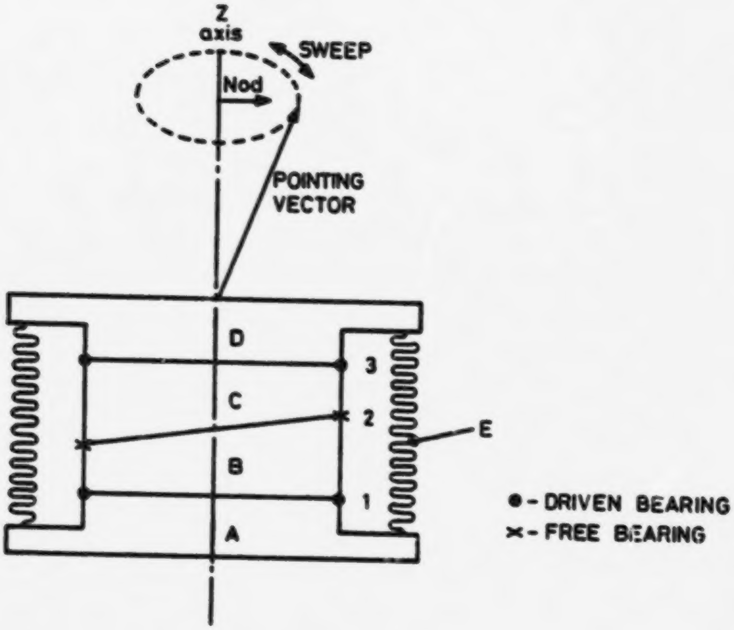
Z
axis
SWEEP
Nod
POINTING
VECTOR
D
C
B
A
3
2
1
E
● - DRIVEN BEARING
× - FREE BEARING

SWASH PLATE POINTING MECHANISM
PRINCIPLE OF OPERATION

FIGURE 1

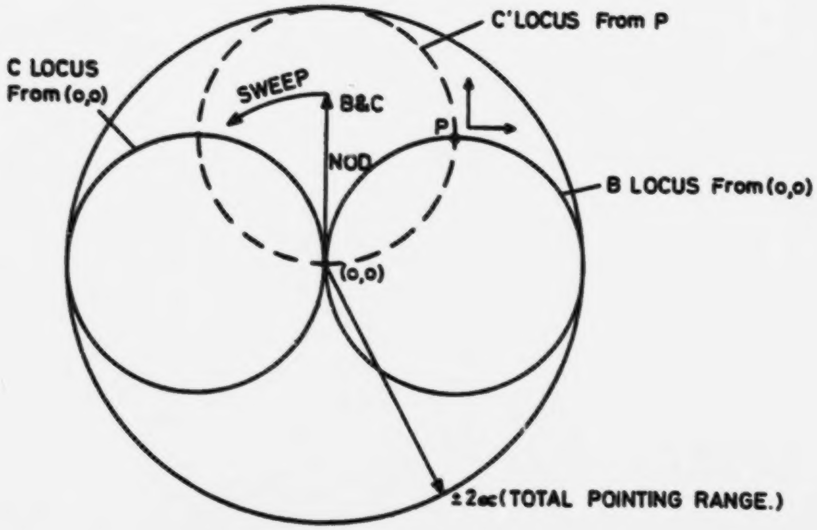
C'LOCUS From P
C LOCUS
From (o,o)
SWEEP
B&C
P
NOD
B LOCUS From (o,o)
(o,o)
±2α(TOTAL POINTING RANGE.)

LOCUS OF POINTING VECTOR DUE TO ROTATION
OF SWASH PLATE

FIGURE 2

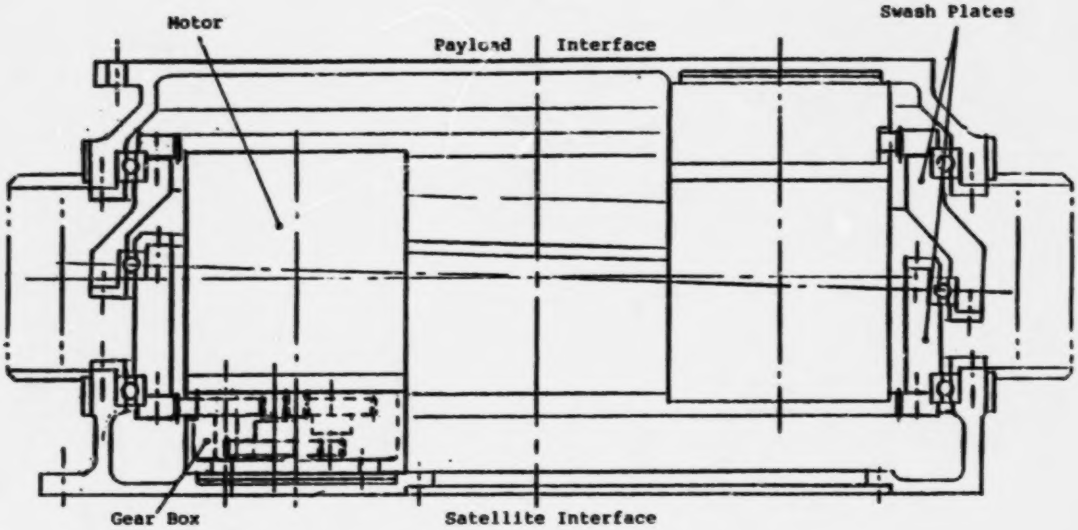
Motor
Payload
Interface
Swash Plates
Gear Box
Satellite Interface

CROSS SECTIONAL VIEW OF HSAPM FIGURE 3

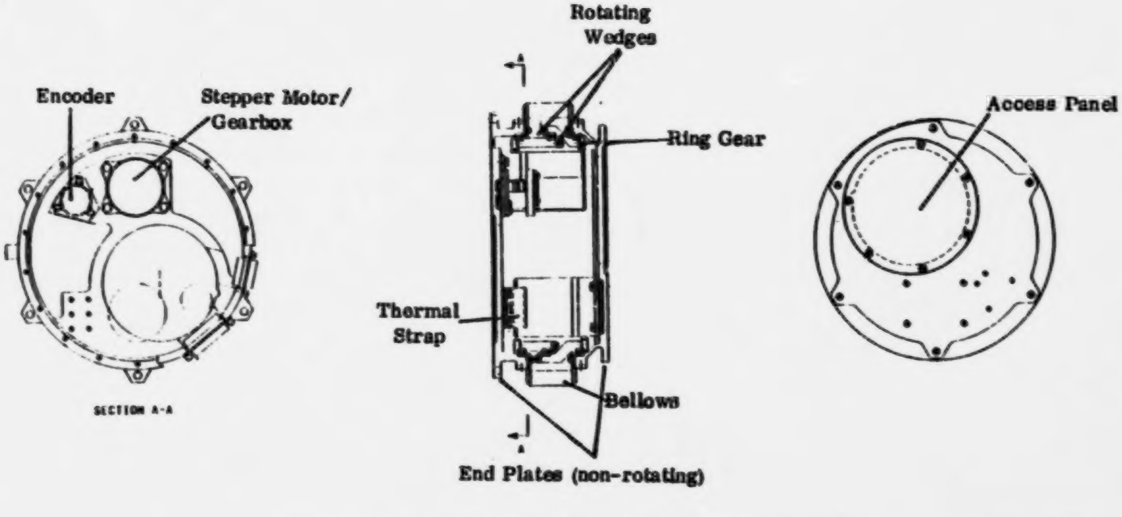
Encoder
Stepper Motor/ Gearbox
SECTION A-A
Rotating Wedges
Ring Gear
Thermal Strap
Bellows
End Plates (non-rotating)
A
Access Panel

HIGH STABILITY ATTITUDE POINTING MECHANISM FIGURE 4

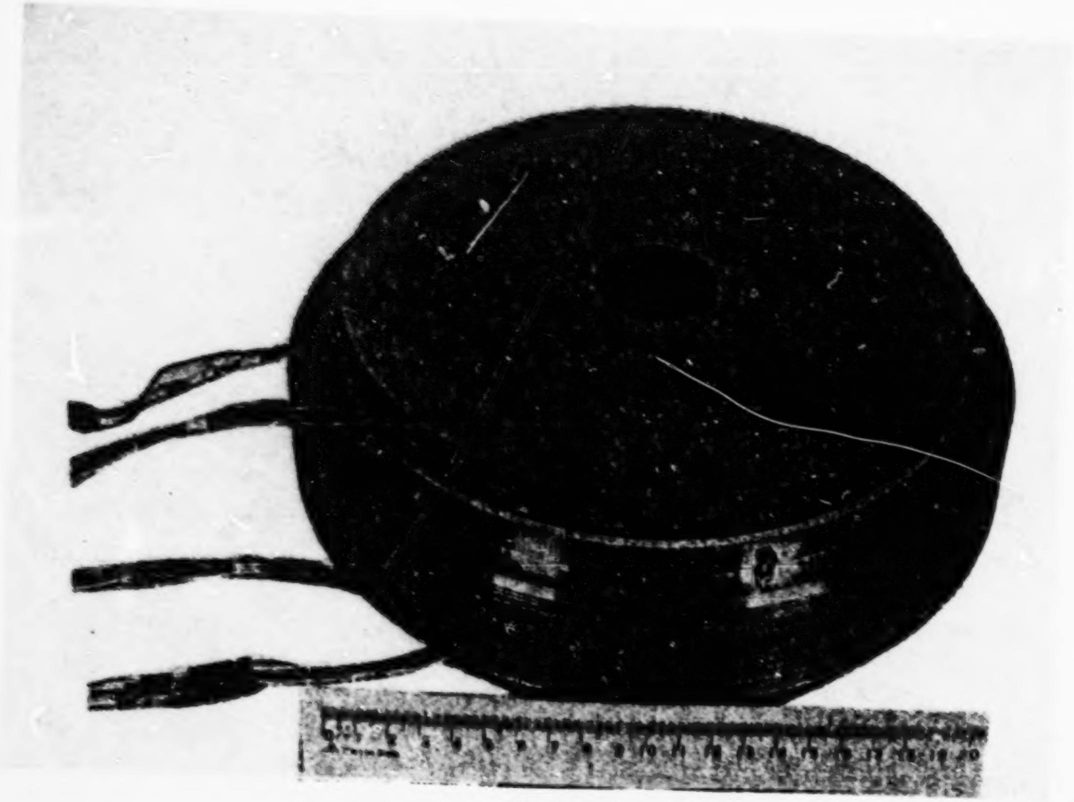

PROTOTYPE HASPM FIGURE 5

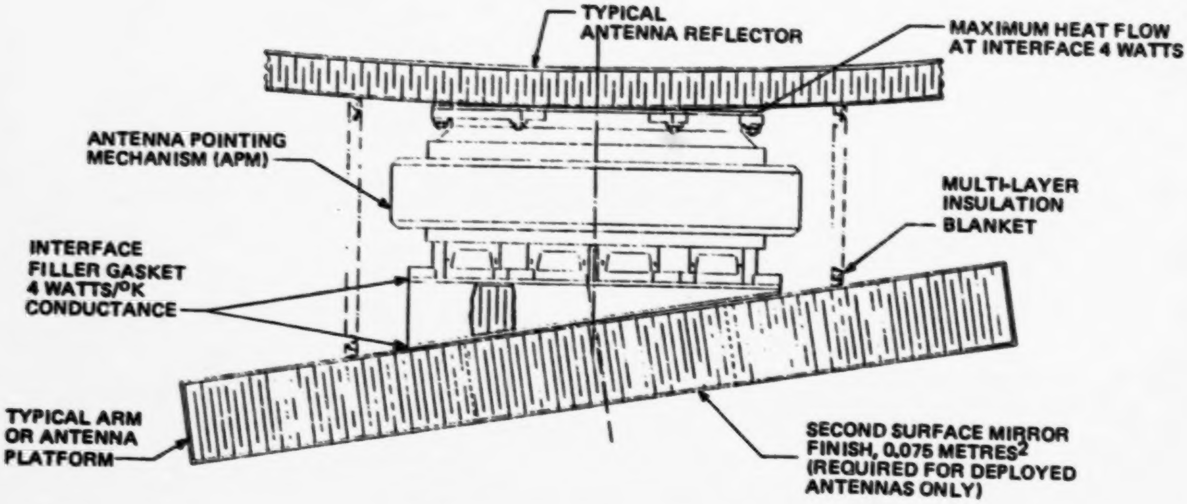
TYPICAL ANTENNA REFLECTOR
MAXIMUM HEAT FLOW AT INTERFACE 4 WATTS
ANTENNA POINTING MECHANISM (APM)
MULTI-LAYER INSULATION BLANKET
INTERFACE FILLER GASKET 4 WATTS/°K CONDUCTANCE
TYPICAL ARM OR ANTENNA PLATFORM
SECOND SURFACE MIRROR FINISH, 0.075 METRES^2 (REQUIRED FOR DEPLOYED ANTENNAS ONLY)

TYPICAL HSAPM INSTALLATION FIGURE 6

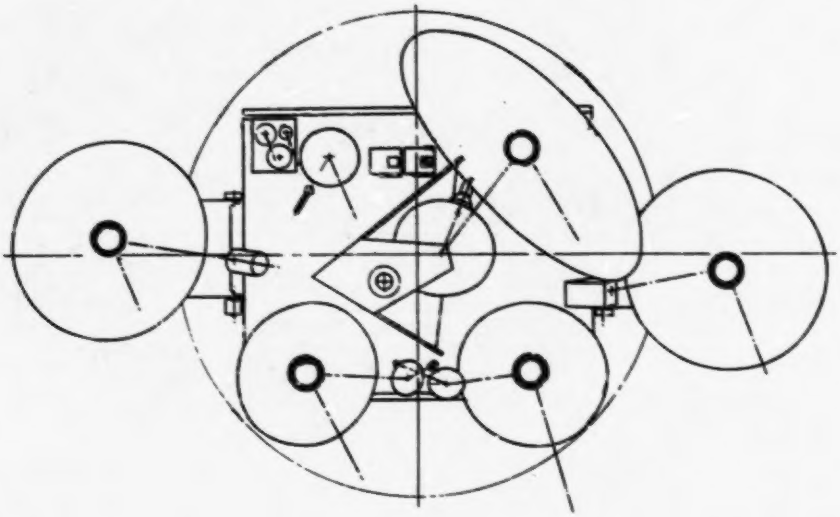

L-SAT CONFIGURATION (5 APM's SHOWN) FIGURE 7

A. J. D. Brunnen
British Aerospace Public Limited Company
Argyle Way
Stevenage, Herts. SG1 2AS
England

Mr. Brunnen has been employed by British Aerospace Dynamics Group, Space and Communications Division, since September 1980. Since joining the company, he has been working on the design of the swash plate pointing mechanism and is currently project leader for the antenna pointing subsystem on the European Communication Satellite, L-SAT. Mr. Brunnen graduated with an Honours degree in Engineering Technology from Robert Gordons Institute of Technology in Aberdeen, Scotland, in 1980.

Co-author of this paper is Mr. R. H. Bentall who is with the European Space Agency (ESTEC), The Netherlands.

Blank Page

COMPUTER-AIDED DESIGN AND ANALYSIS OF MECHANISMS

Frank L. Knight
The Aerospace Corporation

SUMMARY

This paper presents a short introduction to the computer programs which have been developed to assist in the design and analysis of mechanisms. A survey of the various types of programs which are available is given, and the most widely used programs are compared. The way in which the programs are used is discussed, and demonstrated with an example.

INTRODUCTION

Traditional mechanism design methods, both graphical and analytical, can be very complex and time consuming for all but the most simple mechanism systems. Computer software packages facilitate the automation of the trial-and-error process inherent in the design of mechanisms. Instead of cranking through equations by hand, the mechanism designer or analyst can specify characteristics of the mechanism and use the computer to calculate the kinematic and/or dynamic quantities of interest. Two-dimensional pin and paper models used to visualize the operation of proposed designs can be replaced by two- or three-dimensional dynamic visual models shown on a graphic computer terminal. The effect of design changes can be easily seen, and so the time required to develop the desired mechanism is greatly reduced.

Since the late 1960's, many computer programs for mechanism analysis have been developed. A number of these programs have been developed within particular companies and so are proprietary and not generally available. Other programs have been developed for a very specific application and thus are not very useful for general mechanisms work. There are, however, a handful of general programs which are enjoying widespread industrial use, and are actively marketed and maintained commercially. These programs are the subject of this paper.

PROGRAM SURVEY

Table I presents a summary of the characteristics of several of the most commonly used general-purpose mechanism analysis programs. At present, the programs which appear to be in widest use for general kinematic and dynamic analysis are known as ADAMS (for Automatic Dynamic Analysis of Mechanical Systems), DRAM (Dynamic Response of Articulated Machinery) and IMP (Integrated Mechanisms Program). These and other analysis programs operate on similar, but different, analytic principles, the details of which may be found in Reference (1). Of these programs, only ADAMS and IMP have been implemented for three-dimensional systems. A "two-dimensional" package, however, does not require that all of the links of the mechanism being designed must be contained completely in a single plane, but rather that all motions of the mechanism take place in parallel planes. For a large number of mechanisms, this is not a serious restriction, and the two-dimensional formulation provides advantages in computing speed and model simplicity.

ADAMS, IMP, and DRAM are used for the analysis of a mechanical system which has already been designed. These programs are distinctly different from packages which have been developed to assist in the synthesis of mechanisms. Table II compares three of these programs, KINSYN (Kinematic Synthesis), LINCAGES (Linkage Interactive Computer Analysis and Graphically Enhanced Synthesis Package), and MECSYN (Mechanism Synthesis). These programs provide the designer with a "family" of possible solutions to a design problem involving mechanisms which may be modeled as four-bar linkages (pin and slider-jointed planar mechanisms). They do not, however, lend themselves to more general mechanism systems.

Table III is provided as a summary of other more specialized mechanism programs. While these types of programs may be very useful for particular types of analyses, they do not lend themselves to more general mechanism systems. This paper will discuss the most widely used programs, ADAMS, IMP and DRAM, in more detail.

PROGRAM COMPARISONS

In comparing mechanisms programs, one should first attempt to determine for what types of problems the program selected will eventually be used. A three-dimensional program may be necessary for some applications, but a two-dimensional analysis may be sufficient for a wide class of problems. Of course, it is important to determine whether the intended use is one of design analysis or design synthesis, since both types are available.

Beyond distinctions in type, there are other more subtle differences. The most general programs, IMP and ADAMS, offer certain advantages. IMP is less expensive, but ADAMS appears to be more powerful, especially with respect to graphic capabilities. IMP is particularly good in detecting "lock-up" configurations. Both offer a similar menu of joints which may be used to connect the system components. The languages used in IMP and ADAMS to input the geometry of the model are similar. In contrast, programs such as DYMAC use standard computer languages (e.g., FORTRAN).

A major difference in the way these programs operate is that IMP is formulated to analyze systems composed of linkages comprising "closed" kinematic loops, while ADAMS permits open loops. Dummy loops, with masses and stiffnesses equal to zero, may be used in IMP to connect free links to ground. For some types of analyses, the use of dummy loops may not be desirable because of the resulting increases in model complexity and computing time. For aerospace applications, the requirement that all components be connected to ground is particularly inconvenient.

DRAM is similar to ADAMS, mainly because these two programs were developed by the same people. DRAM is two dimensional, however, and so has considerably greater computing speed. It is also a good deal less expensive. A unique feature of DRAM is its generalized impact modeling capability.

PROGRAM USAGE

ADAMS, IMP and DRAM rely heavily on interactive graphics for presenting the results of the design session. In using programs such as these, however, it is first necessary to model the system geometry using alphanumeric program statements. This geometry is not the physical geometry of the system, but rather the kinematic geometry. The distinction is that many details of the physical geometry may be unrelated to the way the mechanism behaves kinematically. The kinematic "shape" of a linkage is defined by the points at which it is connected to other system elements and by its inertial properties. The actual physical shape of the linkage is unimportant unless the shape would cause a condition such as interference.

In addition to describing the kinematic geometry, specification of the forces and constraints which act on the system is necessary to complete the system model. This includes the types of joints which connect the system components, spring stiffnesses, damping constants, and externally applied forces and torques. A wide variety of joints may be used to connect the system components. For example, ADAMS allows the following types of connections: ball joints, U-joints, revolute (pinned) joints, translational contact, cylindrical joints, gear contact, screw joints, flat sliders, and rack-and-pinion gears. IMP offers a similar menu of joints.

Since DRAM is two dimensional, it is limited to translational and rotational contacts. Cam-and-follower-type contact is not currently available in any of the programs; however, this and other special situations may be simulated with user-written subroutines.

Forces and torques may be input as constants or as "conditional" values which only act under certain conditions. In this way, it is possible to model compliant members or simulate impact by specifying that certain forces act only when specific members are within a certain distance of each other.

The development of the system model and entering it into the computer comprises most of the work required to use the programs. The language used to describe the model is "user oriented," in that familiar terms are used to describe the system. For example, the ADAMS statement:

JOINT/3, REVOLUTE, I = 21, J = 14

defines a rotational joint, numbered 3, which connects previously defined points numbered 21 and 14. By using familiar terms such as this, it is intended to minimize the amount of computer programming experience which is required by the user. Once the system geometry is described, the program user is required to enter the initial conditions (displacements, velocities, etc.) for the mechanism, and define the time interval over which the analysis is to be performed. When the system has been fully described, the designer may run the program.

After the program has been run, the user may request a wide variety of graphical and alphanumeric outputs. The most descriptive output feature for kinematics is the computer graphics which is available; however, it will be shown that many other types of useful results can be obtained.

EXAMPLE

As an example of computer-aided mechanism analysis, consider the automobile suspension shown (without its tire or the automobile frame) in Figure 1. An ADAMS model of the suspension was created to examine the kinematic and dynamic properties of the suspension. The model consisted of five major parts with twelve degrees of freedom. Compliance effects were included by modeling the tire stiffness and damping effects, and two mechanical stops, four bushings, a spring and a shock absorber. Also included in the model were three ball joints, one universal joint and rack-and-pinion steering. Figure 2 depicts the computer graphics model created for this suspension. The graphics serve two purposes: verification of the correctness of the input model, and easier interpretation of the simulation results. By combining suspension models with a rigid body model of a truck body, it is possible to model the total vehicle, as depicted in Figure 3. Using the computer graphics model, it is possible to determine the response of the total vehicle without ever building a prototype.

The graphic output may be manipulated in a number of ways. The graphic model shown at various times may be superimposed on one view as in Figure 3, or each interval of time may be viewed individually. The view may be rotated, or zoomed in or out. It is also possible to show three orthographic views, either at individual time increments, or superimposed. This is demonstrated in Figure 4 with a robot arm. By using cameras which are computer controlled to take pictures of the graphics display at each time increment ("frame-by-frame"), it is possible to produce motion pictures which allow the response of the system to be viewed continuously throughout the time increment analyzed. This type of motion picture will be demonstrated at the symposium. Recently, new technology in computer graphics has made it possible to produce a similar graphic display directly on the computer terminal.

While graphic results are the most striking feature of these programs, other types of useful information may be obtained. The user may request plots or tabular listings of forces, displacement, velocities or accelerations as functions of time. An example of a plot produced by the IMP program is shown in Figure 5. These programs may also be asked to compute relative velocities, torques, static equilibrium positions, natural frequencies and the like. That these programs may be used with an alphanumeric terminal is an important economic consideration, since the cost of one of these terminals is quite a bit less than that of a graphics terminal.

While the example discussed previously is from the automotive industry, the use of mechanism analysis programs in aerospace applications is particularly advantageous since the analyst is able to simulate conditions of zero gravity. Since one can "turn off" gravity effects, simulations of mechanical systems which could not be tested on the ground can be performed. The programs have been used to analyze the performance of numerous aerospace systems such as landing gears, ailerons, airplane doors and deployable booms. The interactive nature of the programs allows the designer to quickly determine if a candidate design is able to fulfill the requirements of the desired mechanism. The kinematic properties of the system are clearly seen and the effect of design changes are immediately evident. Consequently, the time required to design a mechanism is reduced and the number of options which may be examined is greatly increased.

CONCLUSIONS

An introduction to the types of programs which are available has been given and some quick comparisons of the most widely used have been made. It has been shown that ADAMS, IMP, and DRAM are the most complete programs for mechanism work, and offer a comparatively wide range of analysis capabilities. Each of the programs offers certain advantages to the user, depending on the type of mechanism to be designed or analyzed. For more details on the programs, the reader is directed to References 1 through 15.

TABLE I

GENERAL ANALYSIS PROGRAMS

	ADAMS	DRAM	DYMAC	IMP	UCIN
Dimensionality	3-D	2-D	2-D	3-D	3-D
Capability	General mechanical systems*	General mechanical systems*	Closed-loop systems	Closed-loop systems*	Open-loop systems
Available from	Mechanical Dynamics, Inc., Ann Arbor, MI	Mechanical Dynamics, Inc., Ann Arbor, MI	B. Paul, U. of Penn. Phil., PA	Structural Dynamics Research Corp. Milford, OH	Univ. of Cincinnati
Graphics	Yes	Yes	No	Yes	No
Availability	Time-share or lease	Time-share, lease or purchase	Purchase	Time-share, lease or purchase	Purchase
Features	Large problems. Open- and closed-loops OK. Excellent graphics. Good support.	Large problems. Open- and closed-loops OK. Excellent graphics. Generalized impact. Good support.	FORTRAN language. Inexpensive	Large probs. Very accurate kinematic results, easy to learn. Excellent documentation. Good support.	Simple Inexpensive
Limitations	No generalized impact. Manual difficult to understand.	Planar mechanisms only. Manual difficult to understand.	Planar mechanisms only. Closed-loops only. No graphics.	Closed-loops only. Somewhat limited graphics. No generalized impact.	Open-loops only. No graphics.

*See text

TABLE II

PLANAR SYNTHESIS PROGRAMS

	KINSYN	LINCAGES	MECSYN
Dimensionality	2-D	2-D	2-D
Capability	Kinematics design synthesis	Kinematics design synthesis	Kinematics design synthesis, dynamics
Available from	Prof. Kaufman, George Washington, Washington, DC	Prof. Erdman, University of Minnesota, Mineapolis, Minnesota	Prof. Myklebust, Florida Atlantic University, Boca Raton, Florida
Graphics	Yes	Yes	Yes
Availability	Time-share (available Spring 1982) or purchase	Time-share or purchase	Purchase or time-share
Features	Interactive, small version to run on Apple computer being developed. Will handle 4-, 6- or 8-bar mechanisms	Interactive Device independence	Interactive Ringed data structure Can specify time-dependent properties 4-, 6- or 8-bar mechanisms
Limitations	No dynamics	No dynamics 4-bar mechanisms only	Cannot display mechanism itself

TABLE III

SPECIALIZED MECHANISM PROGRAMS

PROGRAM NAME	APPLICATION	DEVELOPER AND/OR AVAILABLE FROM
AFL	Static force analysis of four-bar linkage system	Structural Dynamics Research Corp., Cincinnati, Ohio
CAMDES	Design of disk cams	K. W. Chase, Brigham Young Univ., Provo, Utah
CAMDYN	Design of plate cams	B. Paul, University of Penn., Philadelphia, PA
CAMPAC	Synthesis, analysis, and design of cams	Prof. D. Tesar, Univ. of Florida, Gainsville, Florida
COMMENT I	Generalized mechanical design system with linkage cam, gear, spring, shaft and timing-belt design progrmas	IBM Systems, Development Division, Rochester, MN
DKINAL	Dynamic analysis of machinery	Prof. B. Paul, Dept. of Mech. Eng., University of Penn., Philadelphia, PA
DYREC	Dynamic analysis of reciprocating machines with multiple sliders	Prof. B. Paul, University of Penn., Philadelphia, PA
FLYLOOP	Flywheel design	Prof. B. Paul, University of Penn., Philadelphia, PA
FORBAR	Kinematic and dynamic analysis of four-bar linkage systems	Structural Dynamics Research Corp., Cincinnati, Ohio
GODAS	Design of parallel axis gears	D. Hughson, Ford Motor Co., Dearborn, Michigan
IMAGE	Design and analysis of planar mechanisms	Reed and Garrett, University of Texas, Austin, Texas
ISD-FORSS	Force system structural synthesis of four-bar mechanism	Prof. Carson, University of Missouri-Columbia, Columbia, MO
KINAL	Kinematic analysis of planar multiple-loop mechanisms	Prof. B. Paul, University of Penn., Philadelphia, PA
SLIDER	Static and dynamic analysis of slider crank systems	Structural Dynamics Research Corp., Cincinnati, Ohio
STATMAC	Static analysis of planar machines	Prof. B. Paul, University of Penn., Philadelphia, PA

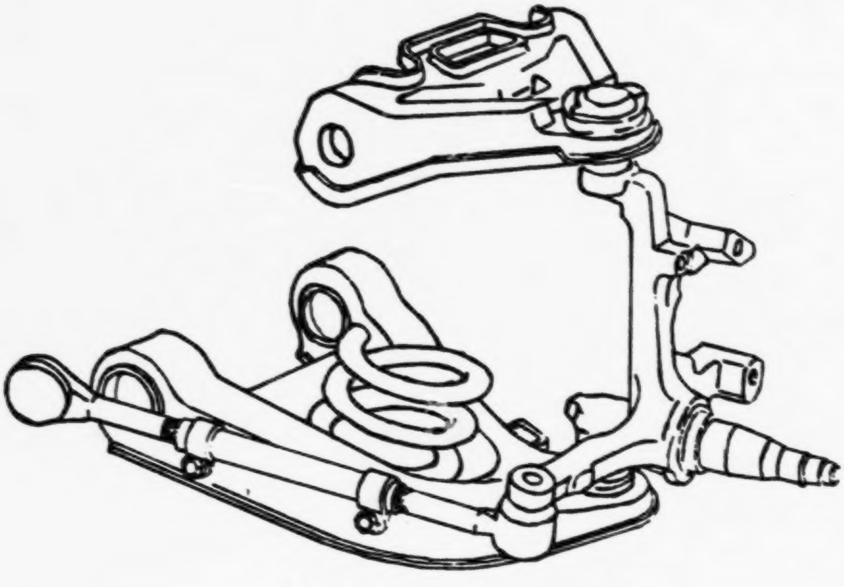

FIGURE 1 - SCHEMATIC OF AUTOMOBILE SUSPENSION
(WHEEL AND TIRE NOT SHOWN)

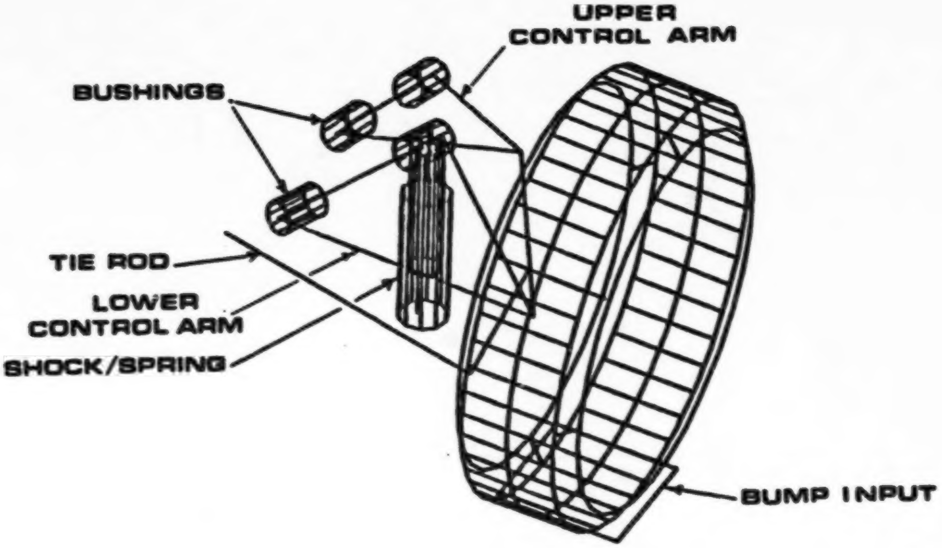
UPPER
CONTROL ARM
BUSHINGS
TIE ROD
LOWER
CONTROL ARM
SHOCK/SPRING
BUMP INPUT

FIGURE 2 - ADAMS GRAPHICS MODEL OF SUSPENSION

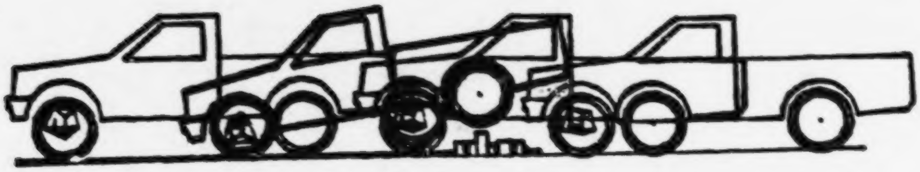

FIGURE 3 - TOTAL VEHICLE SIMULATION

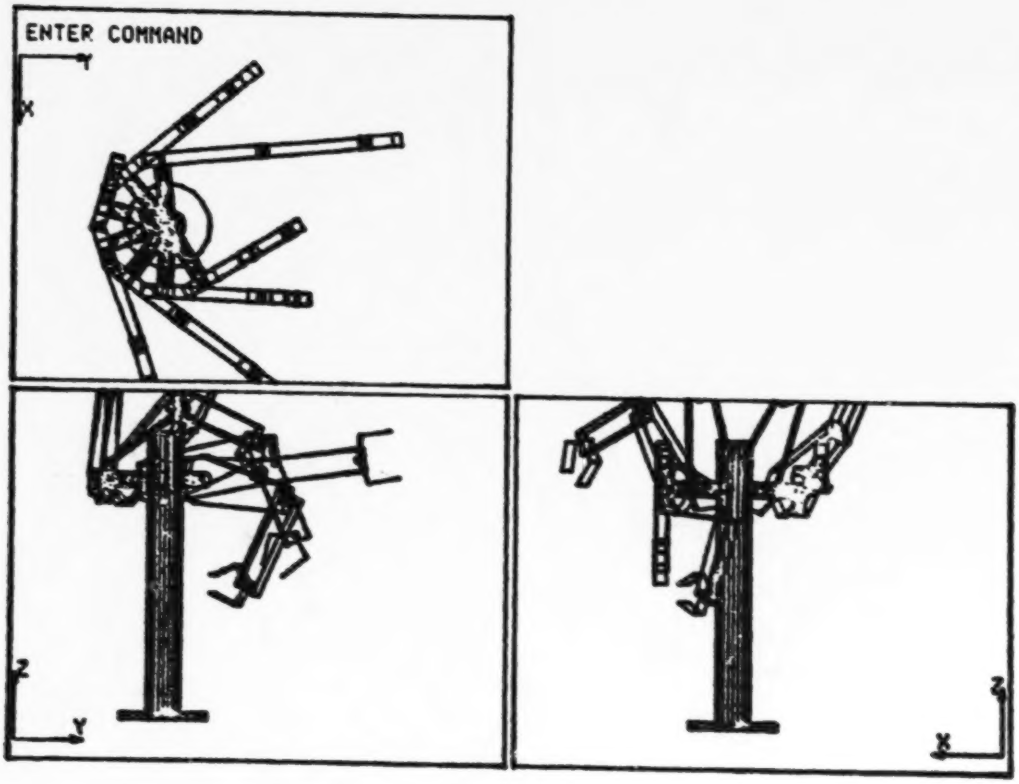
ENTER COMMAND
Y
X
Z
Y
Z
X

FIGURE 4 - SUPERIMPOSED ORTHOGRAPHIC VIEWS
OF A ROBOT ARM

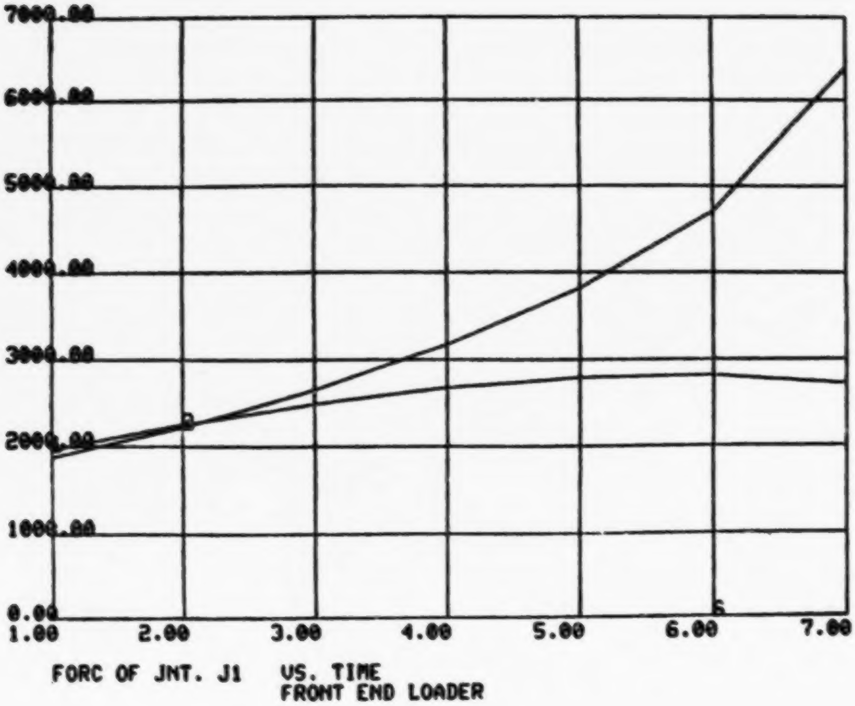

FIGURE 5 - IMP FORCE PLOT

REFERENCES

1. Paul, Burton, "Analytical Dynamics of Mechanisms - A Computer Oriented Overview," *Mechanism and Machine Theory*, 1975, Volume 10, pp. 481-507.

2. Shoup, Terry, *A Practical Guide to Computer Methods for Engineers*, Prentice-Hall Inc., Englewood Cliffs, NJ, 1979.

3. Paul, Burton, *Kinematics and Dynamics of Planar Machinery*, Prentice-Hall Inc., Englewood Cliffs, NJ, 1979.

4. *Users Guide to ADAMS*, Fifth Edition, Mechanical Dynamics, Inc., Ann Arbor, Michigan, 1981.

5. *Users Guide to DRAM*, Fifth Edition, Mechanical Dynamics Inc., Ann Arbor Michigan, 1978.

6. Sheth, P. N., Uicker, J. J., "IMP (Integrated Mechanism Program), A Computer-Aided Design System for Mechanisms and Linkages," ASME, *Journal of Engineering for Industry*, 1972, pp. 454-464.

7. *IMP - Integrated Mechanisms Program*, Structural Dynamics Research Corporation, Cincinnati, Ohio, 1979.

8. Erdman, A. G., Gustafson, J. E., "LINCAGES: Linkage INteractive Computer Analysis and Graphically Enhanced Synthesis Package," Design Engineering Technical Conference, Chicago, Ill., 1977, *ASME Paper No. 77-DET-5*.

9. Paul, B., "Dynamic Analysis of Machinery Via Program DYMAC," International Automotive Engineering Congress and Exposition, Detroit, Michigan, 1977, *SAE Paper No. 770049*.

10. Rubel, A. J., Kaufman, R. E., "KYNSYN III: A New Human-Engineered System for Interactive Computer-Aided Design of Planar Linkages," ASME, *Journal of Engineering for Industry*, May 1977, pp. 440-448.

11. Russon, V. K., Chase, K. W., "Computer-Aided Design of Disk Cams From Numerical Follower Motion Data," ASME Winter Annual Meeting, Chicago, Ill., 1980, *ASME Paper No. 80-WA/DSC-9*.

12. Sivertsen, O., Myklebust, A., "MECSYN: An Interactive Computer Graphics System for Mechanism Synthesis by Algebraic Means," ASME Design Engineering Technical Conference, Beverly Hills, CA, 1980, *ASME Paper No. 80-DET-68*.

13. Chuang, J. C., Strong, R. T., Waldron, K. J., "Implementation of Solution Rectification Techniques in an Interactive Linkage Synthesis Program," *ASME Journal of Mechanical Design*, 1981, pp. 657-664.

14. Carson, W. L., Oladiran, O. B., "An Interactive Computer Program for Force System Structural and Dimensional Synthesis," ASME Design Engineering Technical Conference, Beverly Hills, CA, 1980, ASME Paper No. 80-DET-61.

15. Kramer, S. N., Sandor, G. N., "Selective Precision Synthesis - A General Method of Optimization for Planar Mechanisms," ASME Paper No. 74-DET-68, 1974.

Frank L. Knight
The Aerospace Corporation
P.O. Box 92957
Los Angeles, California 90009

Mr. Knight joined The Aerospace Corporation in 1979 as a member of the Technical Staff in the Vehicle Engineering Division. He received his B.S. and Master of Engineering degrees from the University of South Carolina and is currently pursuing a Doctorate in Mechanical Engineering at the University of Southern California.

ESTIMATION OF BEARING CONTACT ANGLE IN-SITU BY X-RAY KINEMATOGRAPHY

by Peter H. Fowler* & Frank Manders**

The DSCS II Satellite consists of an earth-pointing platform carrying the transponder and antenna farm, mounted on a spinning section providing power and command. Attitude control and pointing are performed entirely in the spinning section. The whole satellite weighs about 650 kg.

The two sections are joined by the "despin mechanical assembly" (DMA), consisting of drive motors, slip rings, and a pair of ball bearings on which the spinning section revolves, all enclosed in a load bearing case (Fig. 1). The system is required to maintain precise earth pointing for at least five years at 60 rpm.

The need arose to measure the bearing contact angles in assembled units which had completed acceptance test. The usual bench methods of estimating contact angle are not applicable to a bearing assembled in an opaque case, and in any case the contact angle as assembled includes the effects of preload and assembly tolerance. Dismantling a flight-accepted unit is both costly and introduces program risk.

The usual methods of measuring bearing contact angle are the Turns method and by measuring internal clearance.

The Turns method is the most popular since it is fairly accurate, requires simple tooling and it can be performed in a relatively short time. This method provides free bearing, preloaded contact angle data. Three marks are located on the outer ring, inner ring and ball cage. These marks are initially aligned. The outer ring or inner ring is rotated a predetermined number of revolutions with the other ring restrained from rotation. The number of ball cage rotations is measured (whole number plus the fraction). The contact angle is then calculated by using the following equation:

$$\beta = \text{arc cos } \frac{E}{d} \left(1 - \frac{2N_E}{N_i}\right)$$

or

$$\beta = \text{arc cos } \frac{E}{d} \left(1 + \frac{2N_E}{N_o}\right)$$

where β is bearing contact angle
E is bearing pitch diameter
d is bearing ball diameter
N_E is number of ball cage revolutions
N_i is number of inner ring revolutions
N_o is number of outer ring revolutions

---

*Peter H. Fowler, TRW Space and Technology Group, Redondo Beach, CA 90278
**Frank Manders, Ball Aerospace Systems Division, Boulder, CO 80306

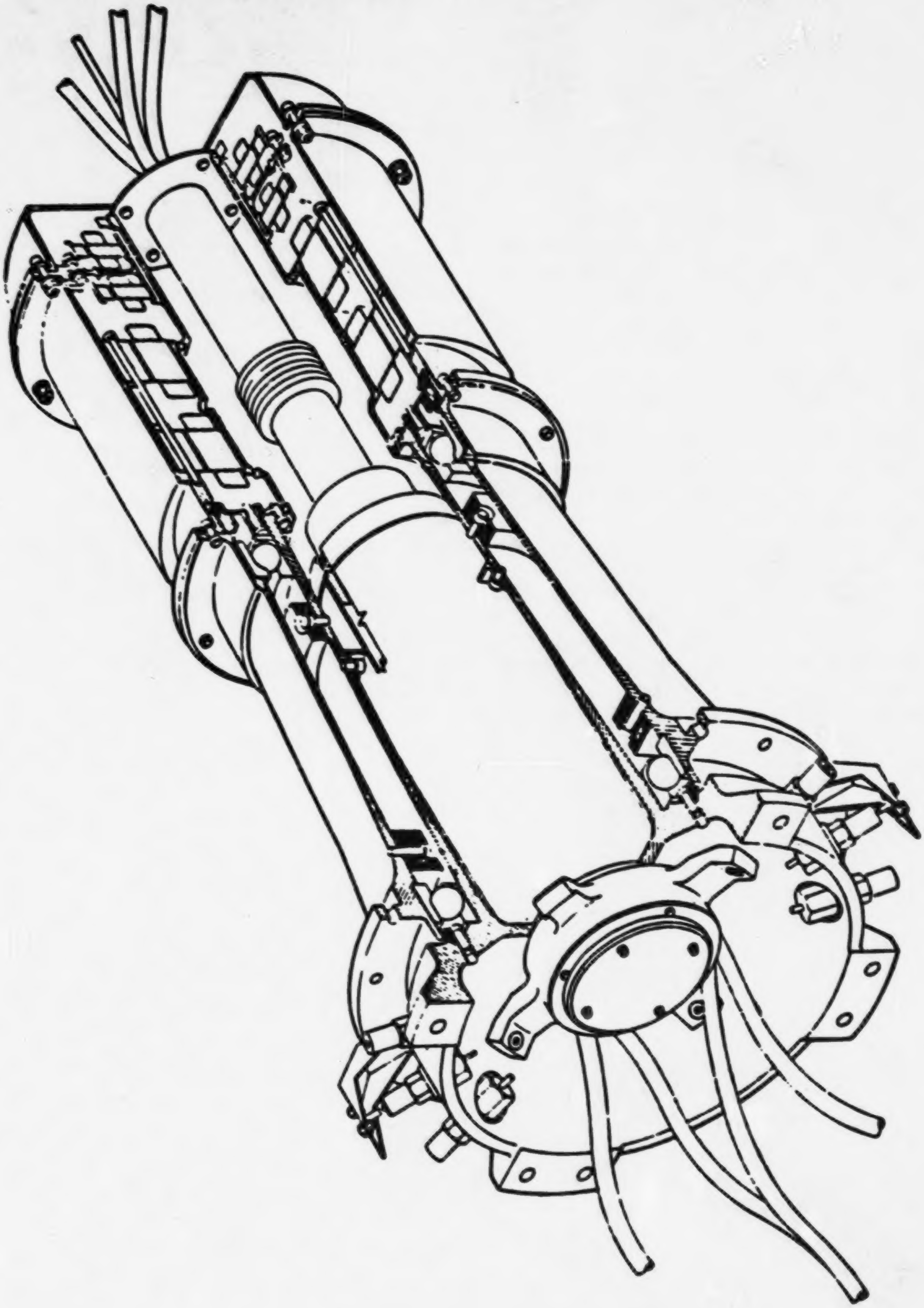

Figure 1. DMA Cutaway View

The internal clearance measurement determines the free bearing, unloaded contact angle. This method is generally used in small bearing production lines since it requires the least amount of time. The outer ring is held, while the inner ring is moved to its extreme radial positions. This motion (C) is measured and the contact angle is calculated by the following equation:

$$\beta = \text{arc cos } \left(1 - \frac{C}{2Bd}\right)$$

here C is the total diametral measurement (called radial clearance)
B is the total curvature constant = $f_o + f_i - 1$
f_o is the ratio of outer race radius to ball diameter
f_i is the ratio of inner race radius to ball diameter.

If, during installation on the shaft and in the housing, the bearing interfaces are slip fits and the bearing preload is equal to the gaged load of the free bearing measurement, the installed bearing contact angle will be as measured by either method. If, however, the bearing is installed with either or both of its interfaces press-fit and/or the preload is different from the gaged load, the mounted, preloaded contact angle is different from any free bearing measurement.

To complicate the situation, in most cases the bearings are not visible after installation in a device. Analysis can be performed to approximate the mounted preloaded contact angle, but this may result in errors of several degrees.

Our problem was to attempt to measure the mounted, preloaded contact angle of the structural bearings in the already assembly DMA.

Initially, it occurred to us that the contact angle could be measured by counter-rotating the inner and outer races at such a speed that the ball train is stationary, hoping to determine this point by x-ray observation.

The free bearing, preloaded contact angle can then be calculated from:

$$\beta = \text{arc cos } \frac{E}{d} \frac{(R_i - R_o)}{(R_i + R_o)}$$

where R_i is the speed of the inner ring
R_o is the speed of the outer ring.

This method is not normally used because the individual speeds or the speed ratio must be known to a high degree of accuracy (on the order of 50 parts per million) for reasonable ($\pm 0.25^o$) accuracy.

We proposed to construct a rather complicated device to counter-rotate the DMA shaft and housing and use this method to calculate the required contact angle.

We located an x-ray facility with a manipulator capable of mounting a DMA and with kinematic display capability. The facility is owned by Test Equipment Distributors, in Detroit. Not being familiar with the state of the art of this type of equipment, we were surprised at the clarity and definition with which moving parts could be seen. Figure 2 is a print of one frame of a video tape of the DMA in motion. The ball positions can clearly be determined with accuracy, even though, of course, the phenolic retainer position cannot be seen. A less complicated modification of the Turns method appeared practical.

Contact angle can be estimated by counting the number of balls passing a given point as a function of number of turns of the shaft. The Turns method is then modified as follows:

The angular distance between the leading edge of one ball and the leading edge of the following ball (ϕ) is:

$$\phi = \frac{360}{n} \text{ (degrees)}, \ \frac{2\pi}{n} \text{ (radians)}$$

where n is the number of bearing balls.

The total angle for ball train motion depends upon the number of balls observed passing a stationary point or:

$$\Theta_E = N\phi = \frac{360N}{n}$$

where N = the number of balls observed passing a stationary point.

The contact angle equation then becomes:

$$\beta = \text{arc cos } \frac{E}{d} \left(1 - \frac{720N}{n\Theta_i}\right)$$

where Θ_i = the shaft angle rotation in degrees.

Using this technique and estimating the bearing individual errors (d, E, Θ_E, Θ_i) the test accuracy can easily be determined.

For the purpose of illustration, let us use one of the DMA bearings as an example. The basic bearing parameters are:

d = 0.5 inch[1]
E = 5.14 inches
β = 15 degrees
n = 23 balls

Ball Diameter Variation

The selection of ball diameter is one of the primary methods of setting free-bearing gaged preload. Ball diameter variation for bearing of the approximate size as the example can vary by ±0.001 inch. The total variation within a single bearing, however, is 0.00001 inch. In our example, we have measured the basic ball size and therefore have knowledge to 10 microinches.

---

[1] Bearing dimensions and tolerances are given in inches, since the design and specifications were pre-SI and an arbitrary translation reduces clarity.

DSCS II
SPECTION
BALLS

Figure 2. Bearing Appearance on Video Monitor

Pitch Diameter Variation

Pitch diameter variation is the most difficult dimensional parameter to determine, since it is made up of several other dimensions which are not normally known by an aerospace applications engineer. For bearings of this size and quality, the range is ±0.001 to ±0.005 inch. For our bearing, the lower figure was used in the error analysis.

Ball Train Uncertainty

If we assume knowledge of the ball in the raceway to ±0.01 inch, the resulting error in ball train angle is about ±0.2 degree.

Shaft Angle Uncertainty

The interface fixture design will dictate the accuracy of shaft angle. If an optical encoder is used, the shaft angle error will be a small part of one degree. For our test, assume a reasonable potentiometer with a readout error of about ±0.25 degree.

Figure 3 shows the contact angle total error for the four parameters using our example bearing, counting 100 balls. This figure shows for equal uncertainty the ball position error is the more critical angular parameter and the ball diameter variation is the more critical dimensional error.

Figure 4 shows the total contact angle error as a function of the ball count and contact angle, for the expected parameters for the example bearing.

As can be easily seen, the contact angle accuracy improves with an increase in ball count and as the contact angle increases.

If we count 300 balls, the calculated contact angle will be accurate to approximately ±0.2 degree. If we increase the count to 700, the error will decrease to about ±0.1 degree. We are thus able to estimate the assembled bearing contact angle with excellent accuracy.

The measurement is made by mounting the assembly shaft on a rotating table, as shown in Figure 5. The x-ray source and imaging system are arranged to view the bearing at a convenient angle so that the balls can be tracked individually. Note that ideally the x-ray axis should be tilted rather than the device axis, as having the weight off-center alters the net preload and side-loads the bearings.

A ball position is marked on the viewing screen, and the shaft rotated slowly some preset number of times. The number of balls is counted, including the fraction. Alternately the shaft may be rotated until some preset number of balls has passed, and the total shaft angle read off. In principle the counting could be automated, but for an occasional measurement on a high-value device this is not worthwhile.

Using a modern image multiplier, the total x-ray dose is very small, insignificant compared with the energies and integrated fluxes of a life in orbit. Radiation damage to lubricant and other parts is thus not a factor in the measurement.

The DMA has a beryllium housing and shaft, with stainless steel balls and races. The x-ray source for clear viewing of the ball positions is about 1 mA at 50 kV. A sharp focus x-ray source and imaging system is capable of showing ball position when the ball is as little as 2% of the total x-ray density. Thus, the measurement could be made as easily if the case and shaft were also stainless steel.

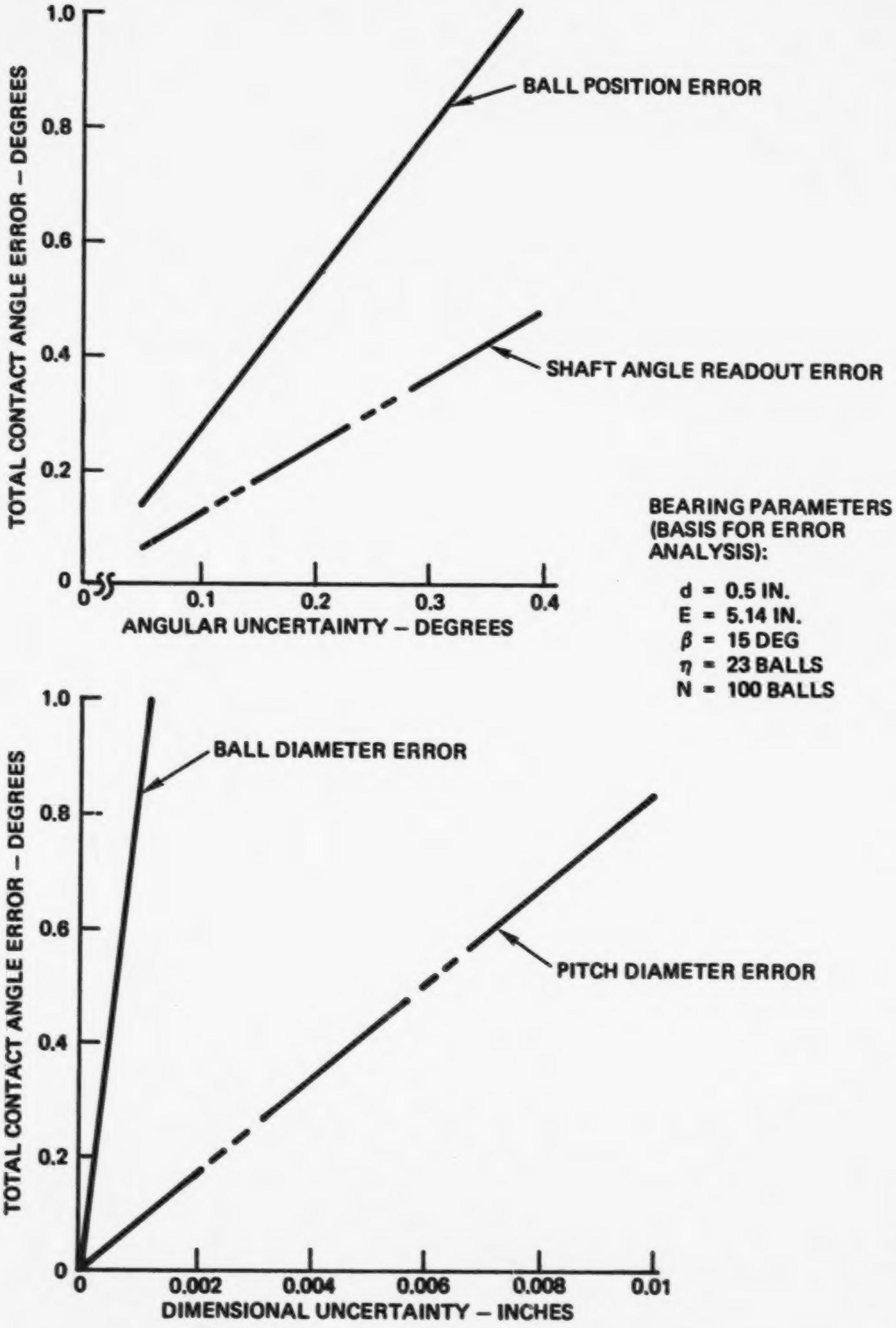

Figure 3. Effect of Measurement Uncertainty on Contact Angle Calculations

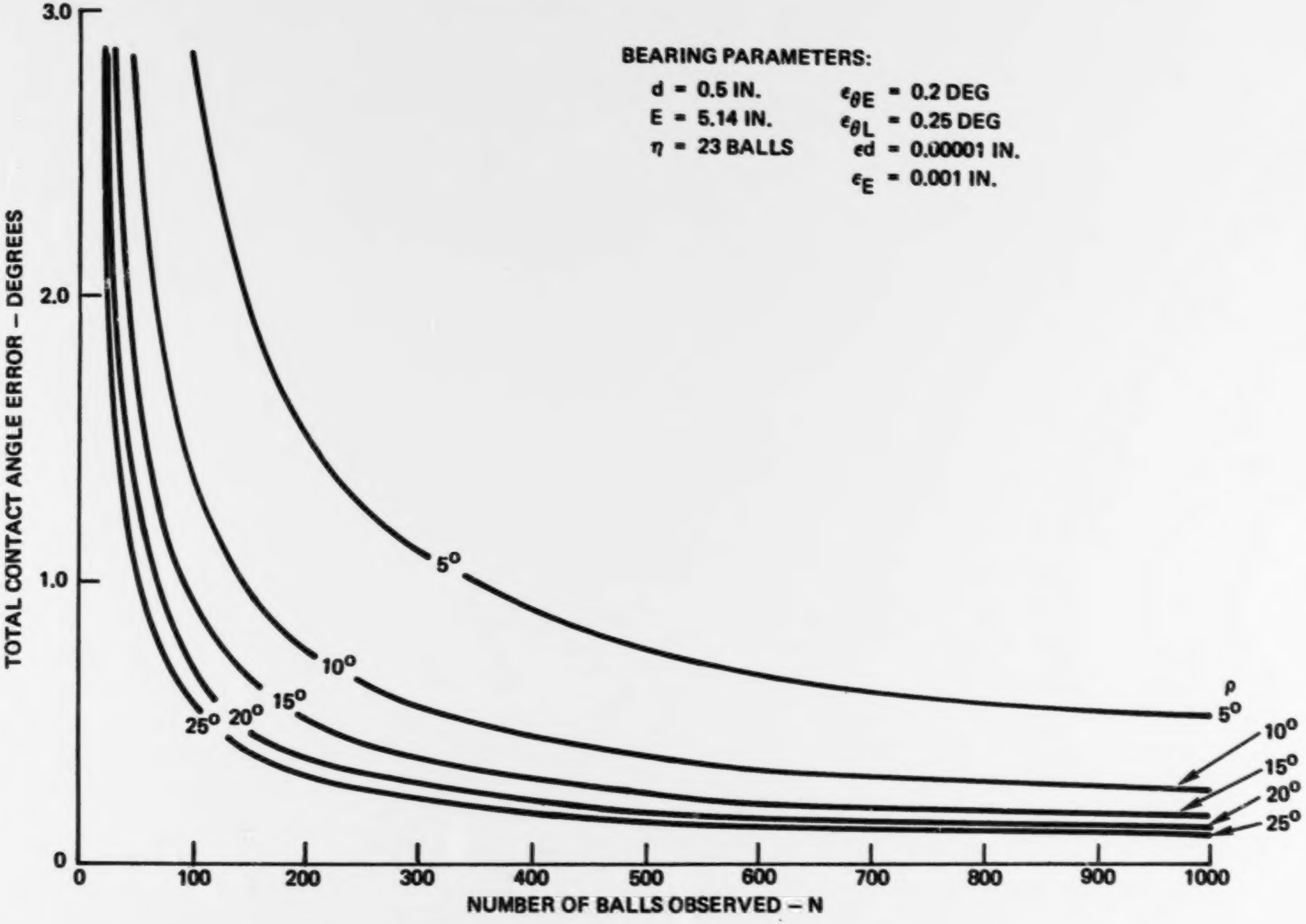

Figure 4. Effects of Ball Count on Contact Angle Calculations

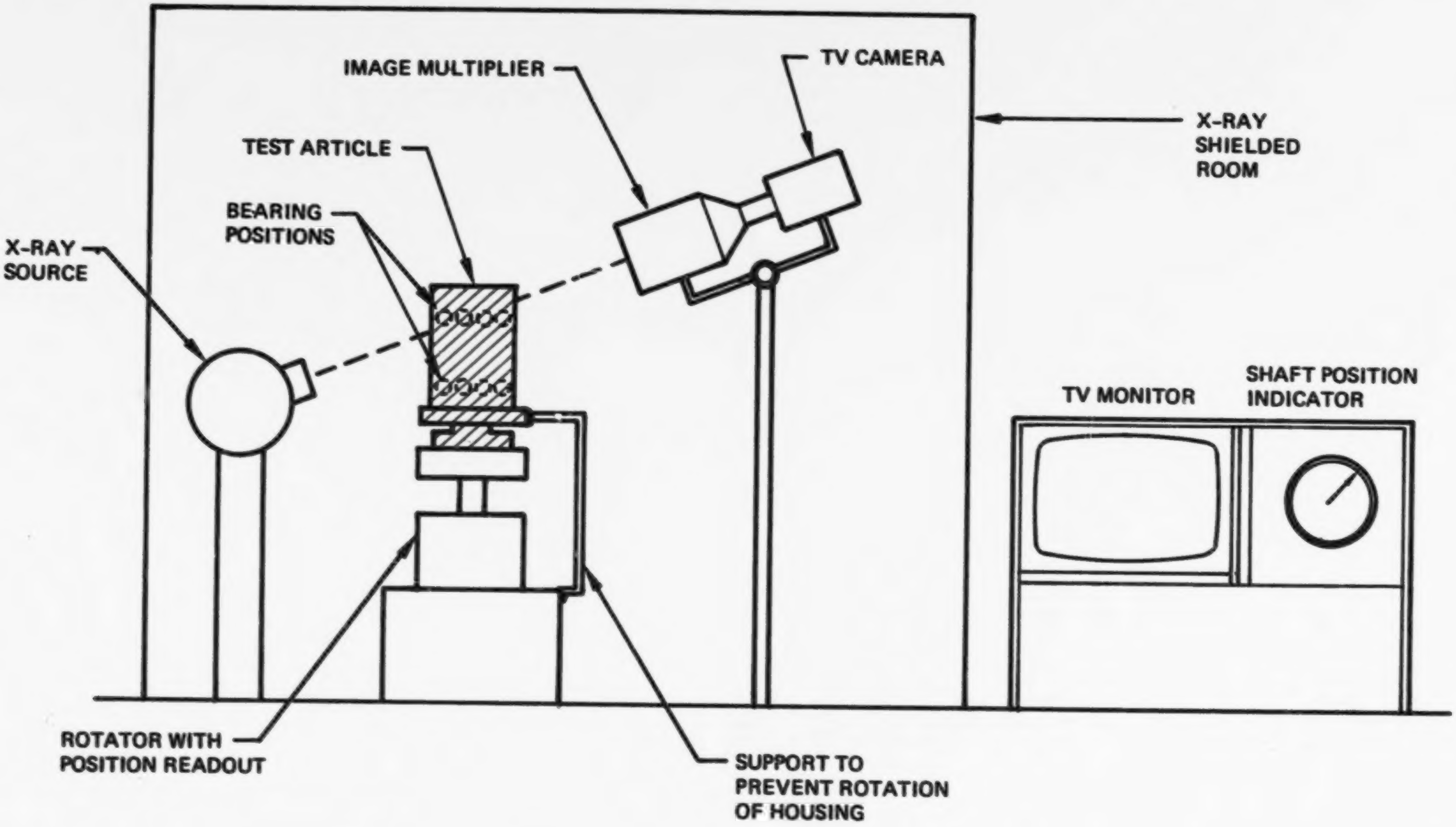
IMAGE MULTIPLIER
TV CAMERA
X-RAY SHIELDED ROOM
TEST ARTICLE
BEARING POSITIONS
X-RAY SOURCE
TV MONITOR
SHAFT POSITION INDICATOR
ROTATOR WITH POSITION READOUT
SUPPORT TO PREVENT ROTATION OF HOUSING

Figure 5. Measurement System

For the DMA, and other comparable-value equipment, it is good practice to make a simultaneous video tape of the monitor as this provides a record of the correctness of the ball count. Since the DMA has a large wire bundle coming out of each end and other connections with opportunity for interference, it is also wise to lock the case with tape or similar easily broken connection. If something hangs up, the case will then pull free and only the measurement is lost.

We suggest that the method described is useful in confirming capability of assembled units, and facilitates in-situ adjustment of preload to obtain a defined contact angle.

Peter H. Fowler
TRW Space and Technology Group
1 Space Park
Redondo Beach, California 90278

Mr. Fowler was educated in England, emigrating to the United States in 1957. He is currently System Engineering Subproject Manager for the Defense Communication Satellite Phase II. Previous responsibility at TRW includes Assistant Project Manager for the Viking Lander biology and meteorology experiments. Prior to joining TRW in 1967, he worked on test equipment design, communication system design, and launch vehicle reliability. He holds patents on a temperature-compensated accelerometer and a pneumatic shock machine. In addition, Mr. Fowler has written papers on wideband shaker design, system pathology, and orbital experience with TWTA reliability.

Co-author of this paper is Mr. Frank Manders who is affiliated with Ball Aerospace Systems, Boulder, Colorado.

Blank Page

NATIONAL GEOTECHNICAL CENTRIFUGE

By James A. Hallam, Nans Kunz, and Wilbur C. Vallotton

NASA, Ames Research Center

A new national resource that may be the world's largest centrifuge is under construction at NASA-Ames Research Center.

The new centrifuge will be able to take a 2700-kg (6000-pound) payload up to 300 G's. The 300 G's will be obtained by spinning the payload with its center of gravity at a radius of approximately 8.8 meters (29 feet) at a speed of 175 rpm. At this speed, the payload bucket will have a tangential velocity of 168 m/s (550 ft/sec), or roughly half the speed of sound. This paper describes some of the design problems encountered in such a high G-ton machine (see figures 1 and 2).

DESCRIPTION

The primary purpose of the new facility will be for the modeling of body force problems in civil engineering. Problems such as the stability of dams and embankments, the bearing capacity of soil foundations, and the dynamic behavior of foundations due to vibration of machinery can be studied using the new centrifuge. The scope of problems that can be addressed by centrifuge modeling include: static, dynamic, thermodynamic, and fluid dynamic processes coupled with body force loading. Some examples include: earthquake response of earth structures, soil-structure interaction, explosive cratering, blast-induced liquefaction, frozen soil behavior, frost heave, etc.

The Geotechnical Centrifuge will be used to verify finite element analyses and help generate new theories and analytical techniques. The new facility, because of its large payload capacity, will be able to carry larger models with greater detail than any centrifuge currently in use for geotechnical work. This will allow greater accuracy in modeling and instrumentation than is currently possible with smaller centrifuge models. This increase in modeling capability will provide for a more precise study of currently used scaling laws, and a more accurate evaluation of the effects of parameters that are difficult or impossible to accurately scale, such as grain size of the soil. The larger model dimensions will reduce inaccuracies due to model boundary effects. The initial research effort with the new facility will hopefully provide a better understanding of these effects, and also provide information for the modification of scaling laws to compensate for them.

The geometric scale of a model which represents an earth structure is inversely proportional to the G-level at which the machine is operating, and the scaling of settling or consolidation time is proportional to the square of the G-level multiplied by the time the centrifuge operates. For example, 40 years of time on a 300-meter section of an earthen dam can be simulated using a 1-meter model at 300 G's in 4 hours. (see figure 3). Other scaling laws have been developed for vibrational frequency, amplitude and duration for seismic events and explosive charge energy for cratering studies.

The new facility and initial research is being funded by grants from the National Science Foundation to NASA-Ames and The University of California, Davis. The Center for Geotechnical Modeling at The University of California, Davis, will provide management and technical expertise for the operation of the new facility. Ames is providing the design and construction management of the facility. The new centrifuge is actually a modification of an obsolete Apollo-program centrifuge. The main existing components that will be used include the motor, the power supply, and the buildings.

DESIGN

The motor that will drive the new centrifuge is a large vertical shaft dc machine built by Westinghouse and originally designed to develop 14,000-kW (18,800-hp) output power for very short durations with a limited duty cycle. The original design speed was 54 rpm. A continuous-duty rating for the motor was not established in the original design.

A recent design study by Westinghouse established a continuous-duty power rating for the motor of 6,700 kW (9,000 hp). It was also determined that 70 rpm would be an acceptable maximum speed at this power level, limited by commutation of the motor. Frequent inspection and commutator servicing would be necessary for operation at this speed and power level.

It was decided to use a speed increaser with a ratio of 1:3 to attain the required 175-rpm output speed for the new centrifuge, thus retaining a maximum motor speed only slightly higher than the original design.

The speed increaser will be an epicyclic configuration to maintain concentric input and output shafts. The large ring gear will have a pitch diameter of approximately 173 cm (68 in) and a face width of 27 cm (10-5/8 in). Lubrication for the gears and bearings is provided by spray lubrication with a dry sump gear case. The lubrication oil reservoir is an annular ring with a 225-liter (60-gallon) capacity that makes up the outer shell of the gear case. This reservoir is kept full by a combination of centrifugal pumping due to rotation of the gearing and a scavenge pump system.

A unique structural design feature of the centrifuge arm is the isolated tension straps (see figure 4). The tension straps carry the centripetal forces of the payload directly from the payload support structure (swing bucket) to the counterweight without going through the main support structure. This force [approximately 27 million newtons (6 million pounds), at full speed], which is equivalent to the thrust of 4 F-1 rocket engines used on Saturn V, is all carried through pivot pins that allow the payload bucket to swing. The tension straps are to be made from high-strength alloy steel, thus allowing the main support structure to be made from mild steel. The main support structure is a box-beam weldment that provides bending and torsional stiffness to the system and carries all of the 1G vertical loads. This structure also sees moderate tensile stress due to centripetal forces from its own mass. Using mild steel for the main support structure greatly reduces the cost of construction since material costs are less and fabrication (especially welding) is easier. The tension straps are attached to the main support structure by a single pin joint at the payload end (see figure 5). This pin joint is capable of handling an unbalanced load up to 10% of payload and carrying it back through the main structure to the spindle bearings. It is located at the payload end to minimize the displacement (due to strain) of the outer ends of the anti-spreader bar with respect to the center of the bar.

The purpose of the anti-spreader bar is to reduce the bending in the tension straps at the first support due to the lateral acceleration force acting on the clevis eyes, bucket walls, and the cantilever portion of the straps. The lateral acceleration is 33 G's on the straps along their entire length, and is supported by hockey-puck-shaped bronze bearing pads that supply support in the lateral direction, yet still allow the straps to slide when stretched by the tension forces (see figures 4 and 5).

The bucket is a swing type; this insures that the acceleration vector remains essentially normal to the floor of the bucket at all times. This is required for many geotechnical studies to keep ingredients, such as sand and loose soil, in place during the entire cycle, from at rest to full speed.

Another interesting design feature is the flexwall bucket design. This insures isolation of the bucket floor loading moment from the pivot pins; the pins are then assured of equal loading in the bucket clevis eyes (see figure 5) The walls of the swing bucket, that attach the payload-carrying surface to the clevis eyes, are made from only 1-inch-thick steel plate. Therefore, they essentially act as a large flexure.

A safety barrier to be constructed within the existing centrifuge building was designed to be capable of containing the entire swing bucket with payload at full speed, should failure occur. The bucket assembly, with payload, weighs about 10,000 kg (22,000 lb.), and is traveling at a tangential speed of about 168 m/s (550 ft/sec); or in other words, the safety barrier will be able to contain the equivalent of a ten-ton truck traveling at 375 miles per hour. The safety barrier is an annulus with an outside diameter of 37 meters (122 ft). The outside wall will be the existing walls of the building which are 0.4-m (16-inch) thick steel reinforced concrete. An inside wall of steel reinforced cinder blocks will retain 6.7 meters (22 ft) of sand fill between the walls. The design assumes fracture or penetration of the inner wall with the sand providing an energy absorption role. Model studies have been performed on a ballistics range to verify the design analysis.

THE CURRENT STATUS OF THIS PROGRAM

The contractor for the centrifuge construction is March Metalfab, Inc., of Hayward, California. Philidelphia Gear Corp. was the successful bidder on a design-and-construct-type contract for the speed increaser. The electrical and controls contract and the safety barrier contract remain to be bid.

A completed gear box is to be delivered by May 1, 1982. Concurrent with this, March Metalfab will fabricate and assemble the centrifuge in their shop so that erection can begin as soon as the speed increaser is installed. The entire facility should be operational by the end of this year.

CENTRIFUGE PERFORMANCE

SPEED	0 - 175 RPM
ACCEL.	300 G (MAX) RAD.
PAYLOAD	2727 KG(MAX) (6000 LB)

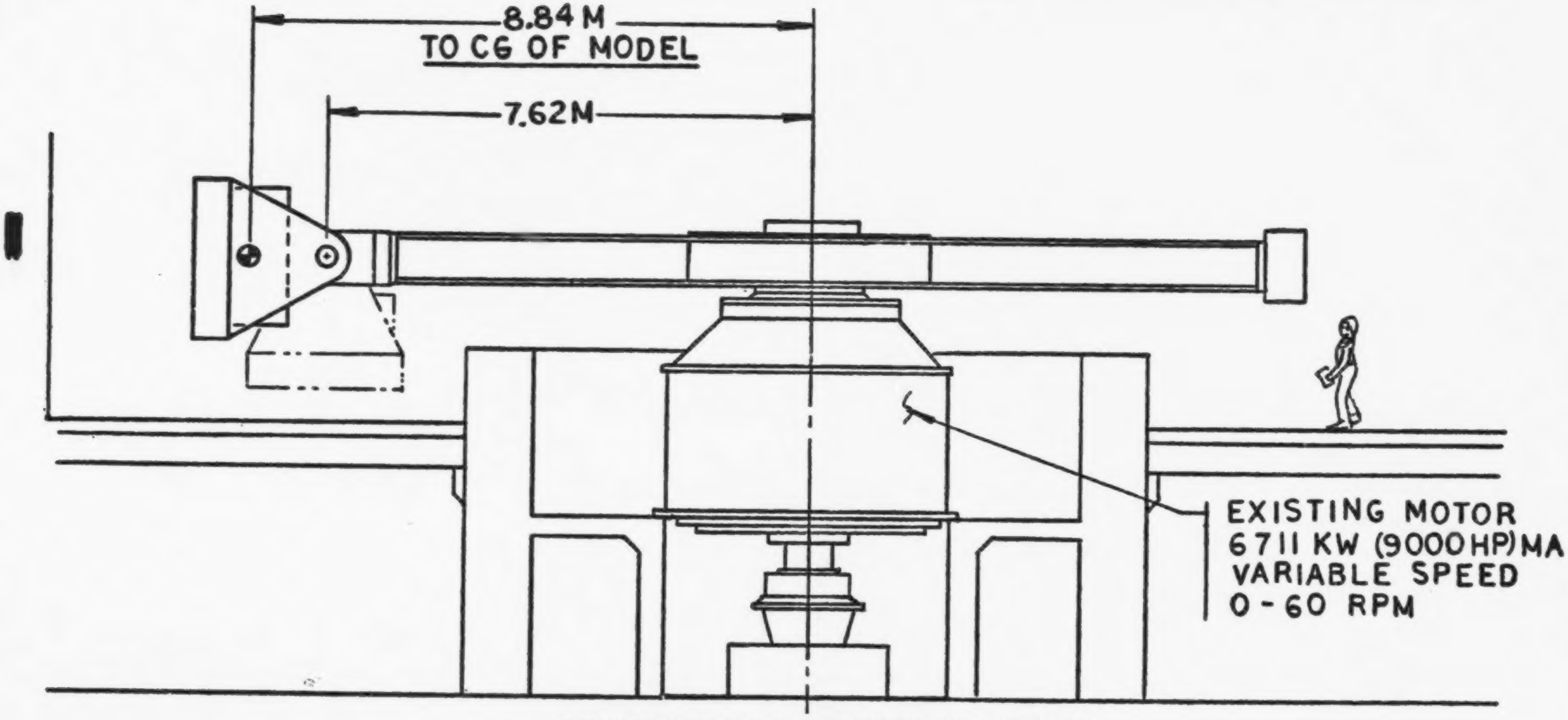
8.84 M
TO CG OF MODEL
7.62M
EXISTING MOTOR
6711 KW (9000 HP) MA
VARIABLE SPEED
0 - 60 RPM

CENTRIFUGE CONFIGURATION

Figure 1

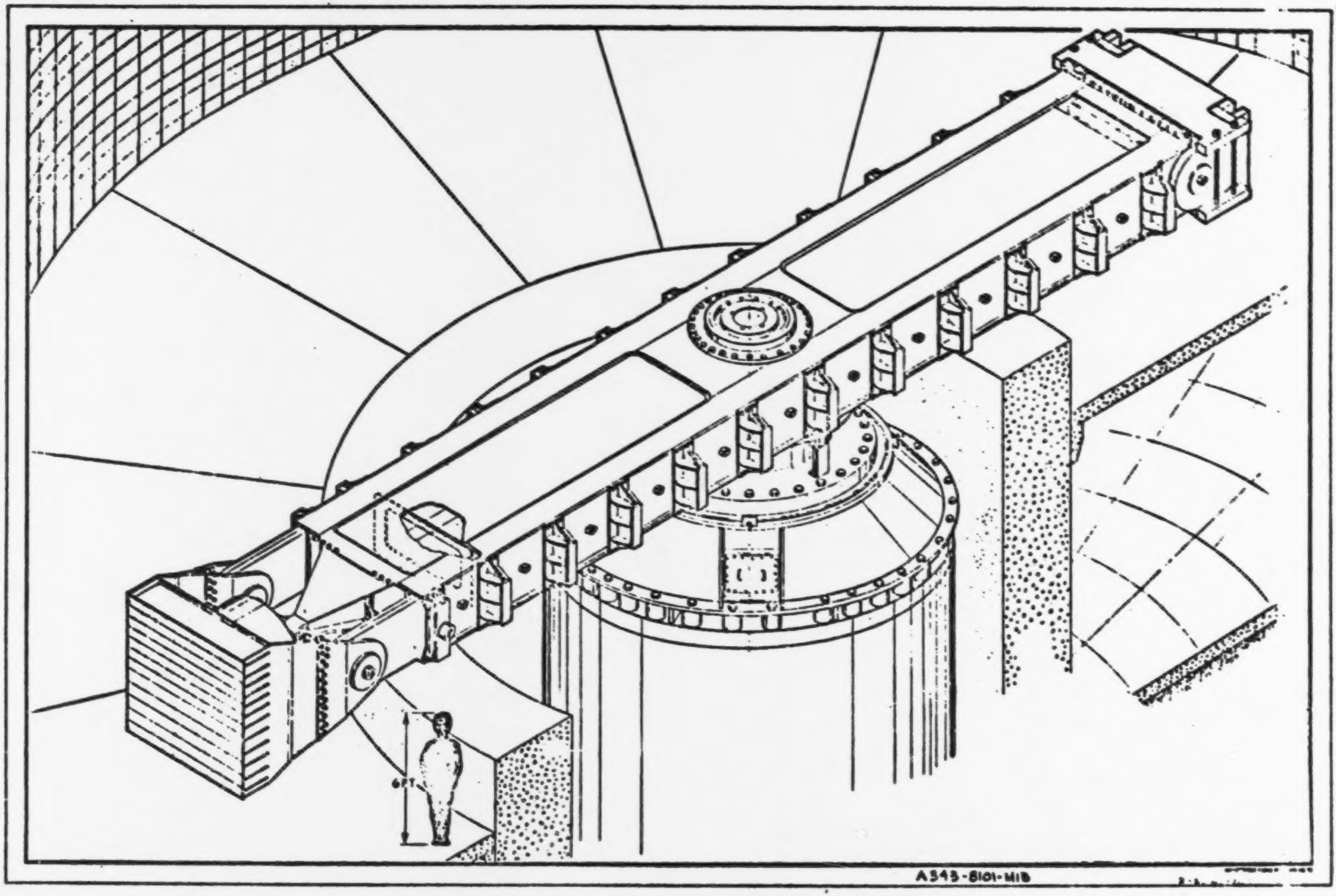
6FT
A343-8101-M1B

CENTRIFUGE PICTORIAL

Figure 2

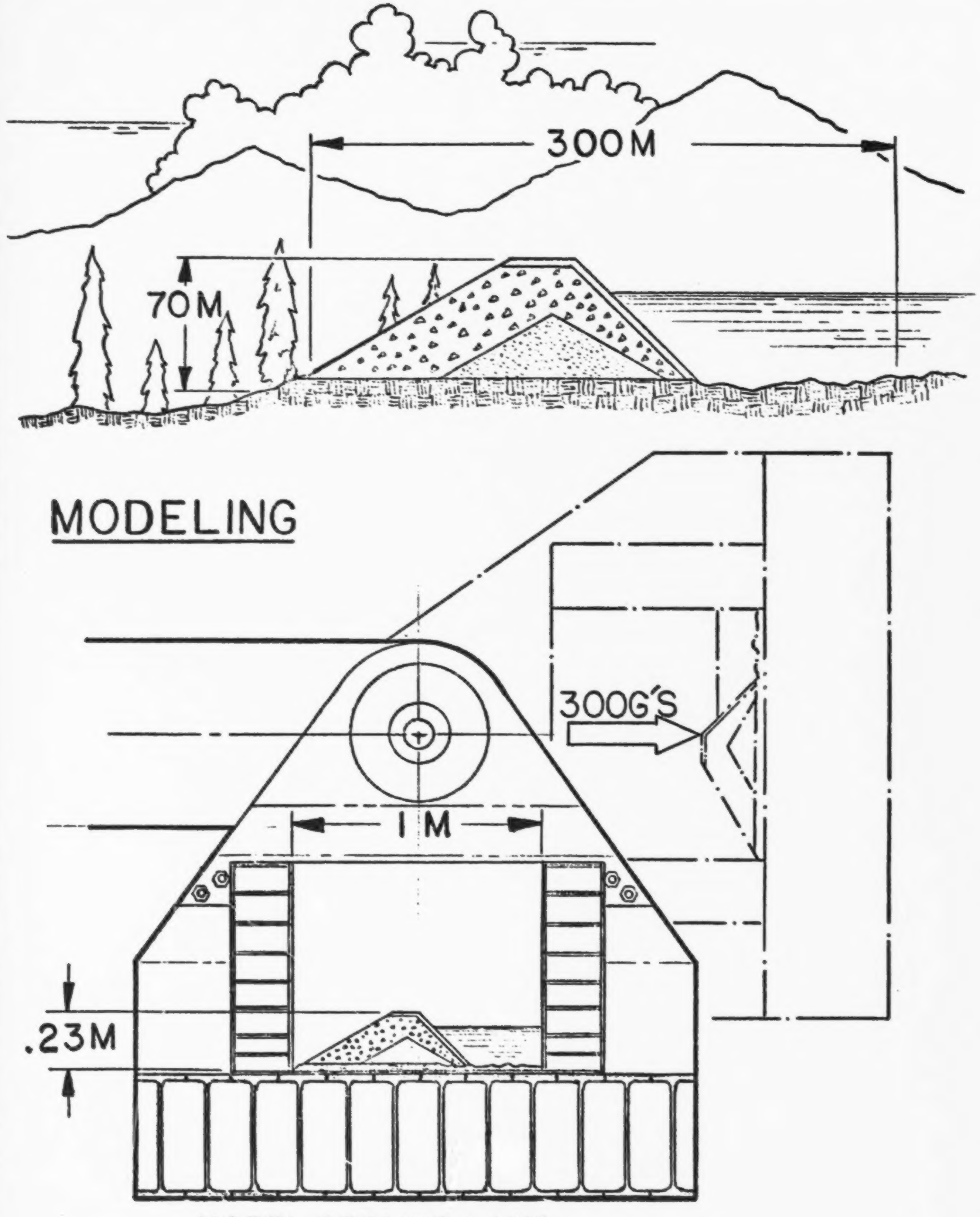
300M
70M
MODELING
300G'S
1M
.23M

MODEL SCALING LAWS

Figure 3

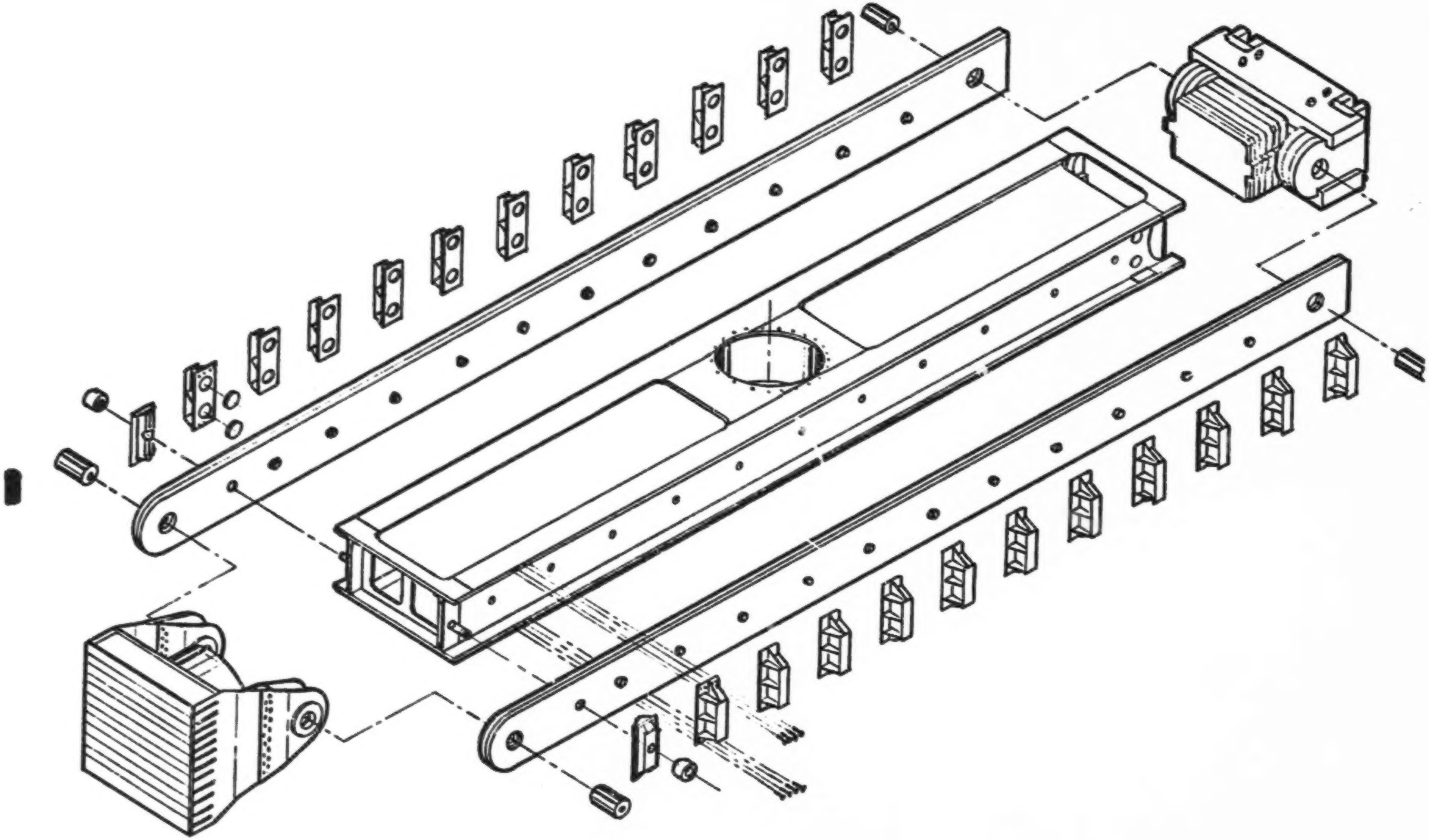

CENTRIFUGE EXPLODED VIEW

Figure 4

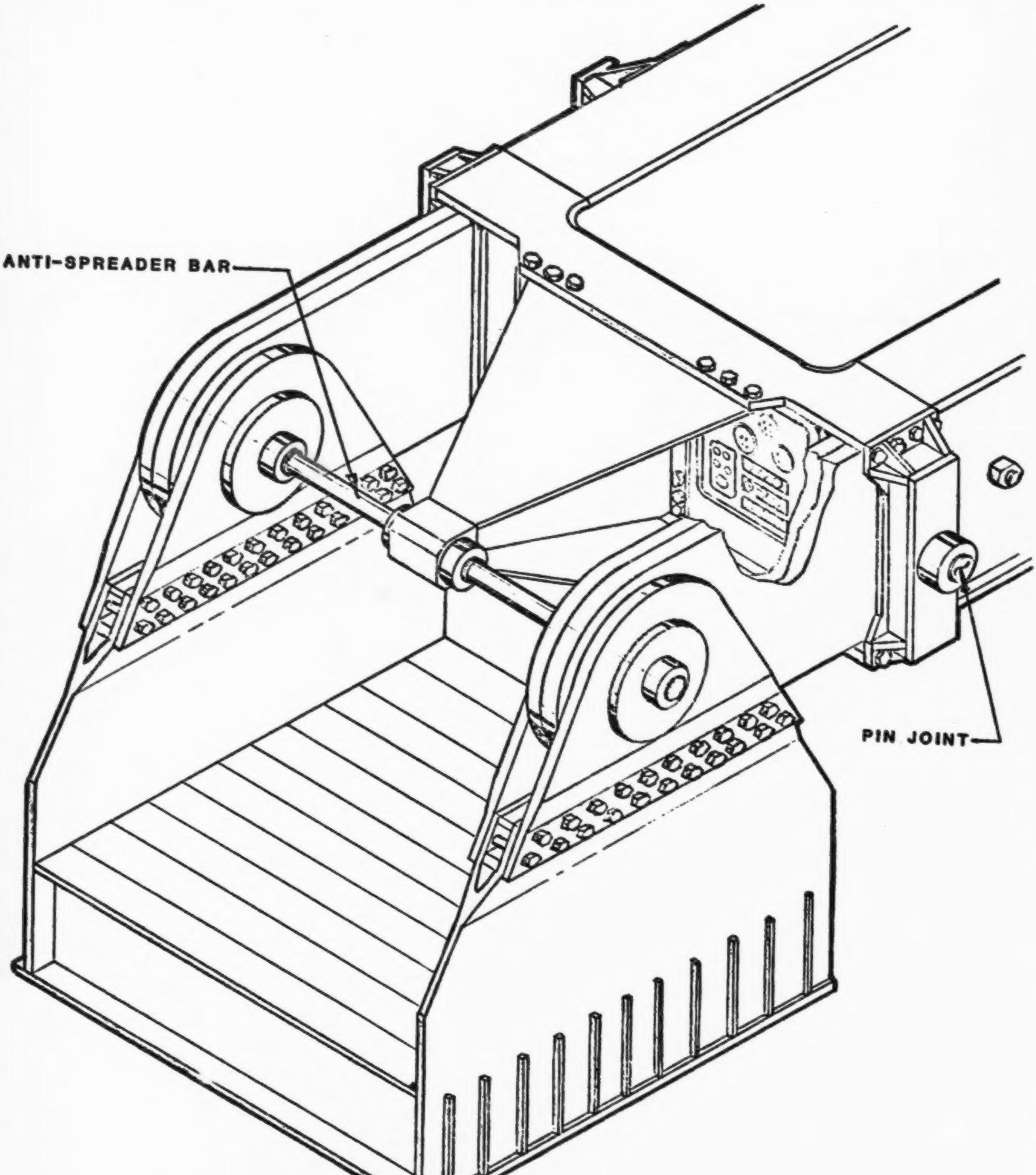
ANTI-SPREADER BAR
PIN JOINT

CENTRIFUGE SWING BUCKET

Figure 5

Nans Kunz
National Aeronautics and Space Administration
Ames Research Center
Moffett Field, California 94035

Mr. Kunz has been working for NASA-Ames Research Center as a research engineer in the Research Equipment Engineering Branch since June 1978. During this time, he has been primarily involved in the design of research equipment such as wind tunnels and aircraft and space flight hardware, as well as finite-element analysis of the same equipment using MSC/NASTRAN. He graduated from Oregon State University in 1978 with a B.S. degree in Mechanical Engineering. Mr. Kunz is currently doing graduate work at Stanford University.

Co-authors of this paper are Mr. James A. Hallam and Mr. Wilbur C. Vallotton who are also with Ames Research Center.

DESIGN AND ANALYSIS CONSIDERATIONS FOR DEPLOYMENT MECHANISMS IN A SPACE ENVIRONMENT

By: P.L. Vorlicek, J.V. Gore, C.T. Plescia
Ford Aerospace & Communications Corporation

ABSTRACT

On the second flight of Ford Aerospace and Communication Corporation's INTELSAT V spacecraft the time required for successful deployment of the north solar array was longer than originally predicted. The south solar array deployed as predicted. As a result of the difference in deployment times a series of experiments was conducted to locate the cause of the difference. Specifically, deployment rate sensitivity to hinge friction and temperature levels was investigated. In conjunction with these experiments a digital computer simulation of the deployment was created to evaluate the effects of parameter changes on deployment. As a result of the experiments and simulation, hinge design was optimized for nominal solar array deployment time for future INTELSAT V satellites. The nominal deployment times of both solar arrays on the third flight of INTELSAT V confirms the validity of the simulation and design optimization.

INTRODUCTION

As satellites grow in size, the need for stowing the satellite within the dimensions of the launch vehicle fairing becomes a serious design constraint. For this reason spacecraft are being built which are stowed in one configuration and then deployed into another configuration once in orbit. An example of such a satellite is the successful Ford Aerospace and Communications Corporation (FACC) INTELSAT V spacecraft. INTELSAT V is powered by two solar arrays that deploy once the satellite reaches geosynchronous orbit.

On the second flight of INTELSAT V the time required for successful deployment of the north solar array was longer than predicted. As a result of this, a series of ground-based experiments was conducted in order to locate the cause. Results of the experiments showed much higher friction levels on the flight hinge assemblies than had been originally predicted. In addition, friction levels increased significantly at the low temperatures expected in orbit. Additional experiments and computer simulations gave additional insight into the solar array deployment mechanisms.

As a result of the experiments and simulations, hinge design was optimized for nominal solar array deployment time for subsequent INTELSAT V satellites. The successful deployment of both solar arrays on the third flight of INTELSAT V confirms the validity of the simulation and design optimization. This paper will present a case study of the analysis and design changes that resulted from the deployment described above. Problems encountered in the analysis of the solar array deployment will be discussed. This is intended to give some insight and guidelines for designers and analysts for use in design of similar mechanisms.

THE SYSTEM

The Spacecraft

The FACC INTELSAT V spacecraft is a communications satellite capable of transmitting 12,000 voice channels and 2 television channels. FACC has been contracted to build 15 INTELSAT V's. INTELSAT V FM-2 was launched December 6, 1980 and is currently operational over the Atlantic Ocean, supplying voice channels between North America and Europe. FM-1, launched May 21, 1981, is also operational over the Atlantic Ocean. The third INTELSAT V, FM-3, was successfully launched December 15, 1981 and is currently undergoing pre-operational testing. Figure 1 is an artist's rendition of the spacecraft.

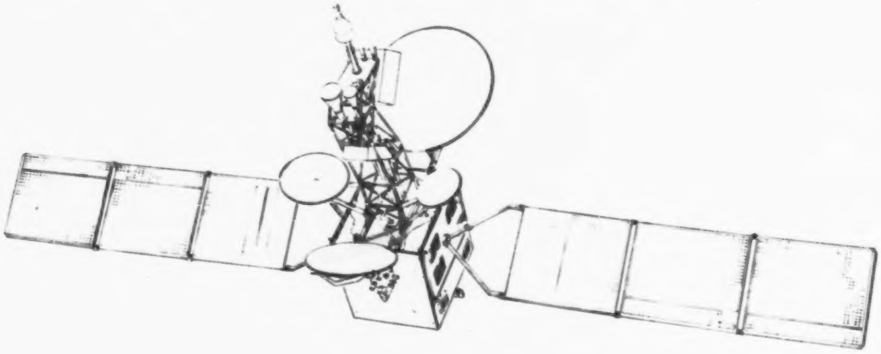

Figure 1. The INTELSAT V Spacecraft

The Solar Array

The solar arrays on INTELSAT V consist of a yoke and three solar panels that deploy in an accordion-type manner (see Figure 2). The array has two deployment mechanisms: (1) torsion springs and (2) closed cable loops. The torsion springs provide the energy to deploy the array. The closed cable loops restrain the deployment of transferring torques between the hinges, synchronizing the hinge deployment angles, and controlling the deployment rate to a point within the structural capability. Springs placed on the closed-cable-loop cables compensate for changes in cable length due to temperature variation. The springs also allow the hinge lines to be at somewhat different angles during deployment and add considerable complexity to the mathematical model of the solar array deployment. See Figure 2 for a description of the deployment mechanism and solar array parameters. Figure 2 also contains drawings of the hinge assemblies.

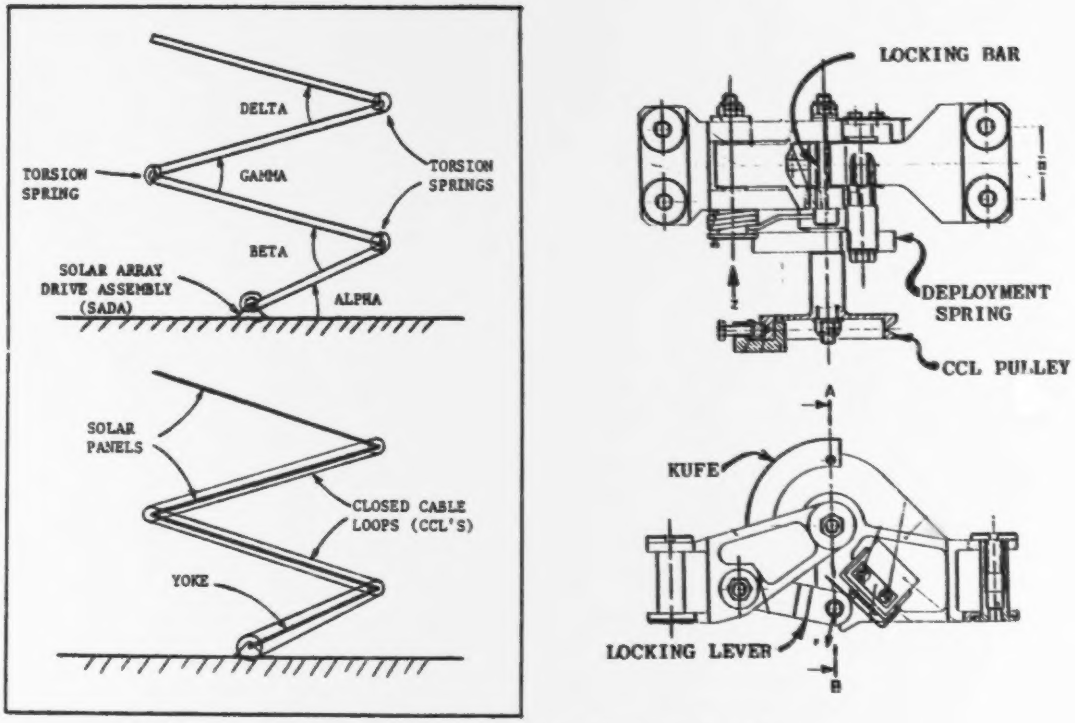
DELTA
TORSION SPRING
GAMMA
TORSION SPRINGS
BETA
SOLAR ARRAY DRIVE ASSEMBLY (SADA)
ALPHA
SOLAR PANELS
CLOSED CABLE LOOPS (CCL'S)
YOKE
LOCKING BAR
DEPLOYMENT SPRING
CCL PULLEY
A
KUFE
LOCKING LEVER
B

Figure 2. The Deployment Mechanisms and Hinges

THE SOLAR ARRAY DEPLOYMENT

On the second flight the south solar array deployment time was 22 seconds. The north solar array almost completely deployed in 22 seconds, but spacecraft roll rate data indicate the array was still moving until 32 seconds after release. Original predictions were for both solar arrays to deploy in approximately 13.5 seconds.

Figure 3 shows the roll rate of the spacecraft during the deployment of both the north and south solar arrays on the second flight. As the arrays are deploying, the roll inertia of the spacecraft increases, which results in a decrease in the spacecraft roll rate. From 0 to 22 seconds the spacecraft roll rate steadily decreases from .34 deg./sec. to .12 deg./sec. Accelerometer data indicated the south solar array locked into the deployed position at around 22 seconds.

Further analysis of the data indicates there is a slow decrease in the roll rate from 22 to 32 seconds, which implies the north solar array was continuing to slowly deploy. The oscillation of the roll rate occurring after 22 seconds is caused by the first bending mode vibration of the south array after it has locked up. This damped oscillation appears to be vibrating around a slowly decreasing roll rate, but due to the quantized nature of the roll rate data, no change in the roll rate is directly measured after the oscillation has damped out.

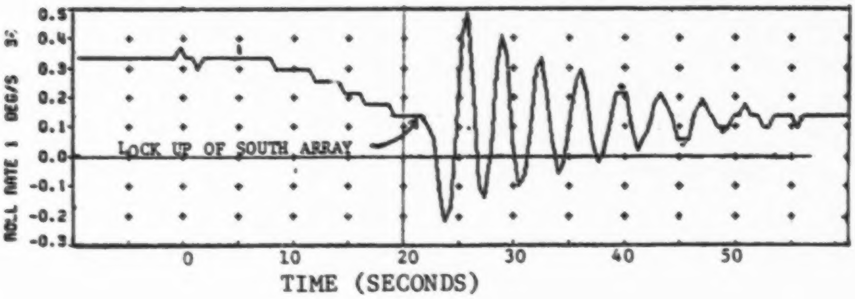

Figure 3. Spacecraft Roll Rate Data From FM-1

EXPERIMENTS

Two sets of ground-based experiments were conducted using an engineering model and flight hinge assemblies in order to locate the cause of the deployment time difference. A series of deployment tests was made with an engineering model of the solar array at FACC. These tests were intended to duplicate the flight experience, or to give insight into the possible causes. The second series of experiments was the measurement of resisting (friction) torques on flight hinge assemblies. These tests were intended to provide better values of the resisting torques in thermal vacuum environments, representative of expected orbital conditions.

Tests on Engineering Model

The deployment tests on the engineering model were divided into two groups:

1. Attempts to duplicate the flight data
2. Deployment tests with simulated hot and cold closed cable loops and hinges, duplicating on-orbit conditions.

A photograph of the test setup is seen in Figure 4. The array deploys horizontally and is supported at the panel centers by a sliding bar support device. The support rig was slightly inclined (2 mm/m) to counteract for the friction of the support device and air drag. At this inclination the array deployed in 22 seconds, the same as the south solar array on the second flight.

The attempts to duplicate the on-orbit results proved unsuccessful. Several test runs were made, varying the inclination of the support rig. No cases were recorded with the type of flight data experienced on-orbit. Additional tests were conducted in which the closed cable loop (CCL) was slipped off of the hinge pulleys. Again, no insight into the deployment time difference was gained.

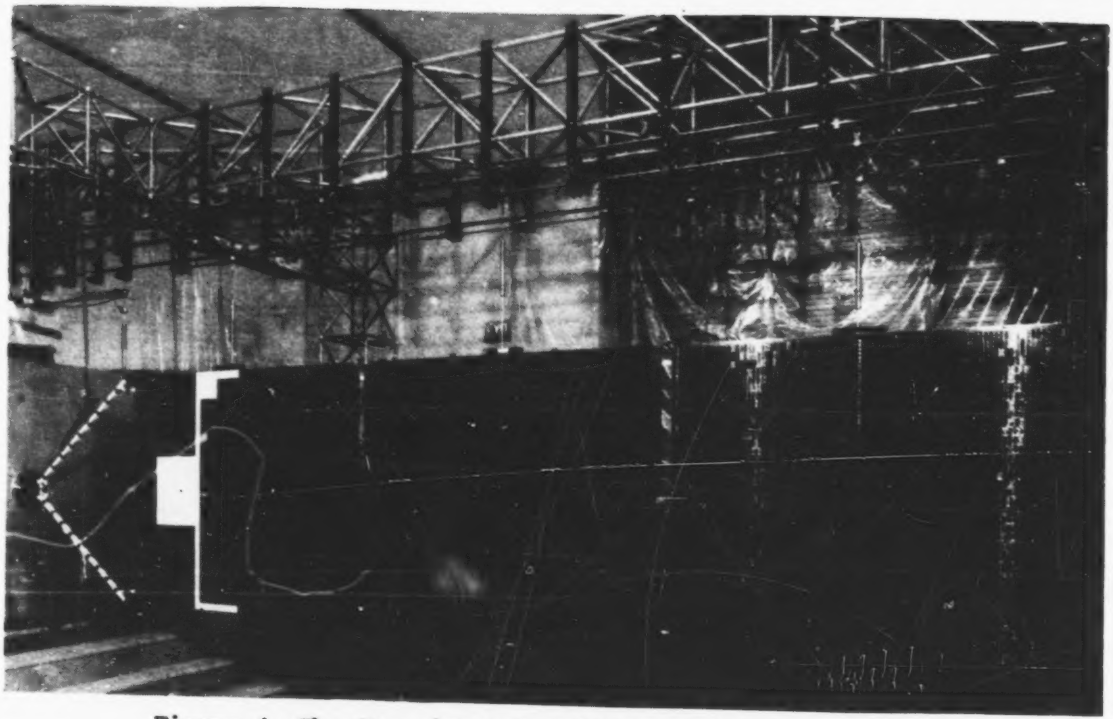

Figure 4. The Experimental Model Test Setup

The second series of tests on the engineering model was conducted to simulate the on-orbit temperature conditions. The orbital configuration of the solar arrays during deployment is edge-on to the sun. This position results in a temperature difference between the sunward and shaded hinges. To evaluate the effects of hot and cold conditions a test was constructed where the upper hinges were heated to 85°C with lamps, and the lower hinges were cooled with gaseous nitrogen to -100°C. The deployment time in this configuration increased to 24.7 seconds. These tests indicated an increasing resistance torque level with decreasing hinge temperature.

Additional tests were conducted to examine the effect of the closed cable loop (CCL) temperatures on deployment times. Temperature changes on the CCL's affect the length of the cables, which will change the point at which the cable will go slack. When the effects of temperature on the CCL's were tested, significant variations in deployment time resulted. Under nominal on-orbit conditions the south array deployment time was three seconds faster than the north array during the tests on the experimental model. On the first flight the south solar array deployed 6.5 seconds faster than the north array. Evidently the temperature of the CCL's contributed to this difference.

Beyond increasing the deployment time, the effect of the CCL temperature on the deployment did not reveal any insight into the deployment experienced on-orbit. Table 1 summarizes the four test runs described above.

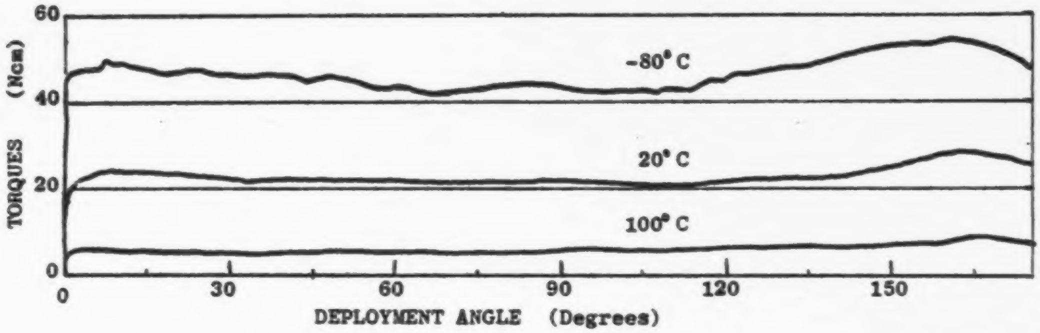

Figure 5. Hinge-Resisting Torque for Original Inter-Panel Hinges

Table 1. Test Runs on Engineering Model

Test	Deployment Times (sec.)		
Number	1st Hinge Lockup	Last Hinge Lockup	Comments
1	21.7	22.0	Rig inclination 2mm/m. Room temperature, baseline deployment
2	24.0	24.7	Rig inclination 2mm/m. Nominal north panel on-orbit conditions. Upper hinges 85°C. Lower hinges -100°C.
3	21.7	22.9	Rig inclination 2mm/m. Nominal north panel taking into account CCL temp. effect.
4	19.0	19.7	Rig inclination 2mm/m. Nominal south panel taking into account CCL temp. effect.

Tests on Hinge Friction Levels

The most important findings of the investigations were the measurements of the resisting torques on flight hinge assemblies. These measurements revealed that the resisting torques at low temperatures in vacuum were much larger than values obtained from measurements obtained on development model assemblies, and much larger than the values obtained in ambient conditions.

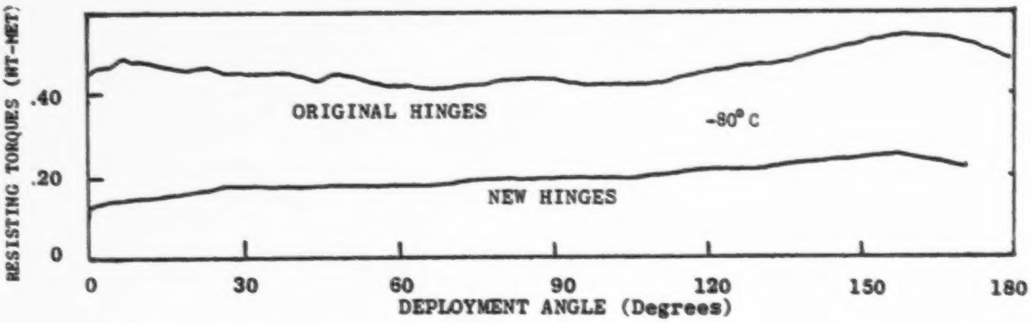

Figure 6. Hinge-Resisting Torques for Modified Inter-Panel Hinges

Figure 5 shows the resisting torque level variation with deployment angle at various temperature levels. The resisting torque does not include the torsion spring torques. The resisting torques at low temperatures are higher than initially estimated. The values are such that beyond a 100° deployment angle of the inter-panel hinges, inertia forces of the moving array are needed to assist the torsion spring torque in the deployment of the array.

As a result of these findings all the hinges were given special lubrication. In addition, the bearing tolerences were increased to allow for greater temperature variations. Results of the hinge friction measurements on the modified hinges are shown in Figure 6. The resisting torque level has been greatly reduced at low temperatures. Further tests showed that the friction level on the modified hinges is not as sensitive to temperature variation as the original hinges.

THEORETICAL ANALYSIS

In conjunction with the laboratory experiments, a theoretical model and digital computer simulation of the solar array deployment was developed. The purpose of the model was to: (1) recreate the on-orbit deployment results, (2) give additional insight into the deployment mechanism dynamics, and (3) provide a tool whereby the data from the friction tests could be evaluated in respect to deployment dynamics. In the simulation the panels and yoke are modeled as rigid elements interconnected with flexible hinges and extendible closed cable loops with accurately modeled temperature compensating springs. The torques acting on the hinges in the simulation include:

1. The torsion springs at the hinges
2. Torques from the closed cable loops
3. Stick-slip coulomb friction torques (stiction).

Stiction is a resisting force that always opposes velocity and accounts for the fact that a finite force is needed to start a body moving. Accurate simulation of stiction is important for both the designer and analyst to consider, as this was eventually found to account for the differences in the north and south panel deployment times.

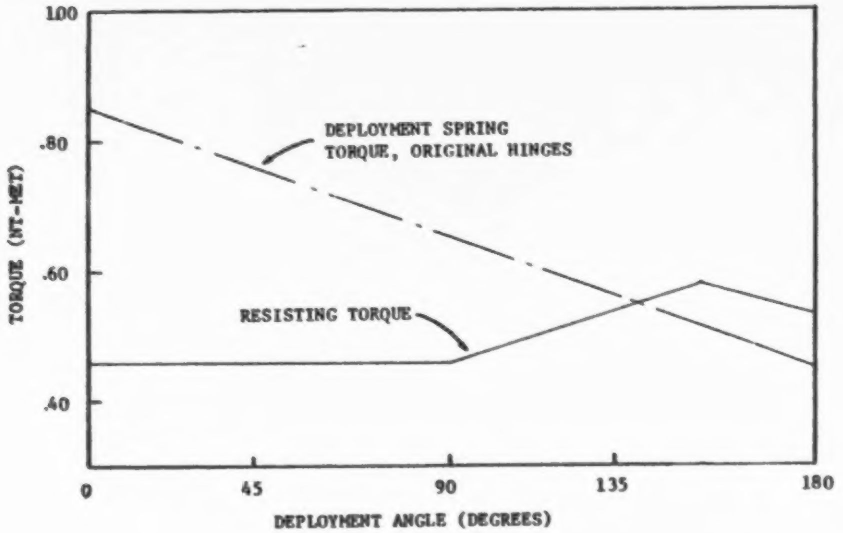

Figure 7. Spring and Resisting Torques Used in the Simulation on the Inter-Panel Hinges

Examination of the results of the hinge friction tests shows the resisting torque to be angle dependent. Since the stiction torque is angle dependent, the torque was represented in the simulation as shown in Figure 7. Figure 7 shows the torsion spring torques and the nominal resisting torques used for the inter-panel hinges in the nominal-case computer simulation.

Several simulation runs were made, varying the driving torques and stiction level at each of the hinges. Results of the simulation are the deployment angles plotted against time. From these curves the deployment time of the panel can be determined. See Figure 1 for a definition of the deployment angles. Figure 8 is the result of a simulation of the deployment of the north solar array with the nominally measured friction levels shown in Figure 7. The deployment time is approximately 18.5 seconds.

Additional runs were made attempting to duplicate a deployment similar to that experienced on orbit. The runs showed that the deployment rate was most sensitive to the friction level on the yoke/solar-array-drive-assembly (SADA) hinge. Raising the stiction on the yoke/SADA hinge 50% and the yoke/inboard-panel hinge 50% yielded a deployment similar to that experienced on orbit. Figure 9 shows these results. The array deploys for approximately 26 seconds at which point it nearly stops, but velocity data indicate the array slowly moves for another 8 seconds, at which point the deployment stops with the array in a partially deployed position.

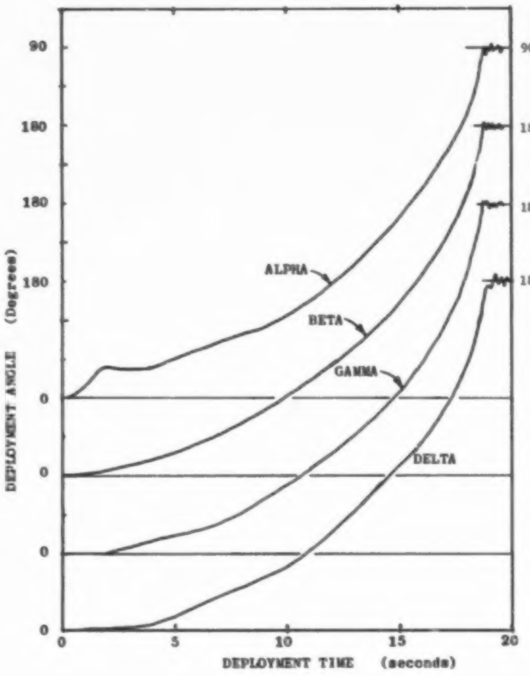

Figure 8. Simulation Results of the Deployment of the North Solar Array Under Nominal Conditions

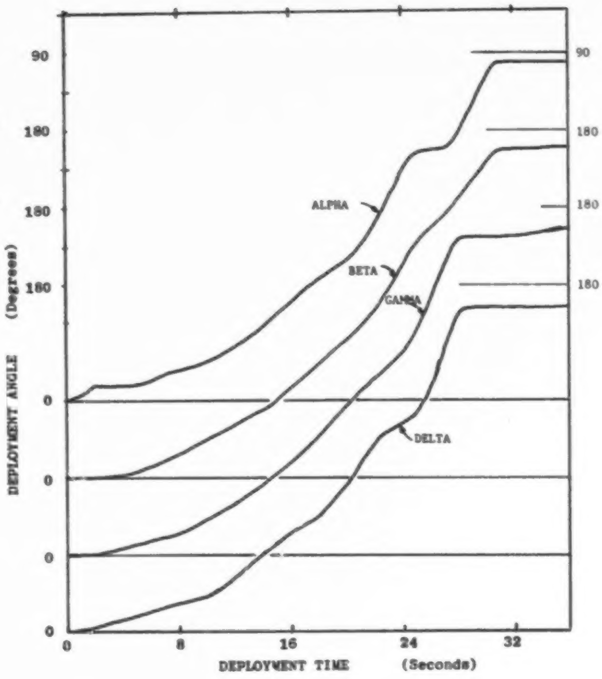

Figure 9. Deployment Similar to That Experienced on Orbit for the North Solar Array

CHANGES TO THE HINGES

As a result of the findings of the simulation runs and the experiments, several changes to the hinges were made. Among the changes are:

1. Special application of lubricant to all moving parts in the hinges
2. Increased bearing tolerances to allow greater variation in temperature
3. Increased polish on locking bars (see Figure 2)
4. Increased torsion spring pretorque level (see Figure 7).

Using the stiction torque level on the modified hinges as given in Figure 5, the predicted deployment time decreased to about 12 to 14 seconds for the south and north solar arrays respectively. Figure 10 shows the simulation results with the modified hinges on the north solar array.

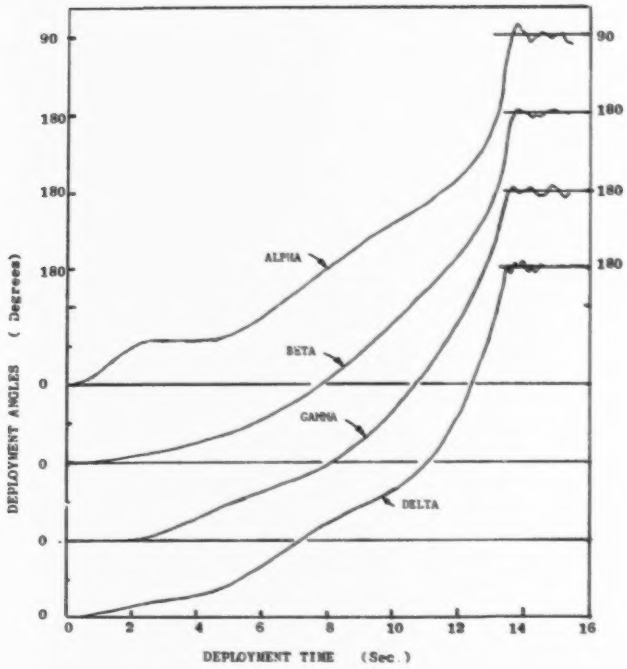

Figure 10. Deployment Simulation With the Modified Hinges on the North Solar Array

RESULTS

The hinge assemblies on the third flight of INTELSAT V incorporated the modifications previously described. The satellite was successfully launched December 15, 1981. Data from the onboard accelerometer, shown in Figure 11, indicate that the first hinge of the south array locked up at 11.8 seconds, and the first hinge of the north solar array began lock up at about 13.8 seconds.

The accelerometer is located on the spacecraft body, near the north solar array. The proximity of the accelerometer to the north solar array makes it more sensitive to accelerations of the north solar array. Therefore, the small initial acceleration disturbance occurring at 11.76 seconds is assumed to be the south solar array locking up, and the larger disturbance at 13.64 seconds is assumed to be the north solar array locking into position. These results are in excellent agreement with the simulation results mentioned in the previous section.

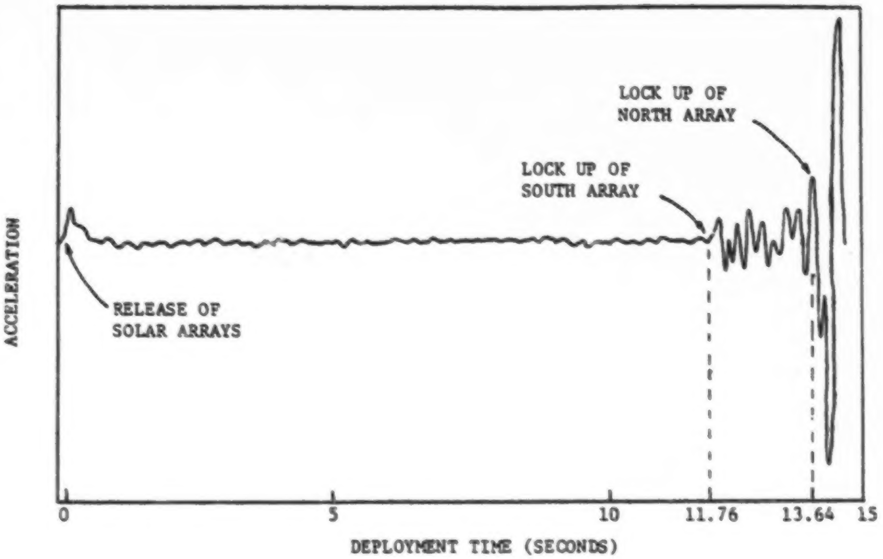

Figure 11. Accelerometer Data From FM-3

CONCLUSIONS

The most probable cause of the deployment time difference has been identified as the variation in the friction level in the hinge assemblies at low temperatures. Some of the changes to the hinges included special lubrication of the guides and bearings and additional polishing of the locking bars. Experiments on the modified hinges showed a reduction of the resisting torque on the hinges by about 50% at low temperatures. When the new friction values were put into the computer simulation, the deployment times of the south and north solar arrays decreased to 11.9 and 13.7 seconds, respectively. The deployment times of the south and north solar arrays on the third flight of INTELSAT V were 11.8 and 13.6 seconds, respectively, in excellent agreement with the theoretical results. These data validate the analysis used in the simulation technique described in this paper. Using techniques similar to those described herein will provide analysts and designers with more accurate simulations and a better basis to evaluate potential problems associated with deployment mechanisms. Points to be stressed are: (1) adequate theoretical analysis of a mechanism should be undertaken, (2) mechanisms should be tested under conditions which duplicate the range of expected orbital environments in order to identify sensitive conditions, and (3) during the ground testing of very large complete assemblies it is very difficult if not impossible to adequately duplicate the orbital conditions.

* The authors would like to thank Dr. A.K. Banerjee and Dr. P.M. Barba for their contributions to the theoretical simulation.

** The work described herein is based, in part, upon work sponsored by INTELSAT. Any views expressed herein are not necessarily those of INTELSAT.

P. L. Vorlicek
Ford Aerospace and Communication Company
3939 Fabian Way
Palo Alto, California 94303

Mr. Vorlicek is currently an engineer in the Systems Analysis Department of the Dynamics and Control Section at Ford Aerospace and Communication Company. He has received both his B.S. degree, in 1979, and his M.S. degree, in 1981, in Aerospace Engineering from Massachusetts Institute of Technology.

Co-authors of this paper are Mr. J. V. Gore and Mr. C. T. Plescia who are also with Ford Aerospace and Communication Company.

A DEPLOYMENT MECHANISM FOR THE DOUBLE ROLL-OUT FLEXIBLE SOLAR ARRAY ON THE SPACE TELESCOPE

T.R. CAWSEY*

ABSTRACT

British Aerospace (BAe), as prime contractor to the European Space Agency (ESA), has developed a Roll-Out Flexible Array which provides more than 4 kW of power for the NASA/ESA Space Telescope (ST). The Array is configured as two wings. The Deployment Mechanism for each wing is based on the flight-proven Hughes Aircraft Company (HAC) FRUSA design. However, modifications have been incorporated to accommodate an increase in size and the ST mission requirements. The assembly and operation of the Deployment Mechanism are described together with environmental and functional tests results.

INTRODUCTION

A double roll-out configuration met all the ESA requirements for the proposed mission. Reliability, cost and flight-proven history were critical factors in the choice of the baseline design. The HAC FRUSA design had completed design, development and test phases and successfully flown on the STP 71/72 mission (Reference 1). It was therefore advantageous to supplement existing European technology with this experience, through a consultancy agreement with HAC, and base the BAe design on this proven mechanism.

An overall view of the ST is illustrated (Figure 1). One Secondary Deployment Mechanism (SDM), which incorporates all those elements for the support, deployment and retraction of two solar cell blankets, is required for each wing.

The SDM with partially deployed solar cell blankets is shown (Figure 2). The two blankets are rolled onto a single Storage Drum with an interleaf of embossed KAPTON film cushion to protect the solar cells (Section BB, Figure 3). The outer edge of each blanket is attached to a Spreader Bar which is connected to and between two BI-STEM booms. As the booms are deployed the blankets are pulled from the Stowage Drum via the Spreader Bar. The cushion rolls onto the spring-driven Cushion Roller and Spring Motors act against drum rotation to ensure tension in each blanket.

REQUIREMENT

Apart from an increase in size (x 1.2 on deployed length and x 1.4 on width) additions and modifications have been incorporated into the FRUSA design to comply with the following major ST mission requirements.

- **5 years' operational life before replacement of components**
- 5 launch/return cycles with only minor refurbishment possible between launches

*British Aerospace P.L.C., Dynamics Group, Bristol Division, England.

- Exposure to 27250 eclipse thermal cycles (-70°C to +70°C)
- The STS (Space Shuttle) launch environment
- Pyrotechnic actuators were prohibited.
- The overall design had to be astronaut compatible (Reference 2).
- Provision of an astronaut over-ride mechanism for manual deployment/ retraction
- Redundancy of all critical components. Where this was not possible, analysis and tests had to be carried out for loads and durations much greater than expected to ensure compliance with the reliability requirements.

DESIGN DESCRIPTION

The Stowage Drum is a one-piece aluminium alloy (Al.Al) tube (203.2-mm O/D, 2-mm wall). It rotates about the static central tube via duplex bearing units in each titanium alloy (Ti.Al) end support (Figure 3). The inner race of the inboard bearing pair is locked to the central tube's Ti.Al seat but the outboard bearing is free to slide axially to accommodate differential expansion between drum and tube. The outboard bearing seat is hard anodised Al.Al coated with a resin-bonded MoS_2. The thin section bearings which are ABEC7 and 440C stainless steel (St.St) have ion-plated lead on the races and a lead bronze cage. They are mounted face to face under a spring pre-load of 22.25 to 40.00 N. The free rotation of the stowage drum is essential for the successful operation of the SDM. To ensure that axial bearing overload does not occur if the sliding interface seizes, the outboard bearing unit is also housed in a diaphragm mount. This diaphragm is 0.5 mm thick with an axial stiffness of 200 N/mm. It is manufactured from a Ti.Al forging with radial gain flow to reduce the possibility of circumferential cracking when deflected. The electrical interface with each blanket is through soldered connections at the drum surface and the mechanical interface is a glass-fibre-reinforced KAPTON strip bonded to the drum with epoxy adhesive. The drum also contains flat flexible harnesses which provide the electrical interface between the rotating drum and static control tube. These harnesses are 1524 mm long and manufactured from a base laminate of 0.068-mm (2-oz) rolled copper foil on 0.051-mm (2-mil) KAPTON film with an overcoat of 0.051-mm KAPTON film bonded with an acrylic adhesive. Each power harness is 311 mm wide and has 20 7A-rated conductors. The data harnesses are 155 mm wide, each with 30 conductors. These harnesses (Figure 3) unwind as a spiral for half the solar blanket's deployed length and then rewind to the completion of deployment to attain a similar wound configuration in the fully deployed state as in the blankets-stowed condition.

Deployed blanket tension (22.25 N) is provided by redundant constant torque springs (Figure 3). The spring storage pulleys are attached to the inboard support brackets which also incorporate an SDM lifting point and a Grapple Fixture interface to enable possible use of the Orbiter's Remote Manipulator System (RMS). The springs are St.St coated with bonded MoS_2. The carbon-fibre-reinforced plastic (CFRP) cushion roller is also driven by constant torque springs which impart a cushion tension of 5.5 N. The cushion roller has St.St. end fittings which rotate in bearing units which comprise a spherical bearing with two small flanged ball bearings fitted into its inner diameter. This arrangement accommodates misalignment, provides redundancy and off-loads the small low friction bearings during launch.

The Boom Actuator comprises two cassette assemblies. Each assembly contains two deployable and retractable BI-STEM Booms (23-mm O/D, 5.85 m long). The cassette assemblies are dry-lubricated, gears are lubricated by a bonded solid lubricant, and the boom element guides are a polymide/MoS_2 composite. The power unit in each two-boom cassette assembly is a size 13PM DC-brushed motor driving through a three-stage epicyclic gearhead (113:1). The gearhead is lubricated with BRAYCOTE 3L-38-RP grease, and the phenolic retainers of the output shaft bearings are vacuum impregnated with BRAYCO 815Z oil. An external molecular seal surrounds the output shaft, and a lip seal is fitted at the motor/gearhead interface to protect the dry-lubricated motor. The spring-loaded radial composite brushes run on a 7-bar commutator of zirconium copper with mica insulators. Anticreep film is used within the gearhead and motor to prevent internal oil migration and leakage from the unit. The two geared motors are connected by a Torque Tube to provide an electrically redundant drive.

The outer edge of each solar cell blanket is attached to a CFRP Spreader Bar (50.8 mm, 2-mm wall) which is located between and attached to the outer tips of each pair of booms via fixed extension rails. The Spreader Bar houses a spring mechanism which compensates for mismatch in boom extension rates and final boom deployed length to maintain a uniform tension across the blankets. The compensator mechanism is connected to the extension rails by St.St tapes and includes a linear potentiometer which senses spring extension, from which the blanket tension is determined. The potentiometer movement is limited to 25.4 mm; and to provide a read-out over full extension rail length, 127 mm, the potentiometer is enclosed by a secondary spring in series with the primary spring such that the load which results in 228.6-mm extension of the primary spring causes the secondary spring to extend 25.4 mm (Figure 6).

The Manual Over-ride gearbox has a ratio of 0.711:1 and is in constant mesh with an output gear on the Torque Tube. The Drum Lock mechanism (Figure 4) also interfaces with the Torque Tube and the design is such that in the locked position the load on the release cam passes through the axis of its carrier shaft which results in a very low torque transfer to the release quandrant.

The overall mass of the SDM is 54.72 kg. However, approximately 10 kg of this is for instrumentation and astronaut EVA interfaces. Apart from thermostatically controlled heaters on the motor units the thermal design is passive with most of the exposed external surfaces covered with self-adhesive aluminised KAPTON film and some internal surfaces black anodised.

OPERATION

A tension of 111.25 N is applied to the solar cell blankets to prevent slippage during launch. This tension is maintained by the Drum Lock mechanism. After primary deployment the SDM is activated and during the initial revolution of the Torque Tube the Drum Lock releases. This is possible because the first revolution of the boom-stowage cassettes is used to open out the elements from their tightly wound condition prior to their exit from the cassette housing. The booms are driven out and the blankets are pulled from the Stowage Drum via the Spreader Bar. The cushion rolls onto the Cushion Roller and the main Spring Motors act against drum rotation to ensure tension in each blanket. At the completion of deployment, or in any interim position, the booms remain locked by virtue of the high gearing within the Actuator Unit. For full deployment the Stowage Drum rotates approximately 8 revolutions and the Cushion Roller 32 revolutions.

For normal deployment and retraction both motors are driven together to deploy or retract one wing at a time. However, if electrical failure occurs in one motor, each motor is capable of driving both boom cassette assemblies and backdriving the failed motor. The drive electronics also has the capability to drive one motor in each SDM to simultaneously deploy or retract both wings. The drive motors are switched off at the completion of deployment or retraction by pre-set microswitches within each cassette assembly. Normal two-motor-drive deployment time is approximately 5 minutes and the manual input torque required for blanket deployment is <5 Nm.

TEST RESULTS

The tests programme is summarized (Figure 7). Structural tests confirmed reserve factors >2 on the maximum predicted loading conditions. The Narrow Blanket Model, using two full-length, 150-mm-wide blankets with a combination of real and dummy solar cells was used to check roll-up geometry and general blanket interface. It was subjected to vibration, acoustic and linear acceleration tests. No solar cell damage occurred. The diaphragm housing successfully completed 45,000 oscillations of +/- 2-mm amplitude without any evidence of cracking. The Sliding Bearing interface also completed 45,000 oscillations of +/- 2 mm in thermal vacuum conditions with 20°C temperature differential between drum bearing housing and central tube. The sliding force was < 10 N, both at high- and low-temperature conditions, and inspection of the bonded MoS_2 film after the tests showed that it was barely worn and thus had more than adequate life. Similarly, the Spring Motor Assembly completed 45,000 drum oscillations of +/- 5° in the fully deployed position and 50 full deploy/retract operations. The Flexible Harnesses completed the same tests in thermal vaccum and while in the deployed configuration a current of 3.7 A was passed through each of the 40 power conductors to simulate the heating effect. The total flexible harness resistance torque (2 power, 2 data) over 9.5 revolutions of the drum at temperatures of +/- 40°C was 0.56 Nm to 0.90 Nm. No de-lamination was observed and continuity was satisfactory during and after tests.

During thermal vacuum testing of the Boom Actuator Unit at -35°C and maximum loading conditions, a problem occurred in the redundant one-motor-drive mode. The detent torque of the back-driven motor increased from its normal 0.42 Nm to about 1.41 Nm (Figure 5). This increase in detent torque, attributed to a reduction in gearhead clearances (backlash) and possibly some increase in lubricant viscosity, was deemed to be a major factor in a drive motor stall condition occurring before retraction was complete.

As a result of this test failure a decision was taken to fit heaters to the gearhead and increase the gear ratio between the gearhead output and cassette drive from 1.943 to 3.579:1 to further reduce the load on the drive motor.

Blanket deployment over water is shown (Figure 9). There was no humidity problem. Provided the water was always colder than the room temperature the relative humidity fell to the general room level (40%) from about 100 mm above the water level. One minor problem with this method of testing is that the stowage drum torque is absorbed in lifting the blankets from the polystyrene floats onto the drum and as a result little or no boom compressive tip load is induced to assist retraction. Therefore, motor currents were higher than expected. Although this test demonstrates the correct function of the SDM/ Solar Cell Blanket interface, representative motor performance is best obtained using a zero blanket mass simulation. The blankets were replaced by terylene cords between the Spreader Bars and Drum, resulting in a good prediction of in-orbit motor and Boom Length Compensator performance.

The SDM integrated with mass-and-stiffness-representative PDM and SAD successfully completed Vibration testing including vertical vibration (Figure 11). In all cases blanket slippage was minimal and did not affect subsequent deployment and retraction. The overall first resonant frequency of the stowed wing was 39 Hz (Requirement 25 Hz). Temperatures recorded during the Thermal Balance tests were generally within 5°to 10°C of predicted values and the Thermal Vacuum Function and Accelerated Life test were completely successful. Solar Cell blanket tensions from these tests are summarised (Figure 8).

CONCLUSION

The adoption of an existing design, coupled with direct access to supporting data, has reduced design and development time. It enabled major effort to be concentrated on design modifications and additions, with the knowledge that the concept was proven. An initial concern was the 5-year life with exposure to approximately 30,000 eclipse thermal cycles. However, the results of the thermal vacuum testing, particularly with regard to the lubrication aspects, have instilled a high degree of confidence in the design and laid the foundation for the future development of this and other mechanisms which have to comply with similar requirements. The mechanism has proven its ability to stow, protect and deploy the solar cell blankets. The final inspection of the blankets after completion of the Qualification programme showed that the cover glass on 28 real cells and 22 dummy cells out of a total of 24,370 cells had been cracked as a result of handling and testing.

ACKNOWLEDGEMENT

The author wishes to thank the Hughes Aircraft Company personnel and, in particular, Mr. G. Wolff, who provided FRUSA data and technical support during the initial design phase.

REFERENCES

1) G. Wolff and A. Withmann, "The Flight of the FRUSA," presented at the AIAA 9th Electrical Propulsion Conference, 1972.

2) NASA. MSFC-STD-512A, "Standard Man/Systems Design Criteria."

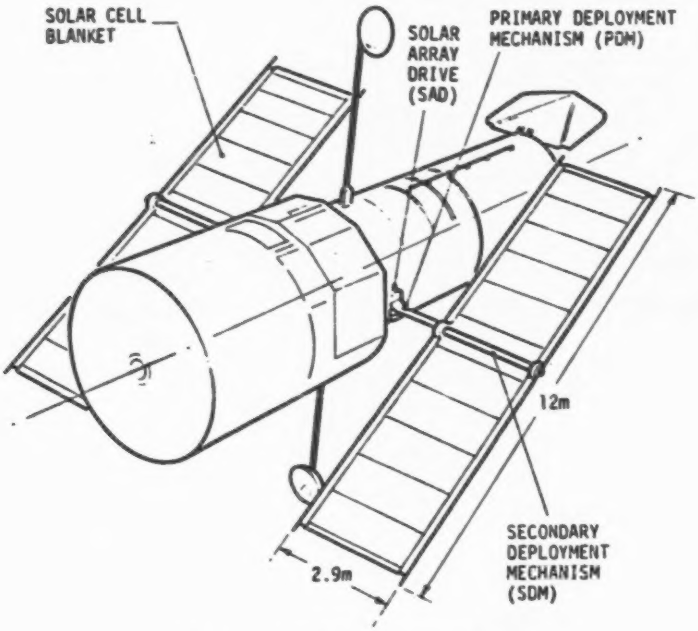
SOLAR CELL BLANKET
SOLAR ARRAY DRIVE (SAD)
PRIMARY DEPLOYMENT MECHANISM (PDM)
12m
2.9m
SECONDARY DEPLOYMENT MECHANISM (SDM)

Fig.1. DEPLOYED SOLAR ARRAY

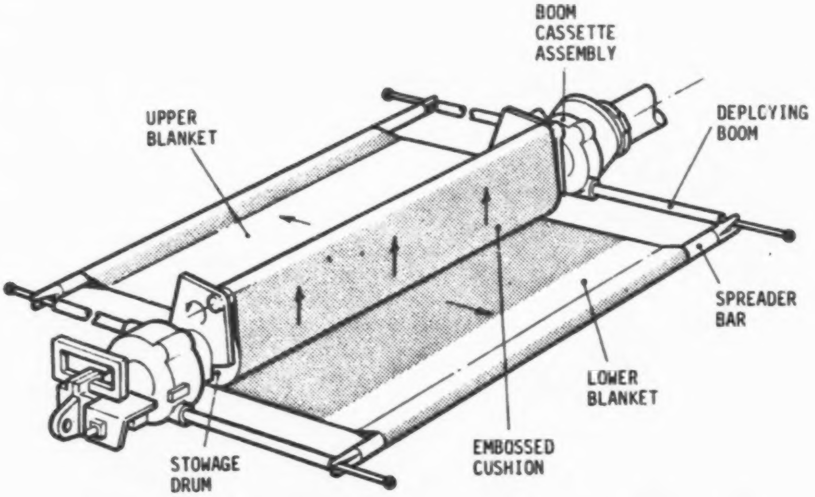
BOOM CASSETTE ASSEMBLY
UPPER BLANKET
DEPLOYING BOOM
SPREADER BAR
LOWER BLANKET
EMBOSSED CUSHION
STOWAGE DRUM

Fig.2. SDM DEPLOYMENT OF SOLAR CELL BLANKETS

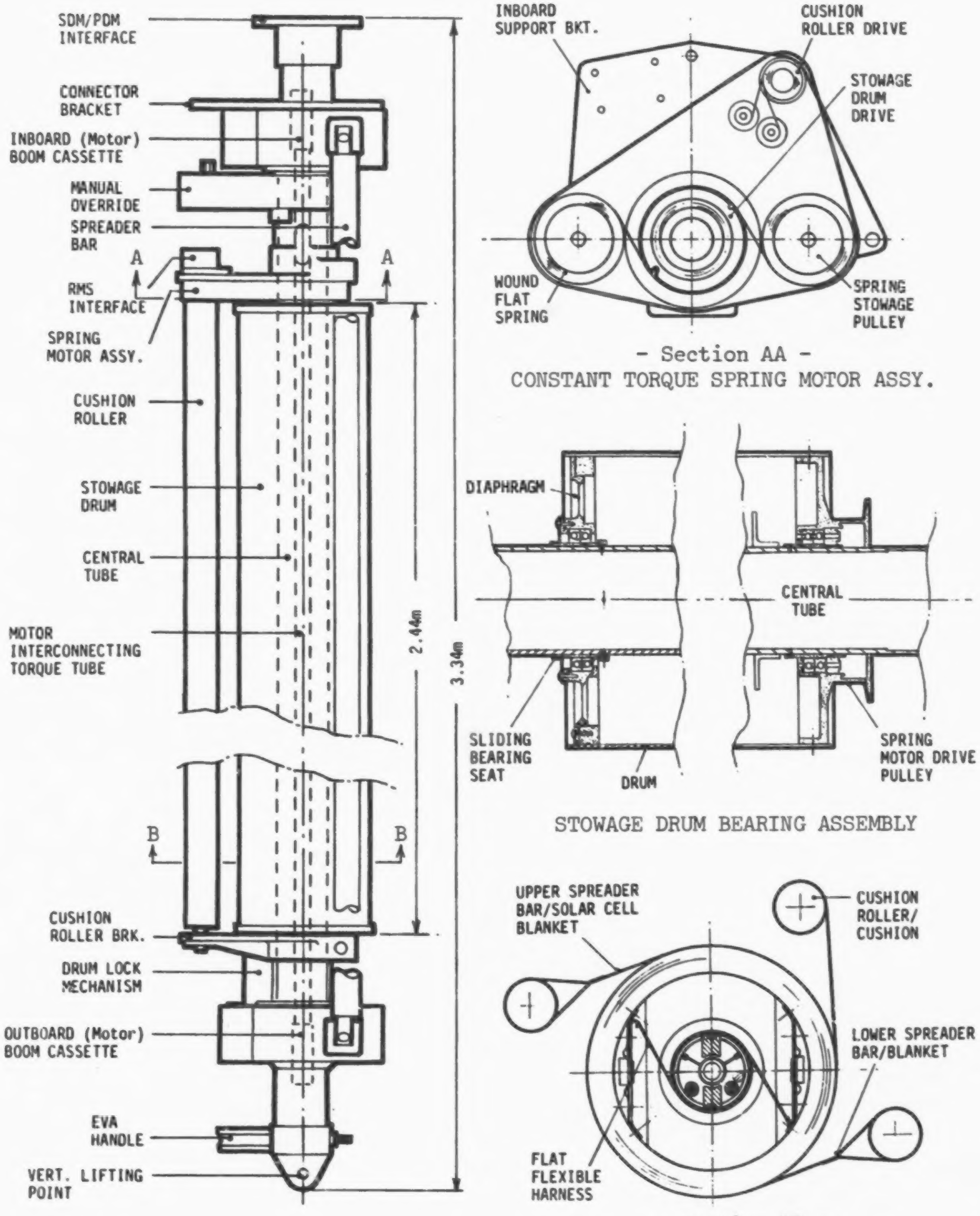
SDM/PDM INTERFACE
CONNECTOR BRACKET
INBOARD (Motor) BOOM CASSETTE
MANUAL OVERRIDE
SPREADER BAR
A
A
RMS INTERFACE
SPRING MOTOR ASSY.
CUSHION ROLLER
STOWAGE DRUM
CENTRAL TUBE
MOTOR INTERCONNECTING TORQUE TUBE
2.44m
3.34m
B
B
CUSHION ROLLER BRK.
DRUM LOCK MECHANISM
OUTBOARD (Motor) BOOM CASSETTE
EVA HANDLE
VERT. LIFTING POINT
INBOARD SUPPORT BKT.
CUSHION ROLLER DRIVE
STOWAGE DRUM DRIVE
WOUND FLAT SPRING
SPRING STOWAGE PULLEY
DIAPHRAGM
CENTRAL TUBE
SLIDING BEARING SEAT
DRUM
SPRING MOTOR DRIVE PULLEY
UPPER SPREADER BAR/SOLAR CELL BLANKET
CUSHION ROLLER/ CUSHION
LOWER SPREADER BAR/BLANKET
FLAT FLEXIBLE HARNESS

- Section AA -
CONSTANT TORQUE SPRING MOTOR ASSY.

STOWAGE DRUM BEARING ASSEMBLY

- Section BB -
HARNESS/BLANKET INTERFACE

Fig.3: SDM MAJOR COMPONENTS

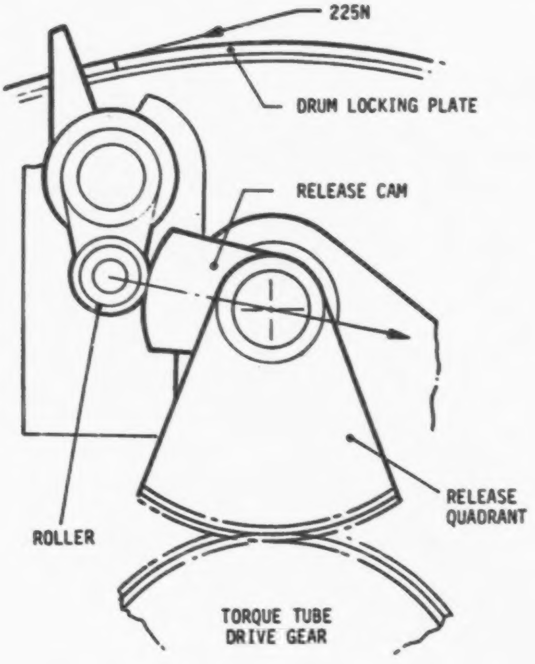
225N
DRUM LOCKING PLATE
RELEASE CAM
RELEASE QUADRANT
ROLLER
TORQUE TUBE DRIVE GEAR

Fig.4. RELEASE MECHANISM LAYOUT

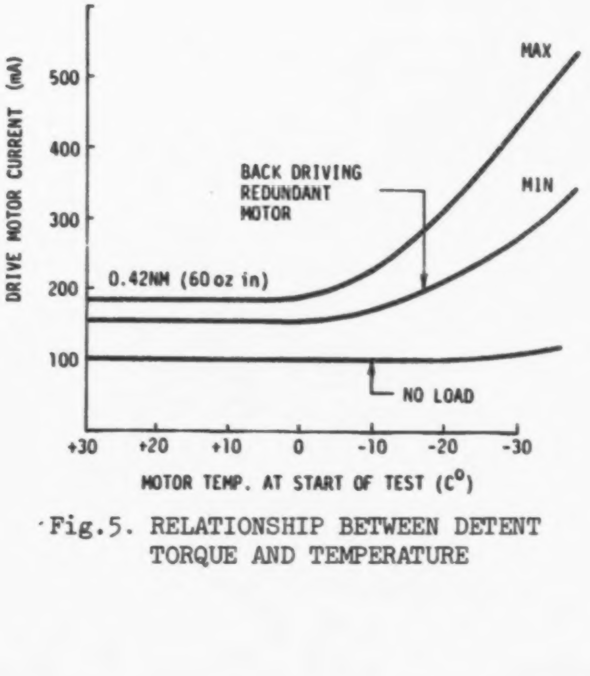

Fig.5. RELATIONSHIP BETWEEN DETENT TORQUE AND TEMPERATURE

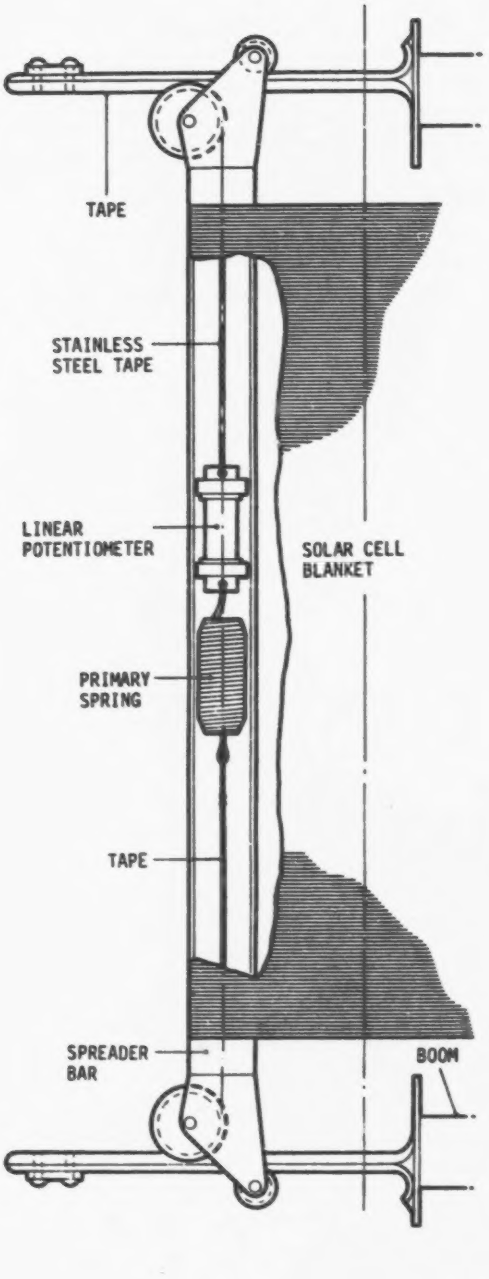
TAPE
STAINLESS STEEL TAPE
LINEAR POTENTIOMETER
SOLAR CELL BLANKET
PRIMARY SPRING
TAPE
SPREADER BAR
BOOM

Fig.6: BOOM LENGTH COMPENSATOR POTENTIOMETER INTERFACE

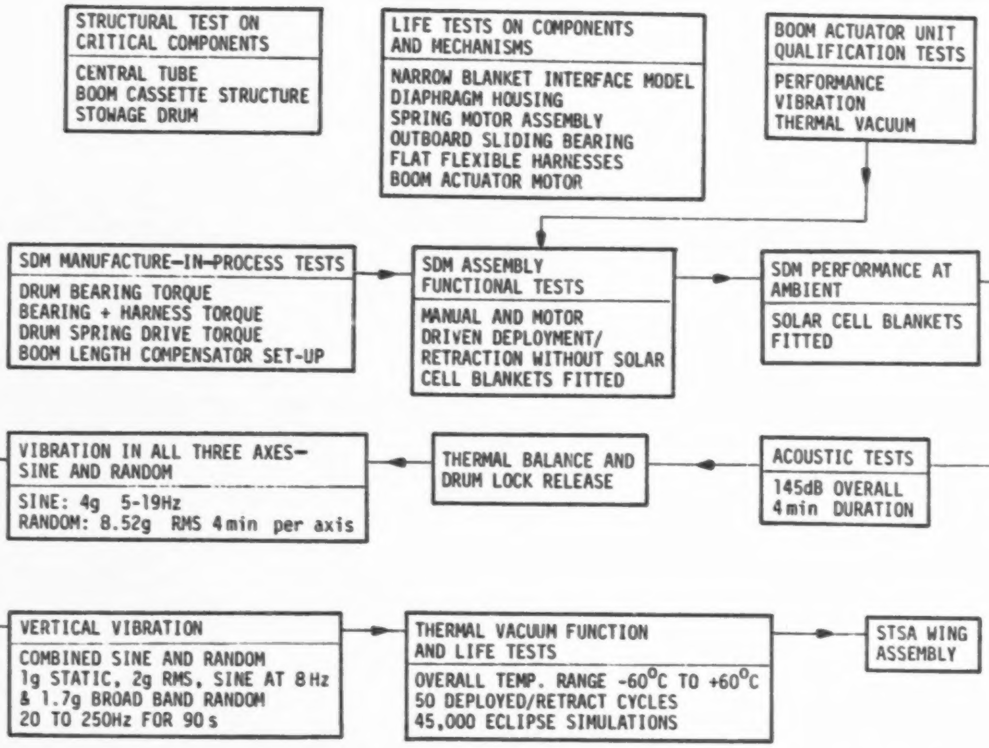
STRUCTURAL TEST ON CRITICAL COMPONENTS
CENTRAL TUBE
BOOM CASSETTE STRUCTURE
STOWAGE DRUM
LIFE TESTS ON COMPONENTS AND MECHANISMS
NARROW BLANKET INTERFACE MODEL
DIAPHRAGM HOUSING
SPRING MOTOR ASSEMBLY
OUTBOARD SLIDING BEARING
FLAT FLEXIBLE HARNESSES
BOOM ACTUATOR MOTOR
BOOM ACTUATOR UNIT QUALIFICATION TESTS
PERFORMANCE
VIBRATION
THERMAL VACUUM
SDM MANUFACTURE-IN-PROCESS TESTS
DRUM BEARING TORQUE
BEARING + HARNESS TORQUE
DRUM SPRING DRIVE TORQUE
BOOM LENGTH COMPENSATOR SET-UP
SDM ASSEMBLY FUNCTIONAL TESTS
MANUAL AND MOTOR DRIVEN DEPLOYMENT/ RETRACTION WITHOUT SOLAR CELL BLANKETS FITTED
SDM PERFORMANCE AT AMBIENT
SOLAR CELL BLANKETS FITTED
VIBRATION IN ALL THREE AXES- SINE AND RANDOM
SINE: 4g 5-19Hz
RANDOM: 8.52g RMS 4min per axis
THERMAL BALANCE AND DRUM LOCK RELEASE
ACOUSTIC TESTS
145dB OVERALL
4min DURATION
VERTICAL VIBRATION
COMBINED SINE AND RANDOM
1g STATIC, 2g RMS, SINE AT 8Hz & 1.7g BROAD BAND RANDOM 20 TO 250Hz FOR 90s
THERMAL VACUUM FUNCTION AND LIFE TESTS
OVERALL TEMP. RANGE -60°C TO +60°C
50 DEPLOYED/RETRACT CYCLES
45,000 ECLIPSE SIMULATIONS
STSA WING ASSEMBLY

NOTE: Between each environmental test performance tests, mechanical inspection and an electrical check of the solar array was carried out.

Fig.7. TESTS PROGRAMME SUMMARY

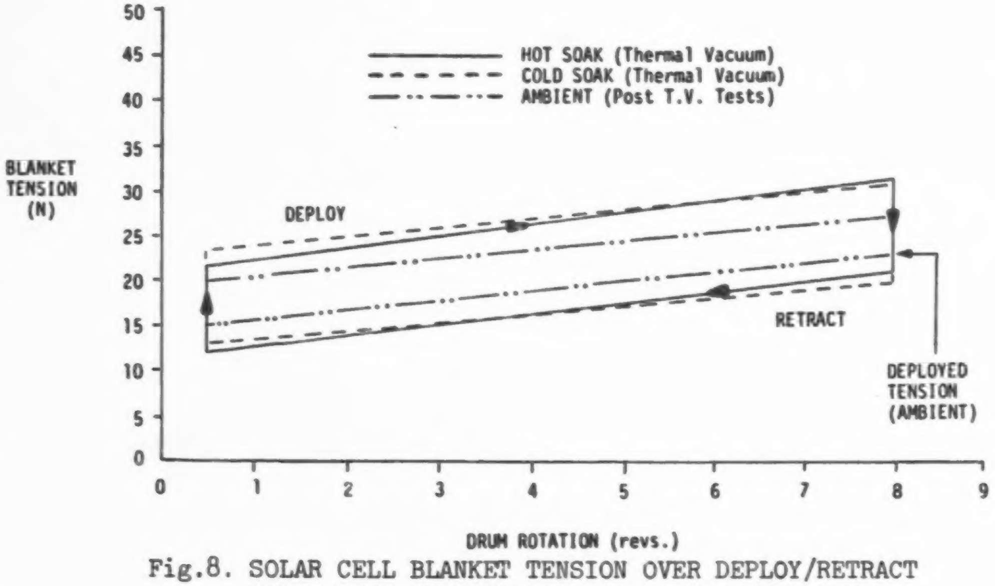

Fig.8. SOLAR CELL BLANKET TENSION OVER DEPLOY/RETRACT CYCLE DERIVED FROM T.V. AND LIFE TESTS DATA

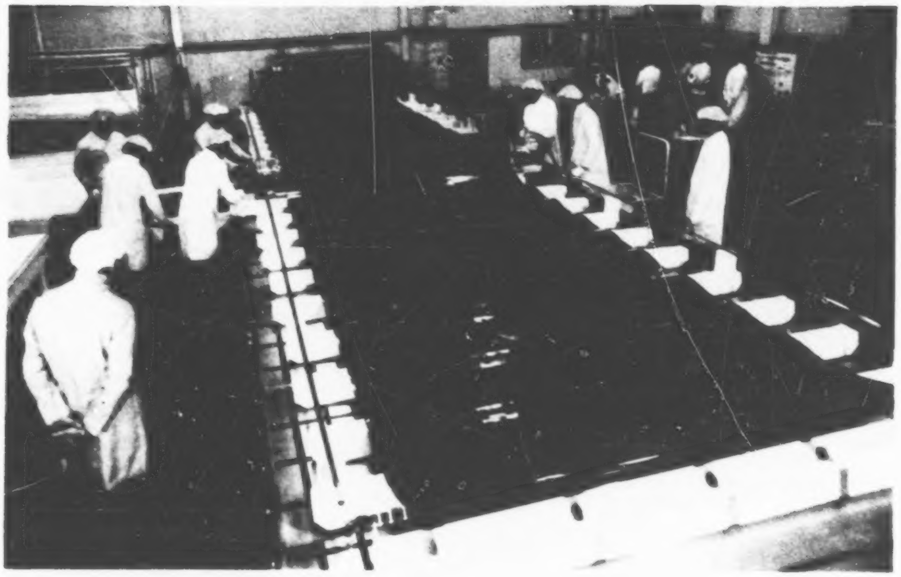

Fig.9. SOLAR CELL BLANKET DEPLOYMENT TEST OVER WATER

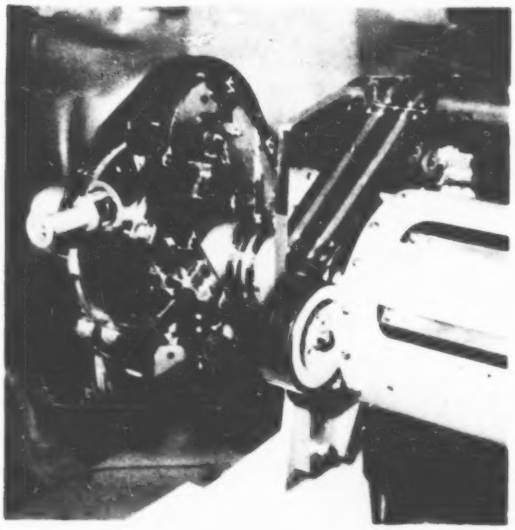

Fig.10. SDM INBOARD BOOM CASSETTE AND CONSTANT TORQUE SPRING MOTOR ASSEMBLY

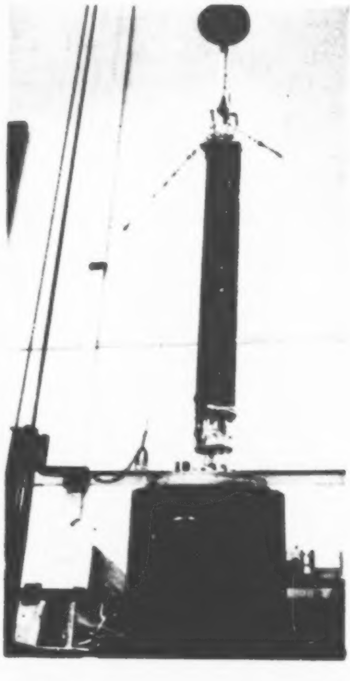

Fig.11. SDM STOWED CONFIGURATION VERTICAL VIBRATION TEST

T. R. Cawsey
British Aerospace
FPC 82, P.O. Box 5
Filton, Bristol BS12 7QW
England

Mr. Cawsey has 20 years' experience in mechanism design, initially on guided weapon systems but since 1969 on spacecraft. This includes the design, manufacture, and test of an early roll-up solar array mechanism; pantograph primary deployment mechanism; and the deployable booms, hinges, and release mechanism for the ISEE-B spacecraft that was launched in October 1977 as part of a joint NASA/ESA program. Since 1978, he has been the design engineer responsible for the space telescope solar array secondary deployment mechanism.

Blank Page

SOLAR DRUM POSITIONER MECHANISMS *

By L. W. Briggs

Hughes Aircraft Company

ABSTRACT

The need for additional power on spinning satellites has required development of deployable solar arrays activated, as on a 3-axis vehicle, after separation from a booster or shuttle orbiter. Mechanisms have been developed at Hughes for telescopically extending a secondary 36.3-kg (80-pound), 2.13-m (84-inch) diameter spinning solar drum for a distance of 2.0 m (80 inches) or more along the spin axis. After extension, the system has the capability of dynamically controlling the drum tilt angle about the spin axis to provide precision in-orbit balancing of the spacecraft.

This approach has been selected for the SBS, ANIK C, ANIK D, WESTAR B and PALAPA B satellites. It has been successfully demonstrated during the in-orbit deployment of the aft solar panels of the SBS F-3 and F-1 satellites, subsequent to the November 1980 and September 1981 launches.

INTRODUCTION

The Hughes HS 376 series of spacecraft utilize deployable, telescoping solar panel drums (see Figure 1) to enhance the on-board power capability. During launch and transfer orbit, the aft (outer) solar drum in its stowed position fits over the forward (inner) solar panel. During the drift orbit, the aft solar drum is extended by the operation of three Solar Drum Positioner (SDP) mechanisms. The mechanisms are located 120 degrees apart at the aft end of the inner solar panel (see Figure 2) with their output pinions engaging three longitudinal gear racks, mounted to the inner surface of the aft (outer) solar panel drum (see Figures 3 and 4). At full extension, each rack is driven into an axial anti-backlash spring located on the SDP. Differential operation of the SDP is then used to tilt the outer drum to provide dynamic balancing of the spinning spacecraft.

Trade-off studies of devices for mechanization of the extension resulted in the selection of a rack-and-pinion system with a stepper motor drive which contains a unique approach to redundancy for the size 11 permanent-magnet stepper motor.

A significant development has been minimizing the backlash or dead zone in the design to insure dynamic control during deployment and controlled in-orbit balancing at the extended position.

---

* Developed under contracts to Satellite Business Systems (SBS) and Telesat, Canada (ANIK).

FUNCTIONAL DESCRIPTION

Prior to deployment of the outer drum, the pyrotechnic locks holding the outer drum at the Solar Drum Positioner locations are released. Three motors (one of two redundant ones on each SDP) are pulsed simultaneously at a relatively slow rate (5 pulses per second) to initiate the outer drum deployment. As the drum extends, it disengages three clevis-type supports at the upper end which provide lateral support during launch. The drum is now constrained by the SDP mechanisms, each of which has a pair of rollers (one spring loaded) riding in longitudinal grooves in the rack. These rollers guide the racks during deployment and provide tangential and radial stiffness.

During the deployment, all three SDP potentiometers are monitored continuously to provide indication of uniform extension of the three mechanisms. Once uniformity of extension is confirmed, the ground-commanded pulse rate is increased to 25 pulses per second. As the outer panel extends, potentiometer dead-band traverses are counted to establish the drum position. Near the end of the deployment stroke, the pulse rate is again decreased to 5 pulses per second and pulsing continues at this rate until the telemetry indicates the rack stops have engaged the SDP anti-backlash springs for a distance of 0.5 centimeters (0.2 inch). During the deployment cycle, the flexible power harness connecting the two drums is gradually unfolded from its stowed position between the two drums.

The axial anti-backlash springs preload the gears to eliminate backlash and provide axial stiffness between forward and aft panels. Travel limit stops at the end of the gear racks prevent overdriving of the panel. The system is now in a position where differential pulsing of the SDP motors can "dewobble" the spacecraft.

DESIGN AND PERFORMANCE CHARACTERISTICS

The key design and performance characteristics of the SDP mechanisms are listed in Tables I and II. The gear ratio was chosen to provide a minimum two-to-one margin (allowing for temperature de-rating) of torque in the extended configuration. The resulting best-case torque capability determined the gear tooth size required. The 2160:1 gear ratio results in a small output step size of 0.0018-cm (0.0073-in) axial displacement. When using the slow step mode (5 steps per second), this small step size enables the telemetry of the position indicator (potentiometer) to be observed and reacted to before sufficient differential travel of any of the racks can cause damage to the panels due to excessive tilt angle. (The allowable detection and reaction time increases with extended distance.)

In the fast pulsing mode, the 25-step-per-second rate is well below the resonant frequency of the motor in combination with the inertia lead, and controlled stepping is assured.

MECHANISM DESIGN DESCRIPTION

Each Solar Drum Positioner Mechanism is comprised of redundant stepper motors, gearheads and worm and wheel sets driving into a common, bevel gear differential whose spider, or trunnion shaft, is keyed to a common output shaft and pinion gear. A redundant element potentiometer provides shaft position indication through the spacecraft telemetry. A set of integral guide rollers secure the gear rack mating with the output pinion, and an axial compression spring engages a stop incorporated at the end of the rack (see Figures 5 and 6). The differential drive provides gear train redundancy up to the output pinion without single-point failure.

The stepper motors are phase-switched, four-phase, permanent-magnet-type motors. Each motor is powered by 28-volt-dc (nominal) square-wave pulses, sequentially applied to the four motor windings.

Each motor is coupled to a gearhead of the same size 11 configuration. The gearhead has a four-stage spur gear drive, with a total reduction of 36:1. The output of the gearhead drives a worm/worm wheel gear stage which has a reduction of 30:1. Each worm wheel is fastened to one side of the differential drive system, which allows either motor or both to drive the output pinion (see Figures 7 and 8). The total reduction from the motor to the output pinion is 2160:1 with a single motor in operation. A 5.1-cm (2-in) pitch diameter pinion meshes with the gear rack (mounted on the outer panel). A 90° step of the motor results in 0.0018-cm (0.00073-in) axial movement of the rack. The outer panel travels 2.1 meters (82.7 inches) for full deployment which corresponds to 13.16 revolutions of the output pinion.

A redundant element potentiometer is mounted to the housing opposite the pinion. The wiper of the potentiometer is pinned to the output shaft which directly couples the wiper to the output pinion. The conductive plastic base of the potentiometer has two resistive elements, each with a 10° dead band. The wiper fingers contact the elements such that the dead bands are 180° out of phase. Thus, an indication of output pinion position is possible for the entire 360° of rotation. The dead bands of the potentiometer elements are set at 90° and 270° when the drum is in its fully stowed condition, so that dead bands are not encountered at fully stowed and fully deployed positions.

Rack-and-pinion gear teeth have been designed to accommodate the tilt capability. The output pinion teeth are crowned, and the rack has added clearance at the top portion to allow for tilting.

BEARINGS AND LUBRICATION

All bearings supporting the worm/wheel gears and differential are preloaded angular contact type. Ground shims are provided to set the proper wavy spring preload forces. These bearings have Duroid 5813 retainers (a glass-filled Teflon/molybdenum-sulphide composite) and the balls and races are lubricated with sputtered MoS_2. The motor and gearhead bearings also have Duroid 5813 retainers and are "run-in" in a controlled atmosphere to transfer MoS_2 lubricant to the balls and races.

The small gearhead spur gears have a 2000-Å-thick coating of ion plated lead and are "run-in" as a gearhead assembly in a controlled atmosphere. The remainder of the gears and the worm shaft are treated with a proprietary solid, bonded lubricant (MoS_2). The bonded MoS_2 is employed at the worm/wheel and bevel gear interfaces because of extensive previous experience with this lubricant in similar space applications where sliding friction occurs.

REDUNDANCY

The differential approach to mechanical redundancy is common to the Solar Drum Positioner mechanism and the Antenna Positioner Mechanism (Reported at the 13th Aerospace Mechanisms Symposium in April 1979).

The differential gear system permits either motor/gearhead/worm and wheel system to drive the output shaft. Any failure in these components is overcome by switching to the standby system, which is unpowered for normal operation. In case of a failure (bearing or bevel gear) in the differential, both motors can be energized simultaneously and will cause the entire differential to rotate as a common member to drive the output shaft. In this mode, the gear ratio is halved and the step size at the output is doubled. The output torque remains the same as for normal operation. Redundancy at the main shaft output bearing is achieved by applying a thin sputtered MoS_2 film to the close-tolerance slip fits of bearing to shaft and bearing to housing. This creates, in effect, a journal bearing at these interfaces that allows operation if the output bearings fail.

QUALIFICATION/LIFE TESTS

The SDP was subjected to a design qualification test and a representative life test.

The key parameters evaluated during the qualification tests included the following:

- Output force (see Figure 9)
- Step accuracy (see Figure 10)

- Repeatability
- Potentiometer position indication
- Stiffness

The unit environmental tests consisted of the following exposures:

- Qualification level random vibration of 21 g's rms overall along each of 3 axes
- Qualification level thermal vacuum tests with a representative inertia load

The required life for the SDP during unit, subsystem, system and in-orbit operation was determined to be approximately 1.2 million steps, with 90% of the testing occurring in air. The planned mode of operation during ground testing is to share the steps between two motors to minimize the wear on the gearheads and the worm/wheel assemblies. Since the solid, bonded lubricant used at the worm/wheel and bevel gear interfaces has a much higher coefficient of friction (and greater wear rate) in air than in vacuum, the life test was conducted in air.

The SDP life test unit was exercised for a total of 2.5 million steps with the appropriate inertia load and a friction load representative of the off-loader mismatch experienced in system testing. The testing was conducted with one motor performing 60% of the steps and the other 40%. Examination of the gearhead spur gears and the worm/wheel and bevel gears subsequent to the test showed the lubricated surfaces still to be in acceptable condition. The backlash increase measured over the 76.2-cm (30-inch) test stroke varied from 0.0025 cm (.001 inch) to 0.005 cm (0.002 inch).

BACKLASH CONTROL

Early in the development program, it was recognized that the backlash inherent in the proposed geared system could have an effect on the dynamic stability of the system during deployment of the panel, since the spacecraft is in a stabilized, minimum momentum situation at that time. A dynamic analysis indicated that a backlash on the order of 0.025 cm (0.010 inch) would be acceptable from a dynamic stability consideration.

Since there was reluctance to accept the complexity, weight and added wear risk that would be incurred by anti-backlash spring loading to eliminate backlash, the decision was made to limit the backlash in the design by close control of the geometry, and by specification of AGMA Class 10 gearing to reduce the variable contributors, such as tooth-to-tooth error, runout and eccentricity.

The major contributors to backlash in the system are the worm and worm gear interface, the bevel gear mating and, of course, the pinion-to-rack interface. The gearhead is a minimal contributor because of a 30 arc-minute backlash control and the 60:1 gear reduction downstream of the gearhead.

The three areas of concern all have a relatively heavy, bonded, solid lubricant applied. For the worm and worm gear sub-assembly, close dimensional control is exercised on the center mounting bores in the housing and a special nominal center fixture is used to check the fit of these parts before and after the lube application and burnishing. The bevel gears are pre-assembled and precisely measured. Special machining cuts and shimming are then performed to establish minimum backlash without interference. The rack-and-pinion interface is adjusted at assembly of the SDP to the spacecraft and the fit is maintained by the spring-loaded guide roller assembly engaging the rack.

The above controls and operations are intended to reduce the backlash during deployment of the panel. At the extended position, engagement of the rack stop into the compression springs reduces the backlash to zero.

During the orbital deployment of the SBS F-3 and F-1 SDP's, the effectiveness of the backlash control was demonstrated. Infrequent actions of the thruster active nutation control were consistent with other expected energy dissipators, and additional firings due to excessive SDP backlash did not take place.

CONCLUSIONS

The system described has operated very well on the two spacecraft launched to date. No evidence of perturbation due to stepping or backlash has been observed during monitoring of the spacecraft during deployment of the panels. The in-flight results demonstrated the effectiveness of the minimum backlash design as well as all other design features.

TABLE 1. DESIGN CHARACTERISTICS

PARAMETER	CHARACTERISTICS
MOTOR SIZE AND TYPE	SIZE 11, PERMANENT MAGNET, 90° STEPPER
MOTOR TORQUE	72 GM-CM (1.0 OZ-IN) RUNNING
GEARHEAD	SPUR GEAR; 36:1 REDUCTION
WORM GEAR STAGE	24 PITCH; 30:1 REDUCTION
DIFFERENTIAL	32 PITCH BEVEL; 2:1 EFFECTIVE REDUCTION
OUTPUT PINION	24 PITCH; 48 TEETH
RACK	24 PITCH; 20° PRESSURE ANGLE
OUTPUT STEP SIZE	0.0018 CM (0.00073 IN) AXIAL
INPUT POWER	15 W AT 28 VDC
SDP WEIGHT	1.72 KG (3.8 LB) EACH

TABLE 2. PERFORMANCE CHARACTERISTICS

PARAMETER	PERFORMANCE
DEPLOYMENT TRAVEL	2.1 M (82.7 IN)
DEPLOYMENT RATE	0.046 CM/S (0.0183 IN/S) AT 25 STEPS/S
OUTPUT FORCE	133 N (30 LB) AXIAL PER MECHANISM
MECHANISM STIFFNESS	>1751 N/CM (1000 LB/IN) IN PRELOAD RANGE
BACKLASH	<0.0178 CM (0.007 IN) DURING DEPLOYMENT 0 EXTENDED
POTENTIOMETER RESOLUTION	0.061 CM (0.024 IN) OF DRUM TRAVEL
STEPPING RATE	
EXTENSION	5 TO 25 STEPS/S
TILT	5 STEPS/S

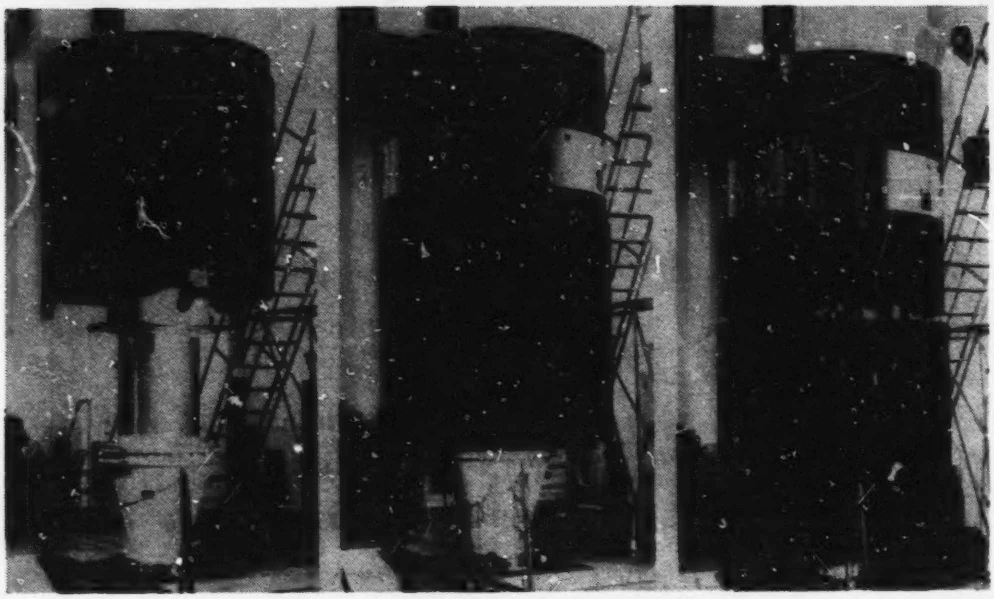

FIGURE 1. DRUM DEPLOYMENT

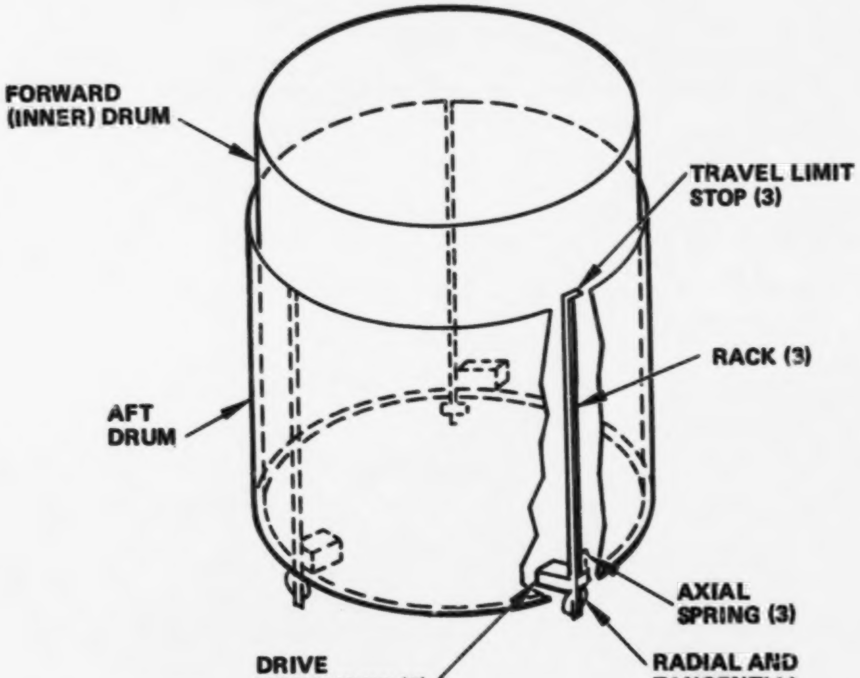
FORWARD (INNER) DRUM
TRAVEL LIMIT STOP (3)
RACK (3)
AFT DRUM
AXIAL SPRING (3)
DRIVE MECHANISM (3)
RADIAL AND TANGENTIAL ROLLERS

FIGURE 2. SOLAR DRUM POSITIONER SYSTEM

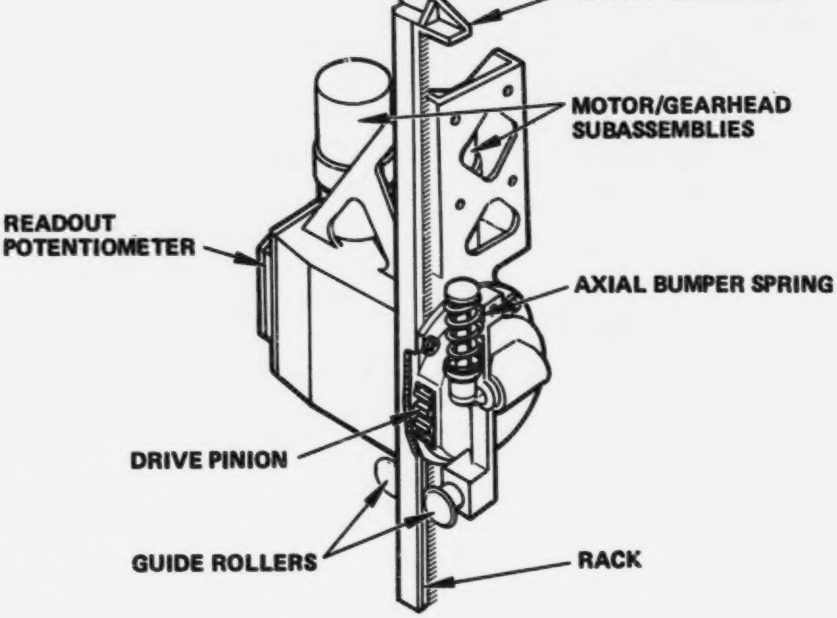
TRAVEL LIMIT STOP
MOTOR/GEARHEAD SUBASSEMBLIES
READOUT POTENTIOMETER
AXIAL BUMPER SPRING
DRIVE PINION
GUIDE ROLLERS
RACK

FIGURE 3. MECHANISM LAYOUT

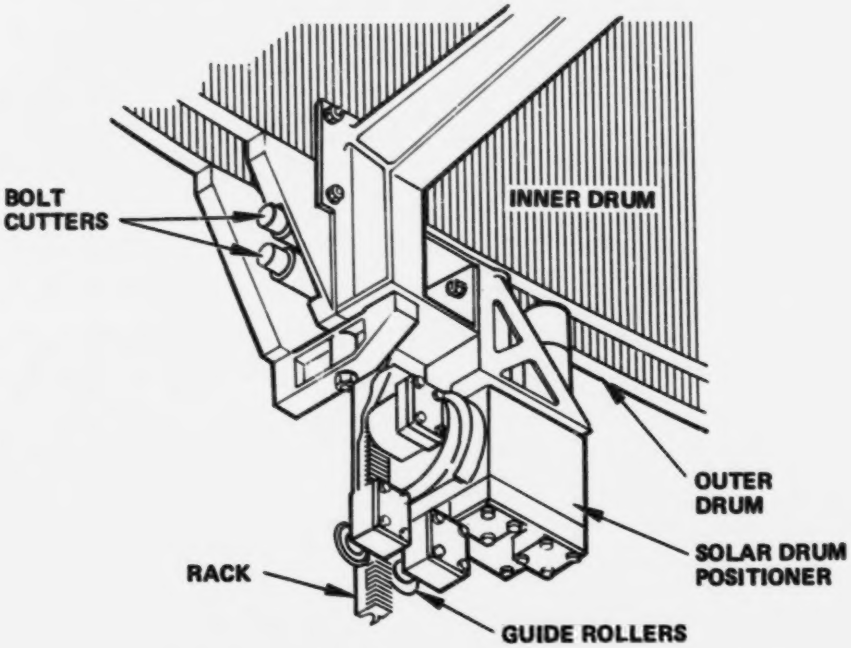
BOLT CUTTERS
INNER DRUM
OUTER DRUM
SOLAR DRUM POSITIONER
RACK
GUIDE ROLLERS

FIGURE 4. INTERFACE

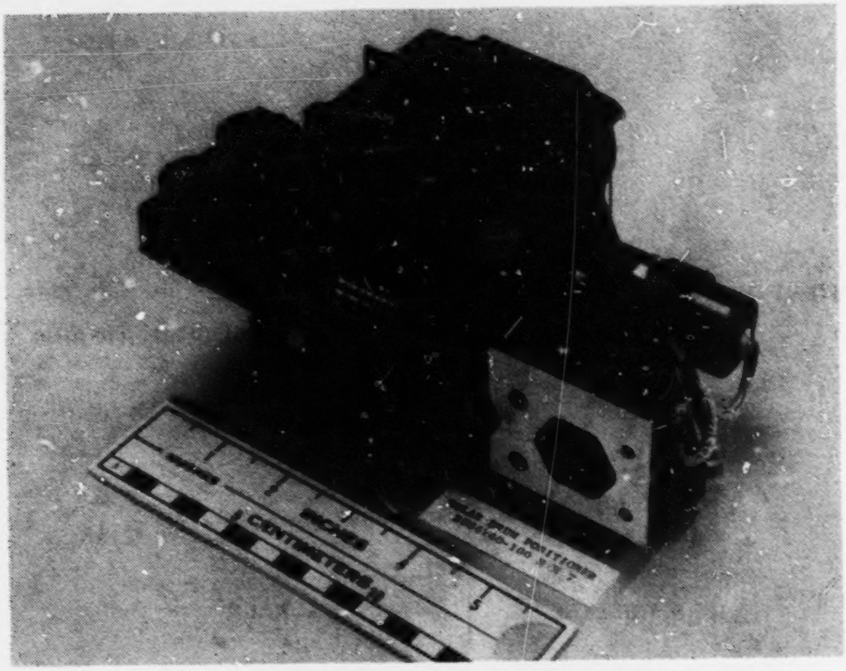
HUGHES
INCHES
CENTIMETERS

FIGURE 5. SOLAR DRUM POSITIONER NEAR SIDE

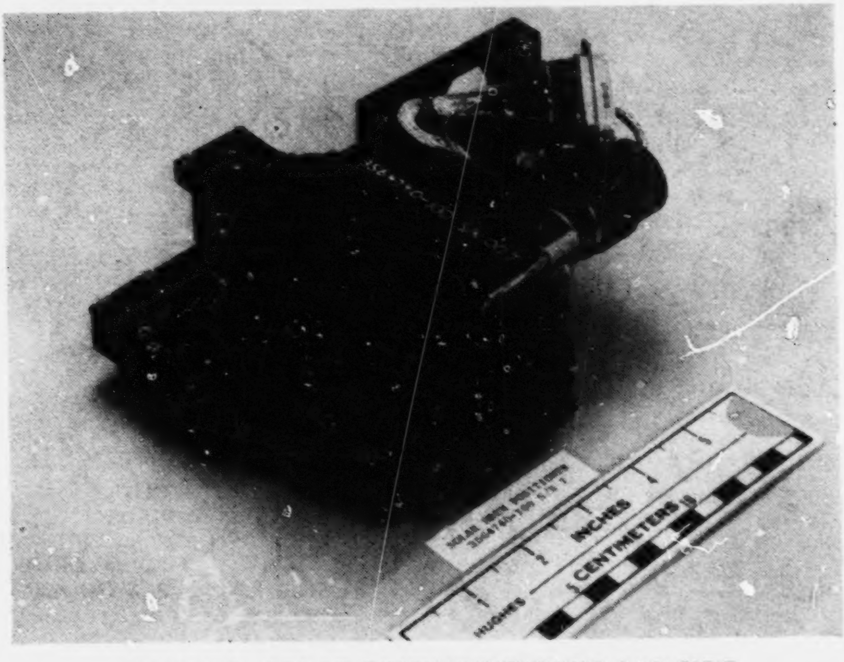
INCHES
CENTIMETERS
HUGHES

FIGURE 6. SOLAR DRUM POSITIONER FAR SIDE

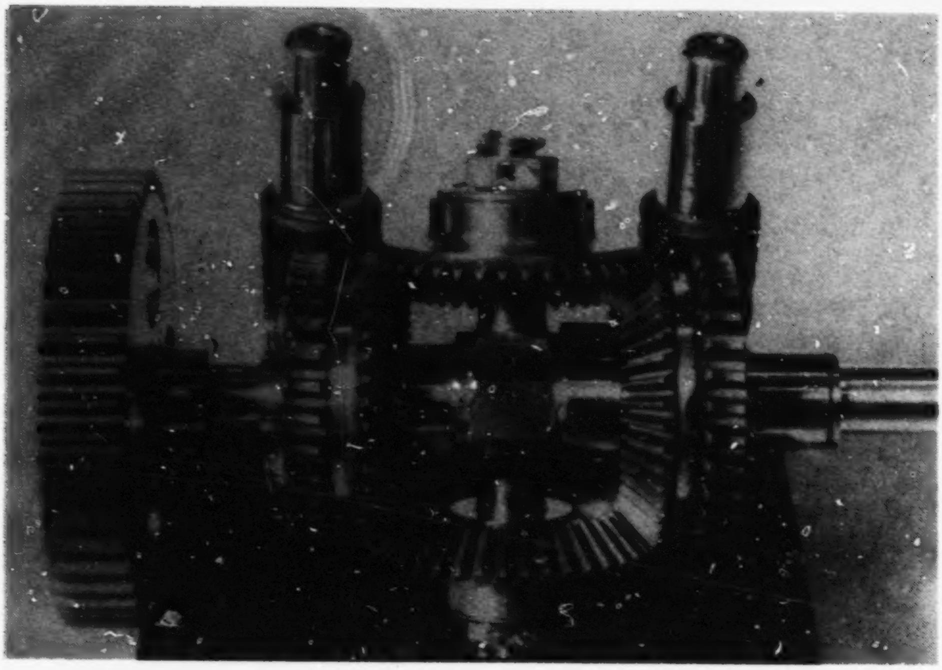

FIGURE 7. DIFFERENTIAL AND WORM GEAR ASSEMBLY

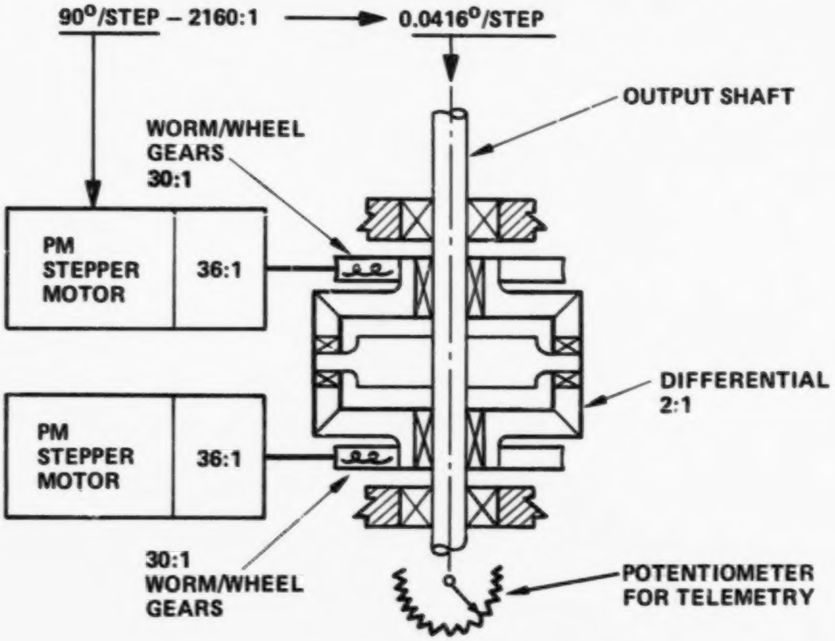
90°/STEP – 2160:1
0.0416°/STEP
OUTPUT SHAFT
WORM/WHEEL GEARS 30:1
PM STEPPER MOTOR
36:1
DIFFERENTIAL 2:1
PM STEPPER MOTOR
36:1
30:1 WORM/WHEEL GEARS
POTENTIOMETER FOR TELEMETRY

FIGURE 8. MECHANICAL SCHEMATIC

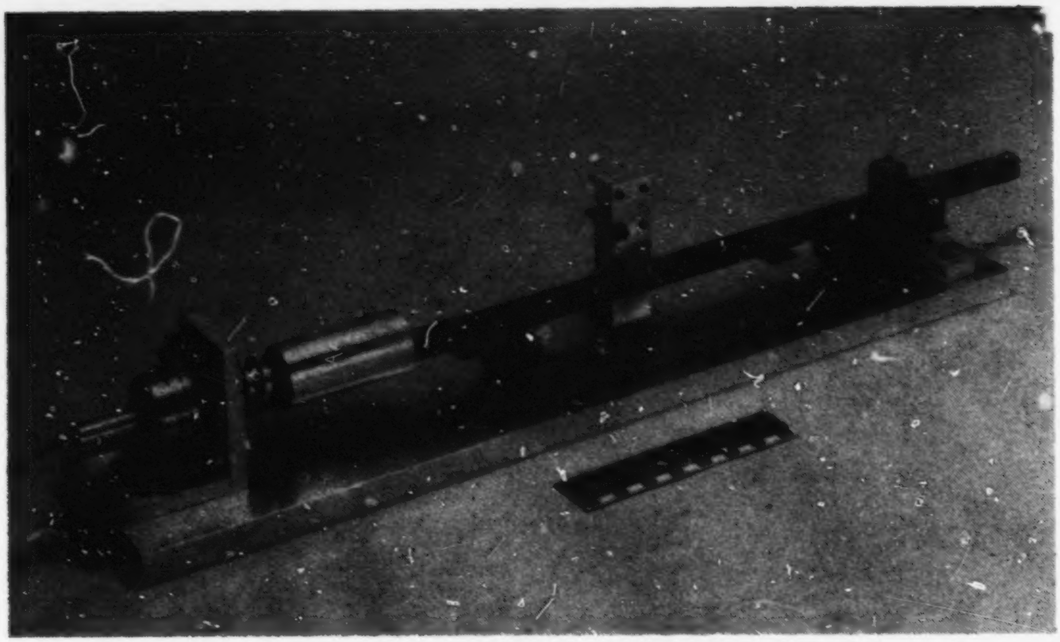

FIGURE 9. RACK TEST SECTION (FORCE OUTPUT)

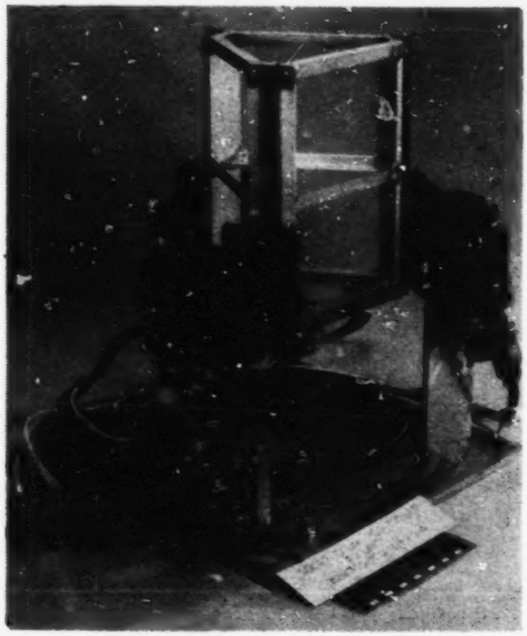

FIGURE 10. UNIT TEST FIXTURE

L. W. Briggs
Hughes Aircraft Company
P.O. Box 9219
Los Angeles, California 90009

Mr. Briggs is currently the senior project engineer in the Technology Division of the Space and Communications Group. He has 30 years' experience in the aerospace field involved in the design of electromechanical components for the Falcon, Phoenix, and Tow missiles; the Surveyor Moon Lander; and commercial and military satellites. During the last 12 years, he has been primarily concerned with the design and technical management of precision positioning and gimballing subsystems for space. Mr. Briggs is a graduate of the Illinois Institute of Technology.

Mr. Briggs was co-author of a paper on the antenna positioner mechanism that was presented at the 13th Aerospace Mechanisms Symposium held at Johnson Space Center in April 1979.

Blank Page

DEPLOYMENT/RETRACTION GROUND TESTING OF A LARGE FLEXIBLE SOLAR ARRAY

Darius T. Chung
Lockheed Missiles and Space Co.

ABSTRACT

In 1974, NASA Marshall Space Flight Center awarded to Lockheed Missiles and Space Co. a contract for a large (4 meter x 32 meter) flexible fold-up solar array. Under this contract a technology program was started at LMSC resulting in conceptual studies, design, fabrication, and ground test of a prototype solar array with the goal of eventual flight of this array as an experiment aboard the Space Shuttle. This paper addresses the simulated zero-gravity ground testing of the solar array consisting of eighty-four full-size panels (.368 meter x .4 meter each) and involving automatic, hands-off extension, retraction, and lockup operations.

Three methods of ground testing were investigated:

1. Vertical testing, similar to that previously conducted in a space station solar array program at LMSC
2. Horizontal testing, using an overhead water trough to support the panels
3. Horizontal testing, using an overhead track in conjunction with a counterweight system to support the panels

Method 3 was selected as baseline.

The test structure is made up of three sections; namely, the wing-assembly vertical support structure, the five-tier overhead track, and the mast-element support track.

The flexible solar array wing assembly was successfully extended and retracted numerous times under simulated zero-gravity conditions. These tests have significantly contributed to the flexible solar array design development and ultimately to the potential success of the solar array shuttle flight experiment.

INTRODUCTION

Lockheed Missiles and Space Co. (LMSC), in conjunction with the National Aeronautics and Space Administration (NASA), Marshall Space Flight Center (MSFC), Huntsville, Alabama has had the responsibility for the design, development, manufacturing, and ground testing of a large-area flexible solar array. The flexible solar array blanket assembly consisting of eighty-three mass-simulated panels and one electrical panel is required to partially extend, fully extend, partially retract, fully retract, and lock up to its fully preloaded stowage mode.* These operations must be performed automatically and demonstrate hands-off, proper unfolding, folding, and lock-up. The simulated zero-gravity, ground test structure developed under this program provided the capability to perform these tasks.

BASELINE SELECTION

During the proposal stage three methods of simulated zero-gravity testing were investigated.

VERTICAL TESTING. This test method was considered first because of LMSC's prior vertical testing experience in connection with a space station solar array contract (NASA Contract NAS9-11039). The total deployed blanket assembly area of this design was approximately 10,000 sq ft, and for ground test one quadrant (2500 sq ft) was automatically deployed sequentially. The quadrant was made up of five individual sub-blanket assemblies, each with a deployed area of 504 sq ft (6 ft x 84 ft), in order to achieve sequential deployment. For ground testing the solar panel container assembly and the mast canister were mounted at floor level. The array was then deployed upward. Automatic counterbalancing of the deploying array was used to counteract the gravity forces. The cover, outboard supports, and each mast element were individually counterweighted, however the solar panels were counterweighted only through the outboard supports at the upper end of the deploying array from which the solar blanket was suspended. In this design, retraction was not a requirement. Consequently, gravity and test personnel were employed to assist in the refolding of the sub-blanket assemblies during a retraction. As a result of sequential deployment and because no retraction was required, vertical testing was the most economically feasible method to use.

---

*NASA Contract NAS8-31352

This test method does not require counterbalancing individual panels. However, the top-most hinge must have the capability to support the total weight of the panels, and the load capability of each adjacent lower hinge can be decreased by the weight of a panel. The alternatives to varying hinge capabilities can be to counterbalance each panel (a very difficult task), or design all the hinges to the maximum capability (a highly over-designed hinge for flight). Counterbalancing, however, must be provided for all other deployed structure such as a cover, outboard supports, and the deployable mast elements.

HORIZONTAL TESTING. This method utilizes an overhead water trough which supports the deploying/retracting blanket assembly through a series of floats. Individual panels and their respective counterweights are vertically supported by the floats and would deploy horizontally. A series of questions resulted from this concept that raised doubts about success, such as:

1. Water leakage and spillage would fall on the assembly and the floor
2. Water on the floor could create a safety hazard
3. Float thickness would negate minimum stack height, which would affect lock-up capabilities
4. Damp atmosphere may create corrosion
5. Stagnant water would have to be replaced periodically.

HORIZONTAL TESTING--BASELINE. This method uses a counterweight system to counterbalance the vertically hung blanket assembly, which deploys and retracts horizontally. As compared to the vertical test method, a single flight-qualified hinge design is all that is necessary, because it is not affected by gravity. However, a ground test support loop at one end of each panel is required to attach the panel to its counterweights. As in vertical testing, the cover assembly and the outboard mechanism assemblies require counterbalancing--but not the deployable mast elements. An inexpensive eight-panel full-scale test model was built and manually operated. The demonstration was very successful and justified the selection of the test method (see Figure 1).

THE BASELINE SIMULATED-ZERO-GRAVITY TEST STRUCTURE

FULL-SCALE WING ASSEMBLY TEST OBJECTIVES. The selection of the test method was made on the basis that it could fulfill all of the test objectives. They are as follows:

- Demonstrate large area solar array hardware handling technology
- Demonstrate development, qualification, and acceptance test techniques
- Demonstrate simulated-zero-gravity, automatic hands-off wing assembly operation
    - Unlocking and locking of the cover assembly
    - Operation of the blanket assembly tensioning system
    - Full and partial deployment/retraction of the mast
    - Simulation of the zero-gravity fold-up
    - Attain planar configuration of deployed or partially deployed blanket assembly

The simulated zero-gravity ground test structure was designed and manufactured by LMSC, and is made up of three sections. The first section is the wing assembly vertical support structure which is supported at each end by bearings, allowing rotation of the wing assembly during extension and retraction. Concentricity of these end bearings was very critical during ground test. The rotation capability was also necessary to install the wing assembly to the test hardware. The second section is the overhead test structure which is made up of a five-tier track section approximately 33.5 meters long. The tracks are the surface for the roller assemblies which support the counterweights and their respective panels, the cover, the locking level mechanism, the mast tip fitting, and the deployed-panel tension distribution bars during extension and retraction operations. The third section is a mast element support track structure approximately 37 meters long which is sloped on one end. This track is the surface for ten wooden dollies that are attached to each other by nine nylon tie strings approximately 3 meters long. Another tie string, 1.5 meters long, attaches the lead dolly to the mast tip fitting of the wing assembly. These dollies and their tie strings are so designed as to provide intermittent support for the mast elements of the Able-Engineering Deployable Mast Assembly during extension and retraction of the wing assembly. During retraction the sloping surface of the track allows the dollies to move away from the retracting mast as it is stowed in its stowage canister (See Figure 2 and Figure 10).

WING ASSEMBLY VERTICAL SUPPORT STRUCTURE. This section of the ground test structure supports the solar array wing assembly through its container assembly. The container is mounted on this support structure at four attach points, which are the same points to be used to mount the solar array wing assembly in the Shuttle for flight. A master hole location tool plate is used to assure precise location of the holes. As shown in Figure 3, the support structure is made up of three sections; namely, the container center crank support assembly, the upper end support assembly, and the lower end support assembly. The center crank structure is an all-aluminum welded assembly made up of a five-inch pipe and its right-angled ends. The two container attach plates are located approximately 40 percent and 80 percent below the top of the pipe. Consequently, the upper container attach point is further away from the top end than its counterpart is from the lower end. To assure a stable top end, the longer upper support was required. The upper end support is a bolted assembly and in turn is attached to structure that is part of the test facility. It houses the upper end support thrust bearing. The lower end support is a stand-off assembly that is merely attached to the floor, and it houses the lower end support bearing. The upper and lower bearings must be vertically aligned to achieve a balanced condition and thus eliminate a built-in tendency of the center crank structure to rotate. Up-and-down adjustment is also necessary to center the container assembly to the vertically supported blanket assembly. In addition, the container attach plates have provisions for attaching a ground handling fixture so that the fully preloaded wing assembly can be installed on the ground test structure.

THE OVERHEAD TEST STRUCTURE. As shown in Figure 2, the overhead test structure is a 33.5-meter-long five-tier track assembly. The five-tier tracks are a bolted assembly, five of which are 6 meters long and one that is 3.5 meters long. Figure 4 is a typical bolted area of the five-tier track. In addition, on top of each track is a 33.5-meter-long continuous steel strip (.042 inch thick). On top and along the outer edge of the strip is a series of square roller guide bars that are butted to each other (they are not shown for clarity). Figure 5 shows the strip, roller guide bars, and roller assembly on a track. It also shows that, the roller assembly is tee-shaped with each pair of vertical rollers supporting the panel and its counterweight, and the pair of horizontal rollers providing guidance. Each roller assembly supports two panels and their respective counterweights, which are at different levels (see Figure 2). This is necessary to allow the counterweights to swing freely as the panels of the blanket assembly travel from their stowed to deployed positions. The first and last roller assemblies, however, support only their own panel and counterweight.

Figure 6a shows the roller assemblies in the stowed position on their respective tier level. Tiering is necessary to assure the thinnest stack of folded panels in the blanket assembly. Figure 6b shows a roller assembly supporting two counterweights and its respective panels in an operating mode. Note the mini-counterweights which are looped around the thin section. They can be moved in either direction to a final position so as to obtain a near-perfectly balanced situation of all the panels in the blanket assembly. Near-perfect balance is when the hinge lines of the folded blanket assembly are in line. This task is very tedious because movement of the mini-counterweight of one panel affects the balanced position of its adjacent panels. It should also be performed in a retracted, but not stowed, position. As a suggestion,one may consider removing the hinge pins, obtaining the near-perfect balance, fixing the position of the mini-counterweight and re-installing the hinge pin. Figure 6c and Figure 7 show the panel edge gound test support loop and the edge support rod that attaches to the counterweight by its support cables. Figure 6d illustrates the three positions of the blanket assembly.

Two other similar roller assemblies are also used to centrally support the intermediate and inner panel tension distribution bars. These bars through a negator spring motor system tension and establish planarity of the partially and fully deployed blanket assembly. The cover assembly and its two-axis counterweight system, the mast tip fitting (see Figure 8), and the whiffletree locking lever assemblies (see Figure 9) are supported by three similar and larger roller assemblies. The two-axis is necessary for the cover assembly because it requires counterbalancing sideways so its edges are parallel with the panel hinge lines and fore and aft to obtain parallelism to the base of the container assembly. The mast tip fitting does not require counterbalancing because it is centrally supported by the overhead structure. Figure 9 shows the whiffletree locking lever assembly is counterbalanced by a rotating weight. Tie cables with adjustable turn-buckles attach to the upper pair of locking levers only. The lower pair is then supported through the locking lever linkage mechanism and the geometry allows simultaneous movement of the levers.

MAST ELEMENT SUPPORT TRACK. This is the third section of the ground test structure and is totally made of wood with one exception, the adjustable steel cable diagonals. The track length is approximately 37 meters long and is made from ten 3.08-meter-long sections and one 6.76-meter-long sloping section. The end of each section is supported to a predetermined height by an offset tee/cross-over diagonal assembly. Every other pair of these assemblies is tied together by the diagonal steel cables and adjusted to its proper tension to assure stability. Under each assembly is a pair of height adjustment screws and two lock nuts per screw to obtain a flat level track. The dolly roller surface is made of particle board, and the butted end of each section of track is filled with wood putty, then sanded to a smooth surface thus eliminating surface irregularities (see Figure 2 and Figure 10). A series of dollies with wheels that are free to rotate support the mast elements as it is deployed. The lead dolly is tied to the mast tip with a nylon tie string. All subsequent dollies then tie to each other, and the maximum length of the tie strings is determined by the maximum length of unsupported mast. This information must be obtained from the mast subcontractor. When the mast is fully stowed, the dollies are butted against each other on the sloping surface of the track. As the mast deploys, the lead tie string, shortly thereafter, becomes taut and pulls the lead dolly up the slope. The dolly is positioned under the mast, thus providing the necessary support for the mast. This operation repeats itself for all subsequent dollies during partial or full deployment operations. During retraction the operation is reversed (see Figure 10).

CONCLUDING REMARKS. The vertical support structure and the mast element structure track were straight-forward designs and did not require any special tooling. Not so for the five-tier overhead support track. The materials used tobuild the five-tier assembly sections were standard aluminum extrusions and engineering accepted them as received. It was imperative that the roller assembly surface be flat, so a tool was designed and manufactured to achieve this. In order to obtain the required flatness, tapered shims were used between the vertical tees and angles (see Figure 4). Another very important reason for the tool is to assure an exact match at the butted end of each five-tier section to its adjacent section.

The first roller assembly did not have the horizontal guide rollers nor did the overhead structure contain the roller guide bars. This was unreliable when demonstrated on the actual structure. Any dirt or surface irregularity resulted in a binding situation and in some cases the roller assembly rotated ninety degrees and fell through the cable clearance gap. The present design was an outstanding solution. In addition, friction in the system is negligible. Another part which contributed to the successful elimination of the roller assembly binding was the continuous steel strip. Initially a .007-inch-thick continuous steel strip was used. When rolled out it was impossible to acquire a flat surface and a single straight edge. The edge was a long curve. Consequently, every instance of straightening the curve resulted in an irregular (puckered) rolling surface.

Simulated zero-gravity testing of the flat-fold flexible solar array wing assembly demonstrated the adequacy and feasibility of the ground test structure. All the objectives were achieved, thus justifying the selected design. The knowledge gained has provided invaluable assistance and has significantly contributed to the design and development of other flexible and rigid solar array systems.

ACKNOWLEDGEMENTS

The author wishes to acknowledge and express his appreciation to the following individuals for their contributions to the success of the Ground Test Program.

Mr. Rick Elms, Program Project Leader, who provided valuable background information for this paper in the form of documented activity reports and various design review presentations.

Mr. Dave Omori, Senior Design Engineer, who was given the responsibility of developing the idea of the test structure and through his ingenuity minimized most of the manufacturing and test problems on his original layout.

Mr. John Cayori, Skunk Works Leadman, had an excellent knowledge of the total design, and as a result resolved most of the manufacturing and test problems. He continuously displayed a natural instinct to create, develop, and build numerous shop aids to minimize and/or eliminate various problems, thus saving the program valuable time and money.

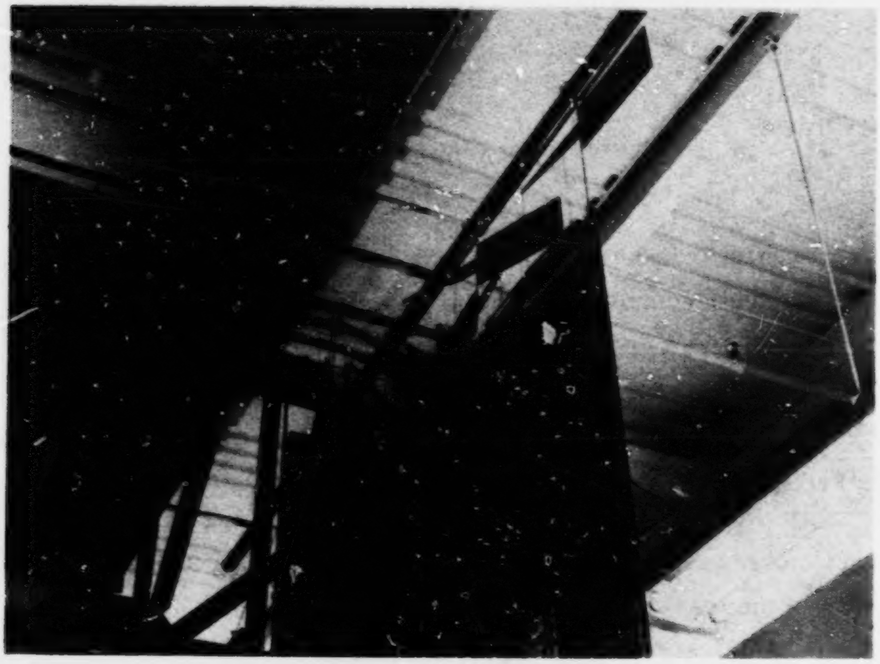

Fig. 1 Eight-panel Full-Scale Demonstration Model

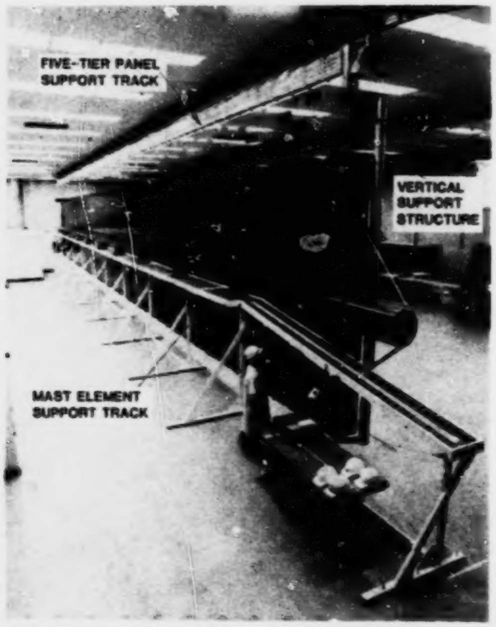
FIVE-TIER PANEL SUPPORT TRACK
VERTICAL SUPPORT STRUCTURE
MAST ELEMENT SUPPORT TRACK

Fig. 2 Fully Deployed Wing Assembly

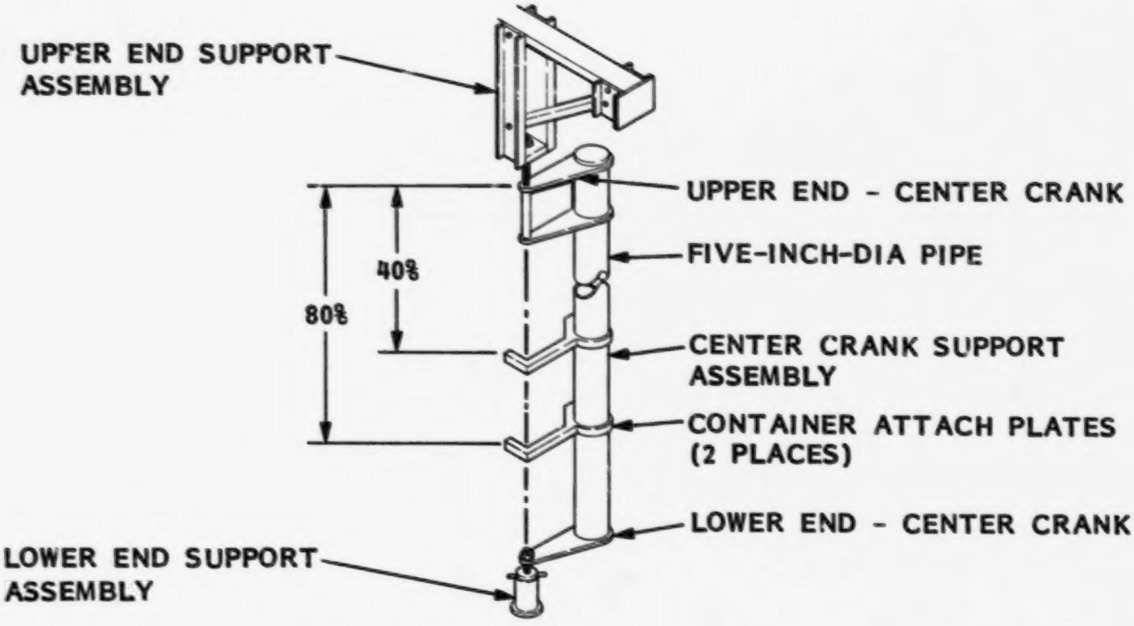
UPPER END SUPPORT ASSEMBLY
UPPER END - CENTER CRANK
FIVE-INCH-DIA PIPE
40%
80%
CENTER CRANK SUPPORT ASSEMBLY
CONTAINER ATTACH PLATES (2 PLACES)
LOWER END - CENTER CRANK
LOWER END SUPPORT ASSEMBLY

Fig. 3 Vertical Support Structure

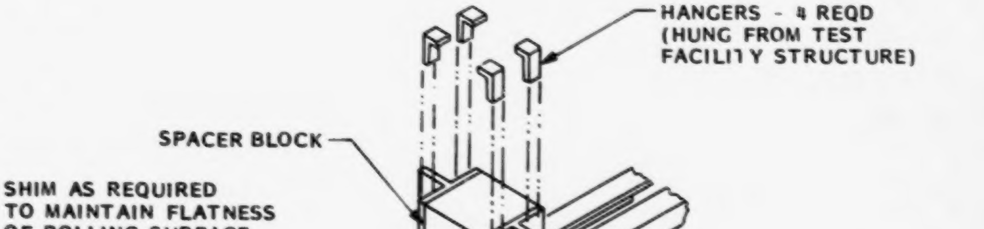
HANGERS - 4 REQD (HUNG FROM TEST FACILITY STRUCTURE)
SPACER BLOCK
SHIM AS REQUIRED TO MAINTAIN FLATNESS OF ROLLING SURFACE (10 PLACES/JOINT)
ROLLER ASSEMBLY ROLLING SURFACE
5-TIER TRACK SECTION EQUALLY SPACED
VERTICAL TEE SECTION 2 REQD

Fig. 4 Typical Bolted Area at the Joints and In between Joints (Strip and Square Bars Not Shown for Clarity)

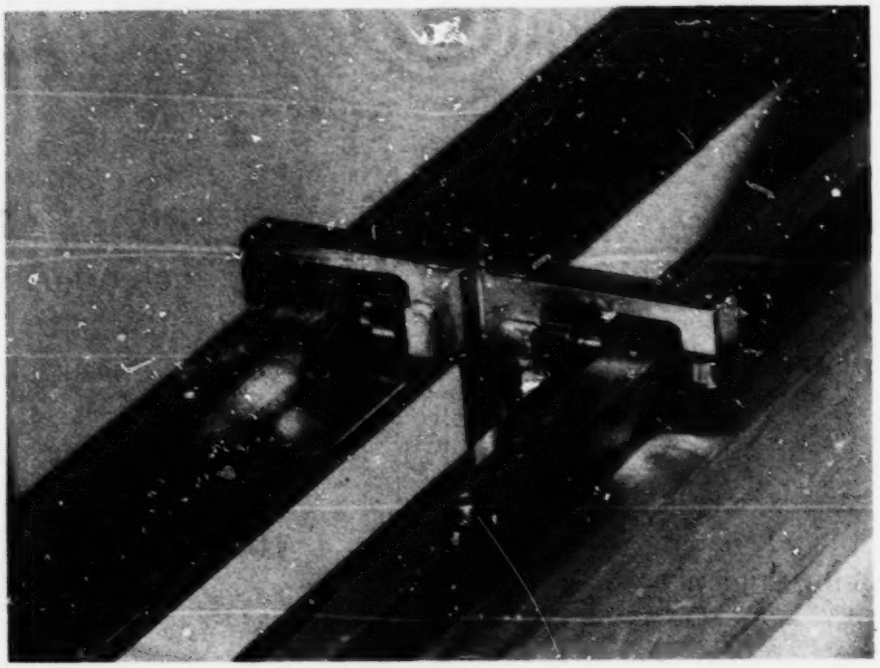

Fig. 5 Panel Roller Support Bearing

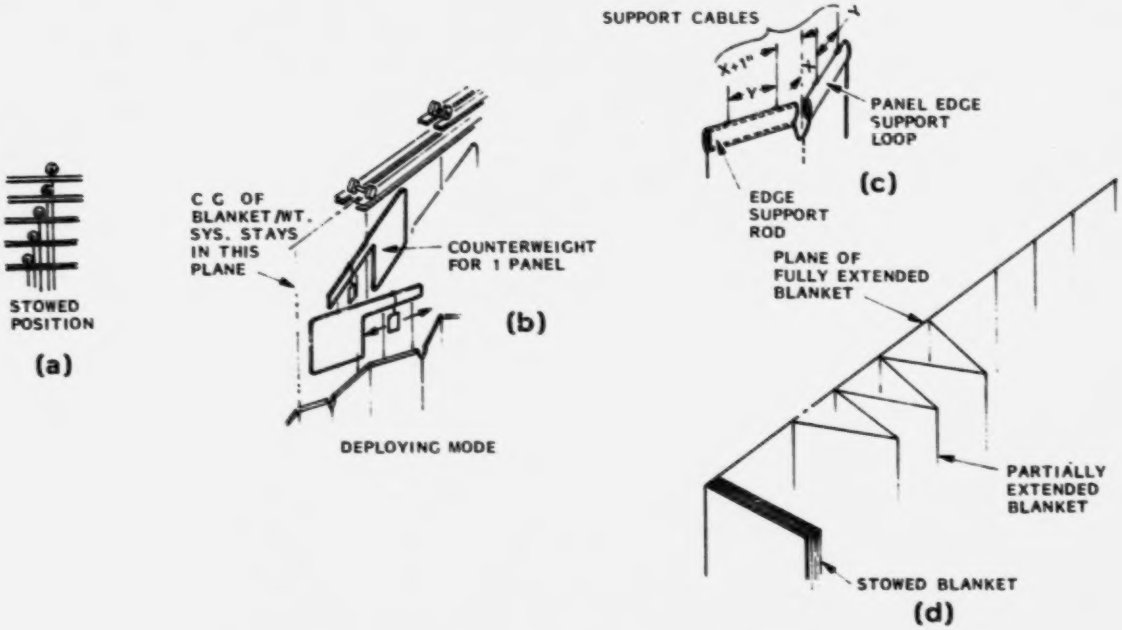
STOWED POSITION
(a)
C G OF BLANKET/WT. SYS. STAYS IN THIS PLANE
COUNTERWEIGHT FOR 1 PANEL
(b)
DEPLOYING MODE
SUPPORT CABLES
X+1"
Y
X
Y
PANEL EDGE SUPPORT LOOP
EDGE SUPPORT ROD
(c)
PLANE OF FULLY EXTENDED BLANKET
PARTIALLY EXTENDED BLANKET
STOWED BLANKET
(d)

Fig. 6 Extension of Flat-fold Array

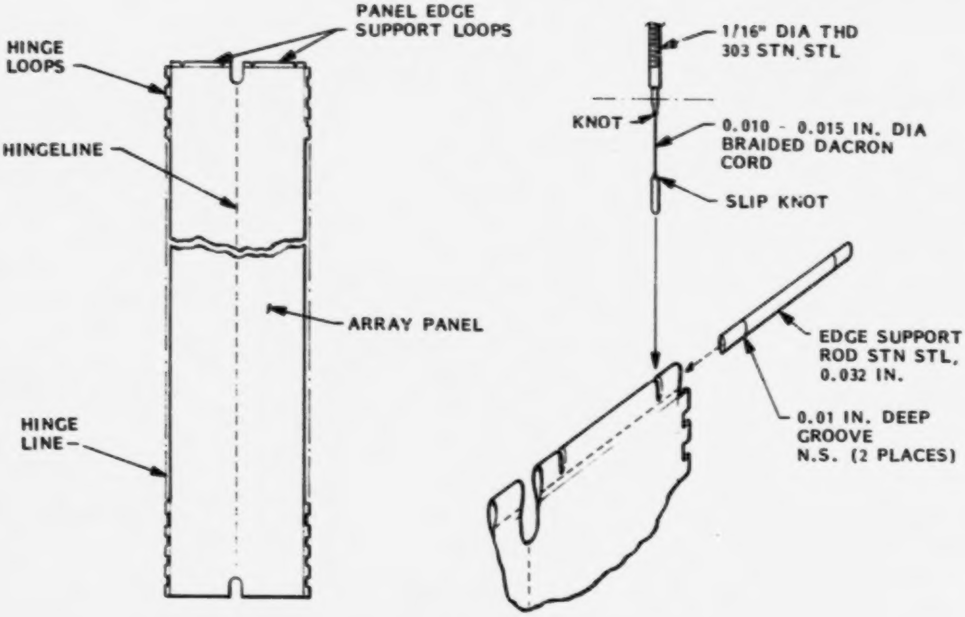
PANEL EDGE SUPPORT LOOPS
HINGE LOOPS
HINGELINE
ARRAY PANEL
HINGE LINE
1/16" DIA THD 303 STN STL
KNOT
0.010 - 0.015 IN. DIA BRAIDED DACRON CORD
SLIP KNOT
EDGE SUPPORT ROD STN STL, 0.032 IN.
0.01 IN. DEEP GROOVE N.S. (2 PLACES)

Fig. 7 Array Panel Edge Support Design

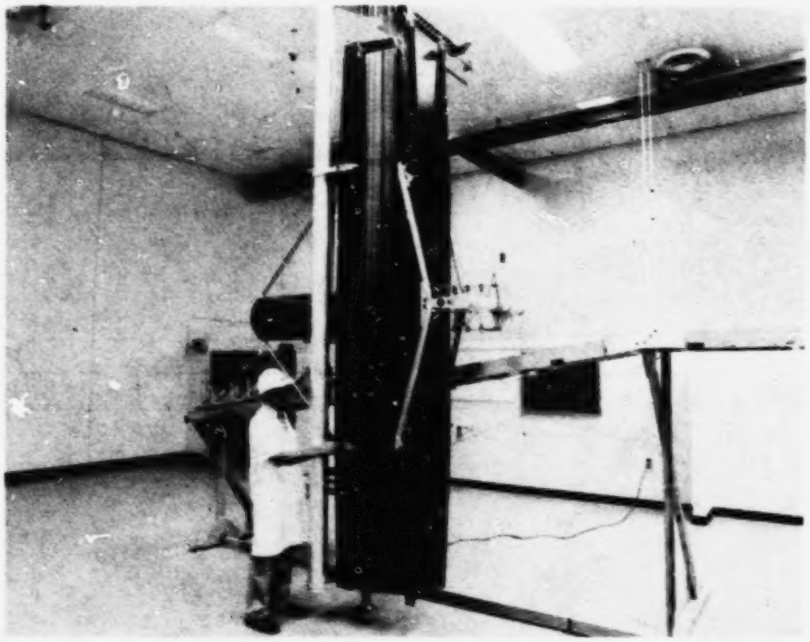

Fig. 8 Cover Assembly Two-axis Counterbalancing System and the Mast Tip Fitting

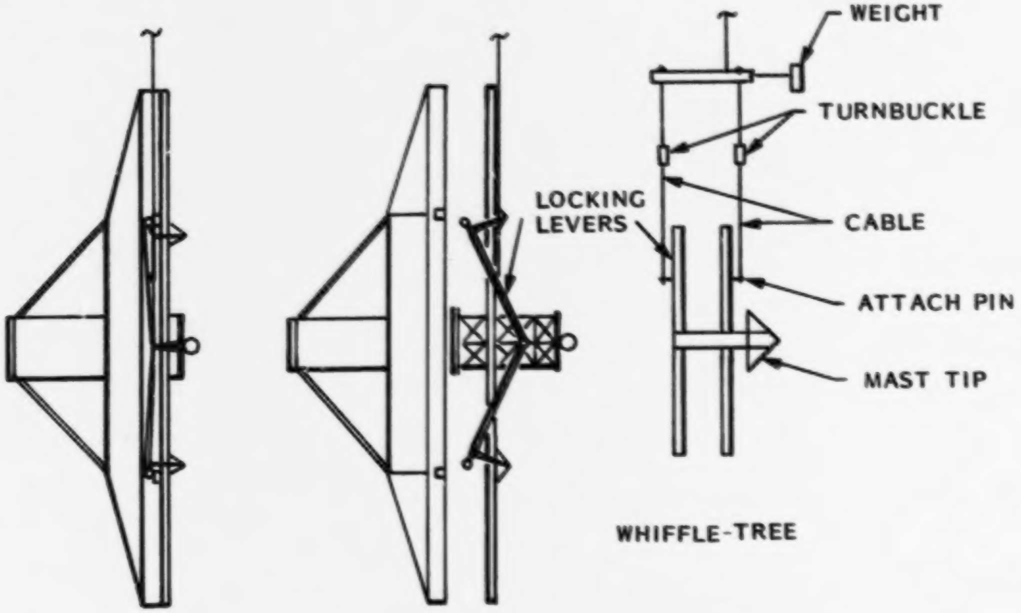
WEIGHT
TURNBUCKLE
LOCKING LEVERS
CABLE
ATTACH PIN
MAST TIP
WHIFFLE-TREE

Fig. 9 Box Cover Locking Mechanism

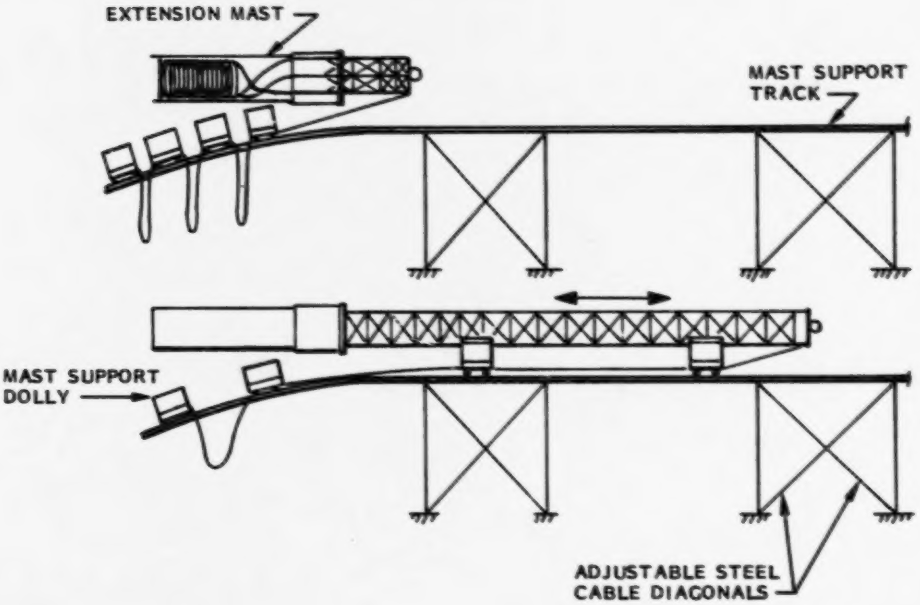
EXTENSION MAST
MAST SUPPORT TRACK
MAST SUPPORT DOLLY
ADJUSTABLE STEEL CABLE DIAGONALS

Fig. 10 Coilable Longeron Extension Mast (CLEM)

Darius T. Chung
Lockheed Missiles and Space Company
P.O. Box 504
Sunnyvale, California 94088

Mr. Chung is presently the responsible engineer for the hold-down and release and the deloyment motor/gearhead mechanisms of the P-375 solar array system. He is also responsible for the Solar Electric Propulsion Solar Array Flight Experiment (SEPSAFE) that will be included in the cargo on one of the Space Shuttle flights. He has been involved in mechanical design with Lockheed since 1961. Specific areas of involvement have been deployable systems such as rigid and large area flexible solar arrays, large area parabolic antennas, and deployable/retractable systems of other large area flexible solar arrays. Since 1976, he has flown on numerous zero-g flights in a specially designed KC-135 aircraft as Lockheed's test coordinator relating to SEP flexible solar arrays.

Blank Page

THE DEVELOPMENT OF A UNIVERSAL DIAGNOSTIC PROBE SYSTEM FOR TOKAMAK FUSION TEST REACTOR

Richard Mastronardi and Richard Cabral
American Science and Engineering, Inc.
Dennis Manos
Princeton University Plasma Physics Laboratory

ABSTRACT

The Tokamak Fusion Test Reactor (TFTR) being built at Princeton Plasma Physics Laboratory is the largest such facility in the U.S. and places tremendous demands on the instrumentation in general and mechanisms in particular. This paper discusses the design philosophy and detailed implementation of a universal probe mechanism for TFTR which utilizes the experience gained by designing and operating aerospace mechanisms.

INTRODUCTION

The Universal Diagnostic Probe System is a mechanism that will insert several types of scientific plasma measuring instruments into the plasma edge of the Fusion Reactor. It must operate from below the reactor substructure and make a reliable and accurate insertion approximately 4.5 meters vertically from the stowed position. Provision is also made for rotating the instrumentation at the probe head and its 16 electrical conductors (2 of which are high voltage) 360 degrees at a varying rate, when in the fully extended or stowed position.

This mechanism must be exposed to harsh environments of temperature (in excess of 200°C), high vacuum (less than 10^{-9} Torr), high radiation levels [4×10^5 rad (Si)], and high magnetic impulses (150 Tesla/sec), without outgassing contaminants to the fusion plasma. It must also operate reliably over an eight-year period, since breaking vacuum to repair the mechanism would be costly when the system is fully operational. It must also not fail in a position or manner that impedes the attainment of scientific data from other diagnostic instrumentation or cause the plasma to be unstable.

This paper discusses the design of the Universal Diagnostic Probe System and demonstrates how the mechanisms achieve their specifications.

Hardware developed for aerospace has traditionally demanded solution of challenging technical problems. Often these challenges are the result of harsh environmental and operational constraints. The design and development of scientific instrumentation for a nuclear fusion reactor such as Princeton Plasma Physics Laboratory's Tokamak Fusion Test Reactor (TFTR) offers engineers and scientists many of the same kinds of problems found in aerospace. In many ways, the environment found on TFTR combines all of the worst constraints we find in aerospace.

Tokamak Fusion Test Reactor

The nation's first magnetic confinement device capable of producing a significant quantity of fusion energy is currently being constructed by Princeton University's Plasma Physics Laboratory (PPPL). The Tokamak Fusion Test Reactor (TFTR), the largest construction project to date in the U.S. fusion program, is scheduled to be operational at Princeton in 1982. The TFTR project is being funded by the U.S. Department of Energy (DOE) as part of its national program to develop nuclear fusion as a safe, economical and environmentally acceptable method of generating electricity for the long term.

Other earlier Tokamaks in the U.S. and other nations were built to study plasma confinement below reactor-level conditions; TFTR has been designed to attain reactor-level plasmas and to yield experimental data relevant to future fusion power plants.

Figure 1 shows an artist's rendition of TFTR.

System Overview

The imposed environments (shown in Figure 2) and requirements placed on this probe system play a significant role in its design.

A cross section of the Tokamak torus is shown at the top of the figure. The probe system is below the torus and extends through the substructure (a 2-meter-thick concrete floor) to the test cell basement floor. The probe system consists of basically four elements: a vacuum envelope which can be isolated from the Tokamak by two gate valves, a guide tube which helps guide and position the probe during its vertical travel, the Vacuum Vessel Interface Section (VVIS) which provides 10-kV electrical isolation and accommodates thermally induced relative motion between the torus vacuum vessel and the rest of TFTR, and the probe tube itself (approximately 4.8 meters long) which resides in the test cell basement area when fully retracted and extends to the plasma edge when fully inserted. The probe tube also contains the mechanism for rotating interchangeable probe heads. The system is noncontaminating and its materials are chosen for their low-outgassing properties, in order to maintain a vacuum better than 10^{-9} Torr.

The external environment is clearly harshest near the plasma. The magnetic flux of 60,000 gauss, the bake-out temperature of 150°C, the probe head temperature of 200°C, and the high radiation levels all place particularly difficult constraints on the choice of materials and limit the techniques acceptable to maintain 2-kV electrical potentials at various points throughout the system and to transmit data signals from the probe head instrumentation to the data-taking computer system with low noise immunity. Noise immunity must be 1 nanoampere or 1 microvolt from frequencies of dc to 1 megahertz.

Design Features

The design of mechanisms for this system must maximize reliability in the TFTR environment. As a result, the probe system design and development have encountered many difficult subproblems including:

- How do you align and maintain alignment of a 9-meter-long vacuum envelope, with 6 interfaces, that experiences a variety of thermal gradients and excursions?
- What materials are best to survive and perform in the imposed environments? This includes lubrication of various mechanisms and guides.
- What structural design best survives the high electromagnetically induced lateral loads during plasma disruptions? These impulse loads can be as high as 1000 kg for 10 milliseconds spread over the top meter of the probe. A bent probe incapable of being withdrawn below the isolation gate valves would necessitate the breaking of system vacuum. When TFTR is fully operational, the cost associated with breaking vacuum can be staggering.
- What is the most reliable way to hoist and lower the probe?
- What is the most reliable way to rotate probe head instruments anywhere along the 4.5-meter vertical stroke?
- What is the most reliable way to get signal and bias wires to the probe head instruments and mechanisms?

The last three subsystems are shown in Figure 3 and will be the focus of our discussion.

Vertical Drive:

The vertical drive system is one of the most crucial subsystems from a reliability standpoint. A failure of this system with the probe in the full-up or even a partially up position would have unacceptable cost and technical implications for the TFTR project. In addition to simply raising and lowering the probe, the system must position the probe relative to the plasma with good precision, repeatability, and knowledge.

Trade-offs were performed on different types of hoist methods to determine which method met the performance requirements with the maximum reliability. Also considered was the ability to incorporate a back-up system for getting the probe down below the gate valves if a failure occurred in the primary drive system.

Three basic types of drive systems were examined: rack and pinion, lead or ball screw and a continuous loop cable hoist. The rack and pinion was chosen for its reliability and its predictable precision.

The vertical drive system is shown in Section B-B and is located at the top of the vacuum envelope. A stepper motor drives a worm gear reducer, which in turn transmits torque to a rack and pinion system through a metal-bellows-type vacuum feed-thru. To reduce torque transmitted by the feed-thru and prolong its life, additional gear reduction is performed inside the vacuum envelope before the rack and pinion drive. A pair of angled guide rollers on the back side of the custom rack maintain proper gear engagement of the rack and pinion throughout the vertical stroke.

Rotary Drive:

A unique feature of this probe system is the rotary drive. It is located at the lower end of the moving probe tube and is contained within its own hermetically sealed housing. Thus, it utilizes conventional wet lubricants for maximum reliability without fear of contaminating TFTR.

Since the rotational drive system is also a critical subsystem, the design was chosen carefully. Particular emphasis was given to designing a system that is both reliable and independent from the vertical drive system. What is meant by independent here is that any type of failure on the rotational system or as a result of the rotation system would not preclude the probe from being withdrawn from the plasma to a position below the gate valves.

The purpose of this mechanism is to rotate the probe head 360 degrees at a selectable speed from 3.6 degrees/second to 90 degrees/second anywhere along the 4.5-meter vertical stroke.

Three basic types of rotational drives were explored; two of these have motors external to the vacuum housing tube and one has an internal motor.

One type of drive system studied involves a scheme whereby a motor external to the vacuum envelope drives a 5-meter shaft through a vacuum feed-thru. The probe tube slides vertically along the shaft.

Another type studied involves a motor outside the vacuum housing which drives a gear through a vacuum feed-thru. This gear engages the probe tube at distinct zones along the vertical stroke.

The design selected for use on this system and shown in Figure 3 has many advantages. The most important one is that no matter what happens in this subsystem, it will not prevent the probe from being safely withdrawn vertically below the isolating gate valve. The wires to drive the stepper motor and to receive encoder signals must however accommodate 4.5 meters of motion. Since the probe head signal and bias wires already have this requirement, it was convenient to combine the wires into one cable.

Electrical Connection:

After many trade-off studies, a cable configuration was chosen that minimizes noise pickup in the high magnetic field, survives the operating environment and minimizes material outgassing. A flexible, shielded kapton sandwich cable has been designed which allows a mixing of conductor types. Flat conductors of various sizes can be combined with twisted pairs of polyimide-covered magnet wire in a single laminated cable. It is shielded with 2300 angstroms of copper electro-deposited around the cable before the last layer is assembled.

The cable is used in a "seat-belt retractor" type mechanism to maintain electrical continuity throughout the probe vertical stroke. The cable is shown in the retracted position in Figure 3. A cross section of the cable laminate is shown in Figure 4 and a photograph of a cable sample is shown in Figure 5.

CONCLUSIONS

The technology developed for the design of aerospace instrumentation has wide-ranging applications; one given here is the development of a universal diagnostic probe system for TFTR. This instrument challenges the designer to formulate a design which operates reliably in each of the worst combinations of environments.

Some of the designs discussed here show that by isolating subsystems, reliability is increased. A failure in any of the many subsystems, such as the vertical insertion stroke drive, the probe head rotary drive and the electrical conductor take-up reel , will not cause a failure in any other subsystem or prevent the probe system from being withdrawn to a safe position below the isolation gate valve. This is an important consideration in the design of this mechanism and is an outgrowth of experience gained in designing complex spaceborne mechanisms where repair is expensive, if not impossible. The philosophy of isolating failures to distinct subsystems proves to be a key ingredient toward mimimizing the impact of failures, if they occur, and providing responsive back-up scenarios. This scheme, coupled with designing simple, reliable mechanisms to start with, gives a mechanical system like the Universal Diagnostic Probe the necessary features to survive and operate satisfactorily in the harsh environment of TFTR.

ACKNOWLEDGEMENT

This work was performed on Princeton Plasma Physics Laboratory subcontract S-01936-H under DOE Contract DE-AC02-76-CHO-3073.

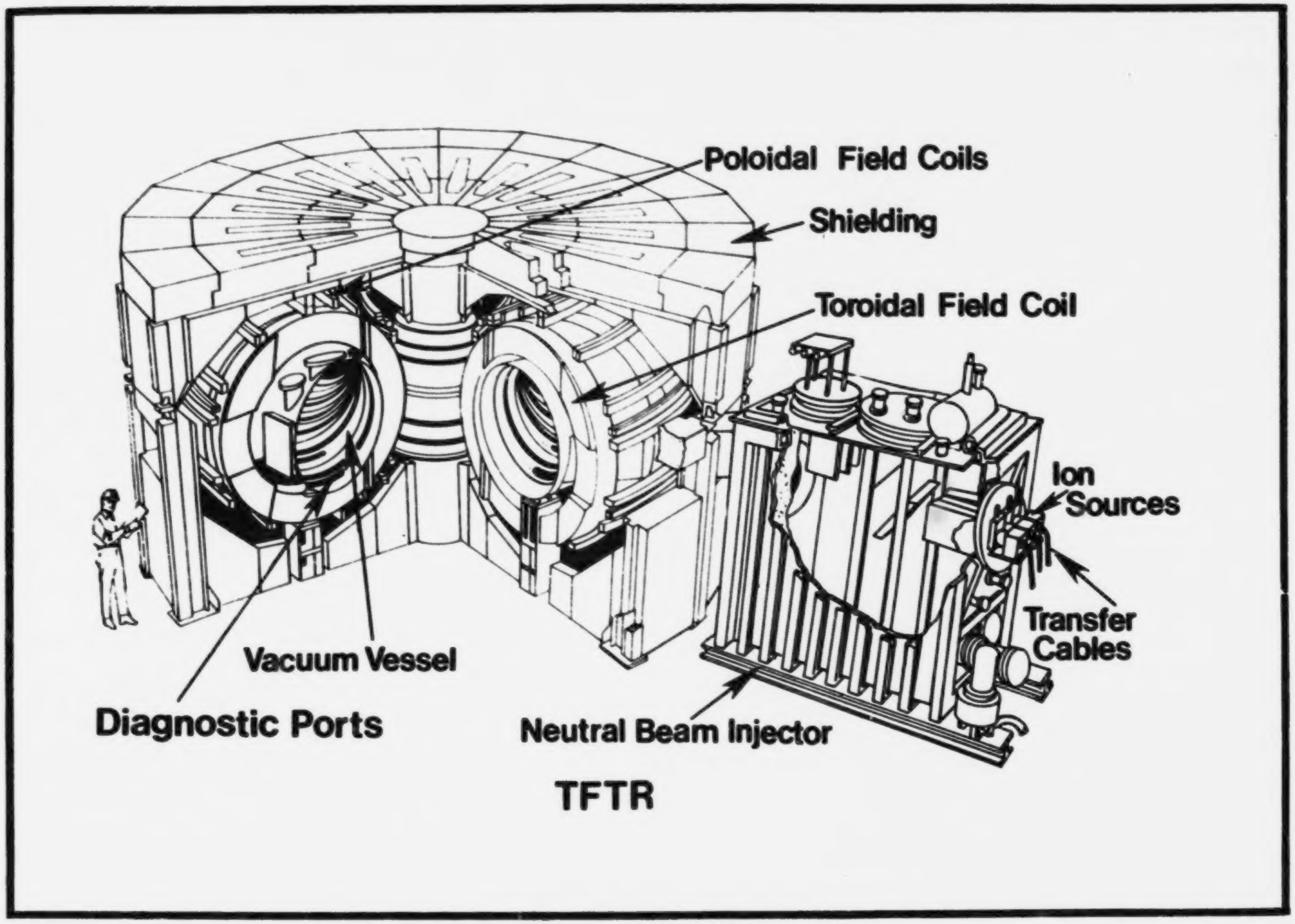
Poloidal Field Coils
Shielding
Toroidal Field Coil
Ion Sources
Transfer Cables
Vacuum Vessel
Diagnostic Ports
Neutral Beam Injector
TFTR

Figure 1. Artist's Rendition of TFTR

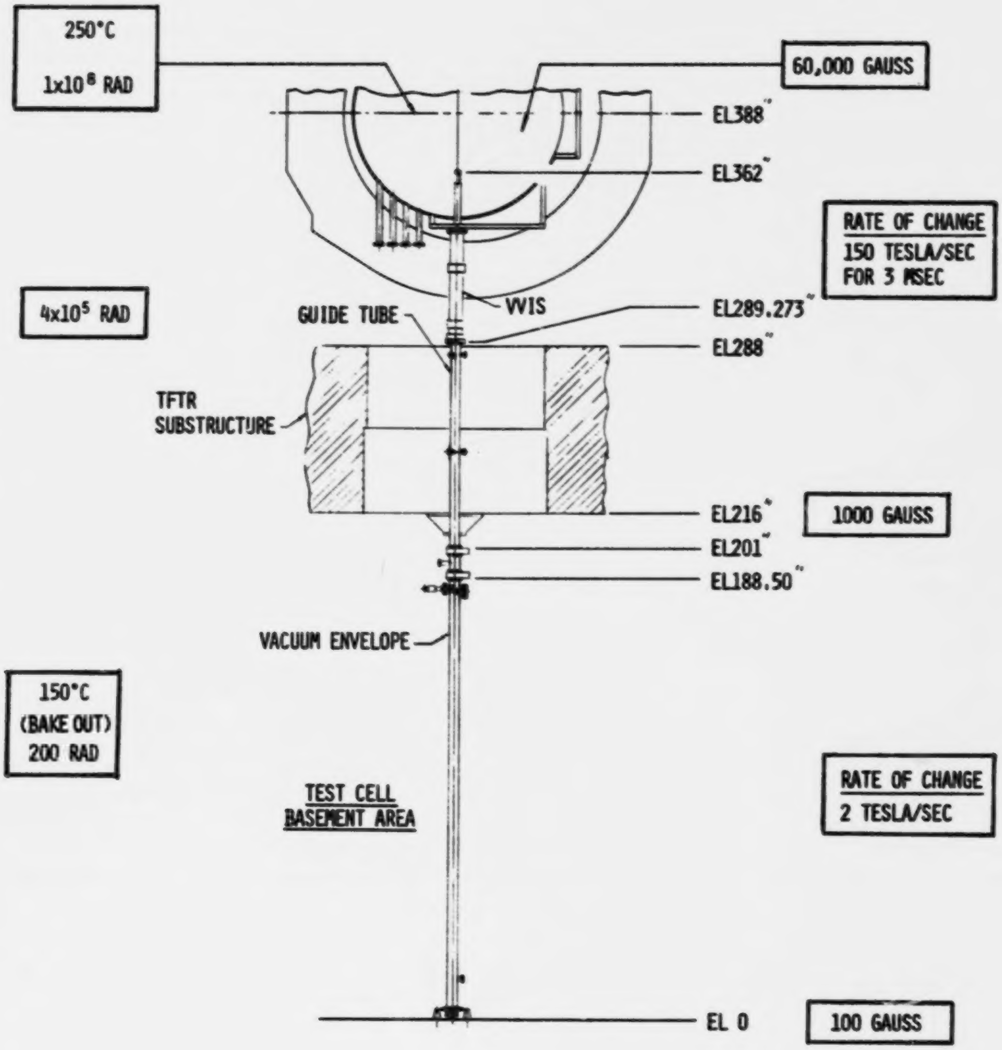
250°C
1x10⁸ RAD
60,000 GAUSS
EL388"
EL362"
RATE OF CHANGE
150 TESLA/SEC
FOR 3 MSEC
4x10⁵ RAD
GUIDE TUBE
VVIS
EL289.273"
EL288"
TFTR
SUBSTRUCTURE
EL216"
1000 GAUSS
EL201"
EL188.50"
VACUUM ENVELOPE
150°C
(BAKE OUT)
200 RAD
TEST CELL
BASEMENT AREA
RATE OF CHANGE
2 TESLA/SEC
EL 0
100 GAUSS

Figure 2. Environmental Schematic

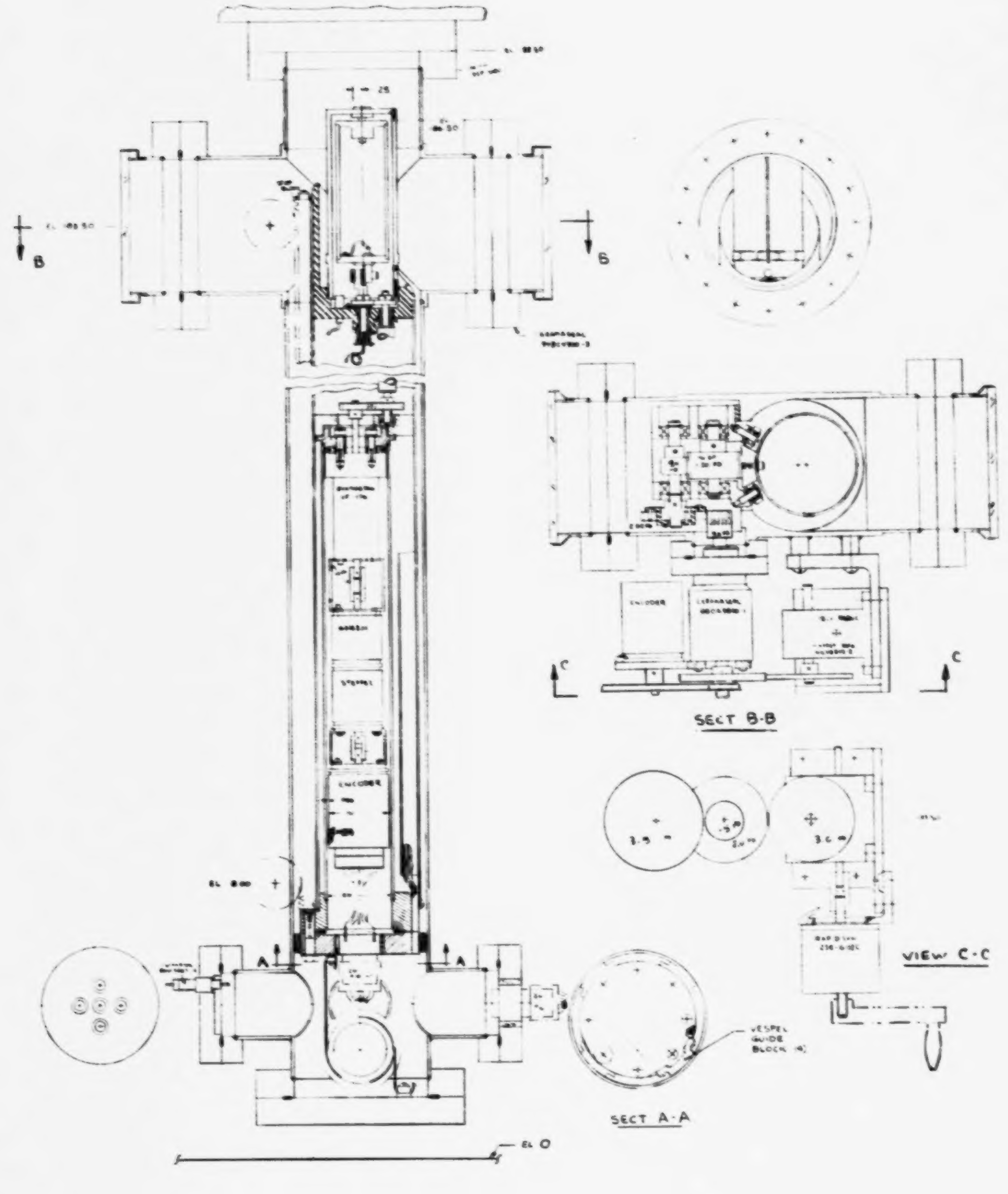
B
B
ENCODER
STEPPER
ENCODER
EL 8.00
A
A
VESPEL GUIDE BLOCK (4)
SECT A-A
EL 0
ENCODER
C
C
SECT B-B
VIEW C-C

Figure 3. Probe System Layout

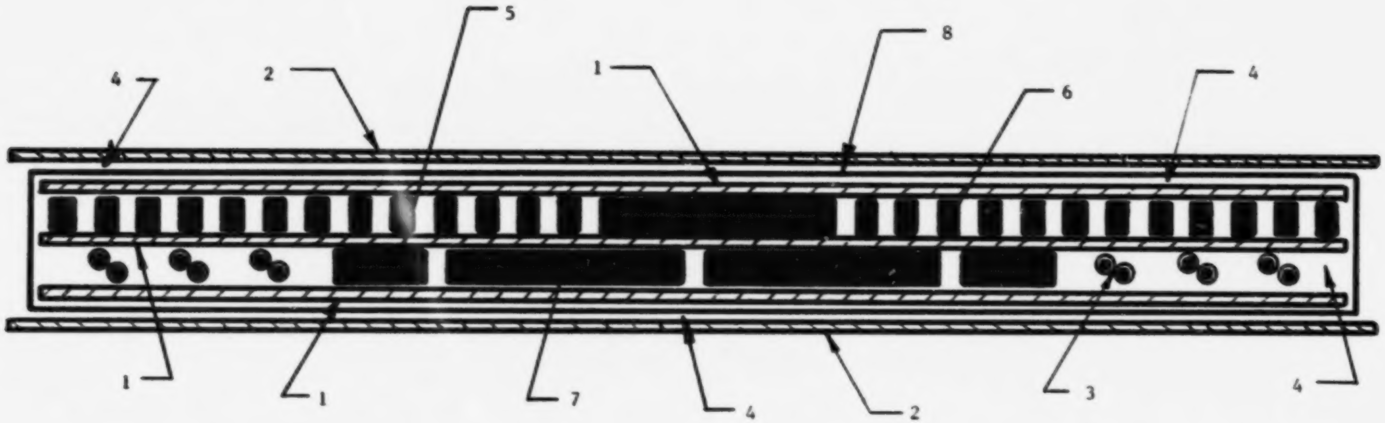

1) 2 MIL KAPTON

2) 1 MIL KAPTON

3) KAPTON COATED MAGNET WIRE IN TWISTED PAIRS, 0.004 IN. DIA. WIRE 0.0003 IN. KAPTON JACKET THICKNESS.

4) .7 MILS ACRYLIC ADHESIVE

5) 5 AMP CONDUCTOR
1.4 MILS (1 OZ.) COPPER, 0.175 IN. WIDE.

6) .125 AMP TO 1 AMP CONDUCTOR
1.4 MILS (1 OZ.) COPPER, 0.040 IN. WIDE.

7) 10 AMP CONDUCTOR
1.4 MILS (1 OZ.) COPPER, 0.450 IN. WIDE.

8) E.M.I. SHIELD
2300 ANGSTROMS COPPER

Figure 4. TFTR Flex Cable Cross Section

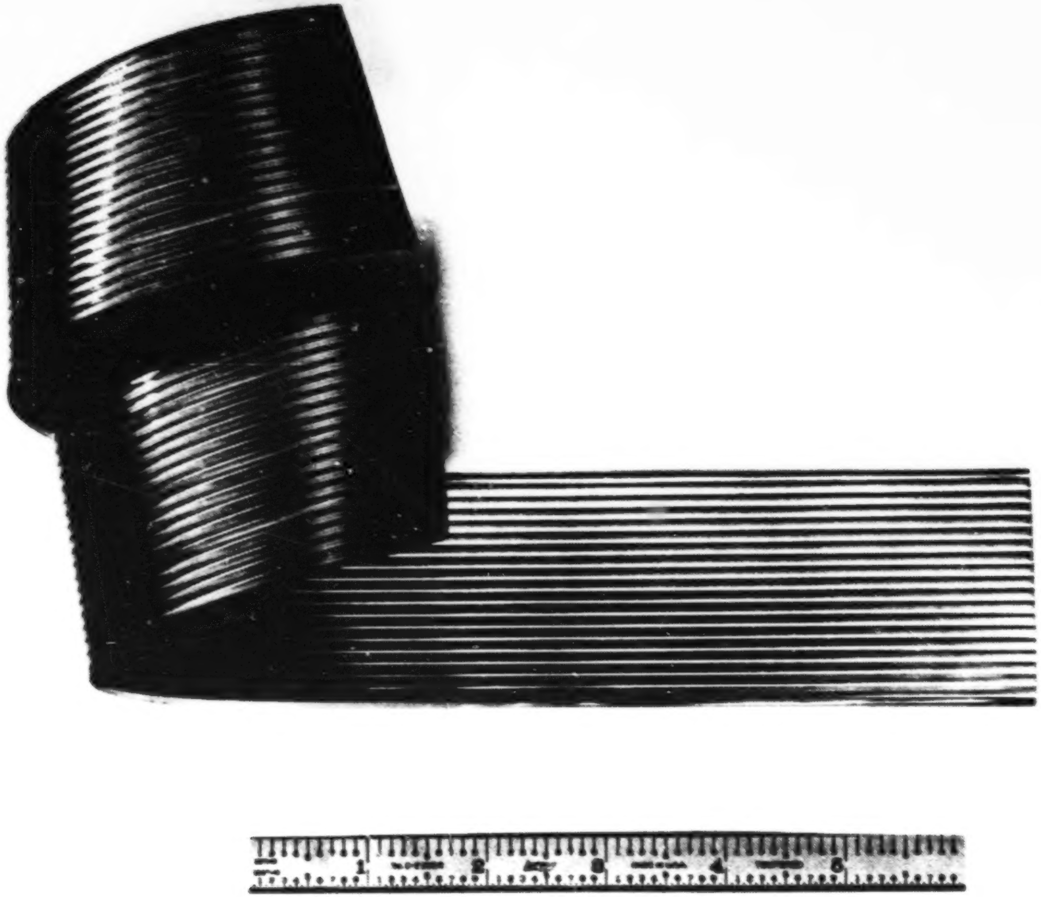

Figure 5. Kapton Sandwich Cable Sample

Richard Mastronardi
American Science and Engineering, Inc.
37 Broadway
Arlington, Massachusetts 02174

Mr. Mastronardi is presently the Manager of Mechanical Engineering at American Science and Engineering. He was previously project engineer on the HEAO-2, High Energy Astronomy Observatory, and other astronomy payloads for NASA. Prior to his employment with American Science and Engineering in 1975, he worked for Atkins & Merrill, Inc., Sikorsky Aircraft, and The Boeing Company. Mr. Mastronardi holds a B.S. degree in Aeronautical Engineering from Rensselaer Polytechnic Institute and an M.B.A. from Northeastern University.

Co-authors of this paper are Mr. Richard Cabral who is also with American Science and Engineering and Mr. Dennis Manos who is affiliated with Princeton University.

Blank Page

ELASTIC SUSPENSION OF A WIND TUNNEL TEST SECTION

Russell Hacker*
Stephen Rock**
Daniel B. DeBra†

INTRODUCTION

As both military and commercial aircraft have become more complex and expensive to operate, designers have looked for ways to increase efficiency and performance. As a consequence, active control systems which influence aircraft aeroelastic behavior are receiving increased attention. These systems use attitude, position, and rate sensors to actuate a variety of control surfaces (e.g., spoilers, ailerons, elevators, flaperons, elevons, and partially inactive spoilers). Their functions include: (a) counteracting wing bending, wing torsion, and fuselage bending; (b) redistributing wing loading; and (c) avoiding flutter [Refs. 1 - 9]. An important benefit is the potential for designing lighter, less rigid structures.

Designing a successful active control system requires a fundamental understanding of an aircraft's aeroelastic behavior. The first solution for unsteady aerodynamic loading was presented in 1934 [Ref. 10] for a wing undergoing simple harmonic motion. The theory for arbitrary motion was still under investigation in 1977 [11], and complete experimental verification is still required.

A program is in progress at Stanford University in the Dept. of Aeronautics and Astronautics to provide experimental verification of the theory describing arbitrary motions of an airfoil and to develop control laws to deal with such motions. The experimental apparatus used in this program is described in this paper. It is a mechanism designed to provide two separate degrees of freedom without friction or backlash to mask the small but important aerodynamic effects of interest.

---

* Lockheed Missiles & Space Company, Sunnyvale, CA, formerly of Stanford University, Dept. Aeronautics and Astronautics

** Systems Control Inc., Palo Alto, CA

† Professor, Dept. Aeronautics & Astronautics, Stanford University

TEST SECTION DESCRIPTION

The experimental apparatus consists of a half-meter square subsonic wind tunnel with a unique airfoil suspension system, which provides two degrees of freedom (DOF) with negligible friction and no coupling of modes through the suspension.

The tunnel is constructed so that an interchangeable 1-meter-long section containing an experiment can be removed and replaced without disturbing the test specimen mounted inside, thus increasing the utilization of the tunnel. Each experiment can be installed in its own test section which is cart mounted for mobility (see Fig. 1).

The test section was designed to support a variety of airfoils. Two versions of this section have been built and, by changing airfoil suspension components, have been used for three research projects [12, 13, 14].

Airfoil test specimens used in recent investigations have been NACA profiles (e.g., 0015, 0009), typically 235-mm chord by 38-mm thickness. The specimen is fabricated with a foam interior covered with three layers of bi-directional weave fiberglass cloth and resin. The foam core consists of two slabs of foam which are grooved to fit around the wing spar (a 19-mm square aluminum tube). These three pieces are glued together and are then cut to shape with a hot-wire cutter guiding on two metal templates. These metal templates are left in place to form end ribs. The fiberglass and resin covering is then applied and final contour is obtained by sanding.

PLUNGE SUSPENSION

The suspension system is designed to provide the airfoil 2 DOF without friction. The airfoil is suspended with the spar vertical so that plunge motion is horizontal and not affected by gravity.

The plunge motion suspension is a set of four folded cantilever springs

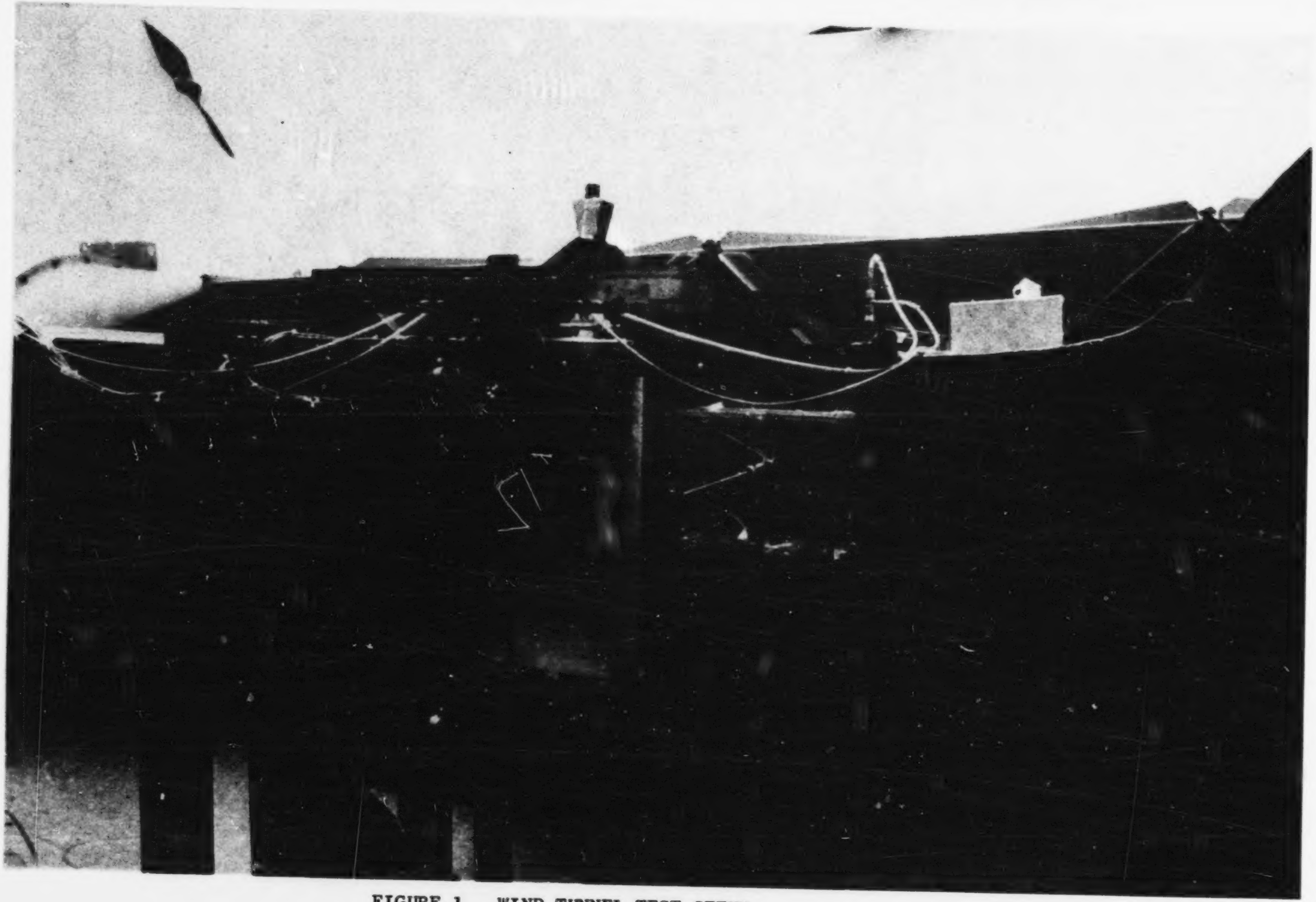

FIGURE 1 WIND TUNNEL TEST SETUP

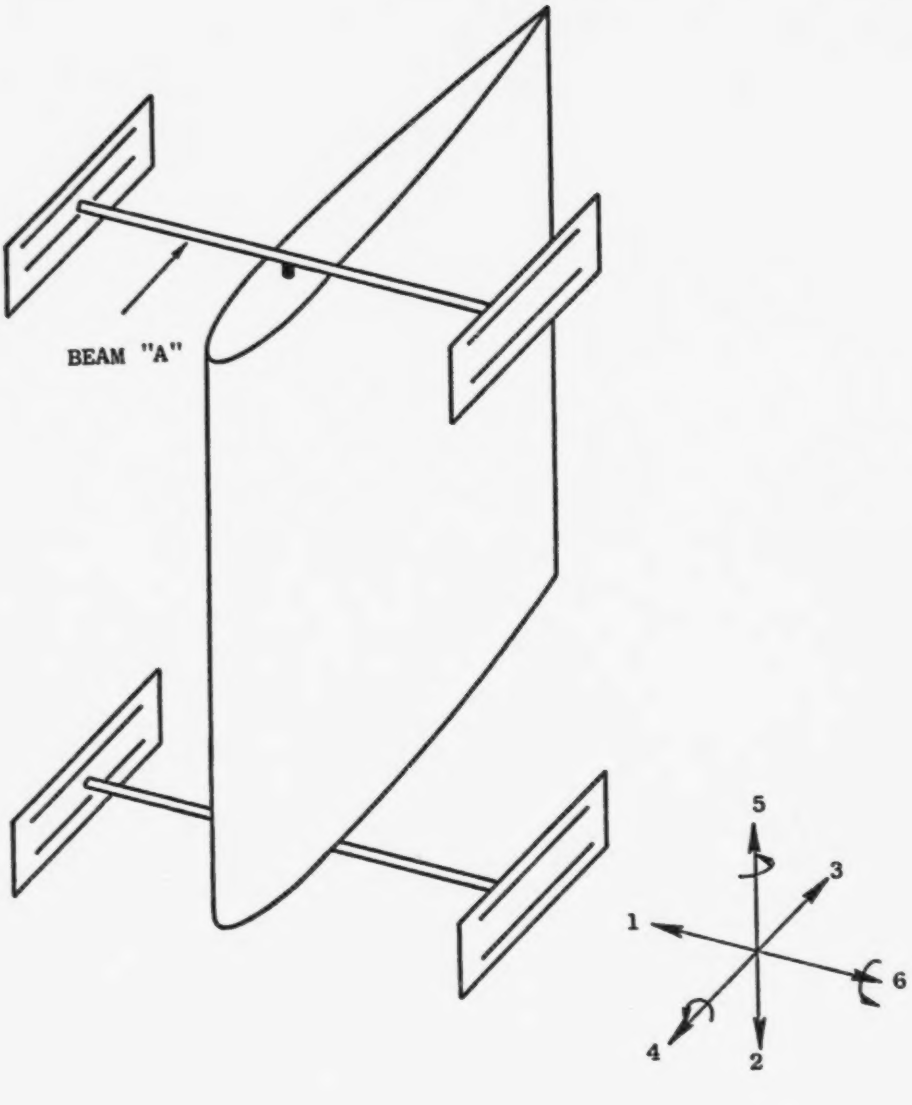
BEAM "A"
5
3
1
6
4
2

FIGURE 2   ARRANGEMENT OF FOLDED CANTILEVERS IN TWO PAIRS
[from Rock, Ref. 12]

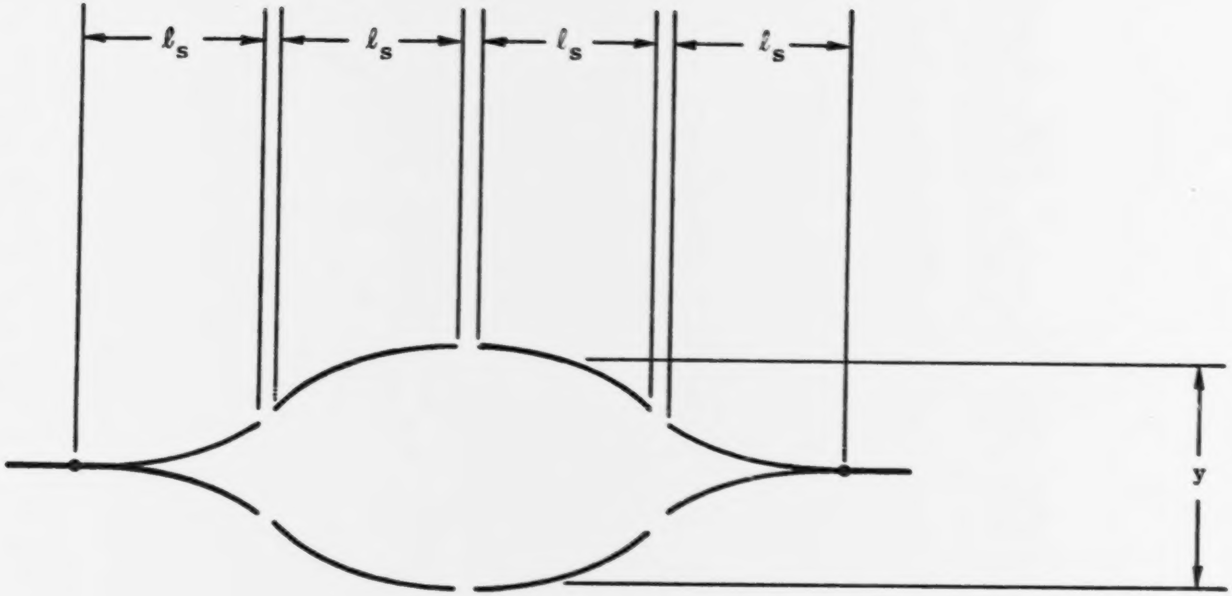
ℓ_s
ℓ_s
ℓ_s
ℓ_s
y

FIGURE 3 DEFLECTION OF SPRING AS A GROUP OF CANTILEVERS [from Rock, Ref. 12]

mounted so they are stiff in the vertical direction to resist gravity and compliant in the horizontal direction to permit airfoil plunge (direction 1) (see Fig. 2).

As the wing plunges, each of the four metal springs deflects as an equivalent group of cantilever beams as shown in Fig. 3, with a spring rate given by

$$K_h = \left[\frac{3EI}{\ell_s^3}\right]\left[1 + \left(\frac{Y}{\ell_s}\right)^2 + \cdots\right]$$

where $I = w_s t_s^3/12$.

In choosing ℓ_s a tradeoff exists. It should be large to minimize the nonlinearity in the spring rate but small to minimize the compliance of the plunge suspension in directions 4 and 5 (Fig. 2). The thickness is determined by vertical strength and stiffness. The springs in current use are 2-mm-thick copper beryllium with $\ell_s = 93$ mm and $\omega_s = 14$ mm. The resulting spring rate is 10.52 kN/m.

This type of folded cantilever spring alone has compliance in directions 4 and 5 which is eliminated by connecting the springs in pairs with cross beams.

The springs are each treated as a group of cantilevers. They are designed to operate on the linear part of the force-deflection curve for the desired maximum deflection. Normally a flat spring will undergo a snap-through action when deflected through its center or zero-deflection position due to its imperfections. In addition, if the suspension is overconstrained as this one is, any imperfection in the nominal positions would require strain in the stiff direction to pass through the undeflected state. This is avoided by biasing each spring approximately $h/4l_s = 0.03$ or about 1.5 times the maximum expected motion from its center position so that in operation the spring does not pass through its zero position. Spring mounting brackets are arranged on the tunnel section to permit changes in spring sizes (widths, length, thickness).

The directions intended to be stiff have some compliance. However, motion in these DOF's can be determined experimentally and filtered electrically

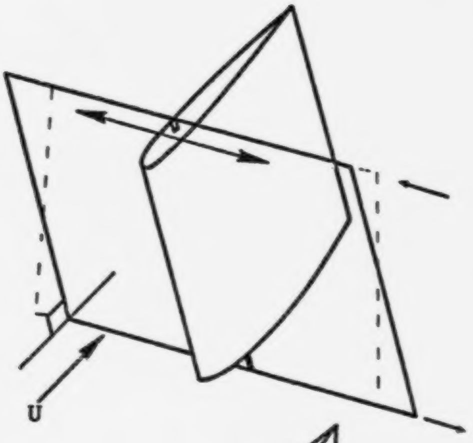

(a) DIFFERENTIAL PLUNGE MOTION

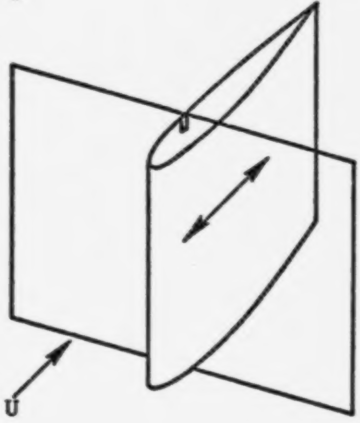

(b) CHORDWISE MOTION

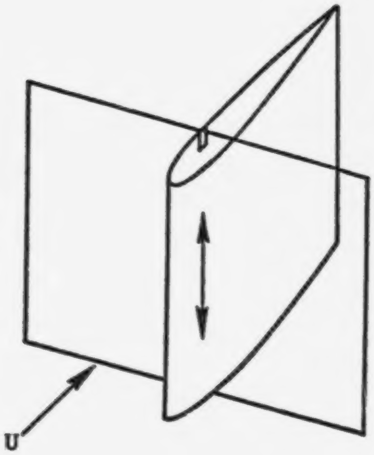

(c) SPANWISE MOTION

FIGURE 4 EXTRANEOUS BENDING DEGREES OF FREEDOM [from Rock, Ref. 12].

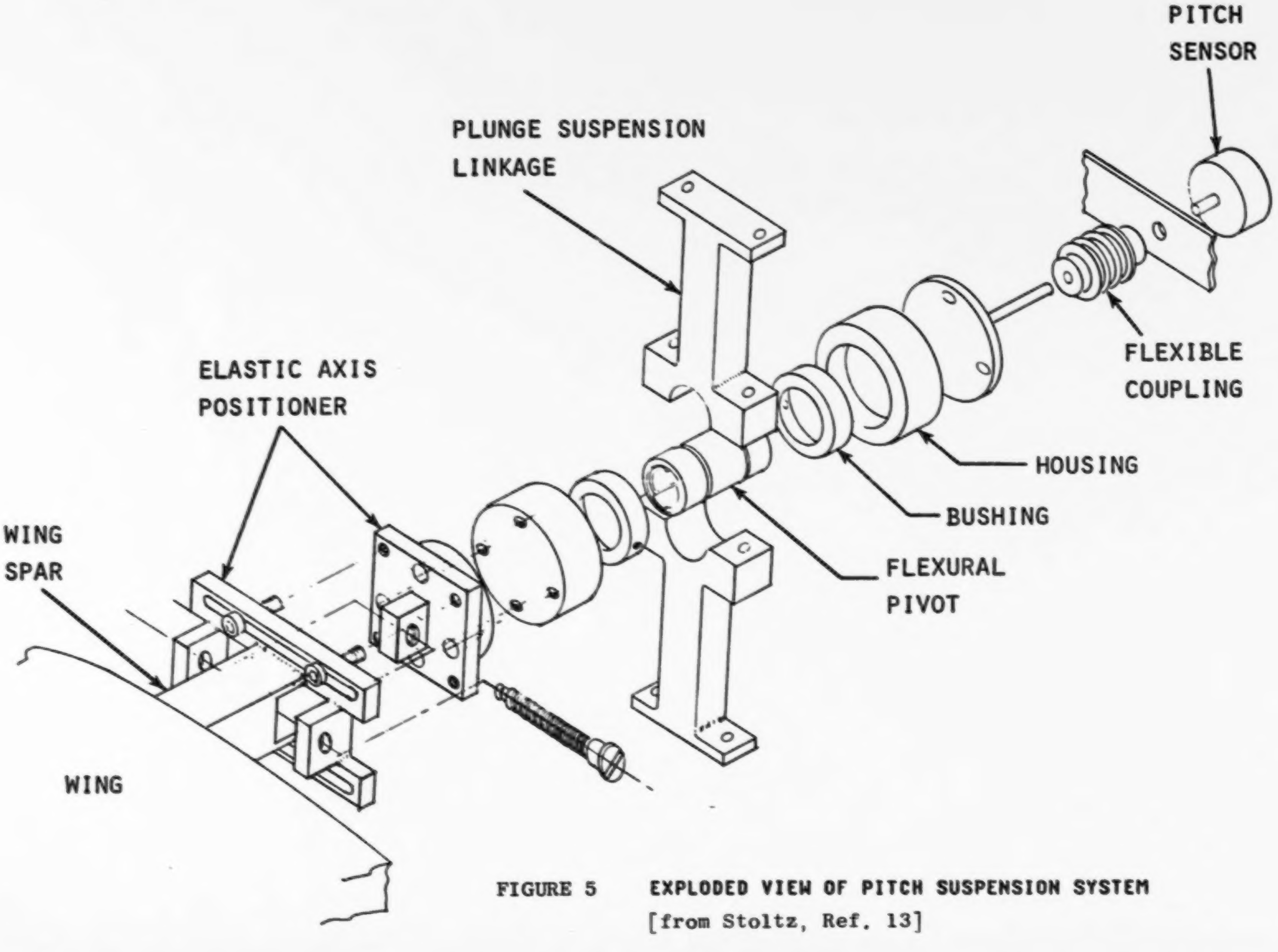
PITCH SENSOR
PLUNGE SUSPENSION LINKAGE
FLEXIBLE COUPLING
ELASTIC AXIS POSITIONER
HOUSING
BUSHING
WING SPAR
FLEXURAL PIVOT
WING

FIGURE 5 **EXPLODED VIEW OF PITCH SUSPENSION SYSTEM**
[from Stoltz, Ref. 13]

from the sensor signals. Shown in Fig. 4 they are:

1) differential motions of the wing in plunge
2) chordwise motion of the wing
3) spanwise motion of the wing

The differential plunge mode is reduced by installing a stiffening beam on the suspension, parallel to the wing spar and external to the tunnel. For experiments requiring external plunge control of the airfoil, a plunge actuator (a cast-off computer-disc-drive linear motor) is attached to the mid-point of this stiffening beam which is the approximate node of the airfoil's differential bending mode. Consequently, the differential mode is not excited by application of an external force. Plunge position is also sensed at this point so the sensor does not measure the differential mode. The transducer used is an LVDT, mounted such that it is isolated from tunnel motions.

PITCH SUSPENSION

Test specimens are permitted to rotate about a pitch axis and may be controlled about that axis by either a control actuator external to the tunnel or by some specimen-mounted device such as a trailing-edge flap.

Each end of the test specimen is attached to housings which are part of the plunge suspension system. Inside each housing there is an arrangement of bushings which accommodates various sizes of Bendix Flex Pivots. These standard commercial pivots are available with a variety of torsional spring rates and radial load capacities.

Brackets built into the spar ends allow adjustment of the wing spar in a chordwise direction relative to the flexural pivot centerline. This was done to permit studies of the effect of chordwise location of the elastic axis (see Fig. 5).

If external pitch control is desired, a control linkage and torque motor are available. A torque motor with peak torque of 2 N-m is currently used, and its mass ($\sim$2 kg) is large enough that direct attachment on the wing pitch axis would result in an unacceptable increase in the total suspended mass.

After considering drives using flexible shafts, belts, metal tape and various linkages, a four-bar linkage was chosen. The linkage is mounted in a horizontal plane under the tunnel section. As the test specimen plunges, its attachment to the plunge suspension is constrained to move in a straight line by the folded cantilever springs. The pitch linkage deflects without imparting torque to the pitch axis because the torque motor is free to rotate and translate. The motor can transmit torque to the pitch axis at any position of plunge, as shown in Fig. 6.

Friction in the linkage is avoided by using Bendix Flex Pivots at all linkage joints as well as in the torque motor since the amount of rotation is limited. Thus, known spring rates replace uncertain friction.

Sensing of pitch motion is done using various angular sensors mounted on the end of the pitch axis. To date, both resolvers and rotary variable differential transformers (RVDTs) have been used. A flexible coupling with synchronizing adjustment has been used for zero setting.

AIRFOIL-MOUNTED PITCH CONTROL

Test specimens having integral means of pitch control, such as a trailing-edge control surface, can be operated in the tunnel by removing the external pitch linkage. One such specimen has been tested. This specimen has a trailing-edge full-span flap with a chord of approximately 24% of the total wing chord (see Fig. 7).

A dc torquer mounted inside the wing at mid-span is connected to the trailing-edge flap by cables routed over pulleys (see Fig. 8).

Installation of the torque motor in the wing was accomplished by first fabricating the wing as previously described, then cutting an opening for installation of a fitting designed to carry the spar loads and house the motor. Wing contour is restored with fiberglass covers held in place with screws, all joints being sealed with putty.

Cables are attached to crank arms mounted on each end of the motor, brought out through span-wise holes in the wing, and routed along the outside of the wing end-rib to the flap hinge.

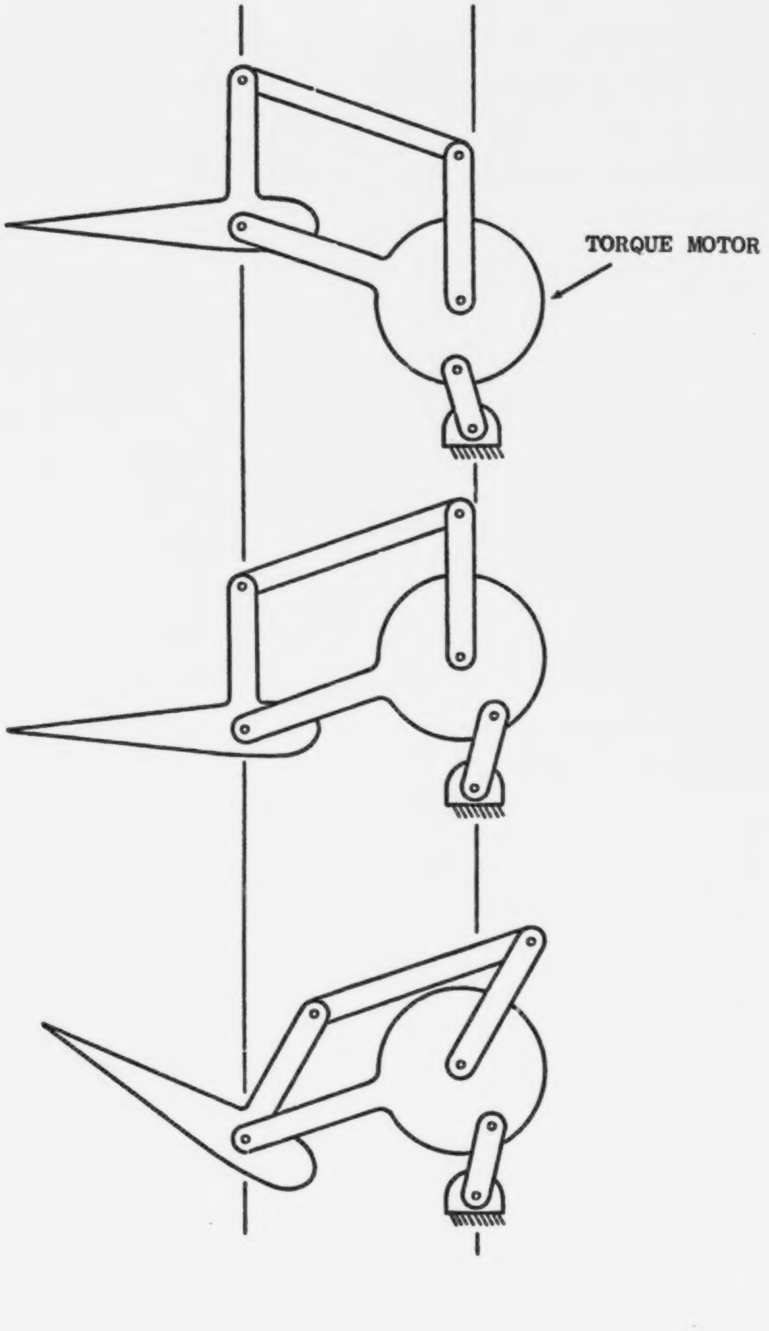
TORQUE MOTOR

FIGURE 6 OPERATION OF FOUR-BAR LINKAGE [from Rock, Ref. 12]

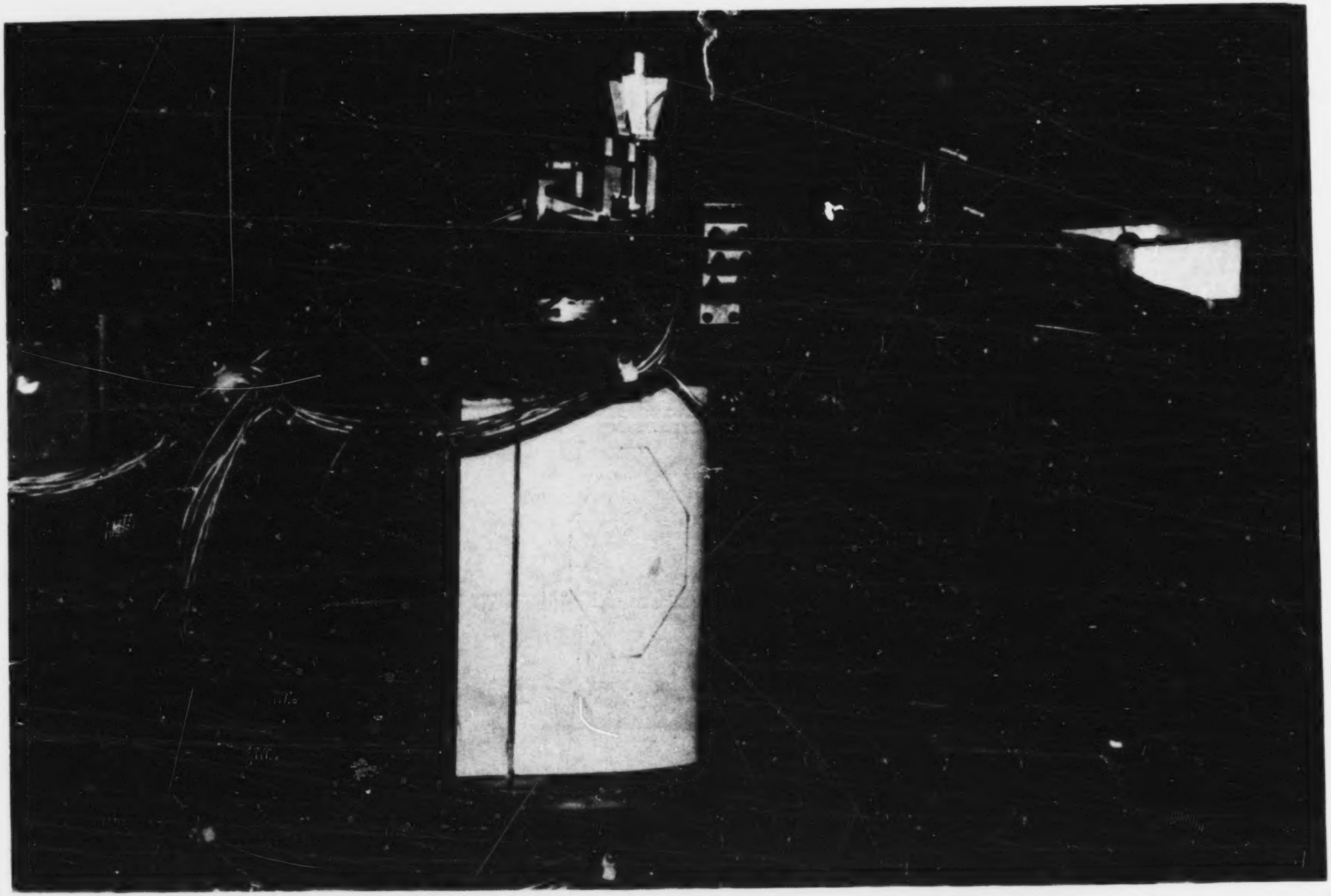

FIGURE 7 TRAILING-EDGE FLAP SPECIMEN

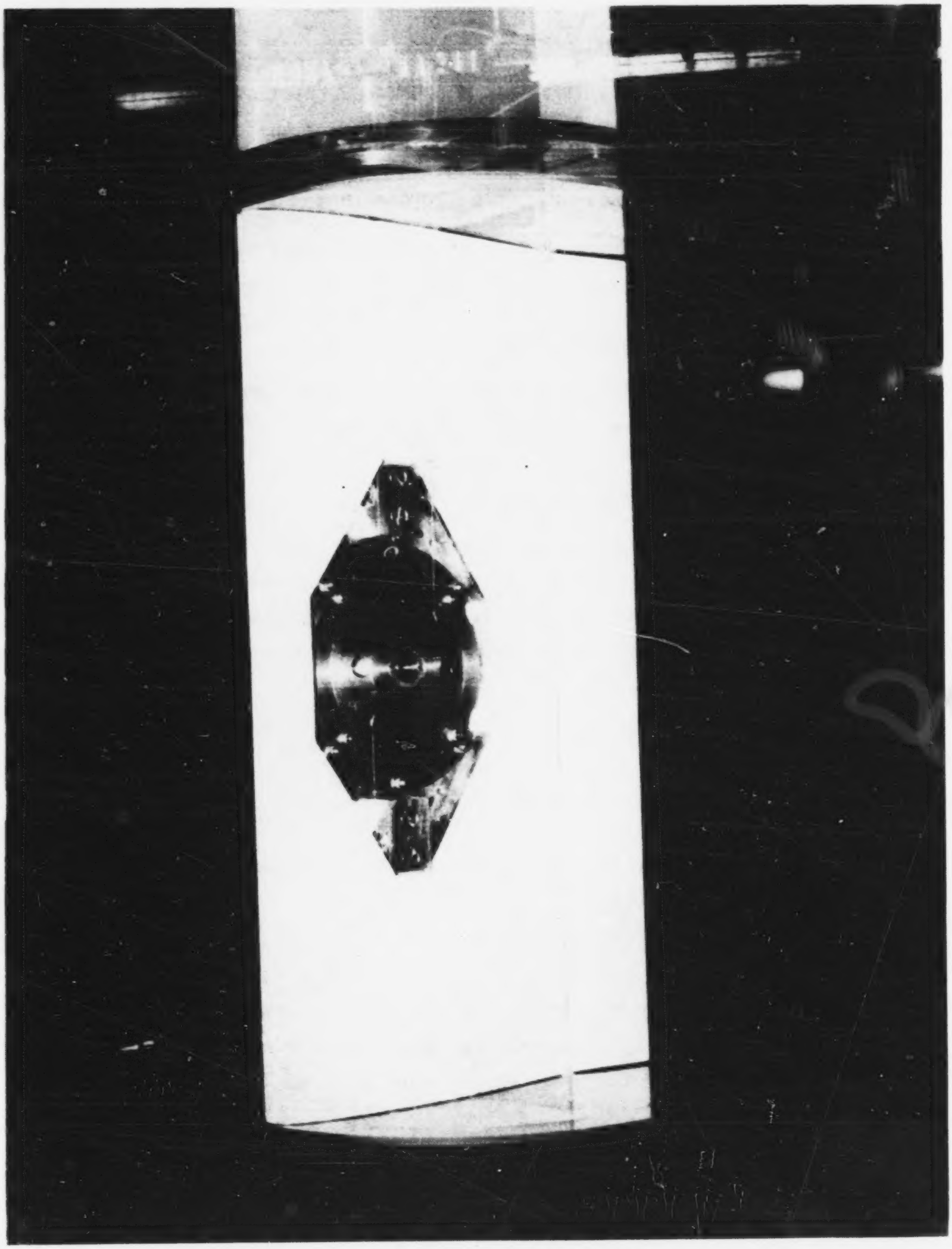

FIGURE 8 WING MOUNTED FLAP CONTROL

The hinge for the flap was designed such that the gap between the flap and the rest of the airfoil could be adjusted to minimize airflow through the gap. To achieve this, the airfoil trailing edge and the flap leading edge were designed with a concave/convex joint and the flap hinge bearings then adjusted to give a clearance of 0.2 mm (0.008 in).

The flap control was designed to provide flap excursions of ± 30 deg although in practice the motion is typically a few degrees.

SUSPENSION PERFORMANCE

The overall performance of the apparatus has been excellent. However, two complicating characteristics have been encountered. The first concerns the four-bar linkage used with the external pitch control motor. The second is excitation of differential modes.

When using the external pitch control motor, torque applied to the elastic axis of the airfoil generates an unbalanced force in the plunge DOF. This is illustrated in Fig. 9. The torque is transmitted through the linkage by axial forces and moments in its members. The motor generates torque, τ, between its case and link "A." This creates force F_1 which acts through link "B" to generate torque T about the elastic axis of the airfoil. From Fig. 9

$$T = F_1 \ell_1 = \left(\frac{T}{\ell_1}\right) \ell_1 = \tau$$

The undesired force is shown as F_2 in Fig. 9. It balances the torque acting on the case of the motor

$$F_2 = \frac{\tau}{\ell_2}$$

This force acts on the wing spar in the plunge direction. A further disadvantage of this force is that it is applied to one end of the wing, which therefore excites not only the primary plunge mode but also the differential plunge mode.

A simple technique has been used to eliminate the excitation of the primary plunge mode by the torque motor. A signal proportional to F_2 is

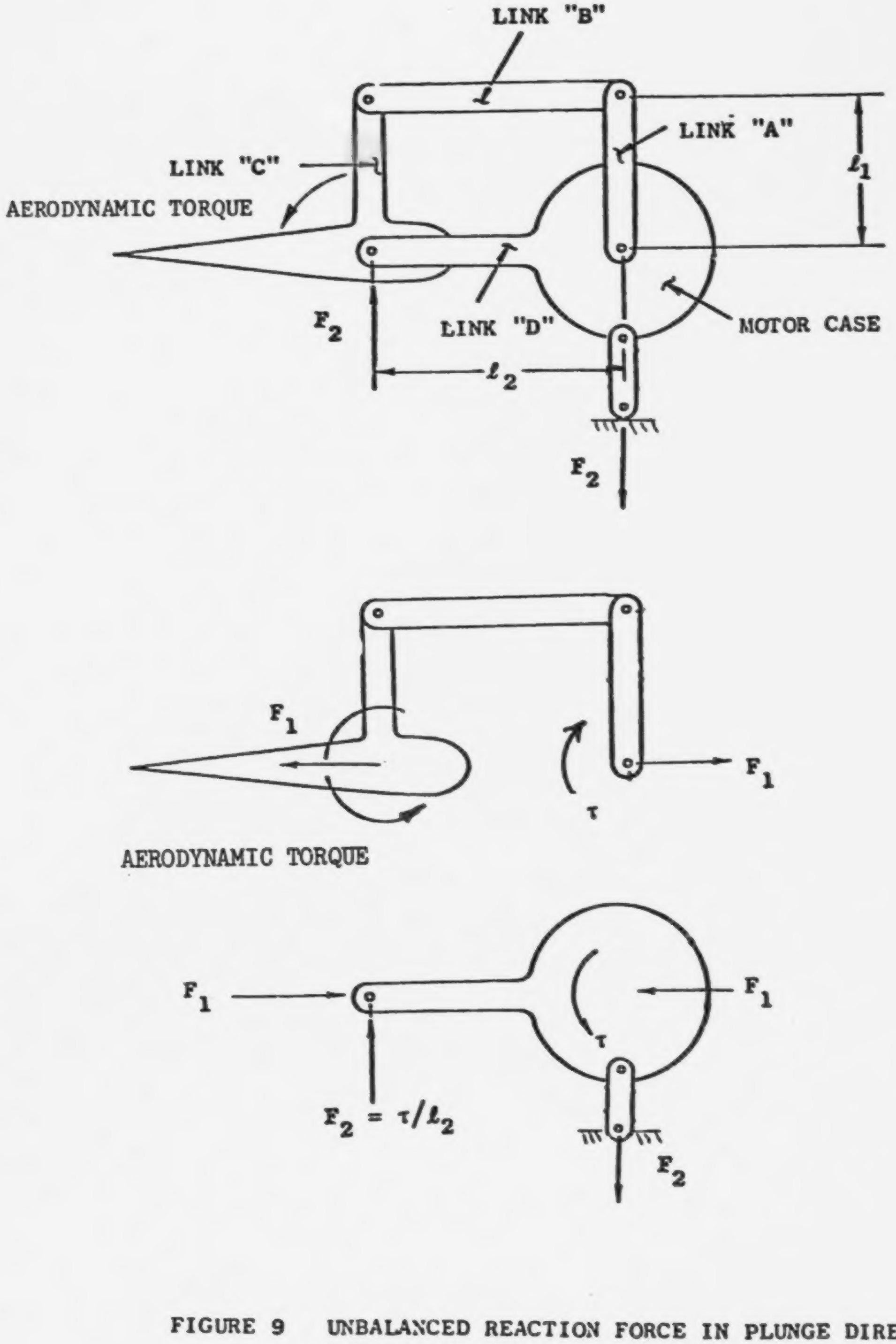
LINK "B"
ℓ
LINK "A"
ℓ_1
LINK "C"
AERODYNAMIC TORQUE
F_2
LINK "D"
MOTOR CASE
ℓ_2
F_2
F_1
F_1
τ
AERODYNAMIC TORQUE
F_1
F_1
τ
$F_2 = \tau/\ell_2$
F_2

FIGURE 9 UNBALANCED REACTION FORCE IN PLUNGE DIRECTION DUE TO APPLICATION OF TORQUE [from Rock, Ref. 12].

created and summed with the command signal to the plunge actuator. The plunge actuator thus cancels F_2.

Two differential modes are excited. One is the differential plunge mode discussed above. The other is a differential twisting of the wing across its span which is excited because torque is applied only to one end of the wing. Natural frequencies are 16.5 Hz for the plunge mode and 79 Hz for the twisting mode.

In open-loop studies (sensor signals not fed back to the actuators), neither of the differential modes is a problem. These motions merely superimpose on the primary motions. They are antisymmetric and therefore do not affect the aerodynamics. Furthermore, the differential twisting mode is much faster (10:1) than system dynamics and can be ignored. The differential plunge mode is less than a factor of two faster, but is not sensed by the plunge position sensor. The only problem occurs when the amplitude of the differential plunge motion becomes large, since this can cause binding of the plunge actuator.

In closed-loop studies, it is theoretically possible to drive the differential modes unstable. This is definitely true of the twisting mode. The angular resolver is located at one end of the wing and senses motions in this mode while the torque motor acts at the other end of the wing and excites the mode. Consequently, when the resolver signal is used as negative feedback to the torque motor (to stabilize the primary mode), a destabilizing positive feedback results on the differential mode. In the experimental procedures carried out, the positive feedback was small enough that no instabilities were encountered.

ALTERNATE SUSPENSIONS

Actuation of airfoil-mounted control surfaces poses one of the more difficult problems for a wind tunnel of this size. If mounted directly in or on the airfoil, a torque motor may exceed the allowable total sprung mass, may be too large to fit within the airfoil cross section, or may not have adequate torque.

An acceptable solution to these problems would result in no unwanted forces being applied to the specimen and no friction being introduced into the system. Two linkages were considered which permit mounting the torque motor external to the test specimen.

The linkage shown in Fig. 10 has the torque motor mounted on a link permitting small fore and aft motions of the torque motor in response to pitch and plunge motions of the wing. This arrangement reduces the sprung mass of the system and is satisfactory for small angle changes of pitch and small displacements in plunge. For the investigation of larger airfoil motions the amount of pitch/plunge/flap angle cross coupling becomes excessive.

The linkage shown in Fig. 11 also permits mounting of the torque motor on an external support. Flap position is effectively decoupled from pitch and plunge. However, most of the linkage mass is mounted on the suspension system. The linkage requires two joints having 2 DOF's on link A and a universal joint on the torque tube.

Both of these linkages, although more complex than the airfoil-mounted cable system which has been used, could be used if

(a) the test airfoil were too thin for a torque motor installation,

(b) the suspended mass were large enough such that the additional mass of a torque motor were unacceptable, and

(c) if the airfoil and control surface motions were small, avoiding cross coupling.

CONCLUSIONS

Elastic elements, which are essential to avoid masking small aerodynamic effects by friction and backlash, can be incorporated in a wind tunnel model suspension. Overconstrained design is more symmetrical and convenient and leads to an acceptable configuration if all flat springs are nominally biased to avoid snap-through. Torquing can be accomplished through linkages to avoid placing a torquer on the sprung mass. A symmetrical configuration could retain independence of plunge and rotation but the duplication of components did not seem warranted. We were able to achieve decoupling by crossfeed compensation.

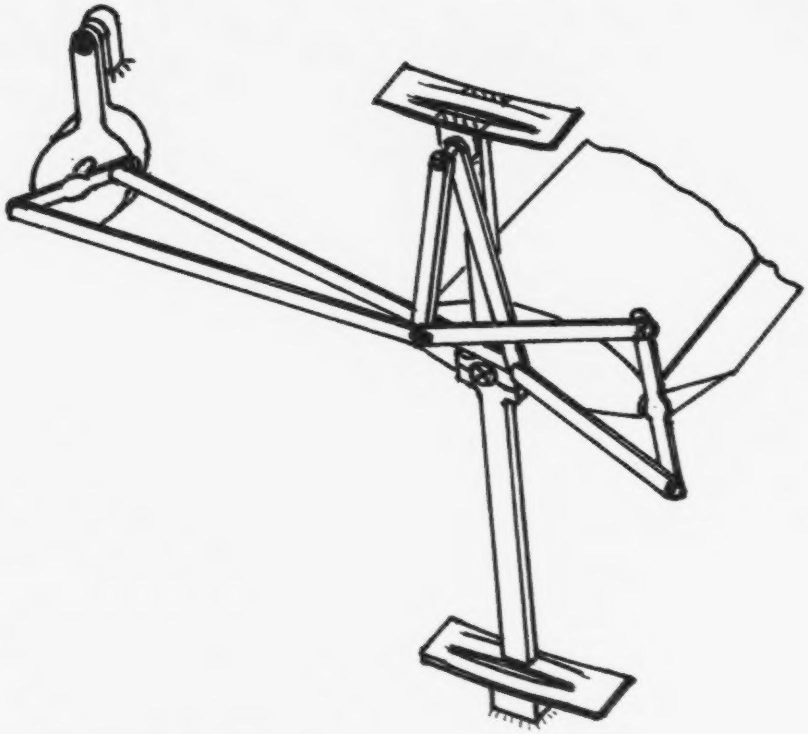

FIGURE 10 ALTERNATE LINKAGE I

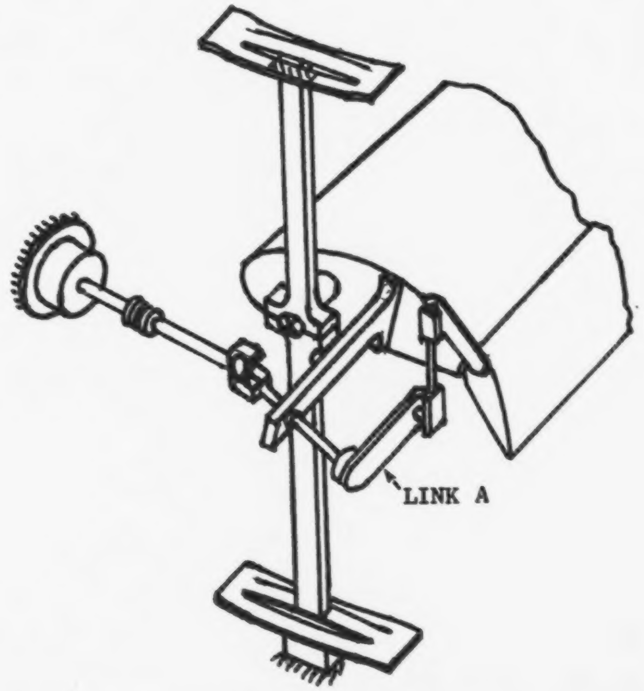

FIGURE 11 ALTERNATE LINKAGE II

ACKNOWLEDGMENTS

We gratefully acknowledge the support of NASA Dryden Flight Research Center for sponsoring the research of S. Rock and P. Stoltz, resulting in their dissertations, under contract No. NSG 4002.

Control torque motor selection, instrumentation, and all associated electric design were performed by R.A. Van Patten of Stanford University. Development and fabrication of the foam core/fiberglass airfoils were performed by Professor DeBra. Certain design requirements and valuable feedback were due to Jim Nathman and Paul Stoltz.

REFERENCES

1. Burris, P.M., and M.A. Bender, "Aircraft Load Alleviation and Mode Stabilization," AFFDL-TR-68-163, Nov. 1969.

2. Rogers, K.L., and G.E. Hodges, "Active Flutter Suppression--A Flight Test Demonstration," J. Aircraft, Vol. 12, No. 6, Jun. 1975, pp. 551-556.

3. "B-52 CCV Control System Synthesis," AFFDL-TR-74-92, Vol. II, Air Force Flight Dynamics Lab., Wright Patterson AFB, Ohio. 1975.

4. Grosser, W.F., W.W. Hollenbeck, and D.C. Eckholdt, "The C-5A Active Lift Distribution Control System," from Impact of Active Control Technology on Airplane Design, AGARD-CP-157, Jun. 1975.

5. Van Dierendonck, A.J., C.R. Stone, and M.D. Ward, "Application of Practical Optimal Control Theory to the C-5A Load Improvement Control System (LICS)," AFFDL-TR-73-122, Oct. 1973.

6. Rynaski, E.G., and N.C. Weingarten, "Flight Control Principles for Control Configured Vehicles," AFFDL-TR-71-154, Jan. 1972.

7. Sandford, M.D., I. Abel, and D.L. Grey, "Development and Demonstration of a Flutter-Suppression System using Active Controls," NASA TR R-450, Dec. 1975.

8. Schoenman, R.L., and H.A. Shomker, "Impact of Active Controls on Future Transport Design, Performance and Operation," SAE Paper No. 751051, Nov. 1975.

9. Doggett, R.V., I. Abel and C.L. Ruhlin, "Some Experiences Using Wind-Tunnel Models in Active Control Studies," Advanced Control Technology and its Potential for Future Transport Aircraft Symposium Los Angeles, Ca., Jul. 1974.

10. Theodorsen, T., "General Theory of Aerodynamic Instability and the Mechanism of Flutter," NACA Rept. 496, 1935.

11. Edwards, J.W., "Unsteady Aerodynamic Modeling and Active Aeroelastic Control," Ph.D. Thesis, Stanford University, Guidance & Control Lab., Dept. Aeronautics and Astronautics, Stanford, CA 94305, SUDAAR No. 504, Feb. 1977.

12. Rock, S.M., "Transient Motion of an Airfoil: An Experimental Investigation in a Small, Subsonic Wind Tunnel," Ph.D. Dissertation, Stanford University, Dept. Aeronautics and Astronautics, Guidance & Control Lab., Stanford, CA 94305, SUDAAR No. 513, May 1978.

13. Stoltz, P.M., "Unsteady Aeroelastic Modeling and Trailing-Edge Flap Control of an Experimental Wing in a Two-Dimensional Wind Tunnel," Guidance & Control Lab., Stanford University, SUDAAR 527, Jun. 1981

14. Nathman, James, "Unsteady Aerodynamic Propulsion," Ph.D. Dissertation, Stanford University, Dept. Aeronautics and Astronautics, Stanford, CA 94305, October 1981.

Russell Hacker
Lockheed Missiles and Space Company
P.O. Box 504
Sunnyvale, California 94086

Mr. Hacker is presently a design specialist in the Structures and Mechanisms Section. During his 30 years with Lockheed, he has been involved in the design of aircraft, spacecraft, and laboratory equipment. The equipment described in this paper was designed while on loan from Lockheed to the Guidance and Control Laboratory of Stanford University. He is a registered professional engineer in California. In addition, Mr. Hacker holds a B.S. degree in Civil Engineering from Northwestern University and received his M.B.A. in 1971 from San Jose State University.

Co-authors of this paper are Mr. Stephen Rock who is affiliated with Systems Control Technology and Mr. Daniel B. Debra, a professor at Stanford University who is Director of their Guidance and Control Laboratory.

Blank Page

SPACE SHUTTLE EXTERNAL TANK
GASEOUS OXYGEN VENT SYSTEM

William G. Franklin
NASA/John F. Kennedy Space Center, Florida

In the summer of 1979, NASA program management was faced with the problem of ice forming on the Space Shuttle External Tank, becoming airborne during launch, and potentially damaging the Orbiter thermal protection tiles. The ice would form during loading of the External Tank propellants as cryogenic gaseous oxygen was vented through the nose cone vent louvers and mixed witn the humid and sometimes wet environment at the launch pad. This ice had to be eliminated to ensure the successful launch of the Shuttle without risking damage to the fragile tiles.

To prevent the ice formation would require a system for removing the cryogenic gaseous oxygen (GOX) from the proximity of the Shuttle and venting it a safe distance away without creating ice on the External Tank (ET) or any of the system hardware. The system had to interface with the ET vent louvers at any location within the stacking envelope of the vehicle at the launch pad and provide an adequate seal, preventing the ice-forming leakage of cold gaseous oxygen in the vicinity of the ET, without altering the design of the ET or placing excessive loading on the tank's surface. The system would be required to track and remain interfaced with the ET in winds of up to 25.2 m/sec (49 knots) and be operational for launch in winds of up to 17.7 m/sec (34.4 knots) while allowing for downward tank shrinkage of approximately 6.9 cm (2.7 inches) as loading of the liquid oxygen proceeded. Although these requirements directed the final design concept, the basic success criteria for the system was "no ice formation."

Two problems had to be solved to assure successful elimination of ice on the ET. First, an access/support structure had to be provided from the Launch Complex 39A Fixed Service Structure (FSS) to the vicinity of the nose cone on the ET approximately 82.3 meters (270 feet) above the surface of the pad and 22.9 meters (75 feet) from the face of the FSS. Second, an umbilical had to be designed and tested that would seal around the ET GOX vent louvers and not allow ice to form on the tank or the umbilical. The umbilical would be designed to be mated to the access/support structure. To solve the first problem, a swing arm subsystem had to be designed to provide the support structure for and to allow access to the umbilical. After consideration of several concepts, the final decision was made in September 1979 to proceed with a modified Apollo service arm as the concept for the swing arm subsystem. To solve the second problem, an umbilical had to be designed which could be remotely disconnected or reconnected with the ET. Again several concepts were considered; and the concept chosen by KSC and MSFC for design and testing was an inflatable vent seal subsystem providing a cloth seal around each vent louver with an internal annulus to provide a path for the gaseous oxygen from the ET to a hard duct on the swing arm. The baseline inflatable vent seal subsystem would require no modifications to the ET.

The system description falls into two major parts: the final design of the swing arm subsystem which provides the access/support structure and the vent seal subsystem which provides interfaces between the swing arm vent pipes and the ET; and the qualification testing required to certify the system for use on the launch pad and to resolve major problems which developed in support of the first Shuttle launch.

FINAL SYSTEM DESIGN

The swing arm subsystem consists of a horizontally rotating, 19.2-m (63-ft) long arm truss hinged at the northeast corner of the FSS, a vent hood with its actuation mechanism, and a hydraulic/pneumatic control console to provide power to retract or extend the arm (see Figure 1). The arm truss, hinges and control console are all modified Apollo/Saturn V service arm hardware.

The arm truss, made of tubular T-1 steel, is a lightweight design supporting the vent hood located at the tip of the arm and providing access to the vent hood for up to six people. The truss and vent hood assembly, longer than any previous cantilevered swing arm used in launch operations, is 24 meters (79 feet) from arm hinge centerline to the tip of the vent hood. The total arm weight is 10,500 kg (23,100 lb) with an additional 5450-kg (12,000-lb) hinge weight. The arm is actuated by two hydraulic cylinders attached at the hinge and supplied with 1.52×10^7 N/m^2 (2200 psig) pressurized hydraulic fluid from the hydraulic/pneumatic control console. Each cylinder develops 364,000 Joules (268,000 foot-pounds) torque to swing the arm about the hinge.

The vent hood, located on the tip of the arm truss, is the carrier for the vent seal subsystem. The aluminum hood is hinged at its connection to the arm truss and is rotated up or down about that hinge line using the vent hood actuation mechanism (a primary or a secondary screw jack operated by vane-type air motors which are driven by a compressed air supply). In operation, the hood is raised at a .84 rad (48°) angle from horizontal when the arm is extended or retracted to allow it to clear the ET. The hood is then lowered to the horizontal position by the screw jack to allow proper location of the vent seal subsystem. To complete positioning of the vent seal subsystem, the arm extend angle is optically aligned with the centerline of the ET and the vent hood is adjusted in or out axial to the arm truss using two large screw jacks. The vent hood is then leveled by adjusting the secondary screw jack. The arm adjustment of $\pm$ 0.017 rad (1°) in extend angle and the vent hood axial adjustment of $\pm$ 11.4 cm (4.5 in) takes care of the $\pm$ Y and $\pm$ Z vehicle stacking tolerances. This locates the vent seal subsystem properly for mating with the ET.

The hydraulic/pneumatic control console provides arm and hood operating pressure with a 1.52×10^7 N/m^2 (2200 psig) hydraulic supply to extend or retract the arm and an 8.62×10^5 N/m^2 (125 psig) air supply to raise or lower the vent hood. It utilizes a bank of 4.14×10^7 N/m^2 (6000 psig) gaseous nitrogen accumulators regulated down to 1.52×10^7 N/m^2 (2200 psig) to pressurize the hydraulic accumulators and thereby maintain system operating pressure. The facility supplies hydraulic fluid, compressed air, and gaseous nitrogen at system operating pressures to the console; however, the console has accumulator capacity so that once charged the arm and hood can be completely cycled (retracted and extended) twice without any fluid or gas replenishment. The control console contains the KSC Launch Processing System (LPS) controlled valving to provide complete redundancy for arm and vent hood extension and retraction with no single failure points.

The vent seal subsystem consists of two soft, inflatable seals supplied with heated gaseous nitrogen (GN_2) from a pressure regulation panel and heater bank which is ducted across the arm truss for distribution to the vent hood. The inflatable seals are the interface of the ground ET GOX Vent System with the Shuttle External Tank. They provide a flexible pipe able to withstand the 92°K (-294°F) temperature (GOX) venting from the ET vent louvers while ducting the GOX to the hard vent pipes on the vent hood, along the arm truss and away from the ET (see Figures 1 and 2).

The vent seals are inflated with the heated GN_2 from the pressure regulation panel and heater located on the 83.8-meter (275-ft) level of the FSS. The panel is supplied with 1.03×10^6 N/m^2 (150 psig) GN_2 and regulates it down to 5170 N/m^2 (0.75 psig) with two redundant, dome-loaded pressure regulators operating in parallel. The regulators sense the vent hood plenum (seal supply) pressure to maintain the inflatable seals with the 2758 ± 690 N/m^2 (0.4 ± .1 psig) tolerance required for proper seal function. The seals are protected from overpressurization by four relief valves located at the regulation panel outlet. The pressure regulation panel is capable of flowing 68 kg/min (150 lb/min) of GN_2 to the heater. The 156-kW heater operating at one-quarter capacity heats the GN_2 to approximately 389°K (240°F). The heat losses in the ducting reduce this to 355°K (180°F) maximum by the time the GN_2 reaches the vent hood plenum and the seals. A temperature-sensing probe is located in the plenum which is routed to the heater controller, maintaining the plenum (seal supply) temperature between 350°K and 355°K (170°F and 180°F) by varying the heater temperature. After exiting the heater the heated GN_2 flows through the main GN_2 shutoff valve (which is controlled by LPS) and to the ducting on the arm truss. The ducting distributes the approximately 45.4 kg/min (100 lb/min) total GN_2 heated flow to three areas: the vent hood plenum at 27.4 kg/min (60 lb/min); the two flexible vent ducts located at the arm truss/vent hood hinge line at 4.5 kg/min (10 lb/min) each; and the two exhaust tips of the GOX vent pipes at 4.5 kg/min (10 lb/min) each.

The vent hood plenum supplies the heated GN_2 to the inflatable seals. Ideally in operation, the inflatable seals are pressurized to approximately 3103 N/m^2 (0.45 psig) with a GN_2 supply temperature of 355°K (180°F) at a flow rate of 10.5 kg/min (23 lb/min) maximum to each seal with an additional 6.4 kg/min (14 lb/min) being dumped to inert the hood annulus. The inflatable seals are constructed of a vinyl-impregnated nylon cloth (Herculite 20 manufactured by Herculite Products) and Beta cloth (a Teflon-coated fiberglass cloth used in making the astronauts' suits during the Apollo Program). The vinyl-impregnated nylon cloth (called nylon cloth for simplicity) is stitched into a segmented column to provide the structural strength to hold the seal shape when inflated. When the seal is inflated against the tank, the nylon cloth is the contact surface of the seal with the ET. The Beta cloth, used as an inner liner to the seal, protects the nylon cloth from the GOX by maintaining its flexibility under the cryogenic flow conditions and insulating the seal (see Figure 3). The use of the Beta cloth was required since the nylon cloth becomes stiff at temperatures below 239°K (-30°F) and cracks when subjected to motion. The Beta cloth, which remains relatively flexible down to 89°K (-300°F), insulates the nylon cloth from the cryogenic gas by using the heated GN_2 flowing through each seal at 10.5 kg/min as a captive boundary layer between the two fabrics. The heated GN_2 passes through an even distribution of .64-cm (.25-in) holes in the nylon cloth, into the boundary layer between the two materials and through a smaller quantity of .64-cm holes in the Beta cloth. The heated GN_2 is then exhausted into the vent pipe providing a limited boundary layer effect on the outside surface of the Beta cloth. Pictures of the inflated vent seals are shown in Figures 4 and 5. When the vent seals are inflated around the two ET vent louvers they provide a complete flexible pipe from the GOX vents to the vent pipe on the hood (see Figure 3 for the shape of the sealing surface with the ET) which is able to track vehicle motion during cryogenic propellant loading and operating winds.

When the cold GOX has been exhausted through the seals, it travels through the vent pipes and is dumped approximately 6.7 m (22 ft) from the ET. The GOX from each vent seal flows through an insulated 0.46-m (1.5-ft) diameter vent pipe on the hood to the flexible vent ducts. The flexible vent ducts provide a lightweight, flexible pipe to allow the vent hood to raise and lower while the arm and hood vent pipes remain connected. The 1.83-m (6-ft) long flexible vent ducts are cylindrical versions of the inflatable vent seals and are clamped to both the vent hood and arm truss vent pipes. From the inflatable vent ducts the GOX travels down two 0.61-m (2-ft) diameter, 8.2-m (27-ft) long insulated vent pipes before being dumped to the atmosphere. On the exhaust tip of each GOX vent pipe is a 0.3-m (1-ft) long, heated annular section which is designed to prevent ice formation on the vent pipe.

SYSTEM QUALIFICATION TESTING

Shuttle Program testing of the vent seal subsystem was conducted in four parts: concept verification tests to determine if the system concept would perform under the required conditions, qualification testing to certify the performance of the designed hardware, pad validation testing to verify system installation and marriage with the pad systems, and system requalification testing required due to the failure of the system to function as designed in support of the first Space Shuttle launch (STS-1).

The concept verification testing (CVT) was conducted in September and October 1979. The prototype vent seal configuration was tested to determine its capability and performance in sealing against the ET under the required vehicle stacking and tracking parameters. To accomplish this test program, a test nose cone was outfitted by MSFC and installed in the KSC Launch Equipment Test Facility (LETF) on an existing vehicle random motion simulator. Liquid nitrogen tanker trucks were connected to the ET nose cone vent valve plumbing to provide cryogenic GOX simulation, and a gaseous nitrogen supply was connected to an existing heater to provide the heated GN_2 for the inflatable vent seals. The test vent seals were installed on a prototype vent hood structure which provided the plumbing for the heated GN_2 supply. Simulations of worst-case venting conditions and all vehicle stacking and tracking parameters were successfully completed. As a result of the successful concept verification testing, the system design was baselined for use on STS-1.

The qualification testing was conducted from April to September 1980 in the LETF. For this test program the pad vent hood, vent seals, hood retract mechanism, and a 1.8-m (6-ft) section of the arm truss (support structure for the vent hood and hood retract mechanism) were installed in the LETF on the test stand about the nose cone simulator. This hardware is called the tip assembly. The pad GN_2 regulation panel was also installed, mated with the heater (used during the CVT program and identical to the pad heater), and the ducting routed to the tip assembly. The pad arm truss GOX vent pipes which for STS-1 were 20.4 m (67 ft) long and 0.3 m (1 ft) in diameter were not installed but were simulated with shorter 4.5-m (15-ft), smaller 0.15-m (.5-ft) diameter vent pipes due to the short test program initially scheduled to meet a September 1980 launch. The cryogenic GOX simulation was the same as for the CVT program.

During the qualification testing a number of minor problems occurred, related to heated GN_2 flow to the inflatable vent seals and flexible vent ducts, which required minor modifications to the hardware and operating procedure. Most notable of these problems was the sensitivity of nylon cloth and stitching to pressure and temperature. The material, originally thought to be structurally sound when supplied with 4137-N/m^2 (.6-psig) GN_2 at 380°K (225°F), became severely damaged. Modifications were made to the seams to add adhesive to minimize stress concentrations at the stitch holes. The seal operating pressure was reduced to 3447 N/m^2 (.5 psig) maximum and the seal supply temperature was reduced to 366°K (200°F) maximum resulting in a maximum seal temperature of 355°K (180°F). Modifications were also made to the hood retract mechanism to install a gear reducer between the air motor and jack screw drive shafts. This was required to meet the hood retract time requirement of 25 ± 5 seconds and the hood extend time requirement of 35 ± 5 seconds.

By the completion of the qualification testing, all Shuttle Program requirements were successfully tested, and all known problems had been resolved. The ET stacking and motion tracking envelopes were successfully tested. ET cyclic venting with the vent valve open for two minutes and closed for three minutes and an opening pressure of 5.5×10^4 N/m^2 (8 psig) quickly dropping off to 1.4×10^4 N/m^2 (2 psig) was tested at temperatures ranging from 273°K (32°F) to 88.5°K (-300°F). ET constant venting was simulated for 5½ hours with the vent valve remaining open and the tank venting from 5.5×10^4 to 1.4×10^4 N/m^2 during that time span. Vent hood retraction and re-extension tests were completed with successful seal disconnect and reconnect, simulating remating with the ET in the event of a launch scrub/abort after the vent hood and arm had been retracted. Following the final qualification tests, the tip assembly and GN_2 regulation panel were removed from the LETF, refurbished and installed at the launch pad.

The pad validation testing was conducted in two phases to allow for parallel testing of the arm and its control system on the FSS at the pad while the critical tip assembly and heated GN_2 supply hardware were being tested in the LETF. Phase I testing (starting in June 1980) verified operation of all arm and control console hardware except the LETF test hardware. A weight cage was constructed and installed on the arm tip to simulate the tip assembly weight and C.G. This allowed arm proofloading and timing tests to be completed to control the arm swing time, allowing the arm to swing as quickly as possible without excessively loading the arm truss chord members. An arm retract time of 45 ± 5 seconds was selected after reviewing strain gauge data and possible failure modes which could increase/decrease arm retract time. This time was minimized due to the vent hood retract sequence starting at T-2 minutes and 35 seconds with arm retraction required by T-30 seconds. After similar analysis an arm extend time of 65 ± 5 seconds was selected. Complete checkout of the control console and verification of the operation and control of all LPS-operated valves was also accomplished. Phase II testing (conducted from October to December 1980) verified the end-to-end operation of the installed pad system as operated by the LPS console in the Launch Control Center (LCC). Following validation of the installed GN_2 regulation panel and tip assembly, the complete system was qualified with LPS; and the system operation times and conditions verified as those required to support a launch. Testing was completed prior to rollout of STS-1 to the launch pad on December 29, 1980.

The ET GOX vent system was supporting the STS-1 LOX tanking test on January 24, 1981, when the first in a series of failures occurred. The vent seal over the southwest ET vent louver leaked at the seal/ET interface, damaging the ET insulation below the louver. Investigation of the failure revealed several factors: when the ET vent valve was opened, the vent hood/arm truss bounced up approximately 2.5 cm (1 in) and the seal pressure increased from 3310 N/ m^2 (0.48 psig) to 4000 N/ m^2 (0.58 psig) indicating a sudden loading of the vent seal due to blast pressure from the ET vent or backpressure in the vent pipe; the vent seal moved 10 cm away from the louver at the initial vent valve opening; the failure occurred at a stage during LOX tanking which was not simulated in the LETF due to a lack of ullage capacity in the facility system; the ET surface in the seal contact area was rougher than specified; another contributing factor to the failure may have been arm truss/vent hood misalignment with the ET. After reviewing these factors, the following modifications were made to the system prior to STS-1. Flight Readiness Firing (FRF): the vent seal pressure was increased to 0.039 kg/ cm^2 (0.55 psig) to force the seal to conform to the ET surface; the vent seal supply temperature was increased to 377°K (220°F) to heat the seal footprint; a fiberglass seal support frame was attached to the vent hood to prevent seal movement; the ET surface was repaired and smoothed as much as possible; seal vent cavity backpressure transducers were added with data recorded in the LCC and a film camera arranged to monitor the seals during venting.

FRF occurred on February 20, 1981, with the vent seals again failing to perform. The southwest vent seal ruptured and damaged the ET during the fourth ET vent valve open cycle with the LOX tank approximately 50% full. Analysis of the failure revealed the following: visible signs of stress in the failed seal (stretch marks, elongated stitch holes) indicated that the higher seal pressure and temperature were contributors to the seal failure; the vent seal pressure increased from 3585 N/m^2 (0.52 psig) to 4690 N/m^2 (0.68 psig) and the vent hood bounced approximately 4.6 cm (1.8 in) when the vent valve opened; backpressure in the seal vent cavity increased to approximately 6895 N/m^2 (1 psig) accounting for the vent seal pressure increase and the hood bounce by the sudden dynamic loading; the fiberglass seal support appeared to pinch the vent seal against the ET as the seal attempted to track the shrinking tank; the vent seal appeared to be too closely confined for its designed length which created a bunching action and may have contributed to the problem. Any or all of these factors may have caused the second failure; however, it was apparent that the blast from the southwest vent louver (the northeast seal had never leaked) and the vent cavity backpressure (coupled with the vent hood bounce) were the major contributors to both seal failures. After FRF the system was returned to the baseline configuration (tanking test configuration) pressures and temperatures with the fiberglass seal support removed. The vent seal inflated length was changed from 0.61 m (24 in) to 0.508 m (20 in) to minimize bunching. The ET was also modified to configure the vent orifice located 8 cm (3 in) inside the vent louver to attempt to break up the blast pressure of the venting gas impinging on the vent seal.

These modifications were all accomplished prior to the third ET tanking test which resulted in a third failure of the vent seal. The vent seal leaked with the ET approximately 70% full. The vent seals were removed from the vent hood following completion of the third tanking test, and the vent hood used in the "umbrella" mode as a cover providing a heated nitrogen purge to the ET for STS-1 launch on April 12, 1981. Some ice or heavy frost was formed on the louver area of the ET in spite of the heated GN_2.

A requalification test program of the GOX Vent System was conducted in the summer of 1981. The GN_2 regulation panel and the tip assembly with the full-length vent pipes were returned to the LETF which was upgraded by the addition of a 106-m^3 (28,000-gal.) dewar to the cryogenic simulation system and by other minor modifications to improve the simulation of the ET cryogenic shrinkage, vent hood bounce, ET vent valve, and ET surface smoothness. The test program started by investigating the STS-1 failures to determine their most probable cause. This testing revealed these problems:

1. The blast pressure from the vent valve on the southwest vent seal was approximately ten times that on the northeast seal resulting in an increased load over a concentrated area.

2. The backpressure in the seal vent cavity at vent valve opening was caused by undersized vent pipes, which at 6895 N/m^2 was five times greater than tested one year before. This resulted in a partial internal collapse of the vent seal which was pressurized to less than one-half that amount.

3. The alignment of the arm/vent hood was critical due to the vent seal proximity to the vent louver and may have been as much as 10 cm (4 in) off for STS-1 first tanking test.

To resolve these problems modifications were made to the ET vent valve, the GOX vent pipes and the vent hood. The ET vent valve, a poppet valve, was modified to limit the stroke of the poppet to 42% of the original stroke, thereby reducing the flow through the valve; and the orifices downstream of the vent valve were removed to allow greater expansion of the GOX prior to exiting the vent louvers and impinging on the vent seals. The existing GOX vent pipes were removed and new ones installed which were twice as large in diameter (0.61 m vs 0.3 m) and less than half as long (8.2 m vs 20.4 m). The vent hood was modified to provide an improved optical alignment capability to assure that the vent seals were centered about the ET vent louvers. After the modifications, the retest of the system was performed with the following results:

1. The blast pressure on the southwest vent seal was reduced by 90% to approximately that of the north vent seal on STS-1 (which did not leak).

2. The backpressure in the seal vent cavity at vent valve opening was reduced by 85% to less than 1034 N/m^2 (0.15 psig).

3. The alignment of the arm/vent hood with the ET could be consistently made within 1.25 cm (0.5 in).

4. The LETF cryogenic system could successfully simulate the predicted STS-2 vent valve cyclings and pressure curves.

The retest program successfully requalified the GOX Vent System tip assembly and GN_2 regulation panel which were reinstalled at the pad and checked out prior to STS-2 rollout.

In support of STS-2 the system performance was excellent (see Figure 6). On September 15, 1981, the system successfully supported the tanking and detanking of the ET with no problems. Prior to launch a new seal set was installed. The system successfully supported the STS-2 launch scrub on November 4, 1981, and the launch on November 12, 1981, with the same set (pair) of inflatable vent seals which were under operating pressure and temperature for a total of 30 hours and cryogenic flow for 16 hours (the longest operational usage for one inflatable vent seal set).

The system is now operational at the launch pad. Although the quality of the vent seal manufacturing is still a minor problem, most of the major problems have been solved. The vent seal was a significant factor in the ability of the system to meet program requirements due to its flexibility in tracking vehicle motions and its ability to conform to the contour of the ET and not allow any leakage of GOX. A significant lesson learned in the testing of the ET GOX Vent System is to "simulate as little as possible and when you have to simulate make sure that it adequately meets the requirements and predicted capability of the system you are simulating".

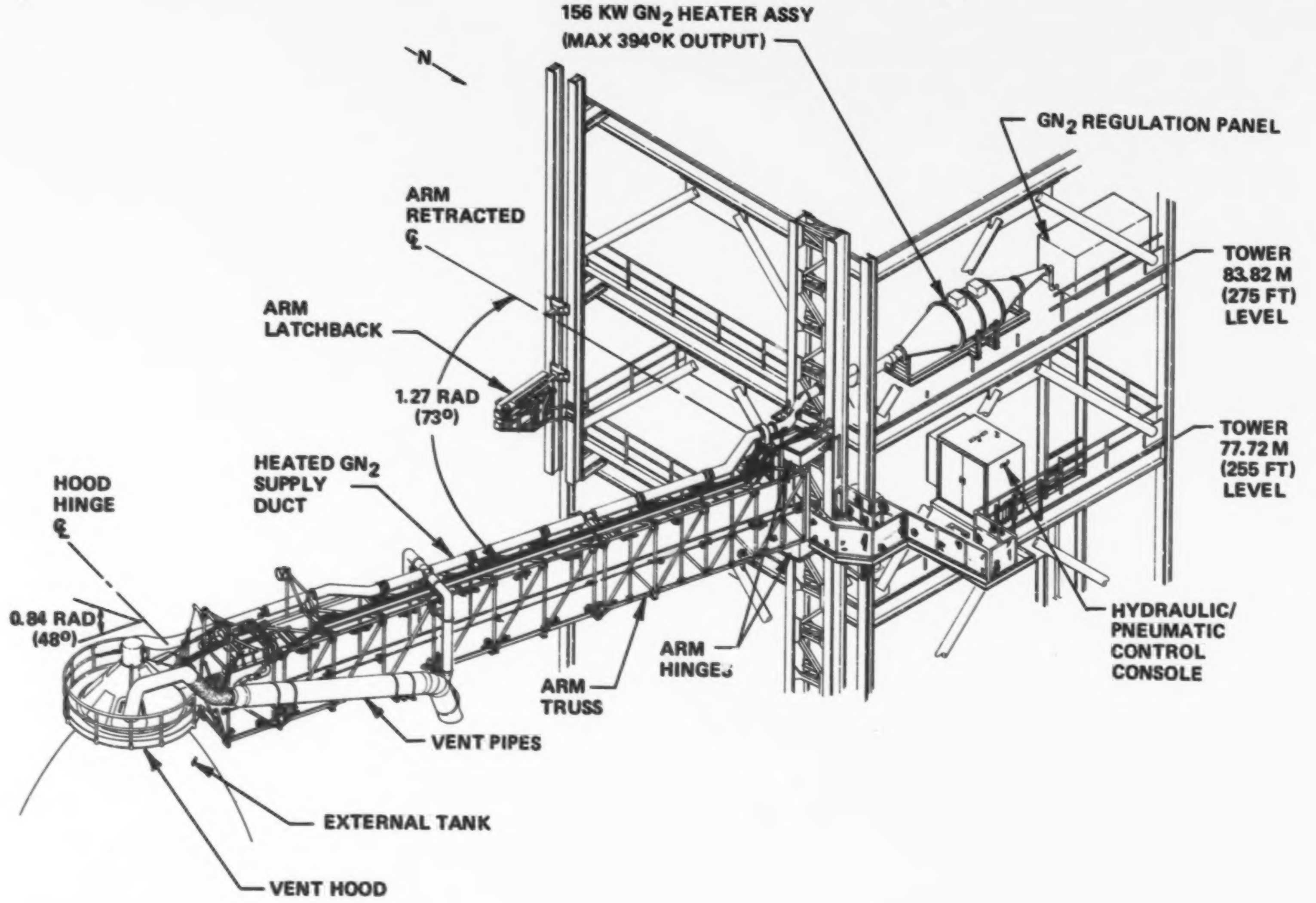
156 KW GN_2 HEATER ASSY
(MAX 394°K OUTPUT)
N
GN_2 REGULATION PANEL
ARM
RETRACTED
℄
ARM
LATCHBACK
TOWER
83.82 M
(275 FT)
LEVEL
1.27 RAD
(73°)
TOWER
77.72 M
(255 FT)
LEVEL
HEATED GN_2
SUPPLY
DUCT
HOOD
HINGE
℄
0.84 RAD
(48°)
HYDRAULIC/
PNEUMATIC
CONTROL
CONSOLE
ARM
HINGES
ARM
TRUSS
VENT PIPES
EXTERNAL TANK
VENT HOOD

Figure 1. ET GOX Vent System Installation at Launch Complex 39A

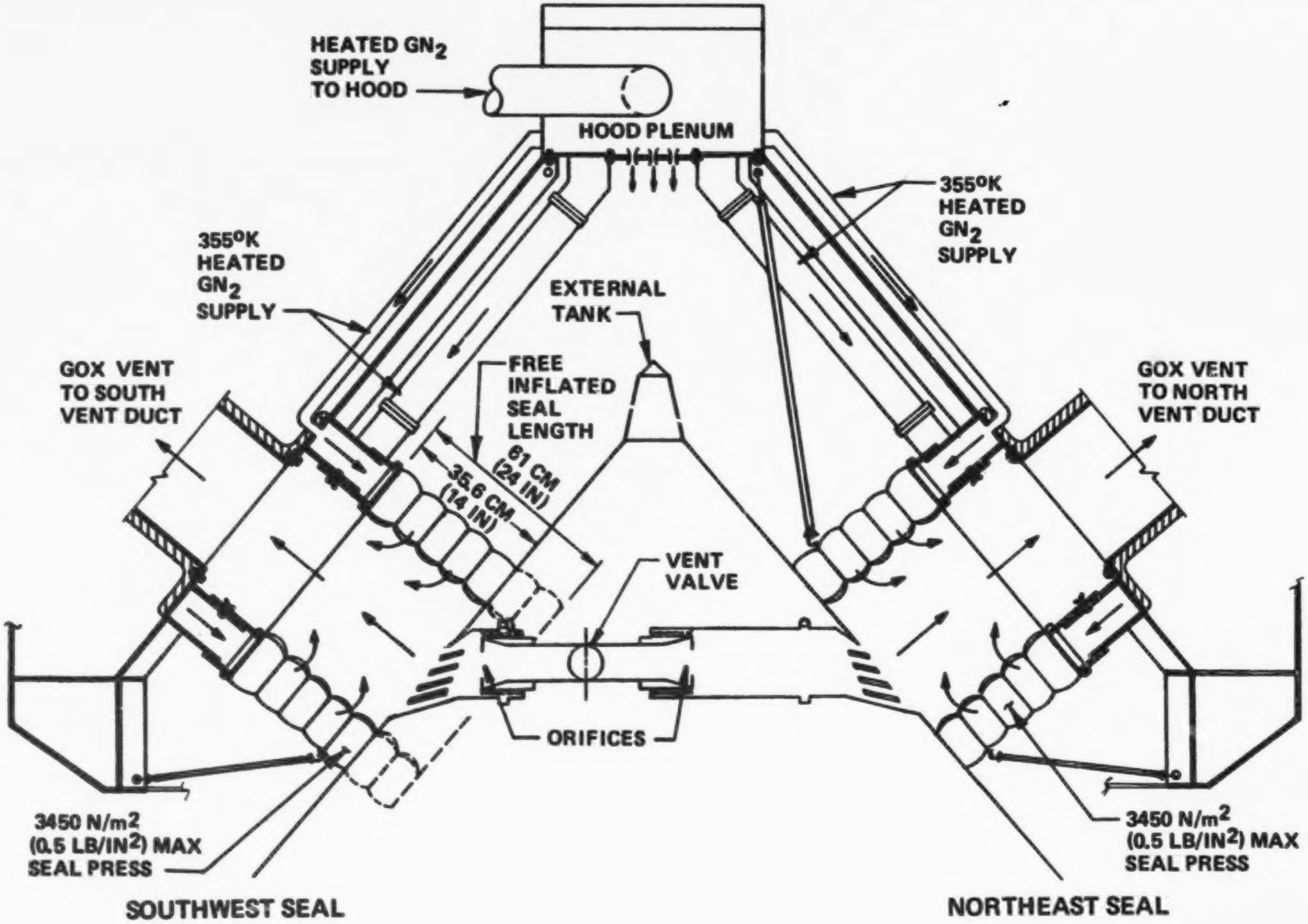
HEATED GN_2 SUPPLY TO HOOD
HOOD PLENUM
355^oK HEATED GN_2 SUPPLY
355^oK HEATED GN_2 SUPPLY
EXTERNAL TANK
GOX VENT TO SOUTH VENT DUCT
GOX VENT TO NORTH VENT DUCT
FREE INFLATED SEAL LENGTH
61 CM (24 IN)
35.6 CM (14 IN)
VENT VALVE
ORIFICES
3450 N/m^2 (0.5 LB/IN^2) MAX SEAL PRESS
3450 N/m^2 (0.5 LB/IN^2) MAX SEAL PRESS
SOUTHWEST SEAL
NORTHEAST SEAL

Figure 2. Vent Hood Cutaway Showing Vent Seals and Interface With ET

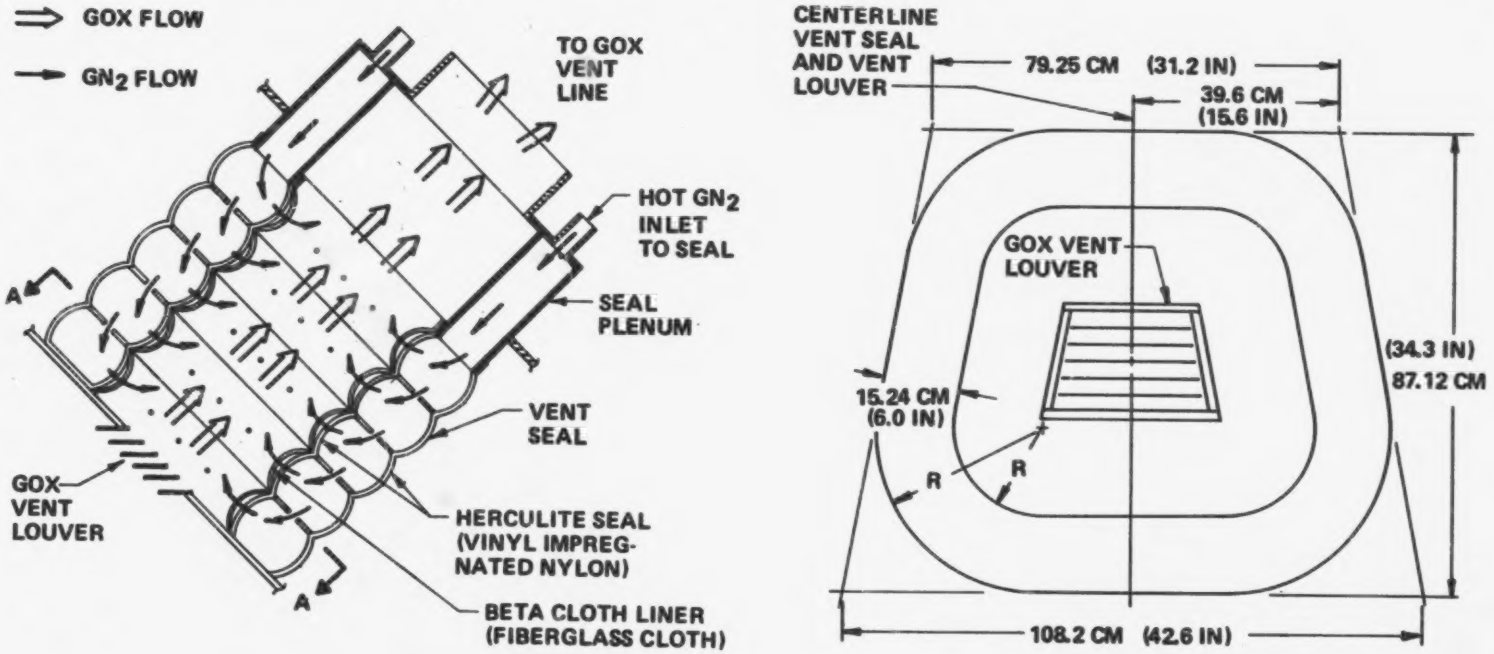
GOX FLOW
GN$_2$ FLOW
TO GOX VENT LINE
HOT GN$_2$ INLET TO SEAL
SEAL PLENUM
VENT SEAL
HERCULITE SEAL (VINYL IMPREGNATED NYLON)
BETA CLOTH LINER (FIBERGLASS CLOTH)
GOX VENT LOUVER
A
A
CENTERLINE VENT SEAL AND VENT LOUVER
79.25 CM (31.2 IN)
39.6 CM (15.6 IN)
GOX VENT LOUVER
(34.3 IN) 87.12 CM
15.24 CM (6.0 IN)
R
R
108.2 CM (42.6 IN)

SEAL CROSSECTION

SECTION A–A
SEAL FOOTPRINT

Figure 3. ET GOX Vent Seal

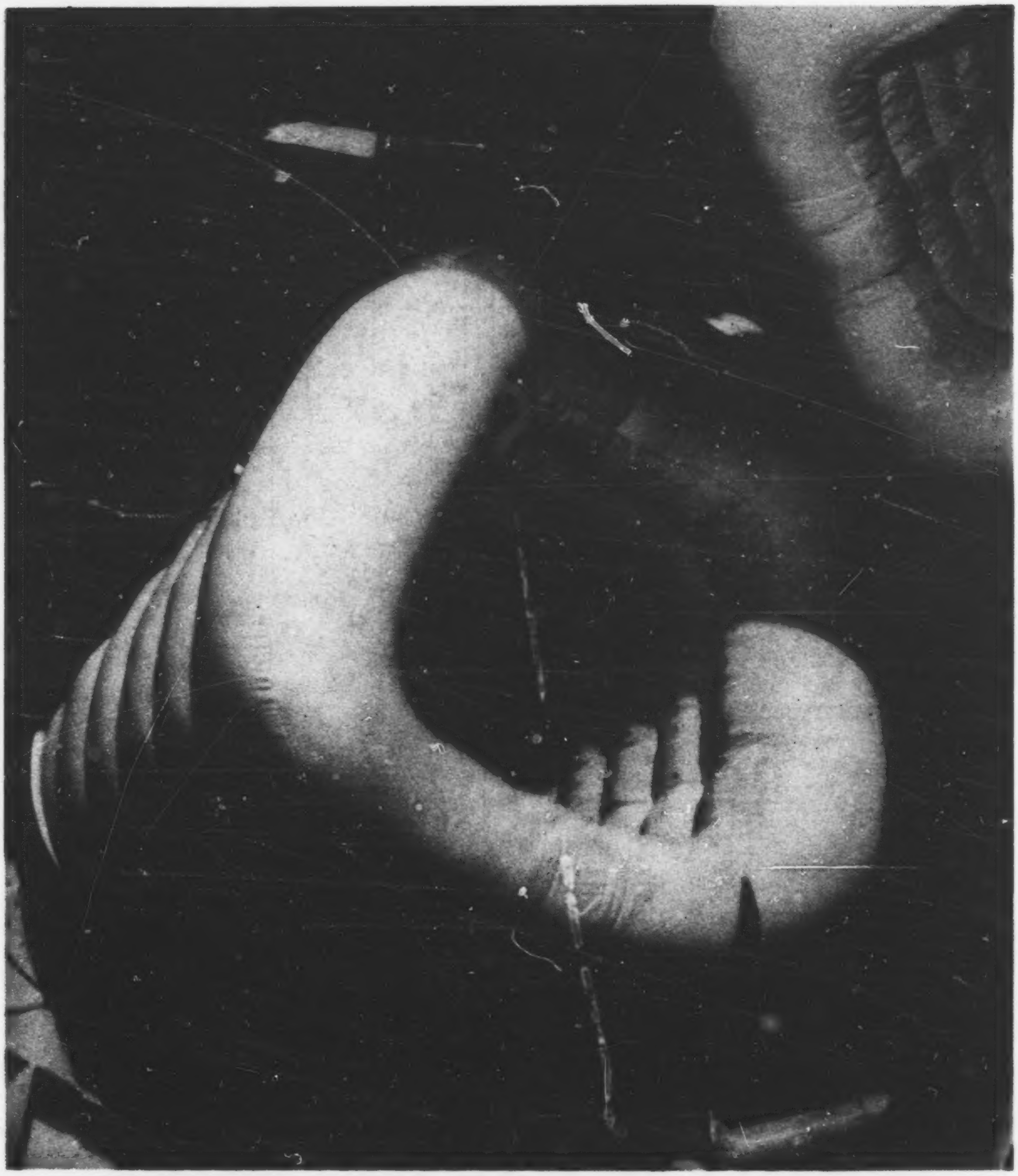

Figure 4. ET GOX Vent Inflatable Seals

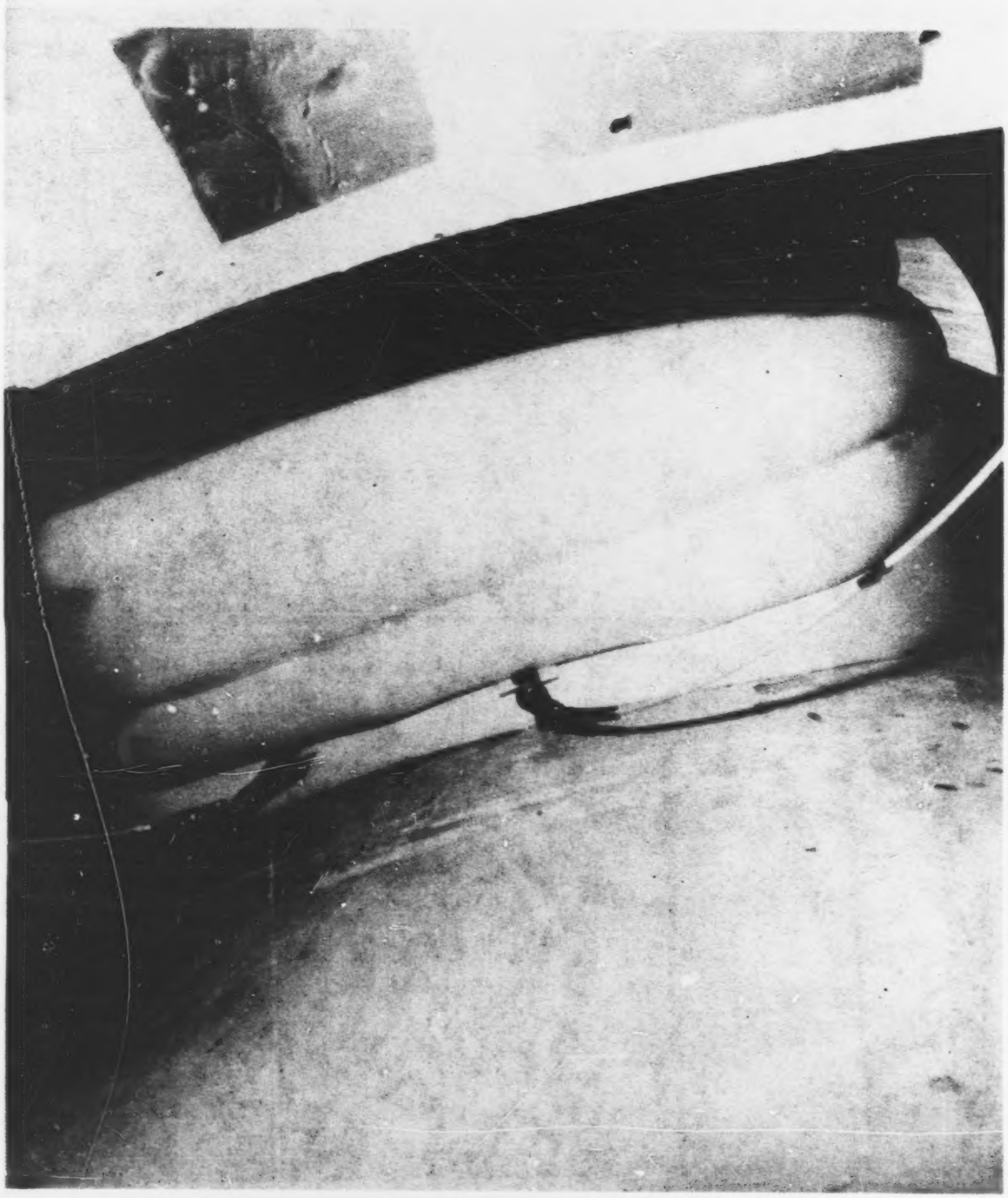

Figure 5. ET GOX Vent Seal Inflated Around ET Vent Louver

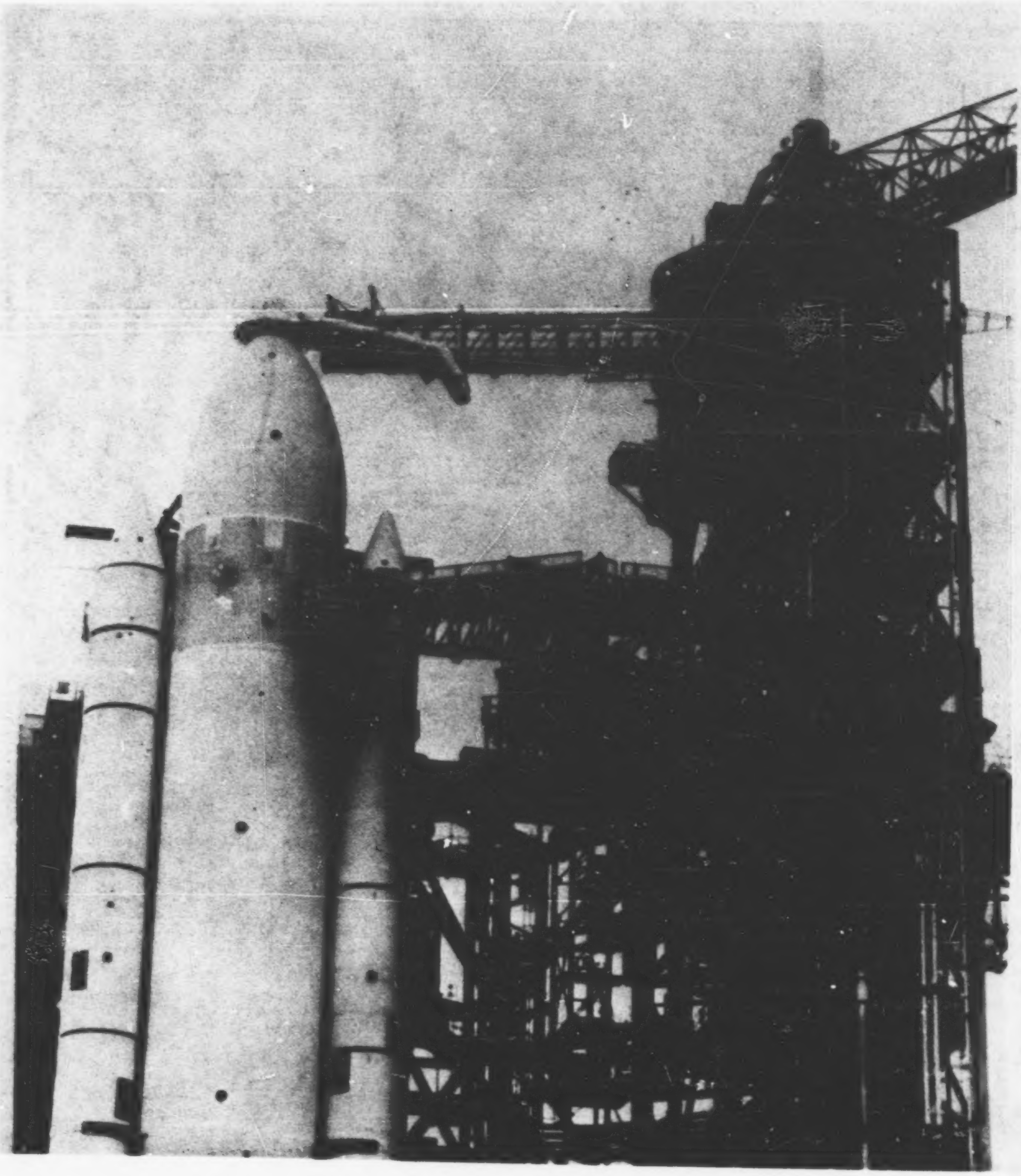

Figure 6. ET GOX Vent System Installed at Pad 39A for STS-2 Launch

William G. Franklin
National Aeronautics and Space Administration
John F. Kennedy Space Center
Kennedy Space Center, Florida 32899

Mr. Franklin has been lead design engineer of the ET GOX vent system for NASA since 1979. Since joining NASA in 1969, he has worked in the Advanced Studies Group and the Launch Accessories Branch of the Design Engineering Directorate. He has been a member of the American Institute of Aeronautics and Astronautics (AIAA) since 1973, serving as chairman of the Cape Canaveral Section from 1978 to 1979. Mr. Franklin received his B.S. degree in Aerospace Engineering from Auburn University in 1973.

Blank Page

DESIGN, DEVELOPMENT AND MECHANIZATION OF A PRECISION DEPLOYABLE TRUSS WITH OPTIMIZED STRUCTURAL EFFICIENCY FOR SPACEBORNE APPLICATIONS

By

N. D. Craighead
T. D. Hult
R. J. Preliasco

Lockheed Missiles and Space Company, Inc.

ABSTRACT

The demand for large space platforms and antenna systems has identified the need for extremely long, stiff deployable booms. This need has prompted Lockheed Missiles and Space Company, under contract to the Jet Propulsion Laboratory, to develop the technology which could provide a space mast structure with a length in excess of the height of the Washington Monument. This structure will be capable of repeatable precision deployments in the space environment without external aids. The lightweight truss structure which also functions as a precision mechanism can be stowed within the Space Shuttle cargo bay. This paper will discuss the design, predicted performance and hardware development of this structure.

The structure, which will be described, is a unique application of a triangulated truss that successfully blends the mechanisms of a deployable structure with those of an efficient extended structure. Individual internal members are double tapered graphite-epoxy tubes for maximum strength/weight ratio and stowed efficiency. The longitudinal members are hinged at the mid point to achieve a simple mechanism joint which provides for a compact folding scheme. Precision alignment and alignment repeatability is provided by a unique prestressed joint design and pretensioned diagonal members which eliminate deadband. These features integrate into a truss system that exhibits a stiffness-per-unit-length ratio and a stowage efficiency unsurpassed by any currently available design approaches. The design synthesis and detailed design work will be presented for the structure in toto as well as the joint details and deployment devices. Also to be summarized are the fabrication and tests on selected critical members and joints, the performance projections based on a mathematical model in the form of parametric results, and a comparison of the theoretical and experimental component test results.

INTRODUCTION

The industrialization and colonization of space will require the establishment of truly large space structures in orbit. Though desirable, the on-orbit assembly and/or fabrication of such structures encounters severe economic and technological limitations for the near future. Thus, the need exists to begin the examination of this new technology through the development of reduced scale systems. Self-contained, deployable structures serving as an investigative foundation for later, more ambitious projects will fill this need. As an economic incentive, these systems should be useful in their own right, while serving as stepping stones toward higher goals.

The "focus mission" concept (Ref. 1) is an effort by NASA to sift the critical technologies required for various mission objectives and combine them into a hypothetical mission which will support their development. One of these critical technologies is the development of a class of large aperture antenna systems (see Figure 1). That model requires reflector apertures ranging from 30 to 300 meters in diameter, operating at radio frequencies from UHF to Ku-band. Lockheed Missiles and Space Company, Inc., under the sponsorship of the NASA/LSST Program, has initiated the development of a 55-meter offset wrap rib antenna demonstration project, scalable to 100 meters, that addresses these requirements (Ref. 2).

Concurrent with this effort, LMSC is proceeding with the development of a deployable feed support boom. As the 55/100-meter antenna system project is a hypothetical mission, no specific mechanical requirements for the boom have been identified. General requirements, however, may be derived from the expressed desires to incorporate specific features into the mission, stowage and weight limitations of the STS and the functional requirements for an antenna system of this size and frequency range. The boom is thus designed to: function with an S-band offset fed reflector up to 100 meters in diameter (possessing booms with a total length of 208 meters, and a positional accuracy of 6 mm between ends), be compatible with the shuttle envelope, and provide a re-stow capability. In addition, the boom will provide a definable stiffness at all phases of deployment and retraction, provide maximum stiffness within the allotted weight and envelope, and weigh no more than 227 kg (500 lbs). Its characteristics have the capability to be tailored to suit other potential uses such as ground-based mobile towers, solar panel support and solar sail booms, and as an elemental building block for large space platforms.

A review of the design synthesis and accompanying analysis is given in this paper.

DESIGN DESCRIPTION

Current deployable truss designs suitable for on-orbit use sacrifice many of their structural characteristics to achieve their deployable function. Recognizing that this mast must function primarily as a stable structure, the design synthesis began by selecting an efficient truss; then a means of mechanization was conceived that did not compromise the primary objective. The result is a feed support consisting of two dedicated subsystems: a folding mast structure and deployment cages containing the mechanisms which extend it.

Structural elements and mast configuration were driven by the need for an efficient truss. The selected arrangement is shown in Figure 2. As designed, the mast is a simple, three-sided, completely triangulated and preloaded truss. This system is an efficient structure wherein all loads are carried in tension or compression along load paths intersecting at node points. Doubly tapered tubes are used for the longerons and battens to achieve a maximum stiffness-to-weight ratio. Simple small-diameter tension rods serve as diagonal members. Pretensioning of these diagonals eliminates clearance in the longeron pivot bearings which ensures structural continuity and provides the majority of torsional stiffness.

The final mast configuration compatible with 55-meter reflector structural requirements is a 122-meter-long, 40-bay mast composed of 3.05-meter-long graphite-epoxy tubes with a 7.62-2.54-cm-diameter taper and a .528-mm wall thickness. Possessing a mass of 172 kg, it has a first mode natural frequency of .105 Hz and stows to a height of 3.32 meters.

TRUSS MECHANIZATION

The design requirements for mechanization were as follows:

- deployment must be automatic and reversible,
- hinges, joints, etc. must have no detrimental effects on extended rigidity,
- mast, reflector and support equipment must stow within STS cargo bay envelope

These requirements were met by incorporating a center joint and pivoting end fittings for each longeron and flexible diagonal members. These features allow the mast to stow as shown in Figure 3. The longerons fold outside the battens while the diagonals stow inside, providing a stowage ratio in excess of 30:1 (55-meter design).

LONGERON CENTER JOINT

The longeron center joint is designed to meet the requirements of low weight, zero deadband, and positive locking at full extension. In addition, it provides a force to aid the deployment of the longeron.

The joint consists of a number of short links connected to fittings attached to the longeron halves. Figure 4 shows the joint in various stages of deployment. The center link pivots about the longeron centerline, facilitating the side-by-side folding of the longeron while avoiding the length extension impacts of a side hinge. As the two halves are allowed to rotate for mast extension, the four-bar linkage formed by the center link, control arm, and end fittings controls the motion of the joint; when fully open the two toggle links extend and lock the joint into position with sufficient preload to eliminate deadband for the orbital loadings.

The locking force is provided by a torsion spring located at the pivot point of one of the toggle links. Due to its placement and the kinematics of the joint, the direction of the resultant force changes during operation. Figure 5 graphs typical values for the moment about the longeron center during joint operation and compares them to predicted values. The positive values denote a moment acting to extend the longeron, while negative values denote a force acting to stow the longeron. The motion is limited by a stop slightly before the toggle links are allowed to reach full extension. This forces them into compression, which in turn causes a tension load in the two center links. This preload eliminates backlash caused by bearing clearances.

A model of the joint is shown in Figure 6. Aluminum was used for ease of manufacture, availability and cost. For flight use titanium or chopped graphite fiber-reinforced plastic materials will be used.

END JOINTS

The longeron end joints are simple clevis connections as shown in Figure 7. The bearing clearances in this joint are eliminated by the tension in the diagonals.

DIAGONALS

The diagonal tension members are designed as several layers of unidirectional graphite/epoxy fibers having a rectangular cross section, typically 1.5 x 5 mm. They are formed with a curve along their length which, when the mast is stowed, causes the diagonals to lie inside the truss, avoiding potential interference with the longerons or deployment mechanism.

EXTENSION/RETRACTION MECHANISM

The mast extension sequence is illustrated in Figure 8. The stowed mast is held in the deployment cages which are functionally divided into two compartments, one for handling the stowed mast and one for extending the bays. The stowed mast is slowly raised toward the forming compartment; the mechanism in the forming compartment lifts a single batten assembly and extends the longerons and diagonals of one bay until the bay is fully formed. The process is repeated at the rate of approximately 1 bay every 2 minutes until the complete mast is fully formed. These steps are reversed to retract the mast. A simplified schematic of the device is pictured in Figure 9 which illustrates the high/low speed drive arrangement and the function of the gear boxes, driver and belts. Not shown are torque tubes interconnecting the drive motors to enhance redundancy and assure speed synchronization. A unique longeron forms the right angle bend in the mast. A significant design feature of the deployment mechanization is that, during deployment, loads are transmitted through the deployed mast sections into the upper deployment cage and around the deploying sections. This feature assures a predictable structural stiffness throughout the entire deployment operation.

Additional considerations were given to the transfer of ascent loads and subsystem interfacing. The cages function as chassis to which the various spacecraft subsystems are mounted and serve to transfer spacecraft loads to the boost vehicle. Loads to the orbiter are transferred through an adaptor ring. Figure 10 shows a complete spacecraft (55-meter configuration) stowed in the orbiter bay.

ADDITIONAL MODELING AND DEVELOPMENT

A full-scale demonstration longeron was constructed of T-300 autoclave-cured graphite epoxy on an aluminum mandrel. Fiber layup of the tube shown in Figure 11 is 0/45/45/0 degrees. This layup represents a compromise between the desires for a low thermal expansion coefficient (CTE = 4.0 x 10^{-6}/°C along the longitudinal axis), adequate torsional stiffness (G = 11 GPA), and a reduction in the probability of microscopic crack propagation due to differences in the ply orientation angle. End fittings and the center joint were bonded in place on a fixture that ensured a precision alignment between ends and a dimensional exactness of the overall part.

As a complement to the ongoing design layout work, a mathematical model of the truss was produced to predict the structural and mass properties of the truss. This model can also be used for both parametric and point design case studies. Functioning as a design tool, such analysis allows member sizing and optimization consistent with design goals and physical constraints.

Figures 12 and 13 are examples of the parametric data generated. They represent the cantilever bending stiffness and mast weight, respectively, as a function of the mast geometry and material thickness.

CONCLUSIONS

Preliminary design and development work at Lockheed Missiles and Space Company, Inc. has resulted in a deployable mast concept which meets the weight, size and stability requirements for a feed support structure for offset antennas up to 100 meters in diameter. A triangulated truss configuration, the use of tapered tubes which exhibit a high strength-to-weight ratio, and low CTE graphite-epoxy material provide an efficient, lightweight and stable truss suitable for an antenna feed support. A low stowage ratio of 30:1 is achieved through a unique preloaded hinge located at the center of each longeron and an autonomous deployment cage with a drive mechanism. Initial analysis and proof of concept hardware have validated the basic mechanism and design assumptions and provided a basis for further investigation. The concept can readily accept variations in member size and thus lends itself to optimization for other potential uses where a stiff, lightweight deployable truss is needed.

REFERENCES

(1) Freeland, R. E. and Campbell, T. G.; Deployable Antenna Technology Development for the Large Space Systems Technology Program; AIAA/NASA Conference on Advanced Technology for Future Space Systems, Hampton, VA, May 8 - 10, 1979, NASA CP-2118.

(2) Wade, W. D. and McKean, V. C.; The Technology Development Methodology for a Class of Large Diameter Spaceborne Deployable Antennas; 15th Aerospace Mechanisms Symposium, Huntsville, AL, May 14 - 15, 1981, NASA CP-2181.

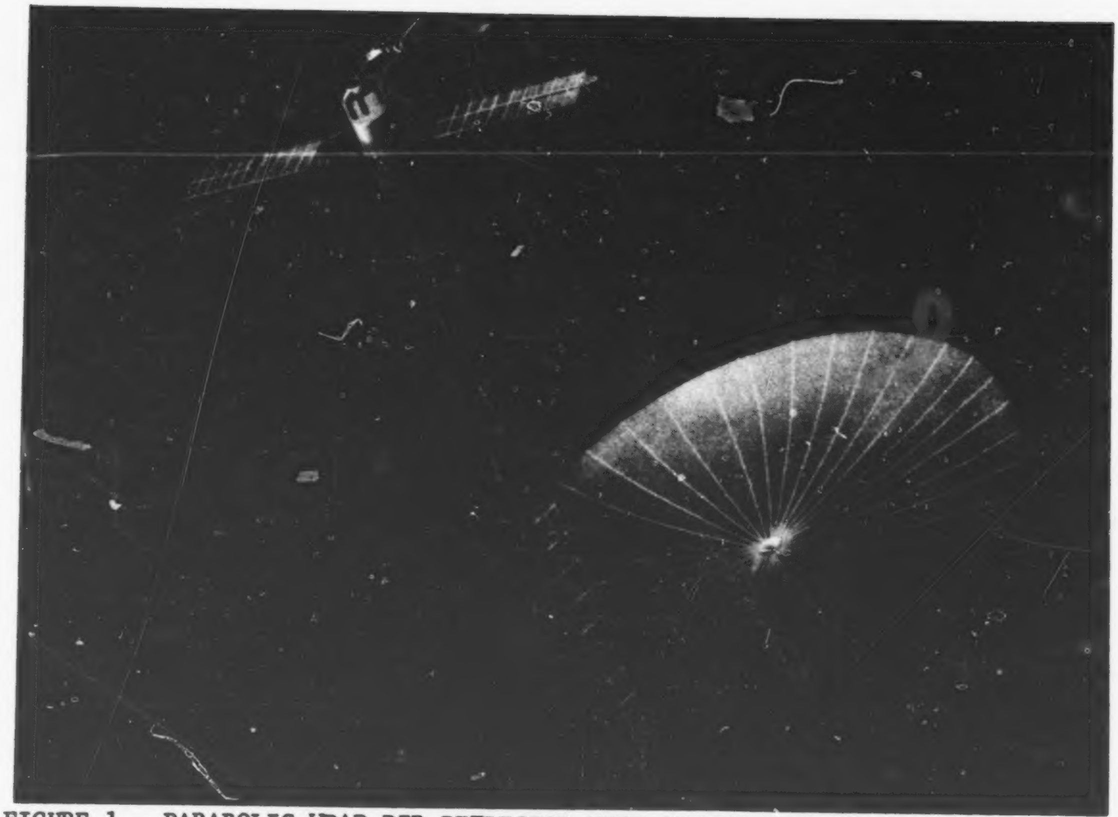

FIGURE 1. PARABOLIC WRAP RIB REFLECTOR WITH OFFSET FEED SUPPORT MAST

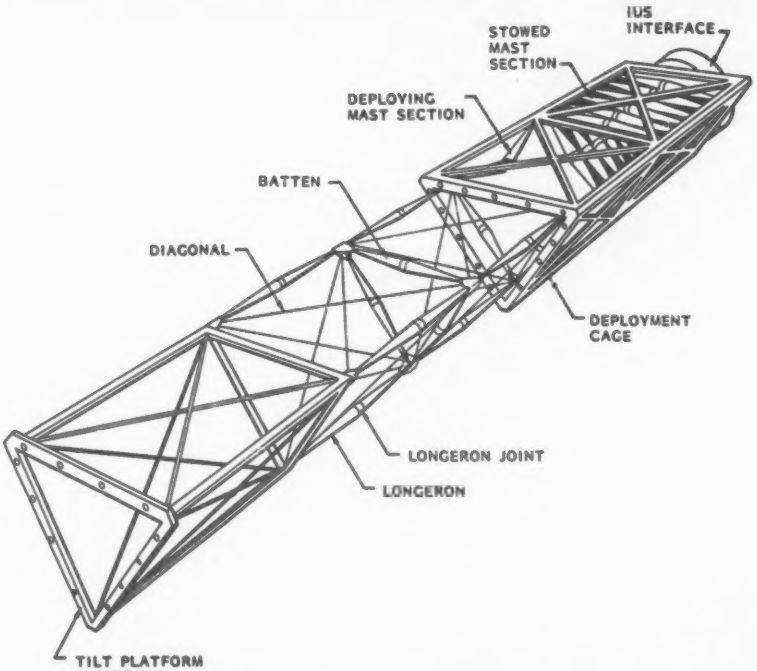
IUS INTERFACE
STOWED MAST SECTION
DEPLOYING MAST SECTION
BATTEN
DIAGONAL
DEPLOYMENT CAGE
LONGERON JOINT
LONGERON
TILT PLATFORM INTERFACE

FIGURE 2. PARTIALLY DEPLOYED MAST
(DEPLOYMENT CAGES ASSURE A DEFINABLE LOAD PATH DURING MAST DEPLOYMENT)

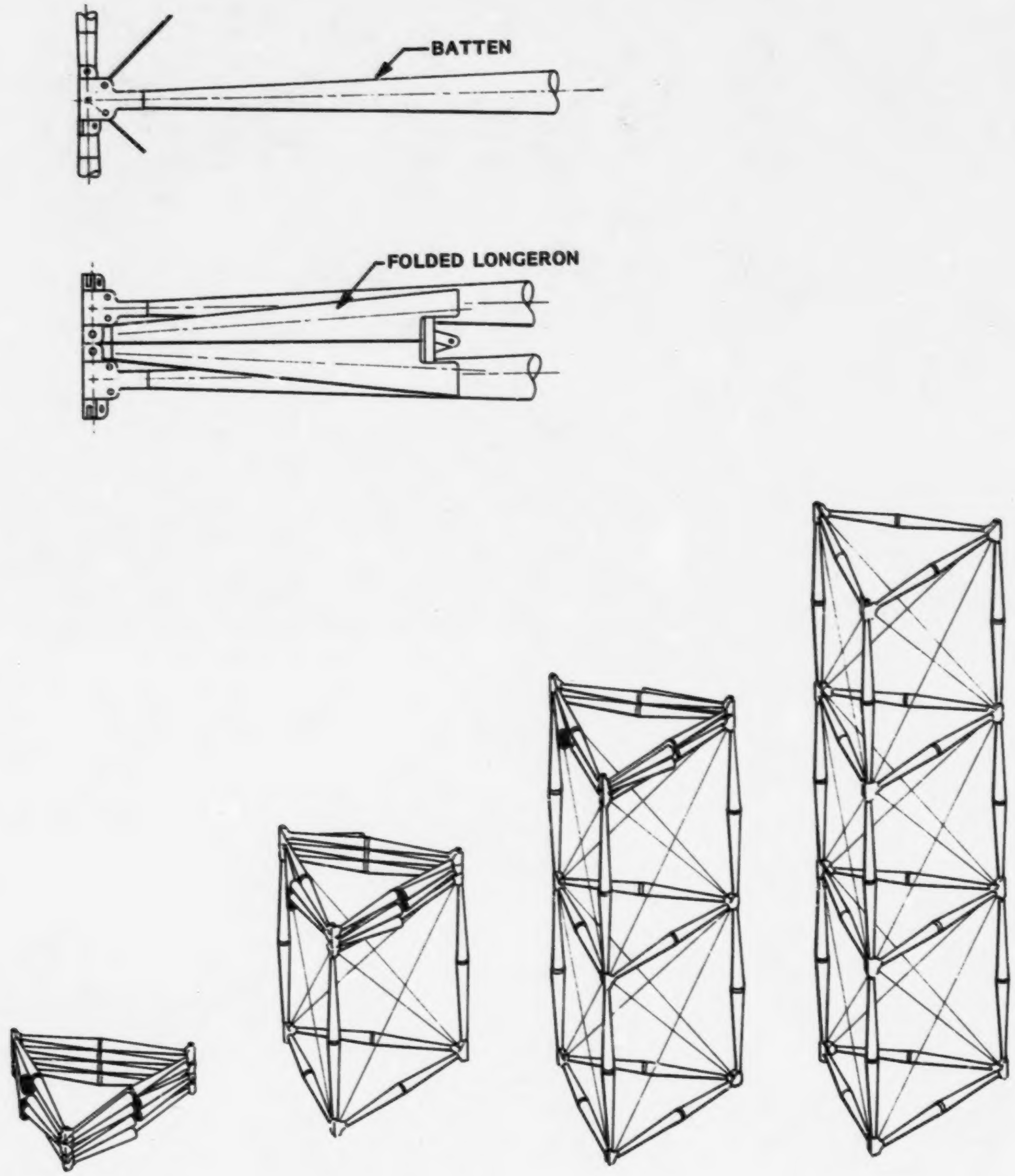
BATTEN
FOLDED LONGERON

FIGURE 3. STRUCTURAL ELEMENT STACKING CONFIGURATION

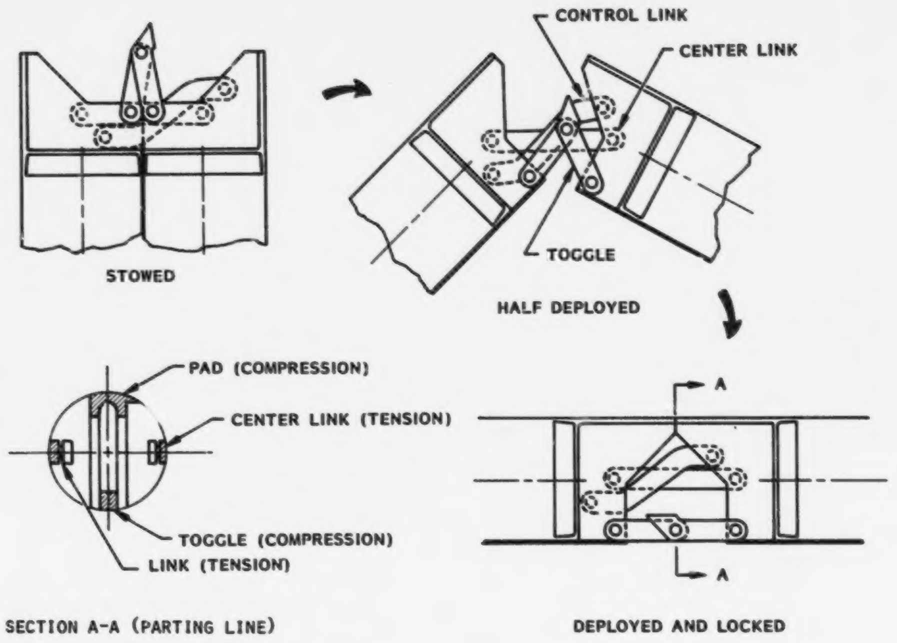
CONTROL LINK
CENTER LINK
TOGGLE
PAD (COMPRESSION)
CENTER LINK (TENSION)
TOGGLE (COMPRESSION)
LINK (TENSION)
A
A

STOWED

HALF DEPLOYED

SECTION A-A (PARTING LINE)

DEPLOYED AND LOCKED

FIGURE 4. LONGERON CENTER JOINT SCHEMATIC

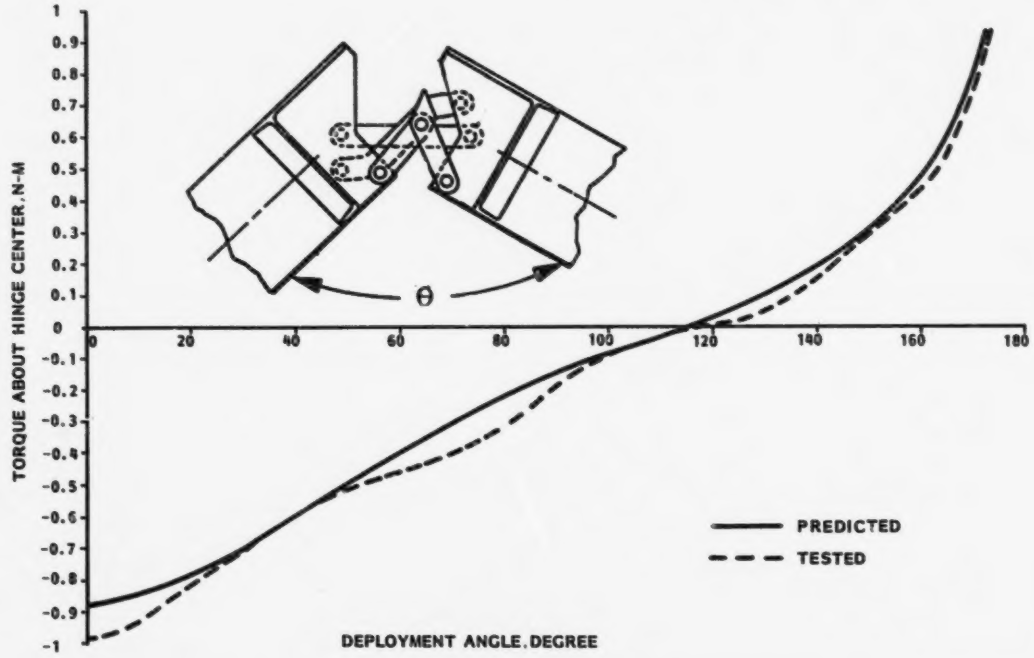

FIGURE 5. TORQUE ABOUT HINGE CENTER VS DEPLOYMENT ANGLE

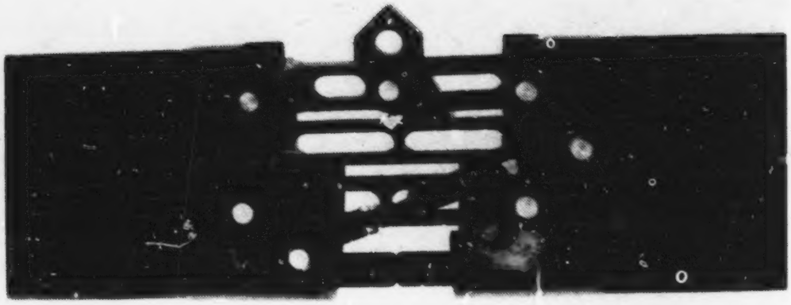

FIGURE 6. LONGERON JOINT-A PRELOADED, OVER-THE-CENTER LATCH THAT IS SELF-LOCKING AND EXHIBITS NO DEADBAND

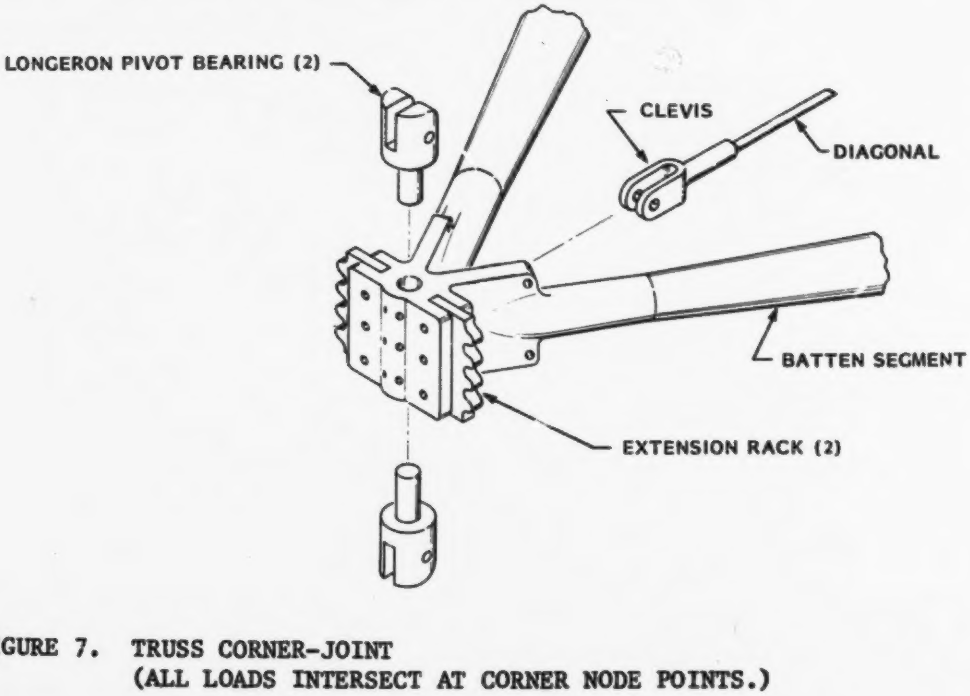
LONGERON PIVOT BEARING (2)
CLEVIS
DIAGONAL
BATTEN SEGMENT
EXTENSION RACK (2)

FIGURE 7. TRUSS CORNER-JOINT
(ALL LOADS INTERSECT AT CORNER NODE POINTS.)

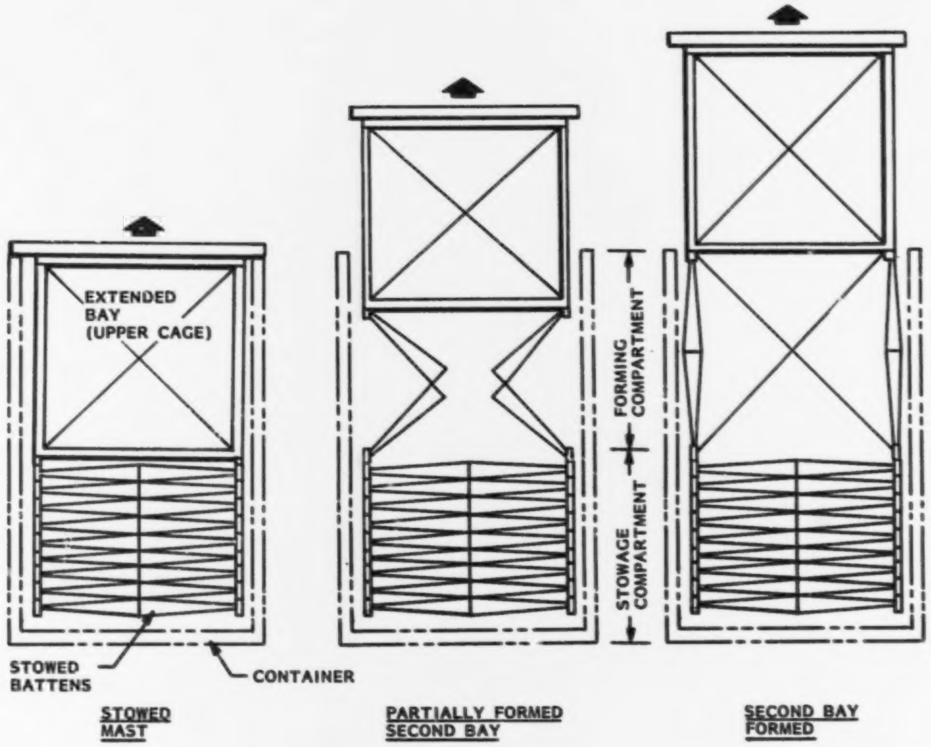
EXTENDED BAY (UPPER CAGE)
FORMING COMPARTMENT
STOWAGE COMPARTMENT
STOWED BATTENS
CONTAINER

STOWED MAST

PARTIALLY FORMED SECOND BAY

SECOND BAY FORMED

FIGURE 8. EXTENSION/RETRACTION PRINCIPLE

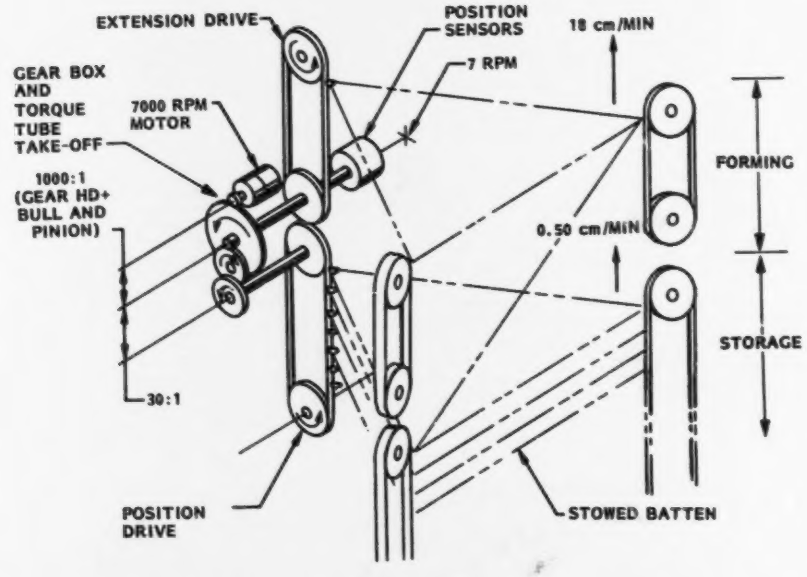
EXTENSION DRIVE
POSITION SENSORS
18 cm/MIN
7 RPM
GEAR BOX AND TORQUE TUBE TAKE-OFF
7000 RPM MOTOR
1000:1 (GEAR HD+ BULL AND PINION)
FORMING
0.50 cm/MIN
STORAGE
30:1
POSITION DRIVE
STOWED BATTEN

FIGURE 9. EXTENSION/RETRACTION DRIVE MECHANISM

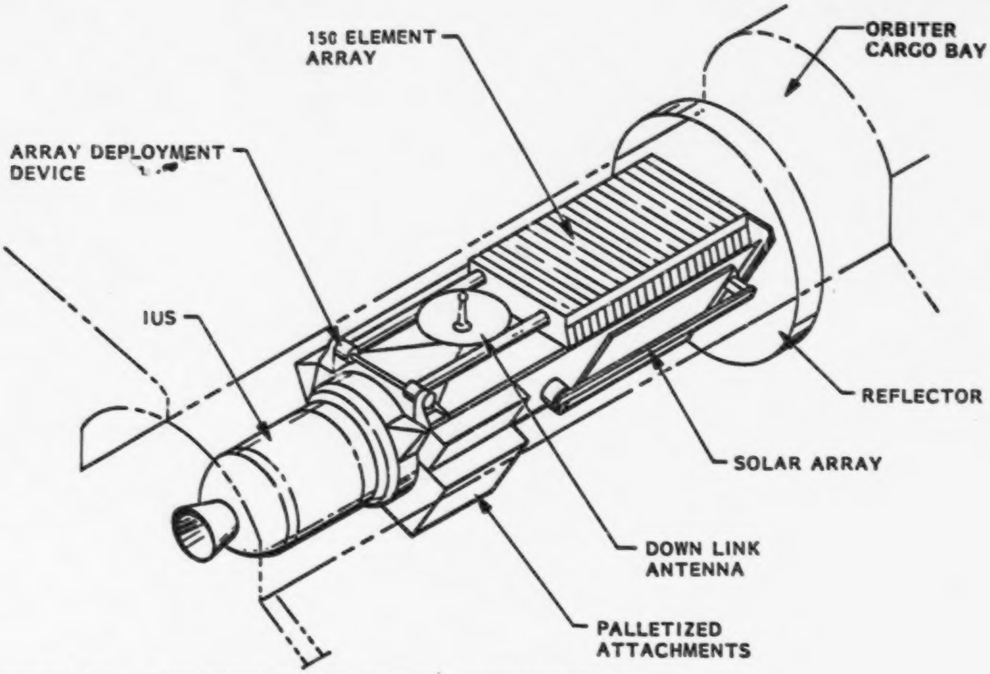
150 ELEMENT ARRAY
ORBITER CARGO BAY
ARRAY DEPLOYMENT DEVICE
IUS
REFLECTOR
SOLAR ARRAY
DOWN LINK ANTENNA
PALLETIZED ATTACHMENTS

FIGURE 10. SPACECRAFT IN STOWED CONFIGURATION

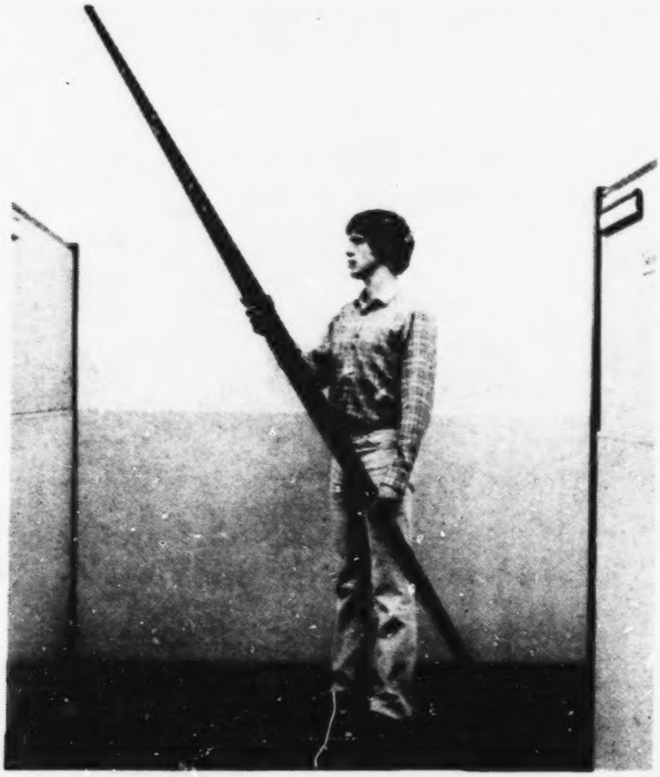

FIGURE 11. TAPERED GRAPHITE TUBES OFFERING HIGH STRENGTH AND LOW WEIGHT

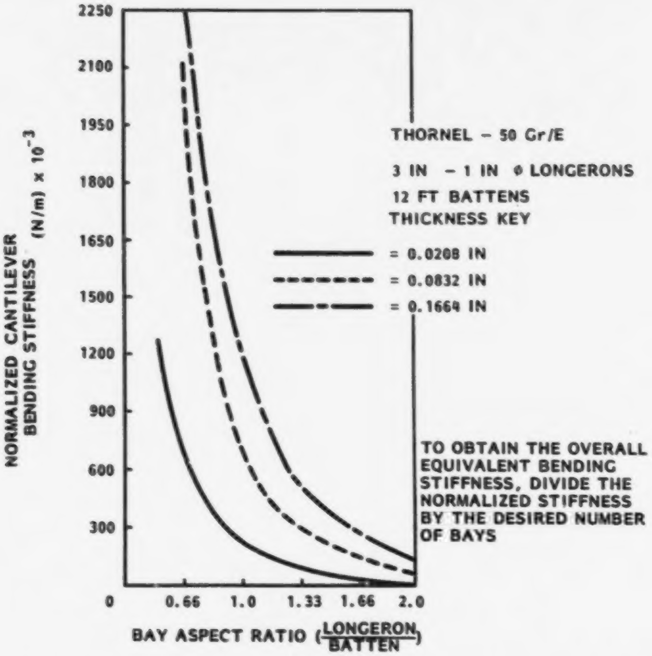

TO OBTAIN THE OVERALL EQUIVALENT BENDING STIFFNESS, DIVIDE THE NORMALIZED STIFFNESS BY THE DESIRED NUMBER OF BAYS

FIGURE 12. EFFECT OF MATERIAL THICKNESS AND ASPECT RATIO ON NORMALIZED BENDING STIFFNESS (NORMALIZED TO BAY LENGTH)

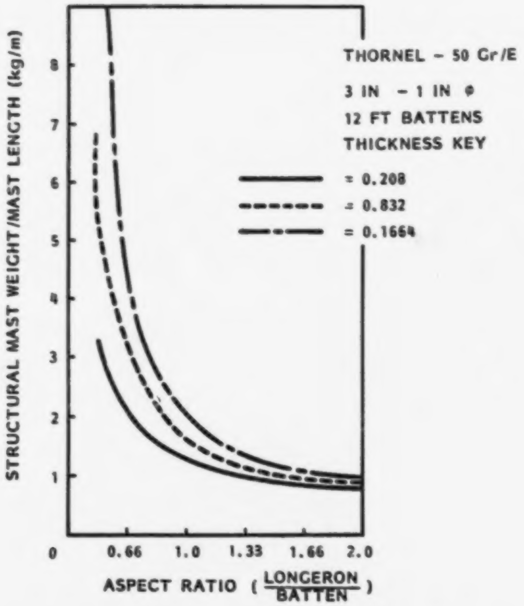

FIGURE 13. EFFECT OF MATERIAL THICKNESS AND ASPECT RATIO ON MAST STRUCTURAL WEIGHT

Timothy D. Hult
Lockheed Missiles and Space Company
P.O. Box 504
Sunnyvale, California 94086

Mr. Hult is presently an associate design engineer in the RF/Antenna Systems Laboratory involved in the engineering of large space deployable reflector systems. He received his B.S. degree in Mechanical Engineering from Clarkson College in 1980.

Richard J. Preliasco
Lockheed Missiles and Space Company
P.O. Box 504
Sunnyvale, California 94086

Mr. Preliasco is currently assigned to the RF/Antenna Systems Laboratory working as an associate design engineer on large space deployable reflector systems. He received his B.S. degree in Mechanical Engineering from Worcester Polytechnic Institute in 1980.

Co-author of this paper is Mr. N. D. Craighead who is also with Lockheed in Sunnyvale.

THE MECHANICAL DESIGN OF A VAPOR COMPRESSOR FOR A HEAT PUMP TO BE USED IN SPACE

By

F. Berner*, H. Oesch*, K. Goetz*,
and C.J. Savage**.

INTRODUCTION

A heat pump is presently being developed for use in Spacelab as a stand-alone refrigeration unit, as well as within a fluid loop system, that will provide an active thermal control for payloads. The sponsor of this work, the European Space Agency, has established the following specifications for the heat pump:

- **Heat removal rates at the source (payload or fluid loop) from tens of watts at subzero (degrees C) temperatures to a few hundred watts during the initial cooling of payloads from room temperature or levels above it**
- **Heat source temperatures from room temperature down to -30°C, arbitrarily selectable**
- **Heat-sink fluid temperatures at condenser inlet between +20°C and +40°C**
- **Minimum reasonable achievable power consumption of the heat pump for each set of the parameters: heat source temperature, heat removal rate at the source, and heat-sink fluid temperature at condenser inlet**

Based on a comparison of different heat pumping schemes including gas cycles, vapor cycles, absorption cycles, and thermoelectric (Peltier) elements, it was decided to meet these requirements with a reversed Carnot cycle heat pump using Freon 12 as working fluid and incorporating a one-cylinder, reciprocating compressor.

For weight reasons and to avoid large deviations from a uniform rotation, the maximum crankshaft speed was fixed relatively high at 1000 rpm. The specified cooling rates then made it necessary to select a cylinder volume of 10 cm^3, which was obtained with a bore of 40 mm and a stroke of 8 mm.

---

*) Swiss Federal Aircraft Factory, 6032 Emmen, Switzerland
**) ESTEC, European Space Agency, 2200 AG Noordwijk, The Netherlands

The engineering model of the vapor compressor has been built and tested in a Freon 12 test loop[1]. Figs. 1 and 2, established for the two heat-sink fluid temperatures of 20°C and 40°C, respectively, show the expected performance of a heat pump incorporating our vapor compressor, based on its experimentally determined performance characteristics.

SOME SPECIAL ELEMENTS OF THE MECHANICAL DESIGN

A section through the vapor compressor is presented in Fig. 3 in which some of the special elements of the mechanical design are called out.

Means for Reducing the Nonuniformity of Rotation

A problem of single-cylinder reciprocating compressors is the nonuniformity of rotation of the crankshaft. In the case of a vapor compressor of a heat pump using Freon 12, this problem is accentuated by the fact that in the range of heat source temperatures of interest from -30°C to +20°C, the saturation pressure - which is close to the minimum pressure in the cylinder - varies from about 1 bar to 5.8 bar. Therefore, even if the compressor were operating in a 1-bar atmosphere, the pressure in the cylinder would generally be well above the ambient pressure during the downward motion of the piston following a compression phase, and the torque in the crankshaft would thus vary from positive values to relatively large negative values during a revolution. To reduce the torque variation, we have incorporated a compression spring between piston and crankshaft housing. Energy is stored in the spring through the latter's compression during the downward motion of the piston, and this energy is returned to the piston during the upward motion. Thus, the spring's effect is similar to that of a flywheel.

Lubrication Under Null Gravity Conditions, Separation of Refrigerant from Lubricants, and Associated Problems

A number of design features have been introduced because of problems associated with the operation in a zero-g environment. The absence of gravity makes oil lubrication impractical because no defined oil level can be maintained. Hence, grease lubrication has been selected in ball bearings and needle bearings. Dry lubrication with a loaded PTFE is employed in some areas, such as the guidance of the tappet and of the stem of the discharge valve and for the piston ring. No lubrication at all is used between tappet and camshaft, whereby the gliding contact between these elements has been replaced by a practically pure rolling contact with the addition of a roller to the tappet head.

Since lubricants exposed to the refrigerant Freon 12 would absorb it at a significant rate [2] (whereby their performance would be impaired if they were not purified from time to time as in fact greases could not be), it was

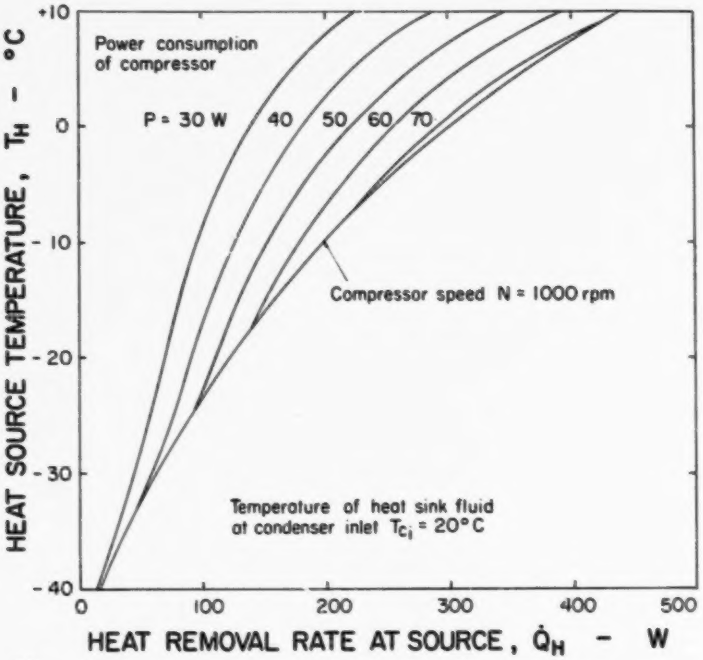

Fig. 1. Performance map of heat pump based on experimentally determined compressor characteristics (T_{ci} = 20°C).

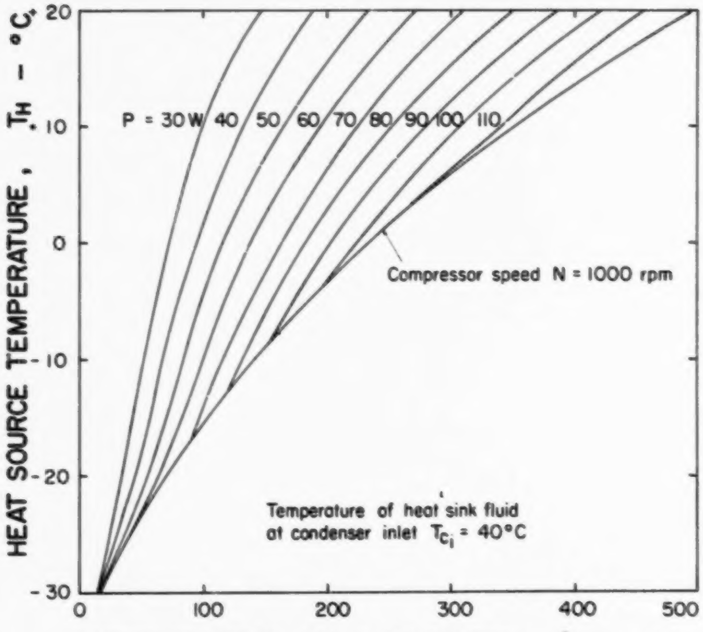

Fig. 2. Performance map of heat pump based on experimentally determined compressor characteristics (T_{ci} = 40°C).

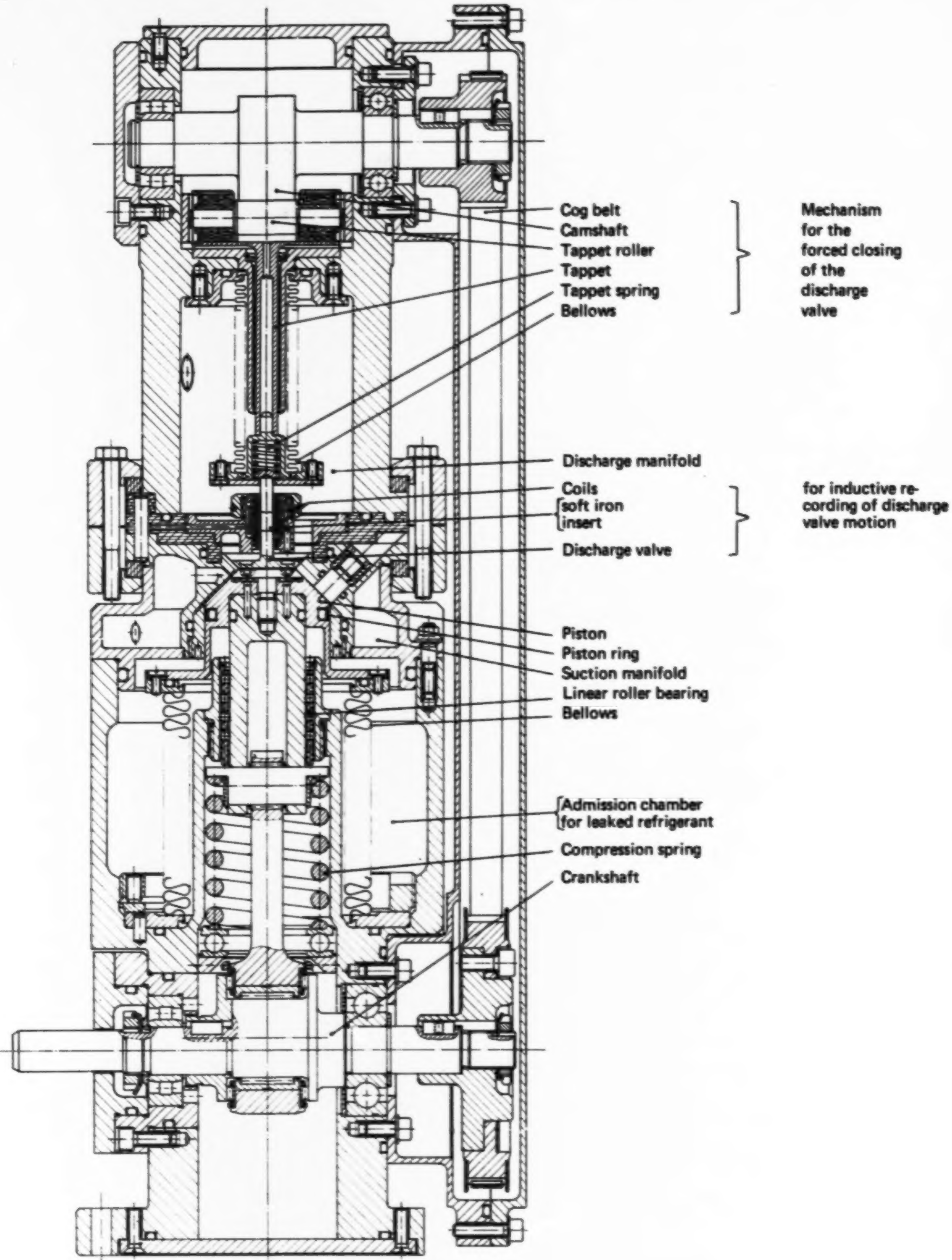
Cog belt
Camshaft
Tappet roller
Tappet
Tappet spring
Bellows
Mechanism for the forced closing of the discharge valve
Discharge manifold
Coils
soft iron insert
Discharge valve
for inductive recording of discharge valve motion
Piston
Piston ring
Suction manifold
Linear roller bearing
Bellows
Admission chamber for leaked refrigerant
Compression spring
Crankshaft

Fig. 3. Section through vapor compressor.

decided to seal off completely the portion of the Freon loop within the compressor from its immediate surroundings. To achieve a hermetic containment of the refrigerant, we have introduced metal bellows between the piston and the lower portion of the compressor housing and between the tappet and the discharge manifold. Both bellows have been subjected to extensive fatigue tests which they passed successfully [3] .

The use of a dry-lubricated piston ring made it necessary to reduce the clearance between piston and cylinder surface below what is standard practice in compressors with oil-lubricated piston rings. Hence a strictly axial piston movement, without any skewing, must be achieved in our compressor. This requirement led to the incorporation of a grease-lubricated, **linear roller bearing**. The rollers of this bearing are contoured such that they match the cylindrical surfaces of piston shaft and guiding bush.

THE SEMI-AUTOMATIC DISCHARGE VALVE

Reciprocating compressors usually are of the automatic type; i.e., they feature suction and discharge valves that open and close automatically in response to a positive or negative pressure difference across their ports. Most designs feature a series of reed-type suction valves and one or two disk-type, spring-loaded discharge valves per cylinder. Whereas reed valves have been found to perform satisfactorily in our application, the characteristics of automatic discharge valves lead to an unacceptably low volumetric efficiency, particularly at high compression ratios and when the compressor is not operated at the speed for which the disk valve was optimized. Hence we have decided to retain the concept of automatic valves for the suction valves only, which in our compressor are a series of reed valves arranged around a centrally positioned disk-type discharge valve. The discharge valve should ideally open when, during a compression phase, the pressure in the cylinder reaches the level of the discharge pressure. This event is delayed if the compression ratio is increased, i.e., the crank angle at which equality of pressures is reached on the two sides of the valve disk increases with the compression ratio. Hence we allow the discharge valve to open automatically, but we have developed a concept for its forced closing such that it hits its seat at a selected crank angle; e.g., when the piston just reaches its upper dead center. This new concept of a semi-automatic discharge valve and the mechanism with which it is realized are described in this section.

Concept of a Semi-Automatic Discharge Valve

Closing of the discharge valve is achieved by pushing on its stem with a tappet, whose motion is controlled by a camshaft that is driven off the crankshaft by means of a cog belt. While the tappet is in permanent contact with the camshaft, it touches the valve stem only during, and a very short time after, valve closing. At other times the valve is either in its seat and the tappet above its lower dead position or, during valve opening, the valve moves toward its open position while the tappet is at its upper dead position. The positions of those extremities of valve stem and tappet that are intermittently in contact with each other are shown as a function of the crank angle in Fig. 4. Notice that the angular velocity of the camshaft is twice that of the crankshaft. Only this higher camshaft speed allows achieving sufficiently fast valve closing for the maximum compression ratio of 10 specified by the client. The additional stroke carried out by the tappet between two closing strokes does not have any influence on the discharge valve because the latter is firmly retained in its seat during this phase due to the positive difference between discharge and cylinder pressures. Notice that the tappet's stroke is slightly larger - in our case 0.5 mm - than the valve's stroke. This difference was introduced for reasons of dimensional inaccuracy. One cannot rigidly push with the tappet against the valve while the latter rests in its seat; i.e., one has to incorporate a spring between actual tappet and valve stem as shown in Fig. 5 (see next page). This spring makes it unnecessary to incorporate special damping means for the prevention of too large a jumping back of the discharge valve from its seat. On the other hand, we have incorporated means for the pneumatic damping of the valve when, at the end of the opening phase, it hits its stop. As can be seen in Fig. 5, they consist of a circular groove on the upper side of the valve disk and a fitting counterpart in the structure that provides the guidance for the valve stem.

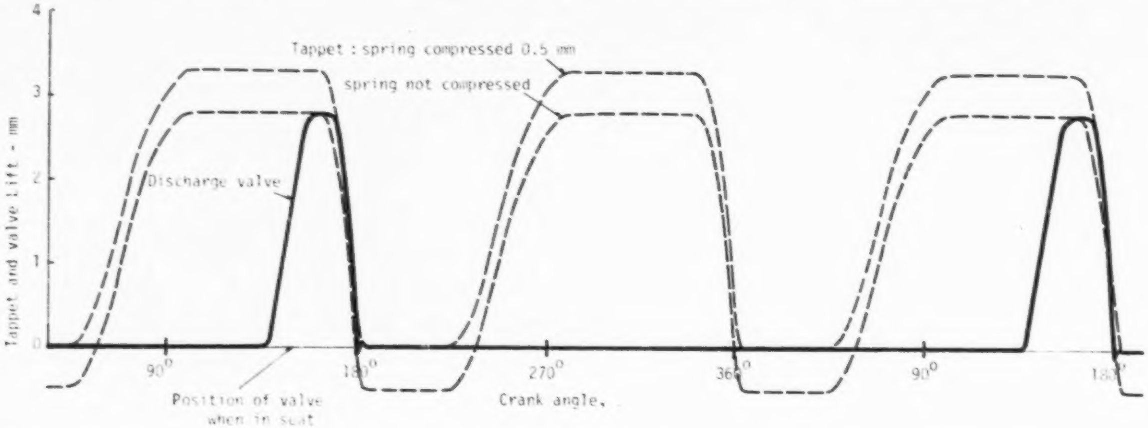

Fig. 4. Position of points on tappet and discharge valve stem, that are intermittently in mutual contact, versus crank angle φ ($\varphi = 180°$: piston is at upper dead center).

Mechanism for the Forced Closing of the Discharge Valve

The camshaft/tappet mechanism makes the duration of the valve-closing phase dependent on the compressor speed so that it is always the same fraction of the time of one revolution. Additional measures are necessary to minimize the valve closing in terms of the crank angle interval. Another

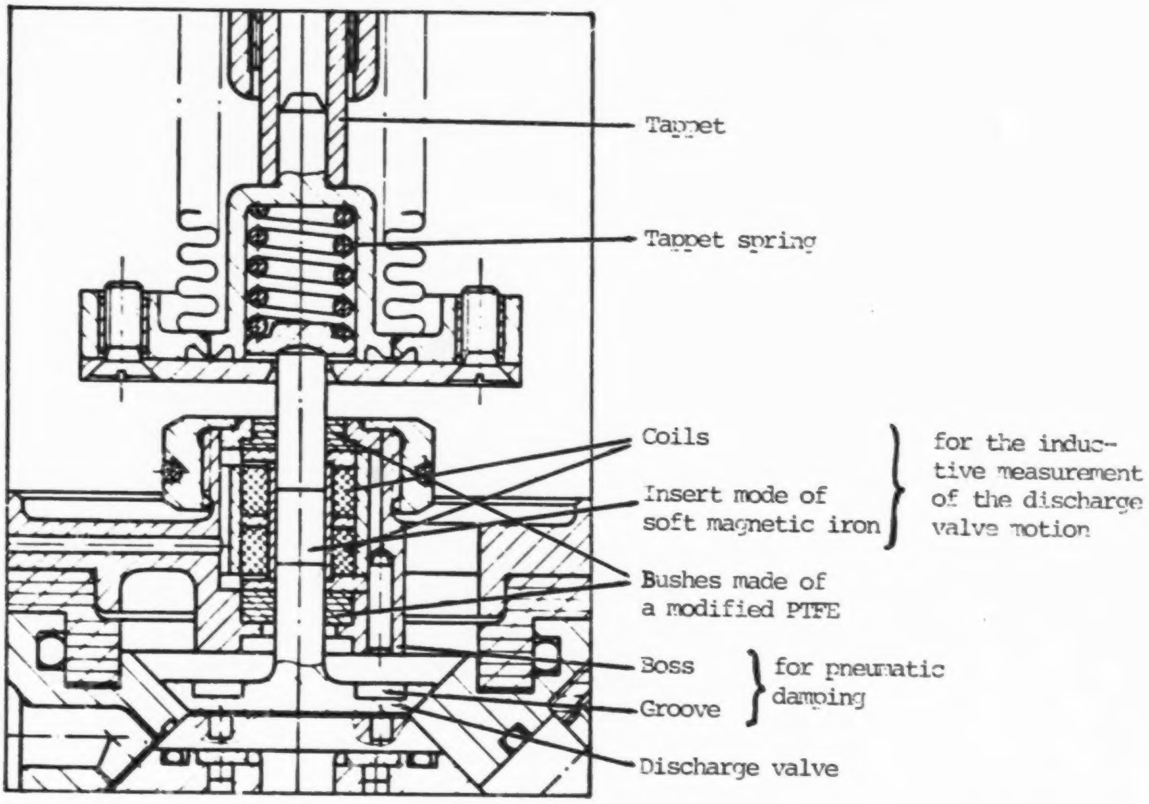
Tappet
Tappet spring
Coils
Insert mode of soft magnetic iron
for the inductive measurement of the discharge valve motion
Bushes made of a modified PTFE
Boss
Groove
for pneumatic damping
Discharge valve

Fig. 5. Details of lower portion of tappet, of discharge valve, and of means for the recording of the valve motion

consideration for the design of the cam contour is the possibly uncontrolled movement of the discharge valve near the end of the closing phase. Ideally, the control mechanism should achieve closing at a very specific crankshaft position. This is not really possible. The tappet, and the discharge valve along with it, is accelerated during most of the closing phase. However, the tappet reaches a position from which it must be decelerated since, slightly later, it must come to a full stop. The valve does not follow this movement; i.e., it remains in contact with the tappet only during the acceleration portion and then proceeds at a constant speed when the tappet is decelerated, meaning that it precedes the tappet from this moment on. Obviously then, a further aim is to postpone the start of tappet deceleration to the last possible moment or, to put it another way, to keep as short as possible the crank angle interval during which the tappet decelerates. There is a limit to the delay of the beginning of the deceleration because the rate of deceleration increases if the deceleration phase is reduced. Noting that during deceleration the tappet roller would jump off the cam if not pushed against it, it is

evident that the larger the deceleration rate, the larger must be the force with which the tappet is pushed against the cam. This force then causes a larger Hertzian surface pressure at all other times and hence an increased wear. Thus a compromise must be found between the duration of the deceleration phase and the mean force with which the tappet is pushed against the cam. To meet the different requirements mentioned above, we had to design a cam of a size that is rather large when compared with the crankshaft [5]. The cam shape is depicted in Fig. 6, which is not to scale but illustrates all relevant features.

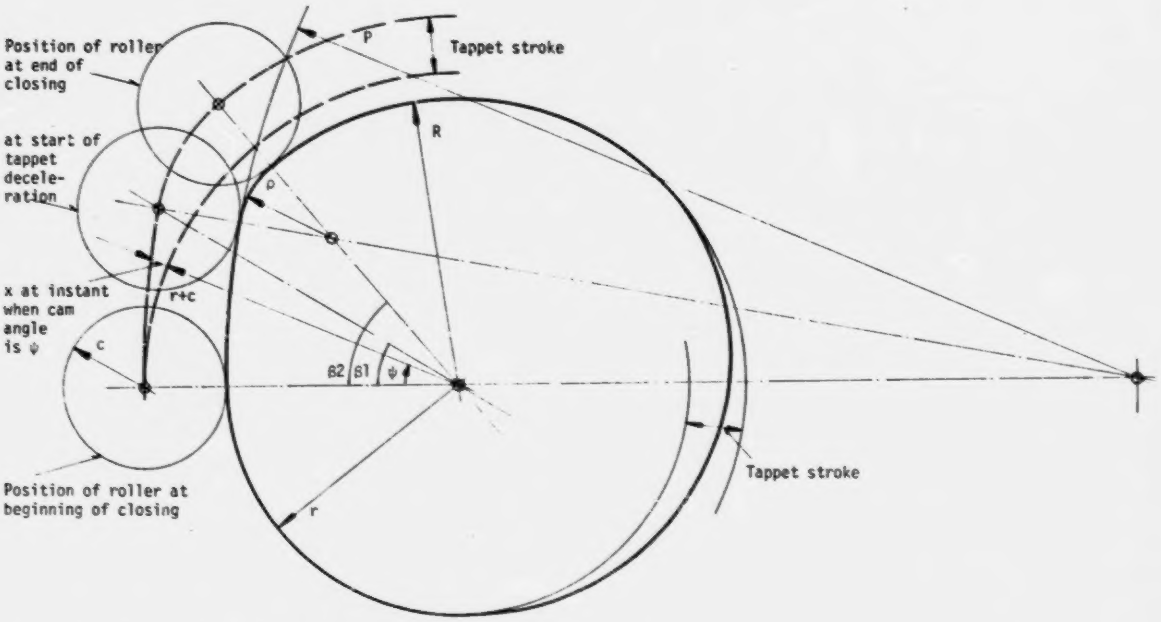
Position of roller at end of closing
at start of tappet deceleration
x at instant when cam angle is ψ
Position of roller at beginning of closing
P
Tappet stroke
R
ρ
r+c
c
β2
β1
ψ
r
Tappet stroke

Fig. 6. Cam geometry and motion of the tappet roller over the cam surface during the closing phase.

The position x of the tappet during the closing phase is also shown as a function of the cam angle ψ in Fig. 7 (see next page) together with the tappet speed and acceleration. Also indicated in this diagram are the actual optimized geometrical parameters (in mm) of the cam and the radius of the tappet roller. Notice that the final acceleration at a cam angle $\psi = \beta_i \approx 35^\circ$ is about 800 m/s^2. Since the valve has a mass of 5 gm, it resists the push by the tappet spring during final acceleration with about $0.005 \times 800 = 4$ N only. The spring being pre-loaded with about 10 N, it does not seem to be compressed at all at the instant when deceleration starts, and the valve is only about 2.8 mm - 2.5 mm = 0.3 mm away from its seat at this instant. In addition, we infer from Fig. 7 that valve closing occurs over a cam angle interval $\Delta\psi \approx 37^\circ$ only; i.e., over slightly more than 5% of one crankshaft revolution.

As noted previously, the discharge manifold is hermetically sealed from the tappet/camshaft assembly by means of a metal bellows. This element has an

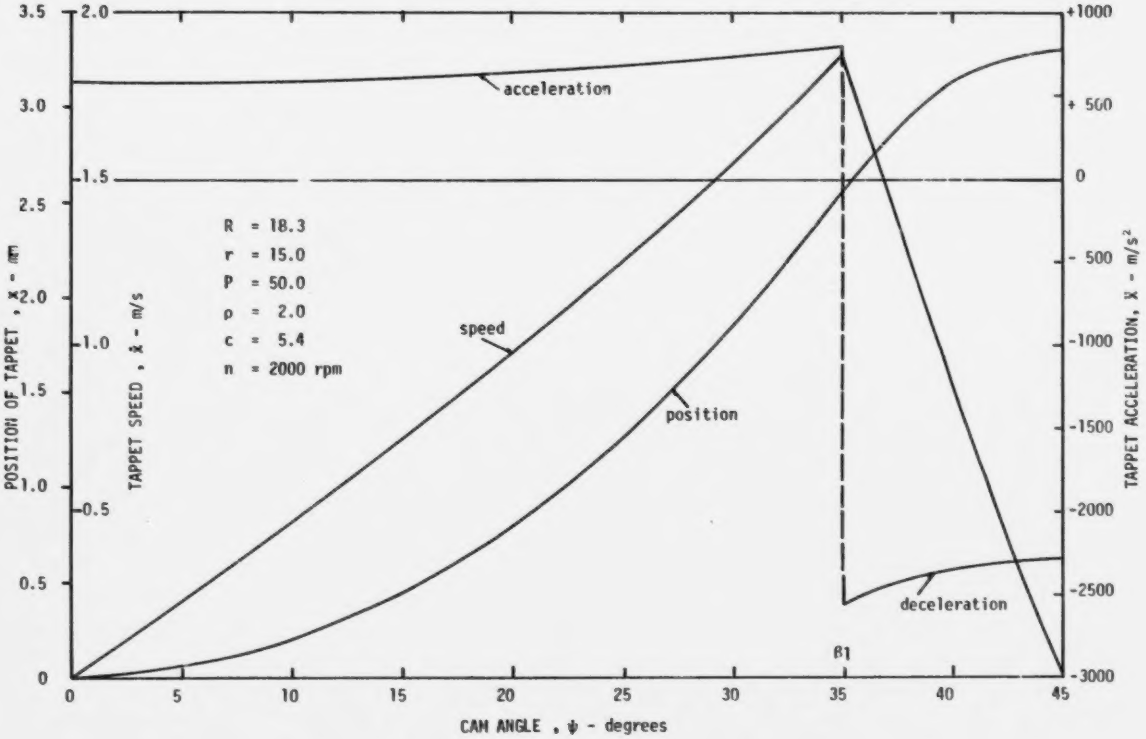

Fig. 7. Characteristics of tappet motion during valve closing.
Camshaft speed: 2000 rpm.

additional function: the pressure in the discharge manifold being typically between 5 and 10 bars higher than in the camshaft housing, the bellows furnishes a pressure force with which the tappet is pushed against the camshaft, thereby assuring a permanent contact between the two elements. With a maximum crankshaft speed of 1000 rpm the bellows is subjected to load cycles at a frequency of 33 Hz. This value is about an order of magnitude above the maximum frequency recommended by the bellows manufacturers. Moreover, the client having specified a minimum operating lifetime of 500 hours at maximum compressor speed, the bellows must survive at least 60 million load cycles, which again is one or two orders of magnitude above manufacturer's specifications. We believe that such a requirement can be met only if, unlike what seems to be general practice, the bellows is deflected only in the strictly elastic range of its material's stress deflection curve [3]. This means that the ratio of the bellows' stroke to its free length has to be limited to a few **percent**. Stroke and free length are 3.3 mm and 60 mm, respectively, in our design.

Tribological Problems

Because of the small size of the compressor, we had initially designed the tappet as a simple, single element. Friction and wear between tappet and cam were reduced through oil lubrication. Unfortunately, we could not maintain a stable oil film between the gliding elements at high camshaft speeds, and excessive wear resulted under these conditions. Since an effective oil lubrication would be even more difficult to maintain under null gravity condition, owing to the absence of a defined level of the oil pool, we have abandoned the gliding contact with oil lubrication in favor of a practically pure rolling contact between the cam and a roller held in the tappet head with miniature ball bearings. Whereas the ball bearings are grease lubricated for life, there is no lubrication at all between roller and cam. Rather extensive testing with camshafts and rollers of different materials, different surface treatments and/or coatings were required to identify that material combination that resulted in the least wear of the cam and roller surfaces. Generally speaking, the camshaft has been found to be the critical element, apparently because of the large radii of curvature of the cam's surface compared with the roller's radius. Specifically, the surfaces of cams made of nitrided steel or coated with tungsten carbide or titanium carbide were found to deteriorate rather rapidly. All roller materials tested performed satisfactorily. These were nitrided steel 34CrAlMo5 and through-hardened steel X102CrMo17 or X165CrMoV12. Excellent results have been obtained with a camshaft made of X102CrMo17 steel, through-hardened and paired with a roller made of the nitrided steel mentioned above. Also very good results were obtained with boronized cam surfaces (material: steel 42CrMo4 boronized to a depth of 100 µm and steel X165CrMoV12 boronized 20 µm deep), paired with rollers made of either one of the three materials mentioned above. With the Hertzian pressure varying between 450 N/mm^2 and 550 N/mm^2 during one revolution of the camshaft, we observed some minor wear of these cams during the first 50 hours of testing at a camshaft speed of 2000 rpm and practically no wear thereafter during several thousand hours of testing.

Guidance of the tappet is provided by a dry bearing material consisting of a layer of sintered bronze that is impregnated with PTFE. The tappet is made of titanium which, according to the dry bearing material's manufacturer, is not hard enough for minimum wear of its material. Therefore we have coated the tappet surfaces with tungsten carbide that is applied with a flame plating process.

Guidance of the discharge valve stem is less critical than tappet guidance because, in contrast to the tappet, the valve is not subjected to significant moments or forces normal to the stem axis. Hence the guiding bushes for the valve stem are made of a modified PTFE only, and the titanium valve is not coated. However, as can be seen in Fig. 5, a piece of soft iron is interposed between upper and lower stem portion. Since titanium is a reasonably good dielectric, this intermediate stem piece, together with the two coils shown in Fig. 5 inside of a tube made of soft magnetic iron, allows the inductive measurement and recording of the discharge valve motion. The path of the discharge valve shown in Fig. 4 has been redrawn from such a recording.

SUMMARY

The most important elements of the mechanical design of a reciprocating compressor have been discussed. Since this compressor is a component of a reversed Carnot cycle heat pump that will be used on space missions, its design is strongly influenced by two requirements: the capability of operating in the absence of gravity, and the necessity of achieving as high an efficiency as possible in order to minimize the heat pump's power consumption.

Because of the zero-g environment, we have replaced oil by grease as a lubricant, which made it necessary to strictly separate the heat pump's working fluid from the lubricants. This requirement led to the incorporation of metal bellows with extremely long operating lifetimes.

The concept of a semi-automatic discharge valve was introduced in order to optimize the compressor efficiency. This valve opens automatically when the pressure in the cylinder starts exceeding the pressure in the discharge manifold, but it is closed by means of a mechanism such that complete closing is reached at a particular crank angle or piston position. The main features of this mechanism have been described.

REFERENCES

1. Berner F., Oesch H. and Goetz K., "Development of a Reverse-Rankine Cycle Heat Pump for Space Use: Design and Testing of the Engineering Model of the Vapor Compressor," Final Report, ESA Contract No. 4094/79/NL/AK(SC), Swiss Federal Aircraft Factory, Doc. No. FO-1568, September 1981.

2. Young J. and Fannin Th., "Vapor Evolution Rates from Oil-Refrigerant Mixtures Following Expansion Through a Nozzle," publ. in Proceedings of the 1972 Purdue Compressor Technology Conf., July 25-27, 1972.

3. Berner F. et al., "Testing of Metal Bellows and Springs in Support of the Development of a Vapor Compressor for Space Flight Application," Final Report, Rider No. 1 to ESA Contract No. 3446/77/Nl/(SC), Swiss Federal Aircraft Factory, Doc. No. FO-1466, April 1979.

4. Berner F., "Initial Development of a Vapor Compressor for Heat Pump to be Used in Spacecraft," Final Report, ESA Contract No. 2447/75 AB (Rider), Swiss Federal Aircraft Factory, Doc. No. FO-1402, December 1977.

5. Berner F., Oesch H. and Jöri O., "Study and Detail Design of the Engineering Model of a Vapor Compressor to be Used in Space," Final Report, ESA Contract No. 3770/78/NL/PP, Swiss Federal Aircraft Factory, Doc. No. FO-1498, December 1979.

Felix Berner
Swiss Federal Aircraft Factory
CH-6032
Emmen, Switzerland

Mr. Berner has been Chief Engineer in the Thermodynamics Section of the Research and Testing Department at the Swiss Federal Aircraft Factory since 1975. In this position, he has been in charge of all work in the field of thermal control for the European Space Agency. From 1966 to 1975, he was a technical specialist in gas dynamics for Swiss Federal Aircraft. As such, he was responsible for the aerodynamics of the front fairing of Europe's launch vehicle, Ariane.

Mr. Berner emigrated to the United States in 1954, becoming naturalized in 1960. Prior to returning to Switzerland in 1966, he was employed as a principal research scientist at the Avco-Everett Research Laboratory. In this position, he worked primarily on classified projects dealing in the areas of reentry physics and ICBM technology. Mr. Berner received his degree in Mechanical Engineering from Swiss Federal Institute of Technology, Zurich, Switzerland, in 1952.

Co-authors of this paper are Mr. H. Oesch and Mr. K. Goetz who are also with the Swiss Federal Aircraft Factory in Zurich and Mr. C. J. Savage who is affiliated with the European Space Agency (ESTEC), The Netherlands.

DESIGN OF A 7kW POWER TRANSFER SOLAR ARRAY DRIVE MECHANISM

J.S. Sheppard *

ABSTRACT

With the availability of the Shuttle and the European launcher, Ariane, there will be a continuing trend towards large payload satellite missions requiring high-power, high-inertia, flexible solar arrays. The need arises for a solar array drive with a large power transfer capability which can rotate these solar arrays without disturbing the satellite body pointing. This paper describes the modular design of such a Solar Array Drive Mechanism (SADM) which is capable of transferring 7kW of power or more. Total design flexibility has been achieved, enabling different spacecraft power requirements to be accommodated within the SADM design.

INTRODUCTION

Since the early 1970's, British Aerospace (BAe), Space and Communications Division, has designed and manufactured Solar Array Drives (SAD) for flight applications. In 1978, the Bearing and Power Transfer Assembly (BAPTA) was qualified for and successfully flown on the Orbital Test Satellite (OTS) for the European Space Agency (ESA). To the present day, suitably modified versions of the BAPTA are being used on a number of European spacecraft including MARECS, ECS, EXOSAT and currently, TELECOM 1, due to be launched in 1983. The BAPTA was also successfully used on the Indian national spacecraft APPLE.

British Aerospace Dynamics Group,*
Space and Communications Division,
Stevenage, England.

The BAPTA, shown in Figure 1, was evolved to orientate medium power (~ 0.5kW) and medium size (~ $5kgm^2$) rigid panel solar arrays at geosynchronous orbit rate. Communication spacecraft of the near future, such as those used for direct television broadcasting with European coverage, will require high-inertia (~ $100-2000kgm^2$), flexible solar arrays providing up to 10kW of power. The operational requirements imposed on the solar array drive by these high-power arrays have necessitated a redesign of BAe's present BAPTA concept.

BAe was awarded a contract in 1978, funded under the Advanced Supporting Technology Programme (ASTP) and coordinated by ESA. This contract was for a design study for an Advanced Solar Array Drive Subsystem (ASADS). The prime objectives were to identify the requirements for and to design an ASADS which would meet the varying needs of different spacecraft applications with a special emphasis on telecommunications. To achieve this, potential satellite market requirements over the next 10 to 15 years were reviewed, together with the types of solar array available to meet the associated higher power levels. It was concluded that an array drive with a power transfer capability of 7kW was required. Several design concepts were evolved, enabling a design trade-off study to be completed. This resulted in a preferred mechanical configuration for the Solar Array Drive Mechanism (SADM) described in this paper.

Design flexibility was a principal objective in designing the SADM in order to satisfy the requirement of being able to meet various spacecraft needs, especially in the area of power transfer. This was achieved by adopting a modular design approach whereby subassembly modules or components can be removed from the mechanical assembly and modified to suit a customer's particular requirements without impacting on the remainder of the mechanism. In meeting its performance objectives, the SADM employs several novel design techniques in the areas of power transfer, bearing support, drive redundancy and pyro/signal transfer.

MECHANICAL CONFIGURATION

The mechanical configuration for the SADM is shown in Figure 2. It consists of four prime modules; namely:

- power slip ring unit
- bearing support unit
- drive actuator unit
- pyro/signal slip ring unit

The power slip ring unit, shown in Figure 3, provides the means of transferring the solar-generated electrical power from the rotating solar array into the stationary spacecraft body. The unit consists of two pancake-type slip ring discs mounted on a titanium array drive shaft. Each disc is double sided with 13 concentric slip rings per side. Two triangular brush block assemblies, mounted diametrically opposite each other, are positioned on each face of the two discs. Each brush block provides 4 contacts on each slip ring by having 13 brushes per side in a leading and trailing 'V' configuration relative to the rotation of the slip ring discs. The brush blocks are mounted on stiffened aluminium diaphragms which act as heat collectors for the power dissipated in the unit. Each slip ring circuit is current rated at 8A for operating voltages up to 100V. The brush contacts are sized on the basis that any three of the four contacts shall be capable of carrying this current should a brush circuit fail.

It was evident during the design evaluation that the large number of slip rings required to meet the 7kW power transfer requirement would be a design driver. Volume constraints, thermal performance, and compatibility with the modular design approach were also important considerations. For these reasons, a pancake-type unit was preferred to the cylindrical-drum-type assembly used on the BAe BAPTA. The pancake-type unit provides an axially compact assembly whose large surface area, provided by each face of the slip ring discs, helps radiate the heat dissipated when carrying high currents, thereby preventing excessive component temperatures within the unit. For the SADM, heat dissipation is minimised by oversizing the brush contacts to carry a larger current than the design requirement. This provides a degree of redundancy in that a single brush failure will not impair the performance of the unit; and, since a larger contact area is required for the higher current rating, the brush contact resistance will be proportionally lower. High friction torque and brush wear are inherent disadvantages with the pancake-type unit due to the increasing radius of contact with each concentric slip ring. The materials selected for the slip rings and brushes will directly influence these parameters.

For this reason, the first choice of materials are those currently developed in Europe and space proven on the BAe BAPTA programmes; i.e., gold-plated copper slip rings contacted by silver-molydisulphide-copper brushes. From test data accrued by BAe, the performance of the SADM using this combination of materials could be readily predicted. The estimated wear on the outermost brush, having the greatest rubbed distance, is on the order of 0.06mm, assuming a 10-year, low-Earth-orbit mission. This will result in little variation in friction torque(~1.5Nm) and contact resistance (~3-10 milliohms) since the brush contact pressure will effectively remain constant at 345kN/m^2. Recent investigations with this combination of materials have revealed the presence of a high-resistant (~90 milliohms) silver-sulphide film on the surface of the gold slip rings. This phenomena appears to be associated with long storage times in air, following running-in and performance testing. Subsequent operation in vacuum appeared to remove the film after several revolutions. For the SADM, with its high current levels, this film would have a significant impact on power dissipation within the unit, increasing the level by a factor of up to 30 times the predicted norm of 2.3W.

This problem may be alleviated using a novel design approach whereby the dry-lubricated, composite silver-molydisulphide-copper brushes are replaced by multi-filament gold wire brushes running in 'U' shaped, gold-plated-copper slip rings. No additional lubricants are used and therefore contamination from oils or from chemical reactions does not occur. In the USA, Polyscientific has carried out extensive research and development into this technique and has demonstrated that, by selecting the correct combination of gold alloys for the brushes and slip rings, a vacuum performance comparable to that of the composite brush design can be achieved. Proprietary test data has revealed that as a result of the low filament contact pressures inherent in the design, extremely low contact wear rates can be achieved. Tests carried out on a brush contact configuration similar to that of the SADM have resulted in over 1.5 billion inches of ring travel under ambient conditions. The multi-filament contact with the slip ring surface provides an extremely low contact resistance (~ 3 milliohms) due to a greater number of asperity contacts; and, since each filament is effectively a wire conductor, a much improved current density (~ 31 X 10^6 A/m^2 in air) can also be achieved. The modular constuction used in the slip ring unit allows either or both slip ring designs to be incorporated in the SADM.

The bearing support unit, shown in Figure 4, provides the major structural element within the SADM, enabling array launch and deployment loads to be transmitted through to the spacecraft structure. The unit consists of a beryllium drive shaft supported on two rigidly preloaded, lead lubricated, angular contact bearings. The bearings are mounted in a beryllium housing which is precision located in an aluminium baseplate. The baseplate provides the basic structure on which all the modular assemblies and other components are mounted.

Rigidly preloaded bearings are very sensitive to thermal gradients across the bearing assembly. Differential expansion within the bearing preload system will result in high bearing loads and friction torques. These effects can be desensitised by using a soft preload system employing springs to absorb the differential movements without causing significant changes in preload and bearing friction. However an off-loading mechanism is required to protect the soft preload system during launch. A considerable mass saving can therefore be made by using a rigid preload method. For the SADM, the bearings are sized to withstand directly the worst-case loads expected during launch (~3000N, 450Nm). Thermal compensation is achieved by using aluminium alloy spacers within the rigid preload system. Detailed bearing analyses performed by the European Space Tribology Laboratory (ESTL) in the UK have found that this choice of spacer material used in conjunction with the steel bearings and beryllium housing/shaft permit temperature differentials of up to 100°C to exist without exceeding the static capacity of the bearings. The maximum predicted temperature differential for the SADM is 20°C.

For low speed applications, good, reliable boundary lubricants must be used to prevent metal contact between the bearing raceway and balls.

This is achieved by using a dry-film lubricant method which has been developed in Europe by ESTL (Reference 1). The process involves ion plating a lead film on the ball bearing raceways to a thickness of 0.2-0.5 microns. Over one million hours' worth of operational test data has been gathered on this process, which has been shown to produce an adherent, good-quality, low-friction lead film with low wear rates. From test data contained in Ref. 1., bearings of approximately BAPTA size (42mm outside diameter, 20mm inner diameter) were rotated in a vacuum at 100-200 rpm for over 2 million revolutions, with an average torque of 0.002Nm. This technique is currently used on all BAe BAPTA programmes with flight experience having been gained with the successful launches of OTS, MARECS and APPLE. This process has also been selected for use on the SPOT, SAD and GIOTTO despin mechanism.

The torque required to rotate the solar array is provided by the drive actuator unit. This unit consists of two main drive stepper motors fixed to a pivoted rocker arm. The rocker arm is connected to an eccentric cam by a hinged rod. The cam is driven by a third stepper motor. The output shaft of each main drive motor terminates in a drive pinion. Either drive pinion, may be brought into mesh with a 30-to-1 main ring gear which is keyed onto the main drive shaft of the bearing support unit. Gear engagement is achieved by slightly rotating the rocker arm using the eccentric cam drive motor. The eccentricity on the cam is sufficient to fully engage one drive pinion, whilst simultaneously disengaging the other. When driving the ring gear, the engaged pinion will exert a radial force on the rocker arm, tending to separate the two gears and backdrive the cam. This is prevented by locating the cam in an over-centre condition such that this separating force will always tend to lock the cam against mechanical end stops as shown in Figure 5.

Mechanical drive redundancy was introduced as a requirement to prevent a single-point failure occurring in the drive system as a result of a tribological breakdown of the gears. Test data for the gear materials used on the SADM, i.e., nitrided nitralloy steel and 440C steel with ion-plated lead, has shown that a gear life of over 50 times that required has been achieved (1.7 million revolutions for a low-Earth-orbit mission) using gears with diametral pitches identical to those on the mechanism (Reference 2).

Control analyses performed for a solar array drive rotating a high-inertia, flexible solar array have shown that a stepped drive system can give an acceptable performance providing the torque impulse applied to the array is sufficiently small. If not, the step motion of the drive is likely to excite the arrays, resulting in unacceptable disturbance torques being applied to the spacecraft body with an associated loss in pointing capability. For the SADM the torque impulse is minimised by reducing the time over which the torque (~15Nm maximum) is applied. This enables a healthy torque margin (~5) to be maintained over the estimated worst-case friction levels. The time period over which the torque is applied will be a function of the motor step size since the output speed is required to be constant.

Therefore the torque impulse per step may be significantly reduced by stepping through smaller angles. This is achieved on the SADM by electronically sub-dividing the basic motor step into smaller mini-steps of 0.06°. The resulting impulse bit has been demonstrated analytically not to disturb the satellite when rotating the arrays at geosynchronous rates and during transition to faster sun acquisition speeds.

The SADM is required to provide a number of slip rings for transferring pyrotechnic firing currents, motor drive currents and control signals to and from the solar arrays. Safety requirements dictated that the slip rings carrying the pyrotechnic firing currents should be totally electrically isolated from the remainder of the slip rings. This was to prevent premature firing of a pyrotechnic device due to electromagnetically induced currents in the pyrotechnic firing circuits.

A novel design solution for this pyro/signal slip ring unit was found for the SADM. The unit is a self-contained assembly consisting of two miniature cylindrical slip ring assemblies concentrically mounted within the main shaft of the bearing support unit. The innermost assembly provides 20 gold-plated slip rings which are contacted tangentially by gold fibre brushes similar to those previously discussed for the power slip ring unit. This assembly provides the pyrotechnic slip ring circuits and therefore is contained within a metallic shield to isolate it from the outermost slip ring assembly. The outermost assembly provides a total of 50 slip rings, identical to those of the inner assembly. These slip rings provide the control and array monitoring functions. Dry-lubricated bearings are used to support the slip ring assemblies within the unit.

Polyscientific has demonstrated lives in excess of 20 million inches of ring travel in a vacuum ($\sim 10^{-8}$ torr) using a 0.5-inch-diameter cylindrical slip ring unit with unlubricated tangential fibre brushes.

The mechanical configuration for the SADM has been evolved to meet the foreseen requirements of large power spacecraft. Its key features may be summarised as follows:

- compact mechanical design
- full mechanical and electrical redundancy
- simple operation
- high reliability
- design flexibility to meet varying system requirements

FUTURE DEVELOPMENTS

At the time of writing, an engineering model SADM is being manufactured and assembled. This unit will undergo functional and environmental testing to qualification levels. This will be followed by a thermal vacuum test and an accelerated life test, designed to simulate a 10-year operational life. The SADM will undergo a strip examination following the life test.

A derivative of the SADM has been successfully bid for use on the European Large Satellite (L-SAT) programme. For this satellite a reduced mass version of the mechanism will be flown, whereby the two main drive motors will be fixed in constant mesh with the ring gear. This approach deletes the need for the redundant actuator mechanism and can be readily achieved without significantly impacting on the remainder of SADM assembly. For L-SAT 1, only a single power slip ring disc is required, further illustrating the flexibility of the SADM design.

ACKNOWLEDGEMENTS

The author would like to acknowledge the valuable advice and direction given by Mr. D.E.L. Tunbridge of ESA, Mr. M.J. Todd of ESTL, and the engineering staff at Polyscientific, Blacksburg, Va., USA.

REFERENCES

(1) Todd, M.J. and Robbins, E.J; Ion-plated Lead as a Film Lubricant for Bearings in Vacuum; ESA Report, ESA (ESTL)26; October 1977.

(2) Vest, C.E., Courtney, W.J. and Farrel, J.J.; Evaluation of Gear Materials for Space Applications; American Society of Lubrication Engineers and American Society of Mechanical Engineers Lubrication Conference, Houston, Texas, October 14-16, 1969.

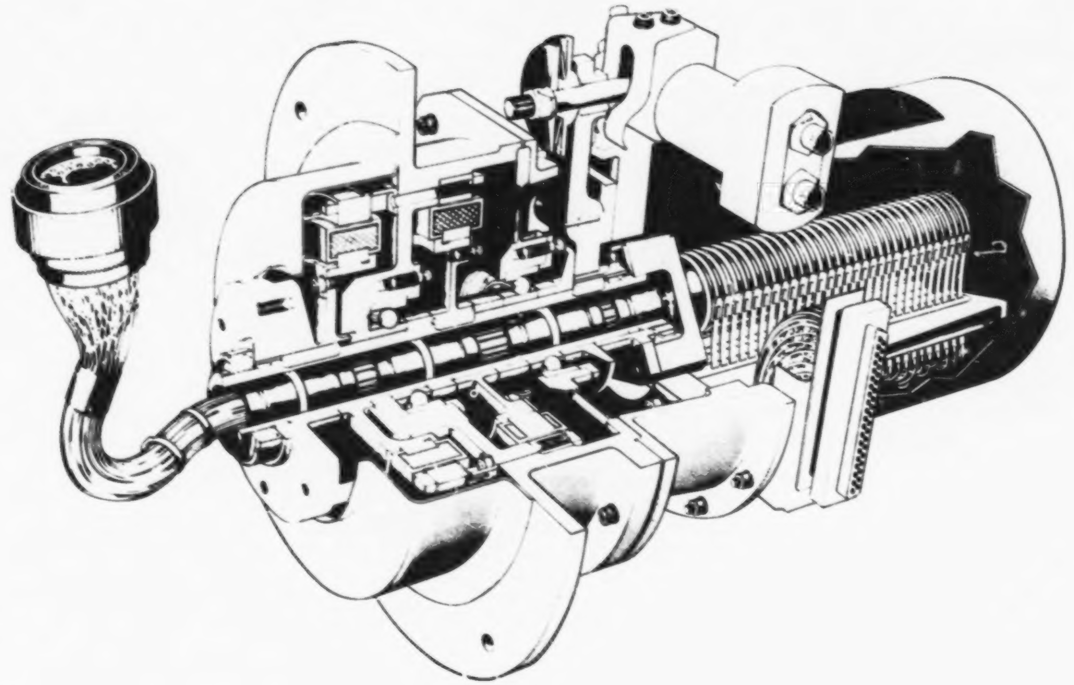

Bearing and Power Transfer Assembly (BAPTA) Fig. 1

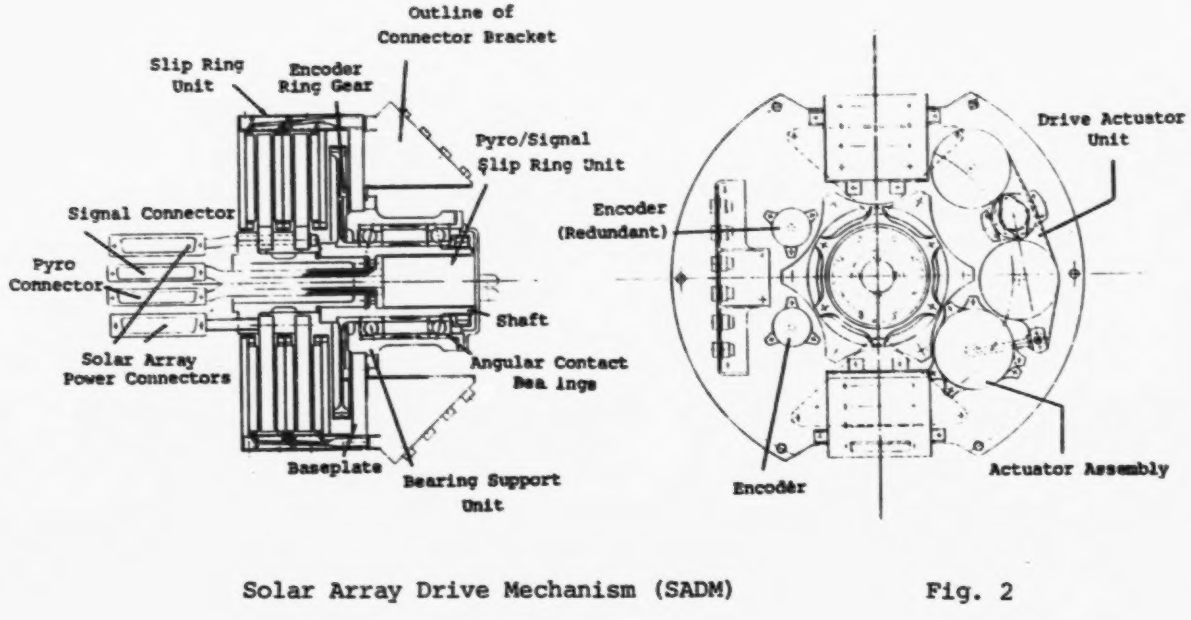
Outline of Connector Bracket
Slip Ring Unit
Encoder Ring Gear
Pyro/Signal Slip Ring Unit
Signal Connector
Pyro Connector
Solar Array Power Connectors
Shaft
Angular Contact Bearings
Baseplate
Bearing Support Unit
Drive Actuator Unit
Encoder (Redundant)
Encoder
Actuator Assembly

Solar Array Drive Mechanism (SADM) Fig. 2

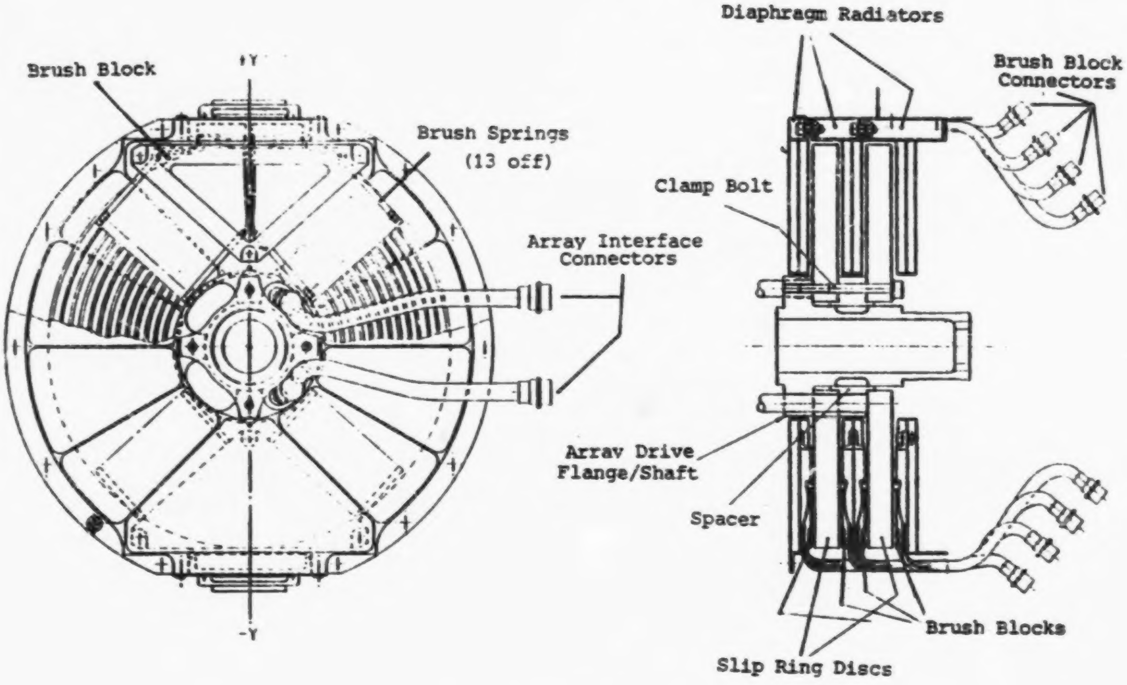
Diaphragm Radiators
Brush Block
+Y
Brush Springs
(13 off)
Brush Block
Connectors
Clamp Bolt
Array Interface
Connectors
Arrav Drive
Flange/Shaft
Spacer
-Y
Brush Blocks
Slip Ring Discs

Power Slip Ring Unit Fig. 3

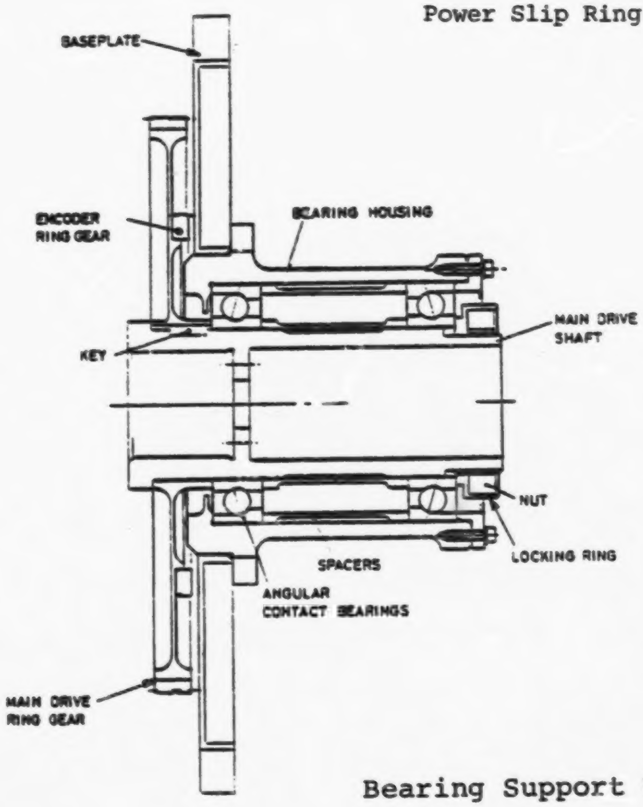
BASEPLATE
ENCODER
RING GEAR
BEARING HOUSING
MAIN DRIVE
SHAFT
KEY
NUT
LOCKING RING
SPACERS
ANGULAR
CONTACT BEARINGS
MAIN DRIVE
RING GEAR

Bearing Support Unit Fig. 4

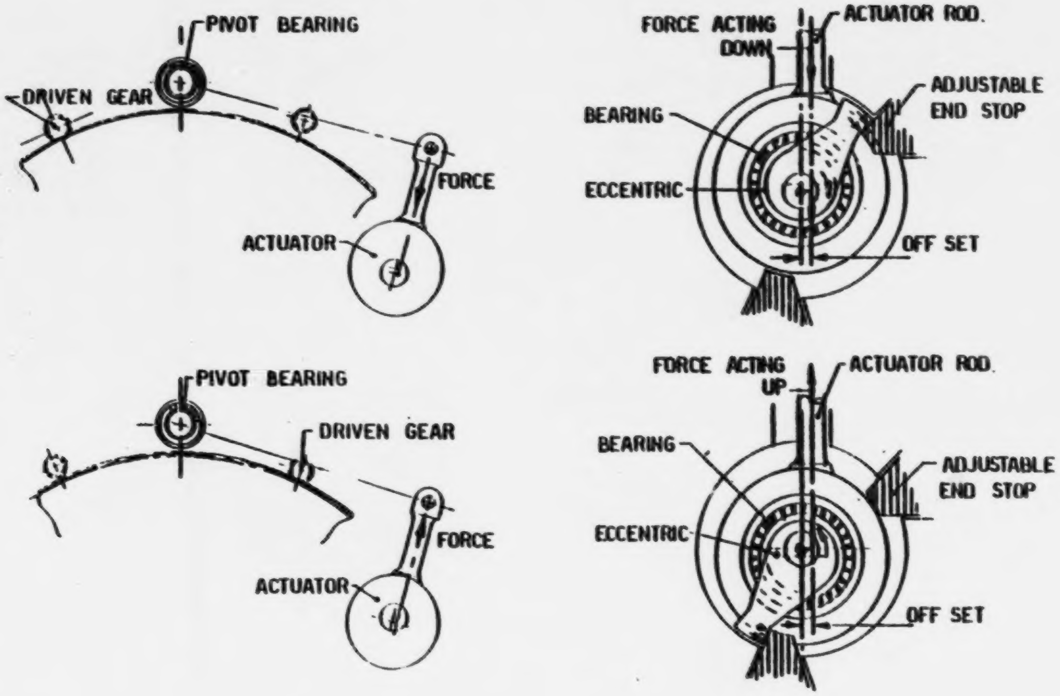
PIVOT BEARING
DRIVEN GEAR
FORCE
ACTUATOR
FORCE ACTING DOWN
ACTUATOR ROD.
ADJUSTABLE END STOP
BEARING
ECCENTRIC
OFF SET
PIVOT BEARING
DRIVEN GEAR
FORCE
ACTUATOR
FORCE ACTING UP
ACTUATOR ROD.
BEARING
ADJUSTABLE END STOP
ECCENTRIC
OFF SET

Eccentric Cam Engagement Mechanism Fig. 5

1. Report No.
NASA CP-2221

2. Government Accession No.

3. Recipient's Catalog No.

4. Title and Subtitle
16TH AEROSPACE MECHANISMS SYMPOSIUM

5. Report Date
May 1982

6. Performing Organization Code
DE-MOO-1

7. Author(s)

8. Performing Organization Report No.

9. Performing Organization Name and Address
John F. Kennedy Space Center
Kennedy Space Center, Florida 32899

10. Work Unit No.

11. Contract or Grant No.

12. Sponsoring Agency Name and Address
National Aeronautics and Space Administration
Washington, DC 20546

California Institute of Technology
Pasadena, CA 91109

Lockheed Missiles & Space Co., Inc.
Sunnyvale, CA 94088

13. Type of Report and Period Covered
Conference Publication

14. Sponsoring Agency Code

15. Supplementary Notes

16. Abstract

The proceedings of the 16th Aerospace Mechanisms Symposium held at the John F. Kennedy Space Center on May 13-14, 1982, are reported in this NASA Conference Publication. Technological areas covered include design of unique ground support equipment, orbiter specialized hardware, payload deployment and positioning. Devices used in space operations are also described.

17. Key Words (Suggested by Author(s))
Ground support equipment
Thermal protection
Remote manipulator
Separation devices
Latching mechanisms
Solar array devices

18. Distribution Statement
Unclassified - Unlimited

Subject Category 31

19. Security Classif. (of this report)
Unclassified

20. Security Classif. (of this page)
Unclassified

21. No. of Pages
360

22. Price
A16

For sale by the National Technical Information Service, Springfield, Virginia 22161

NASA-Langley, 1982